VOLUME 76 FEBRUARY 3, 1972 NUMBER 3

JPCHAx

THE JOURNAL OF PHYSICAL CHEMISTRY

PUBLISHED BIWEEKLY BY THE AMERICAN CHEMICAL SOCIETY

THE JOURNAL OF

PHYSICAL CHEMISTRY

BRYCE CRAWFORD, Jr., *Editor*
STEPHEN PRAGER, *Associate Editor*
ROBERT W. CARR, Jr., FREDERIC A. VAN-CATLEDGE, *Assistant Editors*

EDITORIAL BOARD: A. O. ALLEN (1970–1974), J. R. BOLTON (1971–1975), F. S. DAINTON (1972–1976), M. FIXMAN (1970–1974), H. S. FRANK (1970–1974), R. R. HENTZ (1972–1976), J. R. HUIZENGA (1969–1973), W. J. KAUZMANN (1969–1973), R. L. KAY (1972–1976), W. R. KRIGBAUM (1969–1973), R. A. MARCUS (1968–1972), W. J. MOORE (1969–1973), J. A. POPLE (1971–1975), B. S. RABINOVITCH (1971–1975), H. REISS (1970–1974), S. A. RICE (1969–1975), F. S. ROWLAND (1968–1972), R. L. SCOTT (1968–1972), R. SEIFERT (1968–1972), W. A. ZISMAN (1972–1976)

CHARLES R. BERTSCH, *Manager, Editorial Production*

AMERICAN CHEMICAL SOCIETY, *1155 Sixteenth St., N.W., Washington, D. C. 20036*
FREDERICK T. WALL, *Executive Director*

Books and Journals Division
JOHN K CRUM, *Director*
JOSEPH H. KUNEY, *Head, Business Operations Department*
RUTH REYNARD, *Assistant to the Director*

©Copyright, 1972, by the American Chemical Society. Published biweekly by the American Chemical Society at 20th and Northampton Sts., Easton, Pa. 18042. Second-class postage paid at Washington, D. C., and at additional mailing offices.

All manuscripts should be sent to *The Journal of Physical Chemistry,* Department of Chemistry, University of Minnesota, Minneapolis, Minn. 55455.

Additions and Corrections are published once yearly in the final issue. See Volume 75, Number 26 for the proper form.

Extensive or unusual alterations in an article after it has been set in type are made at the author's expense, and it is understood that by requesting such alterations the author agrees to defray the cost thereof.

The American Chemical Society and the Editor of *The Journal of Physical Chemistry* assume no responsibility for the statements and opinions advanced by contributors.

Correspondence regarding accepted copy, proofs, and reprints should be directed to Editorial Production Office, American Chemical Society, 20th and Northampton Sts., Easton, Pa. 18042. Manager: CHARLES R. BERTSCH. Assistant Editor: EDWARD A. BORGER. Editorial Assistant: WILLIAM T. BOYD.

Advertising Office: Century Communications Corporation, 142 East Avenue, Norwalk, Conn. 06851.

Business and Subscription Information

Remittances and orders for subscriptions and for single copies, notices of changes of address and new professional connections and claims for missing numbers should be sent to the Subscription Service Department, American Chemical Society, 1155 Sixteenth St., N.W., Washington, D. C. 20036. Allow 4 weeks for changes of address. Please include an old address label with the notification.

Claims for missing numbers will not be allowed (1) if received more than sixty days from date of issue, (2) if loss was due to failure of notice of change of address to be received before the date specified in the preceding paragraph, or (3) if the reason for the claim is "missing from files."

Subscription rates (1972): members of the American Chemical Society, $20.00 for 1 year; to nonmembers, $60.00 for 1 year. Those interested in becoming members should write to the Admissions Department, American Chemical Society, 1155 Sixteenth St., N.W., Washington, D. C. 20036. Postage to Canada and countries in the Pan-American Union, $5.00; all other countries, $6.00. Single copies for current year: $3.00. Rates for back issues from Volume 56 to date are available from the Special Issues Sales Department, 1155 Sixteenth St., N.W., Washington, D. C. 20036.

This publication and the other ACS periodical publications are now available on microfilm. For information write to: MICROFILM, Special Issues Sales Department, 1155 Sixteenth St., N.W., Washington, D. C. 20036.

Notice to Authors last printed in the issue of December 23, 1971

THE JOURNAL OF
PHYSICAL CHEMISTRY

Volume 76, Number 3 February 3, 1972

JPCHAx 76(3) 285–458 (1972)

COMMUNICATIONS TO THE EDITOR

AUTHOR INDEX

In papers with more than one author the name of the author to whom inquiries about the paper should be addressed is marked with an asterisk in the by-line.

THE JOURNAL OF
PHYSICAL CHEMISTRY

Registered in U. S. Patent Office © *Copyright, 1972, by the American Chemical Society*

VOLUME 76, NUMBER 3 FEBRUARY 3, 1972

The Reaction of Hydrogen Cyanide and Deuterium behind Reflected Shock Waves[1]

by J. M. Brupbacher and R. D. Kern*

Department of Chemistry, Louisiana State University in New Orleans, New Orleans, Louisiana 70122
(Received August 19, 1971)

Publication costs assisted by the National Science Foundation

A complementary shock tube technique has been employed to study the exchange reaction occurring in equimolar mixtures of HCN and D_2 over the temperature range 2000–3000°K. One shock tube of the complementary system recorded infrared emission from HCN and DCN highly dilute in argon. The second shock tube was coupled to a time-of-flight mass spectrometer in order to monitor mass peaks of interest at 20 μsec intervals. The experiments spanned a total gas density variation of 1.8–4.3 × 10^{-6} mol/cm³. Typical observation periods were about 500 μsec during which time an equilibrium condition was established for the higher temperature runs. Agreement of the results from the two independent techniques was obtained within one standard deviation. The data from both shock tubes were fit to an expression involving mole fractions, $\{1 - f_{DCN}[1 + (f_{HCN}/f_{DCN})_{eq}]\} = \exp(-k[HCN]_0^{1.0}[M]^{0.52}t^2)$, with the rate constant given by $k = 10^{22.27\pm0.19}\exp(-51{,}540 \pm 2080/RT)$, cm³ mol^{-1} sec^{-2} $(M)^{-0.52}$. On a concentration basis, the reaction was found to be second order with respect to reactants and 0.52 with respect to the total density. No attempt was made to determine the individual orders with respect to HCN and D_2. The formation of DCN was found to be a nonlinear function of time which clearly indicates that the mechanism for the exchange is complex.

Introduction

Dynamic sampling of reacting gases in exchange systems involving diatomic molecules has revealed that the product formation is a nonlinear function of time.[2] Whenever possible,[2a] the experiments are conducted with a complementary shock tube technique in which the kinetic data are collected by two independent methods: infrared emission and time-of-flight mass spectrometry (TOF). Reports by other workers of exchange reactions using dynamic techniques have disclosed quadratic time dependence for product formation.[3] An inert gas dependence was indicated for several of these studies although it has been acknowledged that the determination of order was the least accurately established quantity.[2b] However, inert gas dependencies for exchange reactions have been reported in numerous publications that relied upon the single pulse shock tube technique.[4] Two studies have appeared in which the inert gas order was zero.[5]

(1) (a) Support of this work by the National Science Foundation under grant GP-23137 and also funds for equipment from NSF Departmental Science Development Program GU-2632 are gratefully acknowledged; (b) paper presented in part at the Southeast-Southwest Regional meeting of the American Chemical Society, New Orleans, La., Dec 1970.

(2) (a) R. D. Kern and G. G. Nika, *J. Phys. Chem.*, **75**, 171 (1971); (b) R. D. Kern and G. G. Nika, *ibid.*, **75**, 1615 (1971); (c) R. D. Kern and G. G. Nika, *ibid.*, **75**, 2541 (1971).

(3) (a) S. H. Garnett, G. B. Kistiakowsky, and B. V. O'Grady, *J. Chem. Phys.*, **51**, 84 (1969); (b) T. C. Clark, S. H. Garnett, and G. B. Kistiakowsky, *ibid.*, **52**, 4692 (1970); (c) I. D. Gay, G. B. Kistiakowsky, J. V. Michael, and H. Niki, *ibid.*, **43**, 1720 (1965).

(4) (a) S. H. Bauer and E. Ossa, *ibid.*, **45**, 434 (1966); (b) D. Lewis and S. H. Bauer, *J. Amer. Chem. Soc.*, **90**, 5390 (1968); (c) A. Burcat and A. Lifshitz, *ibid.*, **47**, 3079 (1967); (d) A. Burcat, A. Lifshitz, D. Lewis, and S. H. Bauer, *ibid.*, **49**, 1449 (1968); (e) A. Lifshitz, C. Lifshitz, and S. H. Bauer, *J. Amer. Chem. Soc.*, **87**, 143 (1965); (f) P. Schechner, A. Burcat, and A. Lifshitz, *J. Chem. Phys.*, **52**, 337 (1970); (g) W. S. Watt, P. Borrell, D. Lewis, and S. H. Bauer, *ibid.*, **45**, 444 (1966).

There are two instances where comparisons of the results from the dynamic methods[2b,c] have been made with those of the single pulse technique.[4a,b] The former experiments covered the temperature range 1800–3000°K and the latter spanned the interval of 1060–1420°K. After adjustment of the single pulse data for quadratic time dependence, the rate constants for the exchange of $H_2 + D_2$ were found to lie on the same Arrhenius line over the temperature range 1060–3000°K.[2b] Similar agreement was demonstrated for the self-exchange of HD.[2c] Furthermore, in the exchange systems HCl + D_2,[2a] $H_2 + D_2$,[2b] and HD + HD[2c] studied by the dynamic technique, equilibrium conditions were attained during the available observation periods that were in agreement with calculated values.

Hence, there is a thread of consistency that runs through these various studies which allows two general conclusions. The mechanism by which the exchange takes place proceeds through a sequence of reactions rather than one direct step resulting in the exchange product. Secondly, the experimental activation energies are far below the predicted values for either an atomic or molecular mechanism.

The purpose of this study was to apply the complementary shock tube technique to an exchange reaction that may be monitored by infrared emission and the TOF. The exchange has not been studied nor have any kinetic data been obtained for the thermal decomposition of HCN. It will be shown that the homogeneous reaction of HCN with D_2 is complicated by the self-exchange of HD and by the metathetical reaction $2HCN \rightleftharpoons C_2N_2 + H_2$. The reaction $C_2N_2 + H_2 \rightleftharpoons 2HCN$ has been previously investigated under heterogeneous conditions.[6]

Experimental Section

The complementary shock tube facility from which all data were obtained has been described previously.[2] In order to remove hazardous vapors from the working area, exhaust piping was connected to the mechanical pumps.

The experiments were performed using HCN which was prepared by the addition of 100 ml of 50% Matheson H_2SO_4 to 25 g of Baker CP KCN. The gas which evolved was collected at 77°K and subjected to several bulb to bulb distillations before it was placed in the gas handling system for storage. The sample was distilled again at the time of mixture preparation and only the middle fraction was used. Reaction mixtures contained equimolar amounts of HCN and Matheson CP D_2 (99.5%). Nonreacting mixtures contained equimolar amounts of HCN and Matheson Research Grade H_2 (99.9995%). Liquid Carbonic argon (99.99%) was used as diluent for the ir experiments and a Matheson Research grade mixture of 99% Ne–1% Ar served as the diluent for the TOF runs. Typical vacuums in the gas handling system during mixture preparation were on the order of 10^{-6} Torr. Partial pressures of reactants and diluent were measured with Wallace-Tiernan differential pressure gauges 0–10 and 0–400 in. water, respectively. Mixtures were analyzed by the TOF analog units and were found to contain no impurity species at a concentration level greater than background. Mixtures were allowed to stand at least 24 hr in 5-l. storage bulbs before runs were performed.

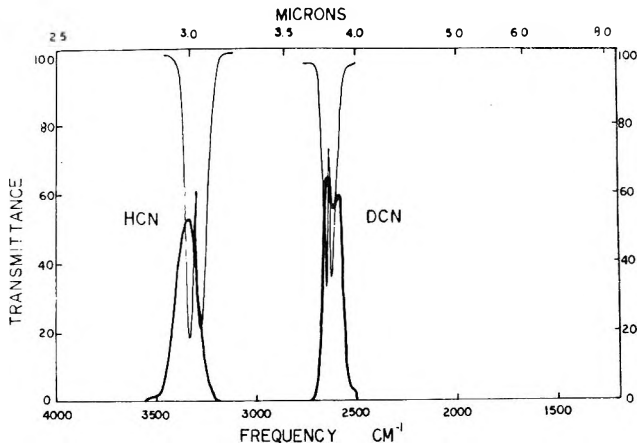

Figure 1. Spectral recording of the vibrational envelopes of HCN and DCN (upper) and their respective filters (lower).

A pair of Infrared Industries interference filters with center wavelengths at 3.0 and 3.8 μ were selected to monitor the emission from HCN and DCN, respectively. The half-band width of the filters is 0.1 μ. An infrared spectrum of the gases and their respective filters is displayed in Figure 1. The emission signals were intense relative to those observed in the HCl–D_2 study. Hence, it was necessary to reduce the slit width through which the radiation passed to 0.5 mm when 2% HCN–2% D_2 experiments were performed at an initial pressure of 10 Torr in order to prevent saturation of the detectors. The slit widths were set at 0.8 mm for the other runs. Outgassing rates in the ir system were less than 0.2 μ/min and as low as 0.05 μ/min prior to all experiments. Repeated shocking of the HCN mixtures resulted in a film buildup at the end wall and on the walls up to 10 cm upstream from the end plate. This film was found to be readily soluble in saturated $NaHCO_3$ solution. In order to monitor the overall cleanliness of the tube, shocks were initiated into argon at 5 Torr. These runs, which were performed between reacting shocks, not only served as a measure of cleanliness but also aided in the cleaning process.

Mass spectra were recorded at 20 μsec intervals on Polaroid 10,000 speed film. Peak heights, which were

(5) (a) H. F. Carroll and S. H. Bauer, *J. Amer. Chem. Soc.*, **91**, 7727 (1969); (b) A. Burcat and A. Lifshitz, *J. Chem. Phys.*, **52**, 3613 (1970).

(6) (a) N. C. Robertson and R. N. Pease, *J. Amer. Chem. Soc.*, **64**, 1880 (1942); (b) N. C. Robertson and R. N. Pease, *J. Chem. Phys.*, **10**, 490 (1942).

shown to be proportional to concentration with nonreacting mixtures, were measured for m/e 27 (HCN) and 28 (DCN). A correction to the DCN peak height due to a HCN contribution at m/e 28 was accomplished by subtracting a constant fraction (0.015) of the HCN peak height from the DCN signal. The fraction was determined by shocking nonreacting mixtures of HCN and H_2. In the TOF experiments, mixtures were analyzed for O_2 just prior to being shocked and for all runs found to be less than 25 ppm in O_2. This level of impurity was established with a known 25 ppm O_2–diluent mixture. Film formation was not observed in the TOF experiments. Outgassing rates in the TOF system were on the order of those reported previously.[2]

Temperatures were determined as described in earlier work.[2] The experimental shock velocities were fit by a least-squares routine and extrapolated to the appropriate observation station. Hydrogen was used exclusively as the driver gas.

Runs at the higher temperatures achieved an equilibrium condition within the available observation times. Statistical thermodynamic formulas were programmed to calculate the equilibrium ratio DCN:HCN as a function of temperature. Thermodynamic data were taken from the JANAF tables.[7] Calculations and plots of data and results were accomplished with the aid of a PDP-10 computer and a digital plotter.

Results

An experimental record on Polaroid 3000 speed film of the emission time history is shown in Figure 2. The contribution to the DCN signal from HCN is due to the shifting of the vibrational envelopes to longer wavelengths at high temperatures. The amount of emission at 3.8 μ due to HCN was determined by shocking equimolar mixtures of HCN and H_2 dilute in argon over the temperature and pressure range spanned by the reacting mixtures. The calibration experiments also served to establish the relation between signal intensities and concentrations.

Photographs of mass spectra are shown in Figure 3. Peak heights of interest from left to right are m/e: 20, 22 (Ne); 26, 27 (HCN); 28 (DCN); and 40 (Ar). The ionizing voltage for the TOF experiments was varied from 30–35 eV. In the beginning of this work, nonreacting mixtures consisted of HCN dilute in argon. However, it was noticed under shock conditions that a peak at m/e 52 increased with time until it reached a constant value. The peak was attributed to cyanogen and its production resulted from the metathetical reaction $2HCN \rightleftharpoons C_2N_2 + H_2$. Additional support for this contention was achieved by taking the square of the C_2N_2:HCN ratio when constant values of each respective peak height were attained. The relative sensitivity of the TOF for C_2N_2:HCN was determined to be 1.054. The resulting number compared favorably with the calculated value of the equilibrium constant[7] ($K = 7 \times 10^{-3}$ at 2500°K). Furthermore, inclusion of 2% H_2 in the mixture shifted the

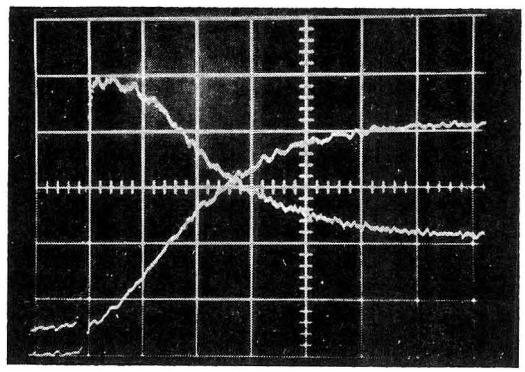

Figure 2. Experimental record of HCN at 3.0 μ (upper trace) and DCN at 3.8 μ (lower trace). Equimolar mixture in argon at 2500°K. The sweep speed is 50 μsec/cm.

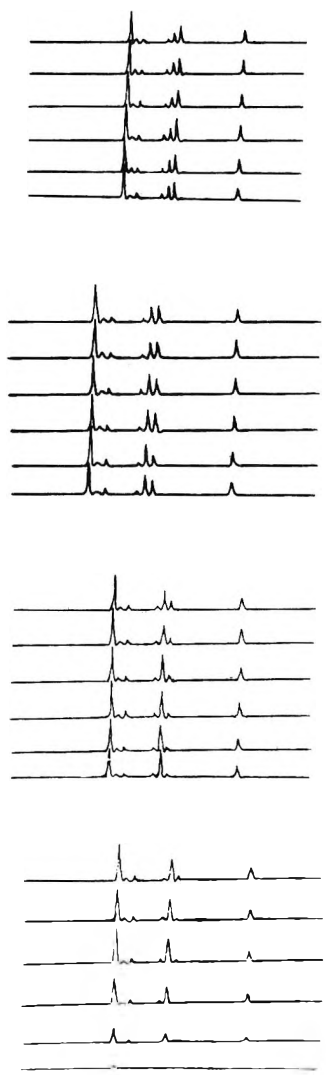

Figure 3. Tracing of TOF experimental record from four sequential photographs for a run at 2700°K. Mass spectra are repeated at 20 μsec intervals.

(7) "JANAF Thermochemical Tables," The Dow Chemical Company, Midland, Mich., 1965.

position of equilibrium far to the HCN side and the peak at m/e 52 was no longer detectable. Hence, calibration mixtures for both TOF and ir experiments were prepared with equal amounts of HCN and H_2 in order to suppress any effects of C_2N_2. It is interesting to note that in those experiments performed on the TOF without hydrogen in the test mixture, equilibrium amounts of HCN and C_2N_2 were observed up to and beyond 500 μsec of observation time. This observation means that mixing of hydrogen driver gas with test mixture was confined largely to the contact surface region during the analysis time.

The data generated by both the TOF and ir-emission shock-tube facilities were fit to the general expression

$$\{1 - f_{DCN}[1 + (f_{HCN}/f_{DCN})_{eq}]\} = \exp(-k't^z) \quad (1)$$

where f_{DCN} is the mole fraction of DCN, k' is the rate constant, and z is the time power for product formation. A plot of the log (−log) of the left hand side of expression 1 *vs.* log of time yields a line whose slope represents the time power. A plot was made for each experiment and z was determined to have a value near 2. It was found that all of the mole fraction reaction profiles were satisfactorily fit with a quadratic time dependence. There was no indication of an induction period.

A specific example of these plots is shown in Figures 4 and 5 for an infrared emission experiment. Reduction of the emission profiles was accomplished as previously described for the HCl–D_2 exchange.[2a]

In the general expression, eq 1

$$k' = k[HCN]_0^x[D_2]_0^{x'}[M]^y \quad (2)$$

where $[HCN]_0$ and $[D_2]_0$ are the initial concentrations of the reactants. The combined order dependence on the reactants, $x + x'$, was determined by studying a 2% HCN–2% D_2 mixture and a 1% HCN–1% D_2 mixture, both at an initial pressure of 10 Torr. Doubling the initial concentration of reactants had the effect of doubling the value of k'. The combined order $x + x'$ was equal to 1 on a mole fraction basis and equal to 2 on a concentration basis since f_{DCN} is defined by $[DCN]/[HCN]_0$.

The order y for the total gas density was determined

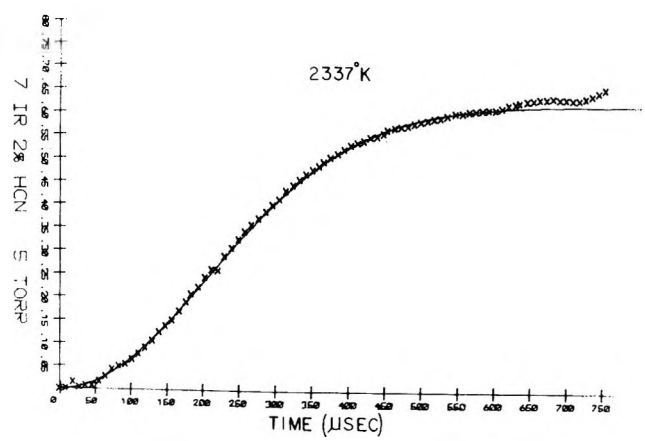

Figure 4. Reaction profile derived from an infrared experiment at 2337°K and fit to a quadratic time dependence.

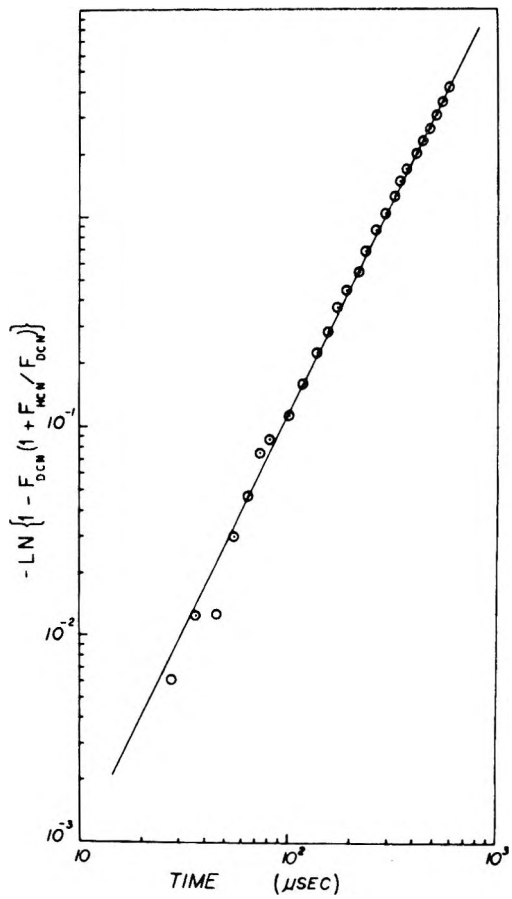

Figure 5. Time power plot of the data shown in Figure 4; slope = 2.07.

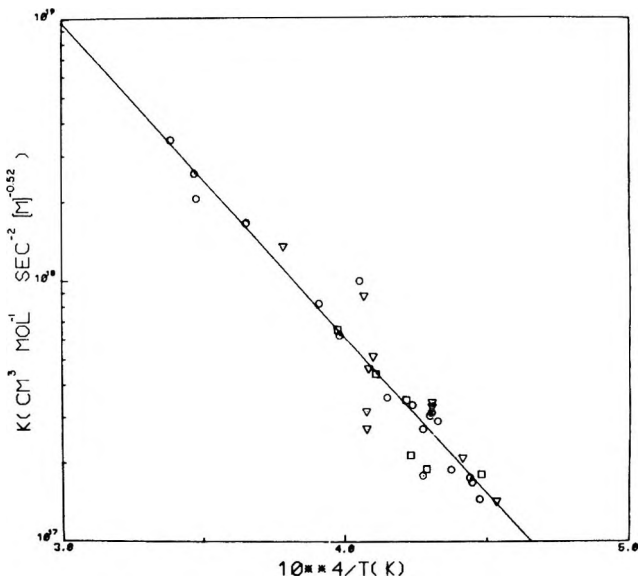

Figure 6. Arrhenius plot of the data in Table I: ⊙, mixture A; ▽, B; ⊡, C.

by comparing k' for a pair of mixtures with the same initial reactant concentration, 2% HCN–2% D_2, but different initial pressures, 5 and 10 Torr. The value of y is 0.52. The rate constants for the ir experiments are listed in Table I and an Arrhenius plot appears in Figure 6. Least-squares treatment of the data yielded values of $\log A = 22.58 \pm 0.28$ and $E^* = 54.84 \pm 3.05$ kcal mol^{-1}.

Table I: Rate Constants for the HCN–D_2 Exchange; Ir Experiments

T, °K	$10^6 \rho$, mol cm^{-3}	$10^{-16} k$, cm^3 mol^{-1} sec^{-2} $[M]^{-0.52}$
Argon Diluent. A. 2% HCN–2% D_2 (P_1 = 5 Torr)		
2233	1.98	14.5
2246	1.98	16.8
2250	1.99	17.6
2284	2.00	18.9
2308	1.99	29.0
2320	2.01	31.3
2324	2.01	30.4
2337	2.02	17.9
2337	2.02	27.0
2357	2.03	33.4
2407	2.08	35.8
2465	2.06	100
2509	2.08	61.9
2555	2.09	82.0
2736	2.13	166
2874	2.18	206
2880	2.18	258
2951	2.20	344
B. 2% HCN–2% D_2 (P_1 = 10 Torr)		
2204	3.95	14.3
2263	4.00	21.0
2319	4.04	33.1
2319	4.02	34.1
2435	4.10	51.4
2445	4.12	46.1
2450	4.16	27.1
2450	4.12	31.6
2455	4.12	87.8
2640	4.23	135
C. 1% HCN–1% D_2 (P_1 = 10 Torr)		
2230	3.84	18.1
2329	3.90	19.0
2360	3.92	21.4
2369	3.92	35.0
2430	3.97	44.0
2513	4.02	65.1

In the TOF experiments, the mole fraction of DCN is given by

$$f_{DCN} = h_{DCN}/(h_{HCN} + h_{DCN}) \quad (3)$$

where h_{HCN} and h_{DCN} are the peak heights of HCN and the corrected peak height of DCN, respectively. The combined reactant order dependence was obtained by shocking two mixtures containing different initial concentrations, 2% HCN–2% D_2 and 1% HCN–1% D_2, Ne–1% Ar diluent, at the same initial pressure 5 Torr over the temperature range 2000–3000°K. The value of k' was different for the two mixtures by a factor of 2. Experiments at higher initial pressures would have increased the TOF ion source pressure beyond prudent operating pressures. A series of runs was made on a mixture dilute in argon. The results of these experiments appear in Table II and Figure 7. The Arrhen-

Table II: Rate Constants for the HCN–D_2 Exchange; TOF Experiments

T, °K	$10^6 \rho$, mol cm^{-3}	$10^{-16} k$, cm^3 mol^{-1} sec^{-2} $[M]^{-0.52}$
Ne–1% Ar Diluent. D. 2% HCN–2% D_2 (P_1 = 5 Torr)		
2004	1.89	4.03
2070	1.84	9.97
2112	1.93	4.98
2160	1.95	11.5
2171	1.96	11.5
2200	1.97	11.3
2237	1.98	16.4
2306	2.01	29.7
2318	2.02	16.9
2581	2.09	54.0
2702	2.13	186
E. 1% HCN–1% D_2 (P_1 = 5 Torr)		
1942	1.76	5.51
2090	1.83	8.79
2099	1.90	8.81
2141	1.84	13.8
2146	1.88	7.26
2152	1.96	13.9
2158	1.89	9.61
2164	1.95	10.7
2181	2.07	9.75
2271	2.03	15.3
2304	1.99	33.2
2310	1.92	29.7
2327	1.86	30.2
2329	1.90	16.0
2380	2.03	33.3
2404	1.99	34.7
2420	1.81	37.0
2468	2.06	33.6
2478	2.06	41.9
2547	2.16	60.1
2614	1.98	206
2691	2.00	101
Argon Diluent. F. 1% HCN–1% D_2 (P_1 = 5 Torr)		
2016	1.82	6.86
2119	1.89	20.5
2181	1.91	11.4
2194	1.90	13.2
2455	1.96	21.9
2565	1.99	80.7
2673	2.06	57.5
2934	2.18	620

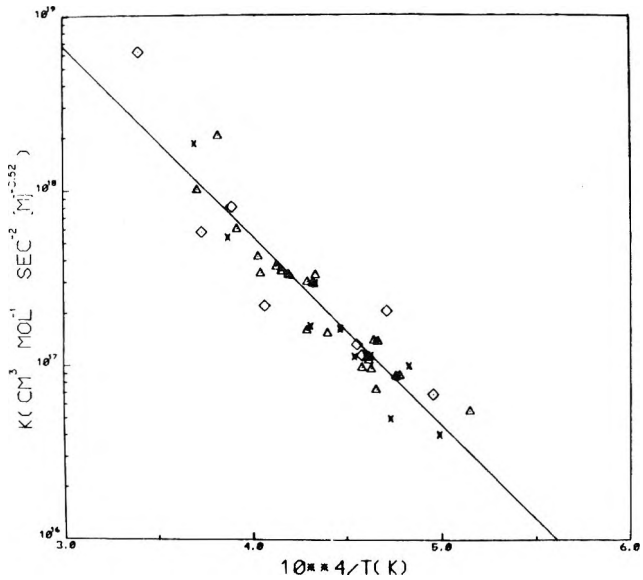

Figure 7. Arrhenius plot of the data in Table II: ×, mixture D; △, E; ◇, F.

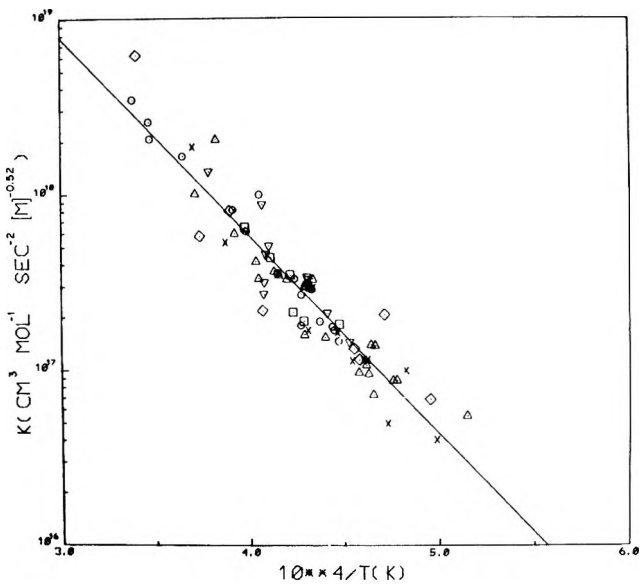

Figure 8. Combined Arrhenius plot of the data in Tables I and II. Same symbols as Figures 6 and 7.

ius parameters are log A = 22.07 ± 0.29 and E^* = 49.53 ± 3.04 kcal mol^{-1}.

The ir and TOF data agree within one standard deviation and an Arrhenius plot of all the data in Tables I and II is shown in Figure 8; log A = 22.27 ± 0.19 and E^* = 51.54 ± 2.08 kcal mol^{-1}. The units of k are cm^3 mol^{-1} sec^{-2} $(M)^{-0.52}$. The unit of M are mol cm^{-3}.

Several experiments were performed on mixture D with the TOF recording the low mass spectra at m/e 2, 3, and 4. The presence of H_2 was confirmed and was attributed to the self-exchange of HD[2a] and the metathetical reaction of HCN. Reaction profiles were constructed using the mole fraction of HD. Quadratic time dependence was observed and rate constants were calculated. In Figure 9, the results of these runs are compared to the Arrhenius line of Figure 8.

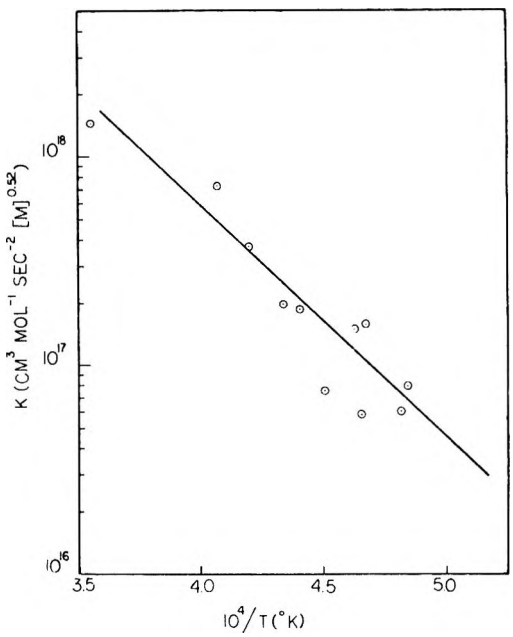

Figure 9. Low mass data points, ⊙. Solid line is taken from Figure 8.

Discussion

It is instructive to tabulate the results of previous studies and this one with respect to rate law parameters

$$\{1 - f_p[1 + (f_r/f_p)_{eq}]\} = \exp(-k[r]^{x+x'}[M]^y t^2) \quad (4)$$

where f_r and f_p are the mole fractions of reactants and products. The results are listed in Table III. The value of y for the exchange of H_2 + D_2 was taken to be one for the purpose of comparing the rate constants with those of a single pulse study. The rest of the entries are experimental quantities. All four exchange reactions were fit to quadratic time profiles.

Various mechanisms have been proposed and rejected for these exchange reactions. Some of the same arguments apply to the HCN–D_2 system. A direct four center molecular mechanism is eliminated because of the nonlinear time dependence for product formation and the inert gas dependence. An atomic mechanism is attractive because the combined reactant order dependence and the quadratic time dependence are in agreement with the predicted value. However, a total

Table III: Rate Law Parameters

Reaction	$x + x'$	y	E^*, kcal mol^{-1}
HCl + D_2[2a]	0	1	34.34 ± 3.13
H_2 + D_2[2b]	0		44.37 ± 2.51
HD + HD[2c]	0	0.57	40.98 ± 2.25
HCN + D_2	1	0.52	51.54 ± 2.08

gas density order of 1 is predicted at the pressures studied here and the observed activation energy is much lower than predicted. Comparison of a product profile calculated with the equation derived from the atomic mechanism with an experimental profile reveals the inadequacy of the mechanism. An atomic mechanism would have an activation energy that reflected the bond energies of the reactants plus the activation energy associated with the subsequent three center atom–molecule reactions. Arguments can be made against a vibrational energy chain mechanism because of the conflict between the predicted linear time dependence and the observed quadratic behavior. This part of the discussion has appeared previously[2] and the reader may easily fill in the elementary reaction steps for the preceding mechanisms applicable to HCN–D_2 exchange.

It is important to distinguish between the vibrational energy chain mechanism described in ref 2 and the vibrational excitation mechanism proposed by Professor S. H. Bauer.[4a] The vibrational energy chain mechanism may be more completely described as a two-state vibrational equilibrium model in contrast to the vibrational excitation mechanism which is a multistate vibrational excitation sequence. The latter postulates that the exchange reaction occurs rapidly when a molecule possesses a critical amount of vibrational energy. The exchange process causes a depletion of the population of vibrational levels above the critical level and prevents the system from attaining a Boltzmann distribution of vibrational energy for a time greater than the vibrational relaxation times. Attempts to solve the coupled differential equations for the vibrational excitation model involved the application of the steady state approximation.[4a,8] A recent development is the solution of this problem without invoking the steady state condition.[9] Using reaction conditions pertinent to the dynamic study of the H_2–D_2 exchange,[2b] the calculation reveals a nonlinear time dependence for product formation which changes over the observation period from a power greater than 3 to 1.2 and the absence of an induction period. Therefore, there is no incompatibility between the results reported earlier[2b] and the multistate vibrational excitation sequence. The application of Dr. Fisher's computer program to the system of interest here is a formidable task at this time because of the increased number of vibrational degrees of freedom for HCN.

There is a reaction pathway available in this system that was absent in the other three,[2] namely, the formation of a stable molecule from a metathetical reaction whose reverse reaction may cause the exchange to take place. The experimental evidence indicates that the reaction of cyanogen and hydrogen occurs *via* a complex mechanism.[6,10] The reaction is currently being studied in this laboratory using the technique of infrared emission and time-of-flight mass spectrometry to accomplish dynamic analysis of the reacting species behind reflected shock waves.[11] The infrared emission observed from the product HCN through a 3.0 μ interference filter displays a nonlinear time dependence which is a diagnostic of a complex mechanism.

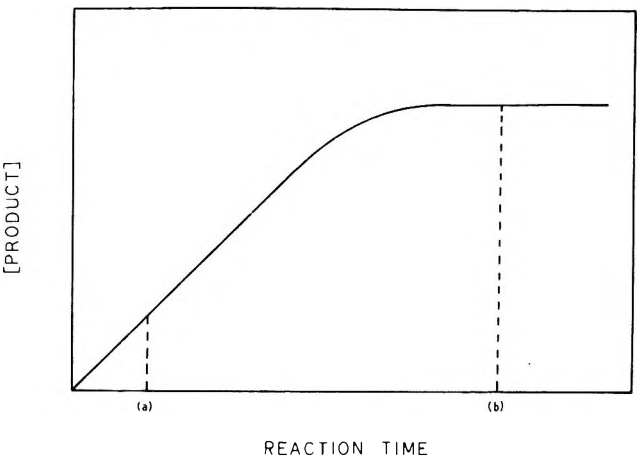

Figure 10. Product formation profile for any elementary reaction.

Figure 10 depicts the profile for *any* elementary reaction. A complex mechanism may also generate a like profile and the horizontal portion may represent a steady state condition rather than an equilibrium level during the available observation time. However, a nonlinear increase in product concentration is a diagnostic of a complex mechanism and such behavior rules out the existence of an elementary reaction for that particular species. The converse is not true.

It is apparent that experimental study of the C_2N_2 + H_2 reaction under homogeneous conditions is necessary before any definitive statements regarding the role of cyanogen in the exchange reaction mechanism may be made. The data presented herein for the exchange of hydrogen cyanide and deuterium support a complex mechanism.

Acknowledgments. The authors wish to express their appreciation to Mr. Darryl Olivier and Mr. Richmond Tankersley whose assistance in experimentation and data reduction was invaluable. The authors also wish to thank one of the referees for bringing to our attention the unpublished calculations of Dr. Edward Fisher.

(8) L. Poulsen, *J. Chem. Phys.*, **53**, 1987 (1970).
(9) Edward Fisher, private communication.
(10) Michael Berger, private communication.
(11) J. M. Brupbacher and R. D. Kern, work in progress.

A Kinetic Analysis of the Shock Wave Decomposition of 1,1,1,2-Tetrafluoroethane[1a]

by G. E. Millward[1b] and E. Tschuikow-Roux*

Department of Chemistry, The University of Calgary, Calgary 44, Alberta, Canada *(Received August 18, 1971)*

Publication costs borne completely by The Journal of Physical Chemistry

The kinetics of the thermal decomposition of 1,1,1,2-tetrafluoroethane have been studied using a single pulse shock tube in the temperature range 1170–1410°K at total reflected shock pressures of about 2850–3800 Torr. Although the main reaction involves the molecular elimination of hydrogen fluoride, $C_2H_2F_4 \xrightarrow{k_1} C_2HF_3 + HF$, a radical mechanism is proposed to explain the formation of additional products derived from the scission of the C–C bond. From the analysis the first-order rate constant was found to be $\log k_1\ (sec^{-1}) = 13.42 \pm 0.28 - (70{,}700 \pm 1700)/2.303RT$. With this value of k_1 it was possible to evaluate the C–C bond dissociation energy, $D(CH_2F\text{–}CF_3) = 92.3 \pm 2.9$ kcal mol^{-1}.

Introduction

Previous work on the decomposition of fluoroethanes has established primarily the Arrhenius parameters for the molecular elimination of hydrogen fluoride. This reaction governs the kinetics of these compounds at temperatures below 1350°K, as has been demonstrated for the series $C_2H_{6-n}F_n$ (where n = 1–3).[2-7] However, studies of the pyrolysis of 1,1,2,2-$C_2H_2F_4$[8,9] and C_2HF_5,[10] using the single pulse shock tube (SPST) technique, have indicated the increasing importance of the parallel C–C bond scission reaction. In these cases the major product was still the fluoroethylene derivative, although several other stable species arose as a result of the radical reactions. Mechanisms, which were consistent with the observed products, were proposed in each instance. From the analysis it was possible to evaluate not only the Arrhenius parameters for HF elimination but also the C–C bond dissociation energies $D(CHF_2\text{–}CHF_2)$ and $D(CHF_2\text{–}CF_3)$. The general trend of the activation energy for HF elimination with additional fluorine atom substitution has been established.[9,10] However, the effect of β-fluoro substitution upon this trend has not been resolved. Additional fluorine substitution seems also to provide a concurrent increase in the C–C bond dissociation energy.

Thus, the present work has three important objectives: firstly, to provide a mechanistic interpretation of the observed reaction products, which is consistent with the previous investigations of 1,1,2,2-$C_2H_2F_4$[9] and C_2HF_5;[10] secondly, to evaluate the Arrhenius parameters for HF elimination from 1,1,1,2-$C_2H_2F_4$ and to examine the effect of structure on the activation energy of this reaction; finally, to estimate the important thermochemical quantity, $D(CH_2F\text{–}CF_3)$.

Experimental Section

The 1,1,1,2-tetrafluoroethane was donated by the Du Pont de Nemours Co., and a gc analysis showed it had a purity of 99.95%. The methyl fluoride, fluoroform, vinyl fluoride, and hexafluoroethane were Matheson Co. research grade gases, as was the argon diluent (99.998% purity). Pentafluoroethane and trifluoroethylene were obtained from Peninsular Chemresearch Inc., and were found to be 99.9% pure. Tetrafluoroethylene was prepared by heating polytetrafluoroethylene (Teflon) shavings *in vacuo*, and the product was purified by trap-to-trap distillation.

(1) (a) Work supported by the National Research Council of Canada; (b) Postdoctoral Fellow, 1970–1971.

(2) D. Sianesi, G. Nelli, and R. Fontanelli, *Chim. Ind. (Milan)*, **50**, 619 (1968).

(3) M. Day and A. F. Trotman-Dickenson, *J. Chem. Soc. A*, 233 (1969).

(4) P. Cadman, M. Day, A. W. Kirk, and A. F. Trotman-Dickenson, *Chem. Commun.*, 203 (1970).

(5) (a) P. Cadman, M. Day, and A. F. Trotman-Dickenson, *J. Chem. Soc. A*, 2498 (1970); (b) *ibid.*, 1356 (1971). In these references errors in the calculated reaction time may arise from boundary layer formation. Small bore (1-in. i.d.) shock tubes are particularly prone to this phenomena, and the problem is magnified in a reflected shock wave environment (see, for example, A. G. Gaydon and I. R. Hurle, "The Shock Tube in High-Temperature Chemical Physics," Chapman and Hall Ltd., London, 1963; or R. L. Belford and R. A. Strehlow, *Ann. Rev. Phys. Chem.*, **20**, 247 (1969)]. However, using a high-frequency pressure transducer to monitor the wave history it is possible to obtain an experimental reaction time. This can then be compared directly with the reaction time calculated from the knowledge of the decomposition of the internal standard.

(6) E. Tschuikow-Roux, W. J. Quiring, and J. M. Simmie, *J. Phys. Chem.*, **74**, 2449 (1970).

(7) E. Tschuikow-Roux and W. J. Quiring, *ibid.*, **75**, 295 (1971).

(8) G. E. Millward, R. Hartig, and E. Tschuikow-Roux, *Chem. Commun.*, 465 (1971).

(9) G. E. Millward, R. Hartig, and E. Tschuikow-Roux, *J. Phys. Chem.*, **75**, 3195 (1971).

(10) E. Tschuikow-Roux, G. E. Millward, and W. J. Quiring, *ibid.*, **75**, 3493 (1971).

Table I: Experimental Results

Shock Mach. No. W_{11}	Shock Mach. No. W_{21}	P_5, Torr	T_5, °K	t, μsec	Product ratios[a] R_1	R_2	R_3	R_4	k_{uc},[b] sec^{-1}	k_1, sec^{-1}	k_{uc}',[b] sec^{-1}	k', sec^{-1}
2.173	1.300	2851	1177	580	0.0010	...	...	...	1.71	1.52	...	...
2.181	1.282	2829	1174	680	0.0013	...	...	...	1.97	1.83	...	...
2.231	1.303	3033	1224	681	0.0039	...	...	...	5.84	5.27	...	...
2.245	1.289	3043	1228	674	0.0054	...	...	...	7.92	7.30	...	...
2.245	1.306	3088	1237	688	0.0058	...	...	...	8.44	7.73	...	...
2.255	1.294	3087	1238	765	0.0080	...	...	...	10.5	9.58	...	...
2.245	1.302	3077	1235	824	0.0086	...	...	...	10.4	9.61	...	...
2.282	1.290	3161	1253	893	0.0125	...	...	...	13.9	12.9	...	...
2.272	1.303	3164	1251	764	0.0137	...	...	...	17.8	16.3	...	...
2.283	1.332	3269	1272	681	0.0136	...	...	...	19.8	18.2	...	...
2.293	1.323	3282	1285	865	0.0197	0.0138	0.0018	...	22.5	20.8	32.4	30.2
2.303	1.314	3288	1278	873	0.0226	0.0090	0.0026	0.0010	25.5	23.2	34.7	31.8
2.288	1.305	3219	1271	779	0.0201	...	...	...	25.6	23.5	...	...
2.314	1.308	3309	1293	835	0.0287	0.0170	0.0024	0.0029	33.7	30.6	49.9	45.7
2.327	1.306	3346	1296	864	0.0310	0.0129	0.0033	0.0038	35.0	32.0	50.5	46.5
2.314	1.329	3364	1304	897	0.0390	0.0036	0.0027	0.0037	42.2	38.7	67.3	62.1
2.336	1.337	3458	1327	916	0.0478	0.0386	0.0039	0.0049	50.2	47.0	73.6	69.2
2.323	1.320	3367	1306	948	0.0503	0.0300	0.0030	0.0040	51.0	47.7	79.9	75.2
2.330	1.350	3473	1325	888	0.0484	0.0455	0.0035	0.0052	52.4	48.7	86.5	80.9
2.345	1.339	3493	1335	840	0.0669	0.0598	0.0044	0.0063	75.5	69.7	122	113
2.367	1.346	3583	1353	857	0.0897	0.0944	0.0085	0.0099	96.1	89.8	164	152
2.350	1.348	3533	1349	840	0.0931	0.0713	0.0067	0.0125	103	94.9	168	158
2.365	1.355	3602	1361	894	0.116	0.111	0.0085	0.0168	118	109	201	188
2.413	1.351	3751	1394	836	0.216	0.238	0.0141	0.0410	215	200	394	370
2.413	1.357	3768	1397	914	0.290	0.369	0.0196	0.0650	251	237	486	460
2.418	1.365	3810	1411	924	0.478	0.546	0.0210	0.0860	372	348	671	630

[a] $R_i = [X_i]/[CH_2FCF_3]$ where X_i = $CHFCF_2$, CHF_3, $CHFCH_2$, CF_2CF_2 for i = 1, 2, 3, 4, respectively, and R_i is determined experimentally. [b] Rate constants uncorrected for the finite cooling rate of the rarefaction fan.

A dilute reaction mixture (1% 1,1,1,2-$C_2H_2F_4$ in Ar) was prepared in a large stainless steel tank and allowed to mix thoroughly before use.

The design and operation of the modified SPST has been fully described previously.[11,12] After evacuation the tube was filled with pure argon, while the ball valve was filled to the same pressure with the reaction mixture. Using amplified signals from two high-frequency pressure transducers, the incident and reflected shock transit times were registered on microsecond counters. Also, the wave history near the end plate was obtained from a photographic record of the oscilloscope trace.

Following each shock a sample of the fully mixed gases was withdrawn and subjected to analysis using a gas chromatograph (Varian, Model 1740). The mixtures were separated on a 12-ft silica gel column at 125° with helium as carrier gas (30 cm^3 min^{-1}). Quantitative identification of the product/reactant ratios was obtained by comparison with standard mixtures prepared for calibration purposes. The conversions ranged from ~0.1% at 1170°K to 46% at 1410°K.

Results

The reflected shock wave parameters P_5 and T_5 given in Table I were calculated from the incident and reflected shock wave Mach numbers W_{11} and W_{21}. The reaction dwell time, t, was determined by a previously described method.[11] The initial cooling rate of the rarefaction fan, $m = (dT_5/dt)_t$, was derived from the oscillographic pressure record. The values of $-m$ varied between 4×10^5 and 1×10^6 °K sec^{-1}.

Between 1170 and 1300°K the major reaction product was C_2HF_3. However, above 1300°K significant amounts of other products were formed. These were identified, by gc, as CH_3F, CHF_3, C_2HF_5, C_2F_6, C_2H_3F, and C_2F_4. Two other products which could not be identified as either C_1 or C_2 fluoro hydrocarbons were present in negligible amounts, compared to the total product formation. Hexafluoroethane had a very low sensitivity to the flame ionization detector, and consequently the peak areas associated with it were practically immeasurable. A discussion of this problem is to be found elsewhere.[10] The product/reactant ratios, with the exception of $[C_2F_6]/[C_2H_2F_4]$, are set out in Table I.

Kinetic Analysis

A simplified reaction scheme is presented below. It is consistent with the observed products and the studies of 1,1,2,2-$C_2H_2F_4$[9] and C_2HF_5.[10] However, it

(11) E. Tschuikow-Roux, *Phys. Fluids*, **8**, 821 (1965).

(12) J. M. Simmie, W. J. Quiring, and E. Tschuikow-Roux, *J. Phys. Chem.*, **73**, 3830 (1969)

should be noted that the mechanism has not been tested for the effects of pressure, concentration, and inhibitors.

$$CH_2FCF_3 \xrightarrow{k_1} CHFCF_2 + HF \quad (1)$$

$$\xrightarrow{k_2} CH_2F + CF_3 \quad (2)$$

$$CH_2F + CF_3 \xrightarrow{k_{-2}} CH_2FCF_3 \quad (-2)$$

$$CH_2F + CF_3 \xrightarrow{k_3} CHF_3 + CHF \quad (3)$$

$$2CF_3 \xrightarrow{k_{-4}} C_2F_6 \quad (-4)$$

$$C_2F_6 \xrightarrow{k_4} 2CF_3 \quad (4)$$

$$2CH_2F \xrightarrow{k_5} CHFCH_2 + HF \quad (5)$$

$$CHF + CH_2FCF_3 \xrightarrow{k_6} CH_2F + CHFCF_3 \quad (6)$$

$$CHFCF_3 \xrightarrow{k_7} CF_2CF_2 + H \quad (7)$$

$$H + CH_2FCF_3 \xrightarrow{k_8} CHFCF_3 + H_2 \quad (8)$$

$$H + R \xrightarrow{k_9} RH \quad (9)$$

The secondary processes that arise from the C–C bond scission are discussed in detail below.

Abstraction Reactions. Under these experimental conditions it can be shown[10] that hydrogen abstraction reactions involving C_1 radicals are slow compared to the combination steps −2 and −4, for example. Thus, the reactions

$$CF_3 + CH_2FCF_3 \longrightarrow CHF_3 + CHFCF_3$$

and

$$CH_2F + CH_2FCF_3 \longrightarrow CH_3F + CHFCF_3$$

are excluded from the scheme. Further evidence that this approximation is valid is provided by the product analysis which indicates that the amount of CH_3F formed is ~2% of the total product formation at the highest temperature.

There is only a sparsity of data on the reactivity of the CHF species. Experiments[13] using tritiated monofluoromethylene showed that the addition of CTF to olefins was stereospecific, but there was no evidence for any insertion reactions. In this case only minute amounts of C_3 compounds were observed, and the addition reaction of CHF is discounted. Concentration restrictions would make 2CHF → CHFCHF unfavorable and in any event CHFCHF was not found experimentally. Triplet methylene, $^3CH_2$, usually produced in thermal systems, is known to abstract hydrogen;[14,15] however, a recent study[16] has indicated that $^1CH_2$ may undergo a similar reaction. Thus, by analogy to CH_2, process 6 is postulated as being the reaction manifold for the CHF species.

Combination Reactions. The scheme includes C_1 radical combination reactions −2 and −4. In the case of CF_3 radical combination the chemically activated adduct may either undergo collisional stabilization or redissociate, reaction 4. An additional reaction manifold exists in the case of the chemically activated CH_2FCF_3* formed in −2 in that HF elimination is also possible, and this is implicitly included in reaction 1. Analogous considerations apply in the case of CH_2F radicals.

$$2CH_2F \rightleftharpoons CH_2FCH_2F^* \quad (10)$$

$$CH_2FCH_2F^* \longrightarrow CH_2CHF + HF \quad (11)$$

$$\xrightarrow{M} CH_2FCH_2F \quad (12)$$

In their chemical activation study Pritchard, *et al.*,[17] have shown that the elimination/stabilization ratio for CH_2F radicals, k_{11}/k_{12}, lay between 0.6 to 3.5 in the temperature range 25–300° and total pressures of about 75 Torr. Under the present experimental conditions the stabilization will be favored due to a 50-fold increase in pressure. However, this will be compensated for by the threefold increase in temperature, since k_{11}/k_{12} increases quite markedly with temperature above 500°K. Thus, the condition that $k_{11}/k_{12} > 1$ is maintained and justifies our omission of reaction 12. This is further corroborated experimentally, since no 1,2-difluoroethane was observed.

The tetrafluoroethyl radical combination reaction $2CHFCF_3 \rightarrow C_4H_2F_8$ and the cross combinations $CH_2F + CHFCF_3 \rightarrow C_3H_3F_5$ and $CF_3 + CHFCF_3 \rightarrow C_3HF_7$ are excluded on the basis of product analysis.

Finally, reaction 9 which accounts for all radicals combining with a hydrogen atom is included to provide a formal chain termination step, but was excluded in the theoretical analysis.

Disproportionation Reactions. The disproportionation reaction 3 has not been previously reported although similar reactions involving fluoromethyl radicals with a total of four or five fluorine atoms do occur.[18,19] The reaction is proposed to explain the formation of relatively large amounts of fluoroform.

Since cross-combination reactions have been omitted, the corresponding cross-disproportionation reactions

$$CH_2F + CHFCF_3 \longrightarrow CH_3F + C_2F_4$$

and

$$CF_3 + CHFCF_3 \longrightarrow CHF_3 + C_2F_4$$

(13) Y.-N. Tang and F. S. Rowland, *J. Amer. Chem. Soc.*, 89, 6420 (1967).

(14) C. H. Bamford, J. E. Casson, and A. N. Hughes, *Proc. Roy. Soc., Ser. A*, 306, 135 (1968).

(15) C. H. Bamford, J. E. Casson, and A. N. Hughes, *Chem. Commun.*, 1096 (1967).

(16) H. D. Roth, *J. Amer. Chem. Soc.*, 93, 1527 (1971).

(17) G. O. Pritchard, M. Venugopalan, and T. F. Graham, *J. Phys. Chem.*, 68, 1786 (1964).

(18) G. O. Pritchard and M. J. Perona, *Int. J. Chem. Kinet.*, 1, 509 (1969).

(19) G. O. Pritchard and M. J. Perona, *ibid.*, 2, 413 (1970).

have also been excluded because radical disproportionation/combination ratios are usually less than unity. However, an unusual feature is the presence of C_2HF_5, amounting to about 1.5% of the total product formation at the highest temperature. In a recent study Cadman, *et al.*,[20] conclude that polar radicals seem to have a much larger disproportionation/combination ratio than nonpolar radicals. Thus, the C_2HF_5 may be originating from

$$2CHFCF_3 \longrightarrow C_2HF_5 + C_2HF_3$$

However, the reaction has been excluded from the scheme, since only small amounts of C_2HF_5 were observed experimentally.

Elimination Reactions. Reaction 7 actually represents two steps, the elimination of a hydrogen atom, then an intramolecular fluorine atom rearrangement. The elimination of a hydrogen atom is preferred over fluorine atom expulsion on the basis of bond dissociation energies. The activation energy for the process, $C_2H_5 \rightarrow C_2H_4 + H$, is about 40 kcal mol^{-1},[21] which is considerably less than the C–H bond energy in C_2H_6 (98 ± 1 kcal mol^{-1}).[22] Although there may be a decrease in the C–F bond energy in $CHFCF_3$ it will not be sufficient to make fluorine atom elimination a competitive reaction.

The elimination of HF from CHF_3 may also occur[23-25]

$$CHF_3 \xrightarrow{k_{13}} CF_2 + HF \qquad (13)$$

but under these experimental conditions, indications[24] are that k_{13} may be a pressure-dependent rate constant. Therefore, we assume the rate of (13) to be slow compared to k_1 [CH_2FCF_3], so that reaction 13 is omitted.

The theoretical carbon mass balance (in terms of product/reactant ratios) was found to be

$$(A)_0/(A) = 1 + R_1 + {}^1/_2R_2 + R_3 + R_4 \qquad (I)$$

where $(A)_0$ is the initial concentration of CH_2FCF_3; (A) = [CH_2FCF_3]; R_1 = [C_2HF_3]/[CH_2FCF_3]; R_2 = [CHF_3]/[CH_2FCF_3]; R_3 = [C_2H_3F]/[CH_2FCF_3]; and R_4 = [C_2F_4]/[CH_2FCF_3]. Assuming that (X) = [CH_2F] ≃ [CF_3] and using the stationary-state equations for transient species, the concentration of C_1 radicals is given approximately by

$$(X)^2 = k_2(A)/2k_{-2} \qquad (II)$$

The depletion of A is given by

$$-d(A)/dt = k_1(A) + k_2(A) - k_{-2}(X)^2 + k_6(CHF)(A) \qquad (III)$$

From the stationary-state equation for the CHF species it is found that

$$k_6(CHF)(A) = k_3(X)^2 \qquad (IV)$$

Substitution of eq IV in III and elimination of the radical concentrations using eq II yields

$$-d(A)/dt = k'(A) \qquad (V)$$

where

$$k' = [k_1 + {}^1/_2k_2(1 + k_3/k_{-2})] \qquad (VI)$$

Integrating eq V with the boundary conditions that (A) = $(A)_0$ at $t = 0$ gives

$$k' = (1/t) \ln [(A)_0/(A)] \qquad (VII)$$
$$= (1/t) \ln (1 + R_1 + {}^1/_2R_2 + R_3 + R_4)$$

The formation of C_2HF_3 is given by

$$d(C_2HF_3)/dt = k_1(A) = k_1(A)_0e^{-k't} \qquad (VIII)$$

Integrating VIII with (C_2HF_3) = 0 at $t = 0$ and substituting k' from eq VII we obtain

$$k_1 = R_1 \ln (1 + R_1 + {}^1/_2R_2 + R_3 + R_4)/[R_1 + {}^1/_2R_2 + R_3 + R_4]t \qquad (IX)$$

The values of k_1 obtained from eq IX are given in Table I as k_{uc}, the uncorrected rate constant. The corrected rate constant is given by[7,11]

$$k_1 = k_{uc}/[1 - (\epsilon/t)] \qquad (X)$$

where

$$\epsilon = (RT_5^2/Em)\{1 - \exp(-E/[RT_5 - (E/\ln \xi)])\} \qquad (XI)$$

In eq XI E is the activation energy obtained to a first approximation from a plot of log k_{uc} *vs.* $1/T$; $m = (dT_5/dt)_t$; T_5 is the reflected shock temperature; and $\xi = 10^{-2}$ is a cut-off parameter.[7] The corrected rate constants are given in Table I, and their temperature dependence is plotted in Figure 1.

From eq VI we obtain

$$(k' - k_1) = {}^1/_2k_2(1 + k_3/k_{-2}) \qquad (XII)$$

which yields an estimate of the rate constant for the C–C bond scission, k_2, provided the value of the disproportionation/combination ratio, (k_3/k_{-2}), for CH_2F and CF_3 radicals is known at high temperatures. The uncorrected and corrected [using eq X and XI] values of k' are given in Table I, and the temperature dependence of the rate constant difference $(k' - k_1)$ is plotted in Figure 2.

Discussion

A least-squares analysis of the high-pressure limiting

(20) P. Cadman, Y. Inel, and A. F. Trotman-Dickenson, *J. Chem. Soc. A*, 1207 (1970).
(21) L. F. Loucks and K. J. Laidler, *Can. J. Chem.*, **45**, 2795 (1967).
(22) J. A. Kerr, *Chem. Rev.*, **66**, 465 (1966).
(23) E. Tschuikow-Roux and J. E. Marte, *J. Chem. Phys.*, **42**, 2049 (1965).
(24) E. Tschuikow-Roux, *ibid.*, **42**, 3639 (1965).
(25) S. F. Politanskii and V. U. Shevchuk, *Kinet. Katal.*, **9**, 496 (1968).

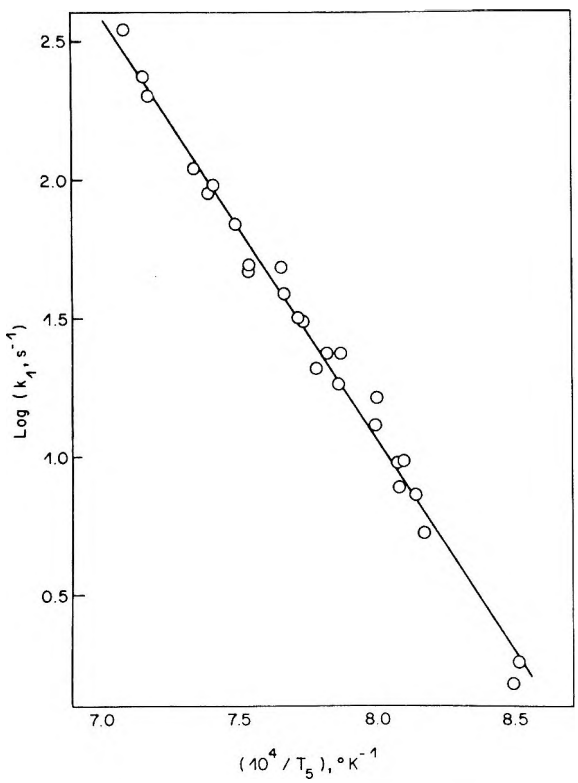

Figure 1. Temperature dependence of the rate constant k_1 for HF elimination from CH_2FCF_3.

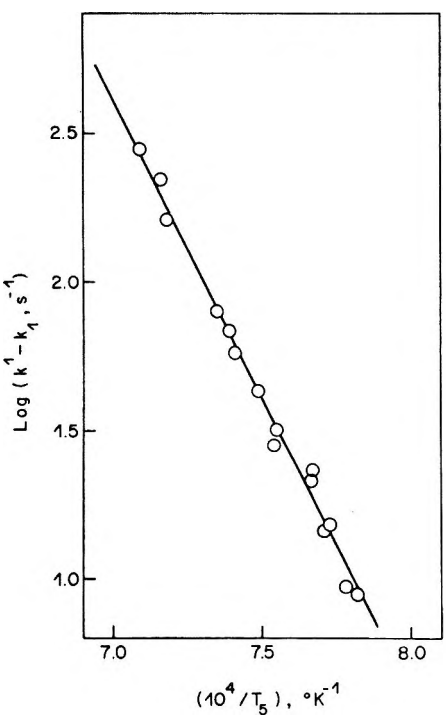

Figure 2. Temperature dependence of $(k' - k_1)$.

rate constants, k_1, reported in Table I yields the Arrhenius expression

$$k_1 \text{ (sec}^{-1}) = 10^{13.42\pm0.28} \exp[-(70{,}700 \pm 1700)/RT]$$

where the error limits are standard deviations. The Arrhenius parameters for HF elimination from fluoroethanes, using several techniques, are shown in Table II. It should be noted that chemical activation studies using the RRK formulation have been omitted since they may be subject to considerable error.[26,27] Two conclusions, concerning the trends in the activation energies, can be drawn from Table II.

Table II: Arrhenius Parameters for HF Elimination from Fluoroethanes

Fluorocarbon	E, kcal mol^{-1}	log A, sec^{-1}	Method	Reference
CH_3CH_2F	62.6	14.4	FS	2
	58.2	13.31	SP	3
	59.9 ± 1.0	13.42 ± 0.3	ST	5a
CH_2FCH_2F	62[a]		CA	28
	63[a]		CA	*b*
CH_3CHF_2	61.9 ± 2.0	13.31	FS	2
	64.97 ± 0.9	13.53 ± 0.3	ST	5b
	61.9 ± 1.8	13.9 ± 0.3	SPST	6
CH_3CF_3	61.4 ± 2.0	12.14	FS	2
	73.64 + 4.1	13.8 ± 0.3	ST	5b
	68.7 ± 2.4	14.0 ± 0.4	SPST	7
CHF_2CHF_2	69.4 ± 3.1	13.3 ± 0.4	SPST	9
CH_2FCF_3	70.7 ± 1.7	13.42 ± 0.28	SPST	This work
CHF_2CF_3	71.6 ± 2.4	13.6 ± 0.4	SPST	10

[a] Critical energy, ϵ_0; FS = flow system; SP = static pyrolysis; ST = comparative shock tube; CA = chemical activation; SPST = single pulse shock tube. [b] J. A. Kerr and D. M. Timlin, *Trans. Faraday Soc.*, **67**, 1376 (1971).

(1) The overall trend is one of increasing activation energy with increasing fluorine substitution. This effect is independent of whether the additional fluorine atom is substituted α or β to existing fluorine atoms. Results from this laboratory indicate that relatively large increases in activation energy arise from additional α fluorination, whereas β-fluoro substitution leads to a minor increase. The following sequence shows the percentage increases in activation energy for the substitution of three fluorine atoms in CH_3CHF_2, $CH_3CHF_2 \xrightarrow{11\%} CH_3CF_3 \xrightarrow{2.9\%} CH_2FCF_3 \xrightarrow{1.3\%} CHF_2CF_3$.

(2) "Rearrangement" of the fluorine atoms in CHF_2-CHF_2 to give CH_2FCF_3 leads to a small increase in activation energy, although both values are within experimental error. Thus, we may predict that similar experiments on the isomers of $C_2H_4F_2$, and $C_2H_3F_3$ should indicate the same trend.

Some *qualitative* evidence that the above hypotheses are correct may be derived from another source. The

(26) G. O. Pritchard and M. J. Perona, *Int. J. Chem. Kinet.*, **2**, 281 (1970).

(27) Some of the earlier chemical activation work has now been reexamined in terms of the more appropriate RRKM theory; see, for example, ref 4.

activation energy for reaction 1, E_1, is linked to the heat of reaction, ΔH, by

$$E_1 = E_r + \Delta H$$

where E_r is the activation energy for the reverse HF-addition reaction. Using known heats of formation[28,29] for the isomers of $C_2H_4F_2$ and $C_2H_3F_3$, then

$$CH_2FCH_2F \longrightarrow CH_2CHF + HF$$
$$\Delta H(14) = 10 \text{ kcal mol}^{-1} \quad (14)$$
$$CH_3CHF_2 \longrightarrow CH_2CHF + HF$$
$$\Delta H(15) = 24 \text{ kcal mol}^{-1} \quad (15)$$
$$CH_2FCHF_2 \longrightarrow CH_2CF_2 + HF$$
$$\Delta H(16) = 14 \text{ kcal mol}^{-1} \quad (16)$$
$$CH_3CF_3 \longrightarrow CH_2CF_2 + HF$$
$$\Delta H(17) = 30 \text{ kcal mol}^{-1} \quad (17)$$

Thus, we find that $\Delta H(17) - \Delta H(15) \simeq 6$ kcal mol^{-1} and from the known activation energies $E_1(17) - E_1(15) \simeq 6.8$ kcal mol^{-1}, and it seems that only minor changes occur within E_r. In contrast, it is seen that the difference in the enthalpies of reaction between isomers is large. Therefore, there must be a substantial difference between the value of E_r for CH_2FCH_2F and CH_3CHF_2 (also in the case of $C_2H_3F_3$ isomers) to account for the apparently small changes in activation energy, E_1, between isomers.

The differences noted in the values of E_r for the above examples may be attributed to the electron-withdrawing effect of the fluorine atom. In the case of CH_3CHF_2 there must be substantial polarization of the C–F bonds, and the substitution of one additional fluorine atom, to give CH_3CF_3, may result in only a relatively minor change in the atomic charge distribution. Thus, the physical properties such as polarizability, dipole moment, and bond lengths, which govern the magnitude of E_r will also change to a minor degree, and hence $E_r(15) \simeq E_r(17)$. However, the change in atomic charge densities in going from CH_2FCH_2F to CH_3CHF_2, for example, must be considerable, because of the increase in the polarization of the α-carbon atom in the latter case. The physical quantities mentioned above change quite markedly in this instance, and hence one expects $E_r(15) > E_r(14)$. Finally, the self-consistent electrostatic (semi-ion pair) model of Benson and Haugen[30] predicts the same value of E_r for reactions 14 and 15. This is because account is not taken of the differences in the transition state polarizabilities and bond lengths in the reverse addition reactions of (14) and (15).

It is interesting to compare some relative rate constants for HF elimination from CH_3CHF_2 and CH_3CF_3 obtained from several laboratories (data are taken from ref 2, 5b, 6, and 7, respectively). For CH_3CHF_2 at 1300°K the ratio of rate constants is 0.25:0.13:1 while for CH_3CF_3 at the same temperature the ratio is 0.24:0.093:1. The agreement between those values obtained in this laboratory[6,7] and those recently obtained by Cadman, *et al.*,[5b] is relatively poor. The discrepancy may lie in some aspects of the comparative shock tube technique as used by Cadman, *et al.*[5] In these studies the reflected shock temperature is calculated from the incident shock velocity; this procedure may cause significant errors.[31] Also, it should be noted that in the comparative technique there is no way of testing whether the instrument is accurately reproducing the Arrhenius parameters of the internal standard.

In Figure 2 the logarithm of the rate constant difference $(k' - k_1)$ is plotted as a function of temperature. A least-squares analysis of these data gives

$$(k' - k_1) = {}^1/_2 k_2(1 + k_3/k_{-2})$$
$$= 10^{16.7\pm0.5} \exp[-(92{,}300 \pm 2900)/RT] \text{ sec}^{-1}$$

where the error limits are standard deviations. The ratio k_3/k_{-2} has not been evaluated for CH_2F and CF_3 radicals. However, we assume the ratio to be 0.2 and temperature independent by analogy to the disproportionation/combination ratio of CHF_2 radicals which is well established.[18] Therefore

$$k_2 \text{ (sec}^{-1}) = 10^{16.9\pm0.5} \exp[-(92{,}300 \pm 2900)/RT]$$

This provides us with the first experimental determination of the C–C bond dissociation energy in CH_2FCF_3. The magnitude of the preexponential factor is consistent with those determined for similar

Table III: C–C Bond Dissociation Energies of Some Fluorocarbon Analogs of Ethane

Fluorocarbon	C–C bond dissociation energy, kcal mol^{-1}	Temp range, °K	Method	Reference
CH_3–CH_3	88.0 ± 2.0	298	*a*	*c*
CH_2F–CH_2F	89.6	298	*b*	*d*
CH_3–CF_3	99.7 ± 2.0	298	*b*	32
CH_2F–CF_3	92.3 ± 2.9	1280–1410	SPST	This work
CHF_2–CHF_2	91.4 ± 3.7	1320–1450	SPST	9
CHF_2–CF_3	93.5 ± 5.2	1300–1450	SPST	10
CF_3–CF_3	94.4 ± 4.0	1300–1600	SPST	*e*
	96.5 ± 1.0	298	*b*	32

[a] Static pyrolysis of CH_3CH_3. [b] Calculated from known thermochemical data. [c] M. C. Lin and M. H. Back, *Can. J. Chem.*, **44**, 505 (1966). [d] See Table II, footnote *b*. [e] E. Tschuikow-Roux, *J. Chem. Phys.*, **43**, 2251 (1965).

(28) H. W. Chang and D. W. Setser, *J. Amer. Chem. Soc.*, **91**, 7648 (1969).

(29) J. R. Lacher and H. A. Skinner, *J. Chem. Soc. A*, 1034 (1968).

(30) S. W. Benson and G. R. Haugen, *J. Amer. Chem. Soc.*, **87**, 4036 (1965).

(31) E. Tschuikow-Roux, J. M. Simmie, and W. J. Quiring, *Astronaut. Acta*, **15**, 511 (1970).

reactions. It should be noted that the use of the assumptions regarding k_3/k_{-2} leads to $k_1/k_2 \simeq 1$ at 1420°K, and $k_1/k_2 < 1$ above this temperature.

Table III gives recently determined values of the C–C bond dissociation energy in ethane and several of the fluoroethanes. The interesting feature is the relatively high value of $D(CH_3\text{–}CF_3)$ calculated from known thermochemical data.[32] It is difficult to fault this result, and CNDO calculations[33] of charge distributions, in CH_3CF_3, indicate that it may be correct. In the past it had been generally thought[33] that the highly electronegative character of the fluorine atom led to a diminishing positive character in a carbon atom chain, *i.e.*, $F^{\delta-} \leftarrow C^{\delta+} \leftarrow C^{\delta\delta+}$. However, the CNDO calculations suggest that the charge distribution should decay as follows: $F^{\delta-} \leftarrow C^{\delta+} \leftarrow C^{\delta\delta-}$. This means that the negative character of the β-carbon atom increases in going from CH_3CH_2F to CH_3CF_3 and decreases in going from CH_3CF_3 to CHF_2CF_3. The maximum charge separation along the C–C bond exhibited by CH_3CF_3 is in accord with a strong C–C bond. The results tabulated are in reasonable agreement with the above hypothesis, but further experimental determinations of $D(CH_3\text{–}CH_2F)$, $D(CH_3\text{–}CHF_2)$, and $D(CH_3\text{–}CF_3)$ are needed to substantiate it.

Acknowledgments. We thank Dr. R. F. Hein of the Du Pont de Nemours Co. for a high purity sample of $1,1,1,2\text{-}C_2H_2F_4$. We also thank Mr. K. Maltman for stimulating discussions.

(32) J. W. Coomber and E. Whittle, *Trans. Faraday Soc.*, **63**, 1394 (1967).

(33) J. A. Pople and D. L. Beveridge, "Approximate Molecular Orbital Theory," McGraw-Hill, New York, N. Y., 1970, p 119.

Quantum Yields in the 58.4-nm Photolyses of Ammonia and Water

by J. B. Tellinghuisen, C. A. Winkler, and L. F. Phillips*

Chemistry Department, University of Canterbury, Christchurch, New Zealand *(Received September 13, 1971)*

Publication costs borne completely by The Journal of Physical Chemistry

Quantum yields have been determined by mass spectrometric analysis and by measurements of the absorption of 58.4-nm radiation by the photolysis products. At pressures where ion–electron recombination is predominantly homogeneous we find the quantum yields of H_2 to be 0.93 ± 0.15 from NH_3 and 2.1 ± 0.5 from H_2O. Yields from H_2O are sensitive to wall effects. The results are discussed in terms of known photofragmentation patterns and ion–molecule reactions, together with less well known dissociative recombination processes and neutral radical reactions. To account for the observed H_2 yield from H_2O (though not for that from NH_3) it is necessary to assume that most of the electron–ion recombination occurs by reactions of the type $H_3O^+ + e^- \rightarrow H_2 + O + H$. The relative effects of 58.4-nm ionizing photolysis and γ radiolysis are compared for H_2O, NH_3, and CO_2.

Introduction

We have recently described studies of processes initiated by 58.4-nm radiation in gaseous CO_2 and other small molecules.[1-3] In a continuation of this work we now report product yields for the ionizing photolysis of NH_3 and H_2O. As before, the results are discussed in terms of known photofragmentation patterns and ion–molecule reactions, together with less well understood dissociative recombination processes and reactions of neutral radicals.

Studies of the γ radiolysis of water and ammonia[4-6] have shown that whereas NH_3 is destroyed quite efficiently ($G_{H_2} = 4.42 \pm 0.1$, $G_{N_2} = 1.45 \pm 0.07$[4]), H_2O is extremely resistant to decomposition ($G_{H_2} \simeq 0.007$[6]). It is therefore of interest to compare the behavior of these two molecules in ionizing photolysis at 58.4 nm. We find that with 58.4-nm (21.2 eV) radiation both are decomposed, the quantum yield of H_2 being greater from H_2O than from NH_3. Some possible reasons for these differences are given in the Discussion.

(1) S. W. Bennett, J. B. Tellinghuisen, and L. F. Phillips, *J. Phys. Chem.*, **75**, 719 (1971).

(2) J. B. Tellinghuisen, S. W. Bennett, C. A. Winkler, and L. F. Phillips, *J. Phys. Chem.*, in press.

(3) C. A. Winkler, J. B. Tellinghuisen, and L. F. Phillips, *Trans. Faraday Soc.*, in press.

(4) J. A. Eyre and D. Smithies, *Trans. Faraday Soc.*, **66**, 2199 (1970).

(5) A. R. Anderson, B. Knight, and J. A. Winter, *Trans. Faraday Soc.*, **62**, 359 (1966).

(6) (a) F. T. Jones and T. J. Sworski, *Trans. Faraday Soc.*, **63**, 2411 (1967); (b) F. T. Jones, T. J. Sworski, and J. M. Williams, *ibid.*, **63**, 2426 (1967).

Experimental Section

The apparatus and procedures have been described previously.[1,2] Briefly, the photolysis system consisted of a Pyrex cell, of volume ~120 cm³, fitted with thin copper wire electrodes and separated from a microwave-powered helium discharge lamp by a thin-film aluminum window. Photon fluxes were obtained from plateaus in the ion-current *vs.* voltage curves measured with hydrogen in the cell. The integrated flux over the course of an experiment was typically 2–6 × 10^{14} photons. Product yields were determined by mass spectrometric analysis and by monitoring the partial pressures of noncondensable products. In the mass spectrometric work the photolysis products were mixed with a known amount of Ar and were analyzed for H_2 abundance by comparison with a standard Ar–H_2 mixture. This standard mixture was itself calibrated using mixing procedures identical with those employed for the unknowns. In the pressure measurements the NH_3 or H_2O was frozen in a side arm of the cell, using liquid air, and product concentrations were determined from the observed ion currents and previously measured absorption coefficients,[1] together with certain assumptions regarding stoichiometry, as discussed below. All experiments were carried out at room temperature, using NH_3 and H_2O which had been purified by trap-to-trap distillation.

Results

Ammonia was photolyzed at pressures from 0.31 to 3.45 Torr and at fluxes 0.8–3.0 × 10^{12} quanta sec^{-1}. The mass spectrometric analyses indicated a yield of 0.93 ± 0.15 H_2 molecules per photon absorbed, with no dependence on either pressure or flux over the range of conditions employed. From the absence of a detectable signal at mass 31 (the second largest peak in the 70 V spectrum of hydrazine) we concluded that, as in high-energy radiolysis,[4,6] no significant amount of N_2H_4 is produced. Separate experiments, in which pressures of noncondensable products were determined from the absorption of 58.4-nm radiation, gave more scatter in the yields than the mass spectrometric results, for reasons mentioned previously.[2] However, with the assumption of a 3:1 ratio of H_2 to N_2 in the products (giving a value of 260 cm^{-1} for the absorption coefficient κ_{av} of the mixture), the average of these measurements agreed with the mass spectrometric value. The pressure measurements demonstrated clearly that the formation of products was linearly dependent on the total number of quanta absorbed.

Water vapor at pressures from 0.5 to 3.7 Torr was photolyzed using fluxes from 0.4 to 8.8 × 10^{12} quanta sec^{-1}. The H_2 yields obtained mass spectrometrically exhibited a much greater scatter than those for NH_3, but there appeared to be no systematic dependence of the yield on pressure or flux over the range of conditions employed. The average H_2 yield was 2.1 with an estimated error of ± 0.5. As for ammonia, product pressure measurements showed that product formation was linearly dependent on the number of quanta absorbed. With the assumption of a 2:1 mixture of H_2 and O_2 (κ_{av} = 290 cm^{-1}) the indicated H_2 yield from these experiments was ~1.5, *i.e.*, somewhat lower than the mass spectrometric values. The apparent disparity of the results from the two sets of experiments probably indicates a deficiency of O_2 in the products, due to wall reactions on both the Pyrex and metal surfaces.[7] Several experiments were performed with a cell containing a cylindrical aluminum sheath, with the initial aim of obtaining more precise ion current plateaus. In these experiments the apparent H_2 yield dropped to 0.4 molecules per absorbed photon. If oxygen is assumed to have been removed quantitatively at the metal surface (giving $\kappa_{av} = \kappa_{H_2}$ = 175 cm^{-1}) the H_2 yield remains anomalously low at ~1.0. These observations show that product yields in the ionizing photolysis of H_2O are strongly dependent on wall processes.

Attempts were made to detect light emission from excited species produced in the 58.4-nm photolysis, such as was previously found with CO_2,[3] but no such emission was observed for NH_3 or H_2O.

Discussion

From the photofragmentation studies of Dibeler, *et al.*,[8] the primary processes at 58.4 nm may be summarized as

$$NH_3 + h\nu \longrightarrow NH_3^+ + e^- \quad (40\%) \qquad (1a)$$

$$\longrightarrow NH_2^+ + H + e^- \quad (60\%) \qquad (1b)$$

$$\longrightarrow NH^+ + H_2 + e^- \quad (<1\%) \qquad (1c)$$

$$H_2O + h\nu \longrightarrow H_2O^+ + e^- \quad (69\%) \qquad (2a)$$

$$\longrightarrow OH^+ + H + e^- \quad (28\%) \qquad (2b)$$

$$\longrightarrow O^+ + H_2 + e^- \quad (3\%) \qquad (2c)$$

With NH_3 the primary ions formed in our system will undergo extremely rapid reactions leading to the formation of the stable charge carriers NH_4^+ and $H(NH_3)_n^+$, according to[9,10]

$$NH_3^+ + NH_3 \longrightarrow NH_4^+ + NH_2 \qquad (3)$$

(k_3 = 1.8 × 10^{-9} cm^3 $molecule^{-1}$ sec^{-1})

$$NH_2^+ + NH_3 \longrightarrow NH_4^+ + NH \qquad (4a)$$

$$\longrightarrow NH_3^+ + NH_2 \qquad (4b)$$

(for thermal energies $k_{4a} = k_{4b}$ = 8 × 10^{-10} cm^3 $molecule^{-1}$ sec^{-1}), and

(7) T. G. Slanger and G. Black, *J. Chem. Phys.*, **54**, 1889 (1971).

(8) V. H. Dibeler, J. A. Walker, and H. M. Rosenstock, *J. Res. Nat. Bur. Stand. Sect. A*, **70**, 459 (1966).

(9) K. R. Ryan, *J. Chem. Phys.*, **53**, 3844 (1970).

(10) W. T. Huntress, Jr., M. M. Mosesman, and D. D. Elleman, *J. Chem. Phys.*, **54**, 843 (1971).

$$NH_4^+ + NH_3 + M \longrightarrow H(NH_3)_2^+ + M \quad (5)$$

where, by analogy with corresponding reactions for H_3O^+, k_5 with M = NH_3 is likely to be of the order of 10^{-27} cm^6 molecule^{-2} sec^{-1}.[11] Thus on a time scale of a few tens of nanoseconds at a pressure of 3 Torr the outcome of the primary photoionization process is described by

$$2.3NH_3 + h\nu \longrightarrow NH_4^+ + NH_2 + 0.3NH + 0.6H + e^- \quad (6)$$

At this pressure the time scale is probably about an order of magnitude larger for reaction 5 than for the bimolecular processes 3 and 4.

Similarly, with H_2O the major primary ions form the stable charge carriers $H(H_2O)_n^+$ by the extremely rapid reactions[11,12]

$$H_2O^+ + H_2O \longrightarrow H_3O^+ + OH \quad (7)$$

($k_7 = 2.6 \times 10^{-9}$ cm^3 molecule^{-1} sec^{-1})

$$OH^+ + H_2O \longrightarrow H_3O^+ + O \quad (8)$$

(at thermal energies $k_8 = 2 \times 10^{-9}$ cm^3 molecule^{-1} sec^{-1})

$$H_3O^+ + H_2O + M \longrightarrow H(H_2O)_2^+ + M \quad (9)$$

(measured $k_9 = 3.4 \times 10^{-27}$ for M = N_2 and 3.7×10^{-27} for M = O_2[11] in units cm^6 molecule^{-2} sec^{-1}). The reaction

$$O^+ + H_2O \longrightarrow OH^+ + OH \quad (10a)$$

is endothermic to the extent of ~2eV and may be neglected. However the exothermic charge-transfer reaction

$$O^+ + H_2O \longrightarrow O + H_2O^+ \quad (10b)$$

would be expected to be fast.[13] Thus after a few tens of nanoseconds we should have effectively

$$2.03H_2O + h\nu \longrightarrow H_3O^+ + 0.72OH + 0.31O + 0.28H + 0.03H_2 + e^- \quad (11)$$

The stable charge carriers $H(NH_3)_n^+$ and $H(H_2O)_n^+$ in turn must ultimately be removed by rapid dissociative recombination processes[14] ($\alpha > 10^{-7}$ cm^3 sec^{-1}), these processes being expected to occur mainly in the gas phase under the conditions of the present experiments[2] but with a possibly significant contribution from wall recombination at the lowest extremes of pressure and photon flux, or in the presence of a large metal surface. At present there is very little information available as to the outcome of such recombination processes. If the neutralization of $H(NH_3)_n^+$ is assumed to produce only H and nNH$_3$ the result of the primary photolysis on a time scale of a few hundreds of microseconds, such that dissociative recombination is essentially finished but neutral radical reactions have hardly begun, is given by

$$1.3NH_3 + h\nu \longrightarrow 1.6H + NH_2 + 0.3NH \quad (12)$$

With the same assumption for the charge carriers in the H_2O case we should have

$$1.03H_2O + h\nu \longrightarrow 1.28H + 0.72OH + 0.31O + 0.03H_2 \quad (13)$$

The radicals on the right-hand side of (12) can take part in a large number of homogeneous and heterogeneous processes, for example[15-17]

$$NH_2 + NH_2 \longrightarrow N_2H_4 \quad (14)$$

$$NH + NH_3 \longrightarrow N_2H_4 \quad (15)$$

$$NH + NH_2 \longrightarrow N_2H_3 \quad (16)$$

$$H + N_2H_4 \longrightarrow NH_3 + NH_2 \quad (17)$$

$$2N_2N_3 \longrightarrow N_2H_4 + N_2 + H_2 \quad (18)$$

and so on. Reaction 15 is rapid enough ($k_{15} \simeq 1.7 \times 10^{-12}$ cm^3 molecule^{-1} sec^{-1} [16]) to result in appreciable N_2H_4 production under the conditions of these experiments; the absence of hydrazine from the products of both photolysis and radiolysis presumably results from the ease with which it can be removed by reactions such as (17). Because of the plethora of possible reactions of neutral species in the NH_3 system our experiments do not allow us to make any firm deductions about the products of dissociative recombination of $H(NH_3)_n^+$.

The radicals on the right-hand side of equation 13 can undergo the following important reactions (assuming ground-state species only)

$$H + OH + M \text{ (or wall)} \longrightarrow H_2O + M \quad (19)$$

($k_{19} = 10^{-31}$ cm^6 molecule^{-2} sec^{-1} for M = H_2O[18])

$$OH + OH \longrightarrow H_2O + O \quad (20)$$

($k_{20} = 3 \times 10^{-12}$ cm^3 molecule^{-1} sec^{-1} [18])

$$O + OH \longrightarrow O_2 + H \quad (21)$$

($k_{21} = 2 \times 10^{-11}$ cm^3 molecule^{-1} sec^{-1} [18])

Other processes that must be considered are the removal of excited O atoms at the wall[2] and of O and OH on metal surfaces, and direct recombination of H and O to H_2 and O_2. Whatever selection of radical reactions is made, however, it is not possible to account for a yield

(11) A. Good, D. A. Durden, and P. Kebarle, *J. Chem. Phys.*, **52**, 212, 222 (1970).

(12) K. R. Ryan, *J. Chem. Phys.*, **52**, 6009 (1970).

(13) E. W. McDaniel, V. Cermak, A. Dalgarno, E. E. Ferguson, and L. Friedman, "Ion-Molecule Reactions," Wiley-Interscience, New York, N. Y., 1970, p 321 ff.

(14) M. A. Biondi, *Can. J. Chem.*, **47**, 1711 (1969).

(15) J. D. Salzman and E. J. Bair, *J. Chem. Phys.*, **41**, 3654 (1964).

(16) K. A. Mantei and E. J. Bair, *J. Chem. Phys.*, **49**, 3248 (1968).

(17) L. J. Stief, *J. Chem. Phys.*, **52**, 4841 (1970).

(18) D. L. Baulch, D. D. Drysdale, and A. C. Lloyd, "High Temperature Reaction Rate Data," No. 2, School of Chemistry, The University, Leeds 2, England.

of more than 1.03 H_2 molecules per photon absorbed on the basis of eq 13. This implies that the assumption behind eq 13, namely that recombination of $H(H_2O)_n^+$ with e^- yields only $H + nH_2O$, must be wrong. In order to account for the observed yield of about $2H_2$ per photon absorbed it is necessary to assume that virtually all of the recombination of $H(H_2O)_n^+$ occurs by a process of the type

$$H_3O^+ + e^- \longrightarrow H_2 + O + H \qquad (22)$$

On the basis of listed dissociation energies and proton affinities[19] process (22) is exothermic to the extent of about 28 kcal mol^{-1}. The lower yield of H_2 in the NH_3 case suggests that the analogous reaction is not significant for NH_4^+, where, on account of the higher proton affinity of NH_3, the formation of $H_2 + NH + H$ would be slightly endothermic or at best thermoneutral. The formation of higher order clusters $H(H_2O)_2^+$, $H(H_2O)_3^+$, $H(NH_3)_3^+$ etc. is exothermic, so that processes similar to (22) should be less favored on energetic grounds at higher gas pressures. Our observation that the H_2 yield from water falls markedly in the presence of a metal surface could be partly due to a difference in the nature of the products between homogeneous and heterogeneous electron-ion recombination. An additional possibility is that whereas a Pyrex surface with no special treatment is effective in removing excited oxygen atoms,[7] the metal might also remove OH by binding on the surface.

We still have to consider the question of the relative stability of water vapor during radiolysis *vs.* its instability during ionizing photolysis, and the contrast with ammonia which is unstable in both situations. In this respect H_2O resembles CO_2, whose apparent stability in the presence of high energy ionizing radiation at moderate dose rates has been attributed to the setting up of a steady state in which CO is reoxidized rapidly.[20] Our observation that CO_2 is decomposed with 20% efficiency by 21.2 eV radiation (under conditions where electron–ion recombination is predominantly homogeneous) would imply that the unidentified species responsible for reoxidizing CO during radiolysis requires a relatively large amount of energy for its formation. Any explanation of the difference in CO yields between the radiolysis and ionizing photolysis experiments should have some relevance to the problem of the unexpected stability of CO_2 in the atmosphere of Venus.[21] One practical difference between the radiolysis and ionizing photolysis experiments is that the former have been carried out at relatively high gas pressures, and often at elevated temperatures, so that the nature of the charge carriers involved in dissociative recombination reactions might be expected to differ. The neutral radical reactions occurring in the H_2O and CO_2 systems appear to be very sensitive to wall effects, and this also might provide a basis for the observed differences. Finally, it is interesting to consider that the ultimate products of the rather violent series of events which constitute radiolysis, namely H_2O, CO_2, and $N_2 + H_2$ in the three cases we have considered, are just what one would have predicted from simple considerations of thermodynamic equilibrium at room temperature.

Acknowledgments. We are grateful to Drs. M. J. McEwan and A. Metcalfe for helpful discussions. This work was supported by the New Zealand Universities Research Committee and by Grant AF-AFOSR-71-2134 from the United States Air Force Office of Scientific Research.

(19) V. I. Vedeneyev, L. V. Gurvitch, V. N. Kondratiev, V. A. Medvedev, and Ye. Frankevitch, "Bond Energies, Ionization Potentials and Electron Affinities," Edward Arnold, London, 1966; A. G. Gaydon, "Dissociation Energies," 3rd ed, Chapman and Hall, London, 1968; J. L. Franklin, J. G. Dillard, H. M. Rosenstock, J. T. Herron, K. Draxl, and F. H. Field, *Nat. Stand. Ref. Data Ser. Nat. Bur. Stand.*, No. 26 (1969).

(20) A. R. Anderson and D. A. Dominey, *Radiat. Res. Rev.*, 1, 269 (1968).

(21) D. M. Hunten, *Can. J. Chem.*, 47, 1875 (1969).

Pulsed Radiolysis and Flash Photolysis of Iodates in Aqueous Solution

by F. Barat, L. Gilles,* B. Hickel, and B. Lesigne

Département de Recherche et Analyse, Centre d'Etudes Nucléaires de Saclay, 91-Gif sur Yvette, France
(Received January 25, 1971)

Publication costs assisted by the French Atomic Energy Commission

The pulsed radiolysis and flash photolysis of aqueous solutions of the iodate ion have been investigated. In both cases, at neutral pH, an absorption band attributed to IO_2 is observed with a maximum at 480–490 nm: $\epsilon_{480}(IO_2) = 800 \pm 100\ M^{-1}\ cm^{-1}$. This transition disappears according a second-order process with $2k = (3.6 \pm 0.8) \times 10^9\ M^{-1}\ sec^{-1}$. Another absorption is also observed that grows in at wavelengths less than 320 nm (band C); in the pulsed radiolysis of 0.1 M IO_3^- it decays with second-order kinetics and $2k/\epsilon_{280} = 5.7 \times 10^6$ cm sec^{-1}. Furthermore, pulsed radiolysis gives rise in neutral media to a second absorption band (band B) centered around 360 nm, formed by the reaction of OH radicals, which is assigned to IO_3. At the same wavelength in alkaline media we have observed another transient species, tentatively attributed to IO_4^{2-}, whose molar extinction coefficient would be about 2600 $M^{-1}\ cm^{-1}$.

Introduction

The results of the numerous studies of the radiolysis of crystalline halates have been discussed in a recent paper by Boyd and Brown.[1] Investigations of the radiolysis and photolysis of aqueous solutions of the same ions are less advanced,[2-8] and with regard to the IO_3^- ion in particular, a disagreement in the attribution of one absorption band has been noted between Amichai and Treinin's work[6,9] and a preliminary flash photolytic study.[7] The aim of this paper is to point out the differences which exist between our results and those of previous studies and which lead to different conclusions. In addition, some new results relative to alkaline media are presented.

Experimental Section

1. Pulsed Radiolysis. The irradiations were performed with electrons whose energy spectrum showed a maximum at 1.8 MeV. The electrons were delivered by an electron gun, Febetron 707, in pulses of half-width 27 nsec with a peak intensity of 4000 A using a magnetic field of 4000 G.

The 1 cm deep cells used are made of high-purity silica (Spectrosil). The optical path through the cell is 2.2 cm long.

The energy deposition in the solution varies with depth in the cell, which results in a concentration gradient of the transient species formed: the effects of a given additive described later were always carried out under identical experimental conditions.

To vary the dose and the effective duration of the electronic pulse in the irradiated solution (measured by observing the Cerenkov emission) two procedures have been simultaneously used: aluminum plates, 5 mm thick, with holes of different diameters were placed in front of the electron exit window; the magnetic focusing field was varied from 0.2 to 0.4 Wb/m^2.

The mean dose per pulse, measured at half-depth of the irradiation cells, ranged from 6 to 150 krads. Doses were measured using 0.1 M ferrocyanide aqueous solution saturated with N_2O taking $\epsilon_{440\ nm}(Fe(CN)_6^{3-})$ 600 $M^{-1}\ cm^{-1}$ and $G_{OH} + G_{e_{aq}^-} = 5.5$.

When the monitoring light source (Osram Xe lamp, 450 W) was intensified during 1 msec,[10] an MQ4 Zeiss Monochromator coupled with 150 CVP (Radiotechnique) and 1 P28 (RCA) photomultipliers was employed. When this source was used without pulsing, the analyzing light was modulated by a rotating disk (100 Hz) to prevent photomultiplier saturation; the illumination time of the photocathode was about 100 μsec/cycle.

For the studies in the infrared region a grating monochromator (Huet, Type M25) or interference filters (Balzers) were used.

The results described were obtained with deaerated solutions and are concerned with single-pulse effects only.

2. Flash Photolysis. The flash photolysis setup has already been described elsewhere.[11] The transient species are formed at micromolar concentrations under a flash of 1300 J with a 4-μsec half-width.

(1) G. E. Boyd and L. C. Brown, *J. Phys. Chem.*, **74**, 3490 (1970).
(2) N. K. Bridge and M. S. Matheson, *ibid.*, **64**, 1280 (1960).
(3) O. Amichai and A. Treinin, *Chem. Phys. Lett.*, **3**, 611 (1969).
(4) O. Amichai, G. Czapski, and A. Treinin, *Isr. J. Chem.*, **7**, 351 (1969).
(5) O. Amichai and A. Treinin, *J. Phys. Chem.*, **74**, 3670 (1970).
(6) O. Amichai and A. Treinin, *ibid.*, **74**, 830 (1970).
(7) F. Barat, L. Gilles, B. Hickel, and J. Sutton, *Chem. Commun.*, 1485 (1969).
(8) F. Barat, L. Gilles, B. Hickel, and B. Lesigne, *ibid.*, 847 (1971).
(9) O. Amichai and A. Treinin, *J. Chem. Phys.*, **53**, 444 (1970).
(10) F. Barat, L. Gilles, B. Hickel, and B. Lesigne, Report CEA-N-1438.
(11) F. Barat, L. Gilles, B. Hickel, and J. Sutton, *J. Chem. Soc. A*, 1982 (1970).

3. Products. The solutions of potassium iodate (Prolabo RP; Analar, Merck) were prepared with triply distilled water and then deaerated by argon (N-55, Air Liquide) or nitrous oxide (N-40, Air Liquide) bubbling. The alcohols—ethanol, 2-propanol, and *tert*-butyl alcohol—and the sodium hydroxide were Merck chemicals used without further purification.

Results

1. Pulsed Radiolysis. A. Results Obtained in Neutral Media. For a dose of 6 krads the absorption spectrum between 280 and 600 nm of a 10^{-1} *M* deaerated iodate solution is presented in Figure 1. Three absorption bands are observed: the first (A) centered around 480 nm is formed immediately (100 nsec) after the pulse and remains approximately constant during 1 μsec, the second (B) centered around 360 nm reaches its maximum intensity after 1.3 μsec, and the third (C) observed at wavelengths less than 320 nm increases continuously in the uv region and is maximal after 200 nsec.

At $[IO_3^-] = 10^{-2}$ *M* the same shape of the spectrum is observed (Figure 2), and if the solution is saturated with nitrous oxide, the intensity of band A decreases by about 60% whereas the intensity of band B notably grows in.

For 2×10^{-3} *M* $\leqslant [IO_3^-] \leqslant 10^{-2}$ *M* an intense absorption was observed during and immediately after the pulse in the 500–750-nm wavelength region. This band had the characteristic shape of the solvated electron absorption and disappeared rapidly, between 200 and 70 nsec, for the concentration range considered. At iodate concentrations greater than 10^{-2} *M* there is no residual absorption in the 700-nm region after 100 nsec whatever the radiation dose.

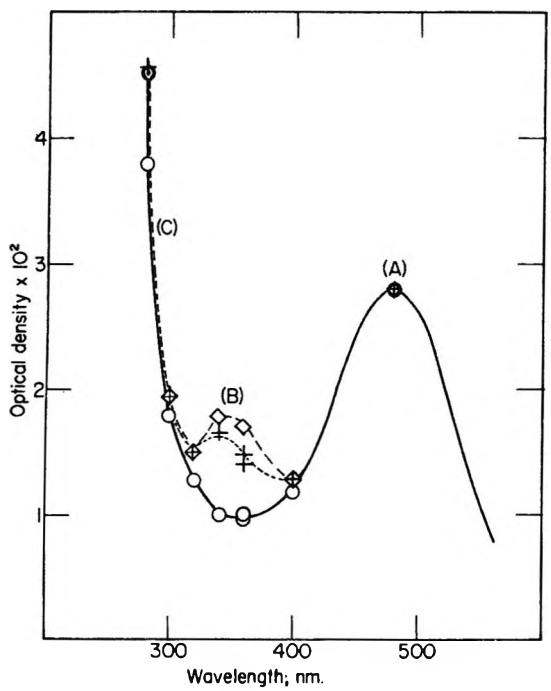

Figure 1. Absorption spectrum for $[IO_3^-] = 10^{-1}$ *M*, dose 6 krads: O, recorded 100 nsec after the pulse; +, recorded 500 nsec after the pulse; ◇, recorded 1.3 μsec after the pulse.

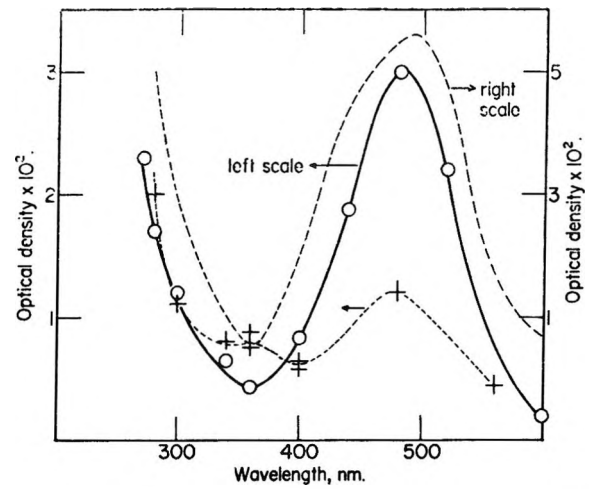

Figure 2. Left scale: absorption spectrum for $[IO_3^-] = 10^{-2}$ *M*, dose 6 krads, recorded 100 nsec after pulse: O, deaerated solution; +, solution saturated with N_2O. Right scale: absorption spectrum for $[IO_3^-] = 10^{-3}$ *M*, recorded 30 μsec after the photolytic flash.

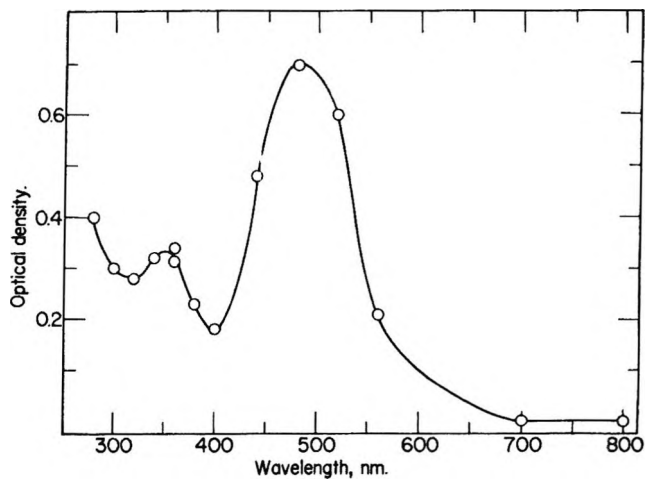

Figure 3. Absorption spectrum for $[IO_3^-] = = 10^{-1}$ *M*, recorded 100 nsec after the pulse, dose ≃150 krads.

At high doses (70–150 krads) the absorption spectrum recorded 100 nsec after the pulse clearly shows the three absorptions mentioned above (Figure 3). The maximum intensity attained by band A remains constant for 10^{-2} *M* $\leqslant [IO_3^-] \leqslant 2 \times 10^{-1}$ *M*, and by band B, for 10^{-1} *M* $\leqslant [IO_3^-] \leqslant 2.10^{-1}$ *M* decreasing in this latter case at lower concentrations.

With a 10^{-2} *M* iodate solution the time required to reach maximum absorption is less than 100 nsec at 480 nm and about 1.5 μsec at 360 nm. Bands A and B disappear according second-order kinetics with $2k/\epsilon_{360} = (5.0 \pm 0.5) \times 10^6$ cm sec^{-1} and $2k/\epsilon_{480} = (4.5 \pm 0.5) \times 10^6$ cm sec^{-1}, ϵ_{360} and ϵ_{480} being the molar extinction coefficients of the transients at 360 and 480 nm.

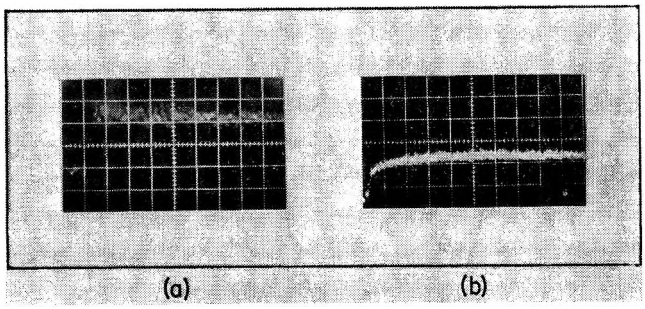

Figure 4. (a) Time of formation of IO_2 (λ 480 nm, $[IO_3^-] = 10^{-2}$ M, dose 6 krads, transmittance 2.4%, 50 nsec/division). (b) Time of formation of IO_3 (λ 360 nm, $[IO_3^-] = 10^{-1}$ M, dose 6 krads, transmittance 2%, 500 nesc/division).

The decay of band C has been measured at 280 nm with a dose of 6 krads. It is a second-order process with $2k/\epsilon_{280} \approx 5.7 \times 10^6$ cm sec^{-1}.

The significant points which emerge from these results follow. Whatever the dose, and for a large range of iodate concentrations, the species absorbing at 480 nm is formed very rapidly in less than 100 nsec (Figure 4a). In all cases where $[IO_3^-] \geq 10^{-2}$ M there is no absorption at 730 nm, 100 nsec after the pulse. Figure 1 shows that the contribution of band C to the absorption at 360 nm is important (about half of the maximum intensity attained) and that at least two species absorb at this wavelength.

Effect of Scavengers. Band Attribution. Ethanol, 2-propanol, or *tert*-butyl alcohol added in concentrations between 10^{-3} and 10^{-1} M to centimolar or decimolar solutions of iodate do not modify the initial intensity or the kinetics of disappearance of the band at 480 nm (band A).

Nitrous oxide (whose effect was always studied by saturating 10^{-2} M iodate solutions ($[N_2O] \approx 2.5 \times 10^{-2}$ M) reduces the intensity of A by about 60% without changing the kinetics of its disappearance (Figure 2).

On the basis of these observations and because varying the iodate concentration does not modify the kinetics of its disappearance, band A is assigned to the radical IO_2 formed by the reaction

$$IO_3^- + e_{aq}^- \xrightarrow{H_2O} IO_2 + 2OH^- \qquad (1)$$

Assuming $G_{e_{aq}^-} = 2.8$, the molar extinction coefficient of IO_2 can be estimated as $\epsilon_{480}(IO_2) = 800 \pm 100$ M^{-1} cm^{-1}.

At low dose (Figure 2) the initial absorption at 360 nm increases when the solution is saturated with N_2O without affecting it between 270 and 300 nm (but the rate of disappearance of the latter absorption is modified and $2k/\epsilon_{280} \approx 2 \times 10^7$ cm sec^{-1}).

At high doses, N_2O does not appreciably change the intensity of band B whereas the addition of *tert*-butyl alcohol (10^{-1} M) completely suppresses this absorption, thus showing that the extinction coefficient of IO_2 is very small at 360 nm. In the presence of alcohol the decay of band B is still second order but the value $2k/\epsilon_{360}$ increases markedly with alcohol concentration. The effect of alcohol has not been studied at lower wavelengths (λ <300 nm) because the hydroxyalkyl radicals absorb in this region.[12]

Thus, the effect of alcohols, ROH, considered as scavengers of OH radicals according to the reaction

$$ROH + OH \longrightarrow R'OH + H_2O \qquad (2)$$

and the effect of N_2O, as observed for a dose of 6 krads, lead us to assign part of the 360-nm absorption to the IO_3 radical formed by the reaction

$$IO_3^- + OH \longrightarrow IO_3 + OH^- \qquad (3)$$

However, the molar extinction coefficient of this species cannot be obtained from our experiments due to the presence of at least one other absorbing species (unspecified) at 360 nm. For the same reasons the ratio $k(IO_3^- + OH)/k(ROH + OH)$ cannot be precisely determined. Some experiments performed with ethanol and 2-propanol have given $k(IO_3^- + OH) \leq 5 \times 10^7$ M^{-1} sec^{-1}.

Considering the reactions

$$OH + OH \longrightarrow H_2O_2 \qquad (k_4 = 5 \times 10^9\ M^{-1}\ \text{sec}^{-1}\ [13]) \qquad (4)$$

$$IO_3^- + OH \longrightarrow IO_3 + OH^- \qquad (k_3 = 5 \times 10^7\ M^{-1}\ \text{sec}^{-1}) \qquad (3)$$

$$IO_3 + IO_3 \longrightarrow P \qquad (2k_5/\epsilon = 5 \times 10^6\ \text{cm}^{-1}\ \text{sec}^{-1}) \qquad (5)$$

the best fit between calculated values[14] and experimental data is obtained with $\epsilon_{360}(IO_3) \sim 300$ M^{-1} cm^{-1} taking into account the contribution of band C to the absorption at 360 nm.

In the same way one may calculate that in 10^{-1} M iodate solution under our experimental conditions, IO_3 reaches its maximum concentration in about 1 μsec, in good agreement with the growth registered in Figure 4b.

The increase in $2k/\epsilon_{360}$ with alcohol concentration may be due to various processes including, for instance, a reaction of IO_3 with the hydroxyalkyl radical R'OH formed in reaction 2 or a modification in the kinetics of disappearance of absorption C. The lack of information concerning this absorption makes it impossible at present to settle this point.

B. Results Obtained in Alkaline Media. Two sets

(12) M. Simic, P. Neta, and E. Hayon, *J. Phys. Chem.*, **73**, 3794 (1969).

(13) M. Anbar and P. Neta, *Int. J. Appl. Radiat. Isotop.*, **18**, 493 (1967).

(14) K. H. Schmidt, Report ANL 7199, a computer program for the kinetic treatment of radiation induced simultaneous chemical reactions, Argonne National Laboratory, Argonne, Ill.

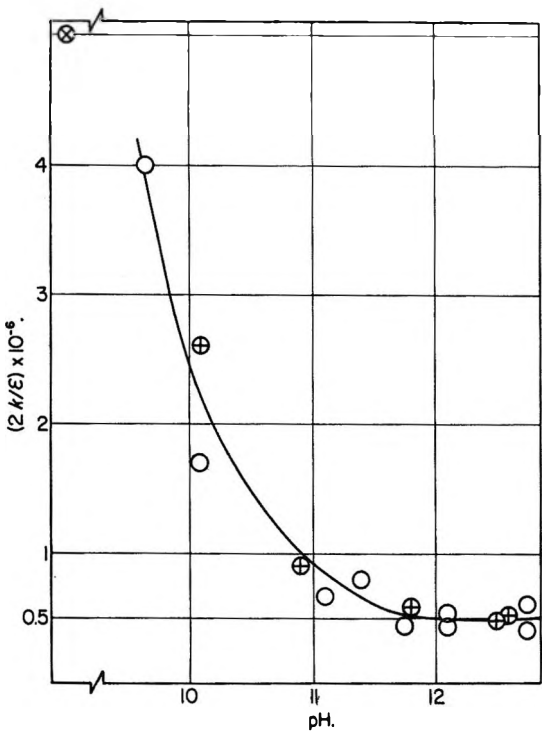

Figure 5. $2k/\epsilon_{360}$ as a function of pH: ○, pulsed radiolysis; ⊕, flash photolysis.

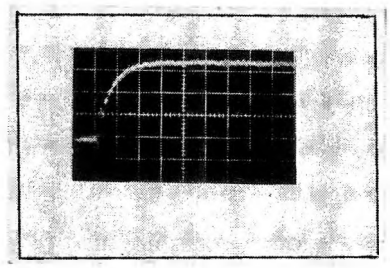

Figure 6. Time of formation of transient species absorbing at 360 nm in alkaline media (pH 12.6, $[IO_3^-] = 10^{-2}$ M, dose 6 krads, transmittance 5.4%, 100 nsec/division).

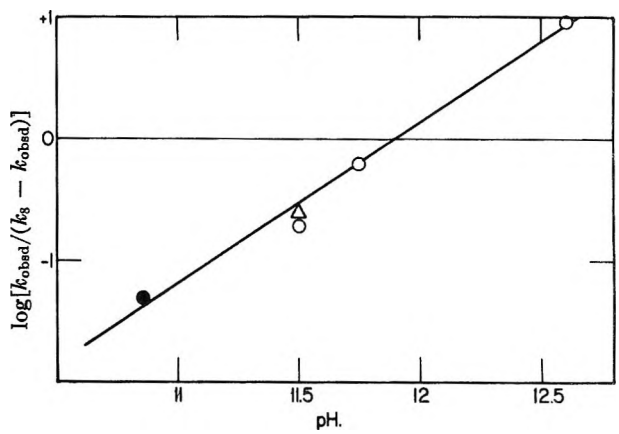

Figure 7. Log $[k_{obsd}/(k_8 - k_{obsd})]$ = f(pH): ●, $[IO_3^-] = 10^{-1}$ M; ○, $[IO_3^-] = 10^{-2}$ M; △, $[IO_3^-] = 10^{-2}$ M (solution saturated with N_2O).

of measurements were made: the first with $[IO_3^-] = 10^{-2}$ M and a dose of 8 krads; the other with $[IO_3^-] = 10^{-1}$ M and a dose of 11.6 krads. Although in the first case a weak absorption of IO_3 is observed in neutral solution (OD $\leqslant 5 \times 10^{-3}$), with increasing pH a band centered around 360 nm grows in. This band disappears by a second-order law and $2k/\epsilon_{360}$ decreases with increasing pH (Figure 5). The addition of 2-propanol causes this band to disappear, whereas addition of N_2O, at a given pH, leads to a further increase in the absorption.

These results suggest that IO_2 does not play a part in the formation of this transient and that O^- intervenes through the reaction

$$e_{solv}^- + N_2O \longrightarrow N_2 + O^- \qquad (6)$$

followed by

$$O^- + H_2O \rightleftharpoons OH + OH^- \qquad (7)$$

Another argument which strengthens this assumption will be reported in the section dealing with flash photolysis. The various results lead us tentatively to ascribe the absorption at 360 nm to IO_4^{2-} formed by the reaction

$$IO_3^- + O^- \longrightarrow IO_4^{2-} \qquad (8)$$

and whose molar extinction coefficient is $\epsilon_{360}(IO_4^{2-})$ 2600 M^{-1} cm^{-1}.

The rate of growth of the 360-nm band increases with the pH and seems proportional to the O^- concentration. In this case and if the rate constant $k(OH + IO_3^-)$ is slow compared to $k(O^- + IO_3^-)$, it is possible to derive the relation[15]

$$\log [k_{obsd}/(k_8 - k_{obsd})] = pH - pK$$

where $pK = -\log ([H^+][O^-]/[OH])$ and where k_{obsd} is the apparent rate of formation of the 360-nm band.

The rate constant $k(O^- + IO_3^-)$ was determined at pH 12.6 (Figure 6) and corrected for the undissociated OH radicals: $k(O^- + IO_3^-) = (3 \pm 0.5) \times 10^9$ M^{-1} sec^{-1}.

Figure 7 shows log $[k_{obsd}/(k_8 - k_{obsd})]$ *vs.* pH in the range where reaction 3 is unimportant: the intercept with the abscissae gives $pK = 11.9$ in good agreement with previous results.[15,16]

Assuming that the following reactions occur

$$IO_3^- + OH \longrightarrow IO_3 + OH^- \qquad (k_3 = 5 \times 10^7\ M^{-1}\ \text{sec}^{-1}) \quad (3)$$

$$IO_3^- + O^- \longrightarrow IO_4^{2-} \qquad (k_8 = 3 \times 10^9\ M^{-1}\ \text{sec}^{-1}) \quad (8)$$

$$OH + HO^- \longrightarrow O^- + H_2O \qquad (k_{9b} = 1.2 \times 10^{10}\ M^{-1}\ \text{sec}^{-1}\ [17]) \quad (9b)$$

(15) J. L. Weeks and J. Rabani, *J. Phys. Chem.*, **70**, 2100 (1966).
(16) J. Rabani and M. S. Matheson, *ibid.*, **70**, 761 (1966).

$$O^- + H_2O \longrightarrow OH + OH^- \qquad (k_{9a} = 9.2 \times 10^7\ \text{sec}^{-1}\ ^{17}) \quad (9a)$$

$$OH + OH \longrightarrow H_2O_2 \qquad (k_4 = 5 \times 10^9\ M^{-1}\ \text{sec}^{-1}) \quad (4)$$

$$O^- + O^- \longrightarrow HO_2^- + OH^- \qquad (k_{10} = 9 \times 10^8\ M^{-1}\ \text{sec}^{-1}) \quad (10)$$

calculation[14] shows that the growth of optical density at 360 nm with pH is in good agreement with experimental data (Figure 8).

It should be noted that the presence of N_2O leads to a diminution in the decay rate of IO_4^{2-} which is no longer a second-order process, but this result is not found in the flash photolysis experiments and remains at present unexplained.

II. Flash Photolysis. Except where otherwise stated the concentration of iodate solution is 10^{-3} M but experiments have been performed with 10^{-5} $M < IO_3^- < 5 \times 10^{-3}$ M.

A. Results Obtained in Neutral Media. The transient spectrum of a deaerated iodate solution in the 280–800-nm region contains an absorption band centered around 480 nm, which was previously ascribed to the IO_2 radical[7] and an absorption that grows in at wavelengths less than 300 nm (Figure 2). The disappearance of IO_2 is a second-order reaction with $2k/\epsilon_{480} = (4 \pm 0.7) \times 10^6$ cm sec^{-1}.

The formation of IO_2 results from the primary mechanism

$$IO_3^-, H_2O \xrightarrow{h\nu} (IO_3^-, H_2O)^* \longrightarrow IO_2 + OH^- + OH \quad (11)$$

as is the case with other halates.

The band of IO_3 which should appear at 360 nm, due to reaction 3, is missing: this perhaps means that other reactions such as (4) and

$$OH + IO^- \longrightarrow IO + OH^- \quad (12)$$

similar to

$$OH + BrO^- \longrightarrow BrO + OH^- \quad (13)$$

with $k_{13} = 4.5 \times 10^9\ M^{-1}\ \text{sec}^{-1}$, as observed in the pulse radiolysis of BrO_3^-,[18] are involved.

Determination of the IO_2 Extinction Coefficient. The photolytic dissociation mechanism of the IO_3^- ion being formulated in reaction 11, it should be possible by adding bicarbonate ions ($[HCO_3^-] = 0.1$ M) to a 5×10^{-3} M iodate solution to scavenge the hydroxyl radicals by the reaction

$$HCO_3^- + OH \longrightarrow CO_3^- + H_2O \qquad (k_{14} = 1.5 \times 10^7\ M^{-1}\ \text{sec}^{-1}\ ^{13}) \quad (14)$$

The relation

$$\epsilon_{490}(IO_2) = \epsilon_{600}(CO_3^-) \times \frac{OD_{490}(\text{exptl}) - \frac{\epsilon_{490}(CO_3^-)}{\epsilon_{600}(CO_3^-)} OD_{600}(CO_3^-)}{OD_{600}(CO_3^-)}$$

derived from reactions 11 and 14 leads to $\epsilon_{490}(IO_2)$ 830 ± 50 M^{-1} cm^{-1} taking $\epsilon_{600}(CO_3^-)$ 1860 M^{-1} cm^{-1} and $\epsilon_{490}(CO_3^-)$ 600 M^{-1} cm^{-1}.[19]

The validity of the method was checked by determining the molar extinction coefficient of BrO_2 at 475 nm during flash photolysis of BrO_3^-. A value $\epsilon_{475}(BrO_2)$ 990 ± 50 M^{-1} cm^{-1} was found, which is in good agreement with that reported by Buxton and Dainton.[17]

B. Results Obtained in Alkaline Media. The flash photolysis of deaerated alkaline solutions of iodate shows an absorption band centered around 350–360 nm, whose intensity grows with pH; as in the case of pulsed radiolysis, the $2k/\epsilon_{360}$ value decreases with increasing pH (Fig. 5).

Addition of N_2O ($[N_2O] = 2.5 \times 10^{-2}$ M) to such a solution does not bring about any change: at a given pH, neither the absorption intensity at 360 nm nor the kinetics of disappearance is modified.

The photolysis of alkaline oxygenated solutions (pH 11.8, $[O_2] \approx 10^{-3}$ M) results in a considerable lowering of the absorption at 360 nm and the appearance of an absorption band centered around 430 nm, due to the ozonide ion, O_3^-, formed by the reaction

$$O_2 + O^- \longrightarrow O_3^- \quad (15)$$

Addition of 2-propanol, $[(CH_3)_2CHOH] = 10^{-3}$ M,

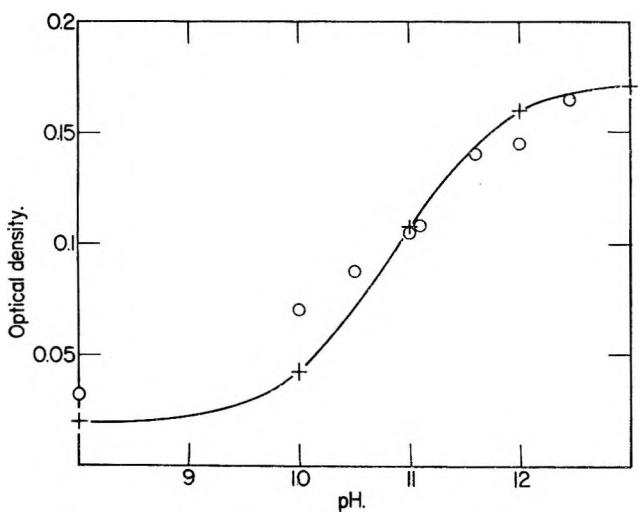

Figure 8. Optical density at 360 nm as a function of pH ($[IO_3^-] = 10^{-1}$ M, dose = 11.6 krads): O, experimental values; +, calculated values, $\epsilon_{360}(IO_4^{2-})$ 2600 M^{-1} cm^{-1}.

(17) G. V. Buxton, *Trans. Faraday Soc.*, **66**, 1656 (1969).

(18) G. V. Buxton and F. S. Dainton, *Proc. Roy. Soc., Ser. A*, **304**, 427 (1968).

(19) J. L. Weeks and J. Rabani, *J. Phys. Chem.*, **70**, 2100 (1966).

at pH 11.7 lowers the absorption at 360 nm by about 70%. These results, compared with those obtained by pulsed radiolysis, lead us to assign the absorption at 360 nm to the species IO_4^{2-} (reactions 9b and 8).

Discussion

The ensemble of the results in neutral media leads us to ascribe the two absorption bands to IO_3 (360 nm) and IO_2 (480 nm), respectively. Though the decay kinetics of these transients and the attribution of the 360-nm band agree with previous results,[6] the assignment of the 480-nm band and the value of $k(IO_3^- + OH)$ do not.

In fact, according to Amichai and Treinin[6] absorption spectrum of the transient species revealed by pulsed radiolysis and flash photolysis of aqueous solutions of iodate at neutral pH shows three maxima at 715, 480, and 360 nm, which they ascribed to IO_2, IO, and IO_3, respectively.

Their mechanism supposed that IO_2 formed in radiolysis by reaction 1 reacts with IO_3^- by a pseudo-first-order process to give IO radicals

$$IO_2 + IO_3^- \longrightarrow IO + IO_4^- \qquad (k_{16} = (3.5 \pm 0.5) \times 10^5\ \text{sec}^{-1}) \quad (16)$$

Moreover, they support their conclusions by a study of pulsed radiolysis and flash photolysis of aqueous solutions of IO^- (pH 13.6): IO is supposed to be formed according to the reaction

$$IO^- + O^- \xrightarrow{H_2O} IO + 2OH^- \quad (17)$$

Finally, their conclusions allow them to interpret the absorption spectrum that they observe in the photolysis of IO_3^- in boric acid glass at 2537 Å.[9]

Considering our own results in alkaline media it is not evident that O^- reacts as OH, so that the products of the reactions $IO^- + OH$ and $IO^- + O^-$ may be different. Nevertheless the following more important results lead us to disagree with the assumptions of Amichai and Treinin:[6] the absence of any absorption, except that of e_{aq}^-, between 700 and 800 nm at high and low doses (from 6 to 150 krads) which eliminates a possible effect of dose; the absence of any absorption in the same wavelength range in the flash photolysis experiments, which eliminates a possible effect of the high dose rates furnished by the Febetron; the absence of an effect of alcohols on the 480-nm band; and the time of formation of the 480-nm band, which would be 200 μsec for $[IO_3^-] = 10^{-2}\ M$ according to Amichai and Treinin[6] and which is always less than 100 nsec in our pulsed radiolysis experiments.

The presence of a relatively strong and, at present, unidentified absorption which increases with IO_3^- concentration, in the same region as a band which grows in with time, makes the assignment of the 360-nm band to IO_3 somewhat difficult. Nevertheless, the assumption that IO_3 radicals absorb at 360 nm leads to a value of $k(IO_3^- + OH)$ much lower than $(9.2 \pm 0.8) \times 10^8$ found by these authors. Indeed, our results do not support a fast reaction between OH and IO_3^-: the rate of appearance of the 360-nm band in neutral media, the effect of IO_3^- concentration, and the addition of alcohols show that, if this band is partly due to IO_3, $k(IO_3^- + OH)$ cannot be greater than $5 \times 10^7\ M^{-1}\ \text{sec}^{-1}$.

In alkaline media the rate of appearance of the 360-nm band gives a more direct determination of $k(IO_3^- + O^-)$ than the indirect method of Amichai and Treinin;[6] the value $k(IO_3^- + O^-) = 3 \times 10^9\ M^{-1}\ \text{sec}^{-1}$ is greater than that given by these authors. The overall results obtained in alkaline media lead us tentatively to attribute the 360-nm band observed under these conditions to IO_4^{2-}. The molar extinction coefficient of this species would be about 9 times that of IO_3.

A New Primary Process in the Ultraviolet Photolysis of Methyl Iodide. The Direct Photolysis to :CHI

by Chi-wing Tsao and John W. Root*

Department of Chemistry, University of California, Davis, California 95616 *(Received July 26 1971)*

Publication costs assisted by the U. S. Air Force Office of Scientific Research

The molecular elimination of H_2 has been shown to contribute to the primary photodissociation mechanism of CH_3I at ultraviolet wavelengths shorter than 3145 ± 20 Å. From these results upper limiting values of 94.2 ± 0.6 and 91.3 ± 1.7 kcal/mol were calculated for the 298°K heat of formation of :CHI and the carbon–hydrogen bond dissociation energy D_0(CHI–H), respectively.

Introduction

For many years the primary photochemical process in methyl iodide has been recognized to be[1-3]

$$CH_3I + h\nu \longrightarrow CH_3 + I \qquad (1)$$

The continuous absorption band for methyl iodide occurs in the ultraviolet from about 3600 Å with the first absorption maximum at about 2600 Å. At short wavelengths two new primary processes become energetically possible.

$$CH_3I + h\nu \longrightarrow :CHI + H_2 \qquad (2)$$

$$CH_3I + h\nu \longrightarrow :CH_2 + HI \qquad (3)$$

The occurrence of reaction 2 in alkanes is well known. Mahan and Mandal demonstrated the formation of H_2 in the vacuum ultraviolet photolysis of CH_4 and concluded that it was produced primarily from an intramolecular process.[4] Herzberg suggested process 2 in CH_3Cl from a theoretical point of view.[5] In recent matrix-isolation studies of the vacuum ultraviolet photolyses of CH_3Cl and CH_3F the spectra of :CHCl and :CHF were identified.[6,7] It was suggested in this latter work that both :CHCl and :CHF resulted from primary processes such as (2), but no attempts were made to detect the postulated molecular elimination of H_2.

The occurrence of reaction 3 at 2288 Å has been verified recently in photolysis experiments with tritium-labeled methyl iodide.[8] The singlet methylene (^{1}:CHT) was detected through the well-known olefin addition and carbon–hydrogen bond insertion reactions.

During the course of our hot methyl radical research program, we suspected that molecular hydrogen was being formed *via* primary process 2 in the ultraviolet photolysis of CH_3I. Another series of experiments was therefore initiated with the tritium-labeled methyl iodide in a dual effort to confirm the existence of CH_2TI photodissociation channel 2 and to measure its photochemical threshold energy.

Experimental Section

Broad spectrum ultraviolet radiation was produced from a Hanovia Type 929B009U, 2500-W Xe–Hg lamp. The collimated light was predispersed by a quartz prism and then concentrated upon the entrance slit of a Bausch and Lomb monochromator. The entrance and exit slits of the monochromator were so adjusted that a reasonably intense beam of light emerged from the monochromator with an effective bandwidth of 40 Å (full width half-maximum). The apparatus and a representative light spectrum are shown on Figures 1 and 2. The quartz optical elements and the light source were carefully aligned by means of a Spectra Physics He–Ne gas laser. The laser beam was passed through the center of each optical element and finally struck the lamp 2 mm below the tip of the tungsten anode. Using this particular optical system it was found that further reductions of the output bandwidth were impractical because of severe intensity losses. Also, the undesirable shoulder at short wavelengths could not be eliminated. The light intensity incident upon the photolysis cells was monitored either by means of an Eppley thermopile and a Keithley nanovoltmeter or a photomultiplier tube and a Keithley electrometer. Except for the quartz windows the reaction cells were constructed from ordinary Pyrex glass and Kontes high

(1) R. D. Doepker and P. Ausloos, *J. Chem. Phys.*, **41**, 1865 (1964).

(2) R. D. Schultz and A. A. Taylor, *ibid.*, **18**, 194 (1950).

(3) G. M. Harris and J. E. Willard, *J. Amer. Chem. Soc.*, **76**, 4678 (1950).

(4) B. H. Mahan and R. Mandal, *J. Chem. Phys.*, **37**, 207 (1962).

(5) G. Herzberg, "Electronic Spectra of Polyatomic Molecules," Van Nostrand, Princeton, N. J., 1967, p 448.

(6) M. E. Jacox and D. E. Milligan, *J. Chem. Phys.*, **53**, 2688 (1970).

(7) M. E. Jacox and D. E. Milligan, *ibid.*, **50**, 3525 (1969).

(8) (a) G. W. Mutch and J. W. Root, unpublished results; (b) C. C. Chou, P. Angelberger, and F. S. Rowland, *J. Phys. Chem.*, **75**, 2536 (1971).

vacuum O-ring stopcocks. Suprasil quartz windows were cemented onto the Pyrex body by means of epoxy glue. The sample cells and vacuum apparatus were absolutely grease free, and connections to the vacuum system were made by means of O-ring ball and socket joints. The photolysis cells were designed to allow their direct incorporation into the flow system of the gas chromatography analytical apparatus.

The entire vacuum gas transfer apparatus was fabricated from copper and brass in order to avoid the hydrogen exchange problems often encountered in photochemical recoil experiments.[9] The brass vacuum valves were Hoke Type 411M, 4B, and the gas pressures were monitored by Hastings gauges in the micron range and by a diaphragm gauge in the Torr range. With the present apparatus ten reaction cells can be filled at once with identical gas mixtures.

For each analysis the reaction cell contents were flushed through a series of liquid nitrogen temperature traps into the gas chromatography column. The eluted tritium-labeled products HT and CH_3T were detected by an internal gas flow proportional counter.[10] To ensure that no CH_2TI was allowed to contaminate the analytical gas chromatography column, a short stripper column consisting of a 5-cm section of Linde Type 5A molecular sieve packed in glass tubing was inserted into the flow stream ahead of the analytical column. The latter column consisted of a 20-ft section of Linde Type 5A molecular sieve. The retention times for HT and CH_3T were 7 and 23 min, respectively, at a helium flow rate of 85 cc/min NTP. Signal pulses generated in the counter passed successively through an Ortec scintillation preamplifier provided with a high-voltage standoff capacitor, a linear amplifier, a discriminator, and a digital output device.

The chemicals employed in these experiments included the following: He, J. T. Baker high purity grade; O_2, Matheson research grade; and CH_2TI, International Chemical and Nuclear Corp., 25 mCi/mmol. In a typical experiment nine photolysis cells were filled simultaneously with 350 μ pressure of the labeled methyl iodide, 20 Torr O_2, and 180 Torr He. The cells containing the reactants were allowed to stand in the dark overnight to ensure complete mixing. One cell from each set was kept in the dark throughout the experiment as a blank run, while the others were irradiated one by one at preselected ultraviolet wavelengths. Because of the low intensity of our narrow bandpass light source, several of the runs required photolysis times as long as 12 hr. Following the irradiations, the reaction mixtures were analyzed as quickly as possible in order to minimize any dark reactions.

Results

The results that we wish to report are summarized in Table I. The reported HT yields represent the signals obtained after corrections for counter background and for the small activities from the blank runs. Absolute quantum yields were not measured in these experiments; instead, the data were normalized by means of the following formula

$$Y = k\frac{N}{I_0Ct} \qquad (4)$$

in which Y is the relative yield of HT; k is an arbitrary constant; N is the net observed HT activity; I_0 is the total light intensity falling on the entrance window of the photolysis cell; C is the concentration of the methyl iodide; and t is the duration of exposure to the ultra-

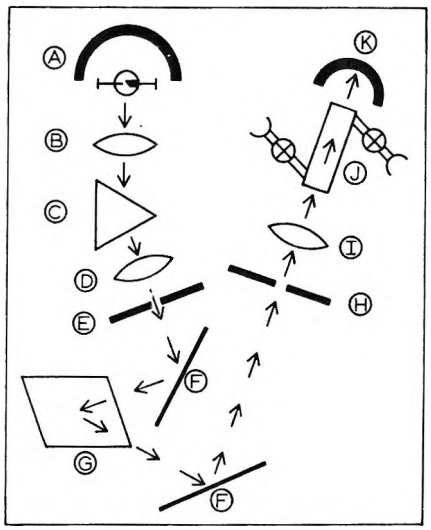

Figure 1. Schematic drawing of the photolysis apparatus. (A) High-pressure Hg–Xe lamp, (B) focusing lens, (C) predispersion prism, (D) focusing lens, (E) variable entrance slit, (F) concave mirror, (G) diffraction grating, (H) variable exit slit, (I) exit lens, (J) photolysis cell, and (K) thermopile or photomultiplier detector.

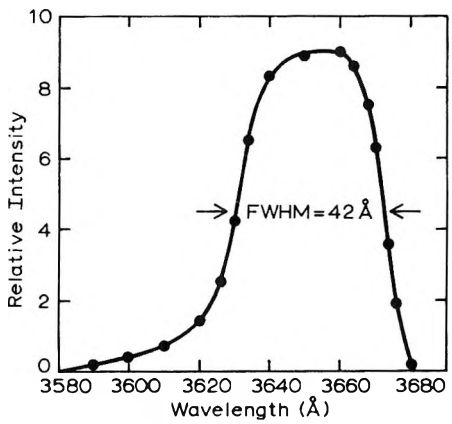

Figure 2. A typical output spectrum of the Bausch and Lomb monochromator at 3650 Å.

(9) (a) R. M. Martin and J. E. Willard, *J. Chem. Phys.*, **40**, 2999 (1964); (b) R. M. Martin and J. E. Willard, *ibid.*, **40**, 3007 (1964).

(10) J. K. Lee, E. K. C. Lee, B. C. Musgrave, Yi-Noo Tang, J. W. Root, and F. S. Rowland, *Anal. Chem.*, **34**, 741 (1962).

violet light. Due to uncontrolled variations in the experimental conditions, the data show fluctuations from run to run. The general trends indicated by these results were quite reproducible, however, and support several conclusions.

Table I: Reaction Yields of HT and CH_3T[a]

Expt	λ, Å	CH_2TI, μ	HT (normalized counts)	CH_3T (normalized counts)	Time, min
I	2804	450	1336 ± 17	18	767
	2967	450	1052 ± 16	0	292
	3025	450	1197 ± 22	18	243
II	3025	350	807 ± 17	...	270
	3130	350	991 ± 23	...	405
	3230	350	0	...	840
	3340	350	78 ± 3	...	720
III	3025	300	258 ± 20	...	120
	3165	300	0	...	300
	3200	300	0	...	300
	3340	300	0	...	700

[a] He = 180 Torr; O_2 = 20 Torr in all the experiments.

Discussion

The experimental results pointed to three unambiguous conclusions. (1) From experiments II and III the threshold wavelength for molecular HT formation was determined to occur in the wavelength interval between 3130 and 3165 Å. Since the effective band width of the light source is 40 Å, full width at half-maximum, our best estimate for this threshold is 3145 ± 20 Å. (2) The total amount of HT produced did not fluctuate appreciably within each set of experiments. (3) In all these experiments the CH_3T yields were small compared to the yields of HT. There are three possible mechanistic paths (5–7) by which HT could be formed in the CH_2TI ultraviolet photolysis experiments

$$CH_2TI + h\nu \xrightarrow{I} :CHI + HT \qquad \Delta H = 4.0 \pm 0.2 \text{ eV} \quad (5)$$

$$CH_2TI + h\nu \xrightarrow{II} CH_2I + T^* \qquad \Delta H = 4.5 \pm 0.07 \text{ eV} \quad (6a)$$

$$T^* + CH_3I \longrightarrow HT + CH_2I \quad (6b)$$

$$CH_2TI + h\nu \xrightarrow{III} \begin{cases} \longrightarrow :CHT + HI & (7a) \\ \longrightarrow :CH_2 + TI & (7b) \end{cases} \qquad \Delta H = 4.12 \pm 0.04 \text{ eV}$$

$$^1{:}CHT + M \longrightarrow {}^3{:}CHT + M \quad (7c)$$

$$^3{:}CHT + O_2 \longrightarrow HT + CO_2 \quad (7d)$$

$$TI + h\nu \longrightarrow T^* + I \quad (7e)$$

$$T^* + CH_3I \longrightarrow HT + CH_2I \quad (7f)$$

The approximate thermodynamic threshold energy for process I is 4.0 ± 0.2 eV based upon a recent electron impact measurement of the heat of formation of :CHI.[11] The uncertainty assigned to the enthalpy change for process 5 represents an estimate, since no accuracy limits were specified in the original reference. The thermodynamic threshold for process II is 4.50 ± 0.07 eV, corresponding to single photon absorption at 2754 Å.[12] The actual photodissociation threshold would probably occur at shorter wavelengths than the 2754 Å value. From recent tabulations of the standard heats of formation of CH_3I, $:CH_2$, and HI the thermodynamic threshold for process III is calculated as 4.12 ± 0.04 eV.[13,14] Our measured threshold for HT formation from the ultraviolet photodissociation of CH_2TI is 3145 ± 20 Å. A 3145 Å photon has an energy of 3.94 eV, which is insufficient for the initiation of either photodissociation process II or III, and we conclude that the observed HT must have come from process I.

Because of the possibility for uncertainties in the thermochemical data, we have also carried out a series of kinetics experiments to substantiate the conclusions derived from the threshold measurements. It has been demonstrated experimentally that triplet methylene reacts very efficiently with oxygen to produce molecular hydrogen as in reaction 7d.[15] No significant changes in our HT yields were observed when otherwise identical samples were photolyzed at 3130 Å with and without added oxygen scavenger. Additional experiments were carried out at 3130 Å in which the samples contained added ethylene. No labeled cyclopropane was detected from the well-known olefin addition scavenging reaction 8

$$^3{:}CHT + C_2H_4 \longrightarrow c\text{-}C_3H_5T \quad (8)$$

The half-pressure for collisional stabilization of the triplet addition product from reaction 8 is about 170 Torr, so that a substantial fraction of the c-C_3H_5T would have survived unimolecular isomerization to C_3H_5T under our experimental conditions. Therefore reaction 7d involving triplet :CHT did not contribute significantly to the HT yields at 3130 Å.[8a] Furthermore, molecular HT is not an expected product from singlet :CHT reactions, and we conclude that process III can be ruled out as a source of molecular HT at wavelengths longer than 3100 Å.

One other possible source for molecular HT might

(11) J. J. De Corpo and J. L. Franklin, *J. Chem. Phys.*, **54**, 1885 (1971).

(12) (a) D. M. Golden and S. W. Benson, *Chem. Rev.*, **69**, 125 (1969); (b) S. Furuyama, D. M. Golden, and S. W. Benson, *Int. J. Chem. Kinet.*, **1**, 283 (1969).

(13) S. W. Benson, "Thermochemical Kinetics," Wiley, New York, N. Y., 1968.

(14) W. A. Chupka and C. Lifshitz, *J. Chem. Phys.*, **48**, 1109 (1968).

(15) R. L. Russell and F. S. Rowland, *J. Amer. Chem. Soc.*, **90**, 1671 (1968).

involve some unspecified reaction of hot CH_2T radicals with O_2. This mechanism is eliminated by the absence of HT in the experiments carried out at wavelengths longer than 3130 Å. Furthermore, the HT yields were not affected by the presence or absence of O_2. Unimolecular decomposition of the hot CH_2T radicals to form either HT or T atoms is not energetically possible at 3145 Å.

By this process of elimination, we conclude that the observed molecular HT yield at 3145 Å must have resulted from molecular elimination photodissociation mechanism I. Herzberg has advanced a theoretical interpretation for photodissociation processes of this kind.[5] According to his model the CH_3I would be excited to an attractive upper state corresponding to H_2 + :CHI. This mode for the unsymmetrical, direct dissociation is depicted in Figure 3. Our observation in Table I that the molecular HT yield is essentially constant at energies immediately above threshold requires that the onset of the upper state vibrational continuum be located directly above the potential minimum for the CH_3I ground state.

The heat of formation for :CHI can readily be estimated from this unsymmetrical direct dissociation model. From our experimental threshold for reaction 5 the heat of formation for :CHI is calculated as 94.2 ± 0.6 kcal/mol. This is an upper limiting value because of the likelihood that the :CHI contains vibrational excitation. This calculated heat of formation for :CHI is in excellent agreement with the independent result of 95 kcal/mol obtained recently by De Corpo and Franklin.[11] Based upon our threshold value and the known CH_2I–H bond dissociation energy,[12] we calculate a 298°K D_0(CHI–H) value of 91.3 ± 1.7 kcal/mol.

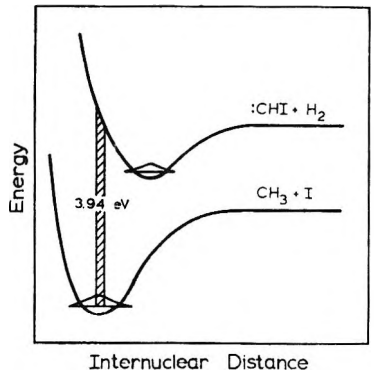

Figure 3. Approximate two-dimensional representation of the dissociation process involved in the photodissociation of CH_3I.

Summary

The existence of a new primary photodissociation process for methyl iodide has been established. This process leads to molecular H_2 and :CHI with a threshold corresponding to ultraviolet absorption at 3145 ± 20 Å.

Based upon Herzberg's unsymmetrical direct photodissociation model, upper limiting values of 94.2 ± 0.6 and 91.3 ± 1.7 kcal/mol were calculated for the 298°K heat of formation of :CHI and the carbon–hydrogen bond dissociation energy D_0(CHI–H), respectively.

Acknowledgment. The authors gratefully acknowledge generous financial support from the U. S. Air Force Office of Scientific Research.[16] We would also like to thank Mr. G. W. Mutch of this laboratory for his assistance with some of the experiments.

(16) This work has been supported under AFOSR Contract AF-AFOSR-68-1493.

The Oxidation of Aqueous Bromide Ions by Hydroxyl Radicals. A Pulse Radiolytic Investigation

by Dov Zehavi and Joseph Rabani*

Department of Physical Chemistry, The Hebrew University of Jerusalem, Jerusalem, Israel
(Received August 18, 1971)

Publication costs borne completely by The Journal of Physical Chemistry

Oxidation of Br^- by OH radicals in neutral and acid aqueous solutions has been investigated. The reaction mechanism involves the following reactions and rate constants: $OH + Br^- \rightarrow BrOH^-$, $k = (1.06 \pm 0.08) \times 10^{10}\ M^{-1}\ sec^{-1}$; $BrOH^- \rightarrow Br^- + OH$, $k = (3.3 \pm 0.4) \times 10^7\ sec^{-1}$; $BrOH^- \rightarrow Br + OH^-$, $k = (4.2 \pm 0.6) \times 10^6\ sec^{-1}$; $BrOH^- + H^+ \rightarrow H_2O + Br$, $k = (4.4 \pm 0.8) \times 10^{10}\ M^{-1}\ sec^{-1}$; $BrOH^- + Br^- \rightarrow OH^- + Br_2^-$, $k = (1.9 \pm 0.3) \times 10^8\ M^{-1}\ sec^{-1}$; $Br + Br^- \rightarrow Br_2^-$, $k \simeq 10^{10}\ M^{-1}\ sec^{-1}$ (previous work). A new absorption peak of Br_2^- at 700 nm is reported. A new equilibrium reaction of Br_2^- with Br^- to produce Br_3^{2-} is proposed.

Introduction

A number of papers have been published concerning steady and pulse radiolysis and photolysis of bromide solutions. Grossweiner and Matheson[1] found an absorption band near 350 nm upon flash photolysis of Br^- solutions. They assigned it to Br_2^- ions. Br_2^- absorption has been observed later in pulse radiolysis.[2-6] Bromide ions have been extensively used in both steady radiolysis and photolysis experiments.[7-14] Matheson, Mulac, Weeks, and Rabani[6] measured the reactivity of OH radicals towards Br^- ions by pulse radiolysis. They concluded that reaction 1 is not a simple electron transfer reaction, but involves an intermediate $BrOH^-$, formed according to reaction 2, which is reversible. Br atoms formed according to reaction 3 react with Br^- to form Br_2^-.

$$Br^- + OH \longrightarrow Br + OH^- \qquad (1)$$

$$Br^- + OH \rightleftharpoons BrOH^- \qquad (2)$$

$$BrOH^- \longrightarrow Br + OH^- \qquad (3)$$

$$Br + Br^- \rightleftharpoons Br_2^- \quad K_4 \geq 10^7\ M^{-1} \qquad (4)$$

Reaction 3 may also be reversible, but the reverse reaction is not important at near neutral pH.[6] The intermediate $BrOH^-$ differs from a usual activated complex by its lifetime, which was estimated to be as long as 10^{-7} sec, and its ability to react with solutes such as H_{aq}^+ and OH_{aq}^-.[6] The results of Matheson, *et al.*,[6] were interpreted assuming that equilibrium 2 was shifted towards the left under their conditions, and that the rate of formation of Br_2^- in near neutral media is controlled by the rate of Br formation *via* reaction 3. In addition, it was assumed that the backward reaction 2 is fast compared with reaction 3. Thus, k_1, defined from the equation: $k_1 = (1/[Br^-])(d/dt) \ln (D_{max} - D_t)$, is an apparent rate constant. D_{max} is the maximum optical density of Br_2^-, corrected for any Br_2^- which have decayed away by radical radical reactions. D_t is the measured optical density at time t.

Recently, we have reported that the competition between ethanol and Br^- for OH did not only depend on the concentration ratio $[Br^-]/[ethanol]$ but also on the absolute concentrations used.[15] Br^- ions were relatively more efficient at higher concentrations. This observation was interpreted as due to a reaction between the intermediate $BrOH^-$ and Br^- ions. This reaction is also supported by the recent results of Behar.[16] Karmann, Meissner, and Henglein[17] proposed a similar

(1) L. I. Grossweiner and M. S. Matheson, *J. Phys. Chem.*, **61**, 1089 (1957).

(2) L. M. Dorfman, I. A. Taub, and R. E. Bühler, *J. Chem. Phys.*, **36**, 3051 (1962).

(3) B. Cercek, M. Ebert, J. P. Keene, and A. J. Swallow, *Science*, **145**, 919 (1964).

(4) B. Cercek, M. Ebert, C. W. Gilbert, and A. J. Swallow, "Pulse Radiolysis", M. Ebert, *et al.*, Ed., Academic Press, New York, N. Y., 1965, p 83.

(5) H. C. Sutton, G. E. Adams, J. W. Boag, and B. D. Michael, *ibid.*, p 61.

(6) M. S. Matheson, W. A. Mulac, J. L. Weeks, and J. Rabani, *J. Phys. Chem.*, **70**, 2092 (1966).

(7) H. A. Schwarz and A. J. Salzman, *Radiat. Res.*, **9**, 502 (1958).

(8) A. O. Allen and R. A. Holroyd, *J. Amer. Chem. Soc.*, **77**, 5852 (1955).

(9) T. J. Sworski, *ibid.*, **76**, 4687 (1954).

(10) C. J. Hochanadel, *J. Phys. Chem.*, **56**, 587 (1952).

(11) J. Jortner, M. Ottolenghi, and G. Stein, *ibid.*, **66**, 2029, 2037, 2042 (1962).

(12) F. S. Dainton and S. A. Sills, *Nature (London)*, **186**, 879 (1960).

(13) (a) V. J. Linnenbom, C. H. Cheek, and J. W. Swinnerton, *Nucl. Sci. Technol.*, **2**, 46 (1962); (b) C. H. Cheek and V. J. Linnenbom, *J. Phys. Chem.*, **67**, 1856 (1963).

(14) A. Hummel and A. O. Allen, *Radiat. Res.*, **17**, 302 (1962).

(15) D. Zehavi and J. Rabani, *J. Phys. Chem.*, **75**, 1738 (1971).

(16) D. Behar, private communication.

(17) W. Karmann, G. Meissner, and A. Henglein, *Z. Naturforsch. B*, **22**, 273 (1967).

reaction in their HS^- system. In view of the importance of Br^- in radiation chemistry, we carried out an investigation with the purpose of elucidating the mechanism of Br^- oxidation by OH radicals.

Experimental Section

The pulsing system, analyzing method, and cell filling technique have been described previously;[15] 20–200-nsec electron pulses (5 MeV, 200 mA) have been used unless otherwise stated. In some experiments, 1.3 A, 50-nsec base width pulses have been used with continuous energy distribution from 0 to 8 MeV (will be referred to as "high current pulses"). A rectangular 4-cm long cell[15] with a light path of 12.2 cm was used in all the experiments. The pulse intensity was monitored with the aid of the inductance current produced in a coil through which the electrons passed before entering the solution. After correcting for the monitor readings, the deviations in the estimation of the pulse doses were <2%. The monitor gave erroneous results when the high current pulses were employed. Therefore we used an internal chemical dosimeter, namely, the absorption of Br_2^- which was always formed in the radiolysis of the Br^- solutions.

Photomultipliers types R 166 for 260–300 nm, I P 28 for 300–650 nm and R 196 above 650 nm were employed. The Bausch and Lomb monochromator gave less than 2% scattered light which was neglected when used with these photomultipliers.

A 556 dual-beam oscilloscope was used. Appropriate light filters were always employed to prevent photochemistry, as well as second-order resolved light. The light source was a 150 W, water cooled xenon lamp. When high time resolution was desired, a high voltage was pulsed between the lamp's electrodes so that a 10–30-fold higher light intensity could be obtained for a period of several hundreds of microseconds.[18] The pulsed lamp signal was always constant with time within the accuracy and time ranges of our measurements. The temperature was 25 ± 2°.

Unless otherwise stated, each reported measurement in the tables represents an average of 4 experiments.

Materials. We employed triply distilled water, Matheson's ultra high purity oxygen, Matheson's purified[6] N_2O, Merck's $HClO_4$ and ethanol (both analytical), Baker's (analyzed) NaBr and KBr, BDH's (Analar) H_2SO_4, and Mallinckrodt's (analytical) methanol.

Results and Discussion

When Br^- is pulse irradiated in O_2 or N_2O aqueous solution, optical absorption is built up as Br_2^- is produced.[3-6] The optical density reaches a maximum, after which it decays away by second order processes.[1,3-6] The formation can be separated from the decay processes, as the first is a pseudo-first-order process while the second is a second-order reaction whose lifetime depends on pulse intensity. In our work, we were interested in determining the optical density of Br_2^-, corresponding to the scavenging of all the OH radicals by Br^-. This was obtained from the maximum optical densities of Br_2^- (on the D *vs.* t scales). In most cases, a small correction (several %) for Br_2^- which had decayed away during its build up had to be made. This was done by appropriate extrapolations from the decay curves.

When an alcohol, RH_2, is also present, it competes with Br^- for OH according to reaction 5

$$RH_2 + OH \longrightarrow RH + H_2O \qquad (5)$$

As a result of this, a decrease of the maximum optical density is observed as the concentration of the alcohol is increased relatively to that of Br^-. The kinetic treatment of the reaction sequence 2–5 leads to a typical competition expression, namely

$$D_{max}^0/D_{max} = 1 + (k_5/k_2)(1 + k_{-2}/k_3)[RH_2]/[Br^-] \qquad (I)$$

where D_{max}^0 and D_{max} are the maximum optical densities (extrapolated) in the absence and in the presence of RH_2, respectively. In terms of the overall reaction 1, the above equation predicts that k_1 (in competition experiments defined as $(G_{(OH + Br^-)}/G_{(OH + RH_2)})k_5[RH_2]/[Br^-]$) be independent of $[Br^-]$ and $[RH_2]$. As pointed out previously, this is not in agreement with the experimental data[15] which show an *increase* in k_1 with $[Br^-]$.

Another definition of k_1 is useful when direct measurements of Br_2^- buildup are investigated, namely:[6] $k_1 = 1/[Br^-](d/dt) \ln (D_{max}^0 - D_t^0)$. D_t^0 is the optical density of Br_2^- at time t, no RH_2 present.

Since k_1 depended on $[Br^-]$ at relatively high Br^- concentrations, we carried out experiments in which the formation process of Br_2^- was observed directly. Had k_1 been a real reaction rate constant, it should have been not only independent of $[Br^-]$, but in addition, the same k_1 value should result from both competition and direct measurements. However, we have found this time that k_1 *decreased* with $[Br^-]$, while in the competition experiments it *increased*. Only at $[Br^-] < 10^{-3}$ M values of k_1 were nearly identical in both sets of experiments, as well as independent of $[Br^-]$. In the following we will describe the experiments and results which helped us to resolve the apparent discrepancy.

I. Competition

Experiments at Near Neutral pH. Competition experiments were carried out between Br^- ions and methanol or ethanol, at various Br^- and alcohol concentrations. The results are presented in Table I and in Figure 1 where D_{max}^0/D_{max} values are plotted *vs.* [alcohol]/$[Br^-]$. Each line corresponds to a constant Br^- concentration. Each of the results in Table I and Fig-

(18) P. Pagsberg, H. Christensen, J. Rabani, G. Nilsson, J. Fenger, and S. O. Nielsen, *J. Phys. Chem.*, **73**, 1029 (1969).

Table I: Irradiation of Oxygenated Br^- (as KBr or NaBr) at 360 nm, Near Neutral pH.[a] Competition with Ethanol (eth) or Methanol (meth)

Curve in Figure 1	Symbol in figure	[Br^-], M	Relative[b] pulse intensity	$D_{max}{}^0$[c]	Slope from Figure 1	$10^{-9}k_1$,[d] M^{-1} sec^{-1}	Remarks
a	●	1.0×10^{-4}	A	0.0307	1.25	1.5	Na^+ eth
b	○	3.0×10^{-4}	A	0.0404	1.70	1.1	K^+ eth
		3.0×10^{-4}	B	0.079	1.33	1.4	K^+ eth
c	×	1.0×10^{-3}	C	0.109	1.79	1.0	Na^+ eth
		1.0×10^{-3}	D	0.186	1.57	1.2[e]	K^+ eth
d	⊗	3.0×10^{-3}	B	0.094	1.54	1.2	K^+ eth
d	⊗	3.0×10^{-3}	E	0.103	1.54	1.2	K^+ eth
e	□	1.0×10^{-2}	F	0.101	0.98	1.9	K^+ eth
f	◒	2.0×10^{-2}	C	0.122	0.91	2.0	Na^+ eth
g	■	3.0×10^{-2}	F	0.101	0.63	2.9	K^+ eth
h	◓	5.0×10^{-2}	C	0.127	0.55	3.3	Na^+ eth
i	▽	0.1	E	0.105	0.39	4.6	K^+ eth
j	◘	0.2	C	0.129	0.30	6.1	Na^+ eth
k	▼	0.3	E	0.105	0.25	7.2	K^+ eth
k	▼	0.3	G	0.369	0.25	7.2	K^+ eth
k	△	2.0	H	0.207	0.25	7.2	Na^+ eth
l	▲	1.0	H	0.195	0.24	7.2	Na^+ eth
		1.0	I	0.188	0.25	7.2[e]	K^+ eth
		3.0×10^{-4}	B	0.079	0.59	1.4	K^+ meth
		0.1	E	0.105	0.20	4.2	K^+ meth

[a] No buffer, pH before pulsing is estimated to be about 7. The 50–150-nsec pulses produced up to 10^{-6} M H^+. [b] All experiments in which the same letter represents the relative pulse intensity were carried out using the same dose. [c] Optical density of Br_2^- in the absence of ethanol, corrected for Br_2^- decay during its buildup (by extrapolation). [d] Based on $k_5 = 1.83 \times 10^9$ M^{-1} sec^{-1} for ethanol and 8.4×10^8 M^{-1} sec^{-1} for methanol.[19] [e] From ref 15, no O_2, N_2O saturated.

ure 1 is an average of eight experiments. The ratio k_1/k_5 increases with the Br^- concentration. Using $k_5 = 1.83 \times 10^9$ M^{-1} sec^{-1} for ethanol and 8.4×10^8 M^{-1} sec^{-1} for methanol[19] gave the same k_1 values at constant [Br^-], no matter whether ethanol or methanol was used for the competition. For the explanation of these results, we invoke reaction 6 which we have tentatively proposed before.[15]

$$BrOH^- + Br^- \longrightarrow Br_2^- + OH^- \qquad (6)$$

On the basis of the reaction mechanism (2)–(6), one may write

$$-d[OH]/dt = k_2[OH][Br^-] - k_{-2}[BrOH^-] + k_5[OH][RH_2] \qquad (II)$$

$$d[BrOH^-]/dt = k_2[OH][Br^-] - (k_{-2} + k_3 + k_6[Br^-])[BrOH^-] \qquad (III)$$

$$d([Br] + [Br_2^-])/dt = (k_3 + k_6[Br^-])[BrOH^-] \qquad (IV)$$

$$d[RH]/dt = k_5[OH][RH_2] \qquad (V)$$

By substituting [OH] from equation (V), and [$BrOH^-$] from (IV) into (II), one obtains (after integration from time zero to time infinity and rearrangement) equation (VI).

$$[Br_2^-]_{max}/[RH]_{max} = (k_2[Br^-]/k_5[RH_2])/(1 + k_{-2}/(k_3 + k_6[Br^-])) \qquad (VI)$$

Equilibrium 4 is far shifted to the Br_2^- side under our conditions.[5] $[RH]_{max}$ (the total [RH] formed according to reaction 5), can be replaced by ($[Br_2^-]_{max}{}^0 - [Br_2^-]_{max}$) where $[Br_2^-]_{max}{}^0$ and $[Br_2^-]_{max}$ (total [Br_2^-] formed in the absence and in the presence of RH_2, respectively) are measured at the same Br^- concentrations. Replacing concentrations of Br_2^- by the appropriate optical densities we obtain

$$D_{max}{}^0/D_{max} = 1 + (k_5/k_2)[RH_2]/[Br^-](1 + k_{-2}/(k_3 + k_6[Br^-])) \qquad (VII)$$

Both equations (VII) and (I) predict straight lines when the ratios $D_{max}{}^0/D_{max}$ are plotted *vs.* $[RH_2]/[Br^-]$ at constant [Br^-], as observed in Figure 1. However, equation (I), based on the old reaction scheme,[6] does not predict the observed dependence of the slopes on [Br^-].

Evaluation of Rate Constants Ratios at Near Neutral Solutions. Let us define

$$Y = 1/(k_2 \times \text{slope}/k_5 - 1) \qquad (VIII)$$

where the "slopes" in equation VIII are the experimental slopes of equation VII. It can be shown that

$$Y = k_3/k_{-2} + (k_6/k_{-2})[Br^-] \qquad (IX)$$

In Figure 2 we demonstrate the linear dependency of Y

(19) P. Neta and L. M. Dorfman, *Advan. Chem. Ser.*, No. 81, 222 (1968).

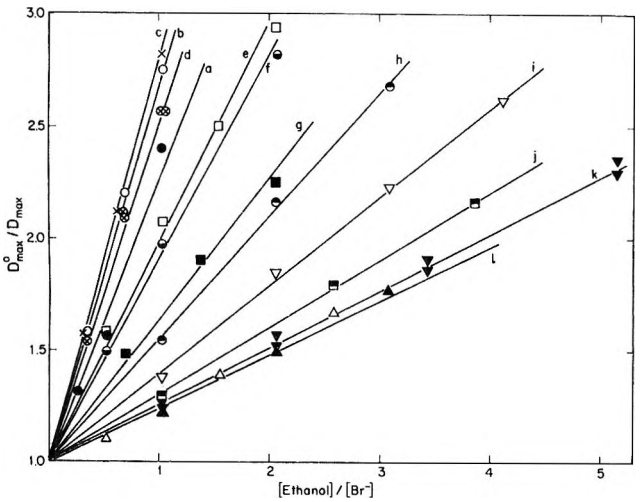

Figure 1. Competition between Br^- and ethanol for OH (neutral pH). Table I includes the explanations for the various curves and symbols.

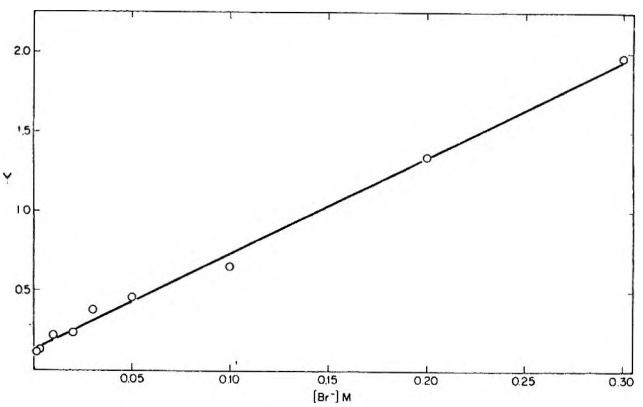

Figure 2. Evaluation of k_6/k_2 from the dependence of Y on $[Br^-]$.

on $[Br^-]$ using $k_5/k_2 = 0.172$ from measurements in the acid pH range (will be discussed later). The straight line (Figure 2) supports our proposed reaction mechanism. From the slope of Figure 2, we obtain $k_6/k_{-2} = 6.1$ (with an estimated uncertainty ± 0.3). Using this value, the intercept of Figure 2 has been calculated from the experiments in which $[Br^-] < 0.2\ M$. This yields $k_3/k_{-2} = 0.127 \pm 0.007$ (The error limit here is the standard deviation.). From the two ratios obtained above, it is possible to calculate $k_6/k_3 = 48$.

Acid Solutions. In Table II, we present competition data in the acid pH range. The intermediate $BrOH^-$ has been proposed to react with H^+ according to reaction 7.[6]

$$BrOH^- + H^+ \longrightarrow Br + H_2O \qquad (7)$$

When reaction 7 is also included, equation VII is modified into X.

$$D_{max}{}^0/D_{max} = 1 + (k_5/k_2)[RH_2]/[Br^-](1 + k_{-2}/(k_3 + k_6[Br^-] + k_7[H^+])) \qquad (X)$$

When $k_7[H^+] \gg k_{-2}$, equation (X) reduces into (XI)

$$D_{max}{}^0/D_{max} = 1 + (k_5/k_2)[RH_2]/[Br^-] \qquad (XI)$$

A plot of $D_{max}{}^0/D_{max}$ *vs.* $[RH_2]/[Br^-]$ in relatively strong acid indeed shows relatively small variation of slope with Br^- concentration. The data of Table II give $k_5/k_2 = 0.172 \pm 0.013$ (mean deviation). From this, $k_2 = (1.06 \pm 0.08) \times 10^{10}\ M^{-1}\ sec^{-1}$ follows (mean deviation).

Table II: Irradiation of Aerated Acidic ($HClO_4$)NaBr in Solutions Containing Ethanol[a]

$[Br^-]$, M	Relative pulse intensity	$D_{max}{}^0$ [b]	$[H^+]$, M	Slope	$10^{-10}\ k_1$,[c] M^{-1} sec^{-1}
3.0×10^{-4}	A	0.049	0.1	0.177	1.03
1.0×10^{-2}	H	0.189	0.1	0.189	0.97
0.10	C	0.128	0.1	0.179	1.02
1.0	H	0.202	0.1	0.166	1.10
1.0×10^{-3}	C	0.127	0.3	0.168	1.09
0.1	C	0.127	0.3	0.153	1.20

[a] Measurements were carried out at 360 nm. Pulse duration was 50–150 nsec. [b] Optical density of Br_2^- in the absence of ethanol, corrected for Br_2^- decay during its formation (by extrapolation). [c] Based on $k_5 = 1.83 \times 10^9\ M^{-1}\ sec^{-1}$.

From our competition experiments $k_2k_3/k_{-2} = 1.35 \times 10^9\ M^{-1}\ sec^{-1}$. This is in excellent agreement with k_1 which has been measured by the buildup of Br_2^- absorption.[6] It can be shown that at relatively low $[Br^-]$, k_1 (from Br_2^- formation) approaches the ratio k_2k_3/k_{-2}.

Due to reaction 6, the results in neutral pH at high bromide concentrations are expected to approach those at low pH's. This is indicated by the results in Table I, when $[Br^-] \geq 0.3\ M$.

The lack of Br^- concentration effect on the slopes above 0.3 M Br^- is not predicted, however: in fact, changing the Br^- concentration from 0.3 to 1 M is expected to decrease the slopes by about 15%, but no such a decrease is observed. The slope at 2 M neutral Br^- should have been not so far above the slopes obtained at the acid range. We have no definite explanation for this. It is not impossible that it is not outside experimental uncertainty. We considered the possible effects of changing viscosity. Taking the viscosity of water as 1, the viscosity of 1 M NaBr was found 1.06. When 3.3 M ethanol was added to the neutral solution, the viscosity increased to 1.8. This might have an effect on the rate constants. However, the viscosities in acid solutions were similar. At the higher concentrations of bromide and ethanol, direct effects may influence the results. Due to such uncertainties, we prefered to use the ratio k_5/k_2 measured in the acid range at relatively low bromide concentrations.

II. Direct Kinetic and Spectral Measurements

Kinetics of Br_2^- Formation in Near Neutral pH—No

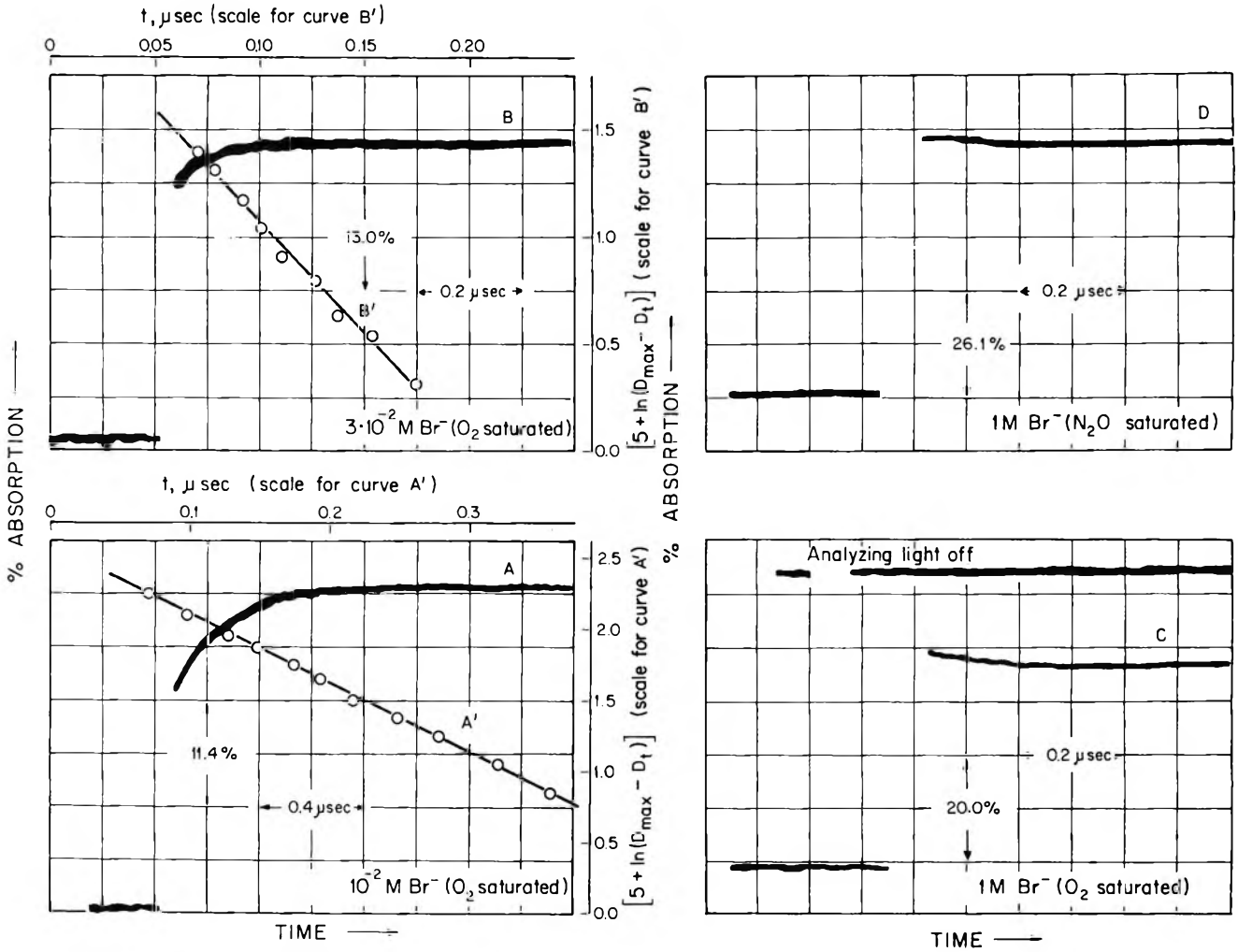

Figure 3. Oscilloscope traces for the buildup of Br_2^- optical absorption; 360 nm, 50-nsec high-current (1.3-A) pulses. Pulsed Xe lamp. Pulse reproducibility was bad and $D_{plateau} = D_{max}$ cannot be a measure for the Br_2^- yields, but rather can be used as a measure for the pulse intensity.

RH_2 Present. The measurement of k_1 by the Br_2^- formation has been described previously.[6] We have extended the previous work to higher $[Br^-]$. In Figure 3 we present some typical oscilloscope traces at high $[Br^-]$. These traces demonstrate the accuracy of our measurements. It can be seen that the plot of ln $(D_{max} - D_t)$ *vs.* time yields a straight line, the slope of which, when divided by $[Br^-]$ equals to k_1 as long as k_4 is sufficiently greater than k_1. This is always the case in the neutral pH. Such straight lines are typical for all the neutral solutions. When the ln $(D_{max} - D_t)$ *vs.* t plots were extrapolated to the middle of the electron pulse (which we chose as an approximation for time zero), $D_0 > 0$ was obtained at the relatively high Br^- concentrations, such as used in Figures 3A and 3B.

The extrapolated values of D_0 increased with the Br^- concentration. We interpret this as due to a very fast formation of $BrOH^-$ to which we assign optical absorption at 360 nm. Thus, the fast increase of optical absorption during the electron pulse is due to reaction 2, and the slower buildup of the optical density is due to the formation of Br_2^- at the expense of $BrOH^-$ and OH. In 1 *M* bromide, an additional process evidently takes place. Br_2^- must already be formed within a time range shorter than our resolution. However after the pulse, part of the optical absorption decays away with a half-life of about 150 nsec (see Figure 3C). We attribute this decay to a new equilibrium reaction of Br_2^- with Br^-.

$$Br_2^- + Br^- \rightleftharpoons Br_3^{2-} \qquad (8)$$

Br_3^{2-} is assumed to possess no optical absorption or a relatively small optical absorption at 360 nm as compared with Br_2^-. Further results and discussion of reaction 8 are given in the section: *High Br^- Concentrations.* It is of particular interest to note that the decay of optical absorption which is discussed above is delayed for a short while when N_2O is used instead of O_2 to react with e_{aq}^- (see Figure 3D). We attribute this to reaction 9 which becomes a rate determining step in the Br_2^- formation in N_2O saturated 1 *M* Br^-.

$$N_2O^- \longrightarrow N_2 + O^- \quad (9)$$

The results give k_9 between 1×10^7 and 2×10^7 sec^{-1}. This value is in agreement with our previously reported one.[15] In Table III we present k_1 as a function of [Br^-]. Above 3×10^{-2} M no precise measurements of k_1 could be made due to the too small and too fast changes in optical density with time.

Table III: Direct Determination of $k_1 = (1/[Br^-])(d/dt)$ ln $(D_{max} - D_t)$ in Near Neutral Solutions of NaBr or KBr Solutions at 360 nm[a]

[Br^-], M	Additive (1 at)	D_{max}[b]	$10^{-5} \times k_1[Br^-]$[c] sec^{-1}	$10^{-8}k_1$[d] M^{-1} sec^{-1}
3.0×10^{-4} K^+	O_2	0.03	3.55 ± 0.20	1.18
3.0×10^{-4} Na^+	O_2	0.04	4.00 ± 0.09	1.33
3.0×10^{-4} K^+	O_2	0.08	4.47 ± 0.25	1.49
3.0×10^{-4} K^+	N_2O	0.03-0.06	3.65 ± 0.19	1.22
1.0×10^{-3} Na^+	O_2	0.11	1.12 ± 0.05	1.12
1.0×10^{-3} K^+	N_2O	0.09	1.06 ± 0.03	1.06
1.0×10^{-3} K^+	N_2O	0.19	1.03 ± 0.01	1.03
3.0×10^{-3} Na^+	O_2	0.15	24.4 ± 0.5	0.81
3.0×10^{-3} K^+	N_2O	0.07-0.08	23.4 ± 1.2	0.78
1.0×10^{-2} K^+	O_2	0.04	45.4 ± 2.0	0.45
1.0×10^{-2} Na^+	O_2	0.18	48.6 ± 2.0	0.49
1.0×10^{-2} K^+	N_2O	0.09	47.0 ± 0.6	0.47
2.0×10^{-2} Na^+	O_2	0.20	67.7 ± 6.5	0.34
3.0×10^{-2} Na^+	O_2	0.19	89.2 ± 8.7	0.30

[a] See footnote *a* to Table I. [b] Pulse intensity may be determined from D_{max} [c] The numbers on the right-hand side are standard deviations. [d] Each value is an average of 2-15 measurements (total of 105 runs).

Kinetic Treatment. The reaction rate constant k_4 is of the order of 10^{10} M^{-1} sec^{-1}.[6] Hence, our results show that reaction 4 is sufficiently faster than (1) at all concentrations of Br^- in neutral pH. Under such conditions, the overall process (1) determines the rate of Br_2^- formation. Moreover, $k_2 = 1.06 \times 10^{10}$ M^{-1} sec^{-1} as reported in a previous section, and hence the equilibrium 2 is established very fast and is not changed by the consecutive reactions 3 and 6. As will be seen later, the assumption of a very fast establishment of equilibrium 2 is also justified from the comparison of the data to the kinetic calculations based on that assumption. Under such conditions, the reaction sequence 2, 3, 4, and 6 leads to the expression

$$-d([OH] + [BrOH^-])/dt = (k_3 + k_6[Br^-])([OH] + [BrOH^-])/(1 + k_{-2}/k_2[Br^-]) \quad (XII)$$

hence

$$k_1 = (k_3 + k_6[Br^-])/([Br^-] + k_{-2}/k_2) \quad (XIII)$$

by rearrangement

$$(k_2k_3/k_{-2} - k_1)/[Br^-] = k_1k_2/k_{-2} - k_2k_6/k_{-2} \quad (XIV)$$

The value of k_1 at low [Br^-] approaches the ratio k_2k_3/k_{-2}. Thus, the left-hand side of equation XIV (will be referred to as X) can be obtained directly from the appropriate experimental data.

An alternative way to calculate X which gives identical results is based on the use of $k_2 = 1.06 \times 10^{10}$ M^{-1} sec^{-1} and $k_3/k_{-2} = 0.127$ as reported in the competition section. Combining this with measured values of k_1 at various [Br^-] yields values of X. When these are plotted *vs.* k_1, a straight line is obtained (Figure 4) yielding $k_2/k_{-2} = 320$ (from the slope) and $k_6 = 1.9 \times 10^8$ M^{-1} sec^{-1} (the negative value of the intercept devided by the slope). These results are consistent with the competition data. From $k_2/k_{-2} = 320$ and $k_2 = 1.06 \times 10^{10}$ M^{-1} sec^{-1} we obtain $k_{-2} = 3.3 \times 10^7$ M^{-1} sec^{-1}. Combination of this with $k_6/k_{-2} = 6.1$ (see competition) yields $k_6 = 2.0 \times 10^8$ M^{-1} sec^{-1}, which is in very good agreement with $k_6 = 1.9 \times 10^8$ M^{-1} sec^{-1} obtained from Figure 4.

The Reaction of $BrOH^-$ with H^+. When reaction 7 becomes important, eq XIII should be modified into (XV).

$$k_1 = (k_3 + k_6[Br^-])/([Br^-] + k_{-2}/k_2) + k_7[H^+]/([Br^-] + k_{-2}/k_2) \quad (XV)$$

Equation XV gives the [H^+] and [Br^-] dependency of the apparent reaction rate constant for Br_2^- formation. It is important to note that equation XV is valid only as long as: (a) k_1 is sufficiently smaller than k_4; (b) equilibrium 2 is established sufficiently fast as compared with reactions 3, 6, and 7. In Table IV we present data obtained at 10^{-2} M Br^-, in the pH range 3.65–5.08. When k_1 values of Table IV are plotted *vs.* [H^+], a straight line is obtained, the slope of which yields $k_7 = (4.4 \pm 0.8) \times 10^{10}$ M^{-1} sec^{-1}.

Table IV: Determination of k_7 in Oxygenated 10^{-2} M NaBr Solutions[a]

pH[b]	$10^{-8} \times k_1$[c] M^{-1} sec^{-1}
5.08	5.20 ± 0.14
4.53	5.73 ± 0.23
3.95	8.27 ± 0.40
3.65	12.6 ± 0.9

[a] Seven to eight parallel measurements have been carried out at each pH. At 360 and 380 nm, using 50-nanosecond high-current pulses (1.3 A), and pulsing the Xe lamp. D_{max} at 360 nm (measured or normalyzed) was 0.130 to 0.145. [b] $HClO_4$ was used for the adjustment of pH. The values reported here were measured prior to pulsing with the aid of a pH meter. [c] Here k_1 is defined as $(1/[Br^-])(d/dt)$ ln $(D_{max} - D_t)$.

Deviations occur at higher [H^+], when $(k_2[Br^- + k_{-2})$ is not sufficiently greater than $k_7[H^+]$. When the pH is further decreased, process (1) is not a rate determining step in the formation of Br_2^-. Reaction 4 be-

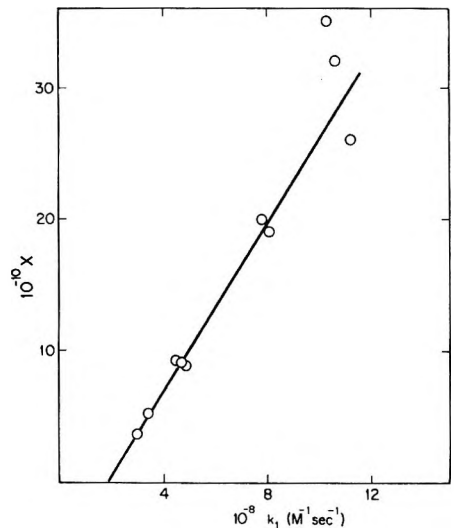

Figure 4. Plot of X *vs.* k_1 for the evaluation of k_2/k_{-2} and k_6.

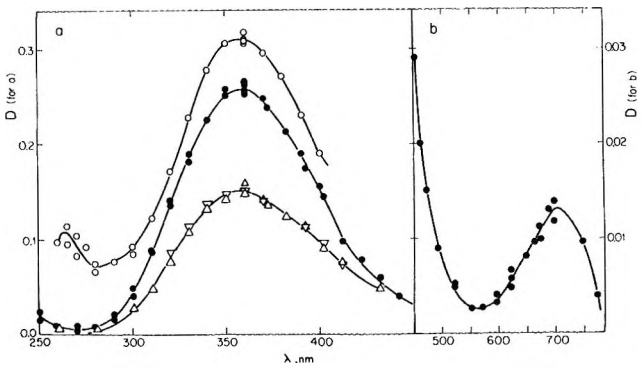

Figure 5. Absorption spectrum of Br_2^-; 0.1-μsec pulses used. Key: ○, 1 M NaBr, neutral, N_2O saturated; ●, 10^{-3} M NaBr, neutral, N_2O saturated; △, 10^{-3} M KBr, pH = 2.0 (H_2SO_4) argonated (no air); ▽, 10^{-3} M KBr, pH = 2.0 (H_2SO_4) oxygenated.

comes comparable in rate to process 1.[6] Indeed, experiments at pH 1 have shown that the plots of ln ($D_{max} - D_t$) *vs.* time do not give the typical first-order straight lines. The competition experiments, however, are free of these complications. It can be seen from Table II that k_1 is independent of [H^+] in the range [H^+] = 0.1–0.3 M. This is due to the fact that in 0.1 M acid, k_7[H^+] $\gg$ k_2[Br^-]. Under such conditions, reaction 2 becomes the rate-determining step in process 1, and $k_1 = k_2$ results. Thus, the competition experiments in 0.1–0.3 M H^+, in which no [H^+] dependency has been found, are not in disagreement with our present investigation of the effect of pH. Careful examination of the data reveals that the experiments in Table IV were all done under conditions which enable the use of our procedure to calculate k_7.

Spectral Measurements. These were carried out in order to find more direct evidence for the $BrOH^-$ intermediate. We have first studied the absorption spectrum of Br_2^-. Our method, using a split analyzing light beam with two monochromators, is more precise than the previous photographic plates method.[1] The spectrum at time zero was obtained by appropriate extrapolations. We have extended the wavelength range (Figure 5) and found a new peak of Br_2^- at near 700 nm. The absorption at the 700 band showed dependence on [Br^-] and [ethanol] identical with that described in the previous sections for the 360-nm band. It is evident that these two bands belong to the same species, namely to Br_2^-. The peak position at 360 nm, as well as the shape of the spectrum, does not depend on [Br^-] nor on the acidity. A third absorption band of Br_2^- is perhaps formed below 250 nm. The peak at 700 nm is analogous to the absorption band at 750 nm for I_2^- reported by Dobson and Grossweiner.[20]

Comparison between the spectra observed in N_2O saturated neutral solutions containing 10^{-3} and 1 M Br^- reveals a new band near 260 nm in the 1 M solutions. This must be due to species formed only at the higher Br^- concentrations. We have not investigated further the nature of this species. It may be Br_3^- formed by combination of 2 Br atoms or Br_2^- radical ions in the spurs.[21] Reactions 3 and 6 are too slow to produce Br in the spurs. $BrOH^-$, in the absence of sufficient amounts of H^+, will live longer than the spurs. However, H^+ is present in the spurs and may produce Br atoms by the very efficient reaction 7. The identification of the absorption at 260 nm as due to Br_3^- is not conclusive. Br_3^{2-}, formed *via* reaction 8, may perhaps also absorb light at 260 nm.

An attempt has been made to measure the absorption spectrum of $BrOH^-$. The spectrum in the wavelength range 300 to 400 nm was obtained by extrapolations from the exponential plots from pictures such as Figure 3, using O_2 saturated, 2×10^{-2} M NaBr solution. $BrOH^-$ was found to possess a peak at 360 nm, similarly to Br_2^-. The peak seems to be broader than the Br_2^- peak: D_{400}/D_{360} = 0.73 for $BrOH^-$, compared with 0.60 for Br_2^-; D_{320}/D_{360} = 0.62 for $BrOH^-$ compared with 0.53 for Br_2^-. However, there is a large error involved in the extrapolation method, since there is already much reaction during the electron pulse. The absorption of $BrOH^-$ at 360 nm is not surprising. Several radical ions of the type XY^-, *e.g.*, Cl_2^-,[1] Br_2^-,[1] I_2^-[1] $ClCNS^-$,[22] $BrCNS^-$,[23] $SHSH^-$,[17] and perhaps IBr^-[1] have optical absorptions between 300 and 400 nm. An optical density of Br_2^- obtained at 360 nm in O_2 saturated solution of 10^{-2} M Br^- was 0.196. A similar pulse produced D = 0.0353 at 420 nm, in N_2O saturated 10^{-3} M ferrocyanide. Taking appropriate G

(20) G. Dobson and L. I. Grossweiner, *Radiat. Res.*, **23**, 290 (1964).

(21) This possibility has been suggested to us by Mr. E. Peled, of our department, on the basis of unpublished data by Khorana and Hamill who found a similar absorption and attributed it to Br_3^-.

(22) M. Schöneshöfer, *Int. J. Radiat. Phys. Chem.*, **1**, 505 (1969).

(23) M. Schöneshöfer and A. Henglein, *Ber. Bunsenges. Phys. Chem.*, **73**, 289 (1969).

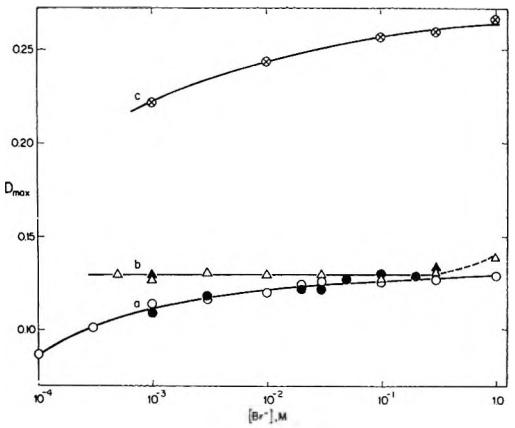

Figure 6. Dependence of Br_2^- optical absorption at 360 nm on $[Br^-]$. All the optical densities are normalized to the same pulse intensity. (a) Neutral NaBr, O_2 saturated: ●, 100-nsec pulses; ○, 50-nsec pulses (the results are normalized to the 100-nsec pulses). (b) Acidified ($HClO_4$, pH = 0.5) NaBr, 100-nsec pulses: △, aerated; ▲, oxygenated. (c) Neutral, N_2O saturated NaBr; 100-nsec pulses.

values for Br_2^- and ferricyanide one may calculate $\epsilon_{Br_2^-}{}^{360} = (1.2 \pm 0.1) \times 10^4\ M^{-1}\ cm^{-1}$, based on $\epsilon_{ferricyanide}{}^{420} = 1000\ M^{-1}\ cm^{-1}$. The extinction coefficient of $BrOH^-$, as estimated from figures similar to Figure 3, is about $8 \times 10^3\ M^{-1}\ cm^{-1}$ (the error here may be as much as 25%). The existence of $BrOH^-$ as an intermediate is supported by esr evidence for $Br-OH^-$,[24] IOH^-[24] and $ClOH^-$.[25]

Effect of $[Br^-]$ on the Optical Absorption. In Figure 6 we present the effect of $[Br^-]$ on the optical absorption at 360 nm. The absorption of Br_2^-, D_{max}, has been measured by extrapolations from the disproportionation kinetics of Br_2^-. Thus, D_{max} does not include the amount of Br_2^- which participated in reaction 8. In oxygen containing acid solutions, the optical absorption is independent of Br^- concentration in the range 5×10^{-4} to $10^{-1}\ M$. It increases (~7%) in 1 M solutions (Figure 6b). If corrected for reaction 8, the increase would have been ~15%. This increase can be explained as a result of both spur reactions and a direct effect. Br^- is known to suppress the molecular yield of H_2O_2 very efficiently.[9] This suppression may be explained as due to the efficient reactions 2 and 7.

The change of D_{max} with $[Br^-]$ in neutral solutions is greater than in acid solutions. This may be explained if the rate constant of the reaction of Br_2^- with e_{aq}^- is different from the corresponding rate constant with H atoms. The large increase at concentrations below $3 \times 10^{-3}\ M$ we attribute to impurity effects. Br^- is 10 times more efficient as an OH scavenger in the acid pH. Therefore, at concentrations less than $10^{-3}\ M$ the impurities compete for OH in the neutral, but not in the acid medium. These results are in agreement with the previous work of Sutton, Adams, Boag, and Michael.[5]

High Br^- Concentrations. Neutral solutions containing 0.1 to 1 M bromide show a partial decay of the optical density of Br_2^- as demonstrated in Figure 3. This decay is observed in both O_2 and N_2O saturated solutions. The formation time of Br_2^- under these conditions is smaller than our time resolution. The decaying fraction increases with the Br^- concentration. The ratios of optical densities at the maxima to the optical densities at the plateau do not depend on wavelength (measurements were carried out with 1 M solutions) in the range 320 nm to 400 nm. This means that the decaying fraction has a spectrum identical with that of Br_2^-. Reaction 8 has been proposed to account for these results. Kinetic measurements in 0.3 and 1 M Br^- showed that the decay was first order. Due to the relatively small optical density changes, there was a large scatter of points around the first-order plots. The results were definitely not second order, as the deviations from such plots were systematic. The half-life of the decay did not depend much—if at all—on the Br^- concentration. A summary of the results is presented in Table V. The reversible reaction 8 is in agreement with these results. If we assume that even at 1 M Br^-, most of the Br atoms are in the Br_2^- and not in the Br_3^{2-} form, the relaxation time is determined by k_{-8} and depends very little on $[Br^-]$, as indeed has been found.

Table V: The fast partial decay of optical absorption in concentrated neutral Br^- solutions[a]

$[Br^-]$, M	$D_{(initial)}$	$D_{(plateau)}$[c]	Approximate half-life (nsec)
0.1	0.192	0.185	110
0.1	0.197	0.193	120
0.2	0.210	0.195	90
0.2	0.200	0.190	40
0.3	0.208	0.192	70
0.3	0.202	0.184	70
1.0	0.205	0.187	80
1.0	0.225	0.205	80
1.0	0 214	0.193	60

[a] 50 nsec, high currant (1.3 A) pulses used. Pulsed lamp used for detection at 360 nm. [b] The optical density measured as close as possible to the end of the electron pulse. [c] The optical density at the end of the decay process. A typical plateau is demonstrated in figure 3 (C).

Acknowledgment. The authors are indebted to Y. Ogdan for his invaluable support in the operation, maintainment, and improvement of the system. We are grateful to E. Peled, D. Behar, and A. Henglein for valuable comments.

(24) I. Marov and M. C. R. Symons, *J. Chem. Soc. A*, 201 (1971).
(25) R. C. Catton and M. C. R. Symons, *Chem. Commun.*, 1472 (1968).

Adsorption Effects in Tungsten–Oxygen–Bromine Reaction

by E. G. Zubler

Lamp Phenomena Research Laboratory, General Electric Company, Nela Park, Cleveland, Ohio 44112
(Received May 13, 1971)

Publication costs assisted by the Lamp Division, General Electric Company

In a microbalance-flow system, the reaction rate of W(s) at 700–900° in Ar, He, and N_2 with 10^{-3} to 10^{-2} Torr oxygen and 0.01 to 3 Torr bromine was linear with oxygen, but a complicated function of bromine and inert carrier gas. Except at the lowest bromine pressures, adsorbed bromine inhibited the reaction and the rate was higher in N_2 than Ar or He where the rate was the same. These observations are explained qualitatively by the two-layer adsorption model proposed by Schissel and Trulson for tungsten oxidation.

In a recent investigation,[1] a microbalance-flow system was used to determine the reaction rate of tungsten foil at 600–950° in nitrogen at atmospheric pressure containing 10^{-4} to 10^{-2} Torr oxygen and 0.3 to 3 Torr bromine. The reaction rate was found to be linear with oxygen but independent of bromine. An empirical rate equation with an apparent activation energy of 31 kcal/mol was obtained and compared with similar rate equations for tungsten oxidation[2-6] at comparable oxygen pressures but temperatures above 1000° where the oxides are volatile. It was concluded that the rate-limiting step was tungsten oxidation followed by the rapid formation of volatile WO_2Br_2 which precluded the formation of an oxide surface layer.

The favorable correlation with tungsten oxidation rate data at low total pressures suggested that the N_2 carrier gas at atmospheric pressure did not affect the reaction kinetics. This conclusion was not consistent with the known strong chemisorption of N_2 on W[7,8] in this temperature region and motivated a continuation of this work. Rate measurements at 700–900° have been made in Ar, He, and N_2 containing 10^{-3} to 10^{-2} Torr oxygen and 0.01 to 3 Torr bromine. The results indicate that the reaction rate was a complicated function of both the carrier gas and the bromine pressure. This dependency negates the simple quantitative interpretation of the previous investigation.[1]

The experimental techniques were essentially the same as used previously. After a reaction series, the condensate on the wall downstream of the W sample was located in three zones. Within the furnace zone, a yellow deposit was observed. Appearance, volatility, and solubility suggested WO_3. Adjacent to the furnace, a yellow brown deposit was located and identified as WO_2Br_2 by X-ray diffraction.[9] Further downstream, red crystals of WO_2Br_2 were identified by X-ray diffraction.[9] With N_2 as the carrier gas, these red crystals of WO_2Br_2 were prevalent. With He as the carrier, there was less crystalline WO_2Br_2 and considerably more WO_3 in the hot zone. Presumably, higher diffusion rates in He allow more $WO_2Br_2(g)$ to reach the wall and undergo decomposition. Kokovin[10] has observed gaseous bromine during sublimation of WO_2Br_2 above 600°K and Gupta[11] has suggested the possibility of dissociation to $WO_2(s) + Br_2(g)$.

In the previous work,[1] the reaction rate was found to be independent of Br_2 in the range 0.3–2.7 Torr. This conclusion was based on rate measurements near the extremes of the oxygen and temperature ranges. Most runs were made with 0.8–1.2 Torr Br_2 and zero-order dependence was assumed. This assumption was erroneous as shown in Figures 1–3. Under certain conditions, zero-order dependence was observed, but in general a complicated dependence on Br_2 pressure and also the carrier gas was observed. The dissociation of Br_2 which was 0.2–0.98 at these temperatures and pressures is ignored here for simplicity. Plots using calculated partial pressures of $Br_2(g)$ and Br(g) are no more revealing. The inability to distinguish between bromine atoms and molecules in these experiments precludes an unambiguous interpretation of the kinetics.

Under the same experimental conditions, the reaction rate in Ar was always within experimental error of that in He and indicates that diffusion effects are not significant. Except at the lowest Br_2 levels, the rate was always higher in N_2 than He (or Ar) at the same O_2 pressure and temperature. Most of the rate curves appear to approach a plateau at the higher Br_2 pressures, 2–3

(1) E. G. Zubler, *J. Phys. Chem.*, **74**, 2479 (1970).

(2) I. Langmuir, *J. Amer. Chem. Soc.*, **35**, 105 (1913).

(3) J. A. Becker, E. J. Becker, and R. G. Brandes, *J. Appl. Phys.*, **32**, 411 (1961).

(4) R. A. Perkins, W. L. Price, and D. D. Crooks, Proc. Joint AIME/Air Force Materials Symposium, Technical Document Report No. ML-TDR-64-162, p 125 (1962).

(5) R. W. Bartlett, *Trans. AIME*, **230**, 1097 (1964).

(6) J. H. Singleton, *J. Chem. Phys.*, **45**, 2819 (1967).

(7) G. Ehrlich, *J. Phys. Chem.*, **60**, 1388 (1956).

(8) G. Ehrlich, *Proc. Third Int. Congr. Catal.*, 113 (1965).

(9) G. A. Kokovin and N. K. Toropova, *Russ. J. Inorg. Chem. (Engl. Ed.)*, **10**, 304 (1965).

(10) G. A. Kokovin, *ibid.*, **12**, 7 (1967).

(11) S. K. Gupta, *J. Phys. Chem.*, **75**, 112 (1971).

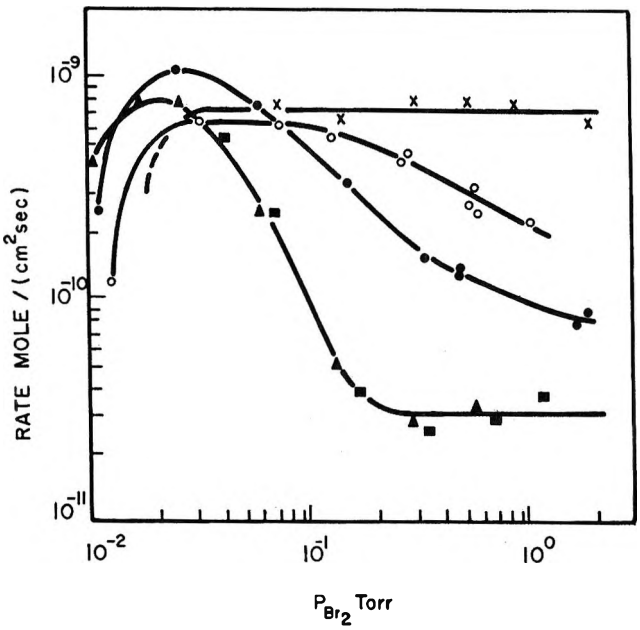

Figure 1. Rate dependence on $Br_2(g)$ in He, Ar, and N_2 with 8.7×10^{-3} Torr O_2: ×, 900°, N_2; ○, 800°, N_2; ●, 900°, He; ▲, 800°, He; ■, 800°, Ar.

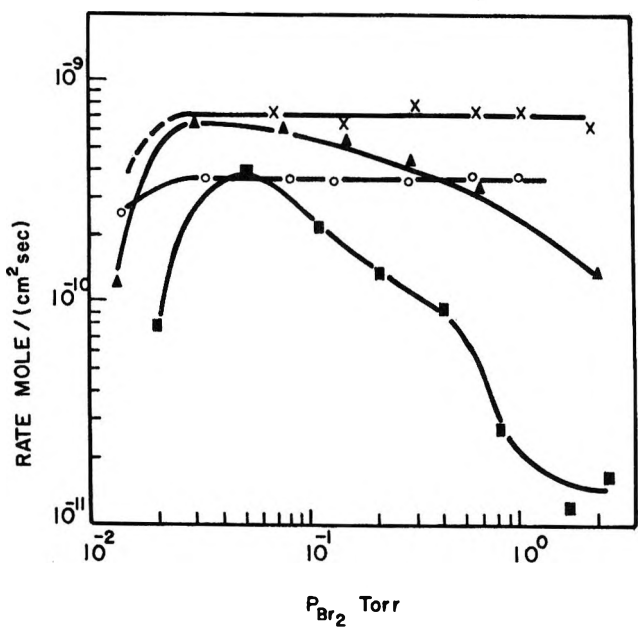

Figure 2. Rate dependence on $Br_2(g)$ in N_2 at various temperatures and O_2 pressures (Torr): ×, 900°, 8.7×10^{-3}; ○, 900°, 4.3×10^{-3}; ▲, 800°, 8.7×10^{-3}; ■, 700°, 8.7×10^{-3}.

Torr. At the lowest Br_2 pressures, the exact shape of the curve was difficult to establish because of problems in controlling and measuring the Br_2.

In N_2 at 900°, the rate was independent of Br_2 from 0.03 to 2 Torr and linear with O_2 pressure as shown in Figure 2. At 700 and 800°, the rate decreased above about 0.05 Torr Br_2 but maintained a linear relation with O_2.

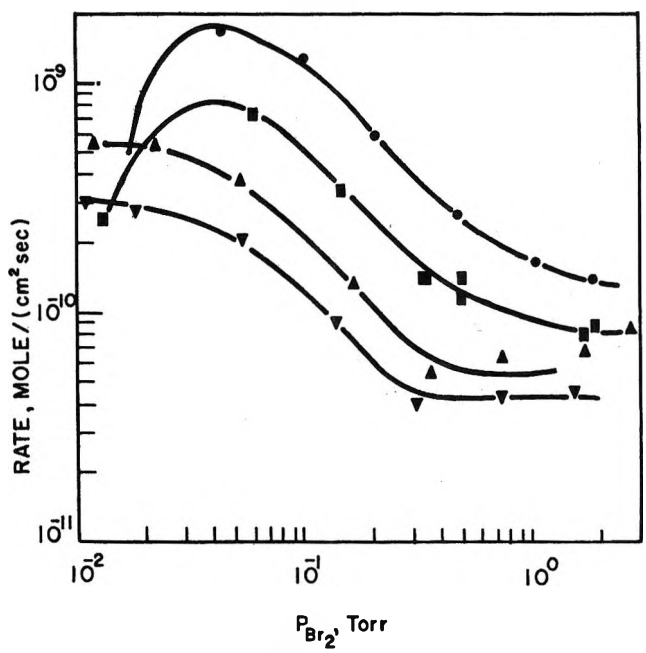

Figure 3. Rate dependence on $Br_2(g)$ at 900° in He with O_2 (Torr): ●, 17.4×10^{-3}; ■, 8.7×10^{-3}; △, 4.3×10^{-3}; ▼, 2.1×10^{-3}.

In He at 900°, the rate decreased above about 0.05 Torr Br_2 but maintained an approximate linear relation with O_2 pressure. This linearity with O_2 pressure was not observed at 800°. At both temperatures, the rate became independent of Br_2 above a pressure (0.2–2 Torr) which increased with O_2 pressure and temperature.

The complexities of this system are great and dictate a limited attempt at interpretation. Previous work in tungsten oxidation has established two distinct binding states or layers of oxygen. Schissel and Trulson[12] have proposed a two-layer model and McCarroll[13] has evidence that the first layer is atomic oxygen. McKinley[14] has applied the two-layer model to the W + O_2 + Cl_2 reaction at 1200–2400° and concluded that the first layer was atomic oxygen and the second layer contained both oxygen and chlorine with the oxygen more extensively adsorbed. Rosner and Allendorf[15,16] have investigated the reaction of W(s) with oxygen–chlorine mixtures (atoms and molecules) and found that at constant O_2 pressure, the apparent reaction order with respect to Cl_2 passed from large positive values to large negative values beyond the rate maximum. Partially dissociated chlorine had a qualita-

(12) P. O. Schissel and C. C. Trulson, *J. Chem. Phys.*, **43**, 737 (1965).

(13) B. McCarroll, *ibid.* **46**, 863 (1967).

(14) J. D. McKinley, "Proceedings of the Sixth International Symposium on Reactivity of Solids," Schenectady, N. Y., Aug 25–30, 1969, Wiley-Interscience, New York, N. Y., 1969, pp 345–351.

(15) D. E. Rosner and H. D. Allendorf, *AIAA J.*, **5**, 1489 (1967).

(16) D. E. Rosner and H. D. Allendorf, "Proceedings of the Third International Symposium on High Temperature Technology," Butterworths, London, 1969, p 707.

tively similar kinetic effect on the tungsten oxidation reaction, but the rate maximum occurred at lower Cl/O element ratios, suggesting an improved ability to competitively chemisorb for Cl atoms.

In the analogous W + O_2 + Br_2 reaction here, it is reasonable to assume the two-layer model where the first layer is formed from a strong selective adsorption of oxygen on W. Both oxygen and bromine, however, are bonded to the first layer to form a second layer with greatly reduced specificity when the Br_2/O_2 ratio is near unity. At the lowest Br_2 pressures used here, the Br_2/O_2 ratio is near unity and the rate increases with increasing Br_2 and/or O_2 which indicates that adsorption sites are available. In this region, the rate may be a linear function of Br_2 and O_2 as McKinley[14] observed for the O_2–Cl_2 system. At higher Br_2 pressures, adsorption of bromine and oxygen in the second layer is complete, and the reaction changes rapidly to zero order. At still higher Br_2 pressures, the bromine displaces some of the oxygen in the second layer and the reaction rate decreases. This decrease in reaction rate is analogous to that observed by Rosner and Allendorf in the W(s)/O_2(g)/Cl_2(g) reaction. With increasing bromine, the rate continues to decrease until the second layer is predominantly bromine and the reaction rate changes to zero order again. At higher temperatures and O_2 pressures, the transitions to zero order would be expected to occur at higher bromine pressures as shown in Figures 1 and 3. The observed increase in rate with increased O_2 pressure indicates that oxygen can successfully compete with a large excess of bromine for adsorption sites. Even with a large Br_2/O_2 ratio, a change in O_2 pressure during a run resulted in an immediate corresponding change in reaction rate.

Nitrogen is strongly chemisorbed on tungsten[7,8] in the temperature range employed here with a binding energy less than that of oxygen[12] but comparable to that of bromine.[17] Chemisorbed oxygen on tungsten is known to prevent chemisorption of molecular nitrogen,[18–20] and there is evidence that oxygen can displace chemisorbed nitrogen on tungsten.[19,20] If nitrogen can displace adsorbed bromine or if adsorbed nitrogen can be displaced by oxygen but not by bromine, the adsorbed oxygen concentration would be greater in the N_2 system and would account for the higher rates observed. The nitrogen effect may be considerably altered when the competition is Br(g) rather than Br_2(g). Unfortunately, temperature and Br atom concentration are not separable in the furnace-type experiments described here and limit this inference.

Acknowledgments. Drs. S. K. Gupta, K. M. Maloney, and L. V. McCarty contributed to many helpful discussions and reviewed the manuscript.

(17) B. McCarroll in "Structure and Chemistry of Solid Surfaces," G. A. Somorjai, Ed., Wiley, New York, N. Y., 1969.

(18) R. E. Schlier, *J. Appl. Phys.*, **29**, 1162 (1958).

(19) J. T. Yates and T. E. Madey, *J. Chem. Phys.*, **45**, 1623 (1966).

(20) H. F. Winters and D. E. Horne, *Surface Sci.*, **24**, 587 (1971).

An Electron Paramagnetic Resonance Study of SO_2^- on Magnesium Oxide

by R. A. Schoonheydt and J. H. Lunsford*

Department of Chemistry, Texas A&M University, College Station, Texas 77843 *(Received July 26, 1971)*

Publication costs assisted by the Environmental Protection Agency

When SO_2 is adsorbed on thermally activated and uv-irradiated MgO, two SO_2^- species are formed. The principal values of the g-tensor are $g_{xx} = 2.0028$, $g_{yy} = 2.0097$, and $g_{zz} = 2.0052$ for SO_2^- (A) and $g_{xx} = 2.0014$, $g_{yy} = 2.0078$, and $g_{zz} = 2.0033$ for SO_2^- (B). The principal values (in gauss) for the ^{33}S tensor are $a_{xx} = 59$ and $a_{zz} = 9.4$ for $^{33}SO_2^-$ (A); $a_{xx} = 55$ and $a_{zz} = 9.4$ for $^{33}SO_2^-$ (B). The values for ^{17}O are $a_{xx} = 36$ and $a_{zz} = 29$ for SO_2^- (A) and SO_2^- (B), respectively. The odd electron, transferred from the surface of MgO to SO_2, occupies a $2b_1''$ antibonding molecular orbital and is mainly concentrated on the S atom. SO_2^- (A) is thermally more stable than SO_2^- (B), and their concentration ratio depends on the pretreatment of MgO. Both SO_2^- (A) and SO_2^- (B) are believed to be located on oxygen ion vacancies. The SO_2^- ion is probably oriented with its oxygen atoms towards the surface. The binding forces are purely electrostatic.

Introduction

The epr spectrum of the radical ion SO_2^- has been described both in solution and in solids. In solution it was first identified as a result of the equilibrium $S_2O_4^{2-} \rightleftarrows 2SO_2^-$ by Rinker and coworkers.[1] This decomposition of the dithionite anion was easily achieved because of the unusually long S–S bond. Atkins, *et al.*,[2] found an isotropic hyperfine coupling constant of 14.5 G which is due to ^{33}S in SO_2^-. The spectrum of γ- or X-ray irradiated solid dithionite was also attributed to SO_2^-.[2,3]

From a comparison of the isotropic hyperfine splitting in SO_2^- and ClO_2, and a consideration of Walsh's energy level diagram[4] it was concluded[2,3] that (a) there is a slight increase of spin density in the 3s orbital of SO_2^- as compared to ClO_2, (b) the odd electron is in a $2b_1''$ orbital and largely concentrated on the central S atom, and (c) a weak spin-orbital coupling exists. The possible d-character of the $2b_1''$ orbital of the odd electron in SO_2^- has only been postulated by Clark and coworkers.[3]

More recently, Dinse and Möbius[5] described the $2b_1''$ molecular orbital of electrolytically generated SO_2^- as consisting of pure 3p and 2p character for S and O, respectively. These authors used the experimental results obtained by Schneider, Dischler, and Räuber[6] to calculate the spin density on the sulfur $3p_z$ and oxygen $2p_z$ orbitals. They found the odd electron largely concentrated on S. By assuming a bond angle of 115° ± 5° they could account also for the shift of the g value from the free-electron value.

This work was confirmed and extended by Reuveni and coworkers[7] on aqueous solutions of $Na_2S_2O_4$ and γ-irradiated, solid $K_2S_2O_5$. By using samples enriched with ^{33}S and ^{17}O these authors obtained experimentally both the ^{33}S and ^{17}O hyperfine tensors of the SO_2^- radical ion. They could account for their experimental results by assuming a pure p type $2b_1''$ molecular orbital for the odd electron. Moreover, the g tensor was asymmetric, but the hyperfine tensors were axially symmetric within the limits of experimental error as one would expect for this type of orbital. The slightly isotropic part of the hyperfine tensors could be accounted for by spin polarization. The d orbitals were neglected from the $2b_1''$ orbital. The bond angle was also assumed to be 115°.

SO_2^- has also been ascribed to epr signals observed in several γ- and X-ray irradiated crystals such as thiosulfates[8,9] and sulfates.[10,11] Usually, SO_2^- is not the only paramagnetic species present in these irradiated crystals. There is no complete agreement among different authors concerning the assignment of the various epr signals to chemical species.[12–15] In general, however, it appears that SO_2^- is well described in the literature and its characteristics established.

Such a radical ion may be an active intermediate in

(1) R. G. Rinker, T. P. Gordon, D. H. Mason and W. H. Carcoran, *J. Phys. Chem.*, **63**, 302 (1959).

(2) P. W. Atkins, A. Horsfield, and M. C. R. Symons, *J. Chem. Soc.*, 5220 (1964).

(3) H. C. Clark, A. Horsfield, and M. C. R. Symons, *ibid.*, 7 (1961).

(4) J. Walsh, *ibid.*, 2266 (1953).

(5) K. P. Dinse and K. Möbius, *Z. Naturforsch. A*, **23**, 695 (1968).

(6) J. Schneider, B. Dischler and A. Räuber, *Phys. Status Solidi*, **13**, 141 (1966).

(7) A. Reuveni, Z. Luz, and B. L. Silver, *J. Chem. Phys.*, **53**, 4619 (1970).

(8) R. L. Eager and D. S. Mahadevappa, *Can. J. Chem.*, **41**, 2106 (1963).

(9) J. M. de Lisle and R. M. Golding, *J. Chem. Phys.*, **43**, 3298 (1965).

(10) N. Hariharan and J. Sobhanadri, *Mol. Phys.*, **17**, 507 (1969).

(11) T. Suzuki and R. Abe, *J. Phys. Soc. Jap.*, **30**, 586 (1970).

(12) J. R. Morton, *Can. J. Chem.*, **43**, 1948 (1965).

(13) V. V. Gromov and J. R. Morton, *ibid.*, **44**, 527 (1966).

(14) J. R. Morton, D. M. Bishop, and M. Randiv, *J. Chem. Phys.*, **45**, 1885 (1966).

(15) K. Aiki and K. Hukuda, *J. Phys. Soc. Jap.*, **22**, 663 (1967).

the oxidation or reduction of SO_2 on metal oxide catalysts. Mashchenko, Pariiskii, and Kazanskii[16] reported the formation of SO_2^- as well as diamagnetic species, on partially reduced TiO_2 by adsorption of SO_2. These authors also presented evidence that the reaction of SO_2^- with O_2 on the TiO_2 surface leads to O_2^- and *vice versa* through intermediate surface sulfates, but they strongly emphasized that the reaction of SO_2^- with O_2 leads mainly to diamagnetic species.

It is our intention in this paper to extend these studies to activated MgO. It is possible to trap electrons on the surface of a suitably prepared MgO sample.[17] Upon adsorption of SO_2 the electron is transferred to the sorbed SO_2 molecule to form SO_2^-. The characteristic molecular parameters of the SO_2^- on the surface of MgO have been determined by evaluating the g tensor and the ^{33}S and ^{17}O hyperfine tensors. These values are compared with those obtained from SO_2^- trapped in solid matrices. Also, the thermal stability of SO_2^- has been investigated, as well as the effects of different pretreatments of the MgO catalyst. The results are interpreted in terms of the molecular orbital of the odd electron in SO_2^- and the nature of the adsorption sites on the MgO surface.

Experimental Section

The MgO used in these experiments was obtained from reagent grade powder supplied by Mallinckrodt Chemical Works. The powder was boiled in distilled water for several hours, dried at 100° until a paste was obtained, extruded into pellets with a hypodermic syringe and dried at 100°. The sample was then heated to 500 or 800° for 5 to 7 hr under high vacuum. The activated MgO was put in contact with very pure H_2 and uv-irradiated with a low-pressure mercury vapor lamp (λ = 2537 Å). The MgO became blue due to electrons trapped at surface centers[18] (S-centers). Uv irradiation at liquid N_2 temperatures produced more S-centers in a much shorter time than at room temperature. Alternately, the uv irradiation was performed after the SO_2 adsorption. In this case no hydrogen was used. Matheson anhydrous grade SO_2 gas was purified several times by the freeze-pumping technique prior to use. Sulfur enriched with 25 and 44% ^{33}S and oxygen enriched with 47% ^{17}O were used to produce enriched $^{33}SO_2$ and $S^{16}O^{17}O$, respectively. Suitable amounts of oxygen and sulfur, respectively, were allowed to react at 450° for 4 hr with the enriched sulfur and oxygen. The evolution of the epr spectra of SO_2^- was followed by allowing very small amounts of SO_2 to adsorb in subsequent steps.

The epr spectra were obtained with a Varian Model V-4500 spectrometer equipped with a 100-kc modulation unit. The cavity resonance frequency was 9500 MHz. Special care was taken to avoid saturation of the signal even at room temperature. The standard used to determine the g values of the radical was phosphorus-doped silicon with g = 1.9987.

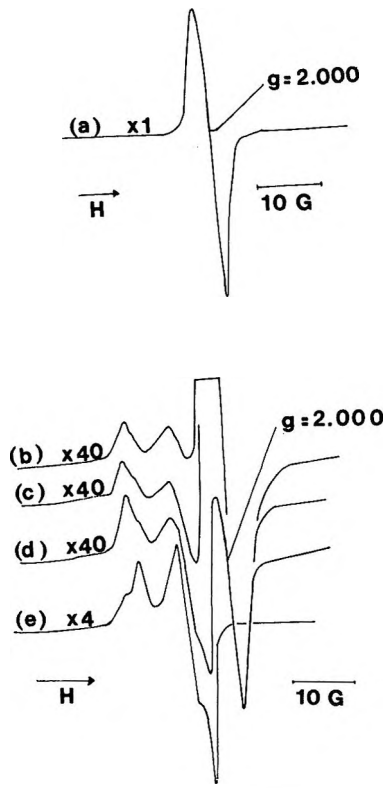

Figure 1. The development of the SO_2^- spectrum from the S-center on MgO pretreated at 500°. (a) Original S-center; (b), (c), (d), increase in intensity of SO_2^- signal with concomitant decrease in intensity of S-center signal; (e) final SO_2^- spectrum.

Results

When SO_2 was allowed to adsorb on previously uv-irradiated MgO, which had been degassed at 500°, the spectra of Figure 1 were obtained. This figure shows a decrease in intensity of the S-center with a simultaneous increase in the SO_2^- spectrum. It is also apparent that two SO_2^- species are formed on the surface of MgO. The species with the highest g values, SO_2^- (A), appeared first followed by the SO_2^- with slightly lower g values, SO_2^- (B). With increased SO_2 adsorption the SO_2^- (B) becomes the predominant species. When all the sites are saturated, the ratio SO_2^- (B):SO_2^- (A) approximately equals two.

When MgO was pretreated at 800°, qualitatively the same results were obtained. The difference being the final ratio of SO_2^- (B):SO_2^- (A): as shown in Figure 2 the ratio for this case is less than unity if one considers the doubly integrated signal.

A sample, previously saturated with SO_2^-, undergoes exactly the reverse behavior when heated under vac-

(16) A. I. Mashchenko, G. B. Pariiskii, and V. B. Kazanskii, *Kinet. Katal.*, 9, 151 (1968).

(17) J. H. Lunsford and J. P. Jayne, *J. Phys. Chem.*, 70, 3464 (1966).

(18) J. H. Lunsford and J. P. Jayne, *ibid.*, 69, 2182 (1965).

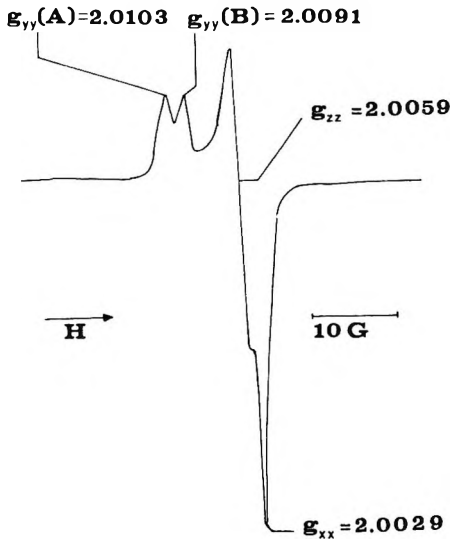

Figure 2. SO_2^- on MgO pretreated at 800°.

uum. Although both SO_2^- species were stable under a dynamic vacuum of 10^{-5} Torr at room temperature, the SO_2^- (B) species disappeared far more rapidly than the SO_2^- (A) species with increasing temperature. Essentially no SO_2^- (B) is apparent following the treatment at 200° for 2 hr under 1×10^{-5} Torr. A temperature of 400° was necessary to remove SO_2^- (A).

Not all of the adsorbed SO_2 is converted into SO_2^-. Analogous to the results on TiO_2[16] the majority of the SO_2 molecules adsorb in a nonparamagnetic form. Indeed, after the MgO was degassed for several hours at 500° under vacuum in order to remove completely the SO_2^- species, and subsequently submitted to uv irradiation, also under vacuum, the SO_2^- spectra reappeared. When the irradiation was performed under a H_2 atmosphere, only the SO_2^- (A) species appeared. The existence of nonparamagnetic SO_2 was further shown by infrared spectroscopy.[19]

The ratio SO_2^- (B):SO_2^- (A) is also influenced by whether the uv irradiation is applied before or after the SO_2 adsorption. If no S-centers were produced prior to the SO_2 adsorption, but uv irradiation was applied after the SO_2 was adsorbed on MgO, the formation of SO_2^- (B) was strongly favored, even when MgO was previously pretreated at 800°. SO_2^- (A) can only be seen as a shoulder on the low-field side of SO_2^- (B). Moreover, SO_2 adsorbed on MgO without uv irradiation, either before or after the adsorption, gave rise to small amounts of SO_2^-. The amounts increase with increasing pretreatment temperature with both SO_2^- species being present. It was thought that this electron transfer from the solid to the SO_2 may create V-type centers; however, attempts to detect them failed.

SO_2 can also be adsorbed on low-surface area MgO after uv irradiation. Both SO_2^- species are present with a SO_2^- (B):SO_2^- (A) ratio equal to one-half.

Table I summarizes the g values for SO_2^- adsorbed on MgO. They are compared with the values obtained for SO_2^- in other environments.

Table I: Principal g Values for SO_2^- Adsorbed on MgO and in Other Matrices

	g_{yy}	g_{zz}	g_{xx}
SO_2^- (A)[a]	2.0097	2.0052	2.0028
SO_2^- (B)[a]	2.0078	2.0033	2.0014
SO_2^- on TiO_2 (16)	2.005	2.001	2.001
$K_2S_2O_5$ (7)	2.012	2.0057	2.0019
Na_2SO_4 (10)	2.0218	2.0076	2.0069
$Na_2S_2O_5$ (9)	2.0102	2.0057	2.0024
KCl (6)	2.0100	2.0071	2.0025
KBr (6)	2.0100	2.0075	2.0050

[a] Every g value is an average of seven independent measurements.

Sulfur-33 and Oxygen-17 Hyperfine Splittings. The ^{33}S (nuclear spin $^3/_2$) hyperfine lines for either of the two SO_2^- species could be determined by a suitable choice of the experimental conditions according to the results reported above. By pretreatment of MgO at 500° spectra were obtained with SO_2^- (B) predominantly present. Heating MgO at 800° gave SO_2^- (B) and SO_2^- (A) in approximately equal amounts. Upon subsequent degassing at 200° only SO_2^- (A) remained.

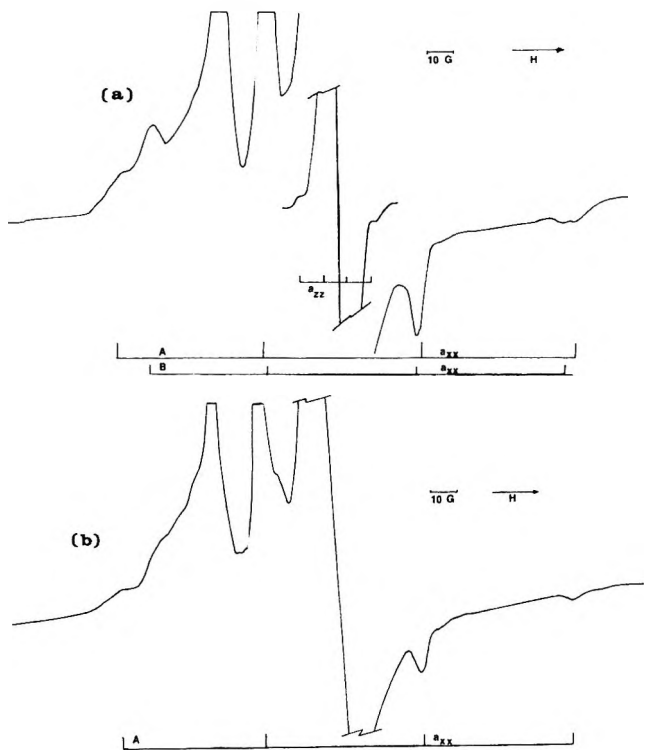

Figure 3. (a) $^{33}SO_2^-$ on MgO pretreated at 800°. Both $^{33}SO_2^-$ (A) and $^{33}SO_2^-$ (B) are present. (b) $^{33}SO_2^-$ on MgO pretreated at 800°, followed by subsequent degassing at 200°; only $^{33}SO_2^-$ (A) is clearly present.

(19) R. A. Schoonheydt and J. H. Lunsford, to be published.

Table II: Principal Values of the ^{33}S and ^{17}O Hyperfine Tensors (gauss) of SO_2^- Adsorbed on MgO and in Other Matrices

	^{33}S			^{17}O		
	a_{xx}	a_{yy}	a_{zz}	a_{xx}	a_{yy}	a_{zz}
SO_2^- (A)	59 ± 1	(6.6 ± 2)[a]	9.4 ± 1	36 ± 1	(3 ± 3)[a]	(3 ± 3)[a]
SO_2^- (B)	55 ± 1	(6.6 ± 2)[a]	9.4 ± 1	29 ± 1	(3 ± 3)[a]	(3 ± 3)[a]
$K_2S_2O_5$ (7)	58 ± 0.5	4 ± 4	4 ± 4	30 ± 0.5	3 ± 3	3 ± 3
KCl (6)	52.5 ± 1	8.6 ± 1	7.1 ± 1	...	...	...
KBr (6)	54.3 ± 1	7.1 ± 1	7.1 ± 1	...	...	...

[a] Estimated from other work.[6,7]

Comparison of the different spectra obtained in this way enabled us to distinguish between the ^{33}S hyperfine splitting constants of SO_2^- (B) and SO_2^- (A) as indicated in Figure 3 and summarized in Table II.

The lines corresponding to the x direction are clearly resolved for $^{33}SO_2^-$ (A) and $^{33}SO_2^-$ (B); however, the hyperfine lines corresponding to the y and z directions overlap with the $^{32}SO_2^-$ spectrum. Of the four lines separated by a_{zz} and centered around g_{zz} only the two extreme lines may be observed as small peaks on the tails of the $^{32}SO_2^-$ spectrum. From the separation between these two lines we calculated $a_{zz} = 9.4 \pm 1$ G. This value should be regarded as a maximum limit to a_{zz}. The four lines centered around a_{yy} could not be resolved from the SO_2^- spectrum. We adopted, therefore, the arithmetic mean of the values of a_{yy} reported by other authors:[6,7] $a_{yy} = 6.6 \pm 2$ G. A nearly axially symmetric ^{33}S hyperfine tensor is obtained in agreement with previous work.[6,7]

The experimental procedure used to obtain the ^{17}O (nuclear spin $^5/_2$) hyperfine tensor is the same as for $^{33}SO_2^-$. Due to the larger number of lines and the overlap with the $S^{16}O_2^-$ spectrum, a_{yy} and a_{zz} could not be calculated from the experimental spectra. Therefore we adopted Reuveni's value[7] of 3 ± 3 G. The spectra are given in Figure 4 and the ^{17}O hyperfine-splitting constants in Table II.

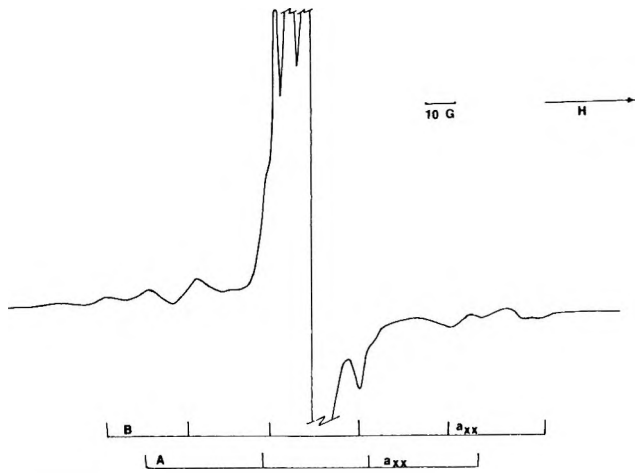

Figure 4. $S^{16}O^{17}O^-$ on MgO pretreated at 800°.

Discussion

The qualitative agreement between the esr spectra obtained with SO_2 adsorbed on MgO before or after uv irradiation of the solid, the similarity of our g values with those of other authors (Table I), and the hyperfine-splitting data unambiguously reveal that our esr signal is due to SO_2^-. Moreover, the two different signals indicate two slightly different adsorption sites on MgO.

Characterization of the SO_2^- Molecule. SO_2^- has 19 valence electrons. The odd electron occupies a $2b_1''$ molecular orbital according to Walsh's diagram.[4] Reuveni[7] and Dinse[5] have given an explicit wave function for this $2b_1''$ MO neglecting the sulfur 3d-orbital contribution

$$\psi(2b_1'') = c_1S(3p_x) + \frac{b_1}{\sqrt{2}}O(2p_{x_1} + 2p_{x_2}) \quad (1)$$

where $1/\sqrt{2}$ is a normalization constant.

The molecular orbital occupied by the odd electron is thus a linear combination of atomic p_x orbitals, perpendicular to the plane of the molecule. According to Reuveni, *et al.*,[7] one expects the following characteristics for the SO_2^- molecule and its g tensor and hyperfine-splitting tensors: (a) two magnetically equivalent oxygens, (b) axially symmetric ^{17}O and ^{33}S hyperfine tensors with their unique components parallel to each other and perpendicular to the molecular plane, and (c) along this unique hyperfine direction the g value should be close to the free-electron value. The maximum g value should be along the O–O direction, which is the y direction.

Sulfur and Oxygen Hyperfine Interactions. The ^{33}S and ^{17}O hyperfine tensor may be resolved into an isotropic part (A_{iso}) and a traceless anisotropic part (A) as described in Table III. The choice of the sign is made so as to be in agreement with A_{iso} for SO_2^- in solution[7] where A_{iso} for $^{17}O = 8.96 \pm 0.05$ G and A_{iso} for $^{33}S = 14.67 \pm 0.05$ G.

For the pure 3s orbital of ^{33}S the coupling is 970 G and for the pure 2s orbital of ^{17}O a value of 590 G is reported.[20,21] Comparing with our values, we conclude that the spin density in the 3s orbital of sulfur and 2s

(20) G. W. Chantry, A. Horsfield, J. R. Morton, J. R. Rowlands and D. H. Whiffen, *Mol. Phys.*, 5, 233 (1962).

(21) Z. Luz, A. Reuveni, R. W. Holmberg and B. L. Silver, *J. Chem. Phys.*, 51, 4017 (1969).

Table III: Isotropic and Anisotropic Parts of the ^{33}S and ^{17}O Hyperfine Tensors (gauss)

	A_{iso}	A_{xx}	A_{yy}	A_{zz}
$^{33}SO_2^-$ (A)	14.3 ± 2	44.7 ± 2	−20.9 ± 3	−23.7 ± 2
$^{33}SO_2^-$ (B)	13 ± 2	42 ± 2	−19.6 ± 3	−22.4 ± 2
$S^{16}O^{17}O^-$ (A)	10 ± 4	26 ± 4	−13 ± 5	−13 ± 5
$S^{16}O^{17}O^-$ (B)	7.7 ± 4	21.3 ± 4	−10.7 ± 5	−10.7 ± 5

orbital of O is between 1 and 2%. This number is negligibly small and can be accounted for entirely by spin polarization. The wave function adopted in the previous section can therefore be considered as a good representation of the molecular orbital of the odd electron, at least in the LCAO scheme.

The coefficients b_1 and c_1 of the $2b_1''$ molecular orbital may then be calculated by comparing the experimental values of A_{zz} with the theoretical values for an odd electron in a p orbital on ^{33}S and ^{17}O, respectively. The theoretical value of A_{zz} for ^{33}S was calculated with the aid of the numerical value, $\langle r^{-3}\rangle_S = 3.41 \times 10^{25}$ cm^{-3}, reported by Dinse and Möbius.[5] Using the value of $\langle r^{-3}\rangle_O = 3.36 \times 10^{25}$ cm^{-3} [22] the theoretical value of A_{zz} for ^{17}O was also calculated. Table IV lists the spin densities on S($3p_z$) and O($2p_{z1} + 2p_{z2}$) together with the total spin density calculated in this manner. It must be remarked that the spin density on the oxygen reported here is higher than for SO_2^- trapped in a solid matrix,[7] while the values for ^{33}S are nearly the same. This difference, however, may only be due to the approximations made during the calculation.

Table IV: $2b_1''$ MO Coefficients and Spin Densities on S and O for SO_2^- on MgO

	SO_2^- (A)	SO_2^- (B)
c_1	0.86	0.84
b_1	0.52	0.48
c_1^2	0.75	0.71
b_1^2	0.27	0.23
$c_1^2 + b_1^2$	1.02	0.94

The g Tensor. The dominant contribution to the g shift comes from mixing the $2b_1''$ orbital with the $3a_1'$ and $2b_2'$ orbitals.[5,7] The wave functions of these orbitals are [5,7]

$$\psi(3a_1') = c_2S(3p_z) + c_4S(3s) + \frac{b_2}{\sqrt{2}}O(2p_{z1} + 2p_{z2}) + \frac{b_3}{\sqrt{2}}O(2p_{y1} - 2p_{y2}) \quad (2)$$

and

$$\psi(2b_2') = c_3S(3p_y) + \frac{b_4}{\sqrt{2}}O(2p_{z1} - 2p_{z2}) + \frac{b_5}{\sqrt{2}}O(2p_{y1} + 2p_{y2}) \quad (3)$$

Exact values for the different coefficients occurring in these wave functions are not available. We assume, as Reuveni[7] did, $c_3 = b_3 = 0$. The ratio c_2/c_4 can be obtained from the bond angle of SO_2^- with the aid of Coulson's relation between the degree of hybridization and bond angle.[23] The bond angle of SO_2^- is not available. We adopted, therefore, the angle of SO_2 in the $^3B_1$ state as calculated by Brand and coworkers.[24] This value is 126.2° and gives $c_2/c_4 = 1.71$.

Assuming with Reuveni[7] that $c_2^2 = 2b_2^2$ and that $b_4 = b_5$, and applying the normalization condition of the wave functions $\psi(3a_1)$ and $\psi(2b_2)$, including overlap,[25] one obtains the following values for the coefficients: $c_4 = 0.36$, $c_2 = 0.63$, $b_2 = 0.40$, and $b_4 = b_5 = 1/\sqrt{2}$. Then the deviations from the free-electron g value are

$$\Delta g_{xx} = 0$$

$$\Delta g_{yy} = \frac{2(c_1c_2\lambda_s + b_1b_2\lambda_0)(c_1c_2 + b_1b_2)}{E(2b_1'') - E(2b_2')}$$

$$\Delta g_{zz} = \frac{2b_1^2b_5^2\lambda_0}{E(2b_1'') - E(2b_2')}$$

where $\lambda_s = 386$ cm^{-1} is the spin–orbit coupling constant for S and $\lambda_0 = 157$ cm^{-1} is the spin–orbit coupling constant for O. The energy differences in the denominators have been estimated by Dinse and Möbius:[5]

$$E(3a_1') - E(2b_1'') = 34{,}500 \text{ cm}^{-1}$$

$$E(2b_2') - E(2b_1'') = 38{,}500 \text{ cm}^{-1}$$

We obtain then for SO_2^- (A) $\Delta g_{xx} = 0$, $\Delta g_{zz} = 0.0011$, and $\Delta g_{yy} = 0.0140$; whereas, for SO_2^- (B) $\Delta g_{xx} = 0$, $\Delta g_{zz} = 0.0009$, and $\Delta g_{yy} = 0.0136$.

The agreement with experiment is only qualitative in the sense that we predict the right sequence of Δg shifts. No conclusion about the bond angle of SO_2^- can be obtained. We adopted the 126.2° bond angle because we feel that the SO_2^- bond angle is closer to that of the $^3B_1$ excited state of SO_2 than to that of the ground state of SO_2. A widening of the bond angle of SO_2^- with respect to SO_2 is not unreasonable when one considers

(22) J. S. M. Harvey, *Proc. Roy. Soc., Ser. A*, **285**, 581 (1965).

(23) P. W. Atkins and M. C. R. Symons, "The Structure of Inorganic Radicals," Elsevier, Amsterdam, 1967, p 257.

(24) J. C. D. Brand, C. di Lauro, and V. T. Jones, *J. Amer. Chem. Soc.*, **92**, 6095 (1970).

(25) R. S. Mullikan, C. A. Rieke, D. Orloff, and H. Orloff, *J. Chem. Phys.*, **17**, 1248 (1949).

Walsh's diagram.[4] The $2b_1''$ molecular orbital increases only slightly in energy in going from 90 to 180° bond angle. The $4a_1'$ orbital which is the highest filled orbital of SO_2 has a much greater energy increase in going from the 90° bond angle to the linear form. A bond angle close to 90° is therefore more likely.

The Nature of the Adsorption Sites. When MgO is degassed and subsequently uv irradiated in a H_2 atmosphere, two different epr signals are developed, corresponding to a pretreatment temperature of 500 and 800°, respectively. The center obtained after the 500° pretreatment has an axially symmetric g tensor and is believed to be an electron trapped at an oxygen ion vacancy.[17,26] The center obtained after the 800° pretreatment was first ascribed to an electron trapped at an anion–cation vacancy pair by Lunsford and Jayne.[17] Nelson and coworkers,[26] however, showed that this epr signal involves a hydrogen hyperfine splitting and that two centers are present.

The existence of two different paramagnetic centers is clearly confirmed in this work by the presence of two different types of SO_2^-. Moreover, each SO_2^- species retains its same asymmetric g tensor whatever the pretreatment of MgO. This suggests that only the relative number of the two adsorption sites changes with changing pretreatment temperatures.

We think that it is reasonable to ascribe both the electron trapping centers and the SO_2^- adsorption sites to oxygen ion vacancies at the surface. As a working model one may consider that the sites giving rise to SO_2^- (B) are oxygen ion vacancies on the edges of the microcrystals: the centers forming SO_2^- (A) are then oxygen ion vacancies on the flat surface of the microcrystals. The change of their relative number with increasing pretreatment temperature is in agreement with this assignment; that is, one can imagine that the decrease in surface area at 800° is due to a smoothing out of the surfaces of MgO crystallites, thus resulting in a decrease in the number of edges present on the nonideal crystal surfaces. The number of sites (a maximum of 10^{19}/g) can easily be accounted for in this manner.

No explicit proof can be offered to show the orientation of SO_2^- with respect to the surface. The odd electron is entirely located on the SO_2^- ion as suggested by our calculations. Since it plays no role in any kind of covalent bond, the bonding forces are purely electrostatic. The oxygen ion vacancies have a positive character and are likely to attract the more electronegative oxygen atoms instead of the sulfur atom. An analogous orientation has been proposed by Bennett and coworkers[27,28] for CO_2^- and CS_2^- bonded to alkali metals.

Acknowledgment. This investigation was supported by research grant AP 01181, Air Pollution Control Office, Environmental Protection Agency.

(26) R. L. Nelson, A. J. Tench, and B. J. Hamsworth, *Trans. Faraday Soc.*, **63**, 1427 (1967).

(27) J. E. Bennett, B. Mile, and A. Thomas, *ibid.*, **61**, 2357 (1965).

(28) J. E. Bennett, B. Mile, and A. Thomas, *ibid.*, **63**, 1 (1967).

Nuclear Magnetic Resonance Studies of Methanol–Boron Trifluoride Complexes

by Kenneth L. Servis*[1a] and Lucy Jao[1b]

Department of Chemistry, University of Southern California, Los Angeles, California 90007 *(Received May 20, 1971)*

Publication costs borne completely by The Journal of Physical Chemistry

Nuclear magnetic resonance spectroscopy has been used to study the interaction of methanol with boron trifluoride in sulfur dioxide solvent. Composition *vs.* chemical shift diagrams served to identify the species present in each concentration range. At methanol to boron trifluoride ratios of greater than 2 : 1, formation of the conjugate base of the 1:1 adduct, $CH_3OBF_3^-$, and the conjugate acid of methanol, $CH_3OH_2^+$, occurs. Rates for methoxyl exchange between the 1:1 adduct and methanol and for fluorine exchange between the 1:1 adduct and boron trifluoride have been determined from the coalescence temperature of the corresponding nmr absorptions.

Introduction

The coordination compounds of boron trifluoride with organic substances serve as active catalysts for alkylation,[2] condensation,[3] polymerization[4] and other reactions.[5] Methanol forms coordination compounds in which there are one or two molecules of organic substance per molecule of boron trifluoride.[6] Such compounds are strongly acidic[7] and are typical of Friedel–Crafts catalysts. Following studies of the mode and extent of complex formation,[8] the mode and rate of exchange of boron trifluoride between different complexes were investigated.[9,10]

For the methanol–boron trifluoride system, conflicting assignments of the observed nmr absorptions in the methoxyl region have been offered. In one study the two upfield resonances were assigned to the mono- and dialcohol complexes,[11] $BF_3 \cdot CH_3OH$ and $BF_3 \cdot 2CH_3OH$, while in the other they were assigned to the monocomplex and bulk solvent.[12] Using composition *vs.* chemical shift diagrams, we have attempted to identify the species present in each concentration range and to assign characteristic chemical shifts to each of the several species present.

Experimental Section

Preparation of Samples. All samples and their internal standards were prepared by high-vacuum techniques. Anhydrous grade sulfur dioxide (Ansul Chemical Co.) was used as solvent; it was degassed and kept over phosphorus pentoxide in a storage bulb of the vacuum line. Reagent grade methanol was purified by refluxing over magnesium for several hours, then distilling into the storage bulb of the vacuum line. All other reagents were distilled at low temperature into the storage bulbs and purified by vacuum fractionation. Known pressures of methanol, of boron trifluoride, and of sulfur dioxide were condensed from a calibrated volume directly into a nmr sample tube which contained a sealed capillary reference tube (precision coaxial spacing of capillary; Wilmad Glass Company, Inc.) with 25% of perfluorocyclobutane (Penninsular Chemresearch Inc.), 25% tetramethylsilane (Matheson Coleman and Bell), and 50% of dichlorodifluoromethane (American Potash and Chemical Corp.). The samples were sealed under vacuum with the contents still at liquid-nitrogen temperature, then stored in a freezer (−15°). No appreciable discoloration occurred on standing for several months at −15°, however, the solutions discolored upon standing at room temperature.

Nmr Spectra. Spectra were obtained on a Varian Associates HA-100 nmr spectrometer operating at 100 MHz for protons and 94.1 MHz for fluorines. The chemical shifts were determined by measuring with respect to the inner external standard at various temperatures: TMS for proton resonance spectra and perfluorocyclobutane for fluorine resonance spectra. Line widths and the chemical shift in fluorine resonance spectra were determined by the audio side band method using a Hewlett-Packard 200 AB audio oscillator. Low temperatures were obtained by passing

(1) (a) Alfred P. Sloan Research Fellow, 1969–1971; (b) National Science Foundation Trainee, 1969–1970.

(2) V. N. Ipatieff and A. V. Grosse, *J. Amer. Chem. Soc.*, **57**, 1616 (1935).

(3) R. D. Morin and A. E. Bearse, *Ind. Eng. Chem.*, **43**, 1596 (1951).

(4) A. M. Eastham, *J. Amer. Chem. Soc.*, **78**, 6040 (1956); J. M. Clayton and A. M. Eastham, *ibid.*, **79**, 5368 (1957).

(5) H. S. Booth and D. R. Martin, "Boron Trifluoride and Its Derivatives," Wiley, New York, N. Y., 1949.

(6) H. Bowlus and J. A. Nieuwland, *J. Amer. Chem. Soc.*, **53**, 3835 (1931).

(7) A. V. Topchiev, Ya. M. Paushkin, T. P. Vishnyakova, and M. V. Kurashov, *Dokl. Akad. Nauk SSSR*, **80**, 381 (1951).

(8) A. V. Topchiev, S. V. Zavgorodnié, and Ya. M. Paushkin, "Boron Trifluoride and its Compounds as Catalysts in Organic Chemistry," Pergamon Press, New York, N. Y., 1959, p 64.

(9) P. Diehl, *Helv. Phys. Acta*, **31**, 686 (1958).

(10) S. Brownstein, A. M. Eastham, and G. A. Latremouille, *J. Phys. Chem.*, **67**, 1028 (1963).

(11) J. Paasivirta and S. Brownstein, *J. Amer. Chem. Soc.*, **87**, 3593 (1965).

(12) A. Fratiello, T. P. Onak, and R. E. Schuster, *ibid.*, **90**, 1194 (1968).

Table I: Temperature Dependence of Proton Nuclear Magnetic Resonance Spectra of Methanol–Boron Trifluoride Mixtures in Sulfur Dioxide

Sample composition, M										
$[CH_3OH] = 0.965$	Temp[c]	−4.0	−20.5	−37.0	−53.8	−67.0	−70.3			
$[BF_3] = 0$	δ_{CH_3}[d]	3.07	3.05	3.03	3.00	2.99	2.98			
	δ_{OH}	2.44	2.98	3.22	3.44	3.55	3.69			
$[CH_3OH] = 0.762$	Temp	−0.7	−18.0	−35.0	−43.8	−54.3	−61.0	−78.0		
	δ_{CH_3}	3.17	3.15	3.13	3.12	3.11	3.10	3.08		
$[BF_3] = 0.190$	δ_{CH_3}	3.40	3.36	3.33	3.33	3.31	3.32	3.28		
	δ_{OH}	5.35	5.58	5.84	5.96	6.09	6.21	6.48		
$[CH_3OH] = 0.689$	Temp	+1.0	−16.3	−33.8	−42.3	−51.0	−59.5	−68.5	−76.8	
	δ_{CH_3}	3.18	3.15	3.14	3.13	3.13	3.12	3.11	3.10	
$[BF_3] = 0.231$	δ_{CH_3}	3.38	3.34	3.34	3.33	3.33	3.31	3.29	3.28	
	δ_{OH}	5.59	5.83	6.08	6.21	6.36	6.48	6.60	6.73	
$[CH_3OH] = 0.648$	Temp	−3.0	−20.5	−37.5	−46.5	−55.0	−64.0	−72.5	−81.3	
	δ_{CH_3}	3.30	3.28	3.26	3.26	3.25	3.25	3.24	3.24	
$[BF_3] = 0.319$	δ_{CH_3}	3.39	3.39	3.36	3.36	3.35	3.35	3.32	3.32	
	δ_{OH}	7.46	7.68	7.87	7.96	8.04	8.16	8.24	8.34	
$[CH_3OH] = 0.567$	Temp	1.5	−16.0	−33.5	−42.3	−51.0	−56.3	−63.7	−70.3	
	δ_{CH_3}	3.45	3.43	3.45	3.33	3.34	3.32	3.31	3.31	
$[BF_3] = 0.335$	δ_{CH_3}				3.47	3.46	3.45	3.44	3.44	
	δ_{OH}	7.36	7.68	7.81	7.86	7.90	7.92	7.96	8.02	
$[CH_3OH] = 0.327$	Temp	2.3	−6.6	−23.5	−40.0	−48.8	−57.0	−65.5	−74.0	−82.0
$[BF_3] = 0.325$	δ_{CH_3}	3.54	3.55	3.53	3.54	3.57	3.57	3.57	3.54	3.54
	δ_{OH}	6.86	6.94	7.02	7.12	7.17	7.22	7.27	7.30	7.36
$[CH_3OH] = 0.391$	Temp	0.5	−16.5	−36.5	−42.0	−50.5	−59.2			
$[BF_3] = 0.529$	δ_{CH_3}	3.68	3.67	3.66[a]	3.65[a]	3.64[a]	3.63[a]			
	δ_{OH}	6.30	6.34	6.39[b]	6.44[b]	6.48[b]	6.51[b]			
$[CH_3OH] = 0.320$	Temp	3.2	−18.6	−32.6	−41.8	−49.3	−58.0	−66.1		
$[BF_3] = 0.625$	δ_{CH_3}	3.66	3.65	3.63[a]	3.63[a]	3.67[a]	3.62[a]	3.62[a]		
	δ_{OH}	6.21	6.29	6.34[b]	6.40[b]	6.44[b]	6.48[b]	6.52[b]		

[a] Doublet with $J = 4.0$ Hz. [b] Quartet with $J = 4.0$ Hz. [c] In °C. [d] Chemical shifts in ppm downfield from tetramethylsilane.

purified gaseous nitrogen from a coiled copper tube immersed in a Dewar filled with liquid nitrogen into a specially designed silvered transfer Dewar connected to the Varian V-4340 variable temperature nmr probe, and measured with a copper–constantan thermocouple and a Leeds and Northrup potentiometer.

Results

Proton and fluorine magnetic resonance spectra were obtained for mixtures of methanol and boron trifluoride in sulfur dioxide at various concentrations and over the temperature range from 0° to near the freezing points of the solutions at about −80°. The ratio of methanol to boron trifluoride was varied from 1:2 up to 4:1. The sum of the methanol and the boron trifluoride concentrations was maintained at about 0.9 to 1.0 M for most of the solutions examined. For these solutions, the measured chemical shifts at various temperatures are presented in Tables I and II.

For samples with a methanol to boron trifluoride ratio larger than 2:1, the two methoxyl group and one hydroxyl group resonances exhibited only small frequency shifts as the sample temperature was lowered. Upon warming, the two methoxyl group resonances for the 2:1 sample coalesced at 15° and for the 1.5:1 sample at −33°. From examination of the methoxyl resonance line shapes, the coalescence temperatures[13] were determined[14] and are presented in Table III.

In the presence of an excess of boron trifluoride, only a single methoxyl and a single hydroxyl resonance were observed. With decreasing temperature, both of these resonances broadened and eventually resolved into a spin-coupled doublet and quartet, respectively. The coalescence temperature for these spin multiplets increased with increasing boron trifluoride concentration.

Samples containing more than one equivalent of methanol exhibited but a single fluorine resonance whose shift was insensitive to sample composition.

(13) H. S. Gutowsky and C. H. Holm, *J. Chem. Phys.*, **25**, 1228 (1956).

(14) J. A. Pople, W. G. Schneider and H. J. Bernstein, "High-Resolution Nuclear Magnetic Resonance," McGraw-Hill, New York, N. Y., 1959, Chapter 10.

Table II: Temperature Dependence of Fluorine Nuclear Magnetic Resonance Spectra of Methanol–Boron Trifluoride Mixtures in Sulfur Dioxide

Sample composition, M									
$[BF_3]$ = 0.973	Temp[a]	−0.75	−19.0	−36.5	−45.5	−54.0	−63.0	−77.0	−81.0
$[CH_3OH]$ = 0	δ_F[b]	−10.49	−10.81	−10.91	−11.06	−11.3	−11.36	−11.51	−11.55
$[BF_3]$ = 0.615	Temp	2.9	−16.0	−35.3	−54.3	−63.8	−73.0	−87.5	
$[CH_3OH]$ = 0.320	δ_F	2.13	1.34	broad	13.43	13.08	12.97	13.20	
					−11.56	−11.71	−11.71	−12.02	
$[BF_3]$ = 0.529	Temp	0.0	−17.3	−34.8	−52.3	−61.0	−69.75	−78.0	
$[CH_3OH]$ = 0.391	δ_F	7.22	7.69	broad	12.79	13.01	13.75	13.75	
								−10.54	
$[BF_3]$ = 0.325	Temp	−4.5	−22.5	−40.2	−53.6	−67.5	−71.8	−80.6	
$[CH_3OH]$ = 0.327	δ_F	13.5	13.23	13.16	12.86	12.90	12.97	12.72	
$[BF_3]$ = 0.319	Temp	−1.5	−17.3	−36.0	−45.5	−55.0	−64.0	−74.0	
$[CH_3OH]$ = 0.648	δ_F	13.66	13.19	12.82	12.60	12.35	12.29	12.02	
$[BF_3]$ = 0.231	Temp	−0.2	−18.0	−36.8	−46.3	−55.5	−64.8	−73.8	
$[CH_3OH]$ = 0.689	δ_F	13.85	13.185	12.58	12.27	12.39	12.00	11.67	
$[BF_3]$ = 0.190	Temp	−2.6	−20.5	−38.5	−46.3	−55.5	−64.75	−74.0	
$[CH_3OH]$ = 0.762	δ_F	13.2	13.00	12.53	12.16	12.15	11.88	12.03	

[a] In °C. [b] Chemical shift in ppm downfield from perfluorocyclobutane.

Table III: Rate of Methoxyl Exchange ir Methanol–Boron Trifluoride Complex

Sample composition, M	$[CH_3OH \cdot BF_3]$	T_c, °K[a]
$[CH_3OH]$ = 1.03[c]		
$[BF_3]$ = 0.81	0.59	228
$[CH_3OH]$ = 0.567		
$[BF_3]$ = 0.385	0.203	240
$[CH_3OH]$ = 0.83		
$[BF_3]$ = 0.48	0.13	253
$[CH_3OH]$[b] = 0.69		
$[BF_3]$ = 0.29	...	288
$[CH_3OH]$ = 0.648		
$[BF_3]$ = 0.319	...	280

[a] Coalescence temperature for the methoxyl resonances. [b] Data from reference 11. [c] R. J. Gillespie and J. S. Hartman, *Can. J. Chem.*, 45, 2244 (1967).

Table IV: Rate of Fluorine Exchange in Methanol–Boron Trifluoride Complex

Sample composition, M	Temp, °C	$\tau_{CH_3OH \cdot BF_3}$, sec[a]	τ_{BF_3}, sec[a]
$[CH_3OH]$ = 0.370	−63.8	3.8×10^{-3}	4.0×10^{-3}
$[BF_3]$ = 0.651	−73.0	6.2×10^{-3}	6.4×10^{-3}
	−82.5	1.2×10^{-2}	1.4×10^{-2}
$[CH_3OH]$ = 0.391	−61.0	6.1×10^{-3}	
$[BF_3]$ = 0.529	−69.8	9.3×10^{-3}	
	−78.0	1.2×10^{-2}	

[a] Calculated from the line half-widths (δ_f); $1/\tau = \pi(\delta_f - \delta_{f0})$ where δ_{f0} is the line width in the absence of exchange.

With more than one equivalent of boron trifluoride, the fluorine resonance shifted markedly as the sample composition was varied. At low temperatures, the fluorine resonance broadened and eventually split to give two resonances. From analysis of the line shapes at the coalescence temperature, the preexchange lifetimes of the fluorines were determined. These results are presented in Table IV.

Discussion

Most authors seem to agree that the primary interaction between methanol and boron trifluoride is formation of the Lewis acid–Lewis base adduct, $BF_3 \cdot CH_3OH$. That formation of this single adduct is not the only occurrence on mixing these two species becomes clear upon examination of composition *vs.* chemical shift diagrams. In Figure 1 the chemical shift of the methoxyl resonance is plotted *vs.* the relative amount of methanol. A notable break in this curve occurs at a 2:1 ratio of methanol to boron trifluoride. As the proportion of methanol is increased, the methoxyl group shift appears to be insensitive to composition up to one equivalent of methanol. At a composition near one equivalent of methanol, this resonance begins to shift upfield. This upfield shift continues up to two equivalents of methanol. At two equivalents of methanol this peak again becomes insensitive to concentration. When just more than one equivalent of methanol has been added, a second methoxy resonance appears; with increasing methanol concentration, this peak shifts progressively toward the pure methanol resonance position.

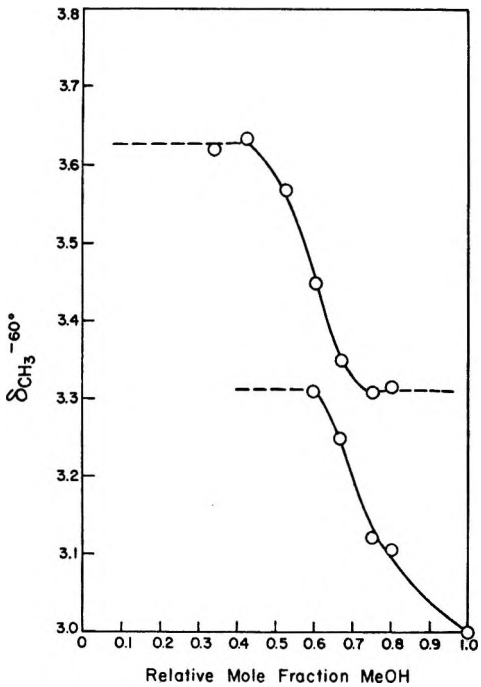

Figure 1. Methoxyl chemical shift (in ppm) as a function of the relative mole fraction of methanol for various mixtures of methanol and boron trifluoride in sulfur dioxide.

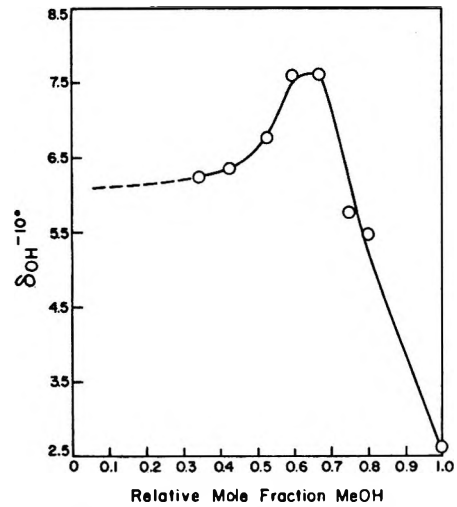

Figure 2. Hydroxyl chemical shift (in ppm) as a function of the relative mole fraction of methanol for various mixtures of methanol and boron trifluoride in sulfur dioxide.

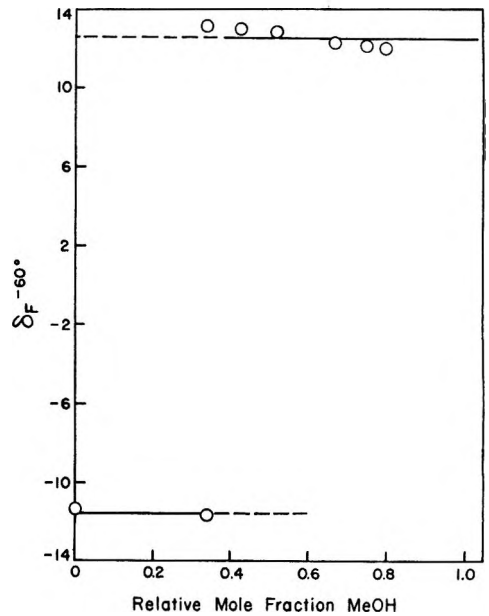

Figure 3. Fluorine chemical shift (in ppm) as a function of the relative mole fractions of methanol for various mixtures of methanol and boron trifluoride in sulfur dioxide.

The combination of these observations seems to require four distinct methoxyl containing species. Two of these can be readily identified as CH_3OH (δ_{CH_3} 3.00 ppm) and $CH_3OH \cdot BF_3$ (δ_{CH_3} 3.62 ppm). The chemical shift of the other two species which are present at intermediate concentrations appear to be nearly identical: δ_{CH_3} 3.30 and δ_{CH_3} 3.32 ppm.

The dependence of the chemical shift of the hydroxyl resonance upon methanol concentration is presented in Figure 2. Up to one equivalent of methanol, the chemical shift of the hydroxyl group is not affected by increasing methanol concentration. At a mole ratio of 1:1, the hydroxyl resonance begins to shift downfield and reaches a maximum downfield shift at a mole ratio of 2:1. As the methanol concentration is further increased, the hydroxyl resonance shifts monotonically towards that for pure methanol. These observations suggest that three hydroxyl containing species occur in these solutions. One of these species is readily identified as CH_3OH (δ_{OH} 2.6 ppm) and another as the monocomplex, $CH_3OH \cdot BF_3$ (δ_{OH} 6.4 ppm).

The dependence of the fluorine resonance position upon relative methanol concentration as shown in Figure 3 is far less informative. In addition to uncomplexed BF_3, only one additional fluorine resonance for the other fluorine containing species seems to occur. The chemical shift of this fluorine resonance shifts by about 0.7 ppm on going from 1 to 4 equivalents of methanol.

Two types of interaction of methanol with the 1:1 adduct, $BF_3 \cdot CH_3OH$, have been proposed. Based on analogy with the reported formation of 2:1 amine–boron complexes,[15] formation of the dimethanol complex (equation 1) has been proposed.[11] If this species is formed, then

$$CH_3OH + BF_3 \cdot CH_3OH \rightleftarrows BF_3 \cdot (CH_3OH)_2 \quad (1)$$

our results require that one of the bound methanols (δ_{CH_3} 3.30 ppm) be capable of rapid exchange with bulk methanol and the other (δ_{CH_3} 3.32 ppm) be capable of exchange with the monocomplex. A dicom-

(15) H. C. Brown, P. F. Stehle, and P. A. Tierney, *J. Amer. Chem. Soc.*, **79**, 2020 (1957).

Table V: Chemical Shifts for Methanol–Boron Trifluoride in Sulfur Dioxide

Assigned structure	Chemical shift[a] δ_{CH_3}[b]	δ_{CH_3}	δ_{OH}	$\delta_{^{19}F}$[c]
CH_3OH	3.33	3.00	2.6	...
$CH_3OH_2^+$	3.76	3.30	7.7	...
$CH_3OBF_3^-$	3.58	3.32	...	12.2
$CH_3OH \cdot BF_3$	3.91	3.62	6.4	12.9

[a] In ppm downfield from tetramethylsilane. [b] Reference 17b. [c] In ppm downfield from perfluorocyclobutane.

ppm to lower field than the ones which we have determined. As a chemical shift reference they added tetramethylsilane to the sulfur dioxide solution; our results were obtained using an internal sealed capillary containing tetramethylsilane. Even after this correction, the methyl chemical shift they report for $CH_3OH_2^+$ is 0.2 ppm to lower field. To obtain this result, data at 0.6 mole ratio BF_3:MeOH was extrapolated up to 1.0 mole ratio.

Assuming that the equilibrium constants for formation of both the mono- and dicomplex are large, the

Table VI: Calculated and Observed Nmr Spectra for Methanol–Boron Trifluoride Samples in Sulfur Dioxide at −60°

Sample composition, M $[CH_3OH]_0$	$[BF_3]_0$	% of methyl area in low-field peak obsd[a]	calcd[f]	Averaged peak positions,[b] ppm High-field methoxyl obsd	calcd[c]	Low-field methoxyl obsd	calcd[d]	^{19}F obsd	calcd[e]
0.762	0.190	17	20	3.10	3.10	3.30	3.33	12.0	12.2
0.689	0.231	23	33	3.11	3.15	3.30	3.33	12.2	12.2
0.648	0.319	41	49	3.25	3.29	3.34	3.33	12.3	12.2
0.567	0.385	60	68	3.31	3.30	3.44	3.46	...	
0.327	0.325					3.57	3.62	12.9	12.9
0.391	0.529					3.63	3.62	7.22	7.26
0.320	0.615	1.0[g]	1.0[g]			3.62	3.62	2.05	2.05

[a] From the ratio of areas of high-field to low-field methoxyl absorptions. [b] Relative to external tetramethylsilane for the methoxyl resonances; relative to external octafluorocyclobutane for the fluorine resonances. [c] $\delta_{calcd} = (n_{CH_3OH} \cdot 3.00 + n_{CH_3\overset{+}{O}H_2} \cdot 3.30)/(n_{CH_3OH} + n_{CH_3\overset{+}{O}H_2})$. [d] $\delta_{calcd} = (n_{\overline{BF_3 \cdot CH_3O}} \cdot 3.32 + n_{BF_3 \cdot CH_3OH} \cdot 3.62)/(n_{BF_3 \cdot CH_3OH} + n_{CH_3\overset{+}{O}H_2})$. [e] $\delta_{calcd} = (n_{BF_3} \cdot -11.7 + n_{BF_3 \cdot CH_3OH} \cdot 12.9 + n_{\overline{BF_3CH_3O}} \cdot 12.2)/(n_{BF_3} + n_{BF_3CH_3OH} + n_{\overline{BF_3CH_3O}})$. [f] $[1 - ([CH_3OH]_0 - [BF_3]_0)/[CH_3OH]_0] \times 100\%$. [g] Ratio of areas of high-field to low-field fluorine absorptions; Calcd value is $([BF]_0[CH_3OH]_0)/[CH_3OH]_0$.

plex containing equivalent methanol moieties[11] cannot be accommodated by the results.[16]

The second proposed type of interaction, equation 2, recognizes the strong acid character of the monocomplex.[17] In this reaction

$$CH_3OH + BF_3 \cdot CH_3OH \rightleftharpoons CH_3\overset{+}{O}H_2 + \overline{B}F_3OCH_3 \quad (2)$$

methanol behaves as a base and forms a salt. The formation of the conjugate base of the 1:1 adduct (δ_{CH_3} 3.32 ppm) and the conjugate acid of methanol (δ_{CH_3} 3.30, δ_{OH} 7.7 ppm) would lead to two additional methoxyl and one additional hydroxyl resonance as required. The ion association indicated by equation 3 can also provide a basis for accounting for the observations since

$$(BF_3 \cdot CH_3OH) \cdot CH_3OH \overset{K_3}{\rightleftharpoons} \overset{-}{B}F_3CH_3O + \overset{+}{C}H_3OH_2 \quad (3)$$

our results would be completely insensitive to the magnitude of the dissociation constant, K_3.

On the basis of methyl chemical shifts alone, Gillespie and Hartman[17b] have arrived at similar conclusions. Their results differ in two important respects. All the chemical shifts they report are 0.3

chemical shifts of Table V were obtained. These have then been used to calculate averaged chemical shifts for methanol plus its conjugate acid and the averaged shift for the monocomplex plus its conjugate base for each sample composition. The calculated and observed values are presented in Table VI. These averaging processes require only a proton transfer from a species to its conjugate base and as expected are rapid on this time scale.[18] The good agreement between the calculated and observed values support the correctness of the chemical shift assignment and the assumption of the magnitude of the K's. Protonation of methanol and protonation of the conjugate base of the monocomplex produce comparable downfield methoxyl shifts of only ~0.3 ppm. Larger shifts might have been expected.

$$\delta_{CH_3\overset{+}{O}H_2} - \delta_{CH_3OH} = 0.3 \text{ ppm}$$

$$\delta_{CH_3OH \cdot BF_3} - \delta_{CH_3O\overline{B}F_3} = 0.3 \text{ ppm}$$

(16) This difficulty has been previously recognized.[12] Exchange of bulk methanol with both the monocomplex and the dicomplex leads to averaging of all the methoxyl resonances.

(17) (a) J. A. Nieuwland, R. R. Vogt, and N. L. Foohey, *J. Amer. Chem. Soc.*, **52**, 1018 (1930); (b) R. J. Gillespie and J. S. Hartman, *Can. J. Chem.*, **45**, 2244 (1967).

(18) E. Grunwald, A. Loewenstein, and S. Meiboom, *J. Chem. Phys.*, **27**, 630 (1957).

Two different mechanisms for the exchange of excess reagent with the complex have been suggested.[9,11] In addition to a mechanism involving direct displacement of BF_3 from the complex by BF_3, an exchange mechanism involving formation of BF_4^- and $CH_3\text{-}\overset{+}{O}H\cdot BF_2$ is consistent with the results. Our results do not offer a clear choice between these bimolecular mechanisms and the unimolecular dissociative mechanism.

In the presence of more than one equivalent of methanol, a different exchange reaction is required. For samples containing more than one equivalent of methanol, two methoxyl resonances were observed at the low temperature extreme (about $-80°$). The coalescence temperature for these methoxyl resonances increased with increasing methanol concentration. This dependence of the methoxyl lifetime on methanol concentration seems to indicate that only the monocomplex and not the conjugate base of the monocomplex is involved in the exchange reaction.

Measurement by nmr integration of the amount of complexed methanol has been reported to be less than that expected based on the amount of boron trifluoride added.[12] We have also observed that the measured relative area of the high-field to low-field methoxyl resonance is larger than that predicted based on the amount of boron trifluoride added. The small difference in the position of the methoxyl resonances may be the source of this difficulty. Measurement of the relative amounts of complexed and uncomplexed boron trifluoride was in accord with expectations.

Acknowledgment. Grants from the National Science Foundation for purchase of the nuclear magnetic resonance spectrometers used in this research are gratefully acknowledged. Support of this research by the Graduate School of the University of Southern California is sincerely appreciated.

Ultrasonic Absorption in Aqueous Solutions of Low-Molecular-Weight Polyamines

by Mostafa M. Emara, Gordon Atkinson,*[1] and Erwin Baumgartner

Department of Chemistry, University of Maryland, College Park, Maryland 20740 *(Received July 19, 1971)*

Publication costs borne completely by The Journal of Physical Chemistry

The absorption of 10–150 MHz ultrasonic waves in dilute aqueous solutions of ethylenediamine, diethylenetriamine, triethylenetetramine, and tetraethylenepentamine has been measured. An excess acoustic absorption has been observed in all cases with a frequency dependence characteristic of a single relaxation. From the dependence of the relaxation frequency on concentration and the dependence of the absorption amplitude on pH, it is deduced that the perturbation of the proton-transfer equilibrium

$$-RNH_2 + H_2O \underset{k_b}{\overset{k_f}{\rightleftharpoons}} -RNH_3^+ + OH^-$$

at a terminal amine group is the process responsible for the excess ultrasonic absorption. Values of k_f and k_b and the standard volume changes for this process are determined. A clear decreasing trend in k_b, which is diffusion-controlled, with increase in molecular weight is observed.

Introduction

A large amount of data has been accumulated on the equilibrium properties of amines, amides, polyamines, and amino acids in H_2O, but the knowledge of their dynamic properties in solution is limited. These compounds are known to undergo extremely fast proton-transfer reactions in dilute aqueous solutions. This fact delayed kinetic studies until the development of relaxation techniques.[2] The ultrasonic absorption properties of dilute aqueous solutions of some amines and amino acids have been studied in recent years.[2–6]

(1) Address correspondence to this author at the Department of Chemistry, The University of Oklahoma, Norman, Okla. 73069.

(2) M. Eigen and L. de Maeyer in "Technique of Organic Chemistry," Vol. VIII, S. Friess, E. Lewis, and A. Weissberger, Ed., 2nd ed, Interscience, New York, N. Y., 1963, Part II, Chapter XVIII.

The observed change of ultrasonic absorption with frequency could be fitted to a single relaxation and has been attributed to the perturbation of the proton-transfer equilibrium of the basic residues

$$-RNH_2 + H_2O \underset{k_b}{\overset{k_f}{\rightleftharpoons}} -RNH_3^+ + OH^- \qquad (1)$$

However, when the ultrasonic studies were extended to aqueous solutions of proteins, the importance of equilibrium (1) compared to conformational changes of the protein molecules remained an open question.[7-10]

In the present study, using the ultrasonic relaxation technique, we have looked at one of the dynamic processes present in dilute aqueous solutions of several low molecular weight polyamines: ethylenediamine (en), diethylenetriamine (den), triethylenetetramine (trien) and tetraethylenepentamine (tetraen). It is highly desirable to know the dynamic behavior of these compounds, since they are of importance in areas of chemistry such as coordination chemistry. In choosing the mentioned compounds, we were able to study the effect of varying the molecular weight on the rates of ion recombination. Also, the chosen low molecular weight amines allow the study of the transition from simple electrolytes to polyelectrolytes. Here we can compare the properties—kinetic in the present case—of this series with the properties observed in the structurally related polyelectrolyte, polyethyleneimine.[11-13]

Experimental Section

Solutions were prepared with deionized water. They were made up at the required concentrations by weight. The organic solutes en (Baker), den (Fisher), trien (Fisher), and tetraen (Eastman) were used without further purification. Measurements were usually made on freshly prepared solutions. Solutions measured more than 2 hr after preparation gave markedly more erratic results.

Sound Absorption Measurements. The absorption coefficient, α, which is defined by the equation $I_x = I_0 e^{-2\alpha x}$ in terms of intensities and distance, was measured in the range 10–150 MHz using a standard send-receive pulse apparatus.[14] The frequency was measured using the heterodyne beat method with a Hewlett-Packard 610 Signal Generator and a Gertsch FM-3R frequency meter. The accuracy of the measured absorption coefficient, α, was on the order of 2% for all frequencies and solutions except for 10 and 15 MHz. At these lower frequencies, where diffraction corrections must be made, the error in α ranged from 3 to 5%. The error in the fixed frequency velocity measurements was less than 0.1% for all solutions. The measurement cell was thermostatically jacketed at 25 ± 0.1° with a Forma constant temperature bath. A complete set of (α, f) data is available from one of the authors (GA) on request.

Sound Velocity Measurements. The sound velocity was determined by the "sing-around" technique[15] using a NUS Laboratory Velocimeter Model 6100, which works at a fixed frequency of 3.6 MHz, together with a Beckman Universal EPUT Meter Model 7350R. The temperature of the solutions was maintained constant to 0.1°.

Results and Their Analysis

The variation of α/f^2 with frequency has been measured at several concentrations for each of the solutes chosen in this work in the frequency range 10–150 MHz. The curves obtained, from which some typical examples are depicted in Figure 1, show the characteristic behavior due to a single chemical relaxation process, which can be described by

$$\alpha/f^2 = \frac{A}{1 + (f/f_r)^2} + B \qquad (2)$$

where α = absorption coefficient, f = measured frequency, B = background absorption due to relaxation processes above the frequency range being examined, A = amplitude factor of the relaxation, f_r = relaxation

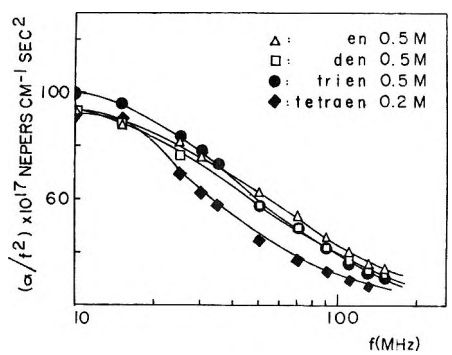

Figure 1. Ultrasonic absorption (α/f^2) *vs.* log f for aqueous solutions of en, den, trien, and tetraen at 25°.

(3) (a) M. J. Blandamer, D. E. Clarke, N. J. Hidden, and M. C. R. Symons, *Trans. Faraday Soc.*, **63**, 66 (1967); (b) M. J. Blandamer, N. J. Hidden, M. C. R. Symons, and N. C. Treloar, *ibid.*, **65**, 2663 (1969).

(4) R. S. Brundage and K. Kustin, *J. Phys. Chem.*, **74**, 672 (1970).

(5) K. Applegate, L. J. Slutsky, and R. C. Parker, *J. Amer. Chem. Soc.*, **90**, 6909 (1968).

(6) (a) R. D. White, L. J. Slutsky, and S. Pattison, *J. Phys. Chem.*, **75**, 161 (1971); (b) M. Hussey and P. D. Edmonds, *J. Acoust. Soc. Amer.*, **49**, 1309 (1971).

(7) R. Zana and J. Lang, *J. Phys. Chem.*, **74**, 2735 (1970).

(8) F. Dunn and L. W. Kessler, *ibid.*, **74**, 2736 (1970).

(9) L. W. Kessler and F. Dunn, *ibid.*, **73**, 4256 (1969).

(10) J. Lang, C. Tondre, and R. Zana, *ibid.*, **75**, 374 (1971).

(11) E. Baumgartner, M. Emara, and G. Atkinson, manuscript in preparation.

(12) S. Lapanje, J. Haebig, H. T. Davis, and S. A. Rice, *J. Amer. Chem. Soc.*, **83**, 1590 (1961).

(13) G. Thomson, S. A. Rice, and M. Nagasawa, *ibid.*, **85**, 2537 (1963).

(14) R. Garnsey and D. W. Ebdon, *ibid.*, **91**, 50 (1969).

(15) R. Garnsey, R. J. Boe, R. Mahoney, and T. A. Litovitz, *J. Chem. Phys.*, **50**, 5222 (1969).

frequency of the relaxation. The amplitude depends only on the normal coordinate thermodynamic parameters of the process and the relaxation frequency depends also on its kinetics. In our present case, all data could be satisfactorily fitted by a least squares technique to eq 2, the differences between observed and calculated relaxation curves being smaller than the experimental errors. The obtained relaxation parameters A_1, f_{r_1}, and B from this analysis are summarized in Table I.

Table I: Relaxation Parameters for the Ultrasonic Absorption of Dilute Aqueous Solutions of en, den, trien, and tetraen from Analysis for a Single Relaxation Frequency

Compound	Molarity C	$A_1 \times 10^{17}$, neper sec^2 cm^{-1}	$f_{r_1} \times 10^{6}$, sec^{-1}	$B \times 10^{17}$, neper sec^2 cm^{-1}
en	0.05	74.8 ± 2.7	19.9 ± 1.1	22.6 ± 1.2
	0.10	69.7 ± 1.7	31.7 ± 1.6	21.5 ± 1.0
	0.30	70.7 ± 1.3	44.5 ± 2.0	24.7 ± 1.7
	0.50	67.4 ± 2.3	53.7 ± 4.4	26.4 ± 2.4
	1.0	62.7 ± 1.9	86.0 ± 4.6	22.8 ± 2.2
den	0.054	100.4 ± 12.2	15.8 ± 1.6	21.4 ± 1.4
	0.116	78.2 ± 2.8	24.8 ± 1.7	22.4 ± 1.3
	0.25	77.2 ± 2.7	35.6 ± 2.9	25.0 ± 2.2
	0.50	70.4 ± 2.0	45.4 ± 3.0	25.8 ± 1.8
trien	0.05	96.5 ± 11.1	13.2 ± 1.8	22.7 ± 1.5
	0.11	74.2 ± 3.7	23.0 ± 2.1	23.6 ± 1.5
	0.20	83.6 ± 1.4	28.0 ± 0.9	23.5 ± 0.7
	0.50	78.2 ± 1.0	43.4 ± 1.3	25.5 ± 0.9
tetraen	0.05	96.3 ± 6.4	13.8 ± 1.1	22.7 ± 1.0
	0.063	62.1 ± 5.0	20.7 ± 2.2	22.7 ± 1.1
	0.10	74.2 ± 0.7	23.9 ± 0.4	22.4 ± 0.2
	0.159	85.9 ± 5.1	26.0 ± 2.3	24.0 ± 1.5
	0.20	77.6 ± 2.2	31.0 ± 1.8	23.7 ± 1.4

The calculated relaxation frequencies f_{r_1} increases with an increase in amine concentration. The B values are all close to the value for water at 25°.[16] This indicates that there are no relaxation processes sensitive to ultrasound at frequencies higher than those experimentally accessible (>150 MHz).

Discussion

We have shown in the above section that the ultrasonic absorption data are fitted well within the experimental errors by a single relaxation. Our next task is to quantitatively account for the observed relaxation. The fact that the relaxation frequencies obtained from the fit for the same compound are concentration dependent (see Table I) seems to exclude the possibility of structural relaxation in our frequency range. As we pointed out in the Introduction, a proton-transfer reaction is known to take place in dilute aqueous solutions of amines. It is justified then to assume that the observed relaxation is due to the perturbation of a chemical equilibrium, and further, that it is a one-step equilibrium similar to the one represented by eq 1. We shall therefore analyze the obtained relaxation parameters in terms of the proton-transfer equilibrium shown in eq 1.

When a relaxation expression based on eq 1 was used for data analysis, neglecting the activity coefficients of the various species, the experimental results fitted reasonably well. But the quotients of the forward and reverse rate constants were found to be in better agreement with the independently determined dissociation constants[17] when activity coefficients were included. The Davies[18] equation (3) was used to calculate the activity coefficients of the species

$$-\ln \gamma_{\pm} = A[\sqrt{I}/(1 + \sqrt{I}) - 0.3I] \qquad (3)$$

where I is the ionic strength, $\gamma_{\pm}$ is the mean activity coefficient, and A a constant (0.221 at 25°). Equation 4 relates the relaxation time to the rate constants and the concentrations of the species involved in eq 1 taking into consideration their activity coefficients

$$1/\tau = 2\pi f_r = k_b^0 \gamma_{\pm}^2 [OH^-]\left(2 + \frac{\partial \ln \gamma_{\pm}^2}{\partial \ln [OH^-]}\right) + k_f^0 \qquad (4)$$

where τ is the relaxation time, k_b^0 and k_f^0 are the rate constants at zero ionic strength and the other symbols have their usual meaning. This relationship can be easily obtained using the standard treatment for chemical relaxations.[2] The concentration of the hydroxide ion can be calculated using the dissociation constant of the first terminal protonated amine group, K, for each compound,[17] eq 5

$$K = a^2C/(1 - a) \qquad (5)$$

where a is the degree of dissociation and C the stoichiometric concentration of the amine.

Figures 2 and 3 show the plot of τ^{-1} *vs.* $\gamma_{\pm}^2[OH^-](2 + (\partial \ln \gamma_{\pm}^2/\partial \ln [OH^-]))$ for en, den, trien, and tetraen at various concentrations. The fit is reasonably good and it is clear from all the figures that a linear behavior holds, as required by eq 4. It should be mentioned, however, that this linearity does not hold at concentrations higher than 1 M for en, 0.5 M for den and trien and 0.25 M for tetraen. A similar behavior was reported by Blandamer, *et al.*, for dilute aqueous solutions of diethylamine.[3a] It is also interesting to note that such deviation is observed even after correcting for the activity coefficients. Possible explanations have been advanced by Blandamer, *et al.*,[3] but we will not attempt to go into details about this particular point. The reasons are unclear at this date and we are mainly interested with the low concentration range.

(16) J. M. Pinkerton, *Proc. Phys. Soc. London, Sect. B*, **62**, 286 (1949); *Nature*, **160**, 128 (1947).

(17) D. D. Perrin, "Dissociation Constants of Organic Bases in Aqueous Solution," Butterworths, London, 1965.

(18) J. N. Butler, "Ionic Equilibrium. A Mathematical Approach," Addison-Wesley, Reading, Mass., 1964.

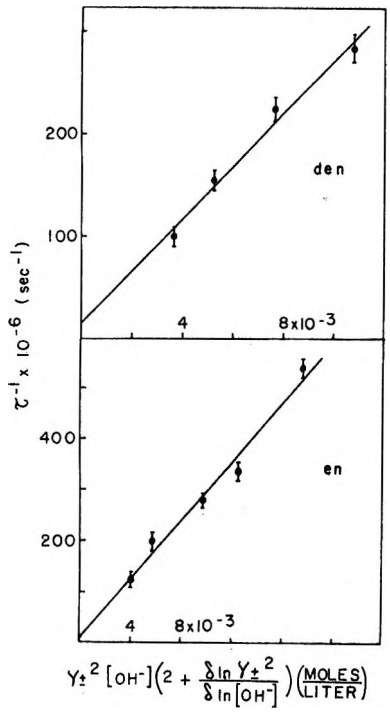

Figure 2. Concentration dependence of relaxation frequency according to eq 4: lower part, en; upper part, den.

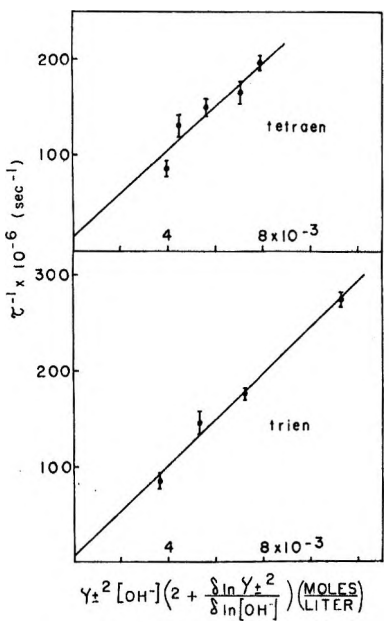

Figure 3. Concentration dependence of relaxation frequency according to eq 4: lower part, trien; upper part, tetraen.

The forward and reverse rate constants in eq 1 were obtained from the intercept and the slope, respectively, Figures 2 and 3. A standard least squares method was used in evaluating both the intercept and the slope. The solid lines shown in Figures 2 and 3 are the "best fit" slopes. The obtained rate constants and the dissociation constants K calculated from them are reported in Table II, together with the calculated values

Table II: Derived Parameters for the Process Represented by Eq 1

Compound	$k_b^0 \times 10^{-10}$, $sec^{-1}\ M^{-1}$	$k_f^0 \times 10^{-7}$, sec^{-1}	$K \times 10^4$, M	ΔV, cm^3/mol
en	2.87 ± 0.12	1.1 ± 0.7	3.8 ± 2.5	25.5 ± 2.0
den	2.56 ± 0.08	1.5 ± 0.9	6.0 ± 3.2	25.5 ± 2.0
trien	2.39 ± 0.10	0.4 ± 0.35	1.8 ± 1.6	25.0 ± 2.0
tetraen	2.27 ± 0.10	1.3 ± 1.0	5.8 ± 5.2	25.0 ± 2.0

of the standard volume changes ΔV for the process represented by eq 1 (see below).

For the process represented by eq 1 A_1 (eq 2) is given by

$$A_1 = \frac{\pi \rho c_0 \bar{V}^2 RT\Gamma}{f_r}\left[\frac{\beta \Delta H}{C_P RT} - \frac{\Delta V}{\bar{V}RT}\right]^2 \qquad (6)$$

where ρ is the density, c_0 the velocity of sound, $\bar{V}$ the volume per mole of solution, β the coefficient of thermal expansion, C_P the molar heat capacity at constant pressure, and ΔH and ΔV the enthalpy and volume changes for the process in question. Γ is given in terms of the molar concentrations of the reactants by eq 7.

$$\Gamma = \left(\frac{1}{[OH^-]} + \frac{1}{[RNH_3^+]} + \frac{1}{[RNH_2]}\right)^{-1} \qquad (7)$$

The previously measured enthalpy change for the process represented by eq 1 is 1.3 kcal/mol and the volume change is reported as 20–30 cm^3/mol. In aqueous solutions at room temperature, where β is relatively small, neglect of the first term in the square brackets in eq 6 alters the calculated value of ΔV by less than 2%. Equation 6 can then be written in the following form

$$Ac_0 f_r = \frac{\pi \Gamma}{\gamma_s RT}(\Delta V)^2 = \frac{\pi ca(1-a)}{\gamma_s RT(2-a)}(\Delta V)^2 \qquad (8)$$

where γ_s is the adiabatic compressibility. A plot of $Ac_0 f_r$ *vs.* $ca(1-a)/(2-a)$ should, therefore, yield a straight line with intercept = 0, the slope being related to ΔV. This is indeed the observed behavior for these systems and the obtained values for ΔV are given in Table II.

It seems necessary at this point to make clear why the dissociation of only the first terminal group of the amines has been taken into account. The reason is obvious in the en case, where the second dissociation constant is three orders of magnitude smaller than the first one. In the cases of den, trien, and tetraen the situation is not as clear because the ratio of the first and the second dissociation constants is 12, 5, 7, respectively.[17] We have calculated the additional concentration of hydroxide ion taking into account the dissociation of the second terminal amine group and even in the most unfavorable case, trien, this concentration is smaller than 2% of the concentration from the dissociation of the first terminal group alone. From this fact and from

the overall good results obtained assuming only one dissociation, we can safely conclude that this assumption was reasonable, at least for a kinetic analysis. An additional fact supporting the correctness of this assumption is that a kinetic analysis of the reaction represented by eq 9 yielded a very poor fit and the obtained rate constants were completely unreasonable.

$$H_2N\text{-}R'\text{-}NH_2 + 2H_2O \underset{k_b}{\overset{k_f}{\rightleftharpoons}} H_3N^+\text{-}R'\text{-}NH_3^+ + 2OH^- \quad (9)$$

We wish to summarize at this point the facts which clearly favor the proposed mechanism represented by eq 1. The linear behavior observed at low concentrations when plotting τ^{-1} *vs.* $\gamma_\pm^2[OH^-](2 + (\partial \ln \lambda_\pm^2/\partial \ln [OH^-]))$ (Figures 2 and 3) indicates that eq 4 holds, which in turn indicates that eq 1 correctly represents the observed process. Second, the linearity observed when calculating ΔV values and their actual value of 25 cm³/mol confirms that an equilibrium of the form shown in eq 1 is responsible for the ultrasonic absorption at low amine concentration. Also, the dissociation constants calculated from the kinetic analysis are in acceptable agreement with the ones obtained potentiometrically, taking into consideration the high error associated inevitably with k_f. The actual values of k_f and k_b are in the same range as the values obtained by other researchers studying different amines (Table II).[2,4-6] Another important factor emphasizing the above argument is the effect of pH on the ultrasonic absorption, which we shall discuss next.

Slutsky, *et al.*,[5,6] have shown that an investigation of the pH dependence of the ultrasonic absorption is another tool to determine if perturbation of an equilibrium represented by eq 1 is indeed the principal source of the observed attenuation. The dependence of the excess acoustic absorption on the equilibrium chemical composition of the solution is largely contained in Γ(eq 7). Expressing the concentration of the amine and its cation in terms of K, the equilibrium constant for eq 1, and the initial concentration of amine c, Γ becomes

$$\Gamma = \frac{[OH^-]Kc}{[OH^-]^2 + [OH^-]K + Kc} \quad (10)$$

From eq 2, 6 and 1 and values of τ the variation of α/f^2 with pH may be deduced. The calculated curve and the experimental points are shown for a 0.5 M solution of trien at 50 MHz in Figure 4. Again, the agreement is sufficiently good to nominate the perturbation of the proton-transfer equilibrium as the principal source of absorption.

An inspection of the k_b^0 values on Table II reveals that they decrease with an increase in molecular weight.

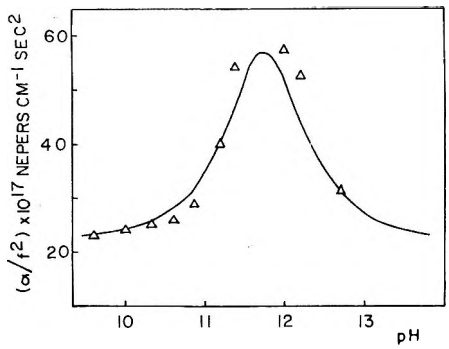

Figure 4. α/f^2 *vs.* pH at 50 MHz for trien at 25°. Key: Δ, experimental points; solid line; calculated behavior by means of eq 2, 6, and 10.

This trend can be explained by taking into account that the backward step in eq 1 is diffusion-controlled. Debye[19] has derived the following expression for this kind of reaction of ions in solution

$$k_{21} = \frac{4\pi N Z_A Z_B e_0^2 (D_A + D_B)}{\epsilon kT[\exp(Z_A Z_B e_0^2/\epsilon r_D kT) - 1]} \quad (11)$$

where N is Avogadro's number, e_0 is the electronic charge, Z_A and Z_B are the algebraic charges of the ions, ϵ is the dielectric constant of the solvent, D_A and D_B are the diffusion coefficients of the reacting ions, and r_D is an effective radius for reaction.

Since one of the ions, OH^-, in the diffusion reaction is constant along the series en to tetraen, the variation of k_{21} within the series will be determined mainly by the diffusion coefficient of the species RNH_3^+. This can be expected to decrease with increase in molecular weight. Rice, *et al.*,[13] have reported coefficients for the uncharged molecules en to tetraen for the corresponding bolaform ions and the fully charged ions. Although they did not measure the diffusion coefficients of the singly charged ions, the trends reported for the other species permit the safe conclusion that in this case too the diffusion coefficient will decrease with an increase in molecular weight. It follows that the observed trend in k_{21} with molecular weight is the expected one. The lack of diffusion-coefficient data for the singly charged ions hampers a more quantitative interpretation of the trend of our k_b^0 data with molecular weight in terms of eq 11.

Acknowledgments. The authors acknowledge the support of the Office of Naval Research under contract N00014-67-A-0239-0017. They gratefully acknowledge the computing support offered by the University of Maryland Computer Science Center under National Aeronautics and Space Administration Grant NsG-398.

(19) P. Debye, *Trans. Electrochem. Soc.*, **82**, 265 (1942).

The Far-Infrared Spectra of Tertiary Ammonium Salts[1a]

by John R. Kludt,[1b] Gilbert Y. W. Kwong,[1b] and R. L. McDonald*

Department of Chemistry, University of Hawaii, Honolulu, Hawaii 96822 *(Received July 7, 1971)*

Publication costs assisted by the National Science Foundation

The far-infrared spectra of several tertiary ammonium salts have been studied in the solid state and in solution. The solution spectra do not reflect the symmetry of the ion aggregates that form in some solvents. The spectra are characterized by two broad bands between 50 and 200 cm^{-1} whose frequencies are anion dependent. The small solvent and concentration effects can be explained if it is assumed that the higher frequency band is the cation–anion stretching mode, and that the lower frequency band is the N^+–H---X^- bending mode, of a hydrogen-bonded ion pair.

Although it has long been assumed that alkylammonium salts associate in nonpolar solvents to form ion aggregates, little if anything is known about the structure of these aggregates. The extensive use of long-chain tertiary and quaternary ammonium salts in solvent extraction has prompted several workers to study the association of these substances in aprotic solvents. However, with the exception of a few light scattering experiments, most investigations have dealt with the measurement of thermodynamic, conductance, or dielectric properties of the solutions.[2,3]

Several years ago Evans and Lo[4] reported the presence of a solute absorption band in the 100-cm^{-1} range for benzene solutions of tetrabutylammonium halides. They postulated that this was a cation–anion stretching mode (ν_σ) of a cyclic dimer (ion quadruplet) of distorted D_{2h} symmetry. To our knowledge, this postulate has not been investigated further.

The present work was undertaken with the hope of obtaining information concerning the structure of the aggregates of tertiary ammonium salts in solution. This class of salts was chosen for several reasons. They are readily soluble in a large number of aprotic solvents; their solution and extraction behavior have been of interest to us in the course of ion solvation studies;[5] and their aggregation equilibria appear to be simpler than those of the quaternary salts.

Experimental Section

Reagents. All solvents used were spectroquality. They were dried over CaH_2 for 24 hr and then distilled from the CaH_2 and stored in a drybox. Eastman tri-*n*-octylammonium chloride (Oc_3NHCl) was recrystallized once from ether and twice from *n*-hexane. Tri-*n*-octylammonium bromide (Oc_3NHBr) was prepared by bubbling HBr through a 0.01 *M* solution of Eastman tri-*n*-octylamine in *n*-hexane. When the solution became slightly pink, the mixture was cooled; the resulting crystals were dried in a vacuum desiccator for several days. Tri-*n*-octylammonium perchlorate (Oc_3NHClO_4) was made by equilibrating a 0.01 *M* solution of recrystallized Oc_3NHCl in ether with successive portions of an aqueous 1 *M* solution of $NaClO_4$ until both phases tested free of Cl^- with $AgNO_3$. The organic phase was evaporated to dryness, and the resulting greenish white crystals were dried in a vacuum desiccator for 72 hr. Triethylammonium chloride (Et_3NHCl) was obtained as a white precipitate when HCl was bubbled through an ether solution of triethylamine. It was recrystallized twice from 1-butanol then dried in a vacuum desiccator for 72 hr. Triethylammonium bromide (Et_3NHBr) was prepared in a manner similar to that for Oc_3NHBr. All solutions for spectral measurements were prepared in a drybox immediately before use.

Procedure. All spectra were obtained at ambient temperature with a R.I.I.C. FS-720 Fourier spectrometer equipped with a FTC 100/7 Fourier transform computer and wave analyzer. A Beckman far-infrared cell with polyethylene windows was used for liquids. The path length varied between 0.1 and 1.0 mm. Solid samples were mixed with powdered polyethylene, then pressed into pellets.

The vapor pressure studies were done at 25° on a Hewlett-Packard Model 302 vapor pressure osmometer using the techniques recommended by the manufacturer. The standards were benzil in CCl_4 and naphthalene in chloroform.

Results

Typical spectra for Oc_3NHCl are shown in Figure 1.

(1) (a) Research supported in part by the Air Force Office of Scientific Research, U. S. Air Force under Grant No. AFOSR-68-1387; (b) NSF Undergraduate Research Participants.

(2) Y. Marcus and A. S. Kertes, "Ion Exchange and Solvent Extraction of Metal Complexes," Wiley-Interscience, New York, N. Y., 1969, pp 757–765, and the references contained therein.

(3) O. Levy, G. Markovits and A. S. Kertes, *J. Phys. Chem.*, 75, 542 (1971).

(4) J. C. Evans and G. Y. S. Lo, *ibid.*, 69, 3223 (1965).

(5) (a) C. V. Kopp and R. L. McDonald, "Solvent Extraction Chemistry," D. Dryssen, *et al.*, Ed., North-Holland Publishing Co., Amsterdam, 1967, pp 447–453; (b) R. E. Jones, Jr., Ph.D. Thesis, University of Hawaii, 1970.

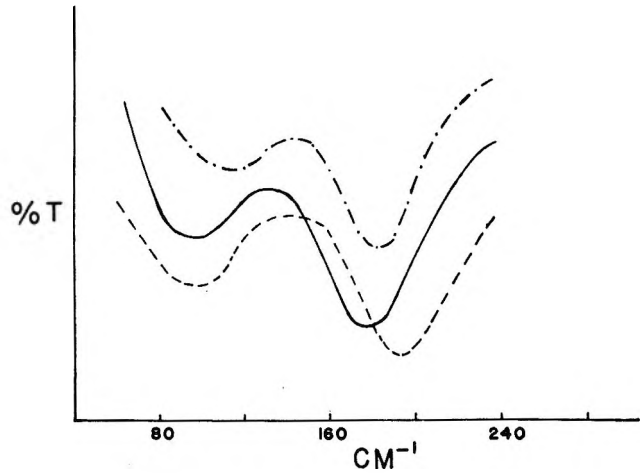

Figure 1. The far-infrared absorption bands of tri-*n*-octylammonium chloride: top curve, 0.050 *M* in $CHCl_3$; middle curve, solid; bottom curve, 0.045 *M* in CCl_4.

The spectra of all tertiary ammonium salts studied (except Oc_3NHNO_3) are characterized by two broad bands, the higher frequency band being more intense. Oc_3N shows no absorption in this region. Spectral data for various salts are tabulated in Table I. It is seen that the frequencies are anion dependent, but are essentially cation independent. Oc_3NHClO_4 exhibits only very weak absorption in either $CHCl_3$ or CCl_4. Bands could not be detected below 0.1 *M;* above that concentration broad weak bands were observed near 70 and 130 cm^{-1}.

Table I: Far-Infrared Absorption Bands of Tertiary Ammonium Salts

Salt	Solvent	Concentration, mol/l.	ν_{max}, cm^{-1} ν_1	ν_2
Oc_3NHCl	Solid	...	94 ± 2	178 ± 2
	CCl_4	0.045	98 ± 4	192 ± 3
		0.077	98 ± 4	190 ± 3
		0.11	96 ± 4	190 ± 3
		0.19	98 ± 4	186 ± 3
		0.21	98 ± 4	186 ± 3
	$CHCl_3$	0.027	114 ± 5	184 ± 3
		0.038	114 ± 5	182 ± 3
		0.050	114 ± 5	183 ± 3
		0.11	112 ± 5	183 ± 3
		0.19	110 ± 5	182 ± 3
	Cyclohexane	0.053	90 ± 8	198 ± 3
		0.11	90 ± 5	196 ± 3
		0.20	86 ± 5	194 ± 3
		0.40	86 ± 5	194 ± 3
Oc_3NHBr	Solid	...	70 ± 5	133 ± 3
Oc_3NHClO_4	Solid	...	66 ± 5	139 ± 3
Et_3NHCl	$CHCl_3$	0.031	110 ± 6	179 ± 3
		0.044	110 ± 6	179 ± 3
		0.052	110 ± 6	180 ± 3
		0.072	110 ± 6	180 ± 3
Et_3NHBr	$CHCl_3$	0.051	75 ± 8	133 ± 3
		0.098	72 ± 6	132 ± 3

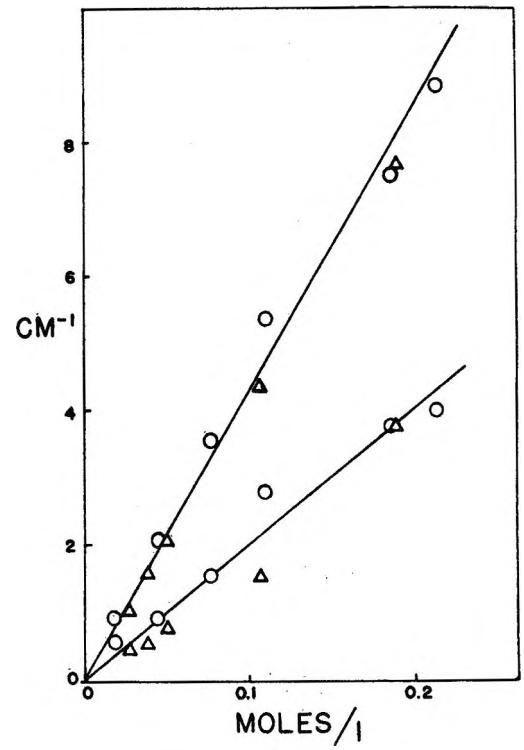

Figure 2. Plots of absorbance/cell path length *vs.* concentration for tri-*n*-octylammonium chloride in CCl_4, O, and $CHCl_3$, Δ. The top line is for the higher frequency bands, and the bottom line is for the lower frequency bands.

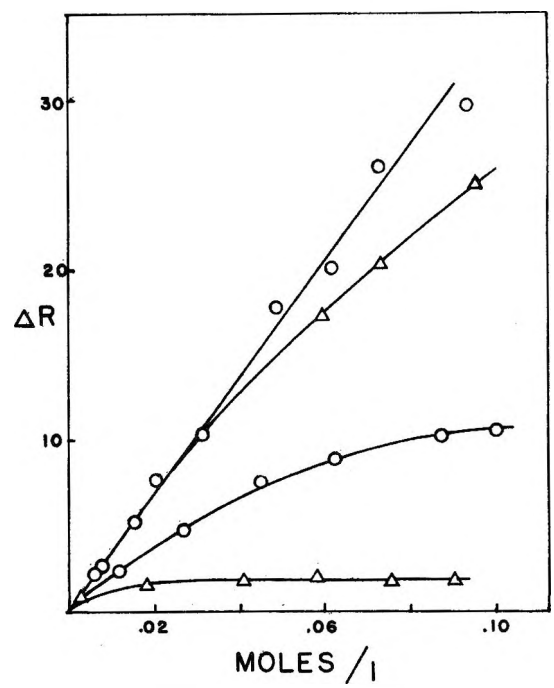

Figure 3. Vapor pressure osmometer data at 25° for tri-*n*-octylammonium chloride, O, and perchlorate, Δ, in $CHCl_3$ (upper curves) and CCl_4 (lower curves). The data for the references lie along the uppermost line.

Figure 2 is a Beer's law plot of the data for Oc_3NHCl in CCl_4 and $CHCl_3$. Both bands obey Beer's law within

the accuracy of the data, and their intensities are independent of the solvent.

Figure 3 shows plots of the data from the vapor pressure osmometer. Oc_3NHCl showed no deviation from dilute solution behavior in $CHCl_3$ and may be assumed to exist as simple ion pairs in this medium. In CCl_4, however, it deviates significantly from dilute solution behavior. Several workers have attributed this type of phenomenon to aggregation of ion pairs.[2] Based on this assumption, the degree of aggregation (*i.e.*, the ratio of the stoichiometric to the apparent concentration) was calculated for Oc_3NHCl in CCl_4 and Oc_3NHClO_4 in both CCl_4 and $CHCl_3$ at various concentrations. These results are tabulated in Table II.

Table II: Average Aggregation Numbers, $\bar{n}$, of Tri-*n*-octylammonium Salts at 25°

Salt	Solvent	Stoic. concn., mol/l.	$\bar{n}$
Oc_3NHCl	CCl_4	0.0051	1.70
		0.0117	1.86
		0.0269	2.01
		0.0454	2.05
		0.0623	2.37
		0.0868	2.99
		0.101	3.21
Oc_3NHClO_4	CCl_4	0.0027	1.96
		0.0050	2.50
		0.0180	4.62
		0.0407	9.04
		0.0584	11.1
		0.0755	16.8
		0.0901	21.8
	$CHCl_3$	0.0200	1.00
		0.0400	1.10
		0.0600	1.17
		0.0800	1.23
		0.100	1.28
		0.120	1.36

Discussion

There are differences in the band positions between the various solutions, but the main features of the spectra are identical. This is of particular interest when viewed in the light of the aggregation data for the salts. The suggestion of Evans and Lo[4] that the symmetry of quaternary salt aggregates in solution is important in determining the infrared absorptions associated with interionic motion does not apply to tertiary salts. A comparison of the spectra for monomeric Oc_3NHCl in $CHCl_3$ and aggregated Oc_3NHCl in CCl_4 (and cyclohexane) shows that neither the number of bands nor their intensities are appreciably affected by aggregation. Furthermore, the most highly aggregated salt, Oc_3NHClO_4, shows only very weak absorption.

There is little doubt that both of the bands arise from interionic vibrations. They are absent in Oc_3N and they are anion dependent. In view of the fact that fairly strong N–H$\cdots$Cl and N–H$\cdots$Br hydrogen bonds have been demonstrated for these trioctylammonium salts in CCl_4,[6] it is assumed that a contact (hydrogen bonded) ion pair is the basic vibrating unit. For the two anions, Br^- and ClO_4^-, the ratios of frequencies, ν_{Cl}/ν_X are *ca.* 1.3 for both bands. (Exception: It is closer to 1.5 for the low frequency band of the triethylammonium salts.) The reduced mass ratios, $(\mu_X/\mu_{Cl})^{1/2}$, are 1.4 for Oc_3NHBr, 1.6 for Oc_3NHClO_4, and 1.3 for Et_3NHBr. This implies that the H-bond force constant is anion independent, a somewhat surprising result for which we have no explanation. The cation effect is negligible; a consideration of masses alone predicts a small increase in frequency for the triethylammonium salts. This may be offset by an increased acidity for the Oc_3NH^+ ion.[7]

The frequency shifts associated with solvent and concentration, although small compared to the bandwidths, are nonetheless real. Using a variety of substituted ammonium salts, we have found that chloroform is the worst, and cyclohexane or CCl_4 the best solvents to use to resolve the two far-infrared bands.[8]

Let us look first at the ν_2 band of Oc_3NHCl. For solutions, it is consistently higher in frequency than the corresponding band in the solid salt. This same result was observed for the quaternary ammonium salts[4] and is probably due to increased interionic bond strengths in these solvents of low solvating power. The decrease in frequency with increasing concentration seen in cyclohexane and CCl_4 is likely due to a weakening of the hydrogen bond with aggregation. This latter effect was proposed by Keder and Burger[6] to explain their nmr data.

In $CHCl_3$ the concentration effect on ν_2 is absent, as expected in a medium where aggregation does not occur. However ν_2 is shifted to a significantly lower frequency. It is known that $CHCl_3$ hydrogen bonds to Cl^- in nonaqueous media.[9] This last fact can explain the effect of $CHCl_3$ on ν_2 if it is assumed that ν_2 is the interionic stretching mode, and that the formation of a ($---Cl^-\cdots HCCl_3$) hydrogen bond has the same effect on the cation–anion stretching frequency as does the formation of a ($\cdots H---Cl^-$) hydrogen bond on the N–H stretching frequency; *viz.* shift it to lower frequencies.[6]

The effect of $CHCl_3$ on ν_1 is noteworthy in that it shifts ν_1 to higher frequencies. When an R_3NH^+ and a Cl^- (or Br^-) combine to form a hydrogen-bonded ion pair, three translational degrees of freedom

(6) W. E. Keder and L. L. Burger, *J. Phys. Chem.*, 69, 3075 (1965).

(7) pK_a for several amines in 70% alcohol increases in the order $(hexyl)_3N < (pentyl)_3N < (butyl)_3N < (propyl)_3N$. L. Spialter and J. A. Poppulardo, "The Acyclic Aliphatic Tertiary Amines," Macmillan, New York, N. Y., 1965.

(8) G. Y. W. Kwong, B.S. Thesis, University of Hawaii, 1971.

(9) R. D. Green and J. S. Martin, *J. Amer. Chem. Soc.*, 90, 3659 (1968).

are converted into vibrational degrees of freedom, only one of which involves cation–anion stretching. The other two are deformations with respect to the hydrogen bond, sometimes called ν_β.[10] We have already assigned ν_2 to the stretching mode. It is well known that the deformation bands in NH_3 are shifted to higher frequencies upon hydrogen bonding.[10,11] As before, we make the reasonable assumption that a (– – –Cl⁻– – – $HCCl_3$) hydrogen bond has the same effect on the cation–anion deformation bands as does a (–H– – – –X) hydrogen bond on the H–N–H deformations. Thus we tentatively assign ν_1 to the degenerate N–H– – – –Cl deformation or bending modes, ν_β.

It is interesting to speculate why ν_2 is at lower (and ν_1 at higher) frequency in CCl_4 than in cyclohexane, in spite of the fact that one finds greater aggregation in the latter solvent.[12] This is probably due to an interaction between CCl_4 and ions, which is, of course, why the ions are less aggregated in CCl_4. The nature of the CCl_4–ion interaction is not known; it has been suggested that CCl_4 forms weak complexes with both acids and bases.[13] The effect of CCl_4 on the spectra is similar to, but less pronounced than $CHCl_3$, thus it is tempting to suggest that CCl_4 interacts with the anion. We are unaware of any convincing evidence to support this suggestion.

To summarize, the far-infrared spectra of tertiary ammonium halides do not reflect the symmetry of the ion quadruplets (or higher aggregates) that form in solution. The spectra can be understood in terms of a simple, hydrogen-bonded cation–anion pair which can undergo additional interactions with either other ion pairs or the solvent. These latter interactions have a relatively small effect on band frequencies and no appreciable effect on band intensities.

Acknowledgment. We wish to thank NSF for partial support of the purchase of the Fourier spectrophotometer under Grant No. GP 8639.

(10) G. C. Pimental and A. L. McClellan, "The Hydrogen Bond," W. H. Freeman, San Francisco, Calif., 1960.

(11) K. Nakamoto, "Infrared Spectra of Inorganic and Coordination Compounds," Wiley, New York, N. Y., 1963.

(12) A. S. Kertes and G. Markovits, *J. Phys. Chem.*, 72, 4202 (1968).

(13) F. L. Slejko, R. S. Drago, and D. G. Brown, Preprint, 1971.

Unimolecular Rate Theory Test in Thermal Reactions[1]

by W. Forst

Department of Chemistry, Université Laval, Québec 10, Canada *(Received August 11, 1971)*

Publication costs assisted by the National Research Council of Canada

The limiting high-pressure unimolecular rate constant k_∞ in thermal systems can be considered as the Laplace transform of the detailed rate constant, or specific dissociation probability, $k(E)$ (E = internal energy). If k_∞ is known from experiment as a function of temperature in the form $k_\infty = A_\infty \exp(-E_\infty/kT)$, $k(E)$ can be obtained by inversion. Using three actual examples, the inversion procedure is exploited to show that k_∞ contains sufficient information for a test of unimolecular rate theory that requires only the knowledge of the molecular properties of the reactant but *not* those of the transition state. Since there are no parameters to adjust, this test, in a thermal system, is therefore more significant than the more usual speculative curve-fitting. Some limitations of the test are noted, and it is pointed out that a more elaborate test cannot be done without additional assumptions; as an example, it is shown that the correct limiting low-pressure rate constant cannot be obtained by this procedure.

Introduction

In thermal systems, experimental data on the temperature dependence of k, the unimolecular rate constant, are usually presented in the familiar Arrhenius form $k = Ae^{-E_a/kT}$, where E_a is the so-called Arrhenius (or experimental) activation energy and A is a temperature-independent parameter. As a consequence of activation by collisions, the rate constant k is a decreasing function of pressure, and only in the limit of high pressures ($p \to \infty$) do we have, in a gas-phase reaction, the pressure-independent relation

$$k_\infty = A_\infty \exp(-E_\infty/kT) \qquad (1)$$

usually obtained by suitable extrapolation of experimental data.[2] Since at all finite pressures $k < k_\infty$, the

(1) Calculations done with financial assistance from the National Research Council of Canada.

gas-phase thermal unimolecular rate constant exhibits a characteristic fall-off with pressure which is useful for comparing theory with experiment.

We propose to show that eq 1 contains sufficient information for a test of unimolecular rate theory that requires only the knowledge of the molecular properties of the reactant but *not* those of the transition state; there being thus no parameters to adjust, this test is therefore more significant than the traditional speculative curve-fitting. However, inasmuch as the information content of eq 1 is limited, the scope of the test is also limited, and it is shown that more elaborate testing requires additional assumptions, or additional (nonthermal) data. The treatment is also useful to delineate more clearly just what sort of information is, or is not, obtainable from purely thermal data.

The High-Pressure Rate as a Laplace Transform

If it is assumed, as in the Rice–Ramsperger–Kassel–Marcus (RRKM) theory, that a molecule does not decompose unless it has accumulated internal energy $E \geqslant E_0$, where E_0 is threshold or critical energy for reaction, the specific dissociation probability $k(E)$ is a function of energy only; in particular, $k(E) = 0$ if $E \leqslant E_0$. It can be shown[3a] that $k_\infty = \langle k(E)\rangle_B$, where $\langle \ldots \rangle_B$ represents an average over a Boltzmann (or thermal) distribution of energies, characteristic of temperature T. Writing out the average explicitly, we have

$$k_\infty = \frac{\int_0^\infty k(E)N(E)e^{-E/kT}\mathrm{d}E}{\int_0^\infty N(E)e^{-E/kT}\mathrm{d}E} \qquad (2)$$

where $N(E)$ is the density of states (number of states per unit energy) of the reactant molecule, and the denominator in eq 2 is its partition function Q. Although the limits of integration in the numerator are $(0, \infty)$, the integrand is in fact zero for $0 \leqslant E \leqslant E_0$. At finite pressures, $k(E)$ in eq 2 is reduced[3a] by $1/(1 + k(E)/Zp)$, where Z is collision number and p is pressure, so that the general-pressure rate is

$$k = \frac{1}{Q}\int_0^\infty \frac{k(E)}{1 + \dfrac{k(E)}{Zp}} N(E)e^{-E/kT}\mathrm{d}E \qquad (3)$$

Suppose now that available thermal experimental data in a gas-phase reaction consist, as is often the case, of (i) the temperature dependence of the high-pressure rate constant in the form of eq 1 (*i.e.*, A_∞ and E_∞ are known); (ii) a part, or even most, of the fall-off with pressure of k at least at one temperature. The question we now ask is the following: what deductions can be made about E_0 and $k(E)$ on the basis of such experimental data? We assume that all molecular parameters of reactant (except E_0) are known from nonkinetic information.

Equating experimental and theoretical expressions for k_∞, we have from eq 1 and 2

$$\int_0^\infty k(E)N(E)e^{-E/kT}\mathrm{d}E = QA_\infty e^{-E_\infty/kT} \qquad (4)$$

We may now observe that the LHS of eq 4 is the Laplace transform of the product function $\mathrm{f}(E) = k(E)N(E)$. If we assume that the experimental relation 1 is exact and is valid for all temperatures, we may obtain $\mathrm{f}(E)$ as a function of energy by inversion, with $s = 1/kT$ as the inversion parameter

$$\mathrm{f}(E) = \mathfrak{L}^{-1}\{Q(s)A_\infty e^{-E_\infty s}\} \qquad (5)$$

where we write $Q(s)$ for Q to indicate that the partition function Q also depends on s. Since we have[4a] $\mathfrak{L}^{-1}\{Q(s)\} = N(E)$, eq 5 represents merely a shift in the zero of energy in $N(E)$ and the result of the inversion is

$$\mathrm{f}(E) = A_\infty N(E - E_\infty)H(E - E_\infty) \qquad (6)$$

where $H(x)$ is the Heaviside step function

$$H(x) = 0,\ x < 0$$
$$H(x) = 1,\ x > 0$$

so that

$$k(E) = \frac{A_\infty N(E - E_\infty)}{N(E)} \quad (E > E_\infty) \qquad (7)$$
$$= 0 \quad (E < E_\infty)$$

a result which may be verified by substituting back into eq 4. The uniqueness theorem[4b] of the Laplace transformation ensures that there is indeed only one function $k(E)N(E)$ which has the transform given by eq 4. Thus a function, $k(E)$, is recovered from its average, a process sometimes referred to as deconvolution. Therefore, if eq 1 is taken at face value, the answer to our question is (a) the critical energy E_0 is given by E_∞; (b) the energy dependence of $k(E)$ is given by eq 7.

The perils of taking eq 1 at face value are, of course, that eq 1 is true only approximately. First of all k_∞ is not an experimental observable and must be obtained by extrapolation, a procedure that inevitably introduces some uncertainty. Second, although E_∞ and A_∞ must be in principle temperature dependent, they are considered in eq 1 as temperature-independent constants, since generally the accuracy of gas phase rate measurements is such that the temperature dependence of A_∞ and E_∞ is lost in experimental error and only the gross overall temperature dependence, corresponding to a

(2) See, for example, I. Oref and B. S. Rabinovitch, *J. Phys. Chem.*, **72**, 4488 (1968).

(3) (a) O. K. Rice, "Statistical Mechanics, Thermodynamics and Kinetics," W. H. Freeman & Co., San Francisco, Calif., 1967, p 556; (b) p 558, eq 1.8.

(4) (a) W. Forst, Z. Prášil, and P. St. Laurent, *J. Chem. Phys.*, **46**, 3736 (1967); (b) for general aspects of the Laplace transformation, see, for example, D. V. Widder, "The Laplace Transform," Princeton University Press, Princeton, N. J., 1941, Chapter II.

constant term in the exponential divided by kT, is detectable. Finally, the validity of eq 1 is usually established only over a small temperature interval (typically 100° or less), although a few systems exist where it has been shown with the help of shock tube technique that eq 1 is reasonably satisfied over an interval of 1000–1500°; however this is still substantially less than an interval comprising "all temperatures," *i.e.*, 0 to ∞.

The combined effect of these uncertainties is that when E_∞ is used for threshold energy, it is afflicted by an error that is likely to be larger than the standard deviation of points on the usual Arrhenius plot ($\log k_\infty$ *vs.* $1/T$) would lead one to believe. Furthermore, because of the exponential relationship between E_∞ and A_∞ *via* eq 1, any error in E_∞ appears magnified in A_∞.

Thus eq 7, even though mathematically correct, is no better than the assumptions involved in treating eq 1 as if it were exact over the whole range of temperatures. Specifically, eq 7 contains the errors inherent in both A_∞ and E_∞; fortunately, the two errors tend to cancel out to some extent, because while the error in E_∞ affects A_∞ nearly exponentially, it appears in $N(E - E_\infty)$ roughly to the power n but in the *opposite* direction (recall[8] that classically $N(E)$ is proportional to E^n, where n is large, usually the total number of vibrational degrees of freedom less one). Nevertheless, since A_∞ and E_∞ are only approximate, the energy dependence of $k(E)$, as given by eq 7, is likewise only approximate. The remainder of this paper is devoted to showing that the approximation is good enough to sustain the test of a thermal system, but not of a system yielding more detailed information, as shown in the section dealing with threshold behavior.

It must be emphasized that eq 2 and 3, being purely theoretical expressions, are not considered as subject to error, in the sense that if the assumptions of the RRKM theory are correct, eq 2 and 3 apply exactly; if the assumptions are not correct, eq 2 and 3 do not apply at all. Similarly, eq 7 does not apply at all if the assumptions of the RRKM theory are incorrect, but, unlike eq 2 and 3, applies only approximately if the RRKM assumptions are correct because eq 7 makes use of imperfect experimental information.

If we wish to include centrifugal effects, *i.e.*, averaging over angular momenta, the theoretical rate in the RHS of eq 2 must be increased by a factor f_∞ which is calculable from the properties of the reactant.[5] The effect is then merely that A_∞ in eq 4–7 is replaced by A_∞' where $A_\infty' = A_\infty/f_\infty$, on the assumption that f_∞ is temperature-independent. This is true for unimolecular reactions in which there is an activation energy for the reverse reaction;[5b] for unimolecular fragmentation with no activation energy for the reverse association of fragments, f_∞ has a small negative temperature coefficient[5] ($-kT/3$ for neutral fragments) that is smaller than the likely error in E_∞ and therefore can be neglected. Thus with sufficient accuracy we have

$$k'(E) = \frac{A_\infty N(E - E_\infty)}{f_\infty N(E)} \quad (E > E_\infty) \qquad (7a)$$

$$= 0 \quad (E < E_\infty)$$

where $k'(E)$ still refers to a purely vibrational potential but is to be used in conjunction with eq 3′ which contains the appropriate corrections to make k' refer to an effective (vibrational + centrifugal) potential.

Equation 7 has been derived before[6] but has not been exploited further in unimolecular rate calculations.

Equation 7 as a Test of Unimolecular Rate Theory

The interesting aspect of eq 7 and 7a is that they involve the density of states $N(E)$ of the *reactant* molecule. On the RRKM model, degrees of freedom involved in $N(E)$ are those that participate in intramolecular energy transfer; these are the so-called active degrees of freedom and their assignment cannot be made entirely without ambiguity. The single assumption is usually made that all vibrational degrees of freedom, including internal torsion, are active, and that also the overall rotation about the symmetry axis in the case of the symmetric top is active.[7] The essential point is that with this one assumption the $N(E)$ of such states can be relatively easily calculated[8] from molecular parameters such as vibrational frequencies, moments of inertia and the like, all of which are available from *non-kinetic* information; thus the ambiguity that enters $N(E)$ is a relatively mild one, as is demonstrated further below in connection with Figure 3.

Inasmuch as the fall-off of k with pressure depends only on the energy dependence of $k(E)$, the test of unimolecular rate theory is complete (in a thermal system) when it is shown that the calculated energy dependence of $k(E)$ leads to the experimentally observed fall-off. In the present case, this entails numerical integration with respect to E using $k(E)$ of eq 7 in eq 3 and varying p.

Fall-off calculations including centrifugal effects are more involved since f_∞ drops somewhat with pressure.[5a] This can be taken into account by rewriting eq 3 in the form

$$k = \frac{f_0}{Q}\int_0^\infty \frac{(f_\infty/f_0)k'(E)}{1 + \dfrac{(f_\infty/f_0)k'(E)}{Zp}} N(E)e^{-E/kT}dE \qquad (3')$$

(5) (a) W. Forst, *J. Chem. Phys.*, **48**, 3665 (1968); (b) E. V. Waage and B. S. Rabinovitch, *Chem. Rev.*, **70**, 377 (1970).

(6) N. B. Slater, *Proc. Leeds Phil. Lit. Soc., Sci. Sect.*, **6**, 259 (1955); *Trans. Faraday Soc.*, **55**, 5 (1959); Eq 16 and 20 in F. P. Buff and D. J. Wilson, *J. Chem. Phys.*, **32**, 677 (1960); H. Labhart, *Chem. Phys. Lett.*, **1**, 263 (1967).

(7) W. Forst and P. St. Laurent, *Can. J. Chem.*, **45**, 3169 (1967).

(8) For a review of available methods, see W. Forst, *Chem. Rev.*, **71**, 339 (1971). Since $N(E)$ is the numerator of eq 7 or 7a it is required at energies from zero onwards, the method used for calculating $N(E)$ must be reasonably accurate at low energies. In the numerical integrations reported further below, the approximation $N(0) \sim 0$ was used, to circumvent extrapolation problems.

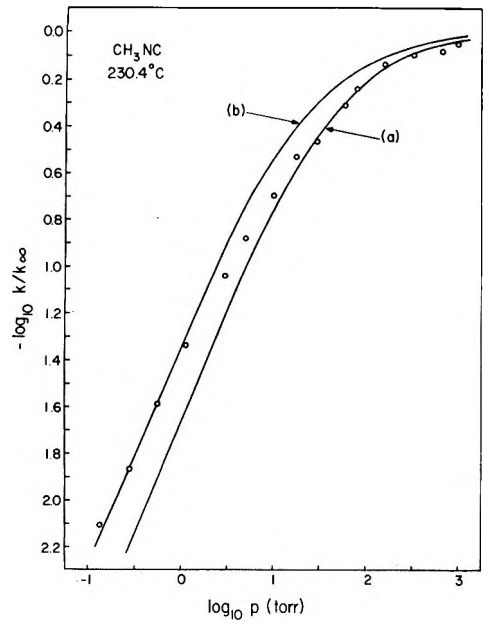

Figure 1. Pressure dependence of unimolecular rate constant for toermal isomerization of CH_3NC at 230.4°. Circles are experimental data of Schneider and Rabinovitch[9] (SR). Curve (a): Calculated from eq 3 and 7 using SR's data $A_\infty = 4.07 \times 10^{13}$ sec^{-1}, $E_\infty = 13{,}413$ cm^{-1}; vibrational frequenceis of CH_3NC as given by SR (ref 9, Appendix III, Table IV; grouped frequencies used). Curve (b): calculated by SR for the "300/600" model of transition state (*cf.* Figure 12 in F. W. Schneider, Ph.D. Thesis, University of Washington, 1962). Collision diameter $\sigma = 4.5$ Å used throughout.

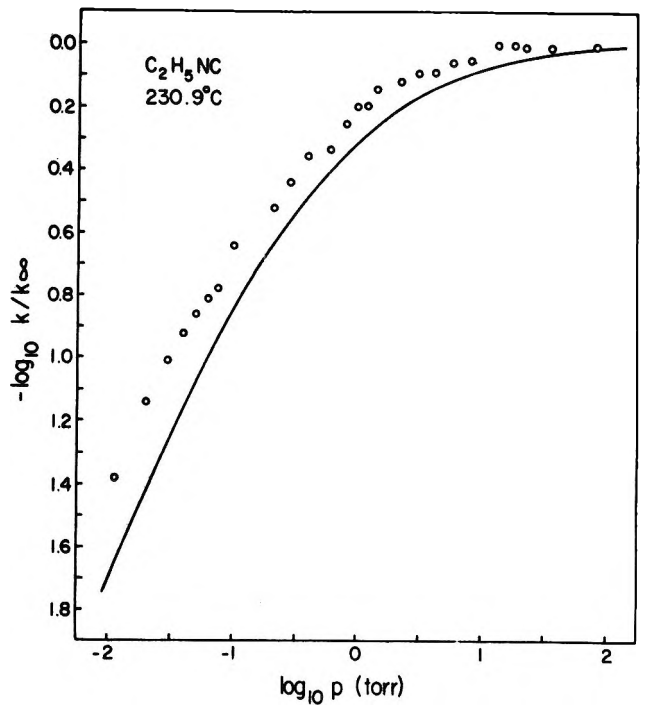

Figure 2. Pressure dependence of unimolecular rate constant for thermal isomerization of C_2H_5NC at 230.9°. Circles are experimental data of Maloney and Rabinovitch[10] (MR). Curve is calculated from eq 3 and 7 using MR's data $A_\infty = 7.76 \times 10^{13}$ sec^{-1}, $E_\infty = 13{,}469$ cm^{-1}; collision diameter $\sigma = 5$ Å. Vibrational frequencies of C_2H_5NC as given by MR (ref 10, Table VIII; grouped frequencies used).

where $k'(E)$ is given by eq 7a and f_0 is the low-pressure centrifugal correction factor ($f_0 < f_\infty$), likewise calculable from molecular parameters of the reactant.[5]

Results obtained from eq 7 and 3 are illustrated on two rather extensively investigated systems, the thermal isomerization of methyl isocyanide[9] and ethyl isocyanide.[10] Figures 1 and 2 show a comparison of experimental (circles) and calculated results (solid lines) for the two systems. Calculations of $N(E)$ were done using the method of steepest descents[11] in the harmonic oscillator approximation; anharmonicity is ignored but it can be shown[12] that in thermal systems this is a reasonably good approximation to the anharmonic $N(E)$. The agreement with experiment is seen to be quite good: the curvature of the calculated curves is about right, and calculated data are not too far displaced from experimental ones along the pressure axis, *i.e.*, the absolute pressure fit is not too bad.[13] Note that the effect of increased molecular complexity (and hence longer lifetime) of C_2H_5NC relative to CH_3NC is correctly rendered by the fall-off curve which in the former case lies at much lower pressures (compare abscissas of Figures 2 and 3).

Omitted in these calculations were centrifugal effects, the inclusion of which would reduce $k(E)$ by the factor f_∞, and, as a result, would shift the high-pressure end of the fall-off curve roughly by log f_∞ toward lower pressures. Note that the calculated curves in Figures 2 and 3 lie generally on the right (high-pressure) side of experimental data, as one would expect when centrifugal effects are not included. The shift required to bring experimental and calculated curves for C_2H_5NC into coincidence is roughly 0.25 log units, which implies $f_\infty \simeq 1.8$, a reasonable magnitude for this type of reaction. The case of CH_3NC is less clearcut as the calculated data (curve a) fail to coincide with experiment only at low pressures.

The left-hand part of Figure 3 shows how the energy dependence of $k(E)$, calculated from eq 7, is affected by a change in molecular parameters of the reactant molecule; reactant in this case is azomethane which may be considered representative of a class of C_4 olefins. Curve b assumes[14a] that internal torsions of the two methyl groups in azomethane are free rotations, and

(9) F. W. Schneider and B. S. Rabinovitch, *J. Amer. Chem. Soc.*, **84**, 4125 (1962).

(10) K. M. Maloney and B. S. Rabinovitch, *J. Phys. Chem.*, **73**, 1652 (1969).

(11) W. Forst and Z. Prášil, *J. Chem. Phys.*, **51**, 3006 (1969).

(12) W. Forst and Z. Prášil, *ibid.*, **53**, 3065 (1970), Figure 3.

(13) This latter point is usually obscured by the practice of shifting curves along the pressure axis to make calculated and experimental fall-off curves coincide at some chosen value of log k/log k_∞.

(14) (a) Table I in W. Forst, *J. Chem. Phys.*, **44**, 2349 (1966); (b) Figure 3.

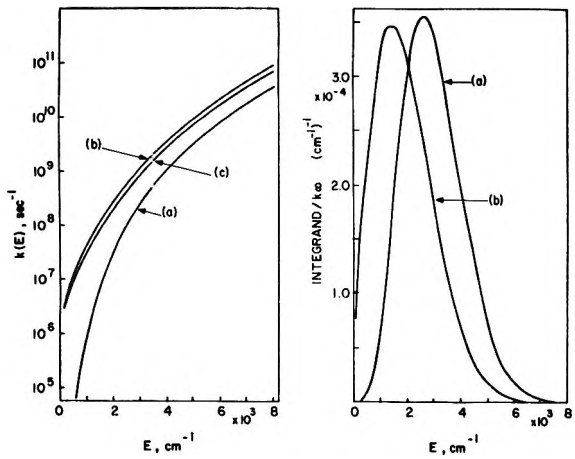

Figure 3. Energy dependence of calculated parameters for the thermal decomposition of azomethane. Left: energy dependence of $k(E)$ (energy E in excess of threshold energy). Curve (a): calculated for "tetrahedral II model" of transition state (W. Forst, *J. Chem. Phys.*, **44**, 2349 (1966)). Curve (b): calculated from eq 7 using azomethane frequencies of W. Forst, *J. Chem. Phys.*, **44**, 2349 (1966), and his experimental data $A_\infty = 2.09 \times 10^{17}$ sec^{-1}, $E_\infty = 19{,}412$ cm^{-1}. Curve (c): calculated from eq 7 using azomethane frequencies of Chang and Rice (Table II in *Int. J. Chem. Kinet.*, **1**, 171 (1969)); other parameters the same as for curve (b). Right: energy dependence of integrand in eq 3. (Energy E in excess of threshold energy.) Curve (a): Calculated with $k(E)$ of curve (a), left; $p = 1000$ Torr. Curve (b): calculated with $k(E)$ of curve (b), left; $p = 1000$ Torr. Area under either curve is 0.9.

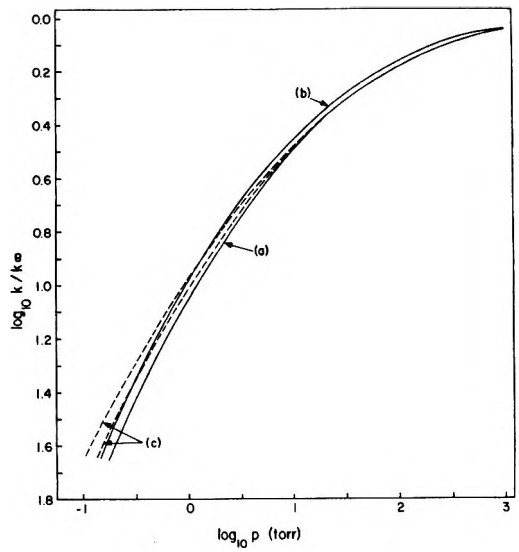

Figure 4. Calculated pressure dependence of unimolecular rate constant for thermal decomposition of azomethane at 303°. Curve (a): calculated using $k(E)$ of Figure 1, curve (b). Curve (b): calculated using $k(E)$ of Figure 1, curve (c). Curve (c): calculated for two versions of "tetrahedral model" of transition state (left curve: "tetrahedral II"; right curve: "tetrahedral I"; *cf.* Figure 1, ref 14).

also that overall rotation about the symmetry axis of the molecule is an active degree of freedom to be included in $N(E)$. Curve c assumes[15] that internal torsions in azomethane are vibrations with frequency 220 cm^{-1} each, and that the overall rotation about the symmetry axis is *not* an active degree of freedom. It can be seen from Figure 3 that the effect on $k(E)$ of these different assumptions is minimal, and as a result, the calculated fall-off is hardly affected at all (Figure 4). Hence $k(E)$ of eq 7 is not overly sensitive to minor changes in the exact value of some of the molecular parameters of the reactant, and this increases the usefulness of eq 7.

Incidentally, the calculated fall-off curve in Figure 4 does not include centrifugal effects, and, as might have been expected, lies to the right of experimental results.[14b] For this system, f_∞ has been calculated[5a] to be ~6, which would shift the curves of Figure 4 to the left by ~0.8 log units, considerably improving absolute pressure fit.

Comparison with "Traditional" Formulation

The treatment of experimental results by means of eq 7 may now be compared with the "traditional" way: usually a transition state structure is first postulated and its parameters adjusted by fitting them to the entropy of activation (*i.e.*, to A_∞). Since adoption of transition state parameters also fixes part of the temperature dependence of the rate constant, the critical energy E_0 is adjusted to make the overall temperature coefficient of the rate equal to the experimental value. Next the sum of states of the transition state $[G^*(E - E_0)]$ is calculated as a function of energy, and then $N(E)$ for the reactant molecule; from $G^*(E - E_0)$ and $N(E)$ there is obtained $k(E)$ as a function of energy, and, finally, the fall-off curve for k is calculated from eq 3. We claim that because of the usually large number of adjustable parameters involved in a transition state, fall-off curves calculated using $k(E)$ of eq 7 represent a more direct and more significant test of unimolecular rate theory in thermal systems since no transition state structure need be assumed and therefore there are no parameters to adjust.

Consider curve (b) in Figure 1 which has been obtained in the "traditional" way, while curve (a) is calculated from eq 7. The fact that (b) also reasonably fits the experimental data attests to the curve-fitting skill of the authors but not necessarily to the exactness of RRKM theory. Similarly, the almost perfect coincidence of the "traditional" curves (c) in Figure 4 with curves (a) and (b) obtained from eq 7 shows only that curve-fitting in case (c) was properly done.

If one subscribes to the view that most of the heuristic value of transition state theory is in the assumption that the transition state is a "molecule like any other" except that in one (or at least only in few) degrees of freedom it is a structure more or less intermediate be-

(15) See Table II in D-R. Chang and O. K. Rice, *Int. J. Chem. Kinet.*, 1, 171 (1969).

tween reactant and product, then postulating a transition state structure is not an entirely pointless exercise since it helps to systematize a good deal of data on a conceptually simple basis. If we dwell here on the curve-fitting aspects of the exercise, it is to underline the usually wide range of adjustment possible, traceable to the fact that transition state parameters are adjusted using the same kinetic information against which the final result of the calculations is later tested.

Threshold Behavior

Since eq 7 gives the energy dependence of $k(E)$ only approximately, we cannot expect that this $k(E)$ will necessarily have the correct behavior at some particular energy, even though when averaged over the thermal distribution of energies it yields the correct k. This may be illustrated by considering the threshold behavior of $k(E)$. At threshold, $E \rightarrow E_\infty$, and from eq 7

$$\lim_{E \rightarrow E_\infty} k(E) = \frac{A_\infty N(0)}{N(E_\infty)} \tag{8}$$

Since strictly speaking, $N(E)$ is a discontinuous string of δ functions, more or less wide-spaced at very low energies, $N(0)$ must be understood as a smooth-function extrapolation of $N(E)$ to $E = 0$.

It can be shown[3b] that threshold behavior on the RRKM model should be

$$\lim_{E \rightarrow E_0} k(E) = \frac{1}{hN(E_0)} \tag{9}$$

where $h = 3.335 \times 10^{-11}$ cm^{-1}-sec (Planck's constant). Therefore we should have at threshold $hA_\infty N(0) = N(E_\infty)/N(E_0) \gtrsim 1$, since in general E_∞ is a few kT higher than E_0, the reason being that the experimental activation energy is larger than E_0 by the difference between average energy of reacting and nonreacting molecules. The only estimate of E_0 available from high-pressure thermal data is $E_0 = E_\infty$, so that we should have $hA_\infty N(0) = 1$. If the lowest excited state of reactant is a vibrational state at, say, 300 cm^{-1}, we have $N(0) = 1/300$ (cm^{-1})$^{-1}$; then if $A_\infty \sim 10^{13}$ sec^{-1}, we find, in fact, $hA_\infty N(0) \sim 1$; this is roughly the case of CH_3NC and C_2H_5NC.

If $A_\infty \gg 10^{13}$ sec^{-1}, and $N(0) \simeq 10^{-3}$ (cm^{-1})$^{-1}$ (case of azomethane), the threshold value of $k(E)$ calculated from eq 8 is much larger than the corresponding value calculated from eq 9. This is shown in Figure 3 (left) where (a) refers to the "traditional" $k(E)$ which behaves at threshold in accordance with eq 9, while (b) and (c) behave at threshold according to eq 8. However, the fact that curve (a) obeys eq 9 does not make it more "correct" than curves (b) and (c) because (a) employs an adjusted value of E_0 (*cf.* first paragraph of the preceding section) which is derived, using one or more assumptions, from the same information that is embodied free of assumptions in curves (b) and (c). The right-hand part of Figure 3 shows how the different threshold behavior of $k(E)$ affects the integrand of eq 3. Since thermal data give only information about the area under the curve in the right-hand part of Figure 3 but not its shape, thermal data alone cannot give information about behavior of $k(E)$ at threshold, or at some other particular energy.

Thus high-pressure thermal systems yield limited information about a unimolecular process, and $k(E)$ of eq 7 represents all the limited information that can be extracted. Any knowledge of $k(E)$ that goes beyond eq 7 requires either additional data (such as rate at threshold, for example), or additional assumptions.

Low-Pressure Behavior

Near the high-pressure limit, the integrand in eq 3 can be expanded in inverse powers of p

$$\frac{k(E)}{1 + \dfrac{k(E)}{Zp}} = Zp \sum_{n=1}^{\infty} (-1)^{n+1} \left(\frac{k(E)}{Zp}\right)^n \tag{10}$$

so that eq 3 becomes

$$k = \sum_{n=1}^{\infty} (-1)^{n+1} \frac{L_n}{p^{n-1}} \tag{11}$$

where

$$L_n = \mathcal{L}\{[k(E)]^n N(E)\}/QZ^{n-1} \tag{12}$$

The first term ($n = 1$) in (11) is k_∞, and the high-pressure limit corresponds to $L_1 \gg L_2/p$.

Near the low-pressure limit, the integrand of eq 3 can be expanded in powers of p

$$\frac{k(E)}{1 + \dfrac{k(E)}{Zp}} = Zp \sum_{n=0}^{\infty} (-1)^n \left(\frac{Zp}{k(E)}\right)^n \tag{13}$$

so that eq 3 becomes

$$\frac{k}{p} = \sum_{n=0}^{\infty} (-1)^n p^n L_{-n} \tag{14}$$

where

$$L_{-n} = Z^{n+1} \mathcal{L}\left\{\frac{N(E)}{[k(E)]^n}\right\} \Big/ Q \tag{15}$$

The first term ($n = 0$) in (14) is k_0, the second-order low-pressure rate constant, and the low-pressure limit corresponds to $L_0 \gg pL_{-1}$.

Using $k(E)$ of eq 7, the relations 10–15 are illustrated for the case of CH_3NC where experimental data are available at both pressure limits. Table I summarizes the calculated values of L_n and L_{-n}. Since the whole development here is predicated on the assumption that the limiting high-pressure rate is known correctly, the high-pressure expansion does not yield any new insights, except, perhaps, to show that the expansion starts to converge very slowly at 10^3 Torr, and the high-pressure limit is attained only at 10^4 Torr (a pres-

sure reached in the experimental study) and above. This suggests that in most cases it would be rather unpromising to attempt obtaining k_∞ by linear extrapolation of a plot of k *vs.* p^{-1} since the linear region is likely to be located at inconveniently high pressures, and alternative methods of extrapolation must be sought.[1] As a check on the calculations, note that L_1 is equal to the experimental value of k_∞.

Table I: Calculated Coefficients in the Series Expansions 11 and 14 for CH_3NC Using $k(E)$ of Eq 7

n	L_n (mol/cm³)$^{n-1}$ sec^{-1}	L_{-n} (cm³/mol)$^{n+1}$ sec^{-1}
0	...	6.610×10^{2}
1	9.250×10^{-4}	6.355×10^{8}
2	2.477×10^{-9}	6.991×10^{14}
3	1.862×10^{-14}	8.242×10^{20}
4	3.864×10^{-19}	1.011×10^{27}

With $k(E)$ of eq 7, the low-pressure expansion (14) converges below 1 Torr in the case of CH_3NC, and the limit $L_0 \gg p\ L_{-1}$ is reached below 10^{-1} Torr, as can be seen from Table I. We shall denote this limiting low-pressure rate constant by $L_0 = k_0^*$, to emphasize that it is based on *high-pressure* information *via* $k(E)$ of eq 7. It turns out (Table I), that k_0^* is smaller than the extrapolated experimental value ($\sim 2 \times 10^3$ cm³/(mol sec) by about a factor of three. This is not unexpected, since using E_∞ for the critical energy at the low-pressure limit amounts to assuming that the experimental activation energy does not deline much from its high-pressure value, contrary to experiment. In fact, in the limit $p \to 0$, eq 3 yields for the second-order rate constant, with E_∞ for the critical energy

$$k_0^* = \lim_{p\to 0}(k/p) = \frac{Ze^{-E_\infty/kT}}{Q} \times \int_0^\infty N(E + E_\infty)e^{-E/kT}\mathrm{d}E \quad (16)$$

which would require the low-pressure *experimental* activation energy E_{a0} to be given by

$$E_{a0} = kT^2\left(\frac{\mathrm{d}\ln k_0^*}{\mathrm{d}T}\right) \sim kT/2 + E_\infty - \langle E\rangle + kT \quad (17)$$

where $\langle E\rangle = kT^2(\mathrm{d}\ln Q/\mathrm{d}T)$, Z is assumed to be given in concentration units and the logarithmic derivative of the integral is given its classical value, kT, which is a good approximation.[7] Equation 17 yields $E_\infty - E_{a0} \simeq \langle E\rangle - (3/2)kT$, which in the present instance works out to $\sim kT/2$, compared with the experimental value[9] $\sim 2kT$. This illustrates that high-pressure experimental data contain insufficient information for treatment of the unimolecular process over the *whole* range of pressures, and therefore $k(E)$ of eq 7 is valid only for a pressure fall-off region well above the low-pressure limit. The reason is, of course, that low-pressure unimolecular rate is governed by the rate of accumulation of energy and this is a process quite different from the internal randomization of energy that governs the high-pressure behavior as embodied in eq 7.

Conversely, low-pressure thermal data add nothing to information about $k(E)$, as the following considerations show. The expression for the second-order rate constant k_0, using the "true" critical energy E_0 and neglecting centrifugal effects, is[7,16] (*cf.* eq 16)

$$k_0 = \frac{Ze^{-E_0/kT}}{Q}\int_0^\infty N(E + E_0)e^{-E/kT}\mathrm{d}E \quad (16a)$$

so that if k_0 (or, better still, its temperature dependence) is known from low-pressure experiment, the critical energy E_0 can be obtained from eq 16a using properties of the reactant as the only input. Thus E_0 need not (and should not) be treated as an adjustable parameter reflecting the properties of the transition state *if low-pressure data are available.* However a known E_0 does not improve our knowledge of $k(E)$ as given by eq 7, and does not substantially modify our previous comments about the threshold behavior of $k(E)$ (eq 8) since E_0 is always sufficiently close to E_∞ to make $N(E_\infty)/N(E_0)$ little different from unity.[17]

Thus in a thermal study all the information about the energy dependence of the detailed unimolecular rate constant $k(E)$, and hence about most of the pressure fall-off of the averaged rate constant k, is contained in high-pressure data. If the object is to test the basic assumption of unimolecular rate theory, the only meaningful test possible, free of unnecessary assumptions, is to show that $k(E)$ of eq 7 [or (7a)] leads to the observed fall-off; this can be accomplished at a fraction of the time and effort that usually goes into the traditional transition-state formulation. Any other test, such as behavior at both the high- and low-pressure limits, requires additional assumptions.

Acknowledgment. Most of this paper was written while the author was on sabbatical leave in the Service de Chimie Physique II, Université Libre de Bruxelles. The author wishes to express his appreciation to Professor I. Prigogine for hospitality and to Université Laval for the award of a leave.

(16) See, for example, W. Forst, *Chem. Phys. Lett.*, **1**, 687 (1968).

(17) The ratio $N(E_\infty)/N(E_0)$ is 1.23 for CH_3NC using E_0 obtained from low-pressure data, and is very close to 2 for azomethane using an "adjusted" E_0. Thus an improved estimate of the critical energy will yield a better $k(E)$ of eq 7 only if simultaneously an improved estimate of A_∞ is available; unfortunately, eq 7 gives no recipe how this could be accomplished without assumptions.

The Two-Body Diffusion Problem and Applications to Reaction Kinetics

by Walter Scheider

Biophysics Research Division, Institute of Science and Technology, University of Michigan, Ann Arbor, Michigan
(Received May 7, 1971)

Publication costs assisted by the National Institutes of Health

The diffusion of a unit point source in the environment of a spherical barrier with given reaction affinity has been used as a means of calculating some classical chemical kinetic results as well as to derive some results for short-range interaction between two single particles in which the spherical symmetry required in previous methods is lacking. An iterative method is used to calculate a set of functions required for the derivation of the time-dependent encounter and reaction probabilities for diffusing particles with Coulomb interaction. The methods developed are applied to the calculation of surface conductance due to "proton migration" near the surface of a macromolecule.

1. Introduction

The use of Fick's law as the basis for calculating the kinetics of processes which involve collisions between particles in solution goes back to Smoluchowski's formulation[1,2] and has since been refined (ref 3–8) and tested (ref 9–14) extensively. The method is established to be valid whenever time intervals of importance are greater than the inverse of the frequency of elementary jumps[15] or "diffusive displacements," which is estimated to be between 10^8 and 10^{11} sec^{-1} (ref 16 and 17), but which for a rapidly diffusing particle such as a hydrogen ion can be calculated to be near the highest of these values. References 17 and 18 are excellent recent reviews of the field of elementary diffusion processes and their relation to reaction kinetics.

The traditional approach has been to solve the homogeneous diffusion equation given the initial condition that at time t_0 a central spherical particle A is surrounded by a uniform and continuous density distribution c_0 of particles B extending from the surface of the "collision sphere" of radius R outward to infinity. R is the center-to-center distance between an A and a B in contact. Developments have included the effect of long-range forces, such as the Coulomb interaction between ions, and efforts to relate the "reactivity" of particles to the boundary condition at the collision sphere. The spherical symmetry of the mathematics involved in this approach has both simplified and limited it.

With the particle density initially uniform, the subsequent particle density $c(r,t)$ depends only on the radial coordinate and time and approaches a steady state in which, in general, there is a positive radial concentration gradient due to the depletion of B by reaction near each A. The conceptual and philosophical problems associated with such a picture are dealt with in excellent fashion by Collins and Kimball,[3] who also rigorously established the commonly used relation between the particle reactivity and the so-called "radiative" boundary condition at the collision sphere. From density distributions one can derive particle flux and, consequently, reaction rates.

This article presents an approach to this problem from the unit-source function point of view. Though this approach is considerably complicated by the lack of spherical symmetry, it affords the following advantages.

(1) It provides a more fundamental form, from which the classical solutions follow immediately as a special case. By the use of suitable superposition integrals, encounter and reaction probabilities can also be obtained for problems with nonuniform and asymmetric initial conditions, in particular those which are intrinsically two-body problems. The secondary recombination of a particle pair created by dissociation is an example of such a problem.

(2) It provides a means for unifying two approaches to the field of diffusion-limited reaction kinetics: the

(1) M. V. Smoluchowski, *Phys. Z.*, **17**, 557 (1916).
(2) M. V. Smoluchowski, *Z. Phys. Chem., Abt. A*, **92**, 129 (1918).
(3) F. C. Collins and G. E. Kimball, *J. Colloid Sci.*, **4**, 425 (1949).
(4) P. Debye, *Trans. Electrochem. Soc.*, **82**, 265 (1943).
(5) H. L. Frisch and F. C. Collins, *J. Chem. Phys.*, **20**, 1797 (1952).
(6) T. R. Waite, *Phys. Rev.*, **107**, 463 (1957).
(7) T. R. Waite, *J. Chem. Phys.*, **28**, 103 (1958).
(8) T. R. Waite, *ibid.*, **32**, 21 (1960).
(9) S. A. Levinson and R. M. Noyes, *J. Amer. Chem. Soc.*, **86**, 4525 (1964).
(10) R. M. Noyes, *ibid.*, **86**, 4529 (1964).
(11) H. A. Schwarz, *Radiat. Res. Suppl.*, **4**, 89 (1964).
(12) J. Q. Umberger and V. K. La Mer, *J. Amer. Chem. Soc.*, **67**, 1099 (1945).
(13) T. R. Waite, *Phys. Rev.*, **107**, 471 (1957).
(14) W. R. Ware and J. S. Novros, *J. Phys. Chem.*, **70**, 3246 (1966).
(15) F. C. Collins and G. E. Kimball, *Ind. Eng. Chem.*, **41**, 2551 (1949).
(16) A. M. North, "The Collision Theory of Chemical Reactions in Liquids," Wiley, New York, N. Y., 1964.
(17) I. D. Clark and R. P. Wayne, "Comprehensive Chemical Kinetics," Vol. 2, C. H. Bamford and C. F. H. Tipper, Ed., Elsevier, Amsterdam, 1969, Chapter 4.
(18) A. M. North, *Quart. Rev.*, **20**, 421 (1966).

diffusion approach already mentioned and the molecular-pair approach.[19,20]

(3) It provides a conceptually satisfying view of this problem by regarding it fundamentally as the two-body problem in Brownian motion.

In the final section, the results of this method will be used to calculate an approximate value for the surface conductance of dissolved serum albumin molecules due to the migration of bound hydrogen ions.

2. The Formulation of the Two-Body Problem

To formulate the two-body diffusion problem, the origin of a system of spherical coordinates (r,θ,λ) is fixed at the center of a spherical particle A of radius R_A. In this coordinate system we let a second spherical particle B of radius R_B be located at time t_0 with its center at $(r_0,0,0)$ (Figure 1). The "collision sphere," whose surface we shall call Σ is then the locus $r = R_A + R_B \equiv R$. We ask, what are the probabilities associated with the subsequent movements of the two particles by diffusion: the probability density of their relative location in space, their mutual encounter, and reaction?

If the diffusion constants for the particles are D_A and D_B, then in the coordinates defined, A is at rest and B moves relative to A with diffusion constant $D = D_A + D_B$. This formulation neglects the angular displacement of the particle axis due to rotary Brownian movement.[20a] In consequence, the angular distribution of the collision and/or reaction locus will be with respect to the initial spatial direction of the line connecting the two particle centers, and not with respect to the physical pole on particle A which coincides with this line at time t_0. It can be shown that for some applications, as for example the one in section 5 (below), the rates and time intervals involved make this factor negligible. For some other cases approximate corrections can be applied.

The two other parameters required are: (1) a reaction affinity parameter α, with units of velocity, defined as the reaction probability per unit time per unit surface area on the collision sphere, per unit volume density of B particles at Σ; and (2) the long range interaction energy U between A and B particles.

The solution is then obtained as a Green's function, $\Gamma(r,\theta,\lambda,t;r_0,\theta_0,\lambda_0,t_0)$. This is the probability density of finding particle B with its center at (r,θ,λ) at time t if at time t_0 it is known to have been at (r_0,θ_0,λ_0). If $\theta_0 = 0$, Γ is λ-independent.

For an arbitrary distribution $c_0(r,\theta,\lambda,t_0)$ at $t = t_0$, the probability density c at time t is given by the general form

$$c(r,\theta,\lambda,t) = \int dv_0 c_0(r_0,\theta_0,\lambda_0,t_0)\Gamma(r,\theta,\lambda,t;r_0,\theta_0,\lambda_0,t_0) \quad (1)$$

where integration is performed over all volume elements dv_0 outside Σ. In an obvious way this can be extended to cases in which there is not merely an initial distribution, but in which particles are created continuously.

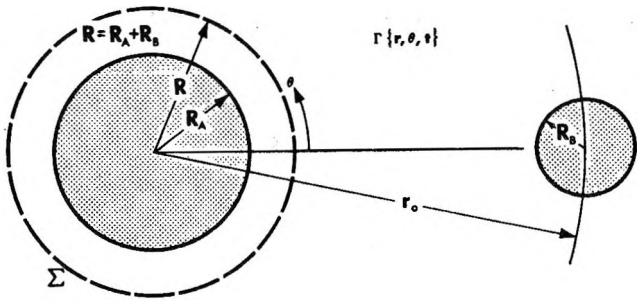

Figure 1. Initial condition of the two-body diffusion problem: a Brownian particle of radius R_B is initially at a distance r_0 from the center of a reference particle of radius R_A. The collision surface Σ is at the locus of the center of particle B when the two particles are in contact. The solution consists in evaluating $\Gamma(r, \theta, t)$, the probability density of finding the center of particle B at the coordinates (r, θ) at time t.

The unit source is introduced as an inhomogeneity in the conservation equation

$$\frac{\partial\Gamma}{\partial t} = -\nabla\cdot\Phi + g(r_0,\theta_0,t_0) \quad (2)$$

where

$$g(r_0,\theta_0,t_0) = -\frac{\delta(r - r_0)\delta(\cos\theta - \cos\theta_0)\delta(t - t_0)}{2\pi r_0^2} \quad (3)$$

and δ is the δ function.

The flux Φ is given by the diffusion equation

$$\Phi = -D(\nabla\Gamma + \Gamma\nabla U/kT) \quad (4)$$

Eliminating Φ from eq 2 and eq 4, we obtain

$$\partial\Gamma/\partial t = D(\nabla^2\Gamma + \Gamma\nabla^2 U/kT + \nabla\Gamma\cdot\nabla U/kT) + g(r_0,\theta_0,t_0) \quad (5)$$

From the definition of the reaction velocity parameter, the boundary condition at $r = R$ is

$$-\hat{n}\cdot\Phi = D\left\{\frac{\partial\Gamma}{\partial n} + \frac{\Gamma}{kT}\frac{\partial U}{\partial n}\right\} = \alpha\Gamma \quad (6)$$

or

$$\frac{\partial\Gamma}{\partial n} = \left\{h - (1/kT)\frac{\partial U}{\partial n}\right\}\Gamma \quad (7)$$

where $\hat{n}$ is the unit normal vector on the surface Σ, and $h = \alpha/D$. Due to its origin in heat conduction problems, this form is known as the "radiative" boundary condition.

Letting $\theta_0 = 0$, eq 5 is solved by separation of variables

(19) R. M. Noyes, *J. Amer. Chem. Soc.*, **78**, 5486 (1956).

(20) R. M. Noyes, *Progr. React. Kinet.*, **1**, 129 (1961).

(20a) NOTE ADDED IN PROOF. The diffusion equation with rotary movement is dealt with in a recent article: K. Šole and W. H. Stockmayer, *J. Chem. Phys.*, **54**, 2981 (1971).

$$\Gamma(r,\theta,t;r_0) = \int_0^\infty S(r,\theta,k)T(t,k)\mathrm{d}k = \sum_{l=0}^{\infty} P_l(\cos\theta)\int_0^\infty \mathrm{d}k f_l(k,r_0)\psi_l(k,r)e^{-Dk^2(t-t_0)} \quad (8)$$

where $P_l(\cos\theta)$ are the Legendre polynomials. Provided U has only radial dependence, is finite and twice differentiable in the domain $r(R,\infty)$, and approaches a constant value at least as $1/r$ for large r, $\psi_l(k,r)$ is, for each value of l, a complete space of functions (orthogonal with weight $r^2\exp(U/kT)$), which are solutions of the space part of the separated homogeneous equation derived from eq 5, and which satisfy eq 7. The distribution function $f_l(k)$ is used to satisfy the inhomogeneity $g(r_0,\theta_0,t_0)$.

3. The Field-Free Problem

If at least one of the Brownian particles is uncharged, and if no long-range interactions other than those of Coulombic origin are considered, ∇U vanishes. In this case, the solution to eq 5 with eq 7 is the Green's function for the analogous heat conduction problem,[21] written in slightly modified form

$$\Gamma(r,\theta,t;r_0,R,h) = (1/2\pi^2R^2)\sum_{l=0}^{\infty}(2l+1)P_l(\cos\theta)\int_0^\infty \times \mathrm{d}k\frac{\psi_l(r)\psi_l(r_0)}{N_l^2}e^{-Dk^2(t-t_0)} \quad (9)$$

where

$$\psi_l(r) = (kR)^2\{[j_l(kr)y_l'(kR) - y_l(kr)j_l'(kR)] - (h/k)[j_l(kr)y_l(kR) - y_l(kr)j_l(kR)]\} \quad (10)$$

and

$$N_l^2 = (kR)^2\left\{\left[\frac{h}{k}j_l(kR) - j_l'(kR)\right]^2 + \left[\frac{h}{k}y_l(kR) - y_l'(kR)\right]^2\right\} \quad (11)$$

Here j_l and y_l are the spherical Bessel's functions.

Since in practice one is often most interested in encounter events, and hence in the values of Γ, c, and Φ at the collision surface, it is noted that

$$\psi_l(R) = (kR)^2W(j_l(kR),y_l(kR)) = 1 \quad (12)$$

where W is the Wronskian. It follows that

$$\Gamma(\text{at } r = R,\theta,t;r_0,R,h) = (1/2\pi^2R^2)\sum_{l=0}^{\infty}(2l+1)P_l(\cos\theta)\times \int_0^\infty dk\frac{\psi_l(r_0)}{N_l^2}e^{-Dk^2(t-t_0)} \quad (13)$$

3.1. Encounter and Reaction Probabilties. From the boundary condition (6) in the absence of long range forces, it is evident that the probability rate of reaction v (per unit surface area), which is given by the inward flux of probability density at $r = R$, is

$$v(\theta,t) = -\hat{n}\cdot\Phi(R) = Dh\Gamma(R,t) \quad (14)$$

The quantity, $w(\theta,t)$, defined as

$$w(\theta,t) = \int_0^t v(\theta,t')\mathrm{d}t' \quad (15)$$

is then the cumulative reaction probability (per unit surface area) due to an instantaneous point source at time t_0, integrated to time t, or alternatively it is the probability rate of reaction at time t due to a continuous point source of unit intensity per unit time located at $(r_0,0,0)$ from time $t_0 = 0$ on.

From eq 13

$$w(\theta,t) = (h/2\pi^2R^2)\sum_{l=0}^{\infty}(2l+1)P_l(\cos\theta)\times \int_0^\infty \frac{\mathrm{d}k}{k^2}\frac{\psi_l(r_0)}{N_l^2}(1 - e^{-Dk^2t}) \quad (16)$$

and, because of the orthogonality property of the Legendre polynomials over the sphere, the cumulative reaction probability (or the probability rate due to a continuous source) over the entire surface Σ is

$$W(t) = \int_\Sigma \mathrm{d}\sigma w(\theta,t) = (2h/\pi)\int_0^\infty \times \frac{\mathrm{d}k}{k^2}\frac{\psi_0(r_0)}{N_0^2}(1 - e^{-Dk^2t}) \quad (17)$$

which comes to

$$W(t) = \frac{\bar{R}}{r_0}\{\mathrm{erfc}(y_0) - e^{x^2+2xy_0}\,\mathrm{erfc}(x + y_0)\} \quad (18)$$

where $y_0 = (r_0 - R)/\sqrt{4Dt}$; $x = \sqrt{Dt}/(R - \bar{R})$. A physical significance will be assigned shortly to $\bar{R}$, which is defined as

$$\bar{R} = \frac{R}{1 + 1/hR} \quad (19)$$

In the case of "totally reactive" particles, those which react on the first collision ($h \to \infty$), the expression (18) becomes

$$\bar{W}(t) = \lim_{(R-\bar{R})\to 0} W(t) = (R/r_0)\,\mathrm{erfc}\left(\frac{t}{\tau}\right)^{-1/2} \quad (20)$$

where $\tau = (r_0 - R)^2/4D$. (See footnote 22.)

When $h = 0$, the reaction probabilities v and w vanish. A quantity of interest which does not vanish in this case

(21) H. S. Carslaw and J. C. Jaeger, "Conduction of Heat in Solids," 2nd ed, Oxford Press, Oxford, 1959.

(22) The same result can be obtained more rigorously by using the boundary condition, $\Gamma(\text{at } r = R) = 0$, instead of the more general condition (7) in the limit, $h \to \infty$.

is the encounter probability, or the particle probability density on the collision sphere

$$G(R,t, \text{at } h = 0) = \int_{\Sigma} d\sigma \Gamma(R,t, \text{at } h = 0) = \frac{1}{r}\left\{\frac{Re^{-(r_0-R)^2/4Dt}}{\sqrt{\pi Dt}} - e^{(r_0-R)/R + Dt/R^2} \times \operatorname{erfc}\left(\frac{\sqrt{Dt}}{R} + \frac{(r_0 - R)}{\sqrt{4Dt}}\right)\right\} \quad (21)$$

3.2. Reciprocity Theorem; Equivalent Virtual Defect Source. To demonstrate some of the versatility of the unit source solutions, we can derive in two alternate ways the well-known result[3]

$$\frac{1}{c_0}c(r,t;c_0) = 1 - \frac{\bar{R}}{r}\{\operatorname{erfc}(y) - e^{x^2+2xy}\operatorname{erfc}(x + y)\} \quad (22)$$

$$y = (r - R)/\sqrt{4Dt};\ x = \sqrt{Dt}/(R - \bar{R})$$

(see footnote 23), where $c(r,t;c_0)$ is the particle probability density when the initial distribution of B particles is uniform and equal to c_0 everywhere outside Σ.

This result can be obtained by straightforward, if cumbersome, application of eq 9 and 1. However, the relationship of eq 22 to the similar-appearing form of $W(t)$ is shown by deriving it from eq 18 by way of a reciprocity theorem of great generality and by showing an equivalence between the condition of uniform initial particle concentration and a constant virtual "defect" source at Σ.

If there is microscopic reversibility in the diffusion process (as is implicit in the use of a diffusion "constant"), and if the absorption properties of all barriers are time-independent, then it is possible to describe the diffusion between two points by a symmetric matrix of random flight transition probabilities **P** in which there is a row and column for each point which is accessible to the diffusing particle. The transition probability $p_{ij}^{(n)}$ for diffusion from point i to point j in time $t = n\tau$, where τ is the time interval for elementary jumps, is given by the i,jth element of $\mathbf{P}^n$. If **P** is symmetric, so is $\mathbf{P}^n$, and hence $p_{ij}^{(n)} = p_{ji}^{(n)}$.

This relation can be written in terms of particle probability densities: if A and B are any two points in a space bounded by any time-independent configuration of barriers, then

$$\Gamma(B,t;A,t_0) = \Gamma(A,t;B,t_0) \quad (23)$$

By obvious extension, the same relationship holds for the "G" functions which are integrals of Γ over a surface. Thus, if A is not a point, but a spherical surface of radius R located just outside a sphere of reactivity h, and B is a point at $(r_0,0,0)$, then, if $W(t)$ of eq 18 is written

$$W(t,r_0) = Dh\int_{t_0}^{t} G(A,t';B,t_0)dt' = Dh\int_{t_0}^{t} G(A,t;B,t_0')dt_0' \quad (24)$$

one can write the following relation between the particle densities

$$c(B,t;c_0,t_0) = c_0 - \int_{t_0}^{t} S(A,t_0')G(B,t;A,t_0')dt_0' \quad (25)$$

where $S(A,t)$ is a virtual "defect," or "depletion" source on the surface A, which is imagined to be located just outside the absorbing surface, Σ.

The net rate at which defect-density diffuses outward from A is given by the reaction rate, $Dhc(\Sigma,t;c_0,t_0)$. Since the defect-density at Σ is $(c_0 - c)$, there is a virtual defect-flux into the surface, equal to $Dh(c_0 - c)$. The net outward defect-flux is then equal to the source intensity minus the inward defect-flux

$$Dh\ c(\Sigma,t;c_0,t_0) = S(A,t) - Dh[c_0 - c(\Sigma,t;c_0,t_0)] \quad (26)$$

Thus, placing a virtual defect source of constant intensity

$$S(A,t) = S(A) = Dhc_0 \quad (27)$$

over the surface of a sphere of reactivity h from time t_0 on, is the equivalent of placing such a sphere initially in an environment of uniform particle density c_0.

With this result and the reciprocity relation, $G(A,t;B,t_0) = G(B,t;A,t_0)$, the eq 25 and 24 give

$$c(r,t;c_0,t_0)/c_0 = 1 - W(t,r) \quad (28)$$

which gives the result (22) immediately from eq 18.

3.3. "Effective Reaction Radius;" Region of Equivalence. For values of t large compared with both $(r_0 - R)^2/D$, and $(R - \bar{R})^2/D$, eq 18 is well approximated by

$$W(t) \approx \frac{\bar{R}}{r_0}\left\{1 - \frac{(Dt)^{-1/2}}{\sqrt{\pi}}(r_0 - \bar{R}) + \frac{(Dt)^{-3/2}}{\sqrt{\pi}} \times \left[\frac{(r_0 - R)^3}{12} + \frac{(R - \bar{R})^3}{2}\right] + O(Dt)^{-5/2}\ldots\right\} \quad (29)$$

and

$$W_\infty \equiv \lim_{t\to\infty} W(t) = \bar{R}/r_0 = \gamma R/r_0 \quad (30)$$

where

$$\gamma = \bar{R}/R = hR/(1 + hR) \quad (31)$$

The dimensionless fraction γ, goes from 0 to 1 as h goes from 0 to infinity, and will be used as a convenient reactivity index.

The quantity $\bar{R}$ represents an "effective reaction radius," in the sense that a particle pair of collision radius R with finite reactivity h, can be represented by a model

(23) Those who will compare this result with that in ref 3 should note that the expression in the cited reference contains a typographical error in sign.

pair of radius $\bar{R}$ which is totally reactive ($h \rightarrow \infty$) and whose cumulative reaction probability $W(t)$ approaches the same limit at large time. This result is non-trivial because eq 31 shows that $\bar{R}$ is independent of the initial center-to-center separation, r_0, and hence is attributable entirely to characteristics of the particles themselves.

Much of the early work in relating reaction kinetics to a particle diffusion model[1,4] was done for so-called "fast reactions," in which it was assumed that an equivalent representation in terms of totally reactive particles could be used. Considerable simplification of the mathematics is achieved by such an assumption. Though frequently used, the limits of its validity have not, to this author's knowledge, been examined previously. It is clear that the "equivalent" representation is completely equivalent only for the reaction probability at $t \rightarrow \infty$. From eq 18 and 20 we can compute the fractional approximation involved in use of the "equivalent" $\bar{W}(t)$ in place of the exact $W(t)$

$$\Delta\bar{W}/W_\infty \equiv (\bar{W}(t) - W(t))/W_\infty = \operatorname{erfc}\frac{r_0 - \bar{R}}{\sqrt{4Dt}} - \operatorname{erfc}\frac{r_0 - R}{\sqrt{4Dt}} + e^{(r_0 - r)/(R-\bar{R}) + Dt/(R-\bar{R})^2}\operatorname{erfc}\left(\frac{\sqrt{Dt}}{R-\bar{R}} + \frac{r_0 - R}{\sqrt{4Dt}}\right) \quad (32)$$

Letting $\beta \equiv Dt/(R - \bar{R})^2$, the "equivalence" is always better than 1% when $\beta > 12.0$, and in general a region of "equivalence" to any given tolerance can be defined entirely in the β-domain

$$\Delta\bar{W}/W_\infty \leq (8\pi e)^{-1/2}\beta^{-1} \quad (33)$$

Figure 2 compares the exact solution with the "effective reaction radius" representation. It is clear from this that recombination problems, in particular the problem discussed in section 5 below, are not among those which can be well approximated by the theory of fast reactions.

3.4. Secondary Recombination and the Never-Return Fraction. Secondary recombination is the term usually applied to the recombination of a particle pair created by some dissociation process in which the particles have become separated by at least one intervening solvent molecule prior to recombination. This is distinguished from primary recombination which takes place while the particles are still contained within the solvent "cage" which initially envelops them.[24]

The kinetics of primary recombination, which generally takes place in less than 10^{-11} sec, is not well represented by a diffusion model. On the other hand, secondary recombination, particularly if at least one of the particles is large compared with solvent molecule dimensions, can be adequately approached by the present model (provided the approximation of fast reactions is avoided), using the special case in which

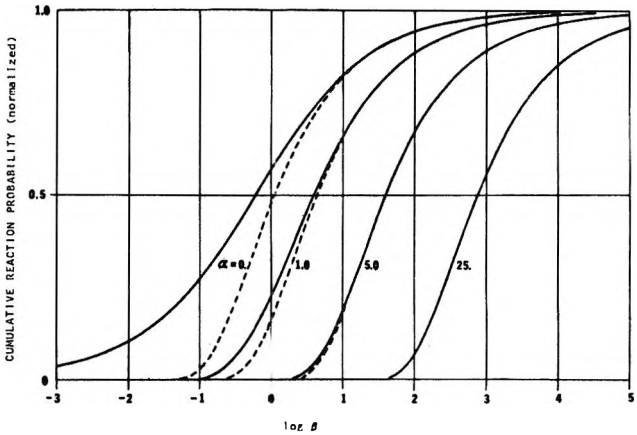

Figure 2. Comparison of "effective reaction radius" calculation of $\bar{W}(t)$, the cumulative reaction probability (dashed), with the exact calculation of the same quantity (solid), showing region of correspondence in the β-domain. $\alpha = (r_0 - R)/(R - \bar{R})$, $\beta = Dt/(R - \bar{R})^2$.

the particles are initially in contact ($r_0 = R$). For this case

$$W(t, \text{at } r_0 = R) = \gamma N(Dt/(R - \bar{R})^2) \quad (34)$$

where

$$N(x) = 1 - e^x \operatorname{erfc}\sqrt{x} \quad (35)$$

which for large x approaches

$$N(x) \longrightarrow 1 - (\pi x)^{-1/2} \qquad \text{valid } x \gg 1 \quad (36)$$

The expression $N(Dt/R^2)$ has the interesting property of being the "never-return" fraction for nonreacting particles ($\gamma = 0$). This is the probability that at time t two particles initially in contact will have separated never to collide again.

3.5. Reaction Rates. For the general two-particle reaction

$$A + B \xrightarrow{k} AB \quad (37)$$

the forward rate constant, k, in the condition of equilibrium between the combination and dissociation processes, is, from the definition of $\mathcal{A}$ and h

$$k = 4\pi R^2 \mathcal{A} = 4\pi RD \cdot hR \quad (38)$$

A so-called "observed reaction rate," k', is defined in reaction kinetics literature as the rate at which AB is formed from A and B assuming that one can initially place A and B particles into solution in random distribution. By this definition, k' is a time dependent function whose transient term represents the depletion of B around A due to reaction. Following Waite,[6] we can derive k' from eq 6 and 22, and obtain, in the present nomenclature

(24) R. M. Noyes, *J. Amer. Chem. Soc.*, **77**, 2042 (1955).

$$k' = \frac{4\pi RD}{1 + 1/hR}\{1 + hRe^{Dt/(R-\bar{R})^2} \times \operatorname{erfc}[\sqrt{Dt}/(R - \bar{R})]\} \quad (39)$$

This approaches the steady-state value

$$k'(\text{at } t \longrightarrow \infty) = 4\pi RD\gamma \quad (40)$$

k' has its primary physical importance in nonequilibrium processes, such as fluorescence quenching[20,14] where a supply of randomly placed reactants is created by externally induced pair formation, and coagulation of colloidal particles in which the time span of reaction is directly observable. In such processes the transient term of eq 39 is significant.

3.6. Reconciling Molecular-Pair Derivation of Reaction Rates with Fick's Law Results. An expression for k', different from eq 39, is obtained by derivations based on the molecular-pair model.[20] Such derivations have sought to avoid making the assumption required in the approach based on Fick's law that the diffusion equations are valid on the scale of dimensions of the encounter process between individual reactant particles.

By use of a result from the unit source function formulation of this article at an appropriate stage in the molecular-pair derivation, we can bring the result into agreement with that based directly on Fick's law. Though this would seem to negate the purpose of using the molecular-pair approach, it has already been pointed out[17] that when pressed to the calculation of kinetic constants, the pair approach has always, in fact, required the use of some assumption equivalent to that of Fick's law. At the point where this has been done, we will simply use an expression which we feel is more appropriate.

The calculation of k' by the molecular-pair approach hinges on the evaluation of a quantity, $\xi(t)$, in terms of which

$$k' = k\left(1 - \int_0^t \xi(t')dt'\right) \quad (41)$$

$\xi(t)dt$ is defined to be the probability that a pair of molecules which have previously reacted with each other will undergo their first subsequent reaction with each other between t and $t + dt$ later. This quantity is usually given in the form $(p \exp(-q/t))/t^{3/2}$, with p and q being parameters to be evaluated by other means. This is the form taken by an expression for the probability that a particle in unrestricted random flight will return to the point of its origin.[25]

In a two-particle system, the point of origin is located on the surface of a spherical barrier, and the model of unrestricted random flight is therefore less appropriate than the model of two-particle diffusion. The result obtained by the former method[20]

$$k' = k\left(1 - \beta' \operatorname{erfc}\frac{\alpha}{\beta'}\sqrt{\frac{\pi}{t}}\right) \quad (42)$$

is thus not only inconsistent with eq 39, but has the additional disadvantage that two parameters, α and β', are left to be evaluated.

Using eq 34 to evaluate $\xi(t)$

$$\int_0^t \xi(t')dt' = W(t, \text{at } r_0 = R) = \gamma\left(1 - e^{Dt/(R-\bar{R})^2} \operatorname{erfc}\frac{\sqrt{Dt}}{R - \bar{R}}\right) \quad (43)$$

which, with eq 38, substituted in eq 41, gives the same resultant expression for k' as was obtained from the Fick's law development in eq 39. This demonstrates, in addition, that the early steps, or foundations, of both approaches are equivalent.

3.7. Latitude-Dependent Solutions. In recombination problems where one of the particles is large and has many equivalent recombination loci (as, for example, a protein molecule with numerous hydrogen ion-binding sites) the latitude-, or θ-, dependence of the form (9) is of interest. The general question is, how does the encounter and reaction probability asym-

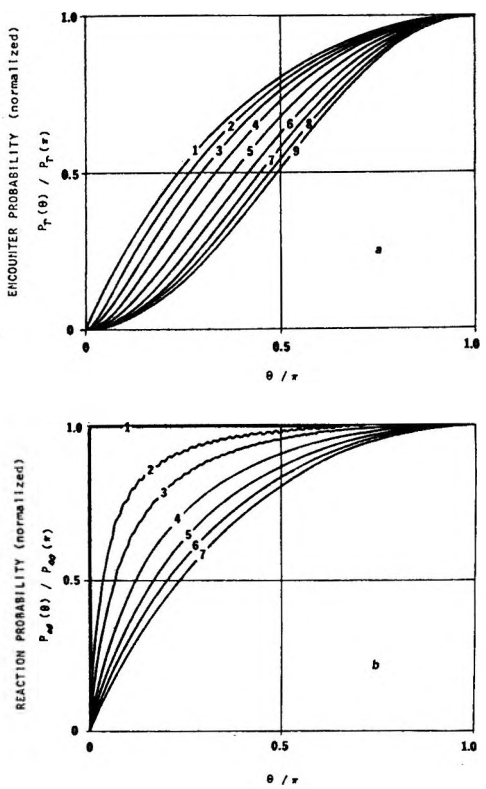

Figure 3. Solutions of latitude dependence of reaction and encounter probabilities. (a) Probability that encounter will occur above latitude θ for nonreacting particles ($\gamma = 0$): r_0/R = 1.0 (1), 1.1 (2), 1.25 (3), 1.5 (4), 2.0 (5), 3.0 (6), 5.0 (7), 10.0 (8), 50.0 (9). (b) Probability reaction will occur above latitude θ for secondary recombination ($r_0/R = 1.0$): γ = 1.0 (1), 0.9 (2), 0.8 (3), 0.6 (4), 0.4 (5), 0.2 (6), lim $\gamma \rightarrow 0$. (7).

(25) S. Chandrasekhar, *Rev. Mod. Phys.*, **15**, 1 (1943).

metry depend upon the initial separation of the two Brownian particles and on the reactivity?

A closed solution for eq 9 retaining both the time and latitude dependence has not been obtained, but its integral to $t = \infty$, the total probability as a function of θ can be obtained from eq 16

$$w_\infty(\theta) = \lim_{t\to\infty} w(\theta,t) = \frac{h}{2\pi^2R^2}\sum_{l=0}^{\infty}(2l+1)P_l(\cos\theta)\int_0^\infty \frac{dk}{k^2}\frac{\psi_l(r_0)}{N_l^2} \quad (44)$$

It can be shown that the integrand is an even function in k. It then becomes possible to integrate the expression in the complex plane

$$w_\infty(\theta) = \frac{1}{4\pi R^2}\sum_{l=0}^{\infty}\frac{hR(2l+1)}{(l+1+hR)}\left(\frac{R}{r_0}\right)^{l+1}P_l(\cos\theta) \quad (45)$$

The sum converges readily except when the particles are initially nearly in contact, $(r_0/R) \approx 1$. The oscillations in curves (2) and (3) of Figure 3b are due to truncation of the sum in eq 45 at $l = 100$. Although round-off is also a severe problem in these slowly converging solutions, the arithmetic was done with 45-decimal place precision, assuring that the oscillations are not related to arithmetic inaccuracy. These solutions which are most difficult to evaluate are, of course, also the ones of greatest interest because it is in those cases that the latitude dependence is most pronounced.

When $\gamma = 1$, eq 45 becomes

$$\bar{w}_\infty(\theta) = \lim_{h\to\infty} w_\infty(\theta) = \frac{1}{4\pi R^2}\sum_{l=0}^{\infty}(2l+1)\times\left(\frac{R}{r_0}\right)^{l+1}P_l(\cos\theta) \quad (46)$$

$$= (1/4\pi R^2)x(1-x^2)/(1-2x\cos\theta+x^2)^{3/2}$$

where $x = R/r_0$ (see footnote 22). This expression, of course, diverges when $(r_0/R) = 1$, as it must for physically obvious reasons.

In Figures 3a,b these results are displayed as integrals over the segment of the sphere bounded by the latitude θ. Plotted are probabilities $P_\Gamma(\theta) = 2\pi R^2\int_0^\theta \cdot \Gamma(R,\theta',t\to\infty)\sin\theta'\,d\theta'$ and $P_\infty(\theta) = 2\pi R^2\int_0^\theta w_\infty(\theta')\sin\theta'\,d\theta'$, that encounter and reaction, respectively, will occur between latitude 0 (head on) and latitude θ. Each curve is normalized to unity at its maximum value, so as to emphasize the latitude dependence rather than the magnitude. Curves are shown for various values of γ, the reactivity index, and r_0/R, the initial separation between the particle centers in units of collision radii.

4. Brownian Particles with Coulomb Interaction

We consider now the two-body diffusion problem in the presence of Coulomb interaction energy between charged spheres. As a first-order approach to this problem we will neglect the effects of counterion shielding. The result will be valid when the ionic strength is sufficiently small; it will also, however, be valid at higher ionic strengths for short-range diffusion problems—in particular for the recombination problem—provided only that the diffusion takes place substantially within the Debye–Hückel radius.

In this model, the long range interaction energy is

$$U = e^2z_Az_B/4\pi\epsilon r \quad (47)$$

where e is the electronic charge, z_A and z_B the valence of the particles, and ϵ the effective dielectric constant between them.

The earliest attempt to extend the calculation of reaction rates from diffusion kinetics to ionic species was by Debye[4] who derived a correction factor, which may be written

$$f = Q/(\exp(Q) - 1) \quad (48)$$

where Q is the dimensionless quantity

$$Q = e^2z_Az_B/4\pi\epsilon kTR \quad (49)$$

such that the steady-state reaction rate for diffusion controlled reactions is obtained by using fR as an "effective" collision radius in the rate equations of Smoluchowski.[1,2] Shortly thereafter, Umberger and LaMer[12] formulated the time-dependent boundary value problem, but solved it by neglecting $QR/2r$ with respect to unity, making the result useful primarily at great distance, and of doubtful value in the study of collision events which occur at $r = R$. (Q takes on the value 1 for two univalent ions of combined radius 7.1 Å in water at 20°.)

We will now attempt to follow the approach of section 2) to obtain a Green's function for charged particles. When U is the Coulombic energy, eq 5 becomes

$$\frac{\partial\Gamma}{\partial t} = D\left\{\nabla^2\Gamma - \frac{QR}{r^2}\frac{\partial\Gamma}{\partial r}\right\} + g(r_0,\theta_0,t_0) \quad (50)$$

and the boundary condition (7) becomes

$$\left.\frac{\partial\Gamma}{\partial n}\right|_{r=R} = (h + Q/R)\cdot\Gamma(\text{at } r = R) \quad (51)$$

A closed solution for $W_\infty(Q)$, the total reaction probability in all time due to a unit source at (r_0,θ_0,t_0), can be found by solving the steady-state form of the homogeneous part of eq 50, in which the left side is set to zero

$$W_\infty(Q) = \frac{e^{QR/r_0} - 1}{e^Q(1 + Q/hR) - 1} \quad (52)$$

It is not possible to define an effective reaction radius for charged particles independent of the initial separation r_0, as we were able to do for uncharged particles in section 3.3. It is convenient, however, to write

$$R' = R(1 - e^{-Q})/Q \quad (53)$$

in terms of which the secondary recombination probability has the familiar form of eq 31

$$W_\infty(Q, \text{at } r_0 = R) = hR'/(1 + hR') \quad (54)$$

The expression for the forward rate constant of the two-particle reaction 37 when the particles are charged is

$$k'(Q, \text{at } t \longrightarrow \infty) = 4\pi RD \cdot Rhe^{-Q}/(1 + hR') \quad (55)$$

which reduces to eq 40 when $Q = 0$. For the special case of "fast reactions" ($h \to \infty$), eq 55 reduces to the modified expression 40 in which R has been replaced by fR, where f is the Debye factor of eq 48.

4.1. The Green's Function with Coulomb Interaction. A closed solution for the unit source function in the presence of Coulomb interaction must be written in terms of the functions $\psi_l(k,r)$ from which the space part of the solution is constructed (eq 8). These functions are not in this case simply combinations of Bessel's functions as in eq 10; they are now combinations of the functions generated by

$$\frac{\partial^2\psi_l}{\partial r^2} + \left(\frac{2}{r} - \frac{QR}{r^2}\right)\frac{\partial\psi_l}{\partial r} + \left(k^2 - \frac{l(l+1)}{r^2}\right)\psi_l = 0 \quad (56)$$

which satisfy

$$\left.\frac{\partial\psi_l}{\partial r}\right|_{r=R} = (h + Q/R)\cdot\psi_l(\text{at } r = R) \quad (57)$$

Equation 56 is recognized as the Bessel's equation but for the term in Q. A scheme for numerical generation of the set of functions $\psi_0(Q,k,r)$ to any desired precision is given in the Appendix. Each such function is generated by finding successive values of the function at $r + \Delta r$ in terms of the value and the slope of the function at r, using increments small enough that in the interval the function may be treated as a Bessel's function perturbed by the term in Q. This requires no assumptions on the magnitude of that term in relation to $2/r$ except for its asymptotic behavior at infinity (see section 2).

The generating program gives two independent functions, $s_1(Q,k,r)$ and $s_2(Q,k,r)$, for any given value of Q and k; as before, $\psi_0(Q,k,r)$ is then that linear combination of s_1 and s_2 which obeys the boundary condition (57).

It is clear that a complete set of s functions for any one value of Q is an infinite set, since k can take any positive value. We are limited in practice to tabulating these functions for discrete values of k over a finite range. The formal solution suggests that truncation of the integral over k at some value k_{max} affects the solution primarily at values of $t < (Dk_{max}^2)^{-1}$.

In a typical solution, the unit source was represented quite adequately in terms of a set of 61 ψ_0-functions for the particular value of Q with the following values of k (in units of R^{-1}): 0.05; at intervals of 0.125 from 0.125 to 1.0; and at intervals of 0.25 from 1.0 to 14.0.

The tabulation of s functions for different values of Q is considerably simplified by the relation

$$s(Q,k,r) = s(aQ,k/a,ar) \quad (a > 0) \quad (58)$$

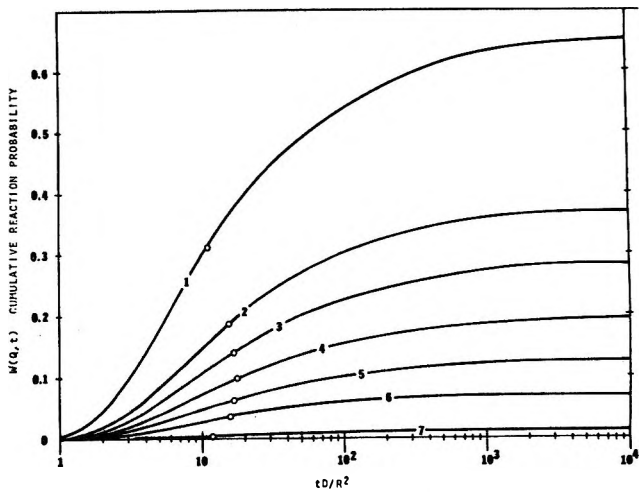

Figure 4. Cumulative reaction probability as a function of time (in units of R^2/D) for totally reacting Brownian particles of initial separation $r_0 = 5R$. $Q = -5.0$ (1), -2.0 (2), -1.0 (3), 0.0 (4), + 1.0 (5), +2.0 (6), +5.0 (7). Circles show $\tau_{1/2}{}^W$, the time at which half the particles have reacted.

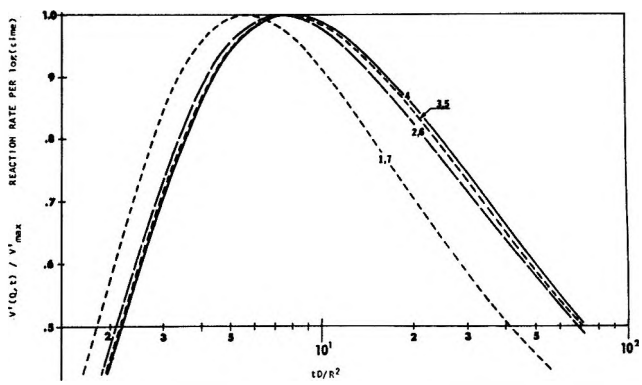

Figure 5. Reaction probability per unit (log time) for totally reacting Brownian particles of initial separation $r_0 = 5R$. $Q = -5.0$ (1), -2.0 (2), -1.0 (3), 0.0 (4), +1.0 (5), +2.0 (6), +5.0 (7). Curves 1 and 7, 2 and 6, and 3 and 5 are so nearly identical over a large part of the range plosted that they are not distinguishable. It should be noted that while the shapes of these pairs of normalized curves are so nearly identical, their magnitudes when not normalized are vastly different, as reflected in column 4 of Table I.

The principal purpose in constructing these numerical solutions was to study the shape of the probability curves along the time axis. For totally reactive particles ($\gamma = 1$), $W(Q,t)$ and the related quantity $V'(Q,t) = \partial W(Q,t)/\partial \ln(t)$, have been plotted in Figures 4 and 5. In Table I, alongside values of the magnitude of these quantities as functions of Q, we have tabulated the half-time, $\tau_{1/2}{}^W(Q)$ for which

$$W(Q,\tau_{1/2}{}^W) = {}^1/_2 W(Q,\infty) \quad (59)$$

and the peak rate time $\tau_{max}{}^V(Q)$ at which $V'(Q,t)$ is a maximum. The graphs and the table show the respective functions calculated at an initial separation $r_0 = 5R$. The results at $r_0 = 2R$ and at $r_0 = 1.1R$ support the conclusions drawn from the tabulated data.

Table I: Reaction and Encounter Probabilities and Indicator Times as a Function of Particle Charge, at $r_0 = 5R$

	Totally reacting particles ($\gamma = 1$)			Nonreacting particles ($\gamma = 0$)	
Net charge parameter Q	Reaction half-time[a] $\tau^1/_2{}^W$	Time[a] of peak reaction rate[b] $\tau_{max}{}^V$	Total reaction probability W_∞	Time[a] of peak encounter density $\tau_{max}{}^G$	Peak encounter density $R\ G_{max}$
−5	11.3	5.6	0.636	7.6	0.239
−2	15.7	7.4	0.381	4.6	0.032
−1	17.0	7.8	0.287	3.9	0.0159
0	17.539	8.000	0.2000	3.682	0.00762
+1	17.0	7.8	0.1289	3.4	0.00361
+2	16.4	7.4	0.0770	3.1	0.00175
+5	12.1	5.6	0.0117	2.35	0.00018

[a] Time expressed in units of (R^2/D). [b] Rate per unit log (time). This rate was chosen for best separation of the curves (see Figure 5).

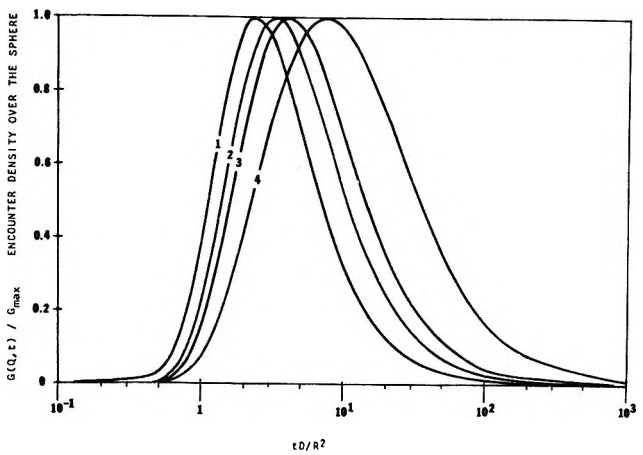

Figure 6. Particle probability density $G(\Sigma)$ at the encounter surface, normalized to unity at its maximum value, for nonreacting Brownian particles of initial separation $r_0 = 5R$. $Q = +5.0$ (1), $+1.0$ (2), -1.0 (3), -5.0 (4).

For nonreacting particles ($\gamma = 0$), $G(Q,R,t)$ is plotted in Figure 6, and for these, Table I lists the peak encounter density time $\tau_{max}{}^G(Q)$ at which G has its maximum value.

In a heuristic way one can conclude that, for particles which do *not* react, Coulomb attraction pulls them together and holds them longer and Coulomb repulsion keeps them apart and pushes them away more quickly. For reactive particles, on the other hand, the reaction occurs most "slowly" for uncharged particles; *both* attraction and repulsion cause whatever reaction does occur to happen "faster" (earlier). Though not necessarily what might have been expected, these conclusions can be reconciled with an intuitive picture.

The more significant conclusion, however, is that the shifts in the shape of the curves along the time axis are small in the range $-5 < Q < +5$, while in the same range the magnitude of the curves varies immensely. For reacting particles the total reaction probability varies by a factor of 50, and for nonreacting particles, the peak encounter density probability varies by three orders of magnitude, while in all cases the indicator times vary by at most a factor of 3. From eq 49 it is clear that particle pairs for which $|Q| > 5$ would be rarely encountered in practice.

It is suggested that for practical purposes, a good approximation to a time-dependent solution for charged particles can therefore be obtained by multiplying the probability density expressions for uncharged particles by a Coulomb interaction factor which is a function of Q but not of time, and which can be derived from the steady-state form of the solution.

Thus, to a good approximation, we obtain from eq 18 and 52

$$W(Q,t) \approx \frac{e^{QR/r_0} - 1}{e^Q(1 + Q/hR) - 1}\{\mathrm{erfc}(y_0) - e^{x^2 + 2xy_0}\mathrm{erfc}(x + y_0)\} \quad (60)$$

where $y_0 = (r_0 - R)/\sqrt{4Dt}$; $x = \sqrt{Dt}/(R - \bar{R})$.

For nonreacting particles, using correspondence of the integral over all time as a criterion for calculating the Coulomb factor, we obtain

$$G(Q,t, \text{ at } h = 0) \approx \frac{e^{QR/r_0} - 1}{RQe^Q}\left\{\frac{e^{-(r_0 - R)^2/4Dt}}{\sqrt{\pi Dt}/R} - e^{(r_0 - R)/R + Dt/R^2}\,\mathrm{erfc}\left(\frac{\sqrt{Dt}}{R} + \frac{(r_0 - R)}{\sqrt{4Dt}}\right)\right\} \quad (61)$$

5. An Application to the Migration of Ions on the Surface of a Protein Molecule

The foregoing has made it possible to estimate the effective surface conductance of a protein molecule in isoionic solution due to secondary recombination of hydrogen ion, provided only that certain chemical quantities about the system are known or can be estimated. Models to predict the effect of such surface conductance on the measured complex dielectric constant of the protein solution are available,[26,27] but no reliable estimate of the magnitude of the surface conductance has previously been made.

In this problem we will slightly redefine the meaning

(26) H. Schwan in *Adv. Biol. Med. Phys.*, **5**, 158 (1957).

(27) C. T. O'Konski, *J. Phys. Chem.*, **64**, 605 (1960).

of the term, secondary recombination, to mean in this case those ions which have dissociated from one binding site on a protein, and which recombine with the same protein molecule but at a different binding site. This is an appropriate definition in this case as the kinetic values which we will use are taken from experiments in which those ions which dissociate but rebind at the same site are never seen, even though they may have become separated from the site by one or several intervening solvent molecules.

We will represent serum albumin as a spherical molecule of radius 30 Å. We will use a recent estimate[28] of 60 as the number of free carboxyl groups which are accessible to hydrogen-ion binding on the surface of the molecule at the isoionic pH, for which we will use the value 5.3. The dissociation kinetics of carboxylic acids measured by Eigen[29] will be assumed to apply. The titration curve of albumin near the isoionic pH gives little reason to believe this is not a fair assumption.

There is, of course, no claim that the results we shall obtain will be of more than order of magnitude accuracy, due to the great over-simplification of the model in many respects, not the least of which is the use of a spherical model, when the molecule is known[30] to be elongated with an axial ratio near 4. Nevertheless, the result as an order of magnitude estimate may be useful.

From Eigen's work, we will use a value

$$k_{21}^{\mathrm{COOH}} = 8 \times 10^5 \ \mathrm{sec}^{-1} \quad (\text{at } 25°) \tag{62}$$

for the generalized reaction

$$-\mathrm{COO}^- + \mathrm{H}^+ \underset{k_{21}^{\mathrm{COOH}}}{\overset{k_{12}^{\mathrm{COOH}}}{\rightleftharpoons}} -\mathrm{COOH} \tag{63}$$

The albumin molecule in its discharged state will be designated by the symbol "P." The 60 carboxyl sites available for hydrogen ion binding at the isoionic pH will be considered equivalent and uniformly distributed over the surface of the protein. The number of hydrogen ions bound when the net charge on the molecule is zero will be called ν_0; thus the valence $Z(\mathrm{P})$ of P is $-\nu_0$ in protonic units. The molecule with ν sites occupied will be designated by (PH_ν). The binding reactions are then described, in principle, by the 60 equations

$$(\mathrm{PH}_\nu) + \mathrm{H} \underset{k_{21}^{P}(\nu)}{\overset{k_{12}^{P}(\nu)}{\rightleftharpoons}} (\mathrm{PH}_{\nu+1}) \tag{64}$$

A set of distribution coefficients $f(\nu)$, the fractions of protein molecules in each state (PH_ν), is then obtained as the solution of the equilibrium conditions

$$f(\nu)[\mathrm{H}^+]k_{12}^{P}(\nu) = f(\nu+1)k_{21}^{P}(\nu) \tag{65}$$

where eq 55 is used to obtain the forward rate constants, with h represented in that equation by $h_0(60 - \nu)/(60 - \nu_0)$ to reflect the effect of the number of free binding sites on the reactivity. The dissociation rate constants are

$$k_{21}^{P}(\nu) = (\nu+1)k_{21}^{\mathrm{COOH}}(1 - W_\infty(Q, \text{at } r_0 = R)) \tag{66}$$

where $(1 - W_\infty)$ is the factor which eliminates recombination ions from being counted as dissociated ions. Equation 54 is used to calculate W_∞.

Although the effect of Debye–Hückel shielding due to the presence of charged protein as counterion in the salt-free solution is small, a first approximation to a correction for this effect was included in the present calculations. A correction factor for the ratio $\Gamma(R)/\Gamma(\infty)$ was obtained from a numerical solution to the steady-state form of eq 5 in which a Debye–Hückel form was used for the interaction energy U.

Of the remaining parameters, Q was evaluated from eq 49, D, the diffusion constant of hydrogen ion, was obtained from the single ion conductivity (giving $D = 9.3 \times 10^{-5}$ cm^2 sec^{-1}), ν_0 was set to the values 6 and 12, corresponding to the choice of 4.3 and 4.6, respectively, for the pK of the carboxyl groups. h_0, and consequently $\gamma_P = h_0R/(1 + h_0R)$, and the 31 distribution coefficients $f(\nu)$, $\nu = 0,1,\ldots 30$, were left to be determined by the 30 equations (65), $\nu = 0,1,\ldots 29$, the normalization condition $\Sigma_\nu f(\nu) = 1$, and the neutrality condition $\Sigma_\nu f(\nu)\, Z(\mathrm{PH}_\nu) = 0$. The states (PH_ν) with $\nu > 30$ are sufficiently rare at the isoionic pH to be neglected.

From the distribution coefficients one can calculate $\langle Z^2 \rangle^{1/2}$, the root-mean-square net charge on the protein. This can be compared with experimental values and with values computed from titration data such as that of Tanford[31] by the statistical functions of Scatchard.[32] In the latter a value of 0.088 calculated from a Debye–Hückel form was used for the electrostatic energy factor w in the equation

$$\log [\alpha/(1 - \alpha)] = \mathrm{pH} - \mathrm{p}K + 0.868wZ \tag{67}$$

where α is the fraction of ionized groups, and Z is the valence.

Tanford and Kirkwood[33,34] have shown that w is in fact strongly dependent on the details of the protein model used. The method of this article, while avoiding the use of this parameter, makes the assumption of the "smeared charge" model which is equivalent to using the simple Debye–Hückel form for w. We have not attempted to include the effects of detailed charge and site geometry in the present calculations, although the most pronounced charge effects may be thus neglected.

The advantage of the method of this article in these calculations is that, in addition to the equilibrium dis-

(28) K. K. Vijai and J. F. Foster, *Biochemistry*, **6**, 1152 (1967).

(29) M. Eigen and J. Schoen, *Z. Elektrochem.*, **59**, 483, (1955).

(30) H. M. Dintzis, Ph.D. Thesis, Harvard University, 1956.

(31) C. Tanford, S. A. Swanson, and W. S. Shore, *J. Amer. Chem. Soc.*, **77**, 6414 (1955).

(32) G. Scatchard, *Ann. N. Y. Acad. Sci.*, **51**, 660 (1949).

(33) C. Tanford and J. G. Kirkwood, *J. Amer. Chem. Soc.*, **79**, 5333, (1957).

(34) C. Tanford, *ibid.*, **79**, 5340 (1957).

tribution $f(\nu)$, it provides separately the forward and reverse rate constants of the reactions (64) and the associated information which is used (below) to calculate the surface mobility of the bound hydrogen ions.

Because the calculations leading to the estimate of surface conductance and the dielectric quantities involve primarily the relations between phenomenological variables, those calculations are least sensitive to the errors in neglecting detailed charge and site geometry. The quantity most sensitive to such error is $\langle Z^2\rangle^{1/2}$, and the relatively good consistency of the calculated values of this quantity with the conductivity data of Figure 7 lends some confidence in the usefulness of the present model.

In Table II are shown the values of $\langle Z^2\rangle^{1/2}$ computed by the two methods with several choices of parameters pK and m, the total number of carboxyl sites accessible at the isoionic pH. The calculated values are to be compared with an experimental value of 1.80 obtained from conductivity of deionized solutions of human and bovine serum mercaptalbumin at 0.3° (Figure 7). In the linear region between the dilution range for hydrogen ion and the high protein concentration saturation range, the slope for both curves is 3.8×10^{-3} (mho/cm)/M, which is almost entirely attributable to conductance of charge-bearing protein. With adjustments for temperature, the root-mean-square net charge is obtained from the conductance K by solving

$$K = \langle Z^2\rangle e^2 D_P c_P / kT \qquad (68)$$

where D_P is the diffusion constant of the albumin, and c_P is the concentration of protein.

Table II: Root-Mean-Square Net Charge on Serum Albumin in Salt-Free Isoionic Solution[a]

Method of calculation	Total no. of accessible binding sites	Assumed pK of these sites 4.0[b]	4.3[c]	4.6[d]
Scatchard[e]	99[b]	1.61	1.86	2.02
	60[c]		1.66	1.86
This paper	60[c]		1.64	1.86

[a] In protonic units. [b] pK = 4.0 calculated from titration curve assuming all 99 groups are equivalently titratable (ref 31). [c] pK = 4.3 with 60 groups titratable at pH = 5.3 according to model of Vijai and Foster (ref 28). [d] pK = 4.6, intrinsic pK for carboxyl groups on small molecules. [e] Reference 32, with w = 0.088.

The results suggest that the value $\langle Z^2\rangle^{1/2} = 3.4$ obtained by Timasheff[35] by light scattering from salt-free albumin solutions is too high. Values of that order of magnitude are predicted only in solutions of high ionic strength where shielding may be considered virtually complete.

The results of section 4.1 showing that the time course of reaction and encounter events is relatively independent of charge allow us to use the latitude dependent solutions of Figure 3b to obtain the locus of recombination of hydrogen ion on albumin.

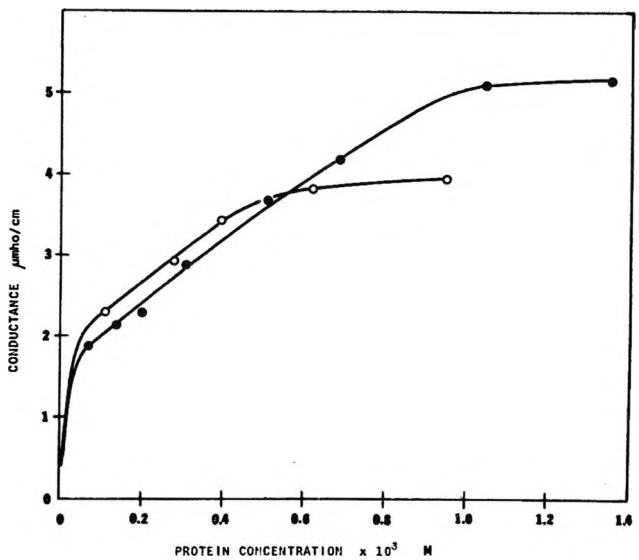

Figure 7. Conductance of isoionic solutions of serum albumin at 0.3°: ●, human mercaptalbumin; ○, bovine mercaptalbumin.

From eq 60 one can calculate that the half-time for recombination of hydrogen ion on albumin is of the order of 2×10^{-11} sec, and that 95% of such recombinations occur in less than 5×10^{-9} sec. Thus dissociation (with rate given by (62)) is the rate-limiting step in the surface diffusion of hydrogen ions, and for the purposes of the Einstein equation (69) the entire recombination path may be regarded as an elementary jump, whose root mean square length $\langle s^2\rangle^{1/2}$ may be obtained from the latitude-dependent solutions. From the values listed in Table III for this distance, one can conclude that most recombination occurs at nearest or next-nearest neighbor sites. On the assumption that sites are distributed uniformly, the nearest neighbor site distance is 14 Å.

The surface mobility μ for hydrogen ion bound to albumin can then be calculated from the relation

$$\mu = e\langle s^2\rangle \gamma_P k_{21}^{COOH}/4kT \qquad (69)$$

and from this, the value of the surface conductance λ is obtained as the product of surface charge density and mobility

$$\lambda = \mu \nu_0 e/4\pi R^2 \qquad (70)$$

This value can be inserted in relationships for dielectric constant given by Schwan[26] and O'Konski,[27] giving for the component of dielectric increment due to hydrogen ion migration, and its relaxation frequency f_0^K, the values shown in Table III. The quantity used for the

(35) S. N. Timasheff, H. M. Dintzis, J. G. Kirkwood, and B. D. Coleman, *Proc. Nat. Acad. Sci., U. S.*, **41**, 710 (1955).

Table III: Calculated Values of Recombination Probability, Surface Conductance, and Dielectric Parameters for Two Values of pK for Dissociable Carboxyl Groups on Model of Serum Albumin

	Value of pK assumed	
	4.3	4.6
Charges bound at $Z = 0$, ν_0[a]	6	12
Recombination probability, γ_P	0.81	0.89
Rms jump distance, $\langle s^2 \rangle^{1/2}$	22 Å	17.5 Å
Surface mobility of H^+ ions, μ	3.0×10^{-7} cm²/sec V	2.26×10^{-7} cm²/sec V
Surface conductance, λ	2.56×10^{-13} mho	3.84×10^{-13} mho
Relaxation frequency, f_0^K	51 KHz	63 KHz
Low frequency dielectric increment per gram/100 ml protein concentration	0.45 ϵ_0	0.66 ϵ_0

[a] Based on 60 accessible binding sites at the isoionic pH (ref 28).

solution conductivity in the Schwan equation was γ_P times the hydrogen ion conductivity at the isoionic pH.

The dispersion calculated in this way could be observed in the region of its relaxation frequency if there were not an alternate way by which the dielectric energy stored by the rearrangement of charge can be dissipated. This way is of course the rotation of the molecule. Since the time constant for this is by a factor of about 20 faster than the characteristic frequency f_0^K, it is important to use the reduced time constant given by a charge fluctuation model[36-38]

$$f_0' \text{ (obsd)} = f_0^K + f_0 \text{ (molecular)} \qquad (71)$$

The principal molecular relaxation frequency for serum albumin at 25° is at about 1.0 MHz.[39] Thus, for a 1% solution of isoionic albumin at 25°, the dielectric increment due to hydrogen ion migration may be expected to be of the order of $0.5\epsilon_0$; the dispersion region, however, will be that of the reduced relaxation time, making this dispersion region experimentally inseparable from the Debye relaxation region. The total increment has been measured as high as $10\epsilon_0$ for a 1% solution of defatted human serum albumin at 0.3°, a figure which would be only somewhat lower at 25°. It is thus clear that the principal polarization mechanism for such molecules is molecular orientation, although according to an earlier estimate[40] it was thought possible that the major dispersion observed may be due to what has been referred to as "proton migration." (Another possible interpretation of that suggestion has been dealt with in a theoretical treatment of dipole vector fluctuations.[38])

Acknowledgment. The author wishes to acknowledge the help and stimulation provided by many discussions of this subject with Dr. J. L. Oncley. This research was supported in part by NIH Grant HE09739 from the National Heart and Lung Institute.

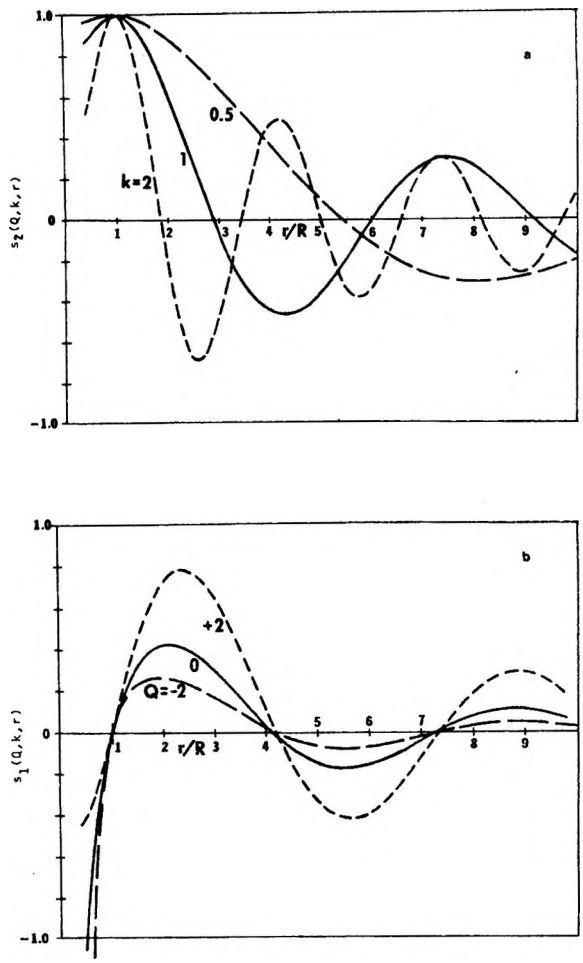

Figure 8. s Functions for the Bessel's equation modified for Coulombic interaction: (a) (top) s_2 functions when $Q = +2.0$, $k = 0.5, 1.0, 2.0$; (b) (bottom) s_1 functions when $k = 1.0$, $Q = -2.0, 0.0, +2.0$ ($Q = 0$ curve is a spherical Bessel's function, graphed for comparison).

Appendix

To find $s_1(Q,k,r)$ and $s_2(Q,k,r)$, two linearly independent solutions of

$$s'' + (2/r - \epsilon)s' + k^2 s = 0 \qquad (72)$$

where ϵ is the perturbation term, $\epsilon = QR/r^2$, we begin at $r = R$ and define two arbitrary but distinct boundary conditions

$$s_1(R) = 0;\ s_1'(R) = 1$$

and

$$s_2(R) = 1;\ s_2'(R) = 0 \qquad (73)$$

and proceed to find at successive points the values of

(36) W. Scheider, *J. Phys. Chem.*, **74**, 4296 (1970).
(37) G. Schwarz, *ibid.*, **71**, 4021 (1967).
(38) W. Scheider, *Biophys. J.*, **5**, 617 (1965).
(39) P. Moser, P. G. Squire, and C. T. O'Konski, *J. Phys. Chem.*, **70**, 744, (1966).
(40) J. G. Kirkwood and J. B. Shumaker, *Proc. Nat. Acad. Sci., U. S.*, **38**, 855, (1952).

$s(r + \Delta r)$ and $s'(r + \Delta r)$ from $s(r)$ and $s'(r)$ with the perturbed difference equation.

First, the unperturbed spherical Bessel's function of zero order through r, having the same value and the same slope at r as does $s(r)$ is determined in terms of two parameters, α and ξ

$$\sigma(r) = (\alpha/r) \sin k(r - \xi) \doteq s \text{ at } r$$

$$\sigma'(r) = \alpha[(k/r) \cos k(r - \xi) - (1/r^2) \sin k(r - \xi)] \doteq s' \text{ at } r \quad (74)$$

$\sigma(r + \Delta r)$ is then the value at $(r + \Delta r)$ of the spherical Bessel's function which coincides in value and slope with s at r. Writing the Taylor expansions of s and of σ in powers of Δr

$$s(r + \Delta r) = s(r) + s'(r)\Delta r + s''(r)(\Delta r)^2/2 + \ldots + s^n(r)(\Delta r)^n/n! + \ldots \quad (75)$$

$$\sigma(r + \Delta r) = \sigma(r) + \sigma'(r)\Delta r + \sigma''(r)(\Delta r)^2/2 + \ldots + \sigma^n(r)(\Delta r)^n/n! + \ldots$$

we can write

$$s(r + \Delta r) = \sigma(r + \Delta r) + a_1\Delta r + a_2(\Delta r)^2/2 + \ldots + a_n(\Delta r)^n/n! \quad (76)$$

But

$$s'(r) = \sigma'(r)$$

$$s''(r) = \sigma''(r) + \epsilon s'(r)$$

$$s'''(r) = \sigma'''(r) + \epsilon s''(r) + \epsilon'(r)s'(r)$$

etc., so that

$$a_1 = 0$$

$$a_2 = \epsilon s'(r) \quad (77)$$

$$a_n = s^n(r) - \sigma^n(r) = \sum_{k=0}^{n-2} \binom{n-2}{k} \epsilon^k s^{n-1-k} \text{ for } n > 2$$

where $\binom{n}{k}$ are the binomial coefficients. The derivatives s^n are computed from

$$s^n = -k^2 s^{n-2} - 2(s'/r)^{n-2} + a_n \quad (78)$$

which comes from the definition of a_n in terms of the perturbed and unperturbed form of eq 72.

Since the computation of a_n involves knowledge only of $s', s'', \ldots s^{n-1}$, eq 77 and 78 permit sequential evaluation of all a_n. Where the series 76 is to be truncated is a computational decision which does not affect the ultimate accuracy of the function generated. The longer the series, the greater the interval Δr can be, and hence the fewer iterations are needed to compute the function s in some range of values of r. In practice, 20 terms can be calculated without difficulty, and convergence tests can be built into the computer program to truncate earlier when warranted.

Several typical functions $s(Q,k,r)$ are graphed in Figures 8a, b. A $Q = 0$ function, which is the appropriate spherical Bessel's function, is plotted in one case for comparison.

Isotope Effects on Hydroxide Ion in Aqueous Solution[1]

by E. A. Walters[2a] and F. A. Long*[2b]

Departments of Chemistry, Cornell University, Ithaca, New York, and the University of New Mexico, Albuquerque, New Mexico (Received August 23, 1971)

Publication costs assisted by Cornell University

A method separating primary and secondary isotope effects on hydroxide ion involved in proton abstraction reactions in mixed aqueous solutions of H_2O and D_2O is proposed. The method is based on the transfer effect formalism of the Gross–Butler theory of solvent isotope effects. A fractionation factor for hydroxide ion of 0.45 and a degenerate activity coefficient for transfer of hydroxide from H_2O and D_2O, explicitly assuming $\gamma_{H_3O^+} = 1.0$, of 1.14 are obtained from water ion product data in mixed aqueous solvents. These are applied to the rate data for detritiation of 1,4-dicyano-2-butene-1-*t* at 25° by the bases hydroxide and triethylamine; the observed hydroxide ion isotope effect, $k_{OH^-}{}^{H_2O}/k_{OD^-}{}^{D_2O} = 0.722$, is factored into a secondary kinetic isotope effect, $k_{OH^-}{}^{H_2O}/k_{OD^-}{}^{H_2O} = 0.57$, and a secondary solvent isotope effect, $k_{OH^-}{}^{H_2O}/k_{OH^-}{}^{D_2O} = 1.27$. The triethylamine isotope effect is totally a secondary solvent effect, $k_{Et_3N}{}^{H_2O}/k_{Et_3N}{}^{D_2O} = 1.24$.

It was pointed out by La Mer and coworkers[3] many years ago and it has been confirmed by many recent investigators[4] that, in dealing with kinetics and equilibrium in H_2O–D_2O solvent mixtures, one must take account of both exchange and transfer effects. Exchange effects are related to the exchange of labile hydrogens with those in the mixed solvents; they are usually discussed in terms of a fractionation factor which is the equilibrium constant for an exchange of the type

$$HA^{H_2O} + {}^1/_2D_2O^{H_2O} = DA^{H_2O} + {}^1/_2H_2O^{H_2O} \quad \phi_{HA} \quad (1)$$

Here, as the superscripts indicate, ϕ is for reaction in the reference solvent water, *i.e.*, it is a medium independent constant.

To go into mixed solvents or into pure D_2O, one introduces a free energy of transfer, usually in the form of a degenerate activity coefficient, to take each species from the reference solvent into the actual solvent. Thus, for the case above, in going from H_2O to D_2O

$$DA^{D_2O} = DA^{H_2O}$$

$$\Delta G^\circ = RT \ln \gamma_{DA} \quad (2)$$

For intermediate solvent mixtures, under the assumption that the free energy of transfer ΔG° is linear in the atom fraction of deuterium, n, the appropriate value of the degenerate activity coefficient is given by $\gamma_{DA}{}^n$.

One reason for this particular formulation is to accommodate the fact that there usually is a "mixed" fractionation factor, ϕ_{HA}', which is often experimentally easier to obtain than ϕ and which is related to a combined exchange and transfer. Thus, for the above exchange, ϕ' for the mixed case is for the process

$$HA^{H_2O} + {}^1/_2D_2O^{D_2O} = DA^{D_2O} + {}^1/_2H_2O^{H_2O} \quad \phi_{HA}' \quad (3)$$

In general, the value of ϕ_{HA}' will vary with deuterium content of the mixed solvent. The link between eq 1 and eq 3 is

$$\phi = \phi'\gamma \quad (4)$$

In the absence of other information, there is an understandable tendency to treat ϕ' as if it were a constant, thus implicitly assuming that the γ term is unity. Enough information on γ values is, however, becoming available to make it increasingly feasible to apply the more correct constants ϕ and γ. Furthermore, the generalized Gross–Butler equations[5] along with the known value[6] for the disproportionation constant for the reaction below give a solid foundation for the application of these equations for exchange and transfer.

$$H_2O + D_2O = 2HOD$$

A formal procedure for obviating the need to use free energy of transfer terms, *i.e.*, to permit use of only exchange terms, is to add waters of solvation to reactants and products and then to assume that some or all of the hydrogens on these waters have ϕ values which differ from unity and hence contribute to the overall solvent isotope effect. In a limited number of cases, *e.g.*, hydronium ion, this procedure is illuminating and useful. More often, however, the number of waters considered is arbitrary and ϕ values for them unknown and unde-

(1) Work supported in part by a grant from the Atomic Energy Commission and by NSF Grant No. GP-10596 to the University of New Mexico.

(2) (a) University of New Mexico; (b) Cornell University.

(3) (a) V. K. La Mer and E. C. Noonan, *J. Amer. Chem. Soc.*, **61**, 1487 (1939); (b) R. W. Kingerley and V. K. LaMer, *ibid.*, **63**, 3256 (1941).

(4) (a) E. A. Halevi, F. A. Long, and M. A. Paul, *ibid.*, **83**, 305 (1961); (b) D. M. Goodall and F. A. Long, *ibid.*, **90**, 238 (1968); (c) V. Gold and B. M. Lowe, *J. Chem. Soc. A*, 936 (1967); (d) V. Gold, *Advan. Phys. Org. Chem.*, **7**, 259 (1969).

(5) (a) P. Salomaa, L. L. Schaleger, and F. A. Long, *J. Amer. Chem. Soc.*, **86**, 1 (1964); (b) *ibid.*, **86**, 410 (1964); (c) For reviews, see A. J. Kresge, *Pure Appl. Chem.*, **8**, 243 (1964), and ref 4d.

(6) L. Friedman and V. J. Shiner, *J. Chem. Phys.*, **44**, 4639 (1966); J. W. Pyper, R. W. Newbury, and G. W. Barton, *ibid.*, **46**, 2253 (1967).

terminable. Hence, such ϕ values turn out only to be adjustable parameters to permit a better fit of the data. More importantly, this procedure leads to a neglect of a growing body of information on γ values for transfer from D_2O to H_2O, information which, in many cases, permits a more explicit analysis of the observations.

This paper proposes an interpretation of deuterium solvent isotope effects for the reaction of hydroxide ion with 1,4-dicyano-2-butene-1-*t* and emphasizes the role of exchange and transfer terms. A useful starting point for the discussion is the thoughtful analysis by Gold and Lowe[4c] of their accurate data for the ion product of water in mixed H_2O–D_2O solvents—especially since the emphasis of this analysis was on the state of hydrogen and hydroxide ions in these solutions.

A first point is that these ion product data can be well fitted by a number of different postulates. The simplest possible one which takes explicit account of exchange and transfer with no assumption about solvation is

$$K_n/K_H = (1 - n + nl')(1 - n + n\phi_1) \times (\gamma_H + \gamma_{OH^-})^{-n}$$
$$= (1 - n + nl')[1 - n + n(K_D/K_H)(b/l')]b^{-1} \quad (5)$$

where l' is a fractionation factor for the species H^+ and where the second formulation introduces the general symbol b for the product $\gamma_+\gamma_-$. Note that the fractionation factor ϕ_1 is given by $(K_H/K_D)(b/l')$. As Gold and Lowe point out, this simple approach of eq 5 can fit the observed data very well. This is not too surprising since both l' and b are treated in the fitting process as essentially unspecified parameters.

A further analysis by Gold and Lowe utilizes the H_3O^+ species with emphasis on the accepted value of $l = 0.69$[7] as the fractionation factor for this species. Assuming $b = 1$, the formulation is

$$K_n/K_H = (1 - n + nl)^3(1 - n + n\phi_1) \quad (6)$$

which contains essentially no free parameters, since l is established and ϕ is $l^{-3}\ K_D/K_H$; this formulation fits the data reasonably well.[5a] The fit can, however, be significantly improved by introducing one further parameter, either as b, stressing the transfer term, or, *via* the solvation approach, with an additional fractionation factor ϕ_2 for the three "inner" solvation hydrogens of a solvated hydroxide ion of the formula $[OH(H_2O)_3]^-$ or $H_7O_4^-$. Gold and Lowe's eq 32[4c] relates to the second. It fits the data well when the parameter ϕ_2 is chosen as 0.92. The other formulation, in terms of transfer is

$$K_n/K_H = (1 - n + nl)^3(1 - n + n\phi_1)b^{-n} \quad (7)$$

where b now refers to the product $\gamma_{H_3O^+}\gamma_{OH^-}$. With $b = 1.14$ and $\phi_1 = 0.45$ an excellent fit of the data is obtained. Gold and Lowe[4c] gave values of $b = 1.26$ and $\phi_1 = 0.53$; these were computed by fitting equation 7 to the nonlinear "least squares" fit of their observed values rather than to the experimental quantities themselves. The present results were obtained by fitting equation 7 directly to the reported K_n/K_H ratios. Both these results and those of Gold and Lowe have standard deviations of 0.005. We choose to employ $b = 1.14$ in this discussion because of the very good agreement of this with $\gamma_{OH^-} \simeq 1.11$ recently given by Salomaa,[8] based on the assumption that $\gamma_{H_3O^+} = 1$, and on adoption the transfer formulation (eq 7) for hydroxide ion. It is obvious that a range of values for b and ϕ_1 could reproduce the observed K_n/K_H ratios with nearly the same accuracy.

It is an interesting and curious fact that another pair of values, namely $b = 3.36$, along with a corresponding value of $\phi_1 = 1.55$, fits the experimental data about as well as the pair with the lower value of $b = 1.14$. Hence it is necessary to consider more carefully whether the validity of either of the two b and ϕ_1 pairs can be substantiated by other data.

The most direct experimental determination of the fractionation factor ϕ_1 for hydroxide ion was made by Heinzinger and Weston,[9] who did a determination of the equilibrium by vapor phase analysis. Their data, using a modern value for the equilibrium constant for disproportionation of H_2O and D_2O, leads to a ϕ_1 value of 0.46. This is for the temperature 13.5° but the temperature coefficient for this should not be significant. These same authors survey earlier analyses which can lead to a value for this same equilibrium constant and conclude that their value of ϕ is in reasonable agreement with a number of other determinations. From this we conclude that the lower value of $b = 1.14$ along with the associated $\phi_1 = 0.45$ are the appropriate numbers from the Gold and Lowe data.

Still other information contributes to this conclusion. The ratio $1/\phi_1(\gamma_{OH^-}/\gamma_{Cl^-})$ may be computed from the literature value for $(\gamma_{D_3O^+}{}^2\gamma_{Cl^-}{}^2)/\phi_{D_3O^+}{}^2 = 18.0$[3b] and the ion product constant ratio[10]

$$\frac{K_C^{H_2O}}{K_C^{D_2O}} = \frac{\gamma_{OH^-}\gamma_{H_3O^+}}{\phi_1\phi_{H_3O^+}} = 7.40$$

as $1/\phi_1\ (\gamma_{OH^-}/\gamma_{Cl^-}) = 1.74$. This value may be substantiated by computing the factor $(\gamma_{D_3O^+}\gamma_{Cl^-})/\phi_{D_3O^+} = 4.24$ from the independently determined standard free energy of 3590 J mol^{-1} for the reaction,[7,11] $HCl^{H_2O} + {}^1/_2D_2O = DCl^{D_2O} + {}^1/_2H_2O$, which

(7) P. Salomaa and V. Aalto, *Acta Chem. Scand.*, **20**, 2035 (1966), and references cited therein.

(8) P. Salomaa, private communication.

(9) K. Heinzinger and R. E. Weston, Jr., *J. Phys. Chem.*, **68**, 2179 (1964).

(10) A. K. Covington, M. Paabo, R. A. Robinson, and R. G. Bates, *Anal. Chem.*, **40**, 700 (1968).

(11) R. Gary, R. G. Bates, and R. A. Robinson, *J. Phys. Chem.*, **68**, 1186 (1964).

Table I: Rate Coefficients for Detritiation in M^{-1} Sec^{-1} Units, 25°

Catalyst	k_2 in H_2O	k_2 in D_2O	Ratio
Hydroxide ion	$1.22(\pm0.03) \times 10^{-1}$	$1.69(\pm0.03) \times 10^{-1}$	0.722 ± 0.025
Triethylamine	$7.56(\pm0.11) \times 10^{-3}$	$6.10(\pm0.13) \times 10^{-3}$	1.24 ± 0.04

leads again to $1/\phi_1(\gamma_{OH^-}/\gamma_{Cl^-}) = 1.74$. A third way of arriving at this ratio comes from an early measurement of $1/\phi_1(\gamma_{OH^-}/\gamma_{Br^-}) = 1.54$ [3b] and the more recent $\gamma_{Br^-}/\gamma_{Cl^-} = 1.14$ [8] to give $1/\phi_1$ $(\gamma_{OH^-}/\gamma_{Cl^-}) = 1.76$. The agreement of these estimations leads us to regard this ratio as established with a value of 1.74.

The free energy of transfer of chloride ion from H_2O to D_2O has been computed from literature values to be 800 ± 80 J mol^{-1} [8] which corresponds to $\gamma_{Cl^-} = 1.38 \pm 0.05$. This is a single ion activity coefficient only in the sense that the calculated value is that of the product $\gamma_{H_3O^+}\gamma_{Cl^-}$ to which the assumption that $\gamma_{H_3O^+} = 1.00$ has once again been applied. Substituting $\gamma_{Cl^-} = 1.38$ and the calculated value for ϕ_1 into the ratio $1/\phi_1(\gamma_{OH^-}/\gamma_{Cl^-}) = 1.74$ leads to $\gamma_{OH^-} = 1.08$. This number compares very favorably with $\gamma_{OH^-} = 1.14$ from the water equilibrium suggesting, at least, that ϕ and γ_{OH^-} computed in this paper are consistent with other data on the behavior of ions in aqueous solution so they may be used to interpret experimental information. The next sections illustrate their application to hydroxide ion catalyzed reactions.

Experimental Results

The experimental procedures for rate determination were identical to those described earlier.[12] Water was doubly distilled; deuterium oxide of 99.7% D was used without further purification. Reaction solutions were brought to an ionic strength of 0.1 with NaCl for the experiments with hydroxide ion and to an ionic strength of 0.4 for triethylamine buffers.

The rate of detritiation of 1,4-dicyano-2-butene-1-*t* has been measured at 25° in the solvents H_2O and D_2O with two catalysts, hydroxide ion and triethylamine. The reaction is known to be a general base catalyzed, slow proton removal.[12]

$$RC\text{-}t + B = RC^- + BH^+$$

The experimental data are summarized in the Table I.

Discussion

The measured rate ratio for reactions of hydroxide ion in the two solvents can be expressed as

$$k_{OH^-}{}^{H_2O}/k_{OD^-}{}^{D_2O} = 0.722$$

where subscripts refer to catalyst and superscripts to solvent. This ratio involves contributions from an exchange isotope effect on hydroxide ion and a medium effect for transferring hydroxide ion from H_2O to D_2O. It may be interpreted either using a medium dependent fraction factor or with utilizations of transfer activity coefficients and a medium independent fraction factor.

In terms of medium dependent fractionation factors the Gross–Butler equation for the H_2O–D_2O isotope effect is

$$k_{OH^-}{}^{H_2O}/k_{OH^-}{}^{D_2O} = \phi_1'/\phi_{\neq}'$$

Alternatively one may use formulations involving additional fractionation factors resulting from attributing specific hydration to hydroxide ion. Using the previously determined value for ϕ_1' and the experimental value of the isotope effect a medium dependent fractionation factor for the transition state of $\phi_{\neq}' = 0.62$ can be calculated. Because of the medium dependence of these fractionation factors no identification of them with secondary solvent or secondary kinetic isotope effects can be made.

Explicit consideration of the transfer effect permits a more illuminating analysis. For this approach the modified Gross–Butler equation is

$$k_{OH^-}{}^{H_2O}/k_{OD^-}{}^{D_2O} = \frac{\phi_1}{\phi_{\neq}} \frac{\gamma_{\neq}}{\gamma_{OH^-}\gamma_{RH}} \quad (8)$$

Recalling that both of these fractionation factors are independent of medium and that the transfer activity coefficients have H_2O as the reference solvent, the exchange effect can be identified with a fractionation factor term for the single solvent, water

$$\phi_1/\phi_{\neq} = k_{OH^-}{}^{H_2O}/k_{OD^-}{}^{H_2O} \quad (9)$$

i.e., this is a kinetic isotope effect for reaction of OH^- *vs.* OD^- in water. Likewise, the transfer effect is simply the activity coefficient ratio

$$k_{OH^-}{}^{H_2O}/k_{OH^-}{}^{D_2O} = \frac{\gamma_{\neq}}{\gamma_{OH^-}\gamma_{RH}}$$

and this can be identified with a secondary solvent isotope effect on hydroxide ion. The attractiveness of this approach is that it permits separation of solvent and kinetic isotope effects in a way which is not possible from the fractionation factor point of view alone.

The kinetic isotope effect, equation 9, can be evaluated separately if the two fractionation factors are known. A value of $\phi_1 = 0.45$ was previously estab-

(12) E. A. Walters and F. A. Long, *J. Amer. Chem. Soc.*, **91**, 3733 (1969).

lished from the ion product data of water. Since $\phi_{\neq}$ is not measurable, an approximation must be made. The proton to which $\phi_{\neq}$ applies is the hydroxide proton; in the transition state this proton is being converted from a hydroxide proton to a water proton. This implies that the fractionation factor lies between 0.45 and 1.0, the exact value being dependent upon the degree of proton transfer. Furthermore, it is not unreasonable to associate the value of $\phi_{\neq}$ with the bond order of the O–H bond being formed in the transition state. Bond order has been shown to be related to the Brönsted coefficient for proton transfer[13] and Gold[14] has used the expression $\phi_a = \phi_b^{1-\beta}$ to calculate values for unmeasured fractionation factors where β is the Brönsted parameter. With bases *other* than OH^- the proton transfer from 1,4-dicyanobutene-2 gives a Brönsted β of from 0.94 to 0.98 implying virtually complete transfer of the proton.[12] However, the rate for OH^- is anomalously low and later studies[15] suggest that the proton in this case is transferred only partially to the OH^-, about to an extent corresponding to $\beta = 0.7$. Employing this β value in the power equation above leads to a value of $\phi_{\neq} = 0.79$. Hence the the calculated kinetic isotope effect is

$$\frac{k_{OH^-}^{H_2O}}{k_{OD^-}^{H_2O}} = \frac{\phi_1}{\phi_{\neq}} = 0.57 \qquad (10)$$

It is evident from this ratio that, compared in the solvent water, deuteroxide is a stronger base than hydroxide ion by almost a factor of two. This substantiates the usual observation that deuteroxide in D_2O is a more effective catalyst at removing protons than hydroxide in H_2O;[16] it also points out that deuteroxide in D_2O is a somewhat weaker base than deuteroxide in the solvent H_2O. The effect of drawing the two basicities fairly close together is a result of the substantial transfer effect on hydroxide ion, γ_{OH^-}.

The secondary solvent isotope effect is also revealing. Substitution of the result of equation 10 into equation 8 gives

$$k_{OH^-}^{H_2O}/k_{OH^-}^{D_2O} = \frac{\gamma_{\neq}}{\gamma_{OH^-}\gamma_{RH}} = 1.27 \qquad (11)$$

Transfer effects on neutral molecules generally fall in the range of 0–10%, *i.e.*, $\gamma_{RH} \simeq 1.0$. Substituting this and the value of 1.14 for γ_{OH^-} into the equation shows that $\gamma_{\neq} \simeq 1.4$ is required. This is a very large value, but in line with what is expected for unsolvated anions.[17]

A similar approach may be used to estimate a related $\gamma_{\neq}$ for a case where no fractionation is involved. Rates of detritiation of 1,4-dicyano-2-butene by the base triethylamine lead to the isotope effect.

$$k_{Et_3N}^{H_2O}/k_{Et_3N}^{D_2O} = \frac{\gamma_{\neq}}{\gamma_{Et_3N}\gamma_{RH}} = 1.24 \qquad (12)$$

As this equation shows, the entire isotope effect is a secondary solvent effect. On the assumption again that the transfer effect on the two neutral species is negligible, we obtain $\gamma_{\neq} \simeq 1.2$. Since the proton is fully transferred in this case, the transition state is a zwitterion-like entity, $RC^-\cdots HN^+Et_3$, for which a $\gamma_{\neq} \simeq 1.2$ is large but plausible. It might also be pointed out that isotope effects in other base catalyzed proton abstraction reactions, but with different base catalysts, are of a similar magnitude. Especially interesting is acetate ion catalyzed bromination of methylacetylacetone for which $k_{OAc^-}^{H_2O}/k_{OAc^-}^{D_2O} = 1.25$.[18] In this case the transition state will have a structure closely analogous to that for dicyanobutene with hydroxide ion since γ_{OAc^-} will be a fairly large number, ~1.3; this required that $\gamma_{\neq}$ be ≃1.6, which is much the same as the transfer activity coefficient arrived at for the transition state in equation 10.

(13) R. A. Marcus, *J. Phys. Chem.*, **72**, 891 (1968).

(14) V. Gold, *Trans. Faraday Soc.*, **56**, 255 (1960).

(15) Zafra Margolin and F. A. Long, personal communication.

(16) S. H. Maron and V. K. La Mer, *J. Amer. Chem. Soc.*, **80**, 2588 (1938); J. Hine, "Physical Organic Chemistry," second edition, McGraw-Hill, New York, N. Y., 1962, p 121.

(17) These numbers are not very sensitive to assumptions on the value of $\phi_{\neq}$. Thus if β is assumed to be 0.94, $\phi_{\neq}$ calculates to 0.96. Then $k_{OH^-}^{H_2O}/k_{OD^-}^{H_2O}$ is 0.47 and $\gamma_{\neq}$ calculates to 1.6. These values are not enough different from those calculated from $\beta = 0.7$ to change any conclusions.

(18) F. A. Long and D. Watson, *J. Chem. Soc.*, 2019 (1958).

Calculation of Rate Constants from Relaxation Spectra of Enzyme Reactions

by John L. Haslam

Department of Chemistry, University of Kansas, Lawrence, Kansas 66044 *(Received January 21, 1970)*

Publication costs borne completely by The Journal of Physical Chemistry

A method is presented which can be used for the calculation of rate constants from the relaxation spectra of linear type enzyme reactions. While the method is applicable to all linear reaction mechanisms of this type, it is especially useful for those in which several elementary reactions equilibrate at comparable rates and are coupled together either by common intermediates or by other rapid reactions. Two cases are considered: the reaction in which the enzyme is not regenerated and that in which both product formation and enzyme regeneration occur. This approach has the advantage that for a sequence of more than two reactions the ordering of rate constants for the individual steps automatically results. Since considerable errors may be present in the experimental data that would be compounded in the calculation of rate constants, a method for obtaining rate constants which "best fit" the experimental data is also presented.

Introduction

A number of papers have presented methods for expressing the relaxation times of various mechanisms as functions of the rate constants and concentration terms.[1-5]

In this paper an approach is presented which can be used to obtain numerical values for the individual rate constants for a linear type mechanism, in which the products of the ith reaction are the reactants of the $i+1$st reaction. This type of mechanism without product and enzyme formation is shown in eq 1

$$\mathrm{E} + \mathrm{S} \underset{k_{-1}}{\overset{k_1}{\rightleftharpoons}} \mathrm{X}_1 \underset{k_{-2}}{\overset{k_2}{\rightleftharpoons}} \cdots \underset{k_{-i}}{\overset{k_i}{\rightleftharpoons}} \mathrm{X}_i \underset{k_{-(i+1)}}{\overset{k_{i+1}}{\rightleftharpoons}} \cdots \underset{k_{-(n-1)}}{\overset{k_{n-1}}{\rightleftharpoons}} \mathrm{X}_{n-1} \underset{k_{-n}}{\overset{k_n}{\rightleftharpoons}} \mathrm{X}_n \quad (1)$$

where E, S, X_i represent the enzyme, the substrate, and the enzyme–substrate complexes, respectively.

Chemical relaxation studies of several enzymes[6,7] have shown that a number of elementary chemical reactions are involved in the complete catalytic process. The calculation of accurate values for the rate constants from experimental data for reactions in which more than three intermediates are involved can be difficult, especially if the relaxation times are functions of several elementary reactions. When this situation exists the reactions involved are "coupled" and the relaxation times become complex functions of the various rate constants and concentrations terms. Castellan[2] has presented a general method for expressing in determinant form the relaxation times as a function of the rate constants and equilibrium concentrations of a system which has received a small perturbation from equilibrium. Hammes and Schimmel[3] present a simple method for expanding this determinant for the mechanism of eq 1 in order to obtain the various coefficients for the different powers of the reciprocal relaxation times. A general method of calculating the individual rate constants from the experimental data and a procedure for refining the rate constants to give a "best fit" of the experimental data are presented here.

General Theory

The general expression for the n relaxation times for the mechanism of eq 1 obtained by the procedure of Castellan[2] is given in eq 2.

$$\begin{vmatrix} k_1' + k_{-1} - \lambda & -k_{-1} & 0 & \cdots & 0 & 0 & 0 \\ -k_2 & k_2 + k_{-2} - \lambda & -k_{-2} & \cdots & 0 & 0 & 0 \\ \cdot & \cdot & \cdot & \cdots & \cdot & \cdot & \cdot \\ \cdot & \cdot & \cdot & \cdots & \cdot & \cdot & \cdot \\ \cdot & \cdot & \cdot & \cdots & \cdot & \cdot & \cdot \\ 0 & 0 & 0 & \cdots & -k_{n-1} & k_{n-1} + k_{-(n-1)} - \lambda & -k_{-(n-1)} \\ 0 & 0 & 0 & \cdots & 0 & -k_n & k_n + k_{-n} - \lambda \end{vmatrix} = 0 \quad (2)$$

For the mechanism of eq 1 this determinant contains zeros at all positions except the major diagonal and the diagonals on each side. The symbol k_1' represents $k_1(\bar{E} + \bar{S})$ in which the barred terms designate the equi-

(1) M. Eigen and L. de Maeyer in "Technique of Organic Chemistry," Vol. VIII, Part II, S. L. Friess, E. S. Lewis, and A. Weissberger, Ed., Interscience, New York, N. Y., 1963.

(2) G. W. Castellan, *Ber. Bunsenges, Phys. Chem.*, **67**, 898 (1963).

(3) G. G. Hammes and P. R. Schimmel, *J. Phys. Chem.*, **70**, 2319 (1966); **71**, 917 (1967).

(4) G. Czerlinski, *J. Theoret. Biol.*, **7**, 435, 463 (1964).

(5) K. Kustin, D. Shear, and D. Kleitman, *ibid.*, **9**, 186 (1965).

(6) G. G. Hammes, *Accounts Chem. Res.*, **1**, 321 (1968).

(7) G. G. Hammes and J. L. Haslam, *Biochemistry*, **8**, 1591 (1969).

librium concentrations of the respective species; the λ's, the reciprocal relaxation times, are those values which make the determinant equal to zero. Equation 2 written as a polynomial equation in λ is

$$(-\lambda)^n + A_1(-\lambda)^{n-1} + A_2(-\lambda)^{n-2} + A_3(-\lambda)^{n-3} + \ldots + A_n = 0 \quad (3)$$

The coefficients, A_i, are given by the method of Hammes and Schimmel[3] as

$$A_1 = \sum_{i=1}^{n} (k_i + k_{-i}) \quad (4)$$

$$A_2 = \sum_{i=1}^{n-1} \sum_{j=i+1}^{n} [(k_i + k_{-i})(k_j + k_{-j})]_R \quad (5)$$

$$A_3 = \sum_{i=1}^{n-2} \sum_{j=i+1}^{n-1} \sum_{k=j+1}^{n} [(k_i + k_{-i})(k_j + k_{-j})(k_k + k_{-k})]_R \quad (6)$$

$$\vdots$$

$$A_n = \prod_{i=1}^{n} [(k_i + k_{-i})]_R \quad (7)$$

In these equations the subscript R stands for the reduced products which means that for the mechanism being considered all of the terms or combination of terms which contain $k_{-i}k_{i+1}$ are eliminated. Again, in these equations k_1 must be replaced by $k_1(\bar{E} + \bar{S})$.

From the relationships between the roots and the coefficients of a polynomial equation, the following equations are obtained

$$A_1 = \sum_{i=1}^{n} \lambda_i \quad (8)$$

$$A_2 = \sum_{i=1}^{n-1} \sum_{j=i+1}^{n} \lambda_i\lambda_j \quad (9)$$

$$A_3 = \sum_{i=1}^{n-2} \sum_{j=i+1}^{n-1} \sum_{k=j+1}^{n} \lambda_i\lambda_j\lambda_k \quad (10)$$

$$\vdots$$

$$A_n = \prod_{i=1}^{n} \lambda_i \quad (11)$$

To use eq 4–7 and 8–11 in calculating the $2n$ rate constants for the system from the n experimental relaxation times, it is observed that the right hand sides of eq 4–7 involve a concentration-dependent and concentration-independent part. A total of n plots of the values determined from eq 8–11 *vs.* $(\bar{E} + \bar{S})$ can be made; each should be a linear plot from which a slope and intercept can be determined. It is from these n slopes and n intercepts that the $2n$ rate constants can be calculated by use of the following equations

$$k_1 = \text{slope I} \quad (12)$$

$$k_{-1} + \sum_{i=2}^{n} (k_i + k_{-i}) = \text{cept I} \quad (13)$$

$$\sum_{i=2}^{n} (k_i + k_{-i}) = \text{slope II}^* \quad (14)$$

$$k_{-2} + \sum_{i=3}^{n} (k_i + k_{-i}) = \frac{\text{cept II} - \text{slope III}^*}{k_{-1}} \quad (15)$$

To obtain the other terms in the series the following procedure is used: the second term in the numerator of eq 15 is written down and then the complete right hand side of eq 15 is substracted after the Roman numerals designating the various slopes and intercepts have been increased by one. Finally the whole expression is divided by the leading rate constant on the left-hand side of the equation being computed reduced in number by one. Other terms in the series are obtained in a similar manner.

As an example, the next two expressions would be formulated as

$$\sum_{i=3}^{n} (k_i + k_{-i}) = \frac{\text{slope III}^* - \left[\dfrac{\text{cept III} - \text{slope IV}^*}{k_{-1}}\right]}{k_2} \quad (16)$$

and

$$k_{-3} + \sum_{i=4}^{n} (k_i + k_{-i}) = \frac{\dfrac{\text{cept III} - \text{slope IV}^*}{k_{-1}} - \left[\dfrac{\text{slope IV}^* - \dfrac{(\text{cept IV} - \text{slope V}^*)}{k_{-1}}}{k_2}\right]}{k_{-2}} \quad (17)$$

The values of the slopes and intercepts are obtained from the plots; for example, slope I and cept I are the slope and intercept of eq 8 plotted against $(\bar{E} + \bar{S})$, and slope II and cept II are obtained from eq 9, etc. Those slopes designated with an asterisk indicate that this slope has been divided by $k_1 \equiv$ slope I.

In calculating these terms, expressions will arise which have slopes and intercepts of numbers larger than n, in which case those particular slopes or intercepts are given values of zero in the computation. The individual rate constants can then be obtained from these equations by subtraction.

Equilibrium constants can now be calculated and compared with the overall equilibrium constant $K = \sum_{i=1}^{n} [X_i]/[E][S]$ which is also equal to slope N/cept N. A comparison of the experimentally determined equilibrium constant and the value calculated from kinetic data can be used to determine if the kinetic data when applied to eq 1 are consistent with the equilibrium data.

As can be seen from eq 8–11 the experimentally determined relaxation times need to be accurate inasmuch as any errors will be compounded in the slopes and intercepts with increasing n. To compare the consistency of the calculated rate constants with the experimental data, the roots of eq 3 can be calculated with the aid of a computer[8] at several substrate concentrations and compared directly with the experimental results. Improvement of the fit with the experimental data may be accomplished by a change in the value of one or more of the slopes or intercepts.

Although an analysis of this type is required for reactions which are coupled, there are several advantages that this approach has for the noncoupled case. First, if the reaction is of the linear type the assignment of rate constants to the different steps in the reaction automatically results. Second, first order reactions, especially those which show little concentration dependence and are, therefore, usually difficult to analyze in terms of defining specific rate constants, can also be analyzed by this method.

The rate constants for certain variations of the linear type mechanism can be calculated by this method. In the mechanism of eq 18 there is product formation and regeneration of the enzyme which, however, has been modified during the course of the reacton so that it is unreactive with substrate.

$$\mathrm{E} + \mathrm{S} = \mathrm{X}_1 = \ldots = \mathrm{X}_l = \ldots \mathrm{X}_{n-1} = \mathrm{E}' + \mathrm{P} \quad (18)$$

If, in the reactions of eq 18, there is a step which is slow relative to the others, then the reaction can be divided in two parts. The reactions preceding and those following the slow step can be analyzed separately and are kinetically of the form of eq 1. The relaxation time for the slow step[3] is then related to the rate constants for this step and the equilibrium constants for the other reactions by

$$1/\tau = \frac{k_l}{1 + \dfrac{1}{(\bar{E} + \bar{S})} \displaystyle\prod_{i=1}^{l-1} \frac{1}{K_i} + \sum_{i=2}^{l-1} \prod_{j=i}^{l-1} \frac{1}{K_j}} + \frac{k_{-l}}{1 + \dfrac{1}{(\bar{E}' + \bar{P})} \displaystyle\prod_{i=l+1}^{n} K_i + \sum_{i=l+2}^{n} \prod_{j=i}^{n} K_j} \quad (19)$$

in which the K's are the corresponding equilibrium binding constants for the reactions of eq 18 and the lth step in the reaction is the slow step.

The calculation of rate constants for the enzyme reaction shown in eq 20 is more difficult because of the common enzyme species involved in both bimolecular steps.

$$\mathrm{E} + \mathrm{S} = \mathrm{X}_1 = \ldots = \mathrm{X}_l = \ldots = \mathrm{X}_{n-1} = \mathrm{E} + \mathrm{P} \quad (20)$$

The various expressions in eq 4–7 for this mechanism are no longer linear functions of $(\bar{E} + \bar{S})$ or $(\bar{E} + \bar{P})$ but involve terms of the form $(\bar{E}^2 + \bar{E}\cdot\bar{P} + \bar{E}\cdot\bar{S})$ as well.

Since the mechanism of eq 20 is of importance in the study of many enzyme systems, an approach is presented which can be used to solve for the rate constants for this mechanism under certain conditions. To do this by the method discussed above, eq 4–7 must be linearized: the terms involving $(\bar{E}^2 + \bar{E}\cdot\bar{S} + \bar{E}\cdot\bar{P})$ must be negligible compared with the terms involving $(\bar{E} + \bar{S})$ and $(\bar{E} + \bar{P})$; that is, the enzyme concentration must be small compared with the substrate or product concentrations. Under these conditions, the term $(\bar{E} + \bar{P})$ can be replaced by $\bar{S}K$ where K is the overall equilibrium constant and then combined with those terms containing $\bar{S}$. All of the eq 4–7 except the nth equation now become functions only of $\bar{S}$ and plots of eq 8–11 except, again, the last one should be linear. Eq 4–7 are then calculated as previously described with the rate constant k_{-n} being replaced by k_{-n} $(\bar{E} + \bar{P})$ and the reduced products now formed by eliminating the terms containing any of the following

$$k_{-i}k_{i+1};\ k_1k_{-n}(\bar{S}\cdot\bar{P});\ \bar{S}\prod_{i=1}^{n} k_i;\ \bar{P}\prod_{i=1}^{n} k_{-i}$$

and finally linearizing the equations by the modifications discussed above. With only $n - 1$ plots available to calculate the slopes and intercepts at least two rate constants will have to be assumed in order to calculate the remaining rate constants.

Equations are presented in the Appendix which can be used to calculate the rate constants for the mechanism of eq 20 up to four intermediates. Once a set of rate constants has been determined, the equilibrium concentrations of the enzyme, substrate, and product can be accurately calculated from the initial values of the enzyme and substrate. The coefficients of eq 3 can then be calculated from eq 4–7. The calculations are simplified if all experiments are performed at the same initial enzyme concentration. The solutions (λ's) to eq 3 can be determined at several different initial substrate concentrations and compared with the experimental values. Changes are made in the assumed rate constants until the best values are found. At this point variations of slopes and intercepts may be made in order to obtain a better fit.

Under the condition that $\bar{S}$ and $\bar{P} \gg \bar{E}$, results of calculations show that the reciprocal relaxation times

(8) Since these polynomial equations usually have very large coefficients, the simple iteration method has given the best results in determining the roots.

A scheme to approximate the largest root in conjunction with Newton's method is first used to obtain a starting value for the iteration. The iteration procedure is always run on the original polynomial expression to reduce cumulative errors. Synthetic division is used to reduce the polynomial equation by one after a root is determined so that the process can be repeated for the next largest root.

for the two bimolecular steps will be functions of equilibrium substrate concentration. At constant initial enzyme concentration one of the reciprocal relaxation times will usually be a linearly increasing function (coupling with another reaction will change it) and the other will be a nonlinear decreasing function. The amplitudes of these functions are complicated functions of the normal coordinates and initial boundary conditions, but with the condition that $\bar{S}$ and $\bar{P} \gg \bar{E}$ the amplitude of the nonlinear function will usually be smaller than the linearly increasing function.

Summary

The results presented here provide a systematic method for the calculation of rate constants for a linear mechanism (whether coupled or not) for an arbitrary number of intermediates. Although accurate results can only be expected when accurate data are obtained for each reaction, refinement of the rate constants is possible such that values can be determined which are consistent with experimental data.

Appendix

Equations are presented which can be used for the calculation of the rate constants of eq 20 in those cases where the terms involving $(\bar{E}^2 + \bar{E}\cdot\bar{P} + \bar{E}\cdot\bar{S})$ can be neglected. The terms V_s, V_p, K_s, and K_p represent the steady-state parameters of maximal velocity and the Michaelis constants for substrate and product.

Case I. One Intermediate ($E + S = X_1 = E + P$). For this case the steady-state parameters give the four rate constants for the reaction. Perturbation kinetics will show two relaxation times. Assume values of k_1 and k_{-1}: k_{-2} = (slope I $- k_1$)/K; k_2 = cept I $- k_{-1}$.

Case II. Two Intermediates ($E + S = X_1 = X_2 = E + P$). Assume values of k_1 and k_{-1}: k_{-3} = (slope I $- k_1$)/K; k_3 = (slope I cept I $-$ slope II $- k_1k_{-1}$)/$k_{-3}K$; $k_{-2} = A/(1 + B)$; $k_2 = A/(1 + 1/B)$; A = cept I $- (k_{-1} + k_3)$; $B = Kk_{-1}k_{-3}/k_1k_3$.

Case III. Three Intermediates ($E + S = X_1 = X_2 = X_3 = E + P$). Assume values of k_1 and k_{-1}: k_{-4} = (slope I $- k_{-1}$)/K; k_4 = (slope I cept I $-$ slope II $- k_1k_{-1}$)/$k_{-4}K$; k_{-3} = cept I $- k_4 -$ (cept II $-$ cept III/$k_{-4}K_p$)/k_4; k_2 = cept I $- k_{-1} -$ (cept II $-$ cept III/k_1K_s)/k_{-1}; $k_{-2} = A/(1 + B)$; $k_3 = A/(1 + 1/B)$; A = cept I $- (k_{-1} + k_2 + k_{-3} + k_4)$; $B = Kk_{-1}k_{-3}$-$k_{-4}/k_1k_2k_4$.

Case IV. Four Intermediates ($E + S = X_1 = X_2 = X_3 = X_4 = E + P$). Assume values of k_1, k_{-1} and k_2: k_{-5} = (slope I $- k_{-1}$)/K; k_5 = (slope I cept I $-$ slope II $- k_1k_{-1}$)/$k_{-5}K$; A = cept I $- k_{-1} - k_2$; k_{-4} = cept I $-$ (cept I slope I $-$ slope III $- k_1k_{-1}A$)/$k_5k_{-5}K$; B = cept II $-$ (cept III $-$ cept IV/$k_{-5}K_p$)/k_5; C = cept II $-$ (cept III $-$ cept IV/k_1k_s)/k_{-1}; k_4 = cept I $- k_{-4} - k_5 - [B - k_5$(cept I $- k_{-4})]/k_{-4}$; k_{-2} = cept I $- k_{-1} - k_{-2} - [C - k_{-1}$(cept I $- k_2)]/k_2$; $k_{-3} = D/(1 + E)$; $k_3 = D/(1 + 1/E)$; D = cept I $- (k_{-1} + k_2 + k_{-2} + k_4 + k_{-4} + k_5)$; $E = Kk_{-1}k_{-2}k_{-4}k_{-5}/k_1k_2k_4k_5$.

Temperature Dependence of the Heat Capacity of Activation ($\Delta C_p^{\ddagger}$) for Solvolysis Reactions in Water

by Svante Wold

Department of Organic Chemistry, Umeå University, S 901 87 Umeå, Sweden *(Received September 8, 1970)*

Publication costs assisted by the Swedish Natural Science Research Council

The temperature dependence of the rate constants of solvolysis reactions in water has been investigated by fitting polynomial spline functions of third degree in $1/T$ to data from 60 different reactions. The average of the resulting parameters indicates that the heat capacity of activation ($\Delta C_p^{\ddagger}$) for these reactions has a temperature-dependent part with a minimum at about 35°.

Introduction

Heat capacities of activation, ($\Delta C_p^{\ddagger}$), have recently been widely used to obtain information concerning the nature of the transition state in solvolysis reactions.[1,2] Most of the $\Delta C_p^{\ddagger}$ values used in these studies have been estimated from experimental data assuming that $\Delta C_p^{\ddagger}$ is independent of temperature.

(1) R. E. Robertson, *Progr. Phys. Org. Chem.*, 4, 213 (1967).

(2) G. Kohnstam, *Advan. Phys. Org. Chem.*, 5, 121 (1967).

Some recent accurate series of measurements[1] show the necessity to adopt a temperature dependent $\Delta C_p^{\ddagger}$ when the measurements reach over large temperature intervals. However, such a temperature dependence can possibly be divided into two parts: one substrate-dependent and one substrate-independent part. The study of the substrate-dependent part demands more accurate data than are available today, but the independent part might be studied by investigating the average behavior of the total temperature dependence of $\Delta C_p^{\ddagger}$, for a large number of test cases.

The purpose of this investigation is to examine the possibility of such a general, *substrate independent*, temperature variation of $\Delta C_p^{\ddagger}$ for solvolysis reactions in water. The investigation has been restricted to these reactions for two reasons; first, the pronounced structure of water is expected to give rise to a large temperature dependence in $\Delta C_p^{\ddagger}$; secondly, the larger part of the experimental data used in the estimation of $\Delta C_p^{\ddagger}$ concerns solvolysis reactions.

Theory

In order to describe the temperature variation of rate constants (k), one usually fits an extended Arrhenius equation to the data. This equation takes the form

$$\ln k_j = A + B(1/T_j - 1/T_0) + C\mathrm{F}(T_j) + \epsilon_j \quad (1)$$

where T_j is the temperature (°K) at which the rate constant k_j is measured and T_0 is the middle point of the experimental temperature interval. The residuals ϵ_j represent that part of the data not described by the parameters A, B, and C. $\mathrm{F}(T)$ is some function of T which may take the form[1-3]

$$\mathrm{F}(T) = (1/T - 1/T_0)^2 \quad (2)$$

or

$$\mathrm{F}(T) = \ln (T/T_0) \quad (3)$$

The parameters A, B, and C may be interpreted according to the transition state theory[4]

$$\ln k = \ln (kT/h) - \Delta H^{\ddagger}/RT + \Delta S^{\ddagger}/R \quad (4)$$

Inclusion of $\mathrm{F}(T)$ in eq 1 results in $\Delta H^{\ddagger}$ and $\Delta S^{\ddagger}$ becoming temperature dependent

$$\Delta C_p^{\ddagger} = \frac{\partial \Delta H^{\ddagger}}{\partial T} = T\frac{\partial \Delta S^{\ddagger}}{\partial T} = -R\frac{\partial}{\partial T} \times \frac{\partial \ln k}{\partial (1/T)} - R = -CR\frac{\partial}{\partial T}\frac{\partial \mathrm{F}(T)}{\partial (1/T)} - R \quad (5)$$

k and h are the Boltzmann and Planck constants, respectively, R is the gas constant, $\Delta H^{\ddagger}$, $\Delta S^{\ddagger}$, and $\Delta C_p^{\ddagger}$ the enthalpy, entropy, and heat capacity of activation.

It is seen that the temperature dependence of $\Delta C_p^{\ddagger}$ is determined solely by the form of $\mathrm{F}(T)$. Equation 3, which is commonly used[1,2] gives $\delta \Delta C_p^{\ddagger}/\delta T = 0$.

In order to determine the form of $\mathrm{F}(T)$ which best fits the experimental data, there are two principally different ways to proceed. The first, most often used, is to try a large number of different forms of $\mathrm{F}(T)$ and to choose the form which best fits the total body of data according to some criterion, *e.g.*, the criterion of the smallest sum of residual squares (least-squares criterion). This method of search has a principal difficulty; it is in principle impossible to exhaust the number of possible $\mathrm{F}(T)$'s in the search for the best one. Thus one must confine oneself to a limited, finite set of $\mathrm{F}(T)$'s and search this set for the member which best fits the data. The choice of this set is by no means obvious and the necessity to choose a small set makes this type of investigation severely restricted. A further difficulty with this approach in connection with the present investigation is that the difference in fit, according to least-squares criteria, for different forms of $\mathrm{F}(T)$, is quite small as can be seen in the previous investigation.[3]

The second method of search which has been used in this investigation is to fit to each individual data series a sufficiently flexible mathematical model to allow for the computation of the behavior of the parameter of interest (in this case the heat capacity of activation, $\Delta C_p^{\ddagger}$) for each data series separately. This behavior is naturally estimated with large uncertainty for each individual data series but by averaging the results it is possible to compute the average behavior of the parameter for all data series (the substrate-independent part of the variation).

This second approach has the advantage that no special form of $\mathrm{F}(T)$ need be specified in advance. If the mathematical equation fitted to the individual series is sufficiently unrestricted, one will obtain the best form of $\mathrm{F}(T)$ quite automatically. The difficulty lies in the choice of this equation. However, with the recent development of polynomial spline functions,[5] this problem has been very satisfactory solved. Spline

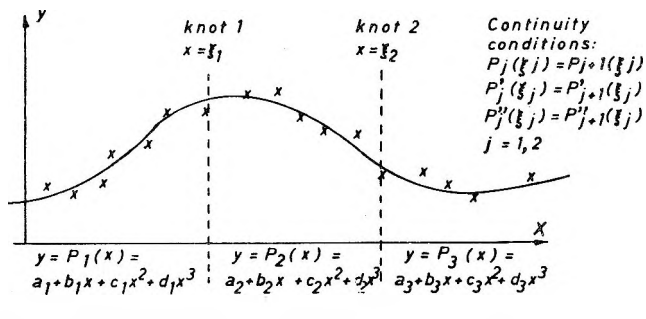

Figure 1. Polynomial spline function of third degree with two knots.

(3) S. Wold, *Acta Chem. Scand.*, **24**, 2321 (1970).

(4) S. Glasstone, K. J. Laidler, and H. Eyring, "The Theory of Rate Processes," McGraw-Hill, New York, N. Y., 1941.

(5) T. N. E. Greville, Ed., "Theory and Applications of Spline Functions," Academic Press, New York, N. Y., 1969.

Table I: Halides (Estimated $\Delta C_p^{\ddagger}$ Values (cal/deg mol) at 25° Using Eq 2, 3, and 12)[a]

Compound	Ref	Temp interval, °C	$\Delta C_p^{\ddagger}$ (25°C) Eq 2	Eq 3	Eq 12	Std dev cal/deg mole	Residual std dev × 10⁴ Eq 2	Eq 3	Eq 12
Methyl fluoride	*b*	80–150	110	66	75	17	15.0	13.8	15.0
Methyl chloride	*c*	50–100	66	49	60	8	5.15	5.25	5.18
Methyl bromide	*c*	35–100	59	46	53	3	4.15	3.76	3.86
Methyl iodide	*c*	50–100	77	56	70	5	3.43	3.66	3.81
Ethyl bromide	*d*	60–90	66	49	60	8	2.08	1.88	1.95
Propyl bromide	*e*	70–100	69	49	60	10	3.95	4.02	3.93
Allyl chloride	*f*	35–85	61	49	55	3	2.30	2.15	2.17
Allyl bromide	*f*	15–65	65	60	59	3	2.29	2.80	2.28
Allyl iodide	*f*	25–70	52	46	47	11	7.70	7.76	7.74
cis-Crotyl chloride	*g*	12–40	66	66	66	2	1.30	1.23	1.43
trans-Crotyl chloride	*g*	6–28	77	82	93	4	2.07	2.07	2.10
2-Methyl-3-chloropropene	*g*	47–88	62	48	57	6	4.70	4.81	4.82
c-$C_3H_5CH_2Cl$	*h*	15–45	83	81	82	5	3.37	3.46	3.34
c-$C_3H_5CD_2Cl$	*h*	15–38	95	95	95	8	2.84	2.83	2.88
Benzyl chloride	*f*	15–65	47	43	42	2	1.70	1.29	1.70
$2\text{-}BrC_2H_5OH$	*e*	75–120	55	37	45	3	2.38	2.49	2.36
2-Chloroethylmethyl sulfide	*e*	1–20	64	71	90	7	2.16	2.16	2.16
$3\text{-}BrC_3H_7OH$	*e*	65–105	66	47	57	5	3.03	3.03	3.04
4-Chlorobutanol	*e*	50–85	53	41	49	5	2.97	2.92	2.90
4-Bromobutylmethyl ether	*e*	35–60	53	46	47	7	2.26	2.24	2.23
Isopropyl chloride	*d*	50–100	51	38	46	4	1.94	2.09	2.02
Isopropyl bromide	*d*	25–75	68	59	60	6	4.24	4.35	4.32
Isopropyl iodide	*d*	25–75	68	58	61	5	5.31	4.70	4.68
Cyclobutyl chloride	*h*	35–60	123	107	107	8	3.13	3.17	3.18
Cyclohexyl bromide	*e*	28–70	68	60	60	3	2.82	2.96	3.01
3-Chloro-1-butene	*g*	1–26	85	92	110	3	1.95	2.00	1.97
3-Bromo-2-methyl-2-butanol	*e*	40–85	95	77	86	8	8.61	8.37	8.27
3-Methyl-2-butyl bromide	*i*	23–51	88	82	79	3	1.16	1.22	1.17
trans-2-Bromocyclohexanol	*e*	60–100	58	42	52	6	4.91	5.01	4.91
tert-Butyl chloride	*j*	1–20	76	83	107	9	1.86	1.88	1.82
tert-Butyl chloride	ref 13	1–35	130	164	159	10	11.4	11.9	10.2
tert-Pentyl chloride	*k*	0–12	96	112	159	30	1.81	1.83	1.75
2,2-Dichloropropane	*l*	27–55	83	75	73	14	4.30	4.29	4.29
2,2-Bromo-, chloropropane	*l*	10–35	92	94	98	4	1.08	1.07	1.23
2,2-Dibromopropane	*l*	20–45	85	80	78	15	3.73	3.67	3.77
2-Chloro-2-methyl-1-propylmethyl ether	*k*	8–40	60	61	64	6	2.24	2.36	2.11
α-Bromoisobutyrate	*m*	10–40	73	73	75	9	3.53	3.52	3.57

[a] The last three columns give the corresponding estimated standard deviations (SD's) of the residuals (ln k_{obsd} − ln k_{calcd}). (The results not agreeing with the original reference have been recalculated.) The estimated SD in column 7 is the mean of the estimated SD's by eq 2, 3, and 12. When T_0 is different from 25°, $\Delta C_p^{\ddagger}$ estimated by eq 2 differs from that of eq 3 due to the temperature dependence of $\Delta C_p^{\ddagger}$ inherent in eq 2. [b] D. N. Glew and E. A. Moelwyn-Hughes, *Proc. Roy. Soc. Ser. A*, **211**, 254 (1952). [c] R. L. Hepolette and R. E. Robertson, *ibid., Ser. A*, **252**, 273 (1959). [d] R. L. Hepolette and R. E. Robertson, *Can. J. Chem.*, **44**, 677 (1966). [e] M. J. Blandamer, H. S. Golinkin, and R. E. Robertson, *J. Amer. Chem. Soc.*, **91**, 2678 (1969). [f] R. E. Robertson and J. M. W. Scott, *J. Chem. Soc.*, 1597 (1961). [g] L. J. Brubacher, L. Treindl, and R. E. Robertson, *J. Amer. Chem. Soc.*, **90**, 4611 (1968). [h] C. Y. Wu and R. E. Robertson, *ibid.*, **88**, 2666 (1966). [i] Y. Inomoto, R. E. Robertson, and G. Sarkis, *Can. J. Chem.*, **47**, 4599 (1969). [j] E. A. Moelwyn-Hughes, R. E. Robertson, and S. E. Sugamori, *J. Chem. Soc.*, 1965 (1965). [k] K. T. Leffek, R. E. Robertson, and S. E. Sugamori, *J. Amer. Chem. Soc.*, **87**, 2097 (1965). [l] A. Queen and R. E. Robertson, *ibid.*, **88**, 1363 (1966). [m] B. N. Hendy, W. A. Redmond, and R. E. Robertson, *Can. J. Chem.*, **45**, 2071 (1967).

functions have the ideal property of being able to describe any continuous variations in the dependent variable and still be computationally facile.

A polynomial spline function of third degree in x ($S(x)$) is defined as a function which is piece-wise defined by a third-degree polynomial in x. These different pieces (P_i in Figure 1) join in the so-called knots (ξ_i in Figure 1) obeying continuity conditions for the function itself and for the first and second derivatives. Once the knots are specified, the least-squares fitting of the spline function to the data is a linear problem,[5] solvable by the ordinary techniques of multiple regres-

Table II: Sulfonates, Sulfates and Others

Compound	Ref	Temp interval, °C	$\Delta C_p^{\ddagger}$ (25°C) Eq 2	$\Delta C_p^{\ddagger}$ (25°C) Eq 3	$\Delta C_p^{\ddagger}$ (25°C) Eq 12	Std dev cal/deg mole	Residual std dev × 10^3 Eq 2	Residual std dev × 10^3 Eq 3	Residual std dev × 10^3 Eq 12
Methylbenzenesulfonate	*a*	10–70	37	34	34	2	1.46	1.62	2.51
Ethylbenzenesulfonate	*a*	10–75	37	34	35	2	2.38	2.46	2.62
n-Propylbenzenesulfonate	*a*	20–80	36	31	32	3	2.69	2.57	2.61
Ethyl-*p*-methylbenzenesulfonate	*g*	10–75	45	40	42	4	5.56	5.41	5.53
Methyl-*p*-methylbenzenesulfonate	*b*	0–80	33	30	32	3	6.87	8.51	6.53
Methyl-*p*-methoxybenzenesulfonate	*c*	35–70	46	39	41	12	4.89	4.84	4.83
Methyl-*p*-bromobenzenesulfonate	*c*	15–65	38	35	35	5	3.51	4.01	3.69
Methyl-*p*-nitrobenzenesulfonate	*c*	25–55	22	20	19	12	3.69	3.73	3.71
Methyl-*m*-nitrobenzenesulfonate	*c*	15–55	34	32	29	15	3.81	3.69	3.81
Methyl-3,4-dimethylbenzenesulfonate	*d*	30–80	46	41	43	5	2.74	2.75	2.80
Methyl-2,4-dimethylbenzenesulfonate	*d*	30–80	43	38	40	5	2.81	2.93	3.02
Methyl-2,4,6-trimethylbenzenesulfonate	*d*	30–80	39	32	35	5	3.23	2.95	2.85
Methyl methanesulfonate	*e*	0–60	37	37	38	2	2.66	3.39	2.64
Ethyl methanesulfonate	*e*	10–80	38	35	36	3	4.05	5.27	4.65
n-Propyl methanesulfonate	*e*	20–90	34	28	30	2	2.91	2.34	2.26
n-Butyl methanesulfonate	*e*	40–90	34	26	29	4	2.36	2.45	2.44
Isopropylbenzenesulfonate	*a*	0–35	39	41	45	5	3.05	3.11	3.05
Isopropyl-*p*-methybenzenesulfonate	*g*	0–40	40	42	45	7	4.47	4.32	4.88
Isopropylmethanesulfonate	*g*	5–33	33	35	38	3	1.15	1.09	1.31
3-Methyl-2-butylmethanesulfonate	*h*	1–25	37	40	48	6	1.61	1.67	1.47
Dimethyl sulfate	*f*	5–45	45	46	48	4	2.74	2.93	2.51
Diethyl sulfate	*f*	5–56	43	43	45	6	4.00	4.19	3.74
tert-Butyldimethylsulfonium ion	*i*	45–90	9	7	8	2	0.988	0.999	0.999

[a] R. E. Robertson, *Can. J. Chem.*, **35**, 613 (1957). [b] R. E. Robertson, *ibid.*, **33**, 1536 (1955). [c] R. E. Robertson, A. Stein, and S. E. Sugamori, *ibid.*, **44**, 685 (1966). [d] G. A. Hamilton and R. E. Robertson, *ibid.*, **37**, 986 (1959). [e] P. W. C. Barnard and R. E. Robertson, *ibid.*, **39**, 881 (1961). [f] R. E. Robertson and S. E. Sugamori, *ibid.*, **44**, 1728 (1966). [g] R. L. Hepolette, *et al.*, *ibid.*, **44**, 677 (1966). [h] Y. Inomoto, *et al.*, *ibid.*, **47**, 4599 (1969). [i] K. T. Leffek, *et al.*, *J. Amer. Chem. Soc.*, **87**, 2097 (1965).

sion.[6] A third-degree spline function is thus a continuous function with continuous first and second derivatives.

Data

The test data consisted of 60 data series from solvolysis reactions in water, measured mainly by Robertson and coworkers. For references see Tables I and II. Data from solvolysis reactions throught to follow reaction mechanisms other than ordinary nucleophilic substitution (SN1, SN2 and possible intermediate types) have not been considered in order to render the material as homogeneous as possible.

Data Analysis

The data analysis has been made in the following way.

Step 1. To each individual data series a third-degree polynomial spline function in $1/T$ has been fitted to the $(\log k, 1/T)$ values.

$$\log k_i = S(1/T_i) + \epsilon_i \qquad (6)$$

$$\Sigma\epsilon_i^2 = \min$$

The number of knots in the spline function was chosen to give at least one knot every 25° at temperatures above 50° and one knot every 15° below 50°. There were no signs of errors in the fittings due to the choice of too few knots.

For each series, $\Delta C_p^{\ddagger}$ was then calculated for grid temperatures within the observed interval, 5° apart, starting at the smallest multiple of 5°. At the temperature T_0

$$\Delta C_p^{\ddagger}(T_0) = \frac{R}{T_0^2}\left[\frac{d^2S(1/T)}{d(1/T)^2}\right]_{T=T_0} - R \qquad (7)$$

Step 2. For the series (index k) which contained the 25° point well inside the experimental interval (between the second and second last points) relative values ($b_k(T)$) were calculated

$$b_k(T) = \Delta C_{p_k}^{\ddagger}(T)/\Delta C_{p_k}^{\ddagger}(25°) \qquad (8)$$

for the grid temperatures (integer multiples of 5°) where $\Delta C_p^{\ddagger}$ values were calculated in step 1.

(6) I. M. Chakravarti, R. G. Laha, and J. Roy, "Handbook of Methods of Applied Statistics," Vol. I, Wiley, New York, N. Y., 1967.

Table III: Resulting Average b Values

	T °C																				
	5	10	15	20	25	30	35	40	45	50	55	60	65	70	75	80	85	90	95	100	105
	$b(T)$																				
	0.64	0.55	0.57	0.88	1.0	0.85	0.83	0.88	0.93	0.82	0.77	0.78	0.72	0.62	0.60	0.80	0.83	0.59	0.59	0.98	0.64
No. of series in b average	8	13	20	21	25	28	28	30	30	30	27	29	26	21	20	15	14	9	7	4	3

From these values, average values (b) were calculated for the grid temperatures, omitting from each series the first and last b_k values since these are less accurate being in the end of the experimental temperature interval.

$$b(T) = \sum_{k=1}^{M} b_k(T)/M \qquad (9)$$

where M is the number of series having the properties: (A) the series has been used in step 2; (B) the series contains T between the second and the second last point. Thus b (T) values were obtained for grid temperatures $T = 5, 10, 15 \ldots .85°$.

Step 3. For all series (index k) *not* yet used in step 2 and which contain the 20° point well inside the experimental interval (analogous definition as in step 2) relative values were computed from

$$b_k(T) = \Delta C_{p_k}^{\ddagger}(T)/\Delta C_{p_k}^{\ddagger}(20°) \cdot b(20°) \qquad (10)$$

where $b(20°)$ was taken from step 2. New *weighted* averages (b) were computed for all relevant temperatures (15, 10 and 5°) from the b values from step 2 and the b_k values from step 3. (The b values were given the weight M if they were calculated from M series in earlier steps, each new b_k value the weight 1).

Step 4. The analogous procedure was repeated for all series not used in step 2 or 3 which contain the 15° point well inside the temperature interval.

Step 5. Analogous procedures were performed for the temperatures 10°, 30°, 35°..... thereby exhausting the number of data series. In each step new b averages for the grid temperatures were computed from the old averages (properly weighted) and the b_k computed in the last step.

In this way average b values were obtained from the total data body in an unambiguous manner; the results are given in Table III. To these b values finally, a spline function with additional smoothing[7] was fitted to obtain a smooth curve representing the *average* behavior (substrate independent part) of

$$\beta(T) = \Delta C_p^{\ddagger}(T)/\Delta C_p^{\ddagger}(25°) \qquad (11)$$

for the investigated data material. This fitting was made with each b value weighted according to the number of series used to compute the b value (line 3 in Table III). The assumed standard deviation of β was 0.08, the reason for which is given below.

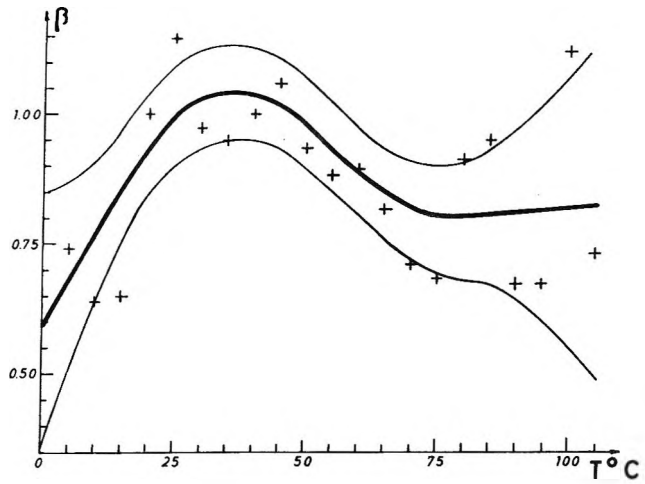

Figure 2. Average variation of $\beta = \Delta C_p^{\ddagger}(T)/\Delta C_p^{\ddagger}(25°)$ with temperature. Thin curves represent upper and lower confidence bands (95%). The crosses are rescaled values from Table III (multiplied by 1.14 to make the curve pass through the point 1.0/25°).

Significance Analysis

Each series was individually fitted and resulted in a rough estimate of the behavior of $\Delta C_p^{\ddagger}$ with temperature for the individual series. The accuracy of these individual estimates can be computed by ordinary statistical methods of multiple regression analysis.[6] It has thus been found that the accuracy (standard deviation, SD) of the individual $\Delta C_p^{\ddagger}$ values was always better than 20%, leading to a maximal SD of the b values (mean values of 20 b_k's in average) of $20/\sqrt{20} \approx 4.5\%$. Since this value gave a less smooth final β-curve a larger value of 8% was used for the SD of the b values in the final fitting. It is hence concluded that the error bands (2 SD's) in Figure 2 represent larger confidence than the 95% claimed in the figure text.

Results

The average behavior of $\beta = b$ is seen in Figure 2. There is a definite maximum of β around 35°, corresponding to a minimum value of $\Delta C_p^{\ddagger}$ since in this investigation all computed $\Delta C_p^{\ddagger}$ values are negative. It is further seen that above 75° the behavior of the curve is highly uncertain owing to insufficient data in this region.

(7) C. H. Reinsch, *Num. Math.*, **10**, 177 (1967).

Tables I and II give the $\Delta C_p^{\ddagger}$ values and SD's for the fitting of each data series to the three-parameter function

$$\log k = A + B(1/T - 1/T_0) + CF(T) \quad (12)$$

where $F(T)$ was chosen to give the same behavior of $b = \Delta C_p^{\ddagger}(T)/\Delta C_p^{\ddagger}(25°)$ as β in Figure 2. It is seen that the fit according to least-squares criteria is not better than when $F(T) = (1/T - 1/T_0)^2$ or $\ln(T/T_0)$ are used. The number of times of better, equal, and worse fit when compared to these functions are 26, 6, 28, and 32, 3, 25, respectively.

Conclusions

A substrate-independent temperature variation of $\Delta C_p^{\ddagger}$ for solvolysis reactions in water supports the assumption that $\Delta C_p^{\ddagger}$ arises from differences in solvation and local solvent structure around the ground and transition states.[1] The minimum in $\Delta C_p^{\ddagger}$ around 35° and the rapid change below this temperature further support this interpretation. Many properties related to water structure[8,9] show an extremum point near 30°, including $\Delta C_p°$ values for the ionization equilibria of some weak acids[9,10] and the bisulfate ion.[11]

An alternative interpretation of the deviations from linearity in the Arrhenius equation based on an equilibrium preceding the rate determining step (referred to by Hulett[12] and Albery and Robinson[13]) would hardly be consistent with a substrate independent variation of $\Delta C_p^{\ddagger}$ with T, considering the large variation in substrates from RCl to $ROSO_2Ar$ with R varying from methyl to *tert*-pentyl and cyclohexyl.

The largest variation in $\Delta C_p^{\ddagger}$ takes place below 25° where the rate of structure change of water is also the largest. This suggests that the T dependence of $\Delta C_p^{\ddagger}$ is smaller in less structured solvents and consequently the assumption that $\Delta C_p^{\ddagger}$ is independent of temperature is more justified for reactions in such solvents.

However, since the variation of $\Delta C_p^{\ddagger}$ with T is not very large even in water, errors made in the estimation of $\Delta C_p^{\ddagger}(25°)$ are seldom large compared with the uncertainty in $\Delta C_p^{\ddagger}$ due to errors of measurement. Therefore the conclusions made by Robertson and others based on $\Delta C_p^{\ddagger}$ values estimated with $F(T) = \ln(T/T_0)$ are not appreciably affected by the results of this investigation.

It must be stressed that this investigation allows no conclusions to be made concerning the total (substrate dependent + substrate independent) temperature variation of $\Delta C_p^{\ddagger}$. The investigation of such phenomena demands a much more accurate estimation of the rate constants since the individual data series must then be examined separately.

Acknowledgments. The author is greatly indebted to Dr. Per Ahlberg for valuable discussions. The access to unpublished data in the Depository of Unpublished Data, National Science Library, NRC, Ottawa, Canada, is gratefully acknowledged.

(8) J. H. Stern and J. T. Swearingen, *J. Phys. Chem.*, **74**, 167 (1970).
(9) F. S. Feates and D. J. G. Ives, *J. Chem. Soc.*, 2798 (1956).
(10) C. S. Leung and E. Grunwald, *J. Phys. Chem.*, **74**, 687 (1970).
(11) J. M. Readnour and J. W. Cobble, *Inorg. Chem.*, **8**, 2174 (1969).
(12) J. R. Hulett, *Quart. Rev. Chem. Soc.*, **18**, 227 (1964).
(13) W. J. Albery and B. H. Robinson, *Trans. Faraday Soc.*, **65**, 980 (1969).

Energy Parameters in Polypeptides. V. An Empirical Hydrogen Bond Potential Function Based on Molecular Orbital Calculations[1]

by R. F. McGuire,[2a] F. A. Momany,[2b] and H. A. Scheraga*

Department of Chemistry, Cornell University, Ithaca, New York 14850 *(Received August 23, 1971)*

Publication costs borne completely by The Journal of Physical Chemistry

Empirical potential functions, based on molecular orbital calculations, are determined for four types of hydrogen bonds, *viz.*, O—H···O<, O—H···O=, N—H···O<, and N—H···O=. These are obtained by first carrying out CNDO/2 calculations of the energy of a number of linear hydrogen bonded dimers. Using empirical energies for all interactions except that between the O and H atoms in the hydrogen bond, the latter function is determined by fitting the empirical expression for the energy of formation of the dimer to the quantum mechanical expression in the region of the *attractive* part of the potential. The O···H empirical interaction potential is further refined by adjusting it so that the minimum in the *total* energy occurs at the experimentally determined depth, and at a distance determined for the cyclic formic acid dimer by gas-phase electron diffraction. In contrast to the *total* interaction energy of the dimer, that for the interaction of the O and H atoms in the hydrogen bond is designated as an empirical general hydrogen bond (GHB) potential. The GHB potential differs for the four types of hydrogen bond cited above, but is the same for a given type of hydrogen bond no matter in which kind of dimer it occurs. On this basis, the total interaction energy in a hydrogen bonded dimer, as computed by the CNDO/2 method, is adequately represented as a sum of empirical nonbonded and electrostatic interactions plus the GHB potential. Without introducing any special angular dependence, the GHB potential, determined in this manner, reproduces the angular dependence (found for hydrogen-bonded linear dimers by the CNDO/2 and other quantum mechanical methods) very well. Thus the nonlinearity of the hydrogen bond (observed in some crystals, and found for some dimers by quantum mechanical calculations) is reproduced by the GHB potential plus the other empirical energies, without resorting to any special angular-dependent term. Further, the GHB potential, obtained for linear dimers, reproduces experimental data for cyclic, doubly-hydrogen-bonded dimers very well.

Introduction

In the first paper of this series,[3] a simple empirical method was used to describe the hydrogen bond interaction by adding an empirical "nonbonded type" of potential function for the interaction of the donor H and acceptor O or N atoms to the usual nonbonded and electrostatic interactions between all other pairs of atoms in the hydrogen-bonded dimer. This empirical potential function was adjusted to fit several experimental quantities and also the long-range monopole electrostatic interactions. One of its main advantages was that it could be very easily included in algorithms for conformational energy calculations on proteins. In subsequent papers,[4-7] we have used several semiempirical molecular orbital methods in order to improve and strengthen the physical basis of the empirical methods which are presently being applied to conformational energy calculations on polypeptides and proteins.[8,9] In this paper, we extend the molecular orbital treatment [using the Complete Neglect of Differential Overlap Theory (CNDO/2) of Pople and Segal[10]], and combine it with experimental gas-phase electron diffraction data and the energy of dimerization, to develop a simple empirical hydrogen-bond-potential function.

It is necessary to have a suitable *empirical* hydrogen-bond-potential function for the study of the conformations of biological macromolecules since the more exact quantum mechanical methods cannot be applied because of the prohibitively high computer size and cost required for the treatment of such large systems; *e.g.*, see Clementi, *et al.*,[11] for an evaluation of the rather astronomical computation times required in more

(1) This work was supported by research grants from the National Science Foundation (GB-28469X and GB-17388), from the National Institute of General Medical Sciences of the National Institutes of Health, U. S. Public Health Service (GM-14312), from the Eli Lilly, Hoffmann-LaRoche, and Smith Kline and French Grants Committees, and from Walter and George Todd.

(2) (a) NIH Postdoctoral trainee, 1968–1969; postdoctoral fellow of the National Institute of General Medical Sciences, National Institutes of Health, 1969–1971; (b) Special Fellow of the National Institute of General Medical Sciences, National Institutes of Health, 1968–1969.

(3) D. Poland and H. A. Scheraga, *Biochemistry*, **6**, 3791 (1967).

(4) J. F. Yan, F. A. Momany, R. Hoffmann, and H. A. Scheraga, *J. Phys. Chem.*, **74**, 420 (1970).

(5) F. A. Momany, R. F. McGuire, J. F. Yan, and H. A. Scheraga, *ibid.*, **74**, 2424 (1970).

(6) F. A. Momany, R. F. McGuire, J. F. Yan, and H. A. Scheraga, *ibid.*, **75**, 2286 (1971).

(7) J. F. Yan, F. A. Momany, and H. A. Scheraga, *J. Amer. Chem. Soc.*, **92**, 1109 (1970).

(8) H. A. Scheraga, *Advan. Phys. Org. Chem.*, **6**, 103 (1968).

(9) H. A. Scheraga, *Chem. Rev.*, 71, 195 (1971).

(10) J. A. Pople and G. A. Segal, *J. Chem. Phys.*, **44**, 3289 (1966).

(11) E. Clementi, J. Mehl, and W. von Niessen, *ibid.*, **54**, 508 (1971).

exact quantum mechanical calculations. These exact methods are even too expensive for treating the rather large number of smaller systems discussed here, and resort is had to the CNDO/2 method, even though it is only an approximation to the more exact procedures. As discussed in previous papers,[4-7] the CNDO/2 method provides valid information when a *group* of related compounds (rather than a few selected ones) is examined, as it is here.

Although a number of empirical hydrogen bond potential functions have been presented in the literature,[3,12-17] their primary emphasis has been on fitting a fixed hydrogen bond length (as observed in crystals) and the energy (from thermodynamic data). Since ranges of bond lengths, bond angles, and energies have been observed for different molecules,[18] involving D–H···A hydrogen bonds, it would seem that the minimum-energy conformation for a particular type of hydrogen-bonded complex [*i.e.*, with particular proton donor (D) and proton acceptor (A) atoms] would depend significantly on *all* the intermolecular interactions and cannot be assumed to depend primarily on the interactions involving only the D, H, and A atoms. Thus, it is necessary to consider the shape of the *total* potential function for the interaction of two molecules in a hydrogen-bonded dimer in order to obtain a correct representation of the D–H···A interaction.

A very important feature of the hydrogen bond interaction, and one which is very poorly understood, is its angular dependence. The origin of this angular dependence has previously been postulated to arise primarily from the "quantum mechanical" nature of the hydrogen bond, which involves the lone-pair electrons on, say, the acceptor oxygen atom in the hydrogen bond. According to molecular orbital theory, these lone-pair electrons are positioned in specific hybridized orbitals (*e.g.*, sp^2 hybridization for an *isolated* C=O group); by *assuming* that this orbital directionality for an *isolated* group is retained upon complex formation, the orbital angular preference would be transferred to the hydrogen bond. This assumption is based on observations of crystals, which indicate that a large number of hydrogen bonds are nonlinear, and in fact close to what one might expect from the sp^2 hybridized orbitals which presumably exist before complex formation. Although considerable angular deviation from pure sp^2 hybridization occurs, there seems to have been an acceptance of the conclusion, stated by Pimentel and McClellan,[15] that "the bond angles display a tendency which reassures us in using the concept of orbital hybridization." However, if one is going to invoke the concept of "hybridization," one should include *all* electron orbital contributions which are mixed in the "hybridization," since additional atoms would perturb the original "hybridization."[19] Thus, as the DH group approaches an oxygen acceptor of an isolated C=O group, the 1s orbital of the hydrogen mixes with the oxygen orbitals, thereby distorting the original sp^2 hybridization of the isolated C=O group. On the basis of this argument, we do not make any *a priori* assumptions about directionality. Thus, instead of assuming, *e.g.*, that the angular dependence displayed by crystal data results primarily from preexisting directed orbitals, we leave open the possibility that the observed angular dependence is a natural consequence of *all* interatomic interactions in the hydrogen-bonded complex. In fact, we will show that the nonlinear hydrogen bond (found in the CNDO/2 calculations) can be reproduced empirically as a sum of all nonbonded and electrostatic interactions among the atoms of the complex, as well as an O···H hydrogen bond interaction which does *not* include any special angular-dependent term.

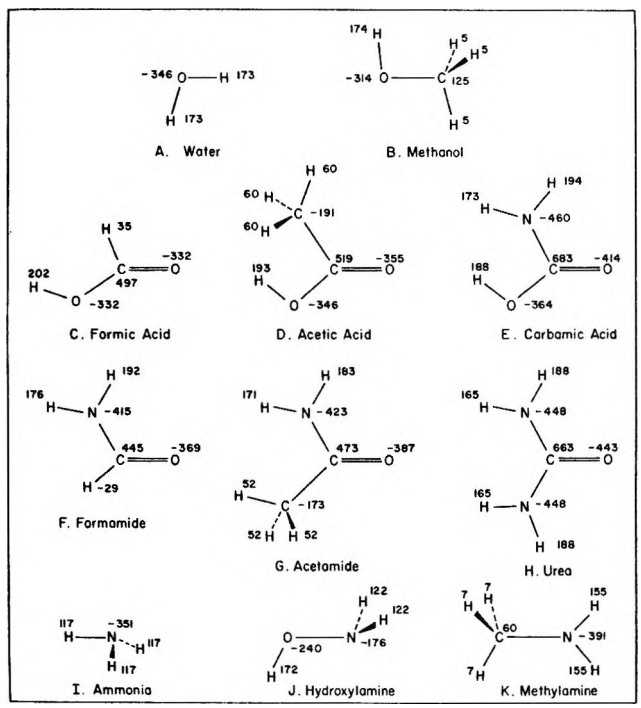

Figure 1. Conformations and partial charges for the monomers used in the hydrogen-bonded model dimers. The overlap-normalized partial charges, calculated by the CNDO/2 method, should be divided by 1000 to obtain electronic charge units.

(12) E. R. Lippincott and R. Schroeder, *J. Chem. Phys.*, **23**, 1099 (1955); *J. Phys. Chem.*, **61**, 921 (1957).

(13) R. Balasubramanian, R. Chidambaram, and G. N. Ramachandran, *Biochim. Biophys. Acta*, **221**, 196 (1970).

(14) N. Salaj, *Acta Chem. Scand.*, **24**, 953 (1970).

(15) G. C. Pimentel and A. L. McClellan, "The Hydrogen Bond," W. H. Freeman, San Francisco, Calif., 1960, p 232.

(16) S. Bratoz, *Advan. Quantum Chem.*, **3**, 209 (1967).

(17) A. S. N. Murthy and C. N. R. Rao, *J. Mol. Struct.*, **6**, 253 (1970).

(18) A. S. N. Murthy and C. N. R. Rao, *Appl. Spectrosc. Rev.*, **2**, 69 (1968).

(19) For example, see C. A. Coulson, "Valence," Oxford University Press, New York, N. Y., 1971 p 197.

Table I: Molecular Geometry[a]

Bond distances		Bond angles	
Bond	Bond length, Å	Bond angle	Value, deg
O(alcohol, water)—H	1.00	$\tau[HO_{water}H]$	105.0
C(methyl)—O(alcohol)	1.36	$\tau[C_{methyl}O_{alcohol}H]$	110.0
C(methyl)—H	1.09	$\tau[HC_{methyl}H]$	109.5
C′(carboxyl)=O	1.23	$\tau[O_{alcohol}C_{methyl}H]$	109.5
C′(carboxyl)—H	1.00	$\tau[C'_{carboxy}O_{alcohol}H]$	110.0
C′(carboxyl)—O(alcohol)	1.29	$\tau[O_{alcohol}C'_{carboxyl}O_{carboxyl}]$	125.0
C′(carboxyl)—C(methyl)	1.53	$\tau[O_{alcohol}C'_{carboxyl}H]$	115.0
C′(carboxyl)—N(amine)	1.32	$\tau[C'_{carboxyl}C_{methyl}H]$	109.5
N(amine, ammonia)—H	1.00	$\tau[O_{alcohol}C'_{carboxyl}C_{methyl}]$	114.5
N(amine)—O(alcohol)	1.46	$\tau[O_{alcohol}C'_{carboxyl}N_{amine}]$	110.5
N(amine)—C(methyl)	1.48	$\tau[C'_{carboxyl}N_{amine}H]$	120.0
		$\tau[N_{amine}C'_{carboxyl}H]$	115.5
		$\tau[HC'_{carboxyl}O_{carboxyl}]$	120.0
		$\tau[C_{methyl}C'_{carboxyl}N_{amine}]$	115.0
		$\tau[C_{methyl}C'_{carboxyl}O_{carboxyl}]$	120.5
		$\tau[N_{amine}C'_{carboxyl}O_{carboxyl}]$	123.0
		$\tau[N_{amine}C'_{carboxyl}N_{amine}]$	114.0
		$\tau[HN_{ammonia}H]$	106.0
		$\tau[N_{amine}O_{alcohol}H]$	103.0
		$\tau[O_{alcohol}N_{amine}H]$	105.0
		$\tau[N_{amine}C_{methyl}H]$	109.5

[a] The geometry in this table was maintained fixed for all conformations studied. The orientations of all end groups are fixed as shown in Figure 1.

To develop a theoretical basis for an empirical hydrogen bond potential function, we have used the CNDO/2 method to compute the energies of a number of linear hydrogen-bonded dimer complexes having the following types of hydrogen bonds: O—H···O<, O—H···O=, N—H···O<, and N—H···O=. The molecules considered are shown in Figure 1 together with the overlap-normalized[20] (CNDO/2) partial charges for each atom in the illustrated conformation; various dimer complexes were formed from these monomers. For amide-type molecules, the geometry chosen was that based on a survey of crystal data for amino acids.[21] The bond lengths and bond angles used in these calculations are shown in Table I (Figure 1). Since variation in the D–H bond length has little effect on the calculated energy, and excessive computer time would be required if the D–H bond length were allowed to vary, the D–H bond length was kept constant in the calculations.[22-25]

The several degrees of freedom which were considered here are shown in Figure 2 and defined as follows: (1) α is the angle between the oxygen axis [defined by a line bisecting the two hydrogen atoms and lying in the H–O–H plane for water (Figure 2A), or the C=O bond for the carboxyl compounds (Figure 2C)] of molecule a and the axis of the H–D (D being the O or N) bond of molecule b, with the O, H, and D atoms being collinear, and both molecules coplanar (with the exception of the hydrogens when necessary) (α = 0° in Figure 2A and 2C); (2) δ is the angle between the oxygen axis (defined above) of molecule a and the H–D bond of molecule b, with the O and H atoms lying along the oxygen axis, and both molecules coplanar as in (1), (δ = 0 in Figure 2A and 2C); (3) θ is the dihedral angle of rotation about the axis defined by the oxygen axis and the H_b and D_b atoms, with the positive direction being clockwise as one looks from a to b and rotates molecule b (θ = 0° in the planar conformation of Figure 2C); (4) $R_{O\cdots H}$ is the distance between the oxygen atom of molecule a and the H(D) atom of molecule b (Figure 2A); for nonlinear hydrogen bonds we will also use $R_{O\cdots D}$, where D is either N or O, shown in Figure 2C; (5) β is the out-of-plane angle which the plane of molecule b makes with that of molecule a with the D–H bond directed toward the O_a

(20) See paper II[4] for definition of overlap-normalized (ON) charges.

(21) R. F. McGuire, F. A. Momany, and H. A. Scheraga, to be published.

(22) While variation in the D–H bond length, especially in hydrogen bonded crystals, has been reported,[23] there is much scatter in the data and it is difficult to detect a trend in the variation of the D–H bond length with, for example, the D···A bond distance. In a few CNDO/2 calculations performed here, in which the D–H bond length was allowed to vary, the results (not shown) indicate that the hydrogen bond energy is not very sensitive to a variation in this bond length. Other more extensive quantum mechanical calculations[11,24,25] do not agree among themselves on this point. Therefore, for these reasons, together with the fact that an empirical function which is intended for conformational energy calculations on macromolecules should be as simple as possible, we have fixed the D–H bond length at the value given in Table I.

(23) W. C. Hamilton and J. A. Ibers, "Hydrogen Bonding in Solids," W. A. Benjamin, New York, N. Y., 1968, p 53.

(24) S. D. Peyerimhoff and R. J. Buenker, *J. Chem. Phys.*, **50**, 1846 (1969).

(25) D. Hankins, J. W. Moskowitz, and F. H. Stillinger, *ibid.*, **53**, 4544 (1970).

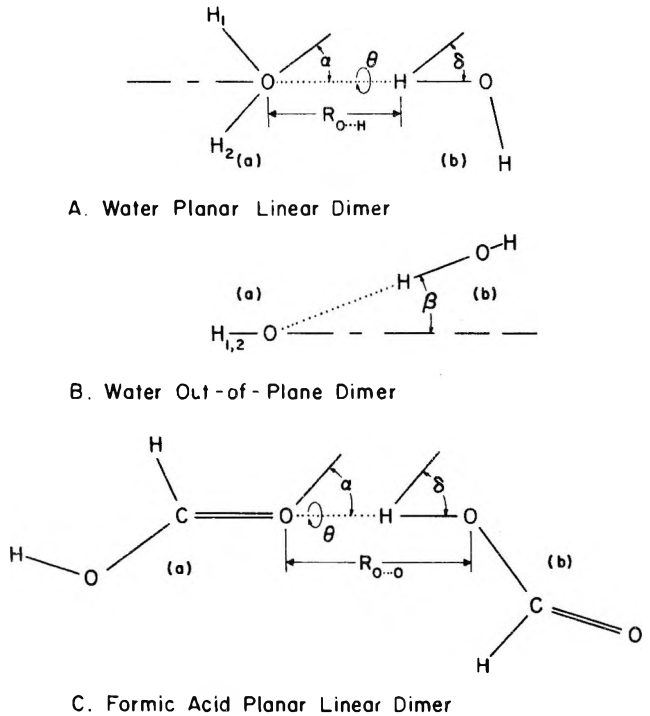

Figure 2. Conformations for the linear hydrogen-bonded dimers studied here. See text for definitions of symbols. $\theta = 0°$ in both Figures A and C.

atom (Figure 2B). Several other conformations were studied in order to compare our results with those previously reported,[5] and these will be noted in the text.

The energies of the complexes were computed as a function of these variables by the CNDO/2 method. The attractive part of these potential curves (computed for the linear dimers as a function of $R_{O\cdots H}$) were fit empirically by adding an empirical potential for the O...H interaction to the nonbonded and electrostatic contributions from all other atoms in the complex. This empirical potential was then refined by requiring that the curve for the total interaction potential energy of the dimer have a minimum (in agreement with thermodynamic data) at a distance corresponding to results from gas-phase electron diffraction data on formic acid. The resulting contribution from the O···H interaction is designated as an empirical general hydrogen bond (GHB) potential. It must be emphasized that the GHB potential is not the *total* interaction energy; the latter is the sum of the GHB potential and all other nonbonded and electrostatic interactions. Further, only the *total* interaction energy, and not the GHB potential, can be compared with experimental data on hydrogen-bonded complexes.

Theory

1. Quantum Mechanical. A brief description of the CNDO/2 method is given in paper II.[4,26] With the exception of the geometry, all input parameters used here were the same as have been used in previous studies.[4,5] Because of limitations on computing time, bond lengths and bond angles within each molecule were not varied, even though it is recognized that the formation of intermolecular hydrogen bonds could lead to changes in these quantities.[22]

2. Empirical. With the exception of the hydrogen bond potential, the empirical functions used here have been reviewed elsewhere.[8] The nonbonded interactions are expressed by a Lennard-Jones 6–12 potential function of the form

$$(U_{ij})_{nb} = \epsilon_{ij}\left[\frac{\langle r_g\rangle_{ij}}{r_{ij}}\right]^{12} - 2\epsilon_{ij}\left[\frac{\langle r_g\rangle_{ij}}{r_{ij}}\right]^{6} \qquad (1)$$

where r_{ij} is the distance between atoms i and j, $\langle r_g\rangle_{ij}$ is the value of r_{ij} at which $(U_{ij})_{nb}$ is a minimum, and ϵ_{ij} is the depth of the potential well at $\langle r_g\rangle_{ij}$. We have recently reevaluated both the $\langle r_g\rangle_{ij}$ and ϵ_{ij} parameters, and these are presented elsewhere,[21] together with all the empirical potential functions, parameters and charges used in conformational energy calculations. The electrostatic interactions are calculated by means of Coulomb's law

$$(U_{ij})_{el} = \sum_{ij}\frac{q_i q_j}{Dr_{ij}} \qquad (2)$$

where D is the apparent dielectric constant, and q_i and q_j are the partial charges (ON) on *all* atoms i and j, respectively, calculated for the monomers by the CNDO/2 method (see Figure 1).

3. Curve Fitting. In order to fit the empirical and quantum mechanical curves for the energies of the hydrogen-bonded complexes, we have used a nonlinear least-squares curve fitting procedure with damping, similar to the method first developed by Levenberg.[27] Briefly, this method may be outlined as follows. Consider a two-dimensional curve described by the experimental coordinates x_i^0 and y_i^0, and suppose one wishes to fit this curve with the expression

$$y_i^c = f(x_i^0, a_1, a_2, \cdots, a_j, \cdots, a_m) \qquad (3)$$

where i varies to indicate the n points used to describe the curve, j is the index for the m variable parameters a_j in the nonlinear function f, and y_i^c is the calculated coordinate corresponding to y_i^0. The m normal equations for the nondamped or Gauss's linear least-squares solution can easily be derived[28] and written in the following form, which includes weighting factors

$$\sum_j^m\left[\sum_i^n F_{ik}F_{ij}w_i\right]\Delta a_j = \sum_i^n (y_i^0 - y_i^c)F_{ik}w_i \qquad (k = 1, 2, \cdots, m) \qquad (4)$$

(26) We are indebted to Professor R. Hoffmann for making the CNDO/2 computer program available to us.

(27) K. Levenberg, *Quart. Appl. Math.*, 2, 164 (1944).

(28) H. Margenau and G. M. Murphy, "The Mathematics of Physics and Chemistry," D. Van Nostrand, New York, N. Y., 1956, p 506.

where the sums are taken over i and j, F_{ij} represents an $n \times m$ matrix with the elements $\frac{\partial f_i}{\partial a_j}$, w_i are weights chosen between 0 and 1, and Δa_j is the change in the variable parameters a_j. According to Levenberg's method, one can rewrite these m normal equations to include a damping parameter, p, as

$$\sum_{i}^{m}\left[\sum_{i}^{n} F_{ik}F_{ij}w_i + p\delta_{kj}\right]\Delta a_j = \sum_{i}^{n}(y_i^0 - y_i^c)F_{ik}w_i \qquad (k = 1, 2, \ldots, m) \quad (5)$$

where δ_{kj} is the kronecker δ

$$\delta_{kj} = 1 \quad (k = j)$$
$$= 0 \quad (k \neq j) \qquad (6)$$

The damping parameter, p, which facilitates convergence, is chosen as follows: initially, p is set equal to zero and the nondamped least-squares solution for the y_i^c's (eq 4) is tested to see if the mean square of the variance

$$\left[MSV = \frac{1}{n(n-1)}\sum_{i}^{n}(y_i^0 - y_i^c)^2\right]$$

has decreased from its initial value. If so, then another iteration is sought. If the MSV value diverges, p is set equal to -0.5, and a new MSV value is obtained. If this new MSV value diverges, p is continually halved until an acceptable solution is found, or until p becomes less than -0.005, at which time the next to last value of p is used as the initial solution for the next iteration. Final convergence is assumed to have occurred when all the a_j's deviate by less than 0.001% from their values in the previous iteration. We have tested this method against several other methods for determining p,[29,30] and found that this method was faster than the others, both in time per iteration and the number of iterations for convergence.

Procedure

The charge distributions and the energies of the monomers shown in Figure 1 were calculated by the CNDO/2 method. Then the energies of a series of linear hydrogen-bonded dimer complexes (listed in Table II) were computed for various values of the $R_{O\cdots H}$ distance (with $\alpha = \beta = \delta = \theta = 0°$) by the CNDO/2 method. To fit an empirical potential to this quantum mechanical potential function, we ignore the repulsive side of the quantum mechanical curve and consider only the attractive side, by proper adjustment of the w_i's in eq 5. This procedure is adopted since it is well known[4-6,31] that the CNDO/2 method underestimates the repulsive interactions, *i.e.*, that it leads to a very short O···H distance in the hydrogen bond, but gives good agreement with experimental data at distances corresponding to the attractive interactions.[4-6,31,32] This fitting is accomplished by first subtracting the empirical nonbonded and electrostatic interactions for all atom pairs between molecules a and b, except that between the H and O atoms in the hydrogen bond. The difference is then fit by an empirical function for the O···H interaction—a different one for each *type* of dimer of Table II. Four general types of hydrogen bond were used since one empirical GHB potential sufficed for describing the O···H interaction for all dimers of a given type. The parameters of the type 2 empirical O···H are then refined to reproduce the gas-phase electron diffraction and thermodynamic data for the cyclic for-

Table II: Various Types of Model Hydrogen-Bonded Linear Dimers

Type	Proton Donor	Proton Acceptor
(1) O—H···O<	Water	Water
	Methanol	Water
(2) O—H···O=	Water	Formic Acid
		Acetic Acid
		Carbamic Acid
		Formamide
		Acetamide
		Urea
	Formic Acid	Formic Acid
		Acetic Acid
		Carbamic Acid
		Formamide
		Acetamide
		Urea
(2a) O—H···O=	Water	Formaldehyde
	Methanol	Formaldehyde
(3) N—H···O<	Ammonia	Water
	Hydroxylamine	Water
	Methylamine	Water
(4) N—H···O=	Ammonia	Formic Acid
		Acetic Acid
		Carbamic Acid
		Formamide
		Acetamide
		Urea
	Formamide	Formic Acid
		Acetic Acid
		Carbamic Acid
		Formamide
		Acetamide
		Urea
	Urea	Formic Acid
		Acetic Acid
		Carbamic Acid
		Formamide
		Acetamide
		Urea
(4a) N—H···O=	Ammonia	Formaldehyde
	Hydroxylamine	Formaldehyde
	Methylamine	Formaldehyde

(29) J. Meiron, *J. Opt. Soc. Amer.*, **55**, 1105 (1965).
(30) J. Pitha and R. N. Jones, *Can. J. Chem.*, **44**, 3031 (1966).
(31) J. R. Hoyland and L. B. Kier, *Theor. Chim. Acta*, **15**, 1 (1969).
(32) A. S. N. Murthy, R. E. Davis, and C. N. R. Rao, *ibid.*, **13**, 81 (1969).

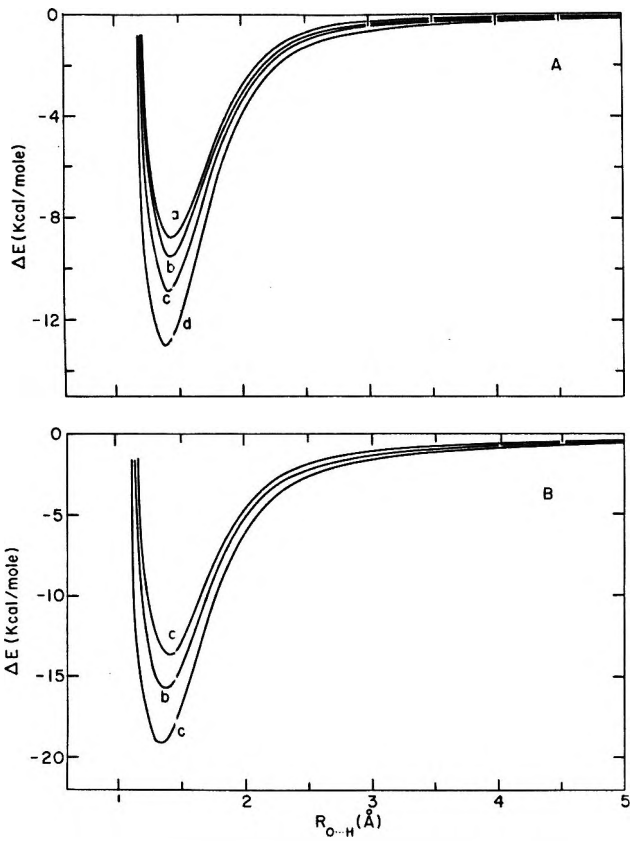

Figure 3. Illustrative CNDO/2 energies for some model linear dimers with hydrogen bonds of types 1 and 2, as a function of the linear distance $R_{O\ldots H}$. For all linear dimers shown, $\alpha = \delta = \beta = 0°$ and $\theta = 0°$. $\Delta E = 0$ for two monomers at infinite separation. (A) Representative dimers with water as the proton donor molecule are: a, water–water (type 1); b, water–formic acid (type 2); c, water–formamide (type 2); d, water–urea (type 2). (B) Representative dimers (type 2) with formic acid as the proton donor molecule are: a, formic acid–formic acid; b, formic acid–formamide, c, formic acid–urea.

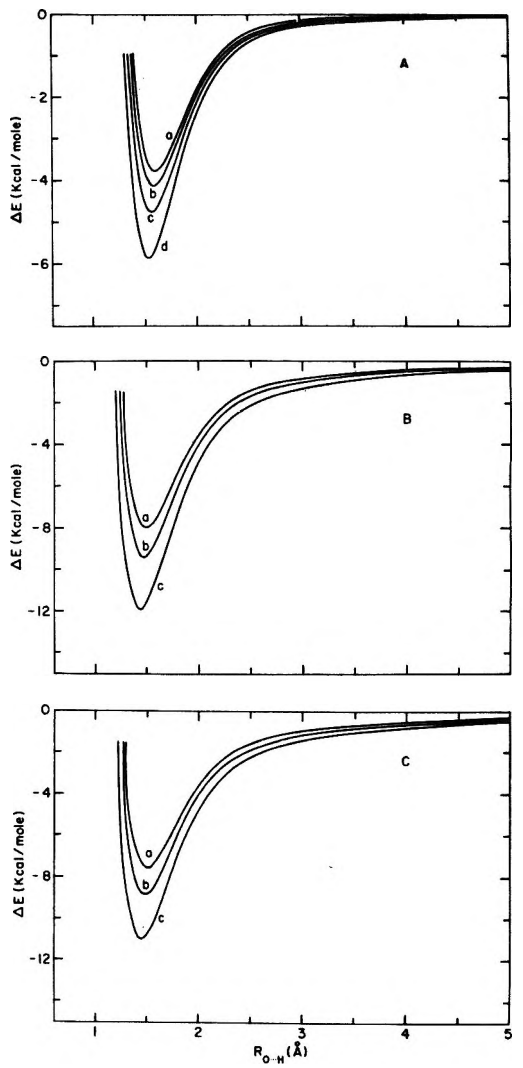

Figure 4. Illustrative CNDO/2 energies for some model linear dimers with hydrogen bonds of types 3 and 4, as a function of the linear distance $R_{O\ldots H}$. For all linear dimers shown, $\alpha = \delta = \beta = 0°$ and $\theta = 0°$. $\Delta E = 0$ for two monomers at infinite separation. (A) Representative dimers with ammonia as the proton donor molecule are: a, ammonia–water (type 3); b, ammonia–formic acid (type 4); c, ammonia–formamide (type 4); d, ammonia–urea (type 4). (B) Representative dimers (type 4) with formamide as the proton donor molecule are: a, formamide–formic acid; b, formamide–formamide; c, formamide–urea. (C) Representative dimers (type 4) with urea as the proton donor molecule are: a, urea–formic acid; b, urea–formamide; c, urea–urea.

mic acid dimer.[33,34] This second adjustment to fit the experimental data did not affect the earlier attained fit to the attractive side of the quantum mechanical potential curve. The empirical function representing the O···H interaction portion of the total energy of the dimer complex is the GHB potential.

As pointed out in the Introduction, no angular dependence is introduced into the empirical potentials. However, we will show (by comparing the total empirical and quantum mechanical energies for the linear dimers) that the angular dependence is accounted for, as a result of the various nonbonded and electrostatic interactions between molecules a and b.

The four types of dimers in Table II contain two subclasses, 2a and 4a, which involve formaldehyde as the proton acceptor. Whereas a specific GHB potential could be obtained for each of the types 1, 2, 3, and 4, for all dimers, this was not true for the dimers of types 2a and 4a. The parameters for the GHB potential fall between those of types 1 and 2 for type 2a, and between types 3 and 4 for type 4a. Since there are many uncertainties about formaldehyde (*e.g.*, its geometry, conformation, and effect of hydrogen bonding thereon), we do not report the results for types 2a and 4a hydrogen bonds here, except to note that they are anomalous.

(33) A. Almenningen, O. Bastiansen, and T. Motzfeldt, *Acta Chem. Scand.*, **23**, 2848 (1969).

(34) W. P. Minicozzi and D. F. Bradley, *J. Comput. Phys.*, **4**, 118 (1969).

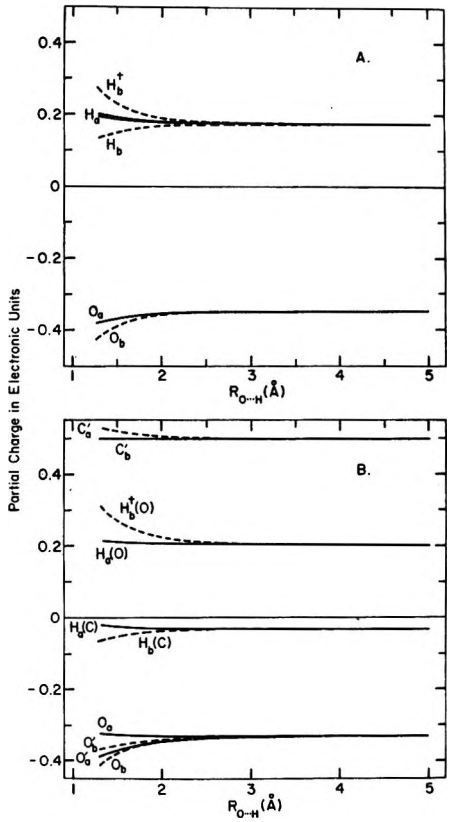

Figure 5. CNDO/2 results for the dependence of partial charge on $R_{O\ldots H}$ for (A) the water–water dimer with $\alpha = \delta = \beta = 0°$ and $\theta = 0°$, and (B) the formic acid–formic acid dimer with $\alpha = \delta = \beta = 0°$ and $\theta = 0°$. The atoms belonging to molecules a or b are designated by subscripts. The dagger indicates the proton in the hydrogen bond, and the primes on the C and O atoms designate the carbonyl groups.

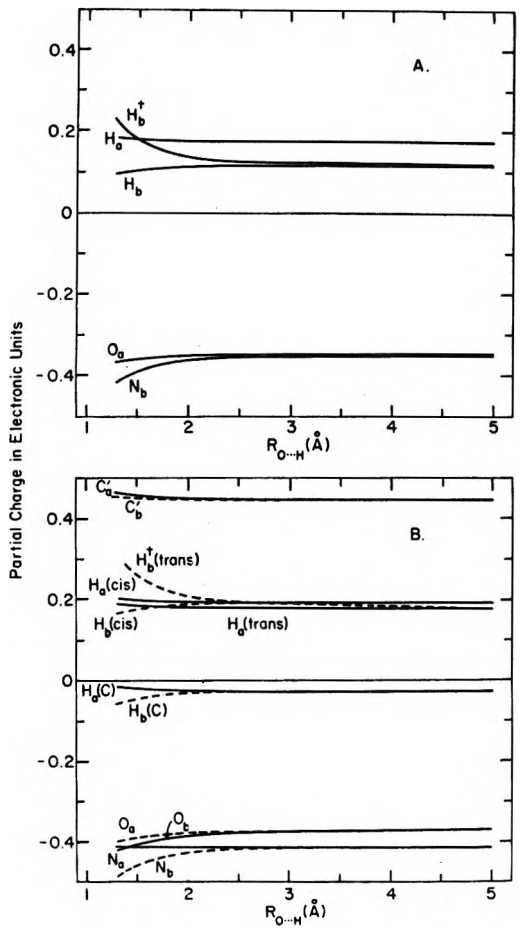

Figure 6. CNDO/2 results for the dependence of partial charge on $R_{O\ldots H}$ for (A) the ammonia–water dimer with $\alpha = \delta = \beta = 0°$ and $\theta = 0°$, and (B) the formamide–formamide dimer with $\alpha = \delta = \beta = 0°$ and $\theta = 0°$. The atoms belonging to molecules a or b are designated by subscripts. The dagger indicates the proton in the hydrogen bond, and the primes on the C and O atoms designate the carbonyl groups. Cis and trans express the position of the hydrogens with respect to the carbonyl oxygen atom.

Results and Discussion

The results are presented and discussed in the following order: (1) CNDO/2 calculations on linear hydrogen-bonded dimers, (2) fitting an empirical GHB potential to the quantum mechanical results, and modifying it to fit experimental data, (3) calculation of total empirical energy of hydrogen-bonded dimer complexes, (4) test of the angular dependence of the total empirical energy of hydrogen-bonded dimer complexes, and (5) comparison of empirical and CNDO/2 results for stacked dimers not linked by hydrogen bonds.

For most of the results, the zero of the energy scale is taken as that of the monomers at infinite separation; for some others, the zero is taken as that of the complex in a specified conformation. In this way, it is easy to see the changes in energy, ΔE, accompanying either the association of two monomers, or the change in the conformation of the complex. These choices of zero energy lead to negative values for a stabilization energy. While a rather extensive number of calculations have been performed, only selected values are reported here for illustrative purposes. All energy differences (*i.e.*, in $U_{CNDO/2}$, in U_{GHB}, or in U_{Total}) are expressed as ΔE.

1. CNDO/2 Calculations on Linear Hydrogen-Bonded Dimers. Assuming the existence of a linear hydrogen bond with a fixed D–H bond length, CNDO/2 calculations of the energy as a function of $R_{O\ldots H}$ were carried out for all of the dimers listed in Table II. In all cases, complete potential curves were constructed for $R_{O\ldots H}$ in the range of 1.3–5.0 Å, similar to those shown for water and formic acid as proton donors in Figure 3, and for ammonia, formamide, and urea as proton donors in Figure 4.

The partial charge distributions (for the O, H, and D atoms) and the *total* energies for all dimers, at several values of $R_{O\ldots H}$, are listed in Table III. Examples of the changes in the charge distributions for all atoms in the dimer, as the hydrogen bond is formed, are shown in Figures 5 and 6.

Table III: Selected CNDO/2 Results for Linear Hydrogen-Bonded Dimers[a,b]

Type	Dimer: Proton Donor	Dimer: Proton Acceptor	$R_{O\cdots H}$ = 1.3 Å: Energy kcal/mol	Partial Charge[c]: O	H	D	$R_{O\cdots H}$ = 1.5 Å: Energy kcal/mol	Partial Charge[c]: O	H	D
(1) O—H···O<	Water	Water	−6.703	−379	269	−420	−8.665	−367	228	−389
	Methanol	Water	−6.949	−382	280	−387	−9.063	−369	235	−356
(2) O—H···O=	Water	Formic acid	−7.201	−371	281	−425	−9.257	−356	238	−394
		Acetic acid	−8.206	−398	286	−429	−9.830	−381	241	−396
		Carbamic acid	−10.295	−453	294	−436	−11.058	−439	249	−402
		Formamide	−9.056	−409	289	−433	−10.358	−394	244	−399
		Acetamide	−9.902	−430	293	−437	−10.853	−414	247	−402
		Urea	−11.901	−482	300	−444	−12.060	−467	254	−408
	Formic acid	Formic acid	−12.525	−386	320	−413	−12.654	−369	273	−381
		Acetic acid	−14.040	−414	325	−418	−13.587	−396	277	−384
		Carbamic acid	−16.851	−469	334	−425	−15.395	−453	285	−390
		Formamide	−15.191	−425	329	−421	−14.331	−408	280	−387
		Acetamide	−16.383	−447	333	−425	−15.037	−429	284	−389
		Urea	−19.026	−498	341	−430	−16.732	−482	291	−393
(3) N—H···O<	Ammonia	Water	3.646	−367	223	−416	−3.351	−359	178	−389
	Hydroxylamine	Water	2.580	−371	233	−242	−3.885	−361	186	−213
	Methylamine	Water	0.792	−373	264	−451	−4.814	−362	218	−425
(4) N—H···O=	Ammonia	Formic acid	2.590	−363	235	−420	−3.832	−349	188	−392
		Acetic acid	1.837	−389	241	−425	−4.253	−374	192	−396
		Carbamic acid	−0.011	−446	251	−431	−5.260	−432	201	−401
		Formamide	1.251	−402	245	−428	−4.595	−387	196	−398
		Acetamide	0.645	−422	249	−430	−4.918	−407	199	−399
		Urea	−0.999	−474	259	−436	−5.816	−461	207	−403
	Formamide	Formic acid	−4.095	−381	304	−481	−7.969	−365	254	−452
		Acetic acid	−5.321	−409	310	−484	−8.706	−391	259	−454
		Carbamic acid	−7.906	−464	321	−488	−10.307	−448	267	−458
		Formamide	−6.276	−420	315	−486	−9.319	−403	262	−456
		Acetamide	−7.324	−441	319	−489	−9.947	−424	266	−458
		Urea	−9.774	−493	329	−493	−11.483	−477	274	−461
	Urea	Formic acid	−3.210	−380	292	−512	−7.558	−363	241	−485
		Acetic acid	−4.457	−407	298	−515	−8.333	−390	246	−487
		Carbamic acid	−7.021	−463	309	−520	−9.939	−448	255	−490
		Formamide	−5.300	−418	303	−518	−8.863	−403	250	−488
		Acetamide	−6.258	−439	308	−520	−9.417	−423	253	−490
		Urea	−8.510	−491	317	−524	−10.804	−476	262	−493

[a] The partial charges (for the O, H, and D atoms) and the *total* energies are given for several values of $R_{O\cdots H}$. [b] The zero reference distribution (ON) in electronic units.

Several interesting trends can be detected in the above results. First, hydrogen bonds of the same type exhibit considerable differences in the depths of their attractive potentials. For example, for a type 2 (O-H···O=) hydrogen bond, there is a spread between ~ -9 to -19 kcal/mol at the energy minimum (see Table III). Further, although in general the attractive potential at the minimum decreases (becomes less negative) in the order type 2 $\geq$ type 4 $\geq$ type 1 $\geq$ type 3, specific examples arise in which this order is not followed (*e.g.*, formamide bonded to carbamic acid, acetamide, and urea, respectively, all show stronger hydrogen bonds than the water–formic acid complex).

Second, as illustrated in Figures 5 and 6, as the strength of the interaction potential increases (*i.e.*, as the two monomers approach each other to form a hydrogen bond), the atoms (especially the hydrogen involved in the hydrogen bond) become polarized. From a comparison of the polarization of this hydrogen atom with the energy at fixed $R_{O\cdots H}$ for different dimers, it is seen that the more negative the energy the greater is the polarization of this hydrogen. However, the polarizations of the H and O atoms are *not* good indicators of the strength of the hydrogen bond for two reasons. (1) Not only the hydrogens, but all atoms in the molecule, become polarized to some extent (see Figures 5 and 6). As the molecules approach each other (even closer than the distance at the minimum of the potential curve), the polarization increases monotonically (*e.g.*, see the ammonia–water data in Figure 6A). It is found by the CNDO/2 calculations that any two atoms which come close together and interact attractively or repulsively, become polarized. (2) Although the partial charge of the hydrogen atom in the hydrogen bond is found to become more positive by as much as $\sim$90–100% at the

$R_{O\cdots H}$ = 1.7 Å				$R_{O\cdots H}$ = 2.0 Å				$R_{O\cdots H}$ = 4.0 Å			
Energy	Partial Charge[c]			Energy	Partial Charge[c]			Energy	Partial Charge[c]		
kcal/mol	O	H	D	kcal/mol	O	H	D	kcal/mol	O	H	D
−6.278	−361	206	−371	−2.855	−355	190	−358	−0.106	−348	175	−348
−6.458	−362	210	−338	−2.912	−355	193	−325	−0.102	−348	176	−315
−6.666	−348	214	−375	−3.131	−341	196	−361	−0.177	−333	177	−349
−6.999	−373	217	−377	−2.292	−366	198	−363	−0.193	−357	178	−349
−7.738	−431	223	−381	−3.674	−425	203	−366	−0.239	−416	179	−349
−7.326	−386	219	−379	−3.463	−379	200	−364	−0.213	−371	178	−349
−7.625	−405	221	−381	−3.621	−398	202	−365	−0.238	−389	178	−349
−8.371	−460	227	−386	−4.021	−453	206	−369	−0.297	−445	179	−350
−8.934	−359	246	−362	−4.531	−350	227	−347	−0.532	−336	205	−334
−9.537	−385	250	−364	−4.886	−376	229	−349	−0.594	−360	206	−335
−10.748	−443	256	−368	−5.630	−435	234	−352	−0.752	−420	207	−335
−10.026	−398	252	−366	−5.170	−389	231	−350	−0.640	−373	206	−335
−10.465	−418	255	−367	−5.416	−408	233	−351	−0.692	−392	207	−335
−11.583	−472	262	−370	−6.081	−463	238	−353	−0.814	−448	208	−335
−3.512	−354	153	−373	−1.820	−351	136	−362	−0.042	−347	120	−353
−3.837	−356	160	−197	−1.965	−352	141	−186	−0.049	−347	124	−177
−4.249	−357	192	−410	−2.091	−352	174	−400	−0.051	−347	157	−392
−3.760	−342	161	−376	−1.955	−337	142	−365	−0.072	−332	122	−354
−4.001	−367	165	−379	−2.071	−361	144	−366	−0.087	−356	122	−354
−4.562	−425	172	−383	−2.328	−420	150	−369	−0.113	−415	123	−355
−4.199	−380	168	−380	−2.163	−375	147	−367	−0.092	−370	123	−355
−4.374	−399	170	−381	−2.238	−394	148	−368	−0.100	−388	123	−355
−4.866	−454	177	−384	−2.450	−449	153	−370	−0.103	−444	124	−355
−6.442	−355	226	−436	−3.550	−347	205	−425	−0.446	−335	183	−416
−6.909	−381	229	−438	−3.818	−373	207	−426	−0.496	−359	183	−416
−7.949	−439	237	−440	−4.434	−432	213	−427	−0.623	−419	184	−416
−7.313	−394	232	−439	−4.055	−386	210	−427	−0.536	−372	184	−416
−7.714	−414	235	−440	−4.291	−405	212	−427	−0.593	−391	184	−416
−8.716	−468	242	−443	−4.885	−461	217	−429	−0.710	−447	185	−416
−6.300	−355	213	−469	−3.587	−348	192	−458	−0.537	−336	169	−449
−6.813	−380	216	−471	−3.905	−372	194	−459	−0.614	−360	170	−449
−7.876	−439	224	−473	−4.561	−432	200	−461	−0.778	−419	171	−449
−7.156	−394	219	−472	−4.103	−386	197	−460	−0.652	−374	170	−449
−7.493	−413	222	−473	−4.289	−405	199	−460	−0.697	−392	171	−449
−8.387	−468	229	−475	−4.814	−460	204	−462	−0.809	−448	172	−450

energy is the sum of the energies of the two planar monomers. [c] These values should be divided by 1000 to obtain the partial charge

calculated (CNDO/2) energy minimum ($R_{O\cdots H} \simeq$ 1.3–1.6 Å), this polarization usually amounts to only a few per cent at values of $R_{O\cdots H}$ (~1.65–2.50 Å) which correspond to *experimentally* observed equilibrium distances. The calculated charge separation (defined as the sum of the positive and negative partial charges of one molecule of the dimer, CS^+ and CS^-, respectively) and the charge transfer (CT, defined as the difference between CS^+ and CS^- for one molecule in the complex[5]) were also examined. In agreement with our previous results (see paper III[5]), there was no correlation between CT and the calculated energy at the minimum. Furthermore, although CS^+ and CS^-, for any particular *type* of hydrogen bond, increase in magnitude as the depth of the potential well increases, we found that this relation did not hold when different types of hydrogen bonds were compared.

Third, concerning the electrostatic nature of the hydrogen bond as predicted by the CNDO/2 method, a comparison of the partial charges on the donor H and acceptor O atoms of the separated monomers (Figure 1) with the energies in Table III shows a good correlation between the magnitude of the charges of these two atoms in the separated monomers and the depth of the interaction potential well. However, this comparison is seen not to hold (Table III) for the D atom (O or N in the proton donor molecule). Hence, although the CNDO/2 results seem to imply that an electrostatic effect contributes to hydrogen bond formation, this electrostatic effect by itself does not appear to account for the total energy; *i.e.*, there is also, presumably, some covalent character to the hydrogen bond.

The above discussion focused attention on the calculated (CNDO/2) energy at the minimum, for illustrative purposes only. Similar conclusions can be drawn from a consideration of other parts of the curve

in the attractive region. Thus, even though we will ignore the CNDO/2 results in the neighborhood of the minimum, in obtaining the GHB potential, for reasons stated earlier, the final GHB potential will still reflect these trends in the attractive region of the potential.

2. Determination of Empirical GHB Potential. The CNDO/2 results presented in section 1 represent all intermolecular interactions for all valence electrons on every atom, and not just the D–H···O atoms; thus, we consider the theoretical interaction potential for the hydrogen bond (*i.e.*, the O···H interaction) as the difference between the CNDO/2 energy and the empirical intermolecular interactions for those atoms not directly involved in the hydrogen bond. That is, a theoretical interaction potential (U_{TIP}) is defined as

$$U_{TIP} = U_{CNDO/2} - \sum[(U_{ij})_{nb} + (U_{ij})_{el}] \qquad (7)$$

where the sum is taken over all atoms of molecule a, with those of molecule b; the O···H interaction[35] is included in $(U_{ij})_{el}$ but is omitted from $(U_{ij})_{nb}$. The empirical GHB potential U_{GHB} is then defined as that empirical function which will reproduce U_{TIP} and be the same for all model systems corresponding to any one *type* of hydrogen bond. The functions $(U_{ij})_{nb}$ and $(U_{ij})_{el}$ are given by equations 1 and 2, respectively.

The O···H potential for a type k hydrogen bond was taken as

$$U_{GBH} = A_k/r_{ij}^{n} - B_k/r_{ij}^{m} \qquad (8)$$

where r_{ij} is the $R_{O\cdots H}$ distance, and A_k, B_k, n and m are constants to be adjusted to yield the best GHB potential. A variety of procedures were tried in order to make U_{GHB} fit well with U_{TIP}, but the only one which was found to be successful was the following:[35] (1) $(U_{ij})_{nb}$ and $(U_{ij})_{el}$ were computed for all pairs of atoms between molecule *a* and molecule *b*, except for the omission of the O···H interaction from $(U_{ij})_{nb}$; (2) the charges in $(U_{ij})_{el}$ were the fixed charges of the separated monomers; and (3) the O···H interaction was assigned as U_{GHB}.

Using the nonlinear least-square fitting procedure, U_{GHB} was fit to U_{TIP}. The following conditions were imposed in this fitting procedure. (1) The fit was carried out only in the attractive region, *i.e.*, where $R_{O\cdots H} \geq 1.65$ Å. (2) For $R_{O\cdots H} < 1.65$ Å, it was assumed that the usual form of the repulsive potential applies; hence n of eq 8 was taken as 12. (3) For $R_{O\cdots H} \geq 5.0$ Å, U_{GHB} should be sufficiently small so that only $(U_{ij})_{el}$ contributes in this region; in order that the residual CNDO/2 contribution correspond to $(U_{ij})_{el}$ at these large distances, it was found necessary to set D equal to 2.0 in eq 2. It is not clear why this apparent dielectric constant of 2.0 was necessary to give agreement between the total empirical energy and the CNDO/2 energy at large distances. However, since the contribution from $(U_{ij})_{nb}$ and U_{GHB} is very small at large distances, *i.e.*, the electrostatic energy dominates, it is presumed that the quantity $D = 2.0$ arises from the way in which the monopole (ON) charges were defined, and is required in order to normalize the energy to a value near the Hartree–Fock limit. Whatever the reason, this value of D is necessary to achieve a fit at large distances.

Applying the least-squares method, to determine A_k and B_k for various values of m, the best results were obtained for $m = 10$. The resulting values of A_k and B_k for the 10–12 GHB potential for the various dimers are listed in Table IV, together with the least-squares standard deviation σ. By weighting the A_k's and B_k's by the standard deviation, weighted average parameters

Table IV: Parameters for the 10–12 GHB Potential Fit to the Theoretical Interaction Potential for Hydrogen-Bonded Dimers

Dimer		A_k, Å^{12} kcal/mol	B_k, Å^{10} kcal/mol	σ, kcal/mol
Proton donor	Proton acceptor			
Water	Water	8741.5	4059.2	0.071
Methanol	Water	8026.8	3815.1	0.096
Water	Formic acid	9502.5	4356.5	0.044
	Acetic acid	4970.1	2853.0	0.261
	Carbamic acid	11558.8	5224.6	0.052
	Formamide	10248.8	4697.5	0.043
	Acetamide	10462.3	4802.2	0.042
	Urea	12396.0	5588.6	0.065
Formic acid	Formic acid	11779.0	5343.0	0.074
	Acetic acid	12618.2	5697.5	0.096
	Carbamic acid	16661.5	7281.5	0.250
	Formamide	16944.2	7299.3	0.144
	Acetamide	14683.0	6534.0	0.168
	Urea	18256.0	7944.0	0.297
Ammonia	Water	4747.9	2187.8	0.101
Hydroxylamine	Water	4568.7	2151.8	0.114
Methylamine	Water	5167.4	2443.1	0.107
Ammonia	Formic acid	3991.4	1930.9	0.135
	Acetic acid	3929.9	1931.2	0.144
	Carbamic acid	5137.3	2446.4	0.114
	Formamide	4643.3	2220.1	0.123
	Acetamide	4488.5	2180.6	0.133
	Urea	5397.4	2580.5	0.121
Formamide	Formic acid	8859.6	3928.7	0.068
	Acetic acid	9370.7	4152.6	0.079
	Carbamic acid	12797.7	5504.2	0.204
	Formamide	10698.1	4677.6	0.119
	Acetamide	11064.1	4838.9	0.136
	Urea	14370.8	6142.8	0.258
Urea	Formic	6321.7	2940.9	0.073
	Acetic acid	7058.6	3245.8	0.080
	Carbamic acid	10935.9	4759.3	0.206
	Formamide	8754.7	3906.9	0.115
	Acetamide	8160.9	3701.5	0.112
	Urea	11331.2	4951.3	0.212

(35) This combination of special H_a and O_b atoms was found to be the best, after having attempted to include other combinations of atoms in constructing the GHB potential. Further attempts to vary the electrostatic interactions as functions of $R_{O\cdots H}$ were also found to be nonproductive.

Table V: Final Parameters for the 10–12 GHB Potential

k	Hydrogen Bond Type		A_k, Å^{12} kcal/mol	B_k, Å^{10} kcal/mol	E_{min},[a] kcal/mol	R_{min},[b] Å
(1)	O—H···O<	Weighted average[c]	8488.8	3972.9	−5.975	1.60
		Fit to formic acid dimer[d]	10341.2	4609.4	−5.432	1.64
(2)	O—H···O=	Weighted average[c]	10951.6	4983.4	−6.512	1.62
		Fit to formic acid dimer[d]	13340.1	5781.2	−5.920	1.66
(3)	N—H···O<	Weighted average[c]	4835.0	2262.2	−3.397	1.60
		Fit to formic acid dimer[d]	5889.7	2624.4	−3.088	1.64
(4)	N—H···O=	Weighted average[c]	7649.3	3458.3	−4.379	1.63
		Fit to formic acid dimer[d]	9318.4	4012.9	−3.981	1.67

[a] E_{min} is the depth of the 10–12 potential well at the minimum, and is $-0.067\ B_k^6/A_k^5$. [b] R_{min} is the value of $R_{O\cdots H}$ at which E_{min} occurs. This is *not* the hydrogen bond minimum distance for any real molecule, but rather a theoretical limit. $R_{min} = [1.2\ A_k/B_k]^{1/2}$. [c] Before adjustment to experimental data. [d] After adjustment to experimental data for the formic acid cyclic dimer.

for the 10–12 GHB potential were obtained for each type of hydrogen bond. These are listed in Table V together with the depth of the potential well (E_{min}) and the value (R_{min}) or $R_{O\cdots H}$ at the minimum of the 10–12 GHB potential. Since the values R_{min} correspond to U_{GHB} rather than to the *total* potential, they are *not* to be compared with experimental data; only the value of $R_{O\cdots H}$ at the minimum of the *total* potential function should be compared with experimental data.

The total interaction potential (in kcal/mol) for two molecules linked by a hydrogen bond is then given by

$$U_{Total} = \sum_{i,j}{}' \epsilon_{ij}\left[\frac{\langle r_g\rangle_{ij}}{r_{ij}}\right]^6\left\{\left[\frac{\langle r_g\rangle_{ij}}{r_{ij}}\right]^6 - 2.0\right\} + \frac{A_k}{R_{O\cdots H}^{12}} - \frac{B_k}{R_{O\cdots H}^{10}} + 166.0\sum_{i,j}\frac{q_i q_j}{r_{ij}} \quad (9)$$

where $\Sigma_{i,j}$ represents summations over all interactions between *all* atoms in molecule a (index i) with *all* atoms in molecule b (index j) and $\Sigma_{i,j}'$ is the same except that only the O...H interaction is excluded.

The use of eq 9 with the parameters A_k and B_k, as thus far determined, would match the CNDO/2 results only in the attractive part of the potential curve. In order to obtain a better fit even at distances less than $R_{O\cdots H} = 1.65$ Å, the values of A_k and B_k were subjected to second-order corrections, using experimental data. The equilibrium value of $R_{O\cdots H}$ was taken as the experimental value for the formic acid cyclic dimer, as determined by gas-phase electron diffraction studies.[33] For the experimental value of $(U_{total})_{min}$, we resort to the data of Minicozzi and Bradley,[34] who used the gas-phase heat of dimerization of the formic acid cyclic dimer to obtain the standard heat of dimerization at 0°K by correcting for the contribution arising from the vibrational zero-point energies. Their value for the energy of dimerization at 0°K, which is not E_{min} but $(U_{total})_{min}$, is −16.2 kcal/mol. Using eq 9 and the A_k and B_k parameters for a type 2 hydrogen bond, the experimental values for the cyclic dimer were fit by only slight modifications of the GHB potential (*viz.*, by multiplying A_k and B_k of Table V by 1.22 and 1.16, respectively). These values are referred to in Table V as "Fit to formic acid dimer." When the refined values of A_k and B_k are used in eq 9, a good fit to the experimental data for the acetic and propionic acid cyclic dimers is obtained, as shown in Table VI.

Table VI: Comparison of Experimental Data with Empirical Calculations for Several Hydrogen Bonded Cyclic Dimers

	Experimental		Calcd	
	$(U_{Total})_{min}$,[a] kcal/mol	$(R_{O\cdots O})_{min}$,[b] Å	$(U_{Total})_{min}$,[a] kcal/mol	$(R_{O\cdots O})_{min}$,[b] Å
Formic acid	−16.2[c]	2.703[e]	−16.17	2.698
Acetic acid	−14.1[d]	2.680[f]	−16.13	2.688
Propionic acid		2.711[g]	−16.23	2.686

[a] $(U_{Total})_{min}$ is the equilibrium energy for the formation of the cyclic dimer. [b] $(R_{O\cdots O})_{min}$ is the distance corresponding to $(U_{Total})_{min}$. [c] This is the *corrected* energy of dimerization at 0°K according to Minicozzi and Bradley.[34] The uncorrected value at 25°C is −14.4 kcal/mol [J. O. Halford, *J. Chem. Phys.*, **10**, 582 (1942)]. [d] Uncorrected values at ~80° [A. E. Potter, Jr., P. Bender, and H. L. Ritter, *J. Phys. Chem.*, **59**, 250 (1955)]. [e] See reference 33. [f] See reference 37. [g] See reference 38.

Since very few other reliable experimental data are available for the formation of hydrogen bonds, unaffected by the environment (such as crystal packing, solvent effects, other bonds, or salts bridges, etc.), we choose to use the above corrections, as determined by fitting our computed parameters to the experimental results for the formic acid cyclic dimer, for all four types of hydrogen bonds. The corrected parameters are listed in Table V (as "Fit to formic acid dimer"), and our final GHB potentials for the four types of hydrogen bonds are shown in Figure 7. In Figure 7, we also show our original GHB potential as determined directly from the CNDO/2 results (at $r > 1.65$ Å) for comparison. It should be pointed out that, although E_{min} and R_{min} have shifted because of the fitting to experimental data, the corrections to A_k and B_k have very little effect on

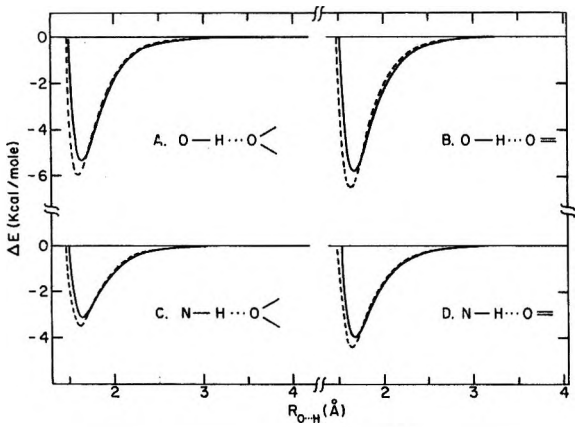

Figure 7. The empirical general hydrogen bond potential (GHB) as a function of $R_{O\ldots H}$, as determined from CNDO/2 results on model dimers (dashed lines), and after fitting to the experimental formic acid cyclic dimer results (solid lines) for the four types of hydrogen bonds studied here. $\Delta E = 0$ for the GHB potential for two monomers at infinite separation.

Table VII: The CNDO/2 Overlap-Normalized Partial Charges[a] Used in the Calculation of the Cyclic Dimers

Formic acid		Acetic acid		Propionic acid	
Atom	Partial charge	Atom	Partial charge	Atom	Partial charge
H(C′)	−0.011	C^{α}	−0.168	C^{β}	−0.051
C′	0.475	$H(C^{\alpha})$	0.063	$H(C^{\beta})$	0.034
O(C′)	−0.330	$H(C^{\alpha})$	0.063	$H(C^{\beta})$	0.034
O	−0.337	$H(C^{\alpha})$	0.063	$H(C^{\beta})$	0.034
H	0.203	C′	0.500	C^{α}	−0.099
		O(C′)	−0.362	$H(C^{\alpha})$	0.044
		O	−0.348	$H(C^{\alpha})$	0.044
		H	0.189	C′	0.490
				O(C′)	−0.368
				O	−0.351
				H	0.189

[a] Charges were calculated for the monomers in the planar cis conformation. Geometries were taken from gas-phase electron diffraction studies.[33,37,38]

the curve for $R_{O\ldots H} > R_{min}$; hence, the final empirical GHB potential still represents the theoretical interaction potential as determined by the CNDO/2 method at distances greater than R_{min}.

3. Total Empirical Energy of Hydrogen-Bonded Dimer Complexes. Since the total energy of a hydrogen-bonded dimer complex is represented not only by U_{GHB} but also by all other intermolecular interactions, we have reconstructed the total potential curve for the cyclic dimer of formic acid in Figure 8A, using eq 9. For the formic acid molecules, we have used the geometry given for the monomers by Almenningen, *et al.*[33] Since the geometry of Almenningen, *et al.*, differs slightly from that used earlier in this paper, we have recalculated the CNDO/2 (ON) partial charges for this geometry, and these are listed in Table VII. The curve of Figure 8A was computed by keeping the C—H bonds of molecules a and b collinear, and varying the $C_a\cdots C_b$ distance. It should be noted that, whereas the parameters given in Table V for the GHB potential for a type 2 hydrogen bond give a value of $E_{min} = -5.92$ kcal/mol at $R_{min} = R_{O\ldots H} = 1.66$ Å, the computed values for the *total* potential energy (Figure 8A) are −8.09 kcal/mol per hydrogen bond at $R_{O\ldots H} = 1.70$ Å. The difference, of course, arises from the fact that U_{GHB} is *not* the total interaction energy.[36] The values for the total energy agree with the experimental ones of −16.2 kcal/mol and $R_{O\ldots O} = 2.703$ Å.

As a test of the GHB potential, computed for *linear* hydrogen bonds, we have calculated the total potential curves for both the acetic acid and propionic acid cyclic dimers (Figures 8B and 8C, respectively), and compared their minimum-energy conformation with those from gas-phase electron diffraction data[37,38] (see Table VI). For both dimers, the same geometry was used as obtained for the monomers.[37,38] Again, because of deviations from "standard" geometry,[21] the overlap normalized CNDO/2 charges were re-computed and are listed in Table VII. In the computations, the two planar monomers were fixed in the same plane with the C_a—C_a' and C_b—C_b' bonds collinear, but pointing in opposite directions so that the carbonyl oxygen atom of molecule a formed a near-linear hydrogen bond with the H—O group of molecule b and, at the same time, the O—H group of molecule a formed a similar hydrogen bond with the carbonyl oxygen atom of molecule b. The potential curves given in Figures 8B and 8C for the acetic acid dimer and the propionic acid dimer, respectively, were constructed by moving molecule b along the common axis, holding molecule a fixed. The calculated equilibrium distances given in Table VI are in excellent agreement with those O···O equilibrium positions experimentally observed for both gas phase dimers.

Having thus tested the empirical GHB potential function on the cyclic dimers, we have used this function to recalculate the total energy of all of the model linear hydrogen-bonded dimers. Examples of the calculated potential curves, representing all four types of hydrogen bonds, are given in Figures 9 and 10. These are compared with the theoretical CNDO/2 curves and with the empirical curves obtained before application of the corrections based on the formic acid dimer data. As can be seen in Figures 9 and 10, both empirical curves match the quantum mechanical one very well for $R_{O\ldots H} > 1.7$ Å. At smaller values of $R_{O\ldots H}$, the final (corrected) empirical potential exhibits a shallower

(36) We have explored the energy surface for the formic acid cyclic dimer in a manner similar to that of Minicozzi and Bradley.[34] Unlike their results, we find only one conformation of significantly low energy. These results are discussed in section 5 of "Results and Discussion."

(37) J. L. Derissen, *J. Mol. Struct.*, 7, 67 (1971).

(38) J. L. Derissen, *ibid.*, 7, 81 (1971).

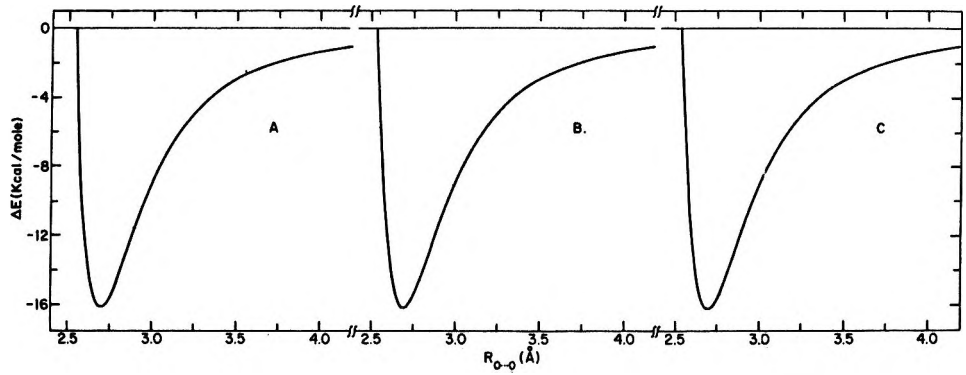

Figure 8. The total empirical potential energy for the formation of the cyclic dimers (A) formic acid, (B) acetic acid, and (C) propionic acid, as a function of the $R_{O\ldots O}$ distance. ΔE represents the total energy including that for the formation of two hydrogen bonds per dimer. $\Delta E = 0$ for two monomers at infinite separation.

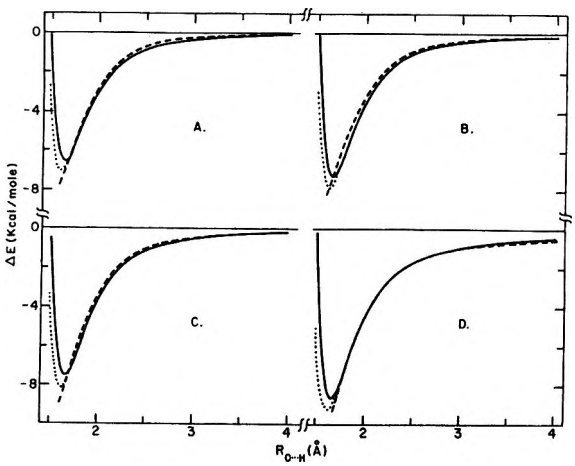

Figure 9. Comparison of the total empirical interaction potential [including the general hydrogen bond (GHB) potential obtained directly from the CNDO/2 calculations (· · · ·) and after improvement using the experimental results for the cyclic dimer of formic acid (—)] with the CNDO/2 results (----) for the hydrogen bond types 1 and 2 as a function of the separation distance $R_{O\ldots H}$. The linear dimers (all with $\alpha = \delta = \beta = 0°$ and $\theta = 0°$) shown are: (A) water–water; (B) water–formic acid; (C) water–formamide; and (D) formic acid–formic acid. $\Delta E = 0$ for two monomers at infinite separation.

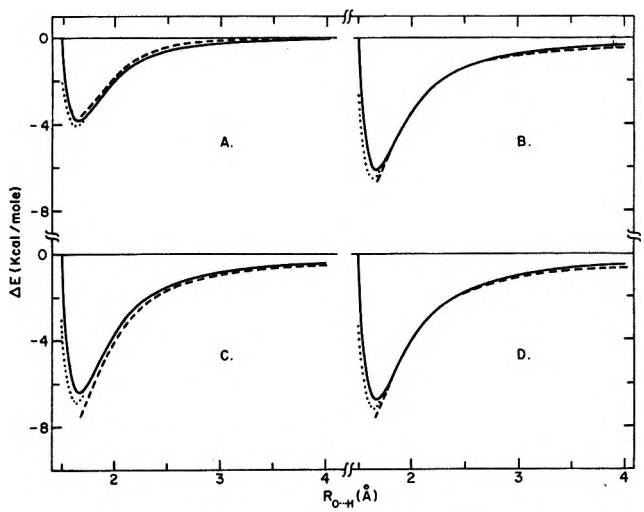

Figure 10. Comparison of the total empirical interaction potential [including the general hydrogen bond (GHB) potential obtained directly from the CNDO/2 calculations (· · · ·) and after improvement using the experimental results for the cyclic dimer of formic acid (—)] with CNDO/2 results (----) for the hydrogen bond types 3 and 4 as a function of the separation kistance $R_{O\ldots H}$. The linear dimers (all with $\alpha = \delta = \beta = 0°$ and $\theta = 0°$) shown are: (A) ammonia–water; (B) formamide–formic acid; (C) formamide–formamide; and (D) urea–formamide. $\Delta E = 0$ for two monomers at infinite separation.

minimum at a somewhat larger equilibrium distance than either of the other two curves.

Several conclusions about the GHB potential may be drawn from the above results. First, for all four types of hydrogen bonds studied here, it is possible to reconstruct the total interaction potential of the complex using only one form of the GHB potential (*i.e.*, the 10-12 form) without requiring any other special interactions. Second, although one set of A_k,B_k is used for a given type of hydrogen bond, different dimers of the *same* hydrogen-bond type have different *total* energy curves, with different equilibrium energies and separation distances (*e.g.*, compare the solid curves in Figures 9B, C and D, all of which represent a type 2 hydrogen bond). Considering *only* the GHB potential, the various types of hydrogen bonds would decrease in stability at any particular value of $R_{O\ldots H}$ as: type 2 > type 1 > type 4 > type 3. However, if one examines the total empirical energy for the following dimers: water–water, a type 1 with a minimum energy of −6.5 kcal/mol; formic acid–formic acid, a type 2 with $\Delta E_{min} = -8.5$ kcal/mol; formamide–formamide, a type 4 with $\Delta E_{min} = -6.4$ kcal/mol; and *N*-methyl acetamide–*N*-methyl acetamide, a type 4 with $\Delta E_{min} = -7.8$ kcal/mol, it becomes clear that the total stability of the dimer does not necessarily depend only on the type of hydrogen bond, but is rather the net result of all intermolecular interactions. This demonstrates not only the importance of the electrostatic and nonbonded in-

teractions, as well as the GHB potential, but also the need to consider these terms when examining the experimentally observable quantities for the hydrogen bond. Finally, when comparing the CNDO/2 results for hydrogen bonded systems either to experimental results or to the results obtained by calculations using this empirical GHB potential, it should be recognized that the CNDO/2 results will predict unreasonably close interaction distances for certain atoms (*viz.*, the oxygen and the hydrogen atoms), while predicting reasonable values for most other interactions.[4-6]

By taking the second derivative of U_{total} in eq 9 with respect to the atom–atom interaction distance r_{ij}, it is possible to calculate the force constant $[k_c = \partial^2 U_{\text{total}}/\partial r_{ij}^2]$ for the stretching vibrations between the two monomers. This is similar to the linear A···D force constant obtained from the stretching frequency ν_σ,[15] except that k_c represents all intermolecular interactions between the two monomers forming the hydrogen-bonded dimer. Figure 11 shows the change in k_c as a function of the O···H distance, for the linear water dimer and for the cylcic dimer of formic acid. Pimentel and McClellan[15] have given estimates of the A···D stretching force constants of between 0.4 and 0.33 mdyn/Å for formic acid, which would correspond to an O···H distance between 1.775 and 1.785 Å in Figure 11, and 0.2 mdyn/Å for water, which would correspond to an O···H distance of 1.753 Å by our calculations. If one compares these distances with the values of $R_{O\cdots H}$ observed experimentally, the agreement is good. However, at the shorter equilibrium position of the formic acid dimer (1.70 Å), the force constant predicted by our potential is large, probably because of the empirical r^{-12} repulsive term of the total interaction potential.

4. Test of the Angular Dependence of the Total Empirical Energy of Hydrogen-Bonded Dimer Complexes. By the angular dependence of the total empirical energy of a hydrogen-bonded complex, we mean the changes in the potential energy surface as the angles α, β, and δ (defined in the Introduction and shown in Figure 2) vary. Even though the angular dependence is thought to be quantum mechanical in origin (see the Introduction), the "correct" angular dependence in a hydrogen-bonded complex can be obtained from the empirical energies (including the GHB potential) *without* the use of an explicit angular-dependent term. The best way to demonstrate this is to compare the calculated empirical energies with those obtained from quantum mechanics, either by the CNDO/2 method or by other methods where such results are available.

The dependence of the total energy on α (with θ, β, and δ fixed at 0°) for two water molecules forming a linear dimer, as predicted by both the CNDO/2 method and by the use of our empirical potential (eq 9), is shown in Figure 12A. Both the CNDO/2 and the empirical potential predict an increase in ΔE as α departs from 0°, with both methods giving almost identical results at $R_{O\cdots H} = 1.80$ Å for α between ±30°. For larger values of α, the empirical results begin to reflect the interatomic repulsions, which are larger than those predicted by the CNDO/2 method for O···H interactions. Thus, the CNDO/2 and the empirical results are very similar for small α. The slight asymmetry in the three curves about $\alpha = 0°$, which is much better demonstrated by the empirical curve for $R_{O\cdots H} = 1.60$ Å, arises from steric interactions between the hydrogen

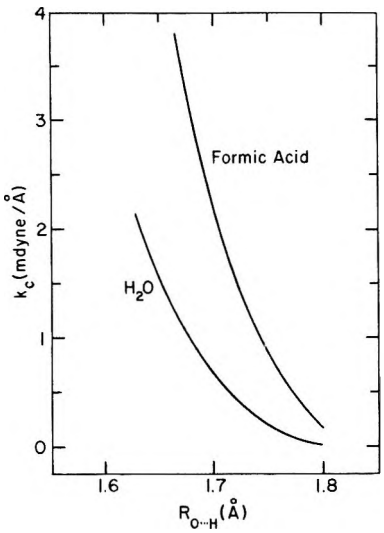

Figure 11. Force constants calculated from the total empirical interaction potential as a function of monomer separation $R_{O\cdots H}$ for the formic acid cyclic dimer and the linear hydrogen-bonded water dimer.

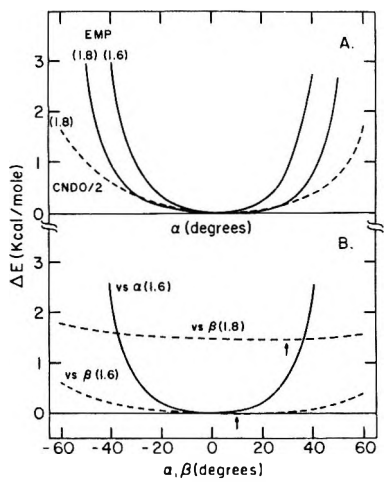

Figure 12. (A) CNDO/2 (---) and empirical results (—) for the dependence of ΔE on α for the linear hydrogen-bonded water dimer at several values of $R_{O\cdots H}$ (in angstrom units), as shown. For all dimers, $\delta = \beta = 0°$ and $\theta = 0°$. $\Delta E = 0$ at $\alpha = 0°$ for each value of $R_{O\cdots H}$. (B) Empirical results for the dependence of ΔE on α (—) (with $\beta = 0°$) and on β (---) (with $\alpha = 0°$) for the linear hydrogen-bonded water dimer at several values of $R_{O\cdots H}$ (in angstrom units), as shown. For all dimers, $\delta = 0°$ and $\theta = 90°$. $\Delta E = 0$ for the water dimer at $R_{O\cdots H} = 1.6$ Å and $\alpha = \beta = 0°$. The arrows indicate the minimum in the total empirical energy at a non-zero value of β.

atoms of molecules a and b, and appears about the same in both the CNDO/2 and empirical calculations. Thus with the exception of the repulsive interactions which differ, both results are in excellent agreement.

Figure 12B shows the empirical results for the same water dimer, except that the second molecule is rotated by 90° ($\theta = 90°$), both as a function of α (solid curve, $\delta = \beta = 0°$) and of β (dashed curves, $\alpha = \delta = 0°$). The dependence on α with $\theta = 90°$ shows the same trends as seen in Figure 12A, except that now the potential is symmetric about $\alpha = 0°$. This is because the hydrogen atoms, which lead to steric interactions at $\theta = 0°$, are farther apart when $\theta = 90°$. The dashed curves indicate a slight preference for $\beta > 0°$, with the magnitude of β_{min} increasing with increasing values of $R_{O...H}$. The actual minimum energy values of β, for several values of $R_{O...O}$, are listed in Table VIII together with the results of a number of quantum mechanical studies, including not only the CNDO/2 method, but also the more exact *ab initio* procedures.[21,31,39-45] The empirical results for the linear water dimer may be summarized as follows. The energetically most stable conformation is found for $R_{O...O} = 2.64$ Å, $\theta = 90°$, $\alpha = 0°$, $\beta = 10°$, and $\delta = 0°$. As $R_{O...O}$ increases, the dependence on α remains substantially unchanged with the most stable conformation being at $\alpha = 0°$, while β_{min} tends toward larger values. Table VIII shows that the nonzero value of β_{min} and its increase with increasing $R_{O...O}$ are consistent with those predicted by quantum mechanics, especially by the more exact *ab initio* calculations. Further, a comparison with the results from one of the more extensive basis sets used to examine the water dimer (see Figure 2 in ref 25) shows that the angular dependences for both α and β are in excellent agreement with our empirical results, even though the quantum mechanical equilibrium value of $R_{O...O}$ (3.00 Å) is larger and of ΔE (−4.72 kcal/mol) is smaller in absolute value than the corresponding empirical values. Since our empirical results do not contain any explicit angular dependence, it is strongly suggested that it is the *total* molecular environment, rather than any particular orbital or atomic property, which dictates the angular dependence.

The above results pertain to a type 1 hydrogen bond, and we consider next some type 2 and 4 hydrogen bonds, *i.e.*, those in which the proton acceptor is a carbonyl oxygen atom. In the latter types of hydrogen bond, the atoms bonded to the carbonyl carbon atom are farther away from those of the proton donor molecule than are those of the proton acceptor molecule in a type 1 hydrogen bond. The dependences of both the CNDO/2 and empirical energies on α at several values of $R_{O...H}$ (all with $\theta = \delta = \beta = 0°$), for several complexes in which H_2O provides the donor proton, are shown in Figure 13. If unperturbed sp^2 hybridization were the origin of the angular dependence, one would expect the CNDO/2 results to exhibit minima at $\alpha = \pm 60°$, and the empirical results (which completely ignore any directionality arising from hybridization) to show very little dependence on α. However, as shown in Figure 13, both the CNDO/2 and empirical results are strikingly similar, *i.e.*, both show a trend toward greater stabilization as α departs from 0°. The quantitative discrepancies between the two methods are greater for the smaller values of $R_{O...H}$ (1.6 Å compared to 1.8 Å) because the total empirical potential exhibits stronger repulsions at the shorter values of $R_{O...H}$. Despite this stronger repulsion in the empirical potential, the general shape and asymmetry about $\alpha = 0°$ are very nearly the same in both methods. Similar data, with formic acid acting as the proton donor, are shown in Figure 14. Again, the very striking asymmetry (but similarity in the results of both methods) is observed. This raises the following question: if the empirical results (with no explicit angular-dependent energy) agree so well with those of the molecular orbital method, does this imply

Table VIII: Calculations for Stable Water Dimers by Different Methods

Reference	Method	$R_{O...O}$, Å	θ,[a] deg	β_{min},[a] deg	ΔE, kcal/mol
This Work	Empirical	2.62	90	10	−6.49
		2.64	0	0	−6.55
		2.64	90	0	−6.56
		2.64	90	10	−6.57
		2.68	90	20	−6.45
		2.75	90	20	−5.76
		2.80	90	30	−5.14
Murthy and Rao[39]	CNDO/2	2.54	0	0	−6.27
Hoyland and Kier[31]	CNDO/2	2.54	90	0	−6.31
Schuster[40]	CNDO/2	2.54	90	[b]	−8.7
Del Bene and Pople[41]	*ab initio*	2.73	90	58	−6.09
Kollman and Allen[42]	*ab initio*	3.00	90	25	−5.3
Morokuma and Pederson[43]	*ab initio*	2.66	90	0	−12.6
Morokuma and Winick[44]	*ab initio*	2.78	90	54	−6.55
Hankins, *et al.*[25]	*ab initio*	3.00	90	40	−4.72
Duijneveldt[45]	Perturbation theory	2.85	90	~10	~−6.0

[a] See text for definition of angles. $\alpha = 0$ and $\delta = 0$ for all dimers listed. [b] Although this author did not study the angular dependence for the water dimer, his mixed dimer calculations would indicate a stable water dimer with β ~10–20°.

(39) A. S. N. Murthy and C. N. R. Rao, *Chem. Phys. Lett.*, **2**, 123 (1968).
(40) P. Schuster, *Theoret. Chim. Acta*, **19**, 212 (1970).
(41) J. Del Bene and J. A. Pople, *Chem. Phys. Lett.*, **4**, 426 (1969).
(42) P. A. Kollman and L. C. Allen, *J. Chem. Phys.*, **51**, 3286 (1969).
(43) K. Morokuma and L. Pederson, *ibid.*, **48**, 3275 (1968).
(44) K. Morokuma and J. R. Winick, *ibid.*, **52**, 1301 (1970).
(45) J. G. C. M. van Duijneveldt-van de Rijdt and F. B. van Duijneveldt, *Theoret. Chim. Acta*, **19**, 83 (1970).

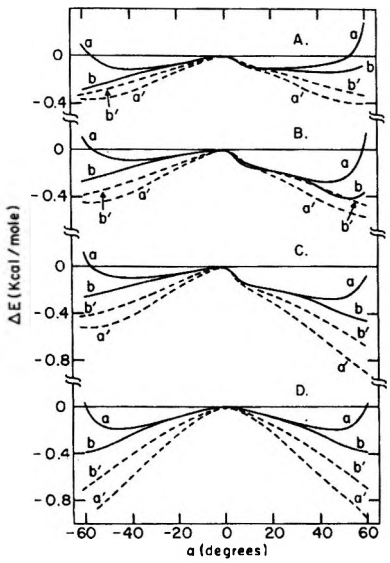

Figure 13. CNDO/2 (—) and empirical (−) results for the dependence of ΔE on α for linear hydrogen-bonded dimers at several values of $R_{O\ldots H}$, *viz.*, a and a′, $R_{O\ldots H}$ = 1.6 Å; b and b′, $R_{O\ldots H}$ = 1.8 Å. (A) water–formic acid; (B) water–acetic acid; (C) water–carbamic acid, and (D) water–urea. For all dimers, $\delta = \beta = 0°$ and $\theta = 0°$. $\Delta E = 0$ at $\alpha = 0°$ for each value of $R_{O\ldots H}$.

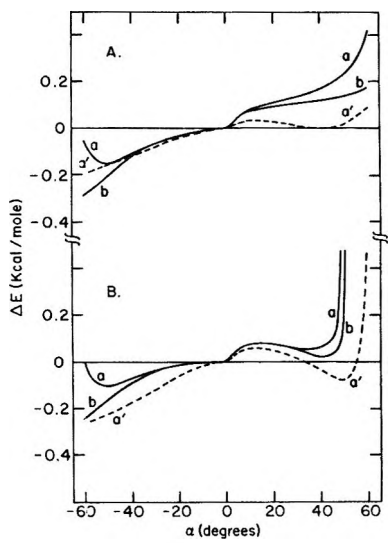

Figure 14. CNDO/2 (—) and empirical (−) results for the dependence of ΔE on α for linear hydrogen-bonded dimers at several values of $R_{O\ldots H}$, *viz.*, a and a′, $R_{O\ldots H}$ = 1.6 Å; b, $R_{O\ldots H}$ = 1.8 Å. (A) formic acid–formic acid, and (B) formic acid–carbamic acid. For all dimers, $\delta = \beta = 0°$ and $\theta = 0°$. $\Delta E = 0$ at $\alpha = 0°$ for each value of $R_{O\ldots H}$.

that the lone-pair directional properties of the acceptor oxygen atom are less important than other more remote interactions arising from the rest of the molecules in the binary complex?

In a similar manner, the angular dependence of the energy of all four types of hydrogen bonds was investigated. Since the results are similar to those discussed above, they are not presented here. Instead, we will consider only a type 4 (N—H···O=C) hydrogen bond, since this is of most interest in conformational energy calculations on proteins. Therefore, we have carried out here a number of empirical calculations for the dimers of formamide and *N*-methyl acetamide (NMA), respectively, and will compare the results with those obtained by the CNDO/2 method (reported earlier in paper III[5]). We retain the same nomenclature for the description of the conformations, and the reader is referred to paper III for the details.

For the formamide linear dimer (ω_1[46] = $\omega_2 = \alpha = \theta = \delta = \beta = 0°$), the *trans* conformation is defined as the one in which the H(N) atom of molecule b, *trans* to the carbonyl of the same molecule, is involved in the hydrogen bond with molecule a; if ω_2 were changed to 180°, the *cis* form would be obtained. The computed empirical energies for both the *trans* and *cis* conformations of the formamide linear dimer are shown in Table IX for both $\theta = 0°$ and $\theta = 180°$; these should be compared with the CNDO/2 results of Table II of paper III.[5] As found for the other dimers discussed earlier in the present paper, we again see the influence of the stronger nonbonded interactions (in the empirical method), leading to a stable hydrogen-bonded complex at $R_{O\ldots H}$ ~ 1.70 Å (for both the *cis* and *trans* forms), compared to the CNDO/2 value of ~1.50 Å. In paper III,[5] it was pointed out that, according to the CNDO/2 method, the most stable conformation of the formamide linear dimer (at $R_{O\ldots H}$ = 1.5 Å) is the *cis* form with $\theta = 0°$, followed (in order of decreasing stability) by the *trans* form with $\theta = 0°$, the *trans* form with $\theta = 180°$, and finally the *cis* form with $\theta = 180°$. According to the empirical results of Table IX, the order of decreasing stability of the complexes (at $R_{O\ldots H}$ = 1.7 Å) is the *trans* form with $\theta = 0°$, the *trans* form with $\theta = 180°$, the *cis* form with $\theta = 0°$, and the *cis* form with $\theta = 180°$. However, aside from the larger equilibrium value of $R_{O\ldots H}$ (obtained by the empirical method), both methods give similar results, with the order of decreasing stability depending on the value of $R_{O\ldots H}$; *i.e.*, for $R_{O\ldots H}$ = 1.5 Å, both methods predict that the *cis* form with $\theta = 0°$ is the most stable one, while, for $R_{O\ldots H}$ = 1.8 Å, they both predict that the *trans* form with $\theta = 0°$ is the most stable one. Also, while the barrier to rotation about the hydrogen bond (for variation of θ from 0° to 180°), at $R_{O\ldots H}$ = 1.7 Å for the empirical method and at $R_{O\ldots H}$ = 1.5 Å for the CNDO/2 method, is lower for the empirical method (0.026 kcal/mol compared to 0.088 kcal/mol), as would be expected for the larger value of $R_{O\ldots H}$ in the empirical method, nevertheless the shape of the curve of ΔE *vs.* θ is similar for the two methods (at 1.7 Å and 1.5 Å, respectively).

The dependence of ΔE on α and δ (by the empirical

(46) ω is the dihedral angle for rotation about the peptide (N–C′) bond, the subscripts 1 and 2 referring to the hydrogen acceptor and donor molecules in the dimer. See paper III[5] for a more complete description.

Table IX: Empirical Results for Formamide Linear Dimer for $\omega_1 = \alpha = \delta = \beta = 0°$

	$R_{O...H}$, Å	ω_2, deg	θ, deg	ΔE,[a] kcal/mol	ΔE,[b] kcal/mol
trans (N–H)	1.40	0	0	24.489	
	1.50	0	0	0.192	
	1.60	0	0	−5.777	
	1.70	0	0	−6.361	
	1.80	0	0	−6.024	
	1.40	0	180	24.526	
	1.50	0	180	0.225	
	1.60	0	180	−5.748	
	1.70	0	180	−6.335	
	1.80	0	180	−5.533	
cis (N–H)	1.40	180	0	24.446	
	1.50	180	0	0.189	
	1.60	180	0	−5.748	
	1.70	180	0	−6.305	
	1.80	180	0	−5.478	
	1.40	180	180	24.659	
	1.50	180	180	0.386	
	1.60	180	180	−5.564	
	1.70	180	180	−6.133	
	1.80	180	180	−5.317	
trans (N–H)	1.70	0	0		0
	1.70	0	30		0.002
	1.70	0	60		0.006
	1.70	0	90		0.011
	1.70	0	120		0.018
	1.70	0	150		0.024
	1.70	0	180		0.026

[a] $\Delta E = 0$ for two planar monomers at infinite separation. [b] $\Delta E = 0$ for *trans* (N–H), $R_{O...H} = 1.70$ Å, $\omega_1 = \omega_2 = \theta = 0°$.

method) for the *trans* form of the formamide linear dimer (with $\theta = 180°$) is shown in Figure 15, and should be compared with the CNDO/2 results in Figure 3 of paper III.[5] The calculations of Figure 15 were carried out for two values of $R_{O...H}$ to demonstrate the effect which the nonbonded interactions have on the shapes of the curves. The curves of Figure 15A have a very similar shape to those of Figure 3A of paper III, indicating that a repulsive potential dominates at positive values of α, and an attractive one at small negative values of α. Since the empirical calculations are less expensive than the CNDO/2 ones, it was possible to examine more details of the angular dependence of ΔE by the empirical method. Thus, it was found (curve b of Figure 15A) that the influence of an attractive potential appears at positive values of α, as $R_{O...H}$ increases. This feature is even more apparent in Figure 15B, where a preference for nonzero values of δ at $R_{O...H} = 1.7$ Å is seen; this behavior was not seen in the CNDO/2 results of Figure 3B of paper III, since the molecular orbital calculations were carried out only for $R_{O...H} = 1.5$ Å. This angular dependence is not a general property of the hydrogen bond, since it is the net result of all intermolecular interactions; thus, it would vary with the nature of the particular molecules forming the hydrogen-bonded complex, and also with the value of $R_{O...H}$.

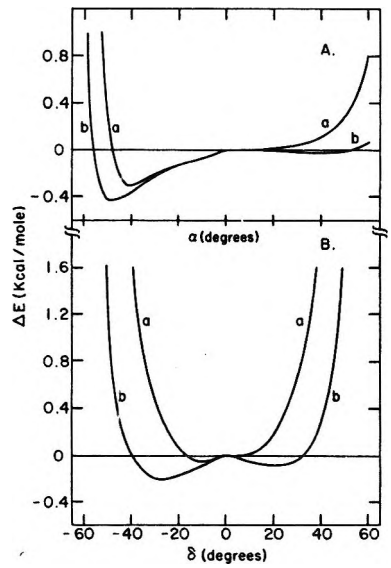

Figure 15. Empirical results for the dependence of ΔE on α and δ, respectively, for the *trans* form of the formamide linear dimer with $\theta = 180°$, and with $R_{O...H} = 1.5$ Å (a) and $R_{O...H} = 1.7$ Å (b). (A) $\delta = \beta = 0°$. (B) $\alpha = \beta = 0°$. $\Delta E = 0$ at $\alpha = \delta = 0°$ for each value of $R_{O...H}$.

For the *N*-methyl acetamide (NMA) linear dimer (with $\phi = 60°$, $\psi = 0°$, $\omega_1 = \omega_2 = \theta = \alpha = \beta = \delta = 0°$), the dependence of ΔE on $R_{O...H}$ (obtained by the empirical method) is shown in Table X. Again, the minimum-energy value of $R_{O...H}$ computed by the empirical method is larger than that obtained in the CNDO/2 calculations of Table VIII of paper III[5] (*viz.*, ~1.7 Å compared to ~1.5 Å), and the empirical value of the energy is less negative (−7.8 kcal/mol compared to −9.4 kcal/mol).

Table X: Empirical Results for *N*-Methyl Acetamide Linear Dimer for $\phi = 60°$, $\psi = 0°$, $\omega_1 = \omega_2 = \alpha = \beta = \delta = 0°$

$R_{O...H}$, Å	θ, deg	ΔE,[a] kcal/mol	ΔE,[b] kcal/mol
1.40	0	23.060	
1.50	0	−1.353	
1.60	0	−7.306	
1.70	0	−7.808	
1.80	0	−6.892	
2.00	0	−4.802	
4.00	0	−0.558	
1.70	0		0
1.70	30		0.142
1.70	60		0.316
1.70	90		0.441
1.70	120		0.439
1.70	150		0.379
1.70	180		0.344

[a] $\Delta E = 0$ for two planar monomers at infinite separation. [b] $\Delta E = 0$ for $\theta = 0°$, at $R_{O...H} = 1.7$ Å.

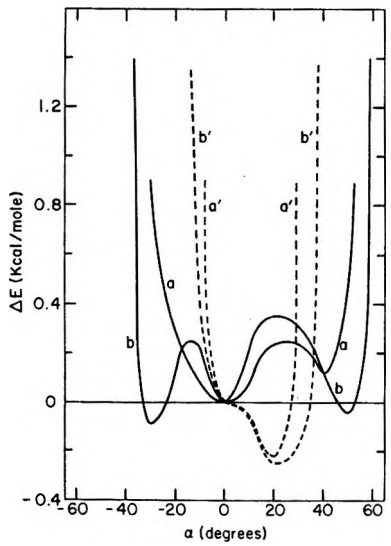

Figure 16. Empirical results for the dependence of ΔE on α for the NMA linear dimer with $\theta = 0°$ (—) and $\theta = 180°$ (---), for $R_{O\ldots H} = 1.5$ Å (curves a and a') and $R_{O\ldots H} = 1.7$ Å (curves b and b'). $\delta = \beta = 0°$. $\Delta E = 0$ at $\alpha = 0°$ for each value of $R_{O\ldots H}$.

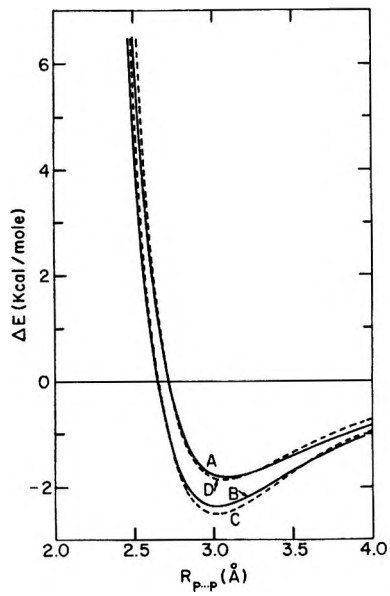

Figure 17. Empirical results for the dependence of ΔE on $R_{P\ldots P}$ for the four models of the formamide parallel-plane dimer with $\omega_1 = \omega_2 = 0°$. $\Delta E = 0$ for infinite separation of the planar monomers of this conformation.

The dependence of ΔE on α for NMA, with $\theta = 0°$ and 180°, respectively, as calculated by the empirical method, is shown in Figure 16. These curves can be compared with the CNDO/2 results of Figure 16 of paper III.[5] For $R_{O\ldots H} = 1.5$ Å, the empirical and CNDO/2 results look similar, the agreement for $\theta = 180°$ being better than for $\theta = 0°$ because the empirical methyl–methyl nonbonded interactions play a lesser role at $\theta = 180°$, *i.e.*, the nonbonded repulsive interactions are not so important in this conformation. As $R_{O\ldots H}$ increases, the empirical curves indicate that α departs from 0° for the most stable conformation with $\theta = 0°$. For $\theta = 180°$, α increases to a larger positive value, as $R_{O\ldots H}$ increases.

5. Comparison of Empirical and CNDO/2 Results for Stacked Dimers Not Linked by Hydrogen Bonds. In paper III,[5] a rarely-considered conformation, that of the parallel-plane dimer, was investigated by the CNDO/2 method, and very highly stable complexes were predicted to occur. Since this type of parallel-plane stacking may be important in the formation of complexes of polar molecules, we have repeated the earlier[5] calculations, using our empirical potentials.[47,48]

In the formamide parallel-plane dimer, the planes are those of the atoms in each planar monomer, and the parallel planes are separated by the distance $R_{P\ldots P}$. Since the C—N bonds can be either parallel or antiparallel and the carbonyl groups either aligned or opposite, there are four possible combinations in this parallel-plane structure, in which $R_{P\ldots P}$ can vary, *viz.*, with (A) the C—N bonds antiparallel and the C=O bonds opposite, (B) the C—N bonds antiparallel and the C=O bonds aligned, (C) the C—N bonds parallel and the C=O bonds opposite, and (D) the C—N bonds parallel and the C=O bonds aligned. The empirical energies for these four parallel-plane dimers as a function of $R_{P\ldots P}$ are presented in Figure 17. All four dimers show stabilization at separation distances slightly shorter than a normal van der Waals contact distance. These results are considerably different from those obtained by the CNDO/2 method,[5] which predicted stabilization energies greater than −40.0 kcal/mol for models A and B at very low values of $R_{P\ldots P}$ (see Figure 10 of paper III[5]). Again, part of this difference arises from the soft repulsions of the CNDO/2 method. Perhaps, if short-range π–π stabilization could be included in the empirical energies, the curves of Figure 17 might be shifted in the direction of more negative energies, but not as much as found by the CNDO/2 method. In the solid state,[49] formamide dimers are stacked in the cyclic conformation with an intersheet spacing of 3.1 Å, which is in excellent agreement with our empirical results, as

(47) It is of interest at this point to consider the most stable conformations of the formic acid and acetic acid dimers, predicted by our empirical procedure and by that of Minicozzi and Bradley.[34] The latter authors constructed an empirical potential function by fitting early gas-phase electron diffraction data[48] for formic acid. They then used this potential function to treat both formic acid and acetic acid dimers, and found not only the cyclic dimer[48] (on which the potential function was based) but also some stacked, nonhydrogen-bonded dimer complexes with energies within 5 to 6 kcal/mol of the hydrogen-bonded cyclic dimer. We have examined their conformations, as well as others, for both formic acid and acetic acid dimers, by exploring the energy surface using our total empirical potentials. In contrast to their results, we find a stable cyclic dimer (of energy ~ −16 kcal/mol) but no other stable complexes within 10 kcal/mol of this energy. However, we do obtain some stable parallel-plane dimers, as discussed in the text, with stabilization energies of −2 to −3 kcal/mol, *i.e.*, ~14 kcal/mol less stable than the cyclic dimer.

(48) J. Karle and L. O. Brockway, *J. Chem. Phys.*, 66, 574 (1944).

(49) J. Ladell and B. Post, *Acta Crystallogr.*, 7, 559 (1954).

shown in Figure 17. It appears that the 2 to 3 kcal of Figure 17 (being more reasonable for a stacking energy in a crystal than the −40 kcal obtained by the CNDO/2 method[5]) would probably be sufficient stabilization energy to lead to planar stacking of these molecules in crystals. In the empirical method, this stabilization arises from the nonbonded and electrostatic interactions.

Conclusion

In conclusion, we have developed an empirical model (based on quantum mechanical calculations, and modified by use of electron diffraction and thermodynamic data for gas-phase formic acid dimers) for the hydrogen-bond interaction. The resulting potential function reproduces the properties of the hydrogen bond without the explicit introduction of an angular-dependent term. By introducing a simple GHB potential (*i.e.*, the 10–12 potential), we have been able to represent the O···H interaction for any particular *type* of hydrogen bond with only one set of parameters (the simplicity of the GHB potential is a very important feature when this function is used for conformational energy calculations in polypeptides and proteins). However, the GHB potential by itself does *not* represent the properties of the hydrogen-bond interaction of a binary complex, *i.e.*, the hydrogen-bond interaction cannot be constructed from any special properties of several isolated atoms alone. Instead, it is an empirical potential required, together with *all* other nonbonded and electrostatic interactions, to represent the total interaction energy in a hydrogen-bonded complex. Consequently, when examining the properties of the hydrogen bond, either by empirical or quantum mechanical calculations or by experimental observation, one cannot single out the properties of specific atoms; instead, one must consider the interactions among all atoms of the complex. Thus, both the stabilization energy and its angular variation can be expected to vary with the nature of the molecules forming the complex.

The parameters of the hydrogen bond potentials, as well as those of other nonbonded interactions, are currently being refined by use of molecular-crystal energy-minimization procedures, and the results will be presented elsewhere.

Acknowledgment. We wish to thank the Cornell Office of Computer Services for use of their facilities, and Mrs. Shirley Rumsey for her assistance in carrying out these calculations.

On the Correlation of Solute Permeability and Reflection Coefficient for Rigid Membranes with High Solvent Content

by Gerald S. Manning

School of Chemistry, Rutgers University, New Brunswick, New Jersey *(Received May 12, 1970)*

Publication costs borne completely by The Journal of Physical Chemistry

Two different models for the diffusion of a binary solution through a membrane are used to derive relations between the solute permeability coefficient ω and the reflection coefficient σ. Since ω and σ are independent phenomenological coefficients, these relations require more data than merely the value of ω in order to predict σ: one must also have data on such quantities as the diffusion coefficient of the solute in pure solution and the diffusion properties of a tracer species of solvent both inside the membrane and in pure solvent. One of the fundamental concepts involved is that a tracer species of solvent is a suitable "reference" solute, since σ must then be zero. There is good agreement between theory and the data of Ginzburg and Katchalsky for two highly porous membranes. An appendix presents a consistent treatment of the diffusion of a binary solution through a membrane, stressing the analogy to ordinary binary diffusion.

Introduction

The linear thermodynamic theory of irreversible processes has been profitably applied to the problem of transport through membranes.[1,2] For a system consisting of a membrane which separates two binary dilute solutions with the same solute (species 1) and solvent (species 2), the transport can be compactly described by three phenomenological coefficients—the

(1) O. Kedem and A. Katchalsky, *Biochim. Biophys. Acta*, 27, 229 (1958).

(2) A. Katchalsky and P. F. Curran, "Non-Equilibrium Thermodynamics in Biophysics," Harvard University Press, Cambridge, Mass., 1965.

solute permeability coefficient ω, the reflection coefficient σ, and the filtration coefficient L_p.

The permeability coefficient ω may be operationally defined by the equation

$$\omega = -(j_1/kT\Delta c_1^0)_{J_v=0} \quad (1)$$

In eq 1, j_1 is the solute flux (molecule cm^{-2} sec^{-1}) and Δc_1^0 is the difference of the solute concentrations (molecule cm^{-3}) of the solutions separated by the membrane. The sign is chosen to be consistent with the theory of diffusion: if Δc_1^0 is positive the flux j_1 is negative (that is, from the solution with higher concentration to the solution with lower concentration), and the coefficient ω is positive. It is noted in eq 1 that the measurement is to be made under conditions for which the volume flow J_v is zero.

The reflection coefficient σ may be defined by the relation

$$\sigma = (\Delta P/kT\Delta c_1^0)_{J_v=0} \quad (2)$$

Here, ΔP is the difference in pressures of the two solutions which must be maintained if the volume flow J_v is to vanish. Equation 2 is the most useful definition of σ for theoretical purposes, although other equivalent relations are usually used for the actual measurement of σ.

The filtration coefficient L_p characterizes nonvanishing volume flow. Since $J_v = 0$ in both eq 1 and 2, L_p plays no role in this article.

Although ω and σ are independent coefficients, and hence can both be determined only by at least two independent measurements, there is a limiting case of direct correlation between them. Thus, if $\omega = 0$ for a particular solute species, then the membrane may be considered as an ideal semipermeable membrane, and σ will equal unity in accordance with van't Hoff's law of osmotic pressure for dilute solutions.

On the other hand, if the solute species is identical with the solvent species (in practice, a tracer isotope of the solvent), then $\sigma = 0$. It is therefore reasonable to ask how well σ and ω are correlated by the following "two-point interpolation formula"

$$\sigma = 1 - (\omega/\omega^*) \quad (3)$$

where ω^* refers to the permeability coefficient when the solute is a tracer of the solvent; for the formula is valid when $\omega = 0$ and is also valid when the solute is a tracer of the solvent, $\omega = \omega^*$. With the definition

$$F(\sigma, \omega; \omega^*) \equiv (1 - \sigma)(\omega^*/\omega) \quad (4)$$

a quantity which will arise in a natural way from the theories to be discussed below, eq 3 reads

$$F(\sigma, \omega; \omega^*) = 1 \quad (5)$$

Ginzburg and Katchalsky[3] have measured values of σ and ω for a series of aqueous solutions with two relatively simple synthetic membranes, dialysis tubing and a commercial wet gel. Table I pertains to the former membrane; Table II, to the latter. The quantity ϕ_w is the volume fraction of water in the membrane; γ^* is defined by eq 32 below. The listed values of ω and σ are those for the lowest concentrations used, since this article restricts itself to dilute solutions. Values of ω^* are taken to be the corresponding measured values of ω for HTO as solute.

The tabulated values of $F(\sigma, \omega; \omega^*)$ in the fourth column clearly show that eq 5 provides a very poor correlation. On a purely intuitive basis, however, it might be expected that the quantity $F(\sigma, \omega; \omega^*)$ is not entirely irrelevant. It is the purpose of this article to derive from two different molecular theories two equations of the form

$$\alpha F(\sigma, \omega; \omega^*) = 1 \quad (6)$$

where α depends neither on σ nor on ω. The first of these equations will be obtained from the energy-barrier model recently developed by the author;[4] the second, from the widely employed frictional-coefficient model.[2,5-7]

Energy-Barrier Model

In an effort to clarify the role of the pressure gradient in osmotic flow through rigid membranes and to derive the thermodynamic equations of flow from a simple kinetic model, the author[4] idealized the membrane by assuming its effect to be equivalent to that of an externally imposed force which acts on the solute but not on the solvent. Since the region occupied by the "energy barrier" contains no tangible membrane material, the model may be described as a membrane with 100% solvent content. To aid in the continuity of reading, a summary of the relevant parts of ref 4 is now given.

The solute species is assumed to execute Brownian motion. The solution is assumed to be sufficiently dilute to allow the neglect of solute–solute interactions. The volume flow J_v is assumed constrained to zero. Variations are allowed only in the x direction. Then the solute flux j_1 at the point x is given by

$$j_1 = -(kT/\zeta_1^0)(dc_1/dx) - c_1(dV/dx)/\zeta_1^0 \quad (7)$$

where ζ_1^0 is the friction coefficient of the solute in pure solvent, and $V(x)$ is the potential energy externally imposed on the solute. To mimic a membrane of thickness h, $V(x)$ is required to satisfy the restriction

$$V(x) \equiv 0; \qquad x \leqslant 0, x \geqslant h \quad (8)$$

The goal is to integrate eq 7 across the membrane (*i.e.*, from $x = 0$ to $x = h$).

(3) B. Z. Ginzburg and A. Katchalsky, *J. Gen. Physiol.*, **47**, 403 (1963).
(4) G. S. Manning, *J. Chem. Phys.*, **49**, 2668 (1968).
(5) K. S. Spiegler, *Trans. Faraday Soc.*, **54**, 1408 (1958).
(6) O. Kedem and A. Katchalsky, *J. Gen. Physiol.*, **45**, 143 (1961).
(7) K. S. Spiegler and O. Kedem, *Desalination*, **1**, 311 (1966).

Table I: Dialysis Tubing Membrane ($\phi_w = 0.68$, $\omega^* = 44.7 \times 10^{-15}$ dyn^{-1} sec^{-1}; $\gamma^* = 0.220$)

Solute	$1 - \sigma$	ω^*/ω	$F(\sigma\ \omega;\ \omega^*)$	α_{eb}	$\alpha_{eb}F$	$\bar{v}_1^0/v_2^0$	α_{fc}	$\alpha_{fc}F$
HTO	1.00	1.00	1.00	1.00	1.00	1.00	1.00	1.00
Urea	0.99	2.15	2.13	0.606	1.29	2.44	0.442	0.943
Glucose	0.88	6.22	5.48	0.296	1.62	6.18	0.180	0.988
Sucrose	0.84	11.40	9.57	0.230	2.20	11.59	0.100	0.957

Table II: Wet Gel Membrane ($\phi_w = 0.77$, $\omega^* = 78.7 \times 10^{-15}$ dyn^{-1} sec^{-1}, $\gamma^* = 0.723$)

Solute	$1 - \sigma$	ω^*/ω	$F(\sigma, \omega; \omega^*)$	α_{eb}	$\alpha_{eb}F$	$\bar{v}_1^0/v_2^0$	α_{fc}	$\alpha_{fc}F$
HTO	1.00	1.00	1.00	1.00	1.00	1.00	1.00	1.00
Urea	1.00	2.49	2.49	0.606	1.51	2.44	0.537	1.34
Glucose	0.98	6.46	6.33	0.296	1.88	6.18	0.242	1.53
Sucrose	0.96	10.30	9.89	0.230	2.27	11.59	0.158	1.56

To this end, define a function $g(x)$ by

$$c_1(x) = c_I \exp[-V(x)/kT]g(x) \tag{9}$$

where c_I is the (uniform) solute concentration in the solution bathing the left side of the membrane, *i.e.*, occupying the region $x \leqslant 0$. If c_{II} is the solute concentration in the solution occupying the region $x \geqslant h$, then $g(x)$ must, because of eq 8, satisfy the following boundary conditions

$$g(0) = 1; \quad g(h) = c_{II}/c_I \tag{10}$$

Substitution of eq 9 into eq 7 yields

$$\zeta_1^0 j_1 \exp(V/kT) = -kTc_I dg/dx \tag{11}$$

With the assumption that the system is in a steady state, so that j_1 is a constant, eq 11 may be directly integrated from $x = 0$ to $x = h$. The result may be put in the form

$$j_1 = -kT\Delta c_1^0/h\zeta_1^0\langle\exp(V/kT)\rangle \tag{12}$$

where

$$\Delta c_1^0 = c_{II} - c_I$$

and

$$h\langle\exp(V/kT)\rangle = \int_0^h \exp(V/kT)dx \tag{13}$$

Equation 12 may now be compared with eq 1, whereupon follows the identification of ω

$$\omega = (h\zeta_1^0\langle\exp(V/kT)\rangle)^{-1} \tag{14}$$

It has been stated that the volume flow J_v is zero. However, since $-c_I dV/dx$ is an external volume force, the pressure P cannot be uniform under these conditions. In fact, the hydrostatic equation is

$$dP/dx = -c_I dV/dx \tag{15}$$

According to eq 8 and 15, P will have a constant value P_I for $x \leqslant 0$ and P_{II} for $x \geqslant h$. Let $\Delta P = P_{II} - P_I$, so that, from eq 15

$$\Delta P = -\int_0^h c_1(dV/dx)dx \tag{16}$$

A convenient expression for the integrand is given by eq 7

$$-c_1(dV/dx) = kT(dc_1/dx) + \zeta_1^0 j_1 \tag{17}$$

or

$$-\int_0^h c_1(dV/dx)dx = kT\Delta c_1^0 + h\zeta_1^0 j_1 \tag{18}$$

If eq 12 for j_1 is used in eq 18 and the result substituted into eq 16, one obtains

$$\Delta P = (1 - \langle\exp(V/kT)\rangle^{-1})kT\Delta c_1^0 \tag{19}$$

Comparison of eq 19 with eq 2 permits the identification of σ as

$$\sigma = 1 - \langle\exp(V/kT)\rangle^{-1} \tag{20}$$

The relation between ω and σ implicit in this model is then obtained from eq 14 and 20

$$\sigma = 1 - h\zeta_1^0\omega \tag{21}$$

Note that measurements of both ω and ζ_1^0 are required in order to obtain σ from eq 21, so that the general criterion that σ and ω be independent is not violated. With this result, the summary of the relevant parts of ref 4 is completed.

The model just described is now applied to a particular solute species, labeled 2*, namely, a tracer species of the solvent. It was specified that the external force $-dV/dx$ does not act on the solvent; hence, for this special case, assuming that the tracer species has exactly the same physical properties as the solvent itself, dV/dx is to be taken as identically equal to zero for all x. With ω^* written for ω in this special case, eq 14 becomes

$$\omega^* = (h\zeta_{2^*}^0)^{-1} \tag{22}$$

where $\zeta_{2^*}^0$ is the friction coefficient of tracer species

2* in pure solvent. Combination of eq 21 and 22 then leads to an expression of the form of eq 6

$$\alpha_{eb}F(\sigma, \omega; \omega^*) = 1 \quad (23)$$

where

$$\alpha_{eb} = \zeta_{2*}^0/\zeta_1^0 \quad (24)$$

and $F(\sigma, \omega; \omega^*)$ is the quantity defined in eq 4. Note that α_{eb} (the subscript indicates the energy-barrier model) does not depend on the properties of the membrane (*i.e.*, on the details of the energy barrier).

Values of α_{eb} from eq 24 may be obtained by applying the Einstein relation

$$\zeta_i^0 = kT/D_i^0 \quad (25)$$

where D_i^0 is the diffusion coefficient of dilute species i, to the diffusion data of Longsworth[8,9] on aqueous solutions; these values are presented in Tables I and II along with the products $\alpha_{eb}F$. The agreement with eq 23 is fair and is certainly a dramatic improvement over that for eq 5. Moreover, it is not to be expected that the energy-barrier model provide a quantitative description, since solvent–membrane interactions are not realistically described. It is easy to gain partial insight into the error thereby introduced by looking at eq 22, which may be rewritten as $\gamma^* = 1$, where γ^* is defined below by eq 32. Experimental values of γ^* are recorded in Tables I and II; they are 0.22 for the dialysis tubing and 0.72 for the wet gel.

Friction-Coefficient Model

For unidirectional flow in a homogeneous, isotropic, multicomponent fluid, the linear Onsager equations[10] may be written in the following form[11,12]

$$d\mu_i/dx = -\sum_{j=1}^{\nu} c_i\zeta_{ij}(u_i - u_j) \quad (i = 1, \cdots, \nu) \quad (26)$$

Equation 26 employs Bearman's notation[12] wherein ν is the number of components, c_i is the concentration of species i, μ_i is the chemical potential (partial molecular Gibbs free energy) of species i, and u_i is the velocity of species i with respect to a frame fixed in the laboratory. The coefficients ζ_{ij} are symmetric

$$\zeta_{ij} = \zeta_{ji} \quad (27)$$

Expressions for the coefficients ζ_{ij} in terms of molecular quantities are given in ref 12. It is assumed that there are no external forces and that the fluid is isothermal. Another restriction required for the validity of eq 26 is that the system be in mechanical equilibrium, a condition to be discussed further in the Appendix. Equation (26), then, provides a description of isothermal diffusion in a homogeneous, isotropic, ν-component solution.

It may be inquired whether an adequate description of diffusion in a membrane could be obtained simply by setting the velocity u_ν of species ν, supposed to correspond to the membrane component, equal to zero. This point of view was taken by Spiegler[5] and by Kedem and Katchalsky,[6] and has been widely, if not always consistently, employed. (In papers pertaining to membranes, coefficients called f_{ij} are often used; the relation between f_{ij} and ζ_{ij} is $f_{ij} = c_j\zeta_{ij}$.) For a two-component solution diffusing through a membrane, one would let species 3 be the membrane, set $u_3 = 0$, and write

$$d\mu_1/dx = -c_2\zeta_{12}(u_1 - u_2) - c_3\zeta_{13}u_1 \quad (28a)$$

$$d\mu_2/dx = -c_1\zeta_{12}(u_2 - u_1) - c_3\zeta_{23}u_2 \quad (28b)$$

From these two equations, and with the use of the usual thermodynamic theory of dilute solutions, we may derive expressions for ω and σ. These expressions and a discussion of their derivations may be found in the Appendix, eq A17 and A23. Having obtained ω and σ, one may now derive the following result (see Appendix)

$$\alpha_{fc}F(\sigma, \omega; \omega^*) = 1 \quad (29)$$

where

$$\alpha_{fc} = (c_2\zeta_{2*2} + c_3\zeta_{2*3})/[c_2\zeta_{12} + c_3\zeta_{2*3}(\bar{v}_1/\bar{v}_2)] \quad (30)$$

where $\bar{v}_i$ is the partial molecular volume of species i inside the membrane. It may be noted that when $c_3 = 0$, α_{fc} (the subscript refers to the friction-coefficient model) reduces to α_{eb}, defined by eq 24, for then $c_2\zeta_{12}$ has precisely the significance of the friction coefficient ζ_i^0 of solute species i in pure solvent, species 2 (see Appendix). The second term in both numerator and denominator of the right side of eq 30 provides for that aspect of the real system not present in the energy-barrier model, namely, tangible membrane material.

As described in detail in the Appendix it is now possible to introduce into eq 30 certain assumptions plausible for a highly porous membrane. They lead to the following approximate expression for α_{fc}

$$\alpha_{fc} = (\gamma^*)^{-1}\{(\zeta_1^0/\zeta_{2*}^0) + (\bar{v}_1^0/v_2^0)[(\gamma^*)^{-1} - 1]\}^{-1} \quad (31)$$

with

$$\gamma^* = h\omega^*\zeta_{2*}^0 \quad (32)$$

and where $\bar{v}_1^0$ is the partial molecular volume of the solute in pure solvent and v_2^0 is the molecular volume of the pure solvent. To obtain some insight into eq 31, note that in the absence of tangible mem-

(8) L. G. Longsworth, *J. Amer. Chem. Soc.*, **75**, 5705 (1953).

(9) L. G. Longsworth, *J. Phys. Chem.*, **67**, 689 (1963).

(10) D. D. Fitts, "Nonequilibrium Thermodynamics," McGraw-Hill, New York, N. Y., 1962.

(11) R. W. Laity, *J. Phys. Chem.*, **63**, 80 (1959).

(12) (a) R. J. Bearman and J. G. Kirkwood, *J. Chem. Phys.*, **28**, 136 (1958); (b) R. J. Bearman, *ibid.*, **31**, 751 (1959); (c) R. J. Bearman, *ibid.*, **32**, 1308 (1960); (d) R. J. Bearman, *J. Phys. Chem.*, **65**, 1961 (1961).

brane material, eq 22 would apply and γ^* would equal unity, thereby reducing eq 31 to eq 24 for α_{eb}.

Values of the ratio of molecular volumes were assumed to be accurately given by the corresponding ratio of apparent molal volumes as measured by Longsworth.[8,9] Values of α_{fc} were then calculated according to eq 31 along with the products $\alpha_{fc}F(\alpha, \omega; \omega^*)$; the results appear in the last two columns of Tables I and II. It is seen that eq 29 is a quantitative description for the dialysis tubing. While agreement with the data is not quite as good for the wet gel, it is significantly better than that obtained with the energy-barrier model. On the other hand, since the wet gel is the more highly porous of the two membranes (it has the higher value of ϕ_w), it is disappointing that eq 29 and 31, the assumptions underlying which should be the more exact as the porosity increases [see particularly the approximation (A28)], provide better correlation for the dialysis tubing. The author can only suggest the appropriateness of more extensive measurements.

Appendix

Mechanical Equilibrium. Because of the symmetry condition $\zeta_{ij} = \zeta_{ji}$, it is easy to see that the result of multiplying each of eq 26 by the corresponding c_i and then adding all ν equations is

$$\sum_{i=1}^{\nu} c_i(\mathrm{d}\mu_i/\mathrm{d}x) = 0 \qquad \text{(A1)}$$

a form of the Gibbs–Duhem relation at uniform pressure. The left side of eq A1 is the negative of the total force exerted on a volume element. Since this force is zero, Newton's second law requires that all accelerations in the fluid vanish. Thus, the velocity of the center of mass of each volume element must be uniform throughout the fluid; in particular, there can be no viscous flow. The fluid is said to be in *mechanical equilibrium*. Thus, eq 26 implies that the solution is in mechanical equilibrium. The condition of mechanical equilibrium may be experimentally attained to a high degree of approximation by constraining the volume flow J_v to be zero. If the volume flow is not zero, additional viscous terms are required in eq 26; the latter equations may therefore be used if $J_v = 0$ but may not be used if $J_v \neq 0$. The complete equations when $J_v \neq 0$ may be found in ref 12. The condition $J_v = 0$ may be written, with $\bar{v}_i$ the partial molecular volume

$$\sum_{i=1}^{\nu} \bar{v}_i j_i = 0 \qquad \text{(A2)}$$

with

$$j_i = c_i u_i \qquad \text{(A3)}$$

The relation

$$\sum_{i=1}^{\nu} c_i \bar{v}_i = 1 \qquad \text{(A4)}$$

is also used in the following. Finally, note that the calculation leading to eq A1 indicates that, of the ν eq 26, only $\nu - 1$ are independent.

Binary Diffusion. If $\nu = 2$ the single independent equation may be chosen as that corresponding to the solute species 1

$$\mathrm{d}\mu_1/\mathrm{d}x = -c_2\zeta_{12}(u_1 - u_2) \qquad \text{(A5)}$$

If the solution is sufficiently dilute that interactions among solute molecules may be neglected, one has

$$\mu_1 = \mu_1^0 + kT \ln (c_1/c_2) \qquad \text{(A6)}$$

where μ_1^0 is a function of temperature and pressure only and hence is uniform for an isothermal fluid with $J_v = 0$. With no approximations whatever (except for the essentially exact one that the $\bar{v}_i$ are independent of x), eq A2–A6 lead directly to a Fick–Einstein relation

$$j_i = -(kT/c_2\zeta_{12})(\mathrm{d}c_1/\mathrm{d}x) \qquad \text{(A7)}$$

From eq A7 it is seen that the Einstein friction coefficient ζ_1^0 is given by

$$\zeta_1^0 = c_2\zeta_{12} \qquad \text{(A8)}$$

as stated in the text in the discussion following eq 30. Moreover, it follows directly from eq A2, A4, and A7 that

$$j_2 = -(kT/c_2\zeta_{12})(\mathrm{d}c_2/\mathrm{d}x) \qquad \text{(A9)}$$

that is, Fick's relation holds, with the same diffusion constant, for the solvent as well as the solute species.

Diffusion in a Membrane Phase. If one is willing to assume that by setting $u_3 = 0$ in a ternary system, one arrives at a realistic model of the interior of a membrane, then one may work with the two independent eq 28 in the text. In eq 28a the chemical potential of solute species 1 is to be written, under the assumption that so little solute is present that solute–solute interactions may be neglected

$$\mu_1 = \mu_1^0 + kT \ln [c_1/(c_2 + c_3)] \qquad \text{(A10)}$$

where μ_1^0 is independent of x. Since $j_3 = 0$, the condition of vanishing volume flow is

$$\bar{v}_1 j_1 + \bar{v}_2 j_2 = 0 \qquad \text{(A11)}$$

To further mimic a rigid membrane, let

$$\mathrm{d}c_3/\mathrm{d}x = 0 \qquad \text{(A12)}$$

With the use of eq 28a, A3, A4 with $\nu = 3$, and A10–A12, the following equation is easily derived

$$j_1 = -kT(c_2\zeta_{12} + c_3\zeta_{13})^{-1}(\mathrm{d}c_1/\mathrm{d}x) \qquad \text{(A13)}$$

In the derivation terms like $c_1\bar{v}_1/[(c_2 + c_3)\bar{v}_2]$ and $c_1\bar{v}_1/c_2\bar{v}_2$ were systematically neglected in comparison with

unity in order to retain consistency with the dilute-solution form of the solute chemical potential. Clearly, eq A13 is a Fick–Einstein equation for the flow of solute in the interior of the membrane phase; the friction coefficient ζ_1 is identified as

$$\zeta_1 = c_2\zeta_{12} + c_3\zeta_{13} \tag{A14}$$

Moreover, it follows directly from eq A13, A12, A11, and A4 with $\nu = 3$ that

$$j_2 = -kT(c_2\zeta_{12} + c_3\zeta_{13})^{-1}(\mathrm{d}c_2/\mathrm{d}x) \tag{A15}$$

Fick's relation for the solvent with the same diffusion coefficient as for the solute. The analogy to binary diffusion [see eq A7 and A9] is complete.

Now suppose one of the membrane–solution interfaces is at $x = 0$, the other at $x = h$. In accord with the dilute solution approximation, the friction coefficient $c_2\zeta_{12} + c_3\zeta_{13}$ is independent of x; assumption of a steady state implies that j_1 is also independent of x. It is also assumed that the solution inside the membrane at the interfaces is in equilibrium with the bulk bathing solutions; the partition coefficient of the solute is denoted by K_1 (ratio of concentration inside membrane to that outside). Then the trivial integration of eq A13 from $x = 0$ to $x = h$ yields

$$j_1 = -K_1h^{-1}(c_2\zeta_{12} + c_3\zeta_{13})^{-1}kT\Delta c_1^0 \tag{A16}$$

whence it follows, on comparison with eq 1, that

$$\omega = K_1h^{-1}(c_2\zeta_{12} + c_3\zeta_{13})^{-1} \tag{A17}$$

This expression for ω is well known and was derived by Kedem and Katchalsky[6] in essentially the same way.

Although the implications of eq 28a are analogous to binary diffusion, a new feature—the reflection coefficient—arises from eq 28b. With the use of eq A3 and A11 and the neglect of $c_1\bar{v}_1/c_2\bar{v}_2$ compared to unity, eq 28b takes the form

$$\mathrm{d}\mu_2/\mathrm{d}x = (j_1/c_2)[c_2\zeta_{12} + c_3\zeta_{23}(\bar{v}_1/\bar{v}_2)] \tag{A18}$$

The dilute-solution approximation allows us to take c_2 as independent of x

$$c_2 = K_2c_2^0 \tag{A19}$$

where c_2^0 is the concentration of pure solvent and K_2 is the solvent–membrane partition coefficient; similarly, the bracketed factor in eq A18 is independent of x. Note also that the chemical potential of the solvent *in the dilute bathing solutions* is given by

$$\mu_2 = \mu_2^0 - kT(c_1^0/c_2^0) \tag{A20}$$

where μ_2^0 is the chemical potential of pure solvent; therefore the difference $\Delta\mu_2$ of chemical potentials in the bathing solutions is

$$\Delta\mu_2 = v_2^0\Delta P - (kT/c_2^0)\Delta c_1^0 \tag{A21}$$

If it is assumed that μ_2 is continuous at the interfaces, the integration of eq A18 from $x = 0$ to $x = h$, combined with eq A19 and A21, yields

$$\Delta P - kT\Delta c_1^0 = (j_1h/K_2)[c_2\zeta_{12} + c_3\zeta_{23}(\bar{v}_1/\bar{v}_2)] \tag{A22}$$

since $c_2^0v_2^0 = 1$. Finally, eq A16 for j_1 is substituted into eq A22, and the result is compared with the definition, eq 2, of the reflection coefficient σ, which is then identified as

$$1 - \sigma = \frac{K_1}{K_2}\frac{c_2\zeta_{12} + c_3\zeta_{23}(\bar{v}_1/\bar{v}_2)}{c_2\zeta_{12} + c_3\zeta_{13}} \tag{A23}$$

This formula for σ was first obtained by Spiegler and Kedem.[7]

Consider now the special case when the solute is a tracer species of the solvent, denoted by species 2*. If 1 is replaced by 2* in eq A23, and if it is noted that $K_{2*} = K_2$, $\bar{v}_{2*} = \bar{v}_2$, and that σ must be zero for such a solute, then eq A23 collapses to the relation

$$\zeta_{23} = \zeta_{2*3} \tag{A24}$$

But the random thermal motion of the tracer species is characterized, according to eq A13 and A14, by the friction coefficient

$$\zeta_{2*} = c_2\zeta_{2*2} + c_3\zeta_{2*3} \tag{A25}$$

It follows from eq A24 that ζ_{23} is related to the random motion of a solvent molecule inside the membrane, and not, as has sometimes been supposed, to the bulk movement of solvent through the membrane; thus, *it is not related to the filtration coefficient* L_p, *which characterizes bulk flow.*[1]

Correlation of ω *and* σ. If ω^* is the value of ω when the solute is the tracer species 2*, then eq A17 leads to

$$\omega^*/\omega = (K_{2*}/K_1)[(c_2\zeta_{12} + c_3\zeta_{13})/(c_2\zeta_{2*2} + c_3\zeta_{2*3})] \tag{A26}$$

Combination of eq A23, A24, and A26, together with the observation that $K_2 = K_{2*}$, then gives eq 29 and 30 of the text.

In remains to show how eq 30 for α_{fc} may be reduced to eq 31. In the first place, for membranes with a high solvent content it is reasonable to approximate the ratio of molecular volumes by the corresponding ratio in pure solution

$$\bar{v}_1/\bar{v}_2 \approx \bar{v}_1^0/v_2^0 \tag{A27}$$

Furthermore, since the coefficient ζ_{12} is a measure of that part of the restoring force due to solute–solvent interactions when the local environment of a solute molecule is perturbed away from its average spherical symmetry,[12] and since the local environment of a solute molecule will consist largely of pure solvent for a highly porous membrane, it seems reasonable to make the approximation

$$\zeta_{12} \approx \zeta_{12}^0 \tag{A28}$$

where ζ_{12}^0 is the corresponding coefficient in pure solvent. Combined with eq A19, the approximation A28 gives

$$c_2\zeta_{12} \approx K_2 c_2^0 \zeta_{12}^0 = K_2\zeta_1^0 \quad \text{(A29)}$$

the last equality having been derived in the discussion of binary diffusion, eq A8. Similarly

$$c_2\zeta_{2*2} \approx K_2\zeta_{2*}^0 \quad \text{(A30)}$$

It is repeated here that ζ_1^0 and ζ_{2*}^0 are friction coefficients (reciprocal mobilities) *in the pure solution.* When the right side of eq 30 is rearranged after using the above approximations, the following expression is obtained

$$\alpha_{fc} = [1 + (c_3\zeta_{2*3}/K_2\zeta_{2*}^0)]/[(\zeta_1^0/\zeta_{2*}^0) + (\bar{v}_1^0/v_2^0)(c_3\zeta_{2*3}/K_2\zeta_{2*}^0)] \quad \text{(A31)}$$

Let us now construct a certain expression involving ω^*. According to eq A17 and A30

$$h\omega^* = K_2(c_2\zeta_{2*2} + c_3\zeta_{2*3})^{-1} \approx K_2(K_2\zeta_{2*}^0 + c_3\zeta_{2*3})^{-1} \quad \text{(A32)}$$

Therefore, with the definition of the quantity γ^*, eq 32, one has

$$\gamma^* = [1 + (c_3\zeta_{2*3}/K_2\zeta_{2*}^0)]^{-1} \quad \text{(A33)}$$

Equation 31 for α_{fc} now follows directly from the substitution of eq A33 into eq A31.

List of Symbols

ω	=	permeability coefficient defined by eq 1, dyn^{-1} sec^{-1}
ω^*	=	permeability coefficient when solute is a tracer species of solvent, dyn^{-1} sec^{-1}
σ	=	reflection coefficient defined by eq 2, dimensionless
j_i	=	flux of species i, molecule cm^{-2} sec^{-1}
c_i	=	concentration of species i, molecule cm^{-3}
J_v	=	volume flux, cm sec^{-1}
$F(\sigma, \omega; \omega^*)$	=	quantity defined by eq 4, dimensionless
α	=	quantity defined by eq 6, dimensionless
α_{eb}	=	value of α predicted by energy-barrier model
α_{fc}	=	value of α predicted by friction-coefficient model
ζ_i^0	=	friction coefficient of solute species i in pure solvent, dyn sec cm^{-1}
D_i^0	=	diffusion coefficient of solute species i in pure solvent, cm^2 sec^{-1}
ζ_i	=	overall friction coefficient of solute species i inside membrane, dyn sec cm^{-1}
ζ_{ij}	=	partial friction coefficient between species i and j, dyn sec cm^{-1}
μ_i	=	chemical potential of species i, erg molecule^{-1}
u_i	=	velocity of species i, cm sec^{-1}
$\bar{v}_i$	=	partial molecular volume of species i, cm^3 molecule^{-1}
$\bar{v}_i^0$	=	partial molecular volume of solute species i in pure solvent, cm^3 molecule^{-1}
Species 1	=	solute species when solute is not a tracer species of solvent
Species 2	=	solvent species
Species 2*	=	solute species when solute is a tracer species of solvent
Species 3	=	membrane material
h	=	width of membrane, cm
γ^*	=	quantity defined by eq 32, dimensionless

A Derivation of the Thermodynamics of Polymer Solutions through Use of the Free Volume Concept. A. The Entropy of Mixing

by Jean Dayantis

C.N.R.S., Centre de Recherches sur les Macromolécules, 67-Strasbourg, France *(Received June 14, 1971)*

Publication costs borne completely by The Journal of Physical Chemistry

A theory is proposed for the entropy of mixing polymer with solvent. The theory originates in Hildebrand's derivation of the combinatorial entropy of mixing polymer with solvent from free volume concepts. The entropy of mixing is considered to be a consequence of the different free volumes available to the molecules in the pure components and in the solution. Two parameters are introduced, a parameter ρ which is the ratio of the free volume fractions in the polymer and in the solvent, and a parameter c' which is closely related to the parameter c introduced by Prigogine and describes the external degrees of freedom of the polymer segments. χ_s, the entropic part of the Flory–Huggins interaction parameter χ, as determined from the theory proposed is in qualitative agreement with experimental values for several polymer–solvent systems.

I. Introduction and Generalities

The more recent theories of polymer solutions have been developed by Prigogine,[1a] by Flory and coworkers[2-7] and by Patterson[8] as a consequence of the shortcomings of the old Flory–Huggins theory. The old theory explains roughly the main features of polymer solutions but fails to give even a qualitative answer to the following points: (a) The Flory–Huggins interaction parameter χ, instead of being constant, according to the theory, is, for most polymer solutions, an increasing function of the concentration. (b) For athermal solutions, and especially at the limit of zero polymer concentration, the χ parameter should be equal to zero. Instead experience shows that χ_0 lies between 0.3 and 0.5. (c) The discovery by Freeman and Rowlinson[9] of the appearance of phase separation in polymer solutions on increasing the temperature (the so-called Lower Critical Solution Temperature or LCST) cannot be explained using the concepts of the old theory.

Guggenheim,[10] in order to explain the temperature and the concentration dependence of the χ parameter, considered that χ is a free energy rather than an energy, being therefore the sum of an enthalpic and of an entropic contribution: $\chi = \chi_H + \chi_s$. Although this assumption was correct, no explanation was given as to the nature of the entropic contribution, which therefore remained rather obscure.

To the above points (a), (b), and (c), one may add point (d), which will illustrate the inadequacy of the old theory to take into account volume changes on mixing.

The newer theory succeeds in explaining at least qualitatively points (a) to (d). In this respect a lattice model is assumed for the structure of the pure components and also the solutions. This enables writing a partition function for the pure components and subsequently extending it to mixtures.[2-3] The thermodynamic functions of mixtures are then derived from the extended partition function in the usual way. Although qualitatively all the features of polymer solutions are explained by the newer theory as developed by Flory and coworkers,[2-7] the quantitative agreement with experiment is perhaps not entirely satisfactory, even considering the rather numerous parameters introduced by the theory and the fact that careful determination of them has been undertaken in some cases.[7] For example, for the system polyisobutylene–benzene the calculated excess volume of mixing differs from the experimental value by a factor of two.[7b] Similarly, in the system polyisobutylene–cyclohexane, χ_0 (*i.e.*, the value of χ for $\varphi_2 = 0$) is theoretically found to be equal to 0.30 where experiment yields a value of 0.44.[7c] In other cases (rubber–benzene[7a]), the shape of the theoretical χ *vs.* concentration curve is in good agreement with the experimental curve except for a rather large translation along the χ axis. Quanti-

(1) (a) I. Prigogine, "The Molecular Theory of Solutions," North-Holland Publishing Co., Amsterdam, 1957, Chapters 15 and 16; (b) Chapter 7; (c) Chapter 16; (d) Chapter 2.

(2) (a) P. J. Flory, R. A. Orwoll, and A. Vrij, *J. Amer. Chem. Soc.*, **86**, 3507 (1964); (b) **86**, 3515 (1964).

(3) P. J. Flory, *ibid.*, **87**, 1833 (1965).

(4) A. Abe and P. J. Flory, *ibid.*, **87**, 1838 (1965).

(5) (a) R. A. Orwoll and P. J. Flory, *ibid.*, **89**, 6814 (1967); (b) **89**, 6822 (1967).

(6) P. J. Flory, J. L. Ellenson, and B. E. Eichinger, *Macromolecules*, **1**, 279 (1968).

(7) (a) B. E. Eichinger and P. J. Flory, *Trans. Faraday Soc.*, **64**, 2035 (1968); (b) **64**, 2053 (1968); (c) **64**, 2061 (1968); (d) **64**, 2066 (1968).

(8) D. Patterson, *J. Polymer Sci., Part C*, **16**, 3379 (1968); see also *Macromolecules*, **2**, 672 (1969).

(9) P. I. Freeman and J. S. Rowlinson, *Polymer*, **1**, 20 (1959).

(10) E. A. Guggenheim, "Mixtures," Clarendon, Oxford, 1952.

tative agreement in this case may be obtained only by introducing a new and somewhat arbitrary parameter Q_{12} which will describe entropic interactions between unlike segments, as the previously introduced X_{12} parameter described enthalpic interactions between unlike segments.

The question now arises if the cell model theory may be further improved so as to take into account more accurately the experimental data. Patterson and Bardin,[11] comparing thermal expansion and compressibility data for *n*-alkanes with theoretical values derived from various cell model theories, have shown that the Flory theory is the one giving best agreement with experiment. More precisely, the slope of the experimental $(\alpha T)^{-1}$ *vs.* log T straight lines, where α is the coefficient of thermal expansion, is best explained taking an inverse volume dependence of the configurational energy. This is what is done in the Flory theory. Therefore the limitations of the Flory theory possibly merely arise from the limitations of the cell model description of the liquid state itself.

Prigogine,[1b] using the cell model, calculates the specific volume of liquid Ar, Xe, and Kr with an agreement with experiment of 10 to 20%. This is perhaps a reasonably good agreement if qualitative or at best semiquantitative results are expected on the basis of a cell model theory. If quantitative agreement is desired, it is doubtful whether the accuracy of a cell model theory, as illustrated by the above example, is sufficient, even if the agreement may be improved by using other interaction potentials than those used by Prigogine.

Barker,[12] in his thorough review of cell model theories of the liquid state, shows that these theories describe the properties of metastable solids rather than true liquids.

Restrictions on the use of partition functions derived from a cell model theory should be even stronger when mixtures and especially mixtures containing macromolecular species are concerned. In this case the possibility of constructing a lattice will depend on the molecular geometry of the mixed species. This point has been stressed by Prigogine.[1c] On the other hand, when macromolecules are concerned, Flory leaves open the definition of the segment.[3] If for instance the repeat unit of the macromolecular species is twice as large in diameter and three times as long as the solvent molecule (assumed to be spherical) then each true segment should be divided in something approaching twelve "segments." This however seems rather artificial, may be physically misleading and modifies at least the combinatorial entropy of mixing.

In view of the above limitations of the cell model description of the liquid state, it is perhaps worthwhile to endeavor to derive the thermodynamics of solutions and especially polymer solutions from free volume concepts, but independently of cell model theories.

The purpose of this series of papers on the thermodynamics of polymer solutions is twofold: (1) To obtain results equivalent to those of Flory and coworkers without reference to any cell model theory. (2) To improve, if possible, the quantitative agreement between theory and experiment. The author however will be satisfied if in this alternative approach point 1 only is achieved, since this will provide a simpler and more intuitive theory of polymer solutions.

The theory as developed below is based on two main assumptions:

(a) The mixing process is equivalent to a Joule–Thomson irreversible expansion of the translational degrees of freedom of the molecules from a given initial free volume to a given final free volume. The free volume is defined as the volume generated by the thermal motion of the molecules. To a first approximation, the free volume is equal at the temperature T°K to the volume at this temperature minus the volume at 0°K. The true free volume is however somewhat greater, since as the temperature increases there is an increased interpenetration of the molecules.

Two kinds of translational degrees of freedom must be distinguished, those associated with the motion of the centers of mass and those independent of the motion of the centers of mass (c.o.m.). For simple molecules, such as the molecules of most usual solvents, it will be assumed that there are no other translational degrees of freedom than those of the c.o.m. For polymer molecules, however, one has to take into account the translational degrees of freedom arising from the motion of the individual segments. These are discussed in section II.

(b) Only the translational degrees of freedom are contributing to the entropy of mixing. This last assumption is equivalent to admitting that the rotational degrees of freedom are internal degrees of freedom not interacting with volume.

Assumption a was first made by Hildebrand[13] when deriving from free volume concepts Flory's combinatorial entropy of mixing polymer with solvent

$$\Delta S = -k[n_1 \ln \varphi_1 + n_2 \ln \varphi_2] \qquad (1)$$

where k is Boltzmann's constant, n_1 and n_2 are the number of molecules of solvent and polymer, and φ_1 and φ_2 the volume fractions.

Assumption b is the one that is usually made and has been introduced by Prigogine.[1d]

It is further assumed that random mixing occurs in the solution. This assumption has always been made when polymer solutions are concerned and is presumably relevant unless special interactions (hydrogen bonding, dipole–dipole interactions) occur in the solu-

(11) D. Patterson and J. M. Bardin, *Trans. Faraday Soc.*, **66**, 321 (1970).

(12) J. A. Barker, "Lattice Theories of the Liquid State," Pergamon, 1963.

(13) J. H. Hildebrand, *J. Chem. Phys.*, **15**, 225 (1947).

tion. The theory therefore does not include associated solvents or solutions with solvation effects. General applicability of the theory to all polymer–solvent systems is not a purpose of this paper.

IIa. The Entropy of Mixing Liquid Polymer with Solvent

Let us assume that we want to mix n_1 moles of solvent of molar volume $V_1^0(T)$ and free volume fraction $v_1(T)$ with n_2 moles of liquid polymer of molar volume $V_2^0(T)$ and free volume fraction $v_2(T)$, each species being at a temperature T_0 lying above the fusion point of the polymer. The free volume available in the solvent will be equal to $(FV)_1 = n_1V_1^0v_1$ and that in the polymer equal to $(FV)_2 = n_2V_2^0v_2$. Assuming mixing without volume change, the free volume in the solution will be equal to $(FV)_m = n_1V_1^0v_1 + n_2V_2^0v_2$. Therefore the c.o.m. of the solvent molecules, following assumption a of section I, will "expand" from the free volume $(FV)_1$ to the free volume $(FV)_m$ and correspondingly the c.o.m. of the polymer molecules will "expand" from the free volume $(FV)_2$ to the free volume $(FV)_m$. This permits the calculation of the entropy of mixing related to the translational degrees of freedom of the c.o.m. However, it may be shown that exactly the same results are obtained if the following procedure is adopted for the mixing process: 1. The solvent is compressed from the volume $\Phi_1^0 = n_1V_1^0$ to the volume $\Phi_1^m = \Phi_1^0[1 - v_1(1 - \varphi_1)(1 - \rho)]$, where ρ is the ratio v_2/v_1 of the free volume fractions of polymer and solvent. Correspondingly the polymer is expanded from the volume $\Phi_2^0 = n_2V_2^0$ to the volume $\Phi_2^m = \Phi_2^0[1 + v_1\varphi_1 \cdot (1 - \rho)]$. At the same time the free volume fractions are varying from v_1^0 to $v_1^m = v_1^0\rho\,[1 + \varphi_1(1 - \rho/\rho)]$ and from v_2^0 to $v_2^m = v_2^0[1 + \varphi_1(1 - \rho)/\rho]$. The volumes Φ_1^m and Φ_2^m have been chosen so that in the compressed solvent and the expanded polymer the free volume fractions are equal to that in the solution if no volume change occurs upon mixing. 2. Compressed solvent and expanded polymer are mixed without volume change. 3. If necessary (occurrence of a significant excess volume of mixing) the solution is compressed or expanded to its true volume.

The above procedure will be followed here to derive the entropy of mixing, as, in a forthcoming paper, the enthalpy of mixing will be derived on the same basis. It is however again emphasized that the results concerning the entropy of mixing derived from free volume concepts are in fact independent of the above scheme for the mixing process.

(1) Entropy of Mixing Associated with the Translational Degrees of Freedom of the c.o.m. To calculate the entropy of mixing associated with the translational motion of the molecules we shall add one by one the terms arising from the procedure described above.

The entropy change due to the compression of 1 mol of solvent is

$$\begin{cases} \Delta S_1^1 = R \ln\left[1 + \varphi_1 \dfrac{1 - \rho}{\rho}\right] \\ \rho = v_2/v_1 \end{cases}$$

That due to the mixing of the solvent is

$$\Delta S_1^2 = R \ln \frac{n_1V_1 + n_2V_2\rho}{n_1V_1\rho\left[1 + \varphi_1 \dfrac{1 - \rho}{\rho}\right]}$$

The sum $\Delta S_1^1 + \Delta S_1^2$ yields, after simple calculations

$$\Delta S_{solv} = -R\{n_1 \ln \varphi_1 + n_1 \ln [1 + \varphi_2(\rho - 1)]\} \quad (2)$$

Similarly, the entropy change due to the expansion and then the mixing with solvent of n_2 moles of liquid polymer is

$$\Delta S_{polym} = -R\left\{n_2 \ln \varphi_2 - n_2 \ln\left[1 + \varphi_1 \frac{1 - \rho}{\rho}\right]\right\} \quad (3)$$

The entropy change associated with the translational degrees of freedom of the c.o.m. of the solvent and the polymer molecules is therefore

$$\Delta S_{c.o.m.} = -R\left\{n_1 \ln \varphi_1 + n_2 \ln \varphi_2 - n_1 \ln [1 - \varphi_2(1 - \rho)] - n_2 \ln\left[1 + \varphi_1 \frac{1 - \rho}{\rho}\right]\right\} \quad (4)$$

The first logarithm containing ρ in the r.h.s. of eq 4 expresses that there is an entropy decrease due to the fact that in the solution there is less free space per unit volume for the solvent molecules in which to move. The second logarithm expresses an entropy increase for opposite reasons related to the polymer molecules.

(2) Entropy of Mixing Associated with the Translational Degrees of Freedom Other than Those of the c.o.m. As already pointed out such degrees of freedom will be considered here to exist only for polymer molecules. However, extension if necessary to solvent molecules should not present special difficulties.

The translational degrees of freedom of the polymer segments are clearly not independent of the position of the c.o.m., that is, if it is true that any polymer segment may occupy through time any position in the solution it is also true that the position of any segment at any moment depends upon the position of the c.o.m. This is why it cannot be considered, a priori, that the expansion of the translational degrees of freedom arising from the motion of the segments is, as in the preceding case, from $(FV)_2$ to $(FV)_m$. Let us then determine the relative space in which these degrees of freedom are moving, first into the pure polymer, then into the solution.

First let us assume that we have a rigid macromolecule. Without loss of generality one may assume that the macromolecule is rod shaped. Although any point D in the rod may take through time any posi-

tion in the solution, this introduces no new degrees of freedom as long as the position of point D is determined from the coordinates, relative to some arbitrary frame of reference of the c.o.m. and two angles. Let us now assume that a segment CB containing point D may have an independent motion, provided that the point C remains attached to the main rod. The position of point D is no longer determined by three coordinates and two angles and the undetermined space in which point D may be found is defined as the relative space in which the translational degrees of freedom introduced by the brownian motion of the individual segments must be considered to move. The free volume related to this relative space will be a function of the density of packing of neighboring molecules, in other words the density of the medium.

Now, for a freely joined chain, the probability density for finding a segment at a distance r from the c.o.m. is given by the well-known relation

$$P(r) = x(a/\pi\bar{r}_0^2)\exp(-9r^2/\bar{r}_0^2) \qquad (5)$$

where $\bar{r}_0^2$ is the mean square end to end distance, x the number of segments, and a the length of each segment. For present purposes it may be assumed, without loss of generality, that there is a uniform distribution of segments inside a sphere of radius $(\bar{r}_0^2)^{1/2}$, all segments having equal probabilities to be found in any point inside that sphere. The relative space is thus in this case the sphere of radius $(\bar{r}_0^2)^{1/2}$ centered at the c.o.m. of the macromolecule.

Neglecting for present purposes any expansion of the chain occuring on mixing, it is seen that the free volume inside this relative space is, in the pure polymer $^4/_3\pi\cdot(\bar{r}_0^2)^{3/2}v_2$, whereas in the solution this free volume is $^4/_3\pi(\bar{r}_0^2)^{3/2}v_m$. If, following Prigogine, we assume that there are c external degrees of freedom per polymer segment, and if w is the ratio of translational to external equivalent degrees of freedom (this ratio is discussed in section IV) the change in relative free volume will introduce the entropy change

$$\Delta S_{segm} = Rn_2w\frac{c}{3}x\ln(v_m/v_2) = Rn_2w\frac{c}{3}x\ln\left[1+\varphi_1\frac{1-\rho}{\rho}\right] \qquad (6)$$

Adding $\Delta S_{c.o.m.}$ and ΔS_{segm} the following expression is found for the total entropy of mixing

$$\Delta S = -R\left\{n_1\ln\varphi_1 + n_2\ln\varphi_2 - n_1\ln[1-\varphi_2(1-\rho)] - n_2\left(1+w\frac{c}{3}x\right)\times\ln\left[1+\varphi_1\frac{1-\rho}{\rho}\right]\right\} \qquad (7)$$

Evaluations of the parameters ρ and c are given in section IV. On the basis of these evaluations it is found that in the last logarithm of eq 7 the unity may be neglected before $wcx/3$ for chains sufficiently long ($x > 100$). Introducing the new constant $c' = w\cdot c/3(V_1/V_2')$ where V_2' is the volume of a mole of segments, eq 7 takes the form

$$\Delta S = -R\left\{n_1\ln\varphi_1 + n_2\ln\varphi_2 - n_1\ln[1-\varphi_2(1-\rho)] - \frac{V_2'}{V_1}n_2c'x\ln\left[1+\varphi_1\frac{1-\rho}{\rho}\right]\right\} \qquad (7')$$

On the other hand, if $c'x$ is small compared to unity, eq 7 reduces to eq 4. This equation was given earlier[14] and is the one relevant for mixtures of simple molecules.

(3) Partial Molar Entropies. The partial molar entropy of mixing of the solvent is defined as

$$\overline{\Delta S_1} = \left(\frac{\partial\Delta S}{\partial n_1}\right)_{T,P,n_2} \qquad (8)$$

From eq 7′ one obtains for $\overline{\Delta S_1}$

$$\overline{\Delta S_1} = -R\left\{\ln(1-\varphi_2) + \left(1-\frac{1}{x}\frac{V_1}{V_2'}\right)\varphi_2 - \ln[1-\varphi_2(1-\rho)] - \frac{1-\rho}{1-\varphi_2(1-\rho)}\varphi_1\varphi_2 - \frac{c'(1-\rho)}{1-\varphi_2(1-\rho)}\varphi_2^2\right\} \qquad (9)$$

Similarly, the partial molar entropy of mixing of the polymer is given by

$$\overline{\Delta S_2} = -R\left\{\ln\varphi_2 + \left(1-\frac{xV_2'}{V_1}\right)\varphi_1 - c'x\ln\left[1+\varphi_1\frac{1-\rho}{\rho}\right] + \frac{c'x(1-\rho)}{1-\varphi_2(1-\rho)}\varphi_1\varphi_2 + \frac{1-\rho}{1-\varphi_2(1-\rho)}\varphi_1^2\right\} \qquad (10)$$

The excess partial molar entropy of mixing of the solvent $\overline{\Delta S_1}^E$, *i.e.*, $\overline{\Delta S_1}$, as given by eq 9, minus $\overline{\Delta S_1}^*$, the Flory–Huggins combinatorial entropy of mixing, is given by

$$\overline{\Delta S_1}^E = +R\left\{\ln[1-\varphi_2(1-\rho)] + \frac{1-\rho}{1-\varphi_2(1-\rho)}\varphi_1\varphi_2 + \frac{c'(1-\rho)}{1-\varphi_2(1-\rho)}\varphi_2^2\right\} \qquad (11)$$

Usually, $\overline{\Delta S_1}/R\varphi_2^2$ is plotted against φ_2. At the limit of φ_2 tending towards zero, the difference between the two curves, *i.e.*, the present theory curve minus the classical Flory–Huggins curve, is given by

(14) J. Dayantis, *C. R. Acad. Sci., Ser. C*, **271**, 276 (1970).

$$\lim_{\varphi_1 \to 0} \{\Delta S_1^E / R\varphi_2^2\} =$$

$$(1 - \rho)(c' - \rho) - {}^1/_2(1 - \rho)^2 \quad (12)$$

Unless c' is significantly greater than one-half, which is quite improbable (see section IV) the present theoretical curve lies below the Flory–Huggins classical curve. For $\rho = {}^1/_2$ and $c' = {}^1/_4$ the limit is equal to -0.25. On the other hand, the newer Flory theory yields for this limit a value varying, following the polymer–solvent system considered, from -0.1 to less than -1.0.[7]

Equation 11 shows that $\overline{\Delta S_1^E}/R\varphi_2^2$ varies typically from about -0.30 for $\varphi_2 = 0$ to about -0.60 for $\varphi_2 = 1$, and depends rather slightly on the values taken by c' when ρ lies between ${}^1/_2$ and ${}^1/_4$.

IIb. The Entropy of Mixing Solid Polymer with Solvent

It is well known that for polymers in the solid state (crystalline or amorphous) the motion of the c.o.m. of the molecules is considerably restricted, and is in fact limited, as for the segments, to motions inside a small cell. Therefore the derivation of the entropy of mixing given in section IIa should not apply, unless the so-called communal entropy of fusion[15] is added to the result

$$\Delta S_{\text{solid}} = \Delta S_{\text{liquid}} + \Delta S_{\text{communal}}$$

where ΔS_{liquid} is the entropy of mixing liquid polymer with solvent and ΔS_{solid} is that of mixing solid polymer with solvent. The question now arises if the communal entropy is an internal or an external entropy change.[16] In the first instance there will be an additional entropic contribution and in the second instance an additional enthalpic contribution. Most authors seem to relate the communal entropy of fusion to the heat of fusion, so that the communal entropy will add an enthalpic contribution to the free energy of mixing. It is out of the scope of the present paper to go through the question, but one may point out that inasmuch as the communal entropy is related to the delocalization of the molecules during the process of fusion, and not related to any volume changes, consideration of the Clapeyron equation opposes the above point of view. If now the communal entropy is an internal entropy change producing no heat exchanges (as in an irreversible Joule–Thomson expansion of a perfect gas) then the communal entropy will add an additional entropic contribution, so that eq 7′ should be modified to

$$\Delta S = -R\Big\{n_1 \ln \varphi_1 + n_2 \ln \varphi_2 - n_1 \ln [1 - \varphi_2(1 - \rho)] - \frac{V_2'}{V_1} n_2 c' x \times \ln\left[1 + \varphi_1 \frac{1 - \rho}{\rho}\right] - g(n_2, c'x)\Big\} \quad (13)$$

where $g(n_2, c'x)$ is some function of the number n_2 of polymer molecules and of the product of the characteristic parameter c' by the number x of segments per molecule. If it is assumed that this communal entropy is just R cal deg^{-1} mol^{-1} as for simple liquids, eq 13 reduces to

$$\Delta S = -R\Big\{n_1 \ln \varphi_1 + n_2 \ln \varphi_2 - n_1 \ln [1 - \varphi_2(1 - \rho)] - \frac{V_2'}{V_1} n_2 c' x \times \ln\left[1 + \varphi_1 \frac{1 - \rho}{\rho}\right] - n_2\Big\} \quad (13')$$

This equation shows that the introduction of the communal entropy does not modify eq 9, 11, and 12, and also the forthcoming eq 17 and 18, except trivially for eq 17.

The important and rather difficult question of the communal entropy of fusion in crystalline polymers and fluidification in amorphous solid polymers will not be pursued any further in this paper.

III. The Flory–Huggins Interaction Parameter χ

Following Guggenheim's assumption the Flory–Huggins χ parameter is the sum of an enthalpic and of an entropic contribution

$$\chi = \chi_H + \chi_s \quad (14)$$

For athermal solutions χ_H should be equal to zero so that the only contribution to χ is entropic. As however χ_s (and generally χ) is concentration dependent, caution should be taken regarding definitions. χ_s determined from integral enthalpy and entropy of mixing will be generally different from χ_s determined from chemical potentials. One should write therefore

$$\Delta G = RT[n_1 \ln \varphi_1 + n_2 \ln \varphi_2 + \chi_s' n_1 \varphi_2] \quad (15)$$

and

$$\mu_1 - \mu_1^0 = \left[\frac{\partial(\Delta G)}{\partial n_1}\right]_{T,P,n_2} = RT\left[\ln (1 - \varphi_2) + \left(1 - \frac{1}{x}\frac{V_1}{V_2'}\right)\varphi_2 + \chi_s \varphi_2^2\right] \quad (16)$$

where $\chi_s' \neq \chi_s$, unless $\partial\chi_s'/\partial\varphi_1 = \partial\chi_s/\partial\varphi_1 = 0$. For nonathermal solutions the same will be true eliminating subscript s in χ_s. Equating now eq 7′ and 9 multiplied by T, respectively, with eq 15 and 16 it is found that

(15) (a) J. O. Hirschfelder, D. P. Stevenson, and H. Eyring, *J. Chem. Phys.*, 5, 896 (1937); (b) J. G. Kirkwood, *ibid.*, 18, 380 (1950); (c) see also G. E. Kimball, "The Liquid State," in "A Treatise of Physical Chemistry," H. S. Taylor and S. Glasstone, Ed., Van Nostrand Co., New York, N. Y.

(16) E. A. Guggenheim, "Thermodynamics," North-Holland Publishing Co., Amsterdam, Chapter I.

$$\chi_s' = -\frac{1}{\varphi_2}\ln\left[1 - \varphi_2(1-\rho)\right] - \frac{c'}{\varphi_1}\ln\left[1 + \varphi_1\frac{1-\rho}{\rho}\right] \quad (17)$$

and

$$\chi_s = -\frac{1}{\varphi_2^2}\left\{\ln\left[1 - \varphi_2(1-\rho)\right] + \frac{1-\rho}{1-\varphi_2(1-\rho)}\varphi_1\varphi_2 + \frac{c'(1-\rho)}{1-\varphi_2(1-\rho)}\varphi_2^2\right\} \quad (18)$$

The limiting values of χ_s' and χ_s for $\varphi_2 = 0$ and $\varphi_2 = 1$ are, respectively

$$\chi_s'^0 = 1 - \rho + c'\ln\rho \quad (19a)$$

$$\chi_s'^1 = \ln\frac{1}{\rho} - c'\frac{1-\rho}{\rho} \quad (19b)$$

and

$$\chi_s^0 = (1-\rho)(\rho - c') + \frac{(1-\rho)^2}{2} \quad (20a)$$

$$\chi_s^1 = \log\frac{1}{\rho} - c'\frac{1-\rho}{\rho} \quad (20b)$$

It is seen that the two functions 17 and 18 converge towards the same limit as φ_2 tends towards one. Since interaction parameters are usually determined from osmotic pressure and vapour pressure measurements, eq 18 should be the one most often used to compare theoretical with measured values of χ_s.

IV. Experimental Determination of the ρ and c Parameters

(1) *The ρ Parameter.* The ratio ρ of the free volume fractions in the polymer and in the solvent may be determined with satisfactory accuracy if liquid polymer and solvent obey the original Tait equation[17]

$$\frac{V_0 - V}{V_0} = \frac{AP}{B + P} \quad (21)$$

where V_0 is the volume at atmospheric pressure, V the volume at the pressure P, A and B two constants. Assuming for present purposes that molecules and segments are rigid and incompressible, it is immediately seen, by letting P go to infinity, that A is the "co-volume" fraction in the species. The free volume fraction will be given by $1 - A$. Unfortunately, the Tait equation is quite unsatisfactory for describing the compression of numerous simple liquids especially in the n-alkane series. In this case the Tait equation will yield only approximate values for v_1. On the other hand, several studies have been devoted to PVT relations in polymers, but it does not seem that in any one of them the applicability of the simplest of these relations, namely the original Tait equation, has been seriously examined. However, Spencer and Gilmore[18] have shown that within a substantial temperature range polystyrene obeys a van der Waals equation with constant internal pressure. For such polymers, the original Tait equation possibly applies, since it may be shown that eq 21 may be derived from the van der Waals equation if the internal pressure is nearly independent of volume.[19]

The free volume fractions may also be derived, neglecting corrections resulting from the interpenetrability of molecules, if the volume at 0°K is known. Doolittle[20] has shown that there are satisfactory empirical relations relating the density of n-alkanes with temperature and molecular weight.[21] At 0°K, Doolittle's relations reduce to

$$\frac{1}{d} = \exp(10/M) \quad (22)$$

where M is the molecular weight and d the density. Using Doolittle's equation and density data reported by Orwoll and Flory,[5] the following table has been established, giving the free volume fractions in the n-alkane series at 170°.

Table I shows that the ratio ρ for polymethylene: hexane is about one-half. On the other hand it may be inferred from the respective densities of styrene and polystyrene (0.907 and 1.09), assuming that v_1 for styrene is about 0.25, that the ρ ratio for polystyrene: styrene has a lower value, perhaps near to one-third. In any case, as the free volume fractions in ordinary solvents at room temperature vary within a rather narrow range of values, it may be inferred that ρ

Table I

Compound	Density 0°K	Density 463°K	Free volume fraction
n-Hexane	0.8904	0.4913	0.448
n-Heptane	0.9050	0.5359	0.408
n-Octane	0.9162	0.5666	0.381
n-Nonane	0.9250	0.5898	0.362
n-Undecane	0.9381	0.6222	0.337
n-Dodecane	0.9430	0.6344	0.327
n-Pentadecane	0.9539	0.6066	0.307
n-Heptadecane	0.9593	0.6729	0.298
n-Eicosane	0.9652	0.6869	0.288
n-Hexacosane	0.9732	0.7060	0.275
Marlex 50 polymethylene	1.0000	0.7662	0.234

(17) P. G. Tait, "Voyage of H. M. S. Challenger 3. Vol. II, 1889. See J. S. Rowlinson, "Liquids and Liquid Mixtures," Butterworth, London, Chapter II.

(18) R. S. Spencer and G. D. Gilmore, *J. Appl. Phys.*, **20**, 502 (1949).

(19) J. Dayantis, *J. Chim. Phys.*, in press.

(20) A. Doolittle, *J. Appl. Phys.*, **22**, 1471 (1951).

(21) Such relations should presumably exist for other homologous series as a result of Prigogine's theorem of corresponding states for x-mers.

will most often lie between one-half and one-third. As the temperature is increased, lower values of ρ may be obtained, as the thermal expansion of simple liquids is more important than that of polymers.

(2) The c Parameter. Much information may be gained concerning Prigogine's c parameter by considering the variation of the thermal pressure coefficient $\gamma = (\partial P/\partial T)_V$ with volume at atmospheric pressure. If one plots $1/\gamma = (\partial T/\partial P)_V$ *vs.* V, it is found that for many simple liquids as well as for polymeric materials like polymethylene the plot is linear, at least within substantial volume (or temperature) ranges. For other simple liquids, however, the plot presents an upwards curvature. Such plots have first been used by Haward.[22] Let us now assume that a simple or polymeric liquid has a linear $1/\gamma$ *vs.* V plot, in a given range of molar volumes. It follows that within the range considered

$$\left(\frac{\partial T}{\partial P}\right)_V = \lambda(V - b) = \frac{V - b}{LR} \qquad (23)$$

where λ is the slope of the straight line, b, the intersection of the straight line with the V axis, R the gas constant, and L another constant. Since, as has been widely observed, liquid isochores are linear, it follows from eq 23, that within the temperature range considered the compound obeys a generalized van der Waals equation

$$P = \frac{LRT}{V - b} + f(V) \qquad (24)$$

where $f(V)$ is a function of volume only. The parameter L has also been introduced by Haward, when plotting $(\partial P/\partial T)_V$ *vs.* molar volume for simple liquids.

The quantity $3L$ may be called the equivalent external degrees of freedom (EEDF). If the $1/\gamma$ *vs.* V plot is not linear, L will be a function of V (or T), that is, the EEDF will be temperature dependent. In Figure 1 are drawn the $1/\gamma$ *vs.* V plots for hexane and polymethylene. For a polymeric material, by equating $3L$ to $cx + 3$, the c parameter is determined. Table II gives the L and c parameters for n-alkanes from n-hexane to polymethylene. Thermal pressure coefficients and density data were taken from Orwoll and Flory.[5] A dash in the temperature column means that L is temperature independent.

Table II

Compound	Temperature, °C	L	$3L$ = EEDF per molecule	c = EEDF per segment
n-Hexane	50	2.115	6.345	1.057
n-Octane	50	2.876	8.628	1.078
n-Hexadecane	50	4.660	13.980	0.874
n-Eicosidiane	50	6.205	18.615	0.846
n-Hexatriacontane	...	9.003	27.00	0.750
Polymethylene, marlex 50, $M = 1 \times 10^4$	...	183.0	549.0	0.768
Polymethylene, marlex 5060, $M = 1.8 \times 10^5$	...	2909	8727	0.678

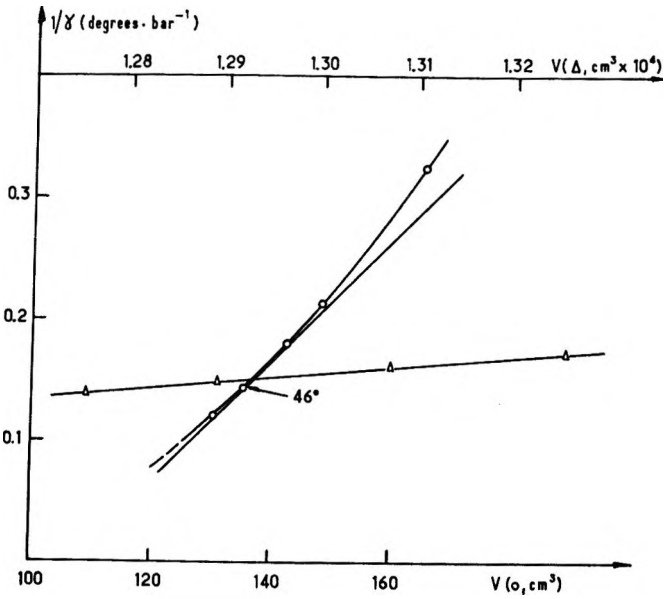

Figure 1. Reciprocal thermal pressure coefficient *vs.* volume at $P = 0$ for n-hexane (circles) and Marlex 50 polymethylene (triangles). Lower scale applies to hexane and upper scale applies to polymethylene. Thermal pressure coefficients and density data have been taken from Orwoll and Flory.[5]

It is thus found experimentally that at infinite molecular weight each segment added adds nearly 0.70 degree of freedom. This is close to the value of one assumed by Prigogine[1] for fixed angle chains. The somewhat lower value found experimentally presumably arises from the interdependence of the degrees of freedom in neighboring segments, since it is quite impossible to rotate a polymer segment without rotating the adjoining segments. Since the energy equipartition theorem requires independent degrees of freedom, the theorem does not apply for the degrees of freedom of polymer segments. However, at least for polymethylene, the experimental value found for the EEDF per segment is in rather good agreement with the equipartition theorem.

V. Discussion

A point of importance in order to apply eq 7′ and 18 is the relation existing between the EEDF of a polymer segment as determined from the variation of the thermal pressure coefficient with temperature and the translational degrees of freedom, which, according to the assumptions made in this paper, are the only degrees contributing to the entropy of mixing. For numerous simple molecules, as shown in Table III, the ratio of translational over EEDF, that is $1/L$, lies between one half and one third. A dash in the tem-

(22) R. N. Haward, *Trans. Faraday Soc.*, 62, 828 (1966).

Table III

Liquid	Temperature, °C	L	$3L$ = EEDF per molecule
Carbon tetrachloride	...	2.52	7.58
Acetone	...	1.61	4.83
Benzene	...	2.79	8.38
Cyclohexane	20	3.83	11.49
Cyclohexane	50	2.90	8.72
Methane	...	2.17	6.51
n-Hexane	50	2.11	6.34
n-Octane	50	2.88	8.63
n-Hexadecane	50	4.66	13.98

perature column means that L is temperature independent, in the temperature range investigated.

Thermal pressure coefficients needed for the calculations in Table III have been determined for carbon tetrachloride, acetone, benzene, and cyclohexane from the ratio α/κ of the thermal expansion coefficient over the isothermal compressibility coefficient. Thermal expansion coefficients have been determined from series expansion given for acetone, benzene, and carbon tetrachloride in Smithsonian Physical Tables[23] and for cyclohexane in International Critical Tables.[24] The isothermal compressibility data used were those of Tyrer[25] for benzene and carbon tetrachloride, of Staveley, Tupman, and Hart[26] for acetone, and of Diaz Pena and McGlashan[27] for cyclohexane. The value of L for methane in the liquid state is that reported by Haward.[22] Results for low molecular weight *n*-alkanes are those already given in Table II and have been computed from data given by Orwoll and Flory.[5]

It seems at present quite hazardous to extend the results for simple molecules given in Table III to the EEDF of polymer segments given in Table II. Very probably the ratio w in eq 7 will depend upon geometrical and stereochemical properties of the segments.

Equation 18 will now be compared with experimental results for several polymer–solvent systems.

(*1*) *Polyisobutylene–Cyclohexane.* This polymer–solvent system has been studied by Eichinger and Flory,[7c] and is nearly athermal, so that $\chi_s \simeq \chi$. According to these authors, equation of state contributions to the free enthalpy are particularly important in this case. The system also affords an illustration of the fact that for athermal solutions χ_0 is not zero.

Let us now assume, by analogy with polymethylene, that for polyisobutylene also the c parameter is near to 0.70. Then, c', according to all possible values of w and V_1/V_2', will lie between 0.10 and 0.30. In Figure 2 are drawn the curves, all within the accepted possible values of w and c', which show the best agreement with experiment. Although quantitative agreement with experiment is not achieved, the qualitative agreement is as good (or, adopting a rather pessimistic view not worse) than that derived from the Flory and coworkers' newer theory of polymer solutions.

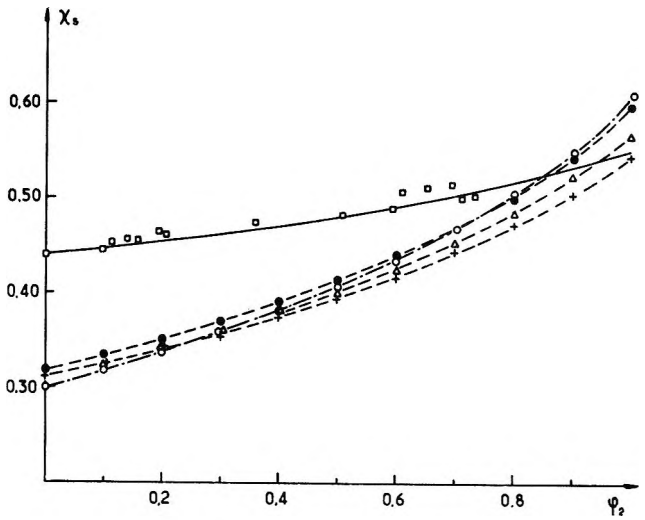

Figure 2. χ_s *vs.* φ_2 for polyisobutylene in cyclohexane. Key: +, $\rho = 0.53$, $c' = 0.125$; Δ, $\rho = 0.50$, $c' = 0.125$; ●, $\rho = 0.48$, $c' = 0.125$; ○, Flory theory;[7c] □, experimental points.[7c]

(*2*) *Polystyrene–Acetone, Polystyrene–Propyl Acetate, Polybutadiene–Chloroform.* Values of $\overline{\Delta S}_1$ for these systems have been taken from the "Reassessment of Published Data" by Booth, Gee, Jones, and Taylor.[28] Polymer–solvent systems containing an associated solvent, like benzene, or showing solvation effects as polystyrene in chloroform have been ignored. Since

$$\overline{\Delta S}_1 = -R\{\ln(1-\varphi_2) + (1-1/x)\varphi_2 + \chi_s\varphi_2^2\} = \overline{\Delta S}_1^* - R\chi_s\varphi_2^2 \quad (25)$$

it follows that

$$\chi_s = \frac{\overline{\Delta S}_1^* - \overline{\Delta S}_1}{R\varphi_2^2} \quad (25')$$

where $\overline{\Delta S}_1^*$ is the combinatorial Flory–Huggins entropy of mixing. In Figure 3 are drawn the curves of χ_s *vs.* φ_2 for the three systems polystyrene–acetone, polystyrene–propyl acetate, and polybutadiene–chloroform, together with three theoretical curves. The experimental curves are somewhat boldly extrapolated to $\varphi_2 = 0$, since vapor pressure data provide χ values only for concentrated solutions. As the experimental points are of limited accuracy it may be assumed that the variation of χ_s for polybutadiene in chloroform is nearly that of

(23) W. E. Forsythe, Physical Tables, Smithsonian Institution, Washington, D. C., Vol. 120, 1954. See Handbook of Chemistry and Physics, 29th ed, the Chemical Rubber Co., Cleveland, Ohio, p 1705.

(24) International Critical Tables, Vol. 3, McGraw-Hill, New York, N. Y., 1928.

(25) D. Tyrer, *J. Chem. Soc.*, **105**, 2534 (1914).

(26) L. A. K. Staveley, W. I. Tupman, and K. R. Hart, *Trans. Faraday Soc.*, **51**, 323 (1955).

(27) M. Diaz Pena and M. L. McGlashan, *ibid.*, **57**, 1511 (1961).

(28) C. Booth, G. Gee, M. N. Jones, and W. D. Taylor, *Polymer*, **5**, 353 (1964).

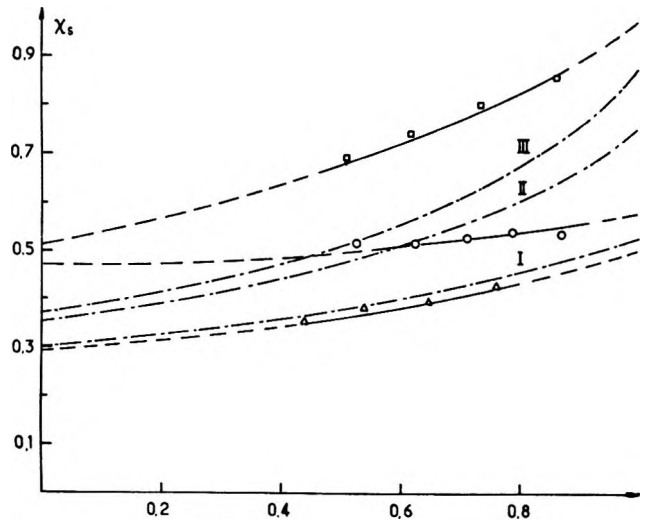

Figure 3. χ_s *vs.* φ_2 for various polymer–solvent systems: Δ, polystyrene–propyl acetate; O, polybutadiene–chloroform; □, polystyrene–acetone. Curve I, $\rho = 0.53$, $c' = 0.125$; curve II, $\rho = 0.4$, $c' = 0.11$; curve III, $\rho = 0.33$, $c' = 0.11$.

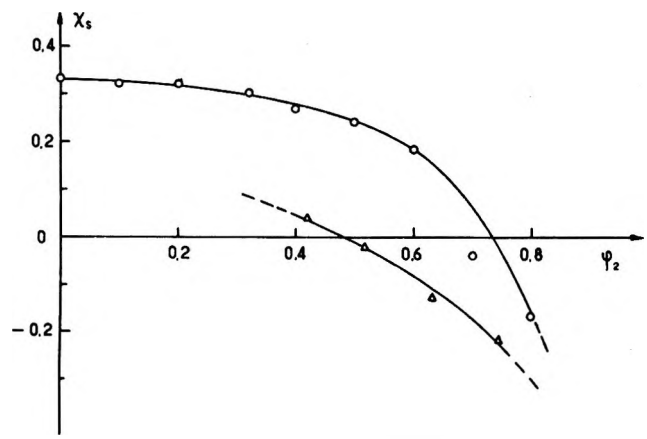

Figure 4. χ_s *vs.* φ_2 for polystyrene in cyclohexane. Δ, from experimental results of Krigbaum and Geymer;[31] O, from results reported by Höcker, Shih, and Flory.[30]

polyisobutylene in cyclohexene. If so, the three above mentioned polymer–solvent systems show at least qualitative agreement with theory.

(3) *Polystyrene–Cyclohexane.* This system provides a striking example of nonapplicability of the theory for a nonassociated solvent forming with the polymer a solution where significant solvation effects are very unlikely to occur. χ_H increases steeply for $\varphi_2 \simeq 0.55$[29,30] and conversely χ_s drops to negative values. In Figure 4 curve I has been drawn from results of Krigbaum and Geymer[31] reassessed in ref 28. Curve II has been drawn from the χ and χ_H curves of ref 30. Although there is not quantitative agreement between the two curves, the decrease of χ_s to negative values seems beyond doubt. This feature cannot be explained on the basis of the theory developed above. However, the steep increase of χ_H at $\varphi_2 \simeq 0.55$ should be an indication that some special phenomenon occurs at the more concentrated solutions.

VI. Conclusions

A theory is proposed giving the entropy of mixing polymer with solvent on the basis of free volume calculations. The theory does not include associated solvents or solutions presenting solvation effects.

The entropy of mixing, following the theory proposed, solely arises from the different free volumes available to the solvent molecules and the polymer segments in the pure components and in the solution. In Flory's and coworkers newer theory of polymer solutions[7,30] there are three distinct contributions to the entropy of mixing: a combinatorial, an "equation of state" contribution, and an interchange between unlike segments contribution. Although the existence of an interchange between unlike segments entropy cannot be disclaimed, its physical significance, in the absence of orientation or solvation effects, remains rather obscure. Such an entropy contribution has not so far been introduced in the present theory. The two first contributions to the entropy of mixing are included in the free volume treatment.

Experimental and theoretical values of χ_s show at least qualitative agreement for several polymer–solvent systems. In the case of polyisobutylene in cyclohexane, the agreement with experiment is about the same as that obtained using Flory's newer theory of polymer solutions. Comparison with more experimental data is needed as well as a better experimental determination of the two parameters ρ and c'.

(29) R. Koningsveld, L. A. Kleintjens, and A. R. Shultz, *J. Polym. Sci., Part A-2*, **8**, 1261 (1970).

(30) H. Höcker, H. Shih, and P. J. Flory, in press.

(31) W. R. Krigbaum and D. O. Geymer, *J. Amer. Chem. Soc.*, **81**, 1859 (1959).

Ion-Molecule Reactions in Gaseous Acetone

by K. A. G. MacNeil and J. H. Futrell*[1]

Department of Chemistry, University of Utah, Salt Lake City, Utah 84112 *(Received May 24, 1971)*

Publication costs assisted by the Air Force Materials Laboratory, Air Force System Command, Wright-Patterson Air Force Base

Ion–molecule reactions in gaseous acetone have been examined in two mass spectrometers, namely in a CEC 21-110 double-focusing, high pressure instrument, and in a modified Varian Associates Syrotron ICR mass spectrometer. The high pressure study (up to 0.6 Torr) has revealed the following reaction products: $(CH_3COCH_3)_mH^+$ (m = 1, ... 4), $(CH_3COCH_3)_mCH_3^+$ (m = 1, ... 4), $(CH_3COCH_3)_mCH_3CO^+$ (m = 1, ... 3), and ions at masses 99, 157, and 215 which correspond to loss of H_2O from the protonated dimer, trimer, and tetramer, respectively. A considerable temperature effect has been noted which results in a shift towards the higher products as the gas temperature is lowered. The ICR mass spectrometer has been used to elucidate the various mechanisms and to measure some of the rate constants of the reactions leading to these products.

I. Introduction

Recently, two separate studies[2] have appeared which concern, at least in part, the ionic chemistry of acetone. The first of these, by Munson,[2a] aims at giving a description of the types of product formed and some discussion of the more important reactions which occur as a result of the ionization of gaseous Brønsted acids; and the second, by Terry and Tiernan,[2b] gives a similar account of the ion–molecule processes in ketones. Although, in the latter case, the product ion distribution resulting from reaction of the major primary ions with the acetone molecule is described, in neither study were any reaction rate constants measured. This present work was undertaken to validate these mechanisms and establish rate constants for the principal ion–molecule reactions in the acetone system.

II. Experimental Section

The high pressure results reported in this paper were obtained using a CEC 21-110 double-focusing mass spectrometer, modified as previously described,[3] to permit operation of the ion source at pressures up to 1 Torr. In the present experiments, source conditions were as follows: ionizing electron energy, 500 eV; repeller voltage 5 V (~12 V cm^{-1} repeller field), and temperature 200° (except in one experiment when this was lowered to 50°). Source pressures were varied up to 0.6 Torr, corresponding to an acetone concentration of 12.3×10^{15} molecule cm^{-3}, and measured using an MKS Baratron Type 77 gauge with a 0–1 Torr pressure sensor.

The low pressure work (up to $\sim 1 \times 10^{-5}$ Torr) and the rate constant measurements were made using a modified Varian Syrotron ICR mass spectrometer as described elsewhere.[4] The only new procedure is that ion residence times, τ, within the source and reaction region of the ICR cell were determined empirically using the pulsing technique described by Smith, *et al.*[5] Selective parent-ion ejection from the source region[6] was achieved by applying an rf field to the negatively biased source drift plate.

The acetone used was analytical reagent grade (Wasatch Chemical Co., Utah) of 99.5% minimum purity.

III. Results and Discussion

1. Pressure Dependence of Ionic Currents. a. Primary Ions. The mass spectrum of acetone was measured over the pressure range 0–600 μ. At low pressures (<10 μ), the major primary ions are CH_3^+ (m/e = 15), CH_3CO^+ (m/e = 43), and $CH_3COCH_3^+$ (m/e = 58$^+$) together accounting for close to 80% of the total ionization. The remaining 20% of ionization is taken up by several minor ions (m/e = 14, 26, 27, 29, 39, 41, 42) which individually amount to only a few per cent of the recorded ion current and whose reactions were consequently ignored in this study.

Decay curves for the ions CH_3^+, CH_3CO^+, and $CH_3COCH_3^+$ over the first 100 μ of the pressure range are illustrated in Figure 1; the most abundant primary ion is CH_3CO^+ which initially gives rise to some 50% of ionization but which falls to 20% by 100 μ and has effectively disappeared from the mass spectrum by 250 μ. Mass 58, $CH_3COCH_3^+$, declines from a low pres-

(1) Alfred P. Sloan Fellow, 1968–1972.

(2) (a) M. S. B. Munson, *J. Amer. Chem. Soc.*, 87, 5313 (1965); (b) J. O. Terry and T. O. Tiernan, Proceedings of the 16th Annual Conference on Mass Spectrometry and Allied Topics, ASTM Committee E14, Pittsburgh, Pa., 1968, p 33.

(3) J. H. Futrell and L. H. Wojcik, *Rev. Sci. Instrum.*, 42, 244 (1971).

(4) R. P. Clow and J. H. Futrell, *Int. J. Mass Spectrom. Ion Phys.*, 4, 165 (1970).

(5) S. Wisniewski, R. P. Clow, D. L. Smith, and J. H. Futrell, Proceedings of the 18th Annual Conference on Mass Spectrometry and Allied Topics, American Society for Mass Spectrometry, San Francisco, Calif., 1970, p B393.

(6) J. L. Beauchamp and R. C. Dunbar, *J. Amer. Chem. Soc.*, 92, 1477 (1970).

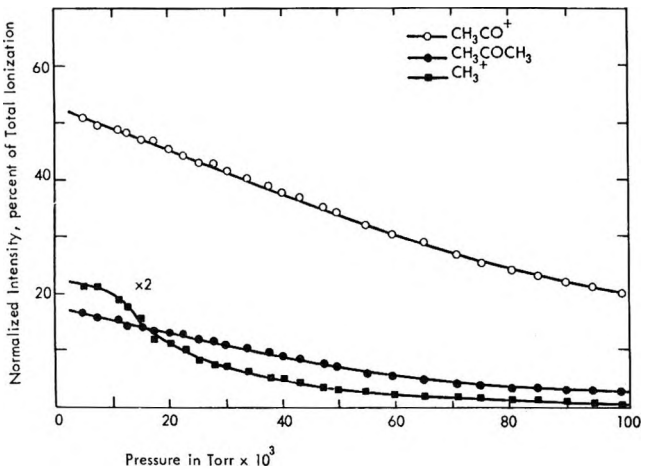

Figure 1. Relative abundances of the major primary ions of acetone as a function of pressure: CH_3CO^+, ⊙; $CH_3COCH_3^+$, ●; 2 × CH_3^+, ■.

sure level of ~17% of all ionization to zero by 150 μ; mass 15, CH_3^+, from ~11% to zero by 100 μ.

b. Secondary and Higher Order Ions. (1) Protonated Solvent Ions. Pressure dependence curves for these species are illustrated in Figure 2a. The first secondary ion to occur to any extent is that of m/e = 59, corresponding to protonated acetone or the monosolvated proton. The relative abundance of this ion rises rapidly to a peak of ~40% of all ionization at a pressure of about 30 μ, falls to less than 5%, and subsequently rises slowly to around 8% (perhaps an artifact resulting from the normalization procedure) at higher pressure. As the monosolvated proton decays, the disolvated proton (m/e = 117) increases to a high relative abundance of 75% and thence declines to ~60% at 600 μ. The trisolvated proton (m/e = 175) appears above 100 μ and steadily increases over the observed pressure range to 10% of total ionization at 600 μ. Although not shown in Figure 2, there is also a trace amount of the tetrasolvated proton species (m/e = 233) present in the mass spectrum at pressures above 300 μ.

Munson[2a] has discussed the reactions of gaseous Brønsted acids with respect to their formation of solvated protons using a model which suggests that the most stable cluster is formed when each hydrogen which is bound to an oxygen atom in the protonated molecule ion is bound to one other solvent molecule. In the case of acetone, where the protonated molecule–ion contains only one such hydrogen, the most stable cluster should consist of two solvent molecules and a proton. Experimentally, Munson[2a] did not observe any such species larger than the disolvated proton at the highest pressures he used (a few tenths of a Torr); neither did Terry and Tiernan[2b] report such species in a study using ion-source pressure up to 1 Torr.

In the present case, however, higher mass clusters are clearly present and, at least for the trisolvated

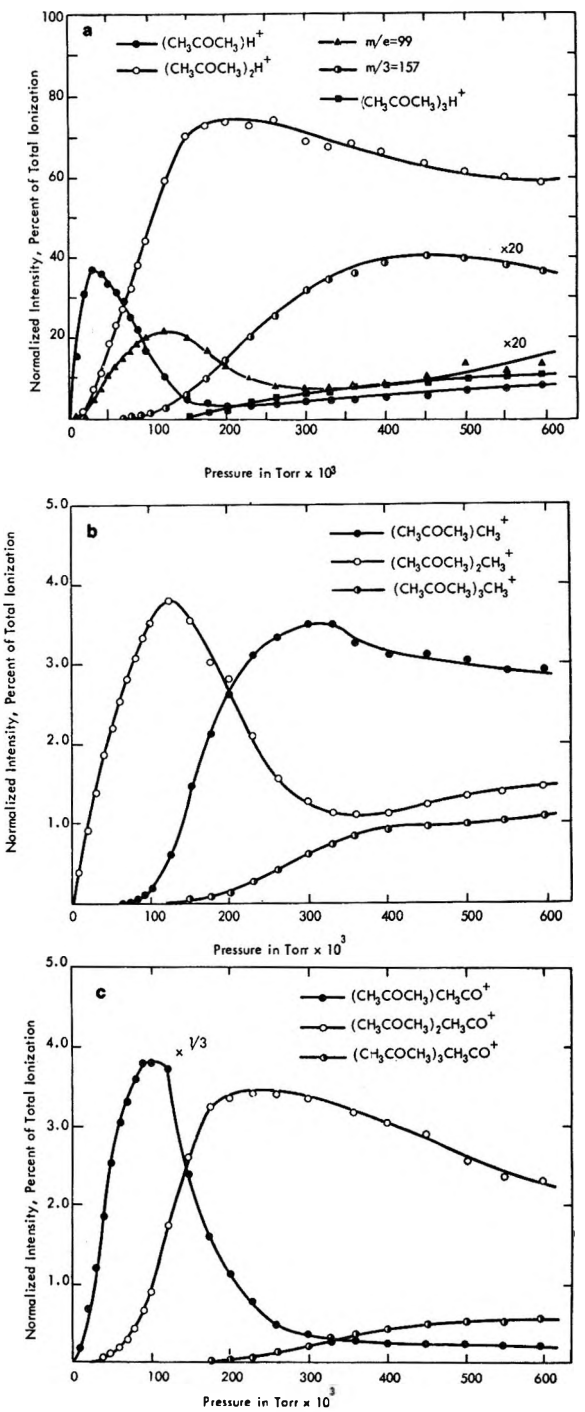

Figure 2. Relative abundances of the major secondary and higher order ions of acetone as a fucntion of pressure. (a) $(CH_3COCH_3)H^+$, ●; $(CH_3COCH_3)_2H^+$, ⊙; $(CH_3COCH_3)_3H^+$, ■; 20 × m/e = 99, ▲; 20 × m/e = 157, ◑. (b) $(CH_3COCH_3)CH_3^+$, ●; $(CH_3COCH_3)_2CH_3^+$, ○; $(CH_3COCH_3)_3CH_3^+$, ◑. (c) 1/3 × $(CH_3COCH_3)CH_3CO^+$, ●; $(CH_3COCH_3)_2CH_3CO^+$, ⊙; $(CH_3COCH_3)_3CH_3CO^+$, ◑.

species, appear to be relatively stable. There is no doubt that there exists a strong tendency to form the disolvated proton over a certain pressure range. In the region of 200 μ this ion accounts for some 75% of all ionization, for example, but above this range its impor-

tance declines and significant amounts of the protonated trimer are formed. It may also be noted that in a study of ion–solvent molecule interactions in water vapor,[7] Kebarle has found no special stability associated with the $(H_2O)_4H^+$ cluster which, for the Munson model, is expected to be particularly favored.

Figure 2a also contains the pressure curves for the two species at m/e = 99 and 157 which correspond to the loss of a water molecule from the disolvated and trisolvated proton, respectively. The latter product likely results from the condensation reaction of acetone with the m/e 99 species. Although there is no direct evidence to suggest that this is the route by which these two species are formed, it is unlikely that they occur through adduct formation by the corresponding primary ion m/e = 41 since this ion constitutes less than 1% of the low pressure mass spectrum. A trace amount of ion at m/e = 215 corresponding to loss of H_2O from the protonated tetramer was observed but is not shown in Figure 2a.

(2) Methylated Solvent Ions. Pressure dependence curves for these species are illustrated in Figure 2b. In general, these ions exhibit relative abundances which are an order of magnitude smaller than their protonated analogs. The methylated monomer ion (m/e = 73) appears at low pressure, achieves some 4% of all ionization at ~125 μ, decays to a low of ~1.3%, and subsequently increases slightly towards higher pressure. The methylated dimer ion (m/e = 131) appears above 50 μ and peaks to 3.5% at a pressure of 300 μ before declining; the methylated trimer ion (m/e = 189) increases steadily above 150 μ. Although not shown in Figure 2b, trace amounts of the methylated tetramer ion (m/e = 247) appeared above 250 μ.

(3) Acetylated Solvent Ions. Pressure dependence curves for these ions are illustrated in Figure 2c. The acetylated monomer ion (m/e = 101) is the most abundant of this series, appearing at low pressure, rising to 12% of ionization at ~100 μ, and falling off at higher pressure to less than 1%. As with the protonated and methylated solvent ions, the acetylated dimer ion (m/e = 159) increases strongly as the monomer decays, in this case reaching a peak of 3.5% of ionization at ~250 μ before depleting. The acetylated trimer ion (m/e = 217) appears above 150 μ and steadily increases over the pressure range. No acetylated tetramer was detected in the pressure range investigated.

2. Temperature Effects. The data reported above were obtained at an ion-source temperature of 473°K. Lowering this temperature to 323°K caused a significant change in the recorded pressure dependences. In general at the same source pressures (or, more strictly, at the same number density of reactant molecules) the lower temperature resulted in a shift towards the higher mass product ions. This can be illustrated by reference to the protonated solvent ions. Figure 3 indicates that the monosolvated proton appears earlier at the lower

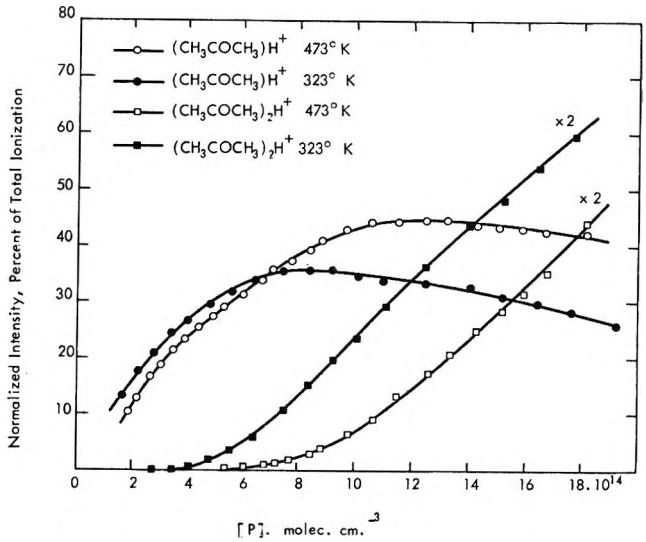

Figure 3. Relative abundances of the protonated monomer and dimer ions of acetone as a function of pressure at two different source temperatures: $(CH_3COCH_3)H^+$, ⊙ (473°K); ● (323°K); 2 × $(CH_3COCH_3)_2H^+$, ⊡ (473°K); ■ (323°K).

temperature but achieves a somewhat lower relative abundance (some 10% less) before declining. Similar early appearances are noted for the protonated dimer ion and the protonated trimer ion (not shown in Figure 3) and for the methylated and acetylated solvent ion series. This dramatic effect of temperature is not unexpected in view of the suggestions that thermodynamic equilibrium may be attained in high pressure sources.[7,8]

It is interesting to note that if one attempts to calculate an equilibrium constant for the reaction

$$(CH_3COCH_3)H^+ + CH_3COCH_3 \underset{}{\overset{k_{eq}}{\rightleftharpoons}} (CH_3COCH_3)_2H^+$$

then the corresponding equilibrium constant

$$K_{eq} = \left(\frac{1}{P_{CH_3COCH_3}}\right)\left(\frac{I_{(CH_3COCH_3)_2H^+}}{I_{(CH_3COCH_3)H^+}}\right) \qquad \text{(E1)}$$

was found to depend on pressure of acetone. Thus ion equilibrium is not achieved under the experimental conditions and the system is kinetically limited. Consequently, while the effects of temperature are qualitatively those anticipated for the increased total internal energy at higher temperature, the data do not support any simple interpretation involving equilibrium concepts.

3. Reaction Rate Constants. Reaction rate constant for the major primary ions of acetone were measured using an ICR mass spectrometer. A previous study[2b] of ion–molecule reactions in acetone had indi-

(7) P. Kebarle, S. K. Searles, A. Zolla, J. Scarborough, and M. Arshadi, *J. Amer. Chem. Soc.*, 89, 6393 (1967); P. Kebarle, *Advan. Chem. Ser.*, 72, 24 (1968).

(8) F. H. Field, *J. Amer. Chem. Soc.*, 91, 2827 (1969); F. H. Field, P. Hamlet, and W. F. Libby, *ibid.*, 91, 2839 (1969).

cated that there were complex interconversion reactions between the ions designated above as "primary," *i.e.*, between CH_3^+, CH_3CO^+, and $CH_3COCH_3^+$ as well as between these ions and the various product ions. The well known ICR double resonance ion-ejection technique[6] is suited to the unravelling of these several mechanisms of reaction.

Before proceeding further it may be useful to give an outline of the kinetic scheme used to obtain the various rate constants presented here. The "beam-model" of Wexler and Jesse,[9] which was further elaborated by Derwish, *et al.*,[10] can be somewhat simplified in the present case. In particular, since the primary and secondary components can normally be separated by the ion-ejection method, there is no need in the reaction scheme to consider separately ions formed purely by electron impact on the neutral molecule and those formed partly in this way and partly as a result of primary ion–parent molecule reactions. Also, secondary ions produced by more than one ion–molecule reaction need not be treated otherwise than secondary ions produced by a single reaction since it is possible to separate contributions from different sources. Thus the reaction scheme is very simple and may be written as follows

$$P \longrightarrow A_i^+ + e \qquad (R1)$$

$$A_i^+ + P \xrightarrow{k_{ij}} S_{ij}^+ + N_{ij} \qquad (R2)$$

$$S_{ij}^+ + P \xrightarrow{k_{ijl}} T_{ijl}^+ + N_{ijl} \qquad (R3)$$

Here, A_i^+'s are primary ions produced directly by ionization of the molecule P, the S_{ij}^+'s are secondary ions resulting from reactions of A_i^+'s with P, and the T_{ijl}^+'s are tertiary ions from the further reaction of the secondaries S_{ij}^+ with P. It should be kept in mind that a secondary ion S_{ij}^+ may be the same species as that formed directly by primary ionization.

For the primary species A_i^+, the rate constant for reaction can be found form the well-known expression

$$[A_i^+]_\tau = [A_i^+]_0 \exp(-k_{ij}'\tau[P]) \qquad (1)$$

where $[A_i^+]_\tau$ and $[A_i^+]_0$ are the intensities of the ion A_i^+ at reaction times τ and zero, k_{ij}' is the sum of the rate constants for the production of all ions S_{ij}^+, *i.e.*, $k_{ij}' = \Sigma k_{ij}$, and [P] is the concentration of neutral molecules in the reaction zone. In practice, instead of the actual intensity $[A_i^+]_\tau$, the relative intensity, *i.e.*, $[A_i^+]_\tau$ divided by the total ion intensity, is used. A semilogarithmic plot of the relative intensity *vs.* [P] gives the rate constant k_{ij}' directly. Any reaction forming the primary ion can be removed by the ejection from the ion source of possible parents.

For the secondary ions S_{ij}^+ formed with a rate constant k_{ij} and depleted to tertiary products with a rate constant k_{ijl}' $(= \Sigma k_{ijl})$, the differential equation describing its intensity is

$$\frac{d[S_{ij}^+]}{dt} = k_{ij}[A_i^+][P] - k_{ijl}'[S_{ij}^+][P] \qquad (2)$$

Replacing $[A_i^+]$ by $[A_i^+]_0 \exp(-k_{ij}'\tau[P])$ and solving gives

$$[S_{ij}^+]_\tau = \frac{k_{ij}[A_i^+]_0}{k_{ijl}' - k_{ij}'}[\exp(-k_{ij}'\tau[P]) - \exp(-k_{ijl}'\tau[P])] \qquad (3)$$

If, following Derwish, *et al.*,[10] we write $k_{ijl}' - k_{ij}' = K$, then

$$\frac{[S_{ij}^+]_\tau}{[A_i^+]_\tau} = \frac{k_{ij}}{K}[1 - \exp(-K\tau[P])] \qquad (4)$$

and differentiating with respect to [P]

$$\frac{d\left[\frac{[S_{ij}^+]_\tau}{[A_i^+]_\tau}\right]}{d[P]} = k_{ij}[\tau \exp(-K\tau[P])] \qquad (5)$$

as $[P] \rightarrow 0$, *i.e.*, at low pressures

$$\left.\frac{d\left[\frac{[S_{ij}^+]_\tau}{[A_i^+]_\tau}\right]}{d[P]}\right|_{P=0} = k_{ij}\tau \qquad (6)$$

Hence k_{ij} can be found from the initial low pressure gradient of a plot of the ratio $[S_{ij}^+]_\tau/[A_i^+]_\tau$ against [P].

It is a peculiarity of the ICR instrument that if the ion detection frequency remains constant and the magnetic field is varied to observe different species, then the ion residence time τ is also varied; increasing the magnetic field increases τ. This can be taken into account by measuring τ for both the primary and secondary ions-(the secondary ion normally has the higher mass requiring a higher magnetic field for its detection and hence corresponding to a larger τ). Assuming that, for the primary ion

$$[A_i^+]_{\tau_2} = [A_i^+]_{\tau_1} \exp(-k_{ij}'\Delta\tau[P]) \qquad (7)$$

where $\Delta\tau = \tau_2 - \tau_1$, a suitable correction for the observed intensities may be deduced.

Derwish, *et al.*,[10] in reference to eq 4 distinguish two limiting modes of behavior which are important enough to mention here.

Case A. $k_{ijl}' > k_{ij}'$, *i.e.*, K is positive. Here a plot of the ratio $[S_{ij}^+]_\tau/[A_i^+]_\tau$ against [P] will have an initial gradient equal to $k_{ij}\tau$, but as [P] tends to infinity, from eq 5, this will tend to zero. The ratio $[S_{ij}^+]_\tau/[A_i^+]_\tau$ will approach a limiting value equal to k_{ij}/K.

Case B. $k_{ijl}' < k_{ij}'$, *i.e.*, K is negative. Here a plot of the ratio $[S_{ij}^+]_\tau/[A_i^+]_\tau$ against [P] will again have an initial gradient equal to $k_{ij}\tau$ but as [P] tends to in-

(9) S. Wexler and N. Jesse, *J. Amer. Chem. Soc.*, **84**, 3425 (1962).

(10) G. A. W. Derwish, A. Galli, A. Giardini-Guidoni, and G. G. Volpi, *J. Chem. Phys.*, **39**, 1599 (1963).

Table I: Thermal Reaction Rate Constants for Primary Ions in Acetone

	Reaction	Rate constant × 10^{-9}, cm³ molecule^{-1} sec^{-1}	k_{ij}/k_{ij}'	$1/\alpha I$ (T and T)[2b]	Theoretical rate constant × 10^{-9}, cm³ molecule^{-1} sec^{-1} [a]
I	$CH_3^+ + CH_3COCH_3 \longrightarrow$ products	2.0 ± 0.1[b]			1.68
II	$CH_3^+ + CH_3COCH_3 \longrightarrow CH_3CO^+$	0.92 ± 0.10	0.46 ± 0.10	0.208	
III	$CH_3^+ + CH_3COCH_3 \longrightarrow CH_3COCH_3^+$	0.20 ± 0.01	0.10 ± 0.01	0.219	
IV	$CH_3 + CH_3COCH_3 \longrightarrow (CH_3COCH_3)H^+$	0.2 ± 0.1		0.044	
V	$CH_3CO^+ + CH_3COCH_3 \longrightarrow$ products	0.43 ± 0.03			1.18
VI	$CH_3CO^+ + CH_3COCH_3 \longrightarrow CH_3COCH_3^+$	0.04 ± 0.02	0.10 ± 0.05		
VII	$CH_3CO^+ + CH_3COCH_3 \longrightarrow (CH_3COCH_3)H^+$	0.39 ± 0.02	0.91 ± 0.10	0.990	
VIII	$CH_3COCH_3^+ + CH_3COCH_3 \longrightarrow$ products	0.54 ± 0.04			1.09
IX	$CH_3COCH_3^+ + CH_3COCH_3 \longrightarrow (CH_3COCH_3)H^+$	0.38 ± 0.04	0.71 ± 0.10	0.442	
X	$CH_3COCH_3^+ + CH_3COCH_3 \longrightarrow (CH_3COCH_3)CH_3CO^+$	0.19 ± 0.01	0.35 ± 0.05	0.473	
XI	$(CH_3COCH_3)H^+ + CH_3COCH_3 \longrightarrow$ products	0.43 ± 0.03			1.08
XII	$(CH_3COCH_3)CH_3CO^+ + CH_3COCH_3 \longrightarrow$ products	<0.54 ± 0.04[d]			0.97

[a] Calculated using the formula[9,10] $k = 2\pi e(\alpha/\mu)^{1/2}$. [b] The error quoted here is a measure of the scatter in values obtained over five or six experimental runs. [c] Obtained from the curvature of the plot of product ion/reactant ion against [P]; see text.

finity, the gradient will also tend to become infinitely large.

Thus the behavior of such plots is an indication of the relative magnitudes of k_{ijl}' and k_{ij}'.

In practice, it has been found preferable to use the limiting gradient eq 6 to obtain k_{ij}, rather than the full expression 4. Apart from the obvious reason that k_{ijl}', and hence K, is not always known (it is known in the case of secondary ions which are also primary ions), use of eq 4 requires considerably more numerical calculation and also calls for the inclusion of a value for K, together with its associated experimental error, twice, in the right-hand side of the expression. Use of eq 6 proved more rapid and consistent, there being little difficulty in deciding what constituted the initial gradient; consequently, this equation is less prone to the accumulation of experimental error.

An equation for the concentration of the tertiary ion, T_{ijl}^+ of (R3), can also be deduced by applying conservation of mass to the overall scheme, if it is assumed that this species does not react further. Thus, remembering that only a fraction k_{ij}/k_{ij}' of A_i^+ reacts to S_{ij}^+ and that, similarly, only a fraction k_{ijl}/k_{ijl}' of S_{ij}^+ reacts to T_{ijl}^+, we have

$$[A_i^+]_0 = [A_i^+]_\tau + \frac{k_{ij}'}{k_{ij}}\left[[S_{ij}^+]_\tau + \frac{k_{ijl}'}{k_{ijl}}[T_{ijl}^+]_\tau\right] \quad (8)$$

Rearranging

$$\frac{[T_{ijl}^+]_\tau}{[A_i^+]_\tau} = \frac{k_{ij}k_{ijl}}{k_{ij}'k_{ijl}'}\left[\frac{[A_i^+]_0}{[A_i^+]_\tau} - 1\right] - \frac{k_{ijl}}{k_{ijl}'}\frac{[S_{ij}^+]_\tau}{[A_i^+]_\tau} \quad (9)$$

and substituting in the expressions for $[A_i^+]_0/[A_i^+]_\tau$ and $[S_{ij}^+]_\tau/[A_i^+]_\tau$ from eq 1 and 3, respectively, gives

$$\frac{[T_{ijl}^+]_\tau}{[A_i^+]_\tau} = \frac{k_{ij}k_{ijl}}{k_{ij}'k_{ijl}'}[\exp(k_{ij}'\tau[P]) - 1] + \frac{k_{ij}}{k_{ij}' - k_{ijl}'}[1 - \exp\{(k_{ij}' - k_{ijl}')\tau[P]\}]\frac{k_{ijl}}{k_{ijl}'} \quad (10)$$

The utility of this relationship will become apparent in subsequent discussion.

Table I summarizes the measured thermal reaction rate constants for the ions CH_3^+, CH_3CO^+, and $CH_3COCH_3^+$ with acetone, together with those for the individual reaction channels. The upper limit, theoretical, thermal reaction rate constants[11,12] are based on the polarizibility of acetone equal to 6.42×10^{-24} cm³.[13]

Figures 4a and b illustrate the method used to calculate rate constants for the various reaction channels; Figure 4a plots the ratio of intensities of the ions $(CH_3COCH_3)H^+$ and CH_3CO^+ against [P]. The full line is that taken as a measure of the initial gradient. At higher pressures there is a clear fall-off in gradient, indicating that the rate constant for the reaction of the ion $(CH_3COCH_3)H^+$ is greater than the overall rate constant for CH_3CO^+. In a similar way, the upward curvature in Figure 4b indicates that the rate constant for $(CH_3COCH_3)H^+$ is less than that for $CH_3COCH_3^+$. Taking these results together, the rate constant for $(CH_3COCH_3)H^+$ is bracketed between (0.43 ± 0.03) and (0.54 ± 0.04) × 10^9 cm³ mol^{-1} sec^{-1}.

(11) P. Langevin, *Ann. Chim. Phys.*, 5, 245 (1905).

(12) G. Gioumousis and D. P. Stevensen, *J. Chem. Phys.*, 29, 294 (1958).

(13) J. A. Beran and L. Kevan, *J. Phys. Chem.*, 73, 3860 (1969).

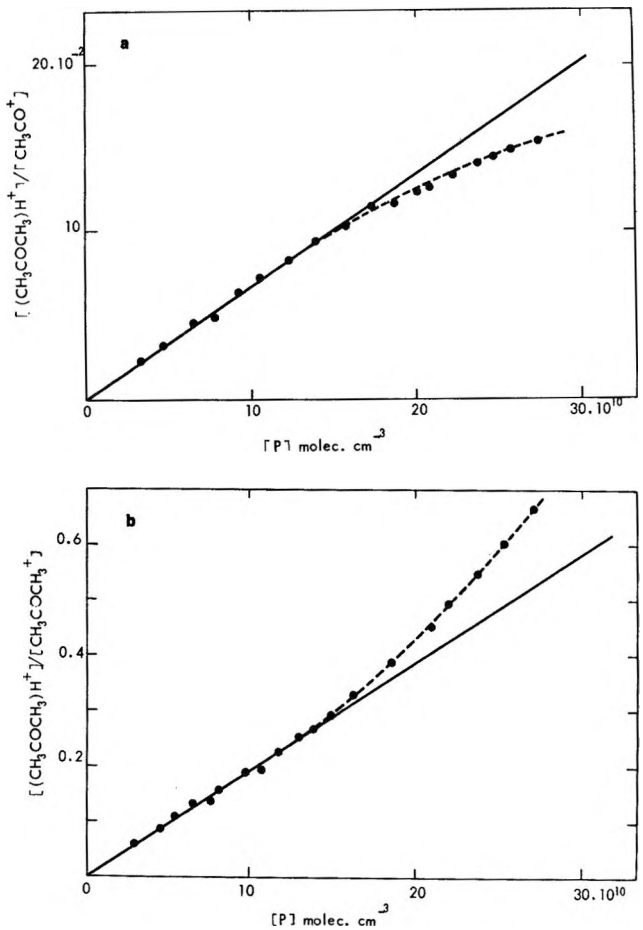

Figure 4. Ratios of intensities of product to parent ions as a function of pressure: (a) $(CH_3COCH_3)H^+/CH_3CO^+$. (b) $(CH_3COCH_3)H^+/CH_3COCH_3^+$. The full line is that used to estimate the initial gradient of the plot.

Although the primary acetyl ion reacts predominantly by proton transfer to the parent molecule, a small amount (~10%) of charge transfer is also observed. For the parent ion, reaction is mainly divided between channels leading to the protonated and to the acetylated monomer. It is instructive to compare the present results with those of Terry and Tiernan (T and T).[2b] This is not completely straightforward, since these authors present their data as relative abundancies of ionic products following reaction in the collision chamber of a tandem mass spectrometer (see Table I) which provides slightly different information than the relative rate constants for individual reaction channels. However, the difference is not great and meaningful comparison can probably be made. Terry and Tiernan report nearly equal partition between these channels (44:47) but we find it somewhat biased towards the protonated species, about 71:35. The protonated monomer is produced[2b] almost equally by proton transfer and by H-atom abstraction, while the acetylated monomer is produced by both acetyl ion transfer and acetyl radical abstraction.

For the methyl ion, the main reaction observed with acetone is the production of the acetyl ion, the rate constant in this case amounting to some 46% of the overall rate constant. T and T observe almost equal amounts of the acetyl and parent ions as products (each about 20%) whereas the present results show the overall rate constant distributed as 46% to acetyl ion production and 10% to the nominal charge transfer process leading to the parent molecule ion. The work of T and T also indicates some reaction forming other minor ions of mass less than that of the parent molecule. Isotopic studies by the same authors[2b] reveal that a major proportion of these ions, together with the acetyl ion, are formed by dissociative charge transfer.

The coupling observed between the primary methyl ion and the proton transfer product is unique amongst the set of reactions described here. Consequently, this behavior warrants a fuller discussion. If for the moment it is assumed that the secondary ion S_{ij}^+ of the reaction scheme described earlier is not consumed by further reaction, *i.e.*, that $k_{ijl}' = 0$, eq 4 simplifies to

$$\frac{[S_{ij}^+]_\tau}{[A_i^+]_\tau} = \frac{k_{ij}}{k_{ij}'}[\exp(k_{ij}'\tau[P]) - 1] \qquad (11)$$

In this case, a plot of $[S_{ij}^+]_\tau/[A_i^+]_\tau$ against $[\exp(k_{ij}'\tau[P]) - 1]$ will give a straight line of gradient k_{ij}/k_{ij}'. If reaction of the secondary does in fact occur, such a plot of the experimental data will show the ionic ratio increasing more slowly than expected, resulting in a curve which falls below the "ideal" straight line.

Now applying eq 11 to the ratio $[(CH_3COCH_3)H^+]/[CH_3^+]$ and using the overall rate constant for CH_3^+ as k_{ij}', it is found that instead of giving a straight line or a concave curve, the observed ratio increases much more rapidly than the exponential term. (This was first noted at an early stage in this study when all such data were treated according to eq 11 rather than to the more correct eq 4.) Clearly, direct reaction from the methyl ion to the protonated acetone ion cannot account for this behavior, and it becomes necessary to invoke at least one two-step mechanism connecting these ions.

From the overall scheme of ionic reactions in this system (see Table I), one plausible ionic intermediate for such a two-step process is the species CH_3CO^+ which is a product of the reaction of the methyl ion with acetone and which also reacts to produce protonated acetone ion. The proposed mechanism is therefore

$$CH_3^+ + CH_3COCH_3 \longrightarrow CH_3CO^+ + \text{neutral} \quad (R4)$$

$$CH_3CO^+ + CH_3COCH_3 \longrightarrow (CH_3COCH_3)H^+ + \text{neutral} \quad (R5)$$

An analogous scheme may be written for $CH_3COCH_3^+$. The final ionic product, $(CH_3COCH_3)H^+$, now behaves as a tertiary ion and, consequently, its concentration is described by eq 10 which was derived earlier. Using

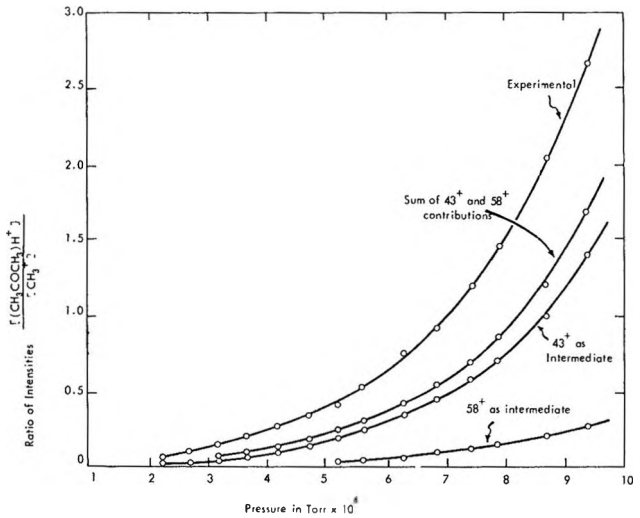

Figure 5. Ratio of intensity of $(CH_3COCH_3)H^+$ to CH_3^+ as a function of ICR chamber pressure. The calculated contribution of the assumed two-step mechanism involving CH_3CO^+ (43+) and $CH_3COCH_3^+$ (58+) as intermediates is shown along with the experimental curve which is the summation of all processes.

the relevant rate constants from Table I, the right-hand side of this equation can be evaluated from various values of [P]; the resulting $[(CH_3COCH_3)H^+]/[CH_3^+]$ ratios are plotted in Figure 5 together with the ratio found experimentally. From the figure it may be seen that a considerable proportion, although not all, of the protonated acetone ion appears to be formed by a two-step mechanism.

If the two-step components are now subtracted from the experimental data and the remainder is plotted as a function of $[\exp(k_{ij}'\tau[P] - 1]$, a straight line is obtained indicating that there is some direct reaction from CH_3^+ to $(CH_3COCH_3)H^+$. The associated rate constant is found to be $(0.2 \pm 0.1) \times 10^{-9}$ cm^3 molecule^{-1} sec^{-1} or $(10 \pm 5)\%$ of the overall rate constant for the methyl ion. For comparison T and T[2b] report the proton transfer to be some 4% of all methyl ion reactions.

Since a correction for two-step reactions is required in the case just considered, the question arises as to whether it is necessary in any of the other reactions described in Table I. It is possible immediately to eliminate from consideration those processes of Table I which refer only to the overall rate constant as a primary ion, since these are independent of any subsequent reaction of products (except, of course, for back-reaction to primary ion). Thus we need not be concerned with processes I, V, VIII, XI, or XII. Similarly, if there is no known path except the one considered between a primary and its products, no correction is required. For example in II the reaction described for the methyl ion leading to the acetyl ion is unique; II, VI, IX, and X can likewise be eliminated from consideration.

Since IV has already been corrected, this leaves III and VII. The reaction from the methyl ion to the acetone ion possibly occurs to some extent *via* the acetyl ion intermediate (II) and reaction of the acetyl ion to form the protonated acetone ion may occur *via* the parent ion (IX). However, if these possible contributions are computed using eq 10, the correction to the $[CH_3CO-CH_3^+]/[CH_3^+]$ ratio from acetyl ion as an intermediate amounts to less than 5% of the observed value at the highest pressure used experimentally and is somewhat lower than this over the pressure range used to estimate the rate constants. Similarly, correction of the $[(CH_3COCH_3)H^+]/[CH_3CO^+]$ ratio attributed to the parent ion as an intermediate is always less than 1% of the uncorrected value. Thus because of a fortuitous combination of relatively large rate constants favoring a two-step mechanism the only reaction path requiring significant correction is reaction IV.

Finally, it is of interest to compare rate constants deduced from ICR measurements in the manner described with those obtained in the high pressure source experiments. Rate constants in the conventional mass spectrometer experiments are deduced from the initial gradient of plots of normalized ion intensities as a function of source pressure. These slopes are the product of the rate constant and the source residence time of that reactant ion. The residence time may be calculated from simple electrostatics (assuming the ions start from rest) and a knowledge of source dimensions and the applied repeller field (12 V/cm in the present experiments). These considerations lead to high pressure total rate constants of 2.4×10^{-9} cm^3 mol^{-1} sec^{-1}, for reaction of CH_3^+, 3.0×10^{-10} cm^3 mol^{-1} sec^{-1} for CH_3CO^+, and 5.1×10^{-10} cm^3 mol^{-1} sec^{-1} for $CH_3-COCH_3^+$. These may be compared with values of 2.0×10^{-9}, 4.3×10^{-10}, and 5.4×10^{-10} cm^3 mol^{-1} sec^{-1}, respectively, obtained for these reactions by ICR. These results are in good agreement within the combined uncertainties of the two experimental techniques.

Acknowledgments. This research was supported for the most part by Contract No. 33615-71-R-1194 with the Air Force Materials Laboratory, Wright-Patterson Air Force Base, Ohio. Partial support was provided by the Air Force Office of Scientific Research through Grant AFOSR 71-1986 and by Grant 5K04GM42390-02 GMK from the Department of Health, Education and Welfare, National Institutes of Health. The financial support of these agencies is gratefully acknowledged.

Statistical Thermodynamics of the Glass Transition and the Glassy State of Polymers

by A. Quach and Robert Simha*

Division of Macromolecular Science, Case Western Reserve University, Cleveland, Ohio 44106
(Received September 24, 1971)

Publication costs assisted by the Petroleum Research Fund and the National Science Foundation

The hole theory of Simha and Somcynsky is applied to an analysis of the liquid-glass boundary and to the equation of state in the region between the glass transition and the β-relaxation. Two systems already studied experimentally are considered, namely, polystyrene and poly(*o*-methylstyrene). The liquid-glass boundary relations are investigated under two sets of conditions corresponding to a low- (LPG) and a high-pressure glass (HPG). The former is formed by cooling the liquid at atmospheric pressure, whereas the latter is obtained by pressurizing the liquid isothermally. The equation of state is analyzed for LPG only. The link between the conventional thermodynamic relations, experiment, and the statistical theory is formed by identifying the vacancy fraction $1 - y$ appearing in the latter with the ordering parameter Z introduced in the thermodynamic theory. For LPG, y_g, the value of y along the boundary, is indeed found to be constant for both polymers. For HPG, $1 - y_g$ is a decreasing function of pressure, as should be expected. The equation $dT_g/dP = (\partial T_g/\partial P)_Z + (\partial T_g/\partial Z)_P \times dZ/dP$ is tested by evaluating the product on the right-hand side by a combination of the statistical theory with experiment. An equation of state for LPG is first computed entirely from theory by assuming that a single constant parameter, $y = y_g$, characterizes not only the liquid-glass boundary line, but the glassy region as well. This results in too low a thermal expansivity, as had been noted earlier by Somcynsky and Simha for several other polymers at atmospheric pressure. Hence, within the frame of the hole theory, y cannot remain constant in the glass but is a function of T and P. It differs, of course, from the function derived by maximization of the configurational partition function of the liquid and is obtained here from experiment. Thus, additional constants enter into the equation of state of the glass, which cannot be obtained solely from the properties of the liquid and the liquid-glass boundary line. On approaching this line, however, the above function reduces to a single constant, *viz.*, y_g.

I. Introduction

The concept of internal ordering parameters (Z_1, Z_2, ...), which assume fixed values at the glass transition temperature, to describe the glass transition process as well as the glassy state, has been proposed by several authors. By applying the formalism of de Donder,[1] Prigogine and Defay[2] obtained for a system characterized by a single ordering parameter, Z, the following identity connecting the changes (Δ) in the thermodynamic derivatives at the transition

$$\Delta\kappa\Delta C_P = VT(\Delta\alpha)^2 \quad (1)$$

Here V and T are the volume and temperature at the transition point and κ, α, and C_P are, respectively, the compressibility, thermal expansivity, and heat capacity. Meixner[3] and Davies and Jones[4] showed that the effect of pressure on the glass transition temperature (T_g) can be described by the relations

$$(\partial T_g/\partial P)_Z = TV\Delta\alpha/\Delta C_P \quad (2)$$

$$(\partial T_g/\partial P)_Z = \Delta\kappa/\Delta\alpha \quad (3)$$

Equation 3 was also obtained by Gee[5] using a slightly different approach. Moreover, if entropy S instead of volume V is chosen as the dependent variable, his procedure readily leads to eq 2.

By equating the right-hand side of relations 2 and 3, eq 1 is recovered, which provides the basis of a rigorous test for a one-parameter theory. When two or more parameters are involved, we have[4,6]

$$\Delta\kappa\Delta C_P \geq TV(\Delta\alpha)^2 \quad (4)$$

but nothing is asserted about dT_g/dP.

Goldstein[7] introduced the concepts of excess volume, entropy, and enthalpy of the liquid over the glass and showed that if either of the latter two is the determining factor, eq 2 holds, while eq 3 is obeyed if the excess volume is the pertinent quantity.

The current experimental evidence is contradictory. Analyses of some authors[5,7,8] have shown that the inequality (4) rather than the equality (1) holds, implying the existence of more than one parameter, while Breuer

(1) Th. de Donder and P. Rysselberghe, "Affinity," Stanford University Press, Menlo Park, Calif., 1936.

(2) I. Prigogine and R. Defay, "Chemical Thermodynamics," Longmans, Green and Co., London, 1954.

(3) J. Meixner, *C. R. Acad. Sci.*, 432 (1952).

(4) R. O. Davies and G. O. Jones, *Advan. Phys.*, 2, 370 (1953).

(5) G. Gee, *Polymer*, 7, 177 (1966).

(6) A. J. Staverman, *Rheol. Acta*, 5, 283 (1966).

(7) M. Goldstein, *J. Chem. Phys.*, 39, 3369 (1963).

(8) J. M. O'Reilly, *J. Polym. Sci.*, 57, 429 (1962).

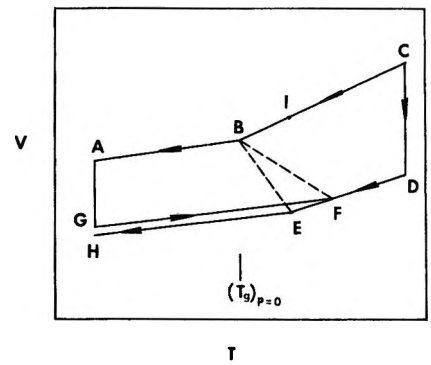

Figure 1. Diagram of cycles to measure T_g as a function of pressure P.

and Rehage[9] observed that for polystyrene eq 2 and 3 are not obeyed but the equality (1) holds. They concluded that a single parameter is adequate to describe the liquid–glass transition behavior.

The conflicting conclusions probably arise in part from the fact that in tests of eq 2 and 3 the requirement of maintaining Z constant has been disregarded. Very few literature data concerning the change of T_g as a function of P satisfy this condition. Bianchi, *et al.*,[10] have carried out experiments in such a way that they expected Z to remain as close to constant as possible. Figure 1 recapitulates the cycle proposed by these authors. The polymer melt at point C is cooled at a fixed rate and atmospheric pressure to point A, where a pressure P is applied to compress the glass to point G. The pressure is then kept constant while the glass is heated isobarically to point D, with a transition point F. By repeating the experiments with different pressures, the locus defined by the dashed line BF is obtained. We shall refer to the glass formed by cooling the melt at atmospheric pressure as low pressure glass (LPG). A different way to form a glass is defined by the path CDEH. In this case the transition point is E and the liquid–glass boundary is marked by the dashed line BE which departs significantly from line BF. A third kind of experiment commonly adopted is to pressurize the melt at point I isothermally. The corresponding liquid–glass transition boundary is not shown in the graph but is expected to differ from both lines BE and BF. The glass formed by the last two types of experiments will be referred to as high pressure glass (HPG). It is not implied, of course, that the dashed portions in Figure 1 are necessarily straight lines. Obviously, only the low pressure glass can possibly satisfy the condition of constant Z.

We have recently reported PVT results for polystyrene (PS) and poly(*o*-methylstyrene) (PoMS) derived from experiments of the third and first type.[11] In this work line GF was obtained by cross-plotting and extrapolating isothermal data rather than directly from isobaric measurements. This is acceptable as long as the transition region itself is avoided. It was shown that eq 3 holds for LPG but not for HPG.[11] If indeed a single ordering parameter characterizes the transition, then $T_g = T_g(P, Z)$, and[10]

$$dT_g/dP = (\partial T_g/\partial P)_Z + (\partial T_g/\partial Z)_P \times dZ/dP \quad (5)$$

where $(\partial T_g/\partial P)_Z = \Delta\kappa/\Delta\alpha$, as is seen from eq 3. Since $(\partial T_g/\partial Z)_P$ should be positive, if Z is a measure of disorder, the relation $dT_g/dP = \Delta\kappa/\Delta\alpha$ only holds if $dZ/dP \equiv 0$.

A purely thermodynamic theory need and does not specify the physical significance of the ordering parameter or parameters. These parameters have been variously associated with such quantities as a free volume, and a single or a spectrum of relaxation time constants. We shall bring molecular theory to bear on first, the properties of the liquid–glass transition line, and second, the equation of state of the low pressure glass. The basis for this is the hole theory of Simha–Somcynsky,[12] which has been successfully used to discuss the equation of state of amorphous polymer systems above the glass temperature.[11,12] In addition to the characteristic volume (V^*), temperature (T^*), and pressure (P^*) quantities, this theory contains an additional parameter pertinent for the present discussion, namely y, the fraction of occupied sites in the quasilattice. It is suggestive then to identify the vacancy fraction $1 - y$ with the thermodynamic parameter Z. At equilibrium, y is determined as a function of V and T by the maximization of the partition function and this fixes then by assumption the value of $y = y_g$ at the glass point. On this basis, Somcynsky and Simha[13] have compared theoretical predictions with experimental thermal expansivities α_g at the glass temperature and atmospheric pressure for a series of polymers. We shall extend this line of investigation by a detailed examination of the two polymer systems mentioned above. To begin with, however, we analyze the liquid–glass transition lines. According to the concepts reviewed above and the postulated relationship between Z and y, the magnitude of y_g at the observed T_g and P_g is determined entirely by equilibrium relations. These are briefly recapitulated in section II, and applied to the transition line in section III. In section IV, an equation of state for the glassy state is developed.

II. Theory

The equation of state expressed in reduced variables ($\tilde{P} = P/P^*$, $\tilde{V} = V/V^*$, and $\tilde{T} = T/T^*$) is[12]

(9) H. Breuer and G. Rehage, *Kolloid-Z. Z. Polym.*, 216–217, 159 (1967).

(10) U. Bianchi, A. Turturro, and G. Basile, *J. Phys. Chem.*, 71, 3555 (1967).

(11) A. Quach and R. Simha, *J. Appl. Phys.*, 42, 4592 (1971); see also A. Quach, Ph.D. Dissertation, Case Western Reserve University, Cleveland, Ohio, 1971.

(12) R. Simha and T. Somcynsky, *Macromolecules*, 2, 342 (1969).

(13) T. Somcynsky and R. Simha, *J. Appl. Phys.*, 42, 4545 (1971).

$$\tilde{P}\tilde{V}/\tilde{T} = [1-2^{-1/6}y(y\tilde{V})^{-1/3}]^{-1} + (2y/\tilde{T})(y\tilde{V})^{-2}[1.011(y\tilde{V})^{-2} - 1.2045] \quad (6)$$

For the equilibrium liquid y is obtained as a function of $\tilde{V}$ and $\tilde{T}$ from the minimization of the Helmholtz free energy by the solution of the following equation for the infinite chain

$$(s/3c)[1 + \ln(1 - y)/y] = [2^{-1/6}y(y\tilde{V})^{-1/3} - 1/3] \times [1 - 2^{-1/6}y(y\tilde{V})^{-1/3}]^{-1} + (y/6\tilde{T})(y\tilde{V})^{-2} \times [2.409 - 3.033(y\tilde{V})^{-2}] \quad (7)$$

where s and $3c$ are, respectively, the number of segments and external degrees of freedom per chain. As previously, we adopt the value of unity for the ratio $s/3c$. This particular choice affects the numerical values of the reducing parameters, but not the generality of the conclusions.[11,12] At a prescribed temperature, the relationship between y and $\tilde{V}$ is most easily computed from eq 7 by Newton's iteration method. However, at constant pressure, $\tilde{T}$ must be eliminated from eq 6 and 7 before the same method can be used.

III. Analysis of the Liquid–Glass Boundary Line

Our previous experimental results for the effect of pressure on T_g and the three characteristic parameters for the two polymers are summarized in Table I. We emphasize that the numerical values of the reducing parameters P^*, V^*, and T^* to be used are those derived from the equation of state of the liquid. By means of these and of eq 6 and 7, the vacancy fraction $1 - y$, a measure of an unoccupied volume, is computed as a function of the transition pressure P_g, corresponding to a transition temperature T_g. The results for both polymers and the two types of glasses appear in Figure 2. For LPG, $Z = 1 - y$ is practically independent of P, *i.e.*, $dZ/dP \simeq 0$, although in the case of polystyrene there is a slight trend of increasing Z with pressure. This may be attributed to the difficulty of extrapolating isobars in the glassy state to locate the transition temperatures of the low pressure glass. There is considerable curvature in the lines for the low pressure region (see ref 11, Figure 5). Therefore, the two temperatures closest to T_g were disregarded, resulting in a somewhat lower value of T_g (see ref 11, Figure 8). Since $Z = 1 - y$ increases linearly with T as will be shown below, a lower T_g would result in a lower value of Z at low pressure and this is actually observed in Figure 2. Another fact to support the above argument is that if Z is to change at all, it should be decreasing with increasing pressure. In any case, the change is small enough to be disregarded for our purposes and a horizontal line was drawn, representing the average value. The fact that $dZ/dP = 0$ for the low pressure glass is in accord with the concept that Z is frozen in the glassy state and does not vary with T and P. On the other hand, it is possible that y remains constant only along the boundary line (see section IV). The identification of $1 - y$ with Z thus provides a physical interpretation as well as a numerical value for the latter. Moreover it attests once more to the validity of the theoretical equation of state, eq 6 and 7. Finally, it permits a prediction of T_g as a function of P, once the glass temperature at atmospheric pressure and hence y_g are known.

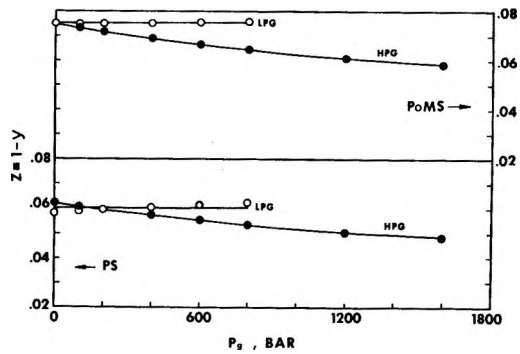

Figure 2. Ordering parameter Z identified with vacancy fraction $(1 - y)$ of the Simha–Somcynsky theory as a function of transition pressure P_g for low and high pressure glasses.

For the high pressure glasses, on the other hand, Z decreases with increasing pressure and dZ/dP is negative. Physically, this is reasonable because the number of vacancy sites at the glass transition is expected to be reduced at elevated pressure.

Now that we have shown that with $Z = 1 - y$, $dZ/dP < 0$ for a high pressure glass, we proceed to compute the derivative $(\partial T_g/\partial Z)_P$ from the molecular theory and examine the validity of eq 5. Figure 3 represents the reduced temperature $\tilde{T}$ as a function of $Z = 1 - y$ for a given reduced pressure $\tilde{P}$ in the region of the glass transition, as calculated from the equation of state, eq 6 and 7. The relation is linear with a slope which increases with $\tilde{P}$. This suggests that T_g should be more sensitive to experimental conditions such as the cooling rate at elevated pressures. With the aid of the results in Figures 2 and 3, the correction term for variable Z on the right-hand side of eq 5 can now be computed. For computational convenience, $dZ/dP = -dy/dP$ was obtained by fitting a least-squares parabola through the points in Figure 2 rather than by analytical evaluation of the derivative from eq 7. The results are shown and compared with the experimental values of dT_g/dP in Figure 4. Except for polystyrene at low pressures, we feel that the extent of agreement observed is quite good, considering the uncertainties involved in computing α_g and κ_g of the HPG by means of an asymptotic value of the Tait parameter B.[11] The residual deviations observed in Figure 4, however, may well be real, and clearly similar analyses of additional polymer systems are highly desirable. These should show whether not only similar magnitudes but also the identical sign of the departures prevail, when the thermodynamic eq 5 is

Table I: Glass Transition Temperatures, Average Pressure Coefficients, and Characteristic Parameters for Polystyrene and Poly(*o*-methylstyrene)[11]

	$(T_g)_{P\to 0}$, °K (HPG)	dT_g/dP, deg/kbar (HPG)	$(T_g)_{P\to 0}$, °K (LPG)	dT_g/dP, deg/kbar (LPG)	$P^* \times 10^{-3}$, bars	$V^* \times 10$, cm³/g	$T^* \times 10^{-4}$, °K
PS	374	31.6	365	74.2	7.453	9.598	1.268
PoMS	404	34.2	404	73.0	7.458	9.762	1.274

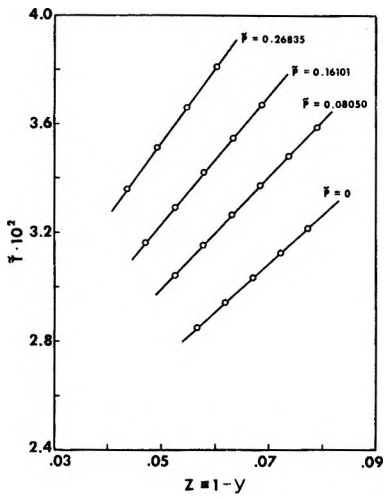

Figure 3. Reduced temperature $\tilde{T}$ as a function of ordering parameter $Z \equiv 1 - y$ at a series of pressures in the region of the glass transition, eq 6 and 7.

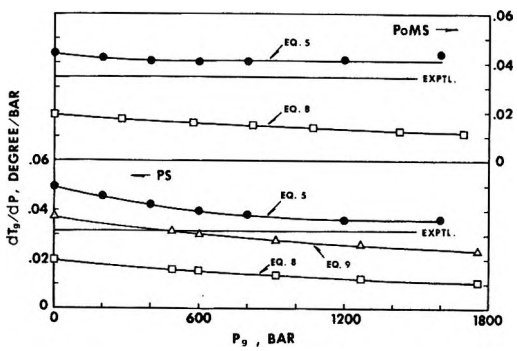

Figure 4. Comparison of various expressions (see text) for the pressure coefficient of T_g of high pressure glasses.

combined with the statistical theory, eq 6 and 7. Such results, of course, have a bearing also on the question of one *vs.* two (or more) ordering parameters.

In Figure 4 there are also plotted the results of two other proposed modifications of eq 3. One, due to Bianchi,[14] introduces the temperature dependence of the volume V_g at T_g, *viz.*

$$dT_g/dP = \Delta\kappa/(\Delta\alpha - d \ln V_g/dT) \quad (8)$$

On the other hand, taking the point of view that in the isothermal experiments a degree of compression f occurs prior to glass formation, Gee[5] proposed the expression

$$dT_g/dP = \Delta\kappa/(\alpha_l - \alpha_{og} + df/dT) \quad (9)$$

where α_{og} is the thermal expansivity of the glass at atmospheric pressure. From Shishkin's densification data,[15] df/dT was estimated to be about 3.3×10^{-4} deg^{-1} for polystyrene.[5]

Equation 8 appears to underestimate significantly dT_g/dP. Equation 9 is quite satisfactory, at least in the low pressure range, with deviations now in the opposite direction from those arising in the molecular theory. On basic grounds and because of the nature of the information required in the application of eq 9, we believe our approach to the thermodynamics of the glass transition to be preferable in the cases of both LPG and HPG.

A final decision regarding the validity of eq 1 and thus of a one-parameter description of the transition boundary requires a knowledge of ΔC_P on the identical sample with identical thermal history. Lacking this information and as a first approximation, we use the value of 0.0525 cal/g-deg for PS given by Wunderlich and Jones,[16] and obtain at $P \to 0$

$$\Delta\kappa\Delta C_P/[TV(\Delta\alpha)^2] \simeq 1.5 \quad (10)$$

Although the ratio does not turn out to be unity, this cannot yet be considered as an argument against the adequacy of the one-parameter concept. Final judgment should be based on appropriate heat capacity measurements at both atmospheric and elevated pressures.

IV. Equation of State (LPG)

In Figure 5 are shown the isobars at atmospheric pressure for PS and PoMS in the region between the β-relaxation and the glass transition temperature, that is, between T_g (see Table I) and about $0.7 \times T_g$.[11] Also indicated are the theoretical results from eq 6 with the assumption of constant $y = y_g$ and $P = 0$. For PS and PoMS the numerical values from Figure 2 are 0.940 and 0.925, respectively. The predicted expansion coefficients are smaller than those observed. This is in accord with previous findings and possible reasons for the discrepancy have been suggested.[13] Within the frame of the hole theory, a single frozen parameter is not sufficient to describe the PVT properties of the glass. Here we wish to explore quantita-

(14) U. Bianchi, *J. Phys. Chem.*, **69**, 1497 (1965).

(15) N. I. Shishkin, *Sov. Phys.-Solid State*, **2**, 322 (1960).

(16) B. Wunderlich and L. D. Jones, *J. Macromol. Sci., Phys.*, **3**, 67 (1969).

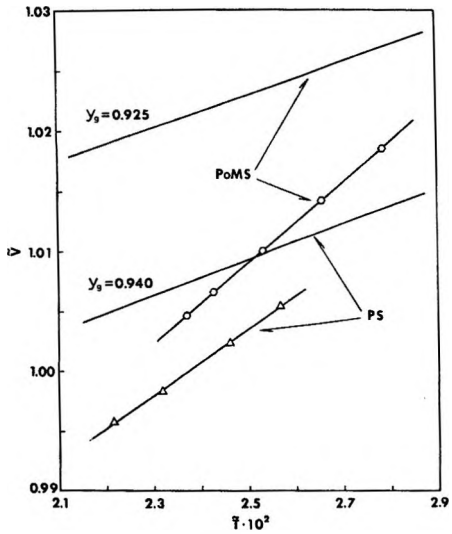

Figure 5. Reduced volume–temperature curve at atmospheric pressure. (Δ) polystyrene, (○) poly(*o*-methylstyrene). Other lines, theoretical, eq 6 with constant $y = y_g$.

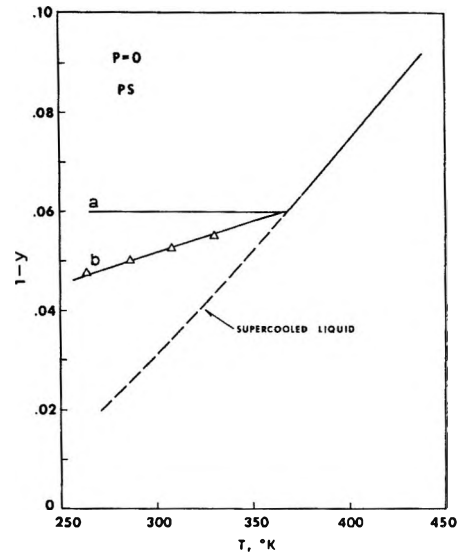

Figure 6. Variation of vacancy fraction $1 - y$ with temperature at atmospheric pressure for polystyrene glass. Dashed line, supercooled liquid, eq 6 and 7. Solid line *a*, assumption of constant $y = y_g$, *b*, from eq 6 and experimental volume–temperature data.

tively one particular suggestion, namely, a nonvanishing temperature and pressure dependence of the vacancy fraction $(1 - y)$ in the glassy state. The functional relationship will be derived from experiment, *i.e.*, from a series of isobars. This is accomplished by intersecting at a given pressure the experimental V–T curve with a net of theoretical lines computed from eq 6 with appropiately chosen values of y. The result for PS at atmospheric pressure is exhibited in Figure 6 and compared with the horizontal line, $y = y_g$, and the curve extrapolated from the liquid region by means of eq 6 and 7. As was to be expected, the actual result is intermediate between these two extremes.

In Figure 7, the values of $1 - y$ for the two glasses are plotted as a function of the temperature difference $T_g(P) - T$ for three pressures. We note that the relationship is linear in T at a given P and may be expressed in the form

$$y - y_g = [T_g(P) - T]A(P) \qquad (10a)$$

The numerical values of the coefficient $A(P) = -(\partial y/\partial T)_P$ are shown in Table II for $P = 0$, 400, and 800 bars. They can be represented by the equations

$$\text{PS} \quad A(P) = 1.36 \times 10^{-4} - 1.52 \times 10^{-7}P + 7.2 \times 10^{-11}P^2$$

$$\text{PoMS} \quad A(P) = 1.82 \times 10^{-4} - 1.44 \times 10^{-7}P + 5.9 \times 10^{-11}P^2 \qquad (10b)$$

Equation 10 represents a variation of the vacancy fraction $1 - y$ which is intermediate between the equilibrium function of the supercooled liquid and the value $1 - y_g$ "frozen" at T_g. In combination with the hole theory, eq 6, and the pressure dependence of T_g, which may be derived either directly from experiment or from the theory by means of low pressure data,

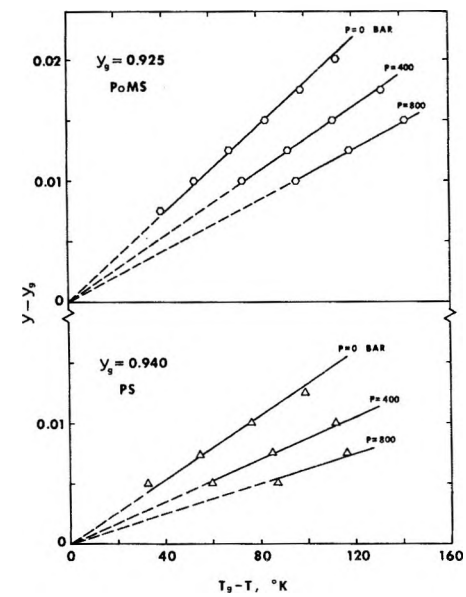

Figure 7. Difference in vacancy fraction $y - y_g = Z_g - Z$ as a function of temperature and pressure, derived from eq 6, pressure dependence of glass transition temperature and value of y at T_g.

it provides an equation of state for LPG above the β-relaxation temperature of the two polymers investigated. Besides the parameters P^*, V^*, T^*, y_g, and $T_g(P)$ which are characteristic of the liquid and liquid–glass boundary line, there appears, in the pressure range explored, also one of the derivatives $(\partial y/\partial T)_P$ or $(\partial y/\partial P)_T$ at $T = T_g(P)$.

Appropriate experimental information for our two polymers required to make similar analyses on HPG is not available.

Table II: Numerical Values for $A(P) = -(\partial y/\partial T)_P$, eq 10a

P, bars	$A(P) \times 10^4$, deg^{-1} PS	PoMS
0	1.36	1.82
400	0.869	1.34
800	0.609	1.05

V. Conclusions

The statistical hole theory of Simha and Somcynsky can be applied to the liquid–glass transition boundary with the vacancy fraction playing the role of a frozen parameter in a limited sense, *i.e.*, remaining constant along the boundary in the case of LPG. For HPG, this fraction is shown to decrease with increasing pressure, since the glassy region is reached from the liquid under different conditions of pressure and temperature. The computed decrease leaves a residual discrepancy between the predictions of the thermodynamic one-parameter theory and experiment.

In order to interpret the equation of state of the LPG within the frame of the hole theory, the vacancy fraction must be permitted to vary with temperature and pressure, converging, however, to a constant value at the liquid–glass boundary. On a different basis involving kinetic arguments, an analogous conclusion regarding the existence of several internal parameters and the reduction to a single one has been reached by Breuer and Rehage.[9]

The usual concept of ordering parameters presumes the existence of quantities which are frozen throughout the glassy region. In this sense the quantity y, which is constant only along the boundary, cannot be considered as such a parameter. Possibly an appropriate two-parameter theory of the equilibrium liquid[18] could be formulated to be in accord with the above concept. On the other hand, one might speculate that this concept requires modification.

Our approach has been applied to polymer glasses. Since not only the thermodynamic but the statistical relations as well are not specific to high-molecular-weight systems, it would be important to examine low-molecular-weight glasses along the same lines.

Acknowledgment. Acknowledgment is made to the donors of the Petroleum Research Fund, administered by the American Chemical Society, and to the National Science Foundation under Grant GK-20653 for support of this research.

Redox Mechanisms in an Ionic Matrix—Kinetics of the Reaction $2O_2^- + H_2O = 2OH^- + 1.5O_2$ in Molten Alkali Nitrates[1]

by P. G. Zambonin,* F. Paniccia, and A. Bufo

Istituti di Chimica Analitica e Generale, Università di Bari, Bari, Italy 70126 *(Received July 21, 1971)*

Publication costs borne completely by The Journal of Physical Chemistry

The kinetics of the homogeneous-phase reaction $2O_2^- + H_2O = 2OH^- + 1.5O_2$ was studied in a molten sodium–potassium nitrate equimolar mixture at 515°K by detecting amperometrically, as a function of time, the concentrations of the species involved in the over-all reaction. At constant concentration of oxygen and water, continuous kinetic curves were recorded by following the limiting current due to the oxidation of superoxide. Within the experimental concentration ranges ($0.7 \times 10^{-5} < [O_2^-] < 8 \times 10^{-4}$; $3 \times 10^{-3} < [H_2O] < 1.8 \times 10^{-2}$; $8 \times 10^{-4} < [OH^-] < 2.3 \times 10^{-2}$; $5 \times 10^{-5} < [O_2] < 1.8 \times 10^{-4}$) the reaction rate can be described by the equation $-d[O_2^-]/dt = k[O_2^-]^2[H_2O]/[O_2]$ which is consistent with the mechanism $2O_2^- \rightleftarrows O_2^{2-} + O_2$ (a); $O_2^{2-} + H_2O \xrightarrow{\text{slow}}$ intermediates (b); intermediates $\xrightarrow{\text{fast}} 2OH^- + {}^1/_2O_2$ (c). Reaction a, characterized by a small equilibrium constant, represents a quasiequilibrium situation prior to the rate-determining step b. The estimated rate parameters are $k = 0.52 \pm 0.03$ mol^{-1} kg sec^{-1}; $k_b = 1 \times 10^6$ mol^{-1} kg sec^{-1}; $k_a \geq \{2 \times 10^3$ mol^{-1} kg sec^{-1}; $k_{-a} \geq 4 \times 10^9$ mol^{-1} kg sec^{-1}.

Introduction

It is known[2] that the reaction of alkali-metal superoxides with water results in the adsorption of water and the liberation of oxygen according to the process

$$2O_2^- + H_2O = 2OH^- + 1.5O_2 \qquad (1)$$

Recently, process 1 has been widely studied because of its numerous practical applications (for reviews see ref 2 and 3). However, very little is known about the possible reaction mechanism, mainly because it could be studied only in heterogeneous phase between solid superoxides and water vapor.

Very recently it has been shown, in this laboratory, that reaction 1 can occur in homogeneous phase in the molten $(Na,K)NO_3$ eutectic, where its equilibrium constant is represented[4] by

$$\frac{[O_2]^{1.5}[OH^-]^2}{[H_2O][O_2^-]^2} = 1 \times 10^3 \text{ mol}^{1/2} \qquad (2)$$

at the temperature of 503°K.

Furthermore it has been seen that all the reagents and products involved can be quantitatively detected[5,6] by a rotated disk electrode (RDE) voltammetric technique.

This favorable situation made possible a kinetic investigation which led to a better understanding of the reaction mechanism. The results of this study, which is part of an extensive research program[4-7] on the chemical and electrochemical behavior of the species superoxide (O_2^-) and peroxide (O_2^{2-}) in molten ionic solvents, are reported and discussed in the present paper.

Experimental Section

Chemical. The solvent was an equimolar mixture (~200 g) of reagent grade molten sodium and potassium nitrate containing water (3×10^{-3} $m < [H_2O] < 1.8 \times 10^{-2}$ m) and maintained at 515 ± 0.5°K. Potassium superoxide (supplied by Alfa Inorganics) was used without further purification. During the experiments the melt was kept under flux of CO_2-free nitrogen containing water vapor at constant partial pressure.[6]

Apparatus and Procedures. The work was performed using the inert material electrolysis cell previously[8] described. The indicator device was an L-shaped, round-corner platinum RDE (area ~2.8×10^{-3} cm^2). This device permitted to minimize the noise due to the development of gas bubbles and to

(1) The work presented at the "Molten Salt Discussion Group" Meeting (Southampton, Sept 23–24, 1971) was carried out by using, in part, facilities of the "Centro di Chimica Analitica Strumentale" of the Italian National Research Council.

(2) I. I. Vol'nov in "Peroxide, Superoxide, and Ozonides of Alkali and Alkali-Earth Metals" (English translation), A. W. Petrocelli, Ed., Plenum Press, New York, N. Y., 1966.

(3) A. Capotosto and A. W. Petrocelli, *Aerosp. Med.*, **35**, 440 (1964); Aerospace Medical Research Laboratories, WP-AFB, Ohio, Report AMRL-TR-68-57, Aug 1968.

(4) P. G. Zambonin, *J. Electroanal. Chem.*, **33**, 243 (1971).

(5) P. G. Zambonin, *Anal. Chem.*, **43**, 1571 (1971).

(6) P. G. Zambonin, V. L. Cardetta, and G. Signorile, *J. Electroanal. Chem.*, **28**, 237 (1970).

(7) (a) P. G. Zambonin and J. Jordan, *J. Amer. Chem. Soc.*, **89**, 6365 (1967); **91**, 2225 (1969); (b) J. Jordan, W. B. McCarthy, and P. G. Zambonin in "Characterization and Analysis in Molten Salts" G. Mamantov, Ed., Marcel Dekker, New York, N. Y., 1969; (c) P. G. Zambonin, *J. Electroanal. Chem.*, **24**, 365, (1970); **24**, Appendix 25, (1970); (d) P. G. Zambonin and A. Cavaggioni, *J. Amer. Chem. Soc.*, **93**, 2854 (1971).

(8) P. G. Zambonin, *Anal. Chem.*, **41**, 868 (1969).

obtain well defined high-sensitivity amperometric recordings. The aluminum block thermostat employed for the cell held a rotating magnet suitable for stirring the solutions. A "three electrode" system was used to collect voltammetric and amperometric data. In this way the potential of the indicator electrode *vs.* the reference (Ag/Ag^+, 0.07 *m*) was potentiometrically detected. At the same time currents were measured in a circuit consisting of the same indicator and of a large area "counter electrode."

Reaction 1 was followed from left to right and initiated by introducting small crystals of potassium superoxide in the melt containing an excess of water. This procedure was possible because the high solubility of superoxide permitted its complete dissolution in about 10 sec under stirring conditions. During this short period the flux of the wet nitrogen was passed through the melt to help the stirring. In the course of the recording period the only stirring was due to the rotated electrode, while the flux of wet nitrogen was maintained over the reacting system.

As mentioned all the reagents and products of reaction 1 could be voltammetrically detected. A representative example of current–potential profiles recorded on the reacting system, far from the equilibrium situation, is represented in Figure 1. The criteria used for identifying the various electrode processes and the way to treat the voltammetric data to define the system quantitatively are described in detail elsewhere.[5,6] For convenience, in Figure 1 is briefly summarized how the concentration of the various species can be obtained from the limiting currents, when the relevant calibration curves are known.

The kinetic processes were followed in two different ways, *i.e.*, by recording sequential voltammograms (see for example Figures 2 and 3) or by detecting amperometrically the decrease of the current h_2 proportional, as seen, to the superoxide concentration. In the last case two strip-chart recorders were used, one to record the current–time curves, the other to test and record rapidly (by instantaneously changing the value of the potential on the polarograph) suitable values of the current h_3 (see for example Figure 4).

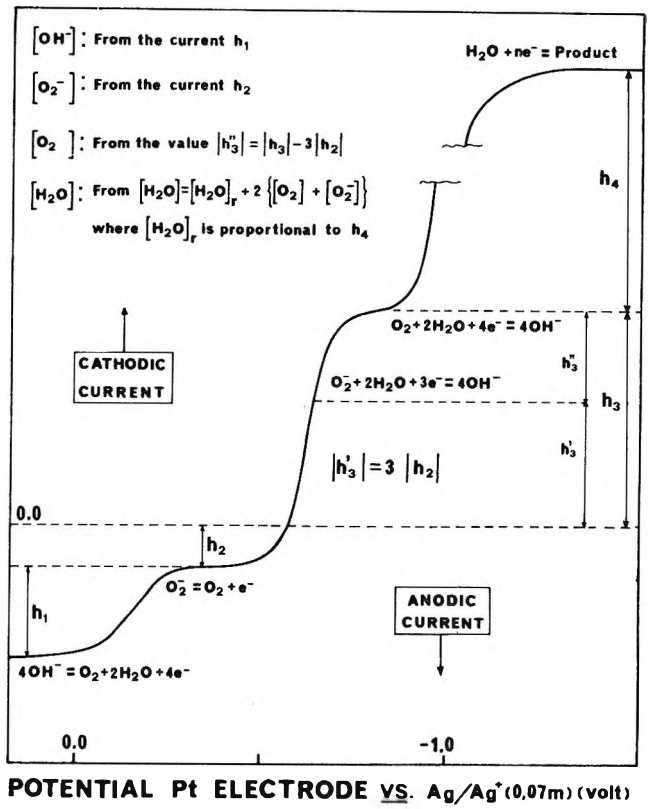

Figure 1. Typical current–potential profile recorded at a rotating platinum indicator electrode on the reacting system (eq 1) far from the chemical equilibrium. Curve corrected for residual current. The way to treat the voltammetric data to obtain the concentrations of reactants and products is briefly summarized.

Results and Discussion

Kinetics Followed by Recording Sequential Voltammograms. A family of voltammograms recorded at various times after the introduction of KO_2 in a melt containing a certain excess of water is reported in Figure 2. It can be seen that the limiting current h_2, proportional to $[O_2^-]$, decreases while h_1, proportional to $[OH^-]$, increases as a function of time.

Only at the beginning and at the end of the followed reaction per cent the complete voltammetric profile was recorded (curves a and e). In the other cases (for example curves b, c, d) the potential was scanned within a narrower potential range (−0.4 to −0.8 V). Not all the recorded curves are reported in Figure 2. The water concentration, present in large excess, was considered constant in the course of the reaction.

The concentrations of superoxide and oxygen calculated from the waves recorded in the course of the described experiment are reported in Figure 3 as a function of time. Figure 3A shows that the concentration of oxygen remained, in first approximation, constant for a certain reaction interval. That is to say that, in this period of time, the quantity of oxygen produced equaled approximately that leaving the supersaturated[9] solution. This "balanced" situation has been verified, under suitable rotation speed of the indicator electrode, for several examples selected in the spectrum of the experimental conditions reported in Table I.

From Figure 3B (curve II) it can be seen that, on assuming the concentrations of oxygen and water to be constant, the disappearance of superoxide is well-represented by a second-order kinetic law.

Kinetics Continuously Recorded. In the previous paragraph it was shown that approximate steady con-

(9) The solubility of oxygen, under the present experimental conditions is, $[O_2] = 5 \times 10^{-6}p$, where $[O_2]$ is expressed in mol kg^{-1} and p in atm (work in progress).

Table I: Kinetic Data Relevant to Reaction 1 in the (Na,K)NO_3 Eutectic Melt Maintained at 515°K. Kinetic Curves Continuously Recorded Except in the Case of the Experiment m, Which is Described in Figures 2 and 3

Run	$[O_2^-]_i \times 10^4$, mol kg^{-1}	$[O_2^-]_t \times 10^4$, mol kg^{-1}	$[O_2] \times 10^4$, mol kg^{-1}	$[H_2O] \times 10^3$, mol kg^{-1}	$[OH^-] \times 10^3$, mol kg^{-1}	Time of reaction, sec	Per cent of reaction	k'', mol^{-1} kg sec^{-1}
a	8.0	4.0	1.8	0.38	2.4	110	50	11
b	5.8	2.9	1.2	0.48	1.9	120	50	15
c	5.4	1.5	0.8	0.45	1.0	180	70	25
d	2.5	0.9	0.85	1.10	2.1	100	65	65
e	3.0	1.2	0.75	1.10	0.8	50	60	75
f	1.5	0.7	0.55	1.10	1.2	70	55	103
g	2.7	1.6	1.6	1.15	1.4	60	40	37
h	2.0	1.0	0.9	1.50	23.1	60	50	85
i	1.7	1.0	0.9	1.55	6.3	30	40	88
j	2.0	0.9	0.8	1.60	1.4	70	55	105
k	2.9	0.9	0.85	1.65	4.0	70	70	108
l	2.8	1.0	1.4	1.75	8.5	70	65	69
m	3.9	1.4	0.55	0.32	0.5	180	65	27

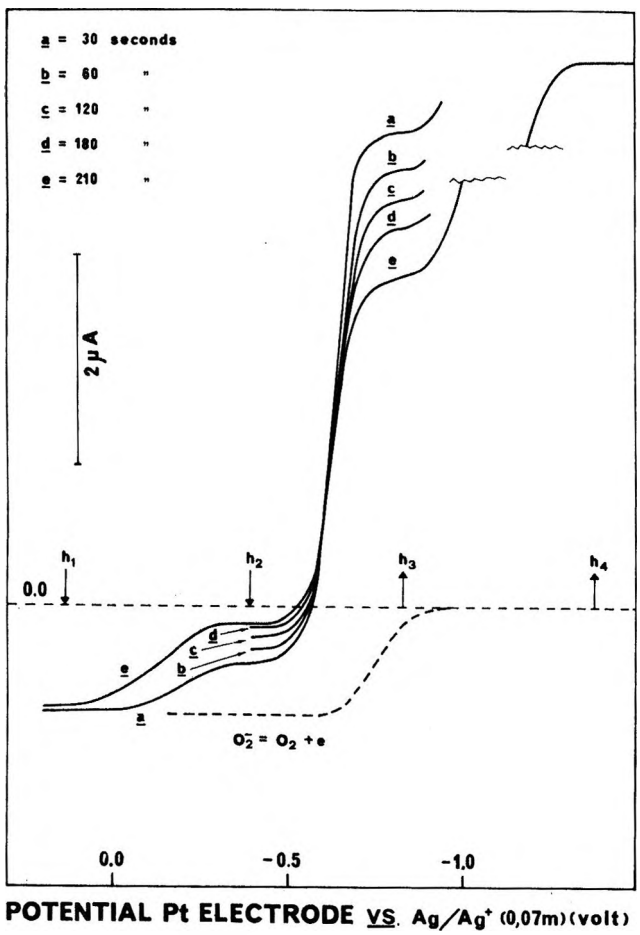

Figure 2. Example of kinetic process followed by recording sequential voltammograms at the specified times. At t = zero 1.0×10^{-2} g of KO_2 was introduced in 186 g of melt maintained at 515°K under a water partial pressure of 4.5 Torr. Indicator electrode rotated at 400 rpm. The curves, recorded at 3 V/min, are corrected for residual current. The dashed wave correspond to the theoretical, initial (t = 0) concentration of superoxide.

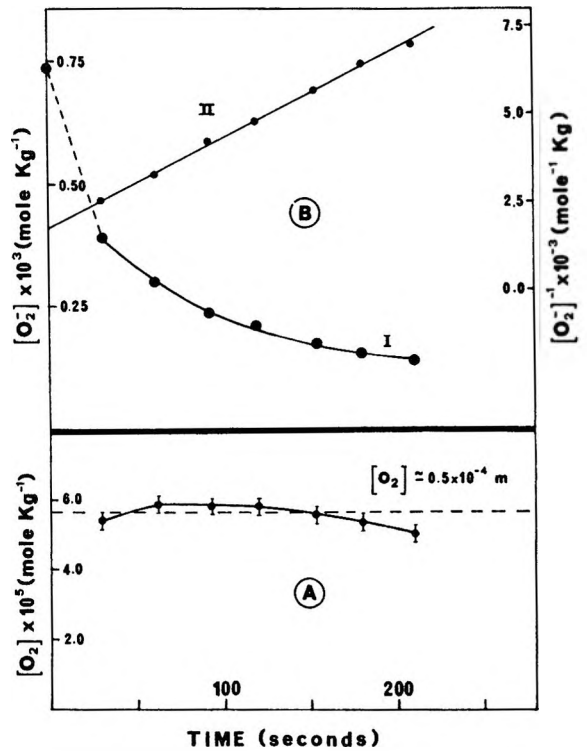

Figure 3. Plots of concentration *vs.* time derived from the experiment described in Figure 2. The points at 90 and 155 sec are obtained from voltammetric profiles not reported in Figure 2. The concentration of superoxide at t = 0 corresponds to the dashed curve in Figure 2.

centrations of oxygen could be obtained during part of a kinetic process. Under these conditions continuous recordings of the kinetics were possible. A representative example of kinetics recorded amperometrically, at −0.4 V, following the disappearance of superoxide, is reported in Figure 4.

At elapsed time corresponding to point B, small crystals of potassium superoxide were introduced in the melt maintained under vigorous stirring. The actual recording started at C, at the end of the magnetic stirring. At D and E the potential was rapidly switched to −0.8 V to record (see the Experimental Section) the

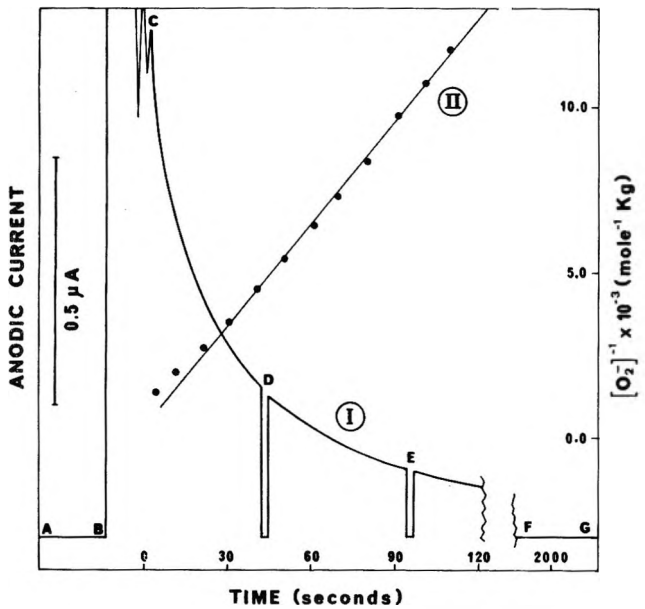

Figure 4. Example of kinetics continuously recorded, by following amperometrically (−0.4 V) the decrease of the concentration of superoxide. Key: $\overline{AB}$ and $\overline{FG}$, pre- and post-reaction base lines; B, introduction of 1.3×10^{-3} g of KO_2 in a melt maintained at 515°K under a water partial pressure of about 23 Torr; $\overline{BC}$, stirring period; D and E, check points for the current h_3 (−0.8 V). The experiment corresponds to k in Table I.

corresponding values of h_3 related (see Figure 1) to the oxygen concentration. In this way suitable controls of $[O_2]$ in the course of the reaction were possible. In particular, for the example described in Figure 4, the concentration of oxygen proved constant in the time interval 25–110 sec.

In accordance with the results reported in Figure 3, as long as the concentrations of oxygen and water were constant, the process was well described (see Figure 4, curve II) by a pseudo-second-order kinetic law.

The results of the experiments are reported in Table I. The second and third columns indicate the superoxide concentration limits for which $[O_2]$ was constant (at least within ±10%) and the process followed a pseudo-second-order kinetic law. Columns VII and VIII show the time elapsed between the reported concentrations of superoxide and the relevant reaction per cents respectively. The concentrations of oxygen, water, and hydroxide, constant in first approximation between the given concentrations of superoxide, are reported in columns IV, V, and VI. The values of the pseudo-second-order kinetic constants (k'', mol^{-1} kg sec^{-1}) are reported in the last column.

Treatment of Data and Proposed Mechanism. Figures 5 and 6 show that straight lines can be obtained by plotting the values of $k''[O_2]$ and $k''[H_2O]^{-1}$ *vs.* $[H_2O]$ and $[O_2]^{-1}$, respectively. No appreciable effect was observed (see Table I and Figures 5 and 6) by changing the concentration of hydroxide. The reaction rate is represented by the relation

$$\text{rate} = -\frac{d[O_2^-]}{dt} = k\frac{[O_2^-]^2[H_2O]}{[O_2]} \qquad (3)$$

where k can be obtained from the slope of the straight lines in Figures 5 and 6

$$k = 0.52 \pm 0.03 \text{ mol}^{-1} \text{ kg sec}^{-1} \qquad (4)$$

The rate law expressed by eq 3 depends on the first power of the inverse oxygen concentration. This suggests[10] that oxygen is produced, prior to the rate-determining step, by a fast process, involving at least one of the reactants. Furthermore this fast process must be involved in a quasiequilibrium situation characterized by a small equilibrium constant so that the concentrations of the reactants are, in practice, not perturbed by this reaction.

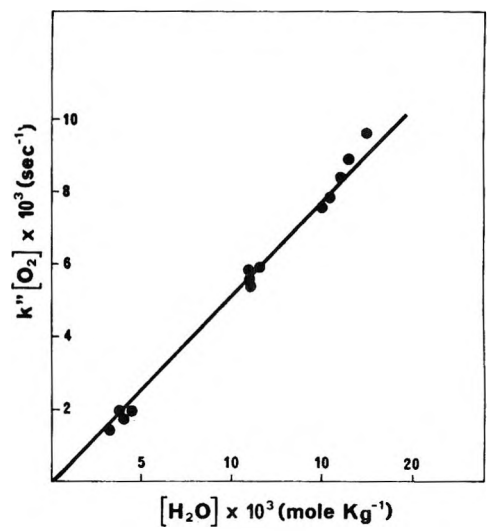

Figure 5. Plot of k'' $[O_2]$ *vs.* $[H_2O]$. Values calculated from the results reported in Table I.

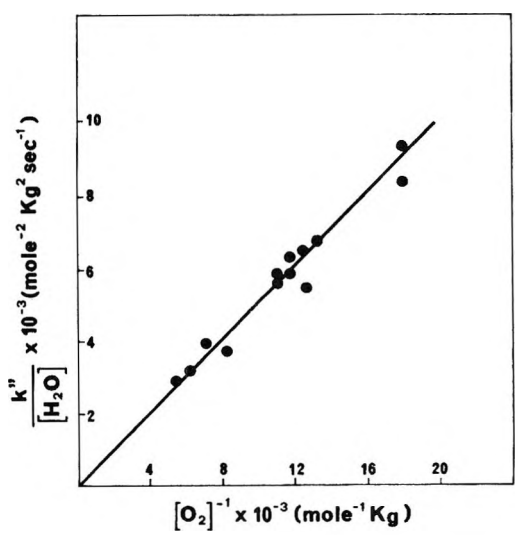

Figure 6. Plot of $k''/[H_2O]$ *vs.* $[O_2]^{-1}$. Values calculated from the results reported in Table I.

(10) J. P. Birk, *J. Chem. Educ.*, 47, 805 (1970).

The observations are consistent with the following reaction mechanism

$$2O_2^- \underset{(k_{-1})}{\overset{(k_1)}{\rightleftharpoons}} O_2 + O_2^{2-} \quad (5)$$

$$O_2^{2-} + H_2O \xrightarrow[(k_2)]{\{H_2O\cdot O_2^{2-}\}^*} \text{intermediates} \quad (6)$$

$$\text{intermediates} \xrightarrow[\text{fast}]{} 2OH^- + {}^1/_2O_2 \quad (7)$$

where reaction 6 represents the rate-determining step leading to the eventual formation of the final products by successive fast processes indicated by reaction 7.

The electron transfer process 5 (well-known[4-7] to occur in molten nitrates) is governed, as required, by a small equilibrium constant[4]

$$\frac{[O_2][O_2^{2-}]}{[O_2^-]^2} = \frac{k_1}{k_{-1}} = K = 5 \times 10^{-7} \quad (8)$$

On the basis of the proposed mechanism, the rate constant, k, can be expressed by

$$k = k_2K \quad (9)$$

and by considering reactions 4 and 8 the second-order rate constant k_2 can be obtained

$$k_2 = \frac{k}{K} = \frac{0.52}{5 \times 10^{-7}} = 1 \times 10^6 \text{ mol}^{-1} \text{ kg sec}^{-1} \quad (10)$$

The proposed mechanism indicates that the forward reaction of process 5 must be (at least) one order of magnitude faster than step 6 for the concentration intervals considered in this study. On this basis minimum values of k_1 and k_{-1} can be computed. By indicating with $[H_2O]_{max}$ and $[O_2]_{min}$ the maximum and minimum concentrations of water and oxygen used

$$k_1 \geq 10k_2K\frac{[H_2O]_{max}}{[O_2]_{min}} = 2 \times 10^3 \text{ mol}^{-1} \text{ kg sec}^{-1} \quad (11)$$

and considering eq 10

$$k_{-1} = \frac{k_1}{K} \geq 4 \times 10^9 \text{ mol}^{-1} \text{ kg sec}^{-1} \quad (12)$$

An interesting point, derived from the present work, is that the dominant path for reaction 1 involves breaking the O–O bond in a peroxide instead of a superoxide compound. This is readily apparent by considering the simplest paths for the decay of the activated complex $\{H_2O\text{–}O_2^{2-}\}^*$ and the relevant successive steps. For example

$$\{H_2O\cdot O_2^{2-}\}^* = OH^- + HO_2^-$$

$$HO_2^- = OH^- + O$$

$${}^1/_2(O + O = O_2)$$

or the less probable

$$\{H_2O\cdot O_2^{2-}\}^* = O^{2-} + H_2O_2$$

$$H_2O_2 = H_2O + O$$

$$O^{2-} + H_2O = 2OH^-$$

$${}^1/_2(O + O = O_2)$$

As in the case of other similar reactions[7d] the prevalence of a "peroxide mechanism" is probably to be ascribed to the minimum bond energy which characterizes[2,11] the species peroxide in the spectrum of the dimeric oxygen species.

In the present context it can be noted that the remarkable stability previously observed for superoxide ions in molten salts[4-7,12-14] appears to be mainly related to the strong tendency of oxygen to be retained by the solution (compare, for example, its capability to form supersaturated solutions) since its formation is controlled (see reaction 5 and relation 11) by a quite high kinetic constant.

Consistency of the Results. Some aspects of the experimental technique used in the course of this study are certainly unusual and may to some appear to be approximate. However, one must consider the difficulties of studying in homogeneous phase a chemical system (reaction 1) involving two gases, one of which (oxygen) is poorly soluble. In this context the technique used, based mainly on the tendency of oxygen to form highly supersaturated solutions, appears, perhaps, unique and in any case the simplest. In practice (see Table I and Figures 5 and 6) the experimental results, obtained in the course of the study, seem sufficiently reproducible to permit the reported mechanistic conclusions.

(11) C. A. Coulson, "Valence," Oxford University Press, London, 1961.

(12) J. Goret and B. Tremillon, *Bull. Soc. Chim. Fr.*, 67 (1966).

(13) E. P. Mignosin, L. Martinot, and G. Duyckaerts, *Inorg. Nucl. Chem. Lett.*, **3**, 511 (1967).

(14) F. L. Whiting, G. Mamantov, and J. P. Young, *J. Amer. Chem. Soc.*, **91**, 6531 (1969).

Kinetic Deuterium Isotope Effects in the Reactions of Methyl Iodide with Azide and Acetate Ions in Aqueous Solution[1]

by Chong Min Won and Alfred V. Willi*[2]

College of Pharmaceutical Sciences, Columbia University, New York, New York 10023 *(Received August 30, 1971)*

Publication costs borne completely by The Journal of Physical Chemistry

The kinetic α-deuterium isotope effect has been determined for the reactions of CH_3I (CD_3I) in aqueous solutions with azide ion from 10 to 40° and with acetate ion at 40°. Kinetic measurements have been carried out in reaction vessels with no gas phase. Rate constants of the reaction of methyl iodide with acetate ion are corrected for simultaneous solvolysis. Results indicate inverse isotope effects: $k_H/k_D = 0.907$ ($CH_3I + N_3^-$), and 0.882 ($CH_3I + CH_3COO^-$) at 40°. The experimental data for the reaction with N_3^- are compared with results of model calculations of isotope effects from force constants with an electronic computer. Reasonable choices are made for the transition state force constants f_{CI}, f_{CN}, f_{12}, f_{HCI}, and the force constants not involving reacting bonds. The bending force constant f_{HCN} (in general: f_{HCY}) is adjusted to fit the experimental isotope effect at one temperature. Good agreement then is obtained between calculated and experimental isotope effects at all four temperatures. In the series $CH_3I + S_2O_3^{2-}$, CN^-, N_3^-, or CH_3COO^-, a very good correlation exists between the values of k_H/k_D and $\Delta G^{\pm}$, but there is no relationship between $\Delta G^{\pm}$ (or the nucleophilic power of Y^-, respectively) and the adjusted value of the bending force constant, f_{HCY}. The particular role of solvation in the SN2 transition state is discussed. The models of the isotope effect calculations must be improved to take care of the solvation of the groups X and Y.

This paper is the third in a series[3,4] referring to experimental studies of secondary α isotope effects in SN2 reactions of methyl iodide (CH_3I in comparison to CD_3I) with various nucleophiles. The work is done in comparison with computer calculations of isotope effects from vibrational force constants in order to gain insight into the nature of the transition states and to arrive at a better understanding of the causes of the isotope effects.

The preceding two papers were concerned with determinations of deuterium isotope effects in the reactions of methyl iodide with cyanide ion[3] and thiosulfate ion.[4] This work refers to deuterium isotope effects in the reactions of methyl iodide with azide ion and acetate ion. Results are now available for deuterium isotope effects in reactions of methyl iodide with four different nucleophiles, and it has become possible to draw some general conclusions.

The reaction of methyl iodide with azide ion is a simple second order process, and the integrated rate equation 1 is adequate for the treatment of the experimental data.

$$\log ([N_3^-]/[CH_3I]) = \log ([N_3^-]_0/[CH_3I]_0) + ([N_3^-]_0 - [CH_3I]_0)k_2t/2.303 \quad (1)$$

The reaction with the weakly nucleophilic acetate ion is complicated by simultaneous first order solvolysis with water according to rate eq 2

$$-d[CH_3I]/dt = k_2[CH_3I][CH_3COO^-] + k_1[CH_3I] \quad (2)$$

The two parallel reactions may be formulated as

$$CH_3I + CH_3COO^- \longrightarrow CH_3COOCH_3 + I^- \quad (k_2)$$

$$CH_3I + H_2O + CH_3COO^- \longrightarrow CH_3OH + CH_3COOH + I^- \quad (k_1)$$

Strong acid formed in the solvolytic reaction is immediately neutralized by acetate ion which is present in excess. Consequently, acetate ion is consumed in both processes which leads to a relatively simple stoichiometric relationship

$$[CH_3I]_0 - [CH_3I] = [CH_3COO^-]_0 - [CH_3COO^-] = [I^-] - [I^-]_0 \quad (3)$$

Combination of eq 2 and 3 and subsequent integration leads to the integrated rate equation 4[5,6]

$$\ln \frac{A_0(A + (k_1/k_2) + B_0 - A_0)}{A((k_1/k_2) + B_0)} = ((k_1/k_2) + B_0 - A_0)k_2t \quad (4)$$

with

$$A = [CH_3I],\ A_0 = [CH_3I]_0,\ B_0 = [CH_3COO^-]_0$$

(1) Taken from the final part of the thesis of Mr. C. M. Won, submitted to the Faculty of Pure Science, Columbia University, New York, N. Y., in partial fulfillment of the requirements for the degree of Doctor of Philosophy.

(2) Address correspondence to this author at Kampenweg 22, D 237 Rendsburg, West Germany.

(3) A. V. Willi and C. M. Won, *J. Amer. Chem. Soc.*, **90**, 5999 (1968).

(4) A. V. Willi and C. M. Won, *Can. J. Chem.*, **48**, 1452 (1970).

(5) E. A. Moelwyn-Hughes, *Proc. Roy. Soc., Ser. A*, **196**, 540 (1949).

(6) Szabo discusses a different case in which the nucleophilic reactant is not neutralized by acid produced in the first order reaction. Z. G. Szabo in "Comprehensive Chemical Kinetics," Vol. 2, C. H. Bamford and C. F. H. Tipper, Ed., Elsevier, Amsterdam, 1969, pp 45, 46.

The rate of formation of acid is equal to the rate of the solvolysis reaction

$$d[\text{acid}]/dt = k_1[CH_3I] \quad (5)$$

Equation 6a describes the increase of the acid concentration as a function of time. It is obtained by combination of eq 2, 3, and 5 and subsequent integration.[5,6]

$$[\text{acid}] - [\text{acid}]_0 = (k_1/k_2) \ln \frac{(k_1/k_2) + B_0}{A + (k_1/k_2) + B_0 - A_0} \quad (6a)$$

Experiments are usually carried out in such a way that $[\text{acid}]_0 = 0$.

As far as the writers know, previous kinetic studies of the reactions of methyl iodide with azide ion or acetate ion have not been published.

Experimental Section

General procedures of purification of reactants and solvent and of the kinetic measurements have been described previously.[3] The reaction vessels with no gas phase were variants of those described by Fahim and Moelwyn-Hughes.[7]

In the measurements of the rates of reaction of methyl iodide with azide ion, 5-ml samples of the kinetic solutions were acidified with 10 ml of 6 N aqueous nitric acid (to prevent precipitation of AgN_3) and then titrated with standardized 0.01 N silver nitrate solution at a silver electrode, utilizing a mercurous sulfate reference electrode. The same procedure was applied in the measurements of the rates of reaction of methyl iodide with acetate ion except that the solution samples were acidified with 1 ml rather than 10 ml of 6 N nitric acid.

The concentration of acid formed in the experiments with acetate ion was determined at 50–60% conversion of methyl iodide, by titration of 5-ml samples with standardized 0.01 N sodium hydroxide solution, using phenolphthalein as an indicator.

The initial concentrations of methyl iodide in the reactions with azide ion were evaluated from iodide ion concentrations in solution samples in which the reaction had gone to 99.9% completion. This procedure was not feasible in the reactions with acetate ion, because of the low rate. However, methyl iodide could be transformed to iodide ion within a reasonable time period by adding a small volume of excess potassium cyanide solution to the solution in the kinetic cell and waiting until the reaction was 99.9% complete. (The reaction time was calculated from known rate constants.[3])

Calculation of Rate Constants from Experimental Data

For each kinetic run of the reaction with azide ion, the best straight line was fitted to the experimental points of $\log([N_3^-]/[CH_3I])$ as a function of t, using a computer with a linear regression program. k_2 was calculated from the slope of the line, according to eq 1.

It was necessary to apply eq 4 and 6a in the calculation of the bimolecular rate constant of the reaction of methyl iodide with acetate ion. The ratio k_1/k_2 was computed from a pair of values of [acid] and $[CH_3I]$ measured at the same time. This was carried out with a method of successive approximations in which a preliminary value of k_1/k_2 was inserted at the right hand side of eq 6b. An improved value of k_1/k_2 then was obtained from eq 6b which was utilized at the right hand side of the equation in the next approximation. This procedure was repeated several times until k_1/k_2 remained unchanged within 0.1%. Two or three separate determinations of k_1/k_2 were carried out in each kinetic run, and the average value was computed. (A value of $k_1/k_2 = 0.094$ M was obtained for the reacting system $CH_3I + CH_3COO^- + H_2O$ at 40°.) In the next step, eq 4 was utilized for the calculation of k_2 from a series of experimental values of $[CH_3I]$ as a function of t. The regression line for the expression at the left hand side of eq 4 as a linear function of t was calculated in a computer with a linear regression program.

$$k_1/k_2 = [\text{acid}]/\ln\{[(k_1/k_2) + B_0]/[A + (k_1/k_2) + B_0 - A_0]\} \quad (6b)$$

Results

In all experiments, the initial concentrations of methyl iodide or methyl-d_3 iodide are *ca.* 2×10^{-2} M, those of sodium azide are *ca.* 5×10^{-2} M, and those of sodium acetate are *ca.* 0.25 M. Plots of $\ln([N_3^-]/[CH_3I])$, or $\ln\{([CH_3I] + (k_1/k_2) + [CH_3COO^-]_0 - [CH_3I]_0)/[CH_3I]\}$, respectively, as functions of t are linear through 2 half-lives. Consequently, the reverse reactions do not interfere under the conditions of these experiments.

Results of second-order rate constants and isotope effects, obtained at different temperatures, are collected in Table I. Each rate constant is the average value of three to five determinations in separate kinetic runs.

Table I: Rate Constants and Isotope Effects in the Reactions of Methyl Iodide (RI) with Azide Ion and Acetate Ion in Water

Nucleophile	Temp, °K	R = CH_3 10^5k_2, sec^{-1} mol^{-1} l.	R = CD_3 10^5k_2, sec^{-1} mol^{-1} l.	k_H/k_D
azide ion	283.2	0.6819	0.7550	0.903 (±0.004)
azide ion	293.2	2.962	3.254	0.901 (±0.007)
azide ion	303.1	11.91	13.20	0.903 (±0.011)
azide ion	313.2	40.45	44.68	0.907 (±0.019)
acetate ion	313.2	0.826	0.936	0.882 (±0.012)

(7) R. B. Fahim and E. A. Moelwyn-Hughes, *J. Chem. Soc.*, 1035 (1956).

Arrhenius parameters of the reaction with azide ion are given as follows: for $CH_3I + N_3^-$, $A = 2.48 \times 10^{13}$ ($\pm 22\%$) sec^{-1} mol^{-1} l., $E_a = 24.05$ (± 0.41) kcal; for $CD_3I + N_3^-$, $A = 2.82 \times 10^{13}$ ($\pm 22\%$) sec^{-1} mol^{-1} l., $E_a = 24.05$ (± 0.41) kcal; isotope effect, $A_H/A_D = 0.879$ (± 0.033), $E_{aH} - E_{aD} = -3$ cal.

Discussion

Relationships between Isotope Effect and Nucleophilic Power. Inverse α-deuterium isotope effects are found in the reactions of methyl iodide with azide ion and acetate ion both of which are relatively weak nucleophiles. Inverse isotope effects have been observed previously in the reactions of methyl iodide with stronger nucleophiles such as tertiary amines,[8] cyanide ion,[3] and thiosulfate ion,[4] and in the solvolyses of the methyl halides in water.[9] However, normal isotope effects occur in the iodide exchange reaction of methyl iodide[10] and in the reactions of methyl, ethyl, and *n*-propyl bromides with thiosulfate ion.[11] Normal deuterium isotope effects are found also in the chloride exchange reaction[12,13] and in the solvolysis[14] of benzyl chloride, as well as in the reaction of benzyl chloride with cyanide ion.[14]

Seltzer and Zavitsas[10] observed a linear relationship between the α-deuterium isotope effect and the difference in nucleophilic powers of the entering and leaving groups (Edwards' E_n constants[15]). If the isotope effects of the reactions of methyl iodide with thiosulfate ion[4] (20°), cyanide ion[3] (20°), azide ion (30°), and acetate ion (40°) in aqueous solution are plotted *vs.* the $\Delta G^{\ddagger}$ values, a straight line is obtained with surprisingly good precision (Figure 1). The point for the iodide exchange reaction[10] is above the line, however. If, on the other hand, the isotope effects in the four SN2 reactions studied by the writers are plotted *vs.* $E_n - E_I$, the experimental points form a straight line (with some scattering) 0.04 unit below the original line drawn by Seltzer and Zavitsas.[10] (The point for the iodide exchange reaction of methyl iodide is far above the line.)

A correlation of similar appearence is obtained if α-deuterium isotope effects in SN reactions of methyl compounds are plotted *vs.* the difference of the Swain–Scott[16] nucleophilic constants of the entering and leaving groups, $n_n - n_I$. It is necessary to use the *n* values of the halide ions suggested by Petty and Nichols.[17]

The reactions which yield a fairly good linear correlation between isotope effects and nucleophilic powers are "downhill" processes, *i.e.*, the products are more stable than the reactants, no matter whether the kinetic "nucleophilic power" of the entering group is greater or smaller than that of the leaving group. (It was emphasized in a previous paper[18] that the Swain–Scott and Edwards scales refer to rates but not to equilibria.) On the other hand, the equilibrium constant of the iodide exchange reaction of methyl iodide must be approximately equal to 1, except for a small iodine isotope effect.

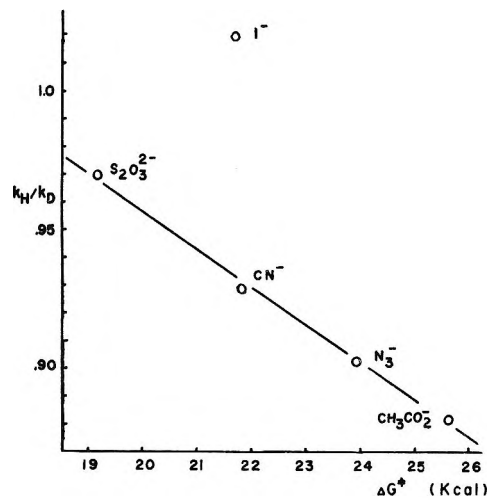

Figure 1. Relationship between α-deuterium isotope effect and free energy of activation.

Comparison with Calculations of Isotope Effects from Force Constants. Model calculations of isotope effects from vibrational force constants for the reaction of methyl iodide with azide ion have been carried out with the aid of the Wolfsberg–Schachtschneider[19] program. The geometry and the force constants of the model of the reactant methyl iodide are the same as in previous calculations.[3,4,20] In the model of the transition state, the central CH_3 group is planar, with $\angle HCH = 120°$, $\angle HCI = \angle HCN = 90°$, and the following bond lengths: r_{CH}, 1.08 Å; r_{CI}, 2.14 Å + 10% = 2.35 Å; r_{CN}, 1.47 Å + 10% = 1.62 Å. According to the cutoff method suggested by Stern and Wolfsberg,[21] the azide group in the transition state is represented by two points, the one being the reacting N atom, the other one the N_2 group, with $r_{NN} = 1.24$ Å[22] and $\angle CNN = 120°$.

Transition state force constants are chosen as follows: $f_{NN} = 9.12$ mdyn/Å,[23] $f_{CNN} = 0.1$ mdyn Å, $f_{HCNN} =$

(8) K. T. Leffek and J. W. McLean, *Can. J. Chem.*, **43**, 40 (1965).
(9) J. A. Llewellyn, R. E. Robertson, and J. M. W. Scott, *ibid.*, **38**, 222 (1960).
(10) S. Seltzer and A. A. Zavitsas, *ibid.*, **45**, 2023 (1967).
(11) K. T. Leffek, *ibid.*, **42**, 851 (1964).
(12) B. Ostman, *J. Amer. Chem. Soc.*, **87**, 3161 (1965).
(13) H. Strecker and H. Elias, *Radiochim. Acta*, **7**, 22 (1967).
(14) A. V. Willi and Chih-kuo Ho, to be published.
(15) J. O. Edwards, *J. Amer. Chem. Soc.*, **76**, 1540 (1954); **78**, 1819 (1956).
(16) C. G. Swain and C. B. Scott, *ibid.*, **75**, 141 (1953).
(17) W. L. Petty and P. L. Nichols, *ibid.*, **76**, 4385 (1954).
(18) A. V. Willi, *Z. Phys. Chem. (Frankfurt am Main)*, **66**, 317 (1969).
(19) M. Wolfsberg and M. J. Stern, *Pure Appl. Chem.*, **8**, 225 (1964).
(20) A. V. Willi, *Can. J. Chem.*, **44**, 1889 (1966); *Z. Naturforsch. A*, **21**, 1377, 1385 (1966).
(21) M. J. Stern and M. Wolfsberg, *J. Chem. Phys.*, **45**, 4105 (1966).
(22) The Chemical Society, "Tables of Interatomic Distances and Configurations in Molecules and Ions," Burlington House, London, 1958.
(23) W. Engler and K. W. F. Kohlrausch, *Z. Phys. Chem., Abt. B*, **34**, 214 (1936).

Table II: Calculated Isotope Effects in the Reaction of Methyl Iodide with Azide Ion

Transition state force constants[a]					k_H/k_D			
f_{CI}	f_{CN}	f_{12}	f_{HCI}	f_{HCN}	10°	20°	30°	40°
0.20	0.20	1.50	0.295	0.340	0.895	0.900	0.905	0.909
1.01	2.85	4.43	0.295	0.320	0.896	0.900	0.905	0.909
1.09	2.80	4.64	0.295	0.320	0.892	0.897	0.902	0.905
Experimental results					0.903	0.901	0.903	0.907

[a] Stretching force constants are given in mdyn/Å and bending force constants are given in mdyn Å.

0.1 mdyn Å (torsion). The values of the force constants for the CH stretching (f_{CH} = 5.05 mdyn/Å in all calculations in this paper), HCH bending, and CH_3 out-of-plane bending motions, as well as the interactions among these motions, are the same as in previous calculations[3,4,20] for transition state models of the general type $I\cdots CH_3\cdots Y$.

The remaining five force constants are related to reacting bonds. Sample calculations are done with three different sets of values for f_{CN}, f_{CI}, and f_{12} (interaction between the CN and CI stretches). The bending force constant f_{HCI} is kept constant at 0.295 mdyn Å (the value found for the transition state $I\cdots CH_3\cdots I$) while for each of the three sets of f_{CN}, f_{CI}, f_{12} the bending force constant f_{HCN} is adjusted to fit the experimental isotope effect.

The three sets of stretching force constants of the reacting bonds have been selected on the following bases:

(1) $f_{CN} = f_{CI}$ = 0.2 mdyn/Å, f_{12} = 1.5 mdyn/Å (no particular theoretical model).

(2) The force constants are calculated from a semi-empirical model of the energy barrier with the aid of a Johnston-type equation.[24] The model has been described previously.[18] Starting from $V_1 = V_2$ = 37.2 kcal, p_1 = 2.26, $V_{max} = \Delta G^{\pm}$ = 23.90 kcal, the following values are obtained: p_2 = 2.73, n = 0.477 (CI bond order), f^* = 2.53 mdyn/Å (force constant describing the curvature of the barrier).

(3) The same model is applied, but it is assumed that $V_2 > V_1$, as the products are more stable than the reactants. The values of V_1 = 37.2 kcal, V_2 = 45.7 kcal (arbitrary assumption, a well-founded value may be computed from the equilibrium constant which has not yet been measured), p_1 = 2.26, and V_{max} = 23.90 kcal lead to p_2 = 2.90, n = 0.486, f^* = 2.74 mdyn/Å.

The force constants of sets (2) and (3) are calculated from n and f^* with the aid of eq 7, 8, and 9[24]

$$f_{CN} = F_{CN}(1 - n) \quad (7a)$$

$$f_{CI} = F_{CI}n \quad (7b)$$

$$f_{12} = [f_{CI}C^2 + f_{CN} + (1 + C^2)f^*]/2C \quad (8)$$

$$C = (1 - n)/n \quad (9)$$

(F_{CN} = 5.45 mdyn/Å[25] and F_{CI} = 2.25 mdyn/Å[26] are the values of the stretching force constants in stable molecules.)

Results of isotope effect calculations based on these three sets of transition state stretching force constants are collected in Table II. The experimental value for k_H/k_D is obtained if the transition state bending force constant f_{HCN} is adjusted to a value in the range 0.320 to 0.340 mdyn Å. In all three examples, calculated and experimental isotope effects agree within experimental error at all four temperatures.

In Table III, transition state bending force constants[3,4,20] involving one reacting bond are compared with bending force constants for the corresponding bonds in stable molecules.[25-28] In all four examples, the transition state bending force constant is equal to 47–63% of the bending force constant in the stable molecule. There is no relationship between the nucleophilic power of Y^- and the transition state bending force constant, f_{HCY}, or the ratio, f_{HCY}/F_{HCY}.

Table III: Transition State Bending Force Constants

Reaction	Transition state: $f_{HCI} + f_{HCY}$ mdyn Å	Transition state: f_{HCY} mdyn Å	Stable molecule F_{HCY} mdyn Å	f_{HCY}/F_{HCY}
$CH_3I + S_2O_3^{2-}$	0.595[a]	0.300[a]	0.525[b]	0.572
$CH_3I + I^-$	0.590[c]	0.295[c]	0.55[d]	0.537
$CH_3I + CN^-$	0.695[e]	0.400[e]	0.64[f]	0.626
$CH_3I + N_3^-$	0.615[g]	0.320[g]	0.681[h]	0.470

[a] Reference 4. [b] Reference 27. [c] Reference 20. [d] Reference 26. [e] Reference 3. [f] Reference 28. [g] This work. [h] Reference 25.

The Role of Solvation in the Mechanism of the SN2 Reaction. As found recently by Bohme and Young[29] applying the flowing afterglow technique, the reactions of methyl chloride with hydroxide or alkoxide ions in the gas phase are fast. Experimental rate constants are of the same order of magnitude as calculated collision rate constants. The same is probably true for

(24) H. S. Johnston, *Advan. Chem. Phys.*, 3, 131 (1961).

(25) J. W. Linnett, *J. Chem. Phys.*, 8, 91 (1940).

(26) P. F. Fenlon, F. F. Cleveland, and A. G. Meister, *ibid.*, 19, 1561 (1951).

(27) H. Siebert, *Z. Anorg. Allg. Chem.*, 271, 65 (1952).

(28) G. Herzberg, "Infrared and Raman Spectra of Polyatomic Molecules," Van Nostrand, New York, 1945, p 193.

(29) D. K. Bohme and L. B. Young, *J. Amer. Chem. Soc.*, 92, 7354 (1970).

many other reactions of methyl halides with charge-localized anions in the gas phase. The rate of the gas phase reaction of methyl chloride with alkoxide ions is strongly decreased if the anion is solvated by one alcohol molecule.

On the other hand, reactions of methyl halides with anions in solution are slow; they possess activation energies in the approximate range of 15–25 kcal. The rates of these reactions are strongly dependent on the solvation of the anion.[30] It is appropriate to reopen the discussion of the mechanism of the SN2 reaction of a methyl halide with a nucleophile in solution with regard to the findings of Bohme and Young. There are three possibilities:

(a) The slow step is the desolvation of the anion (and the methyl halide). The free particles react in a fast subsequent step which must be diffusion controlled. (In this case, the rate of combination of the reactants is assumed to be faster than the rate of solvation.)

(b) The solution contains very small equilibrium concentrations of the unsolvated reactants. The slow step is the diffusion-controlled combination of the reactants. (The rate of solvation is faster than, or of the same order of magnitude as, the rate of combination of the free reactants.)

(c) The concentrations of unsolvated reactants in the solution are too low to maintain an appreciable reaction rate, and *reaction takes place between solvated particles.* If the reactants are solvated by more than one solvent molecule, it may be necessary to remove one solvent molecule from the coordination shells of each of the reactants before the alkyl halide can combine with the anion to form the transition state. (Both reactants still are partially solvated in the transition state.) Activation energy is required in the SN2 reaction of the solvated particles.

A decision among these three possibilities can be made on the basis of observed primary carbon isotope effects in the reactions of methyl halides with water,[31] amines,[31] hydroxide,[31,32] and cyanide[32] ions (k_{12C}/k_{13C} = 1.03–1.07). Bond cleavage between central carbon atom and leaving group must occur in the rate-determining step. Therefore, mechanism (a) may be excluded immediately. Furthermore, mechanism (b) cannot be correct because the carbon-13 isotope effect on the rate of diffusion of the methyl halide must be much lower than 3%. Consequently, mechanism (c) must be correct, *i.e.*, the reaction takes place between solvated reactants, and it is slow because a solvated nucleophile is less reactive than a free one.

There is a wealth of evidence for the bimolecular nature (solvent molecules not counted) of the SN2 reaction in solution and the occurrence of backside attack by the entering nucleophile.[33] One or several solvent molecules must be bonded directly to the entering nucleophile in the transition state. According to the principle of microscopic reversibility, the leaving group in the transition state must be solvated, also. Another way of describing the transition state of the reaction of a methyl halide with an anion would be as follows: the methyl halide and the attacking anion are in the same solvent cage, and the entering and leaving groups are strongly bonded to the walls of the cage.

Conclusions Concerning the Transition State Model in Isotope Effect Calculations. The considerations about the importance of transition state solvation are relevant with respect to the model chosen for the isotope effect calculations. A correlation is observed between the nucleophilic power of the attacking anion and the experimental α-deuterium isotope effect, but there is no clearly visible relationship between the nucleophilic power of Y^- and the bending force constant, f_{HCY}, or the sum of the bending force constants, $f_{HCl} + f_{HCY}$, respectively.

As far as the calculations are concerned, one might expect a relationship between $f_{HCl} + f_{HCY}$ and the isotope effect, with little dependence on the mass and geometry of Y. Large values of $f_{HCl} + f_{HCY}$ would correspond to low values of k_H/k_D. However, sample calculations with the same value of $f_{HCl} + f_{HCY}$ lead to different results of k_H/k_D for transition states with different groups Y. For example, a higher value of k_H/k_D is calculated for the reaction with CN^- than for the reaction with N_3^-. Therefore, $f_{HCl} + f_{HCY}$ must be adjusted to a higher value in order to obtain agreement with the experimental isotope effect in the reaction with CN^-, even though the experimental value of k_H/k_D is lower in the reaction with N_3^- (Table III).

Obviously, the influence of the mass and geometry of Y is not negligible. The isotope effect also depends on the particular way how the motions of H (D) and Y are coupled in some bending vibrational modes of the transition state. The influence of these factors is substantial in comparison to the relatively small range of observed values of k_H/k_D in SN2 reactions.

On the basis of these considerations and the results of sample calculations, a good correlation between isotope effects and values of $f_{HCl} + f_{HCY}$ would not be expected for different transition states. The same refers to correlations between isotope effects and nucleophilic powers of Y^- which affect reacting bond orders and transition state force constants. A very good correlation between isotope effect and reactivity does exist, however, according to Figure 1. Consequently, the models applied in these calculations cannot be fully adequate.

The influence of masses and geometry of entering and leaving groups on the transition state bending frequen-

(30) A. J. Parker, *J. Chem. Soc.*, 1328 (1961); *Quart. Rev. (London)*, **16**, 163 (1962); *Advan. Org. Chem.*, **5**, 1 (1965).

(31) M. L. Bender and D. F. Hoeg, *J. Amer. Chem. Soc.*, **79**, 5649 (1957).

(32) K. R. Lynn and P. E Yankwich, *ibid.*, **83**, 53, 790 (1961).

(33) C. K. Ingold, "Structure and Mechanism in Organic Chemistry," Cornell University Press, Ithaca, N. Y., 1953.

cies will be smaller, if it is considered in the model that these groups are solvated by clusters of associated water molecules. Solvation causes some restriction of the motions of X and Y in the transition state. It is planned to carry out new model calculations of isotope effects with consideration of solvation of the reactant and the transition state.

Acknowledgments. The authors are pleased to acknowledge financial support of this work by the U. S. Atomic Energy Commission through Contract No. AT(30-1)-3796. Furthermore, they wish to thank Professor R. C. Kerber (State University of New York, Stony Brook) for reading the manuscript prior to submission.

Effect of Transfer from Water to 1.0 *M* Water in Dimethyl Sulfoxide on the Reaction of Nucleophiles with Phenyl Esters

by R. Goitein[1] and Thomas C. Bruice*

Department of Chemistry, University of California, Santa Barbara, California 93106
(Received July 26, 1971)

Publication costs assisted by the National Institutes of Health

Solvent S is defined as 1 *M* H_2O in DMSO. In solvent S, water structure is eliminated, solvation of charged centers is reduced, the solvation characteristics of a polar aprotic solvent are approached, but water remains an effective nucleophile. For a series of nine oxyacids, a plot of pK_a determined in S *vs.* pK_a in water is of slope 2.2 as is a plot of the log of the second-order rate constants for acylate ion displacement on substituted phenyl acetates in S and H_2O, respectively. These data, together with previous observations of the alteration of ΔS for ionization and $\Delta S^{\ddagger}$ for acylate ion displacement, are suggested to show that departure of phenoxide is important in the critical transition state. On transfer from H_2O to S the second-order rate constant for HO^- attack on *p*-nitrophenyl acetate is increased 10^6-fold while the constant for $(CH_3)_3N$ attack is increased by only 3.3-fold. Comparison of equivalent ionic conductivities suggests that the increase in activity of HO^- on transfer from H_2O to S is due to a decrease in the activity of H_2O which solvates the HO^- ion rather than to desolvation of this species.

In transferring from H_2O to 1 *M* H_2O in DMSO, water structure is eliminated, solvation of polar or charged centers by water is reduced,[2] the solvation characteristics of a polar aprotic solvent are approached,[3] while water remains an effective nucleophile.[4] Herein are described observations on the change of pK_a values accompanying transfer from water to 1 *M* H_2O–DMSO ("solvent S") and the values of equivalent conductivities of ions in solvent S. These experimental parameters are employed to provide a better description of the critical transition state for acylate ion attack on phenyl acetate esters and the role of solvation for HO^- nucleophilic displacement on these esters.

In solvent S the usual quantitative approach to acid–base chemistry is possible since pH is determinable[4] *via* procedures originally described by Ritchie.[5] The pK_a's of several phenols and trifluoroethanol have been determined in solvent S by the method of half neutralization employing the apparatus previously described.[4] The same apparatus was employed to determine the ionization constants of water (pK_w) in solvent S using the method of Harned and Fallon.[6]

In Figure 1 are plotted the values of the pK_a's of a series of oxyacids in solvent S *vs.* the pK_a values in water. The least-squares slope of the line of Figure 1 is 2.2. In a recent paper by Bruice and Turner[4] the rate constants for the nucleophilic attack of acylate ions upon substituted phenyl acetates in water (k_{H_2O}) and solvent S (k_S) were reported. A plot of log k_S *vs.* log k_{H_2O} was found to be linear and also of slope 2.2. That the slope for the ionization of phenols is identical with the slope

(1) Material submitted by R. G. in partial fulfillment of the requirement for the M.S. degree in Chemistry, University of California at Santa Barbara.

(2) C. H. Langford and T. R. Stengle, *J. Amer. Chem. Soc.*, **91**, 4015 (1969).

(3) A. J. Parker, *Chem. Rev.*, **69**, 1 (1969).

(4) T. C. Bruice and A. Turner, *J. Amer. Chem. Soc.*, **92**, 3422 (1970).

(5) C. D. Ritchie and R. E. Uschold, *ibid.*, **89**, 1721 (1967).

(6) H. S. Harned and L. D. Fallon, *ibid.*, **61**, 2374 (1939).

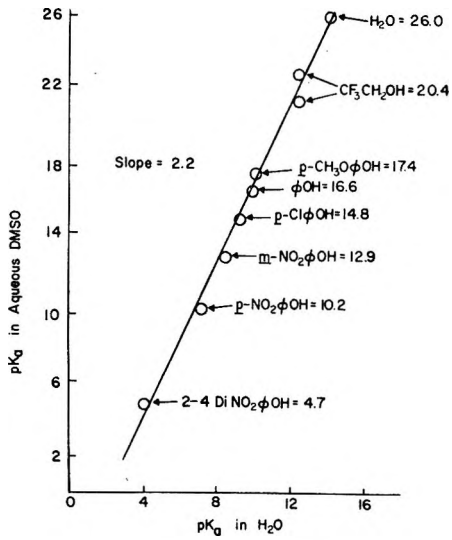

Figure 1. Plot of pK_a of oxyacids in solvent S *vs.* pK_a in water (30°).

for acylate ion attack upon phenyl esters strongly supports a mechanism for acylate ion nucleophilic attack upon phenyl esters in which bond breaking to the leaving phenoxide ion is of paramount importance in the critical transition state. This conclusion reinforces that of Gaetjens and Morawetz[7] who noted that substituent (electronic) effects upon both the ionization of phenol and the rate constants for acylate ion displacements upon phenyl esters were due to changes in entropy (ΔS_i and $\Delta S^{\ddagger}$, respectively) rather than enthalpy. In addition, these workers also pointed out that the ρ values for the ionization of phenols and acylate ion displacement reaction were akin. In reference to eq 1,

$$AcO^- + AcOPh \underset{k_2}{\overset{k_1}{\rightleftharpoons}} CH_3COPh(O^-)(OAc) \xrightarrow{k_3} AcOAc + PhO^- \quad (1)$$

these combined observations support mechanisms in which $k_3 > k_2$ so that nucleophilic attack and departure of phenolate are concerted (no tetrahedral intermediate) or $k_2 > k_3$ so that the formation of the tetrahedral intermediate occurs in an equilibrium step prior to departure of the phenolate ion. That solvent S exhibits a greater sensitivity to electronic effects for both the ionization of phenols and acylate ion nucleophilic displacements upon substituted phenyl acetate may be related to the known greater solvation of charged dispersed systems in DMSO.[3]

On transfer from water to solvent S we find a 10^6-fold rate enhancement for HO^- attack on *p*-nitrophenyl acetate but only a 3.3-fold rate enhancement for trimethylamine attack on *p*-nitrophenylacetate. Large rate enhancements for the alkaline hydrolysis of esters accompanying an increase in the mole fraction of DMSO in DMSO–H_2O systems have been attributed to reduced solvation of the HO^- ion.[8-10] However, conductivity data would indicate that the HO^- ion is not completely desolvated in solvent S. The equivalent conductivities at infinite dilution (Λ_0) of several salts have been determined in solvent S and are listed in Table I.

Table I: Equivalent conductivities at Infinite Dilution (Λ_0) in Solvent S (30°).

Salt	Λ_0
NaCl	34.0 ± 0.2
CsCl	36.5 ± 0.2
Ph_4AsBPh_4	18.5 ± 0.5
CsOH	28.5 ± 0.5
Ph_4AsCl	29.5 ± 0.2

By making the assumption that the equivalent ionic conductivity of tetraphenylarsonium ion equals that of tetraphenylboride ion[11] we may determine the equivalent ionic conductivities of each of the ions listed in Table II. If we assume that the equivalent ionic conductivities are a reflection of the mobility of the ions in solvent S (the resistance to its motion through the solution) then we note that the HO^- ion has a mobility closer in magnitude to that of Ph_4B^- than to Cl^-. Since mobility is a reflection of the size of an ion in solution[11] we are led to conclude that hydroxide ion is heavily solvated in solvent S. Perhaps this finding should not be of great surprise since it has previously been noted that association of carboxylate ions with their conjugate acids occurs in solvent S. The increase in pK_w from 14 to 25 on transfer from H_2O to solvent S is as anticipated for ionization of an acid of type AH on

Table II: Equivalent Ionic Conductivities at Infinite Dilution (λ_0) in Solvent S

Ion	λ_0 ± 0.5
Ph_4B^-	9.3
Ph_4As^+	9.3
Cl^-	20.2
Na^+	13.8
Cs^+	16.3
HO^-	12.2

(7) E. Gaetjens and H. Morawetz, *J. Amer. Chem. Soc.*, 82, 5328 (1960).

(8) E. Tommila and M. L. Murto, *Acta Chem. Scand.*, 17, 1947 (1963).

(9) E. Tommila and I. Palenius, *ibid.*, 17, 1980 (1963).

(10) M. Hojo, M. Utaka and Z. Yoshida, *Tetrahedron Lett.*, No. 1, 25 (1966).

(11) Arguments in favor of this assumption have been presented by: (a) H. S. Harned and B. B. Owen, "The Physical Chemistry of Electrolytic Solutions," 3rd ed, Reinhold, New York, N. Y., 1958, p 232; (b) A. J. Parker in ref 3.

transfer from water to a solvent of lower dielectric constant, and the decrease in pK_a for $(CH_3)_3NH^+$ from 9.76 to 8.6 on transfer from H_2O to solvent S is as anticipated for an acid of type AH^+. The increase of 10^6 in the second-order rate constant for reaction of HO^- with *p*-nitrophenyl acetate is attributable to an increase in the activity of the solvated ion compared to that of the

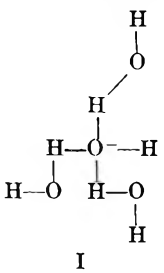

I

transition state. Both the low mobility and enhanced nucleophilicity of the hydroxyl ion in solvent S may be related, at least in part, to a structure as I. Contribution to the high activity of I in solvent S arises from the decreased activity of H_2O in solvent S. The reaction can be written as in (2). For $(CH_3)_3N$ this magnitude

$$HO^-(H_2O)_3 + X \longrightarrow [HO^-X]_{\ddagger} + 3H_2O \quad (2)$$

of rate enhancement is not seen indicating little alteration of the relative activity of ground and transition state on solvent transfer.

Acknowledgment. This work was supported by a grant from the National Institutes of Health. Appreciation is expressed to an unknown referee who suggested we consider structure I.

Electrolyte Viscosities in Associated Solvents[1]

by John P. Bare and James F. Skinner*

Department of Chemistry, Williams College, Williamstown, Massachusetts 01267 *(Received May 5, 1971)*

Publication costs assisted by Williams College

Jones–Dole viscosity *B* coefficients have been determined at 25° for NaI, KI, and CsI in a number of hydrogen-bonded solvents. *B*(NaI) increases from 0.357 to 1.135 for the series of solvents: glycerol, 1,3-propanediol, 1,2-propanediol, methanol, 1-propanol, 2-propanol, 1-butanol, 1-pentanol, and 1-hexanol. This increase has been attributed to a corresponding decrease in the hydrogen-bonded association of the solvents. In the two dihydric alcohols, *B* decreases with increasing crystallographic cation radius, *B*(CsI) being negative. The values of *B*(NaI) in 2-aminoethanol and 2,2′,2″-nitrilotriethanol are similar to the values in the monohydric alcohols, while *B*(CsI) assumes small but positive values in these solvents. *B*(KI) and *B*(CsI) are both more negative in D_2O than in H_2O correlating with the previously reported enhanced association in the former solvent.

Introduction

The concentration dependence of the viscosity of aqueous,[2-4] nonaqueous,[5-7] and mixed solvent[8,9] electrolytic solutions has been interpreted in terms of the semiempirical Jones–Dole equation[10]

$$\eta/\eta_0 = 1 + AC^{1/2} + BC \quad (1)$$

where η and η_0 are the solution and solvent viscosities, C is the molarity, and A and B are adjustable parameters. The square-root term represents the contribution to the viscosity from the ion–ion coulombic interactions, taken into account by Falkenhagen[11] in terms of limiting equivalent conductances and solvent properties.

For monatomic ions in aqueous solution, the *B* coefficient has been interpreted in terms of specific ion–solvent interactions:[2] positive values being attributed to an enhancement of the solvent association by the electrolyte and negative values being attributed to a

(1) This work is based in part on the honors thesis of J. B., 1970.

(2) H. S. Frank and W.-Y. Wen, *Discuss. Faraday Soc.*, **24**, 133 (1957).

(3) R. H. Stokes and R. Mills, "Viscosity of Electrolytes and Related Properties," Pergamon Press, Elmsford, N. Y., 1965.

(4) B. R. Breslau and I. F. Miller, *J. Phys. Chem.*, **74**, 1056 (1970).

(5) G. Jones and H. J. Fornwalt, *J. Amer. Chem. Soc.*, **57**, 2041 (1935).

(6) L. M. Mukherjee, *J. Phys. Chem.*, **74**, 1942 (1970).

(7) R. Gopal and P. P. Rastogi, *Z. Phys. Chem. (Frankfurt am Main)*, **69**, 1 (1970).

(8) D. Feakins, D. J. Freemantle, and K. G. Lawrence, *J. Chem. Soc. D*, 970 (1968).

(9) D. Singh, V. S. Yadav, and B. K. Goel, *Z. Phys. Chem. (Frankfurt am Main)*, **68**, 242 (1969).

(10) G. Jones and M. Dole, *J. Amer. Chem. Soc.*, **51**, 2950 (1929).

(11) H. Falkenhagen and M. Dole, *Phys. Z.*, **30**, 611 (1929).

weakening of the hydrogen bonding in the solvent. In a previous communication from this laboratory,[12] the first negative B values in nonaqueous media were reported.

The present investigation represents an extension of our study of electrolyte viscosities to a variety of alcoholic solvents. While hydrogen-bonded association would be expected to be a significant factor in determining the behavior of all of these solvents and solutions therein, an effort has been made to select solvents in which the relative importance of this phenomenon could be systematically evaluated through viscosity measurements. In studying the properties of the alkali halides in nonaqueous solvents, one is restricted in the choice of solute by the extreme hygroscopicity of the lower formula weight compounds and the low solubility of the higher formula weight compounds below a solvent dielectric constant of about 30. For these reasons, the number of alkali halides whose specific viscosities have been measured is limited.

The purposes of the present study were fourfold. First, importance of the cation in the electrolyte B coefficient in highly structured solvents was elucidated through a study of NaI, KI, and CsI in 1,2-propanediol (ϵ_{20} = 32.0) and 1,3-propanediol (ϵ_{90} = 35.0) and NaI in glycerol (1,2,3-propanetriol) to complement the previous work[12] on KI and CsI in the last solvent. Second, B(NaI) was determined in six monohydric alcohols—methanol, 1-propanol, 2-propanol, 1-butanol, 1-pentanol, and 1-hexanol—to illustrate the effect of increased alkyl chain length in the solvent. Third, viscosities of 2-aminoethanol and 2,2′,2″-nitrilotriethanol (triethanolamine) solutions of NaI and CsI were studied which, in conjunction with B coefficients for these electrolytes in comparable hydroxylic solvents, enabled an estimation of the relative importance of the amino and hydroxyl groups in ion–solvent interactions as exhibited in electrolytic viscosities. Finally, it has been suggested that heavy water (D_2O) is more associated than ordinary water (H_2O), and as this should be reflected in the B coefficients of alkali halides, the viscosities of CsI and KI have been studied in these two solvents.

Experimental Section

Cesium iodide (A. D. Mackay Inc., 99.9%), potassium iodide (J. T. Baker, analyzed reagent) and sodium iodide (Alfa Inorganics, Ultrapure) were used as received, after drying at 110°. While the sodium salt was adequately soluble in the monohydric alcohols of three or more carbons, neither of the other salts was sufficiently soluble for viscosity measurements.

The D_2O (Mallinckrodt, 99.8% isotopic purity) was handled in a drybox and the H_2O was twice distilled. The methanol (Mallinckrodt, anhydrous analytical reagent) was refluxed over magnesium filings under nitrogen for 3 days and fractionally distilled: boiling range of fraction collected, 64.5–64.7 (lit.[13] bp 64.509); density, 0.78652 g/ml (lit.[14] value 0.78655).

The remaining solvents, 1-propanol (A), 2-propanol (B), 1-butanol (C), 1-pentanol (D), 1-hexanol (E), 2-aminoethanol (F), 2,2′,2″-nitrilotriethanol (G), 1,3-propanediol (H), 1,2-propanediol (I), and glycerol (J), were dried in the dark for 3 weeks over one of the following dehydrating agents: Na_2SO_4–K_2CO_3 (I), $CaCl_2$–K_2CO_3 (II), Na_2SO_4 (III). The solvent was then fractionated under dry nitrogen either at 1 atm (heated 75-cm column of glass helices) or at reduced pressure (heated 40-cm Vigreux column), a middle fraction being collected. The purified solvent was stored in the dark under nitrogen. It was necessary to perform two distillations on the 1-hexanol to give a solvent which did not discolor on the solution of the sodium iodide. The details of the individual purifications are shown in Table I.[15–23]

All solutions were prepared by weight in flasks previously flushed with dry nitrogen and were stirred overnight in the dark prior to use. All measurements were made at 25 ± 0.01°. Densities were measured in Sprengel-type pycnometers (22 ml) calibrated with distilled water. Viscosities were measured in a Cannon–Ubbelohde viscometer for the water, heavy water, and methanol solutions and in Cannon–Fenske routine viscometers for the other systems. The viscometers were modified for use in a closed, dry atmosphere. Flow times (400–600 sec) were reproducible to ±0.1 sec.

Specific viscosities, η_{sp}, were determined from

$$\eta_{sp} = \eta_r - 1 = t\rho/t_0\rho_0 \qquad (2)$$

where ρ, ρ_0, t, and t_0 are the densities and flow times for the solution and solvent, respectively. The A and B coefficients were determined from the plots of $\eta_{sp}/C^{1/2}$ against $C^{1/2}$ (Figures 1–4). The linear dependence of solution density on electrolyte molarity was evaluated from

(12) K. Crickard and J. F. Skinner, *J. Phys. Chem.*, **73**, 2060 (1969).

(13) "Organic Solvents, Physical Properties and Methods of Purification," John A. Riddick and Emory E. Toops, Jr., Ed., Interscience, New York, N. Y., 1955.

(14) M. A. Coplan and R. M. Fuoss, *J. Phys. Chem.*, **68**, 1177 (1964).

(15) J. Timmermans, "Physico-Chemical Constants of Pure Organic Compounds," Elsevier, Amsterdam, 1950.

(16) "Handbook of Physics and Chemistry," Robert C. Weast, Ed., 49th ed, Chemical Rubber Publishing Co., Cleveland, Ohio, 1968.

(17) F. Hovorka, H. P. Lankelma, and S. C. Stanford, *J. Amer. Chem. Soc.*, **60**, 820 (1938).

(18) J. N. Pearce and L. F. Berhenke, *J. Phys. Chem.*, **39**, 1005 (1935).

(19) P. W. Brewster, F. C. Schmidt, and W. B. Schaap, *J. Amer. Chem. Soc.*, **81**, 5532 (1959).

(20) "Dictionary of Organic Compounds," Eyre and Spottiswoode Publishers, Ltd., London, 1965.

(21) A. F. Gallaugher and H. Hibbert, *J. Amer. Chem. Soc.*, **59**, 2514 (1937).

(22) T. T. Puck and H. Wise, *J. Phys. Chem.*, **50**, 329 (1946).

(23) H. T. Briscoe and W. T. Rinehart, *ibid.*, **46**, 387 (1942).

Table I: Purification of Solvents[a]

Solvent	Supplier	Drying agent	Boiling range, °C	Density, ρ_0	Refractive index
A	Fisher	II	96.8–97.1 (97.15, 13)	0.79998 (0.79950, 13)	1.3829 (1.3835, 13)
B	Aldrich (99%, anh.)	I	81.0–82.0 (82.40, 13)	0.78093 (0.78095, 13)	1.3747 (1.3747, 13)
C	Eastman (White Label)	I	117.3–117.5 (117.73, 13)	0.80581 (0.80572, 15)	...
D	Eastman	III	138.0–138.2 (138.06, 13)	0.81096 (0.81104, 16)	...
E	Eastman	III	157.4–157.6 (157.47, 13)	0.81583 (0.81556, 17)	...
F	Eastman (White Label)	III	63.8–64.0 (32 mm) (65.0 (5 mm), 18)	1.0117 (1.0117, 19)	1.4533 (1.4539, 20°, 13)
G	Eastman (White Label)	III	168.3–168.8 (1 mm) (175.0 (2 mm), 18)	1.12081 (1.1242, 20°, 16)	1.4832 (1.4852, 20°, 20)
H	Aldrich	I	115.8–115.9 (12.5 mm)	1.04892 (1.050, 21)	1.4380 (1.4396, 20°, 13)
I	Aldrich	III	97.3–97.5 (17 mm)	1.03267 (1.0328, 22)	...
J	Eastman	III	139.2–140.1 (1 mm)	1.25824 (1.2583, 23)	...

[a] Densities and refractive indexes at 25° unless otherwise noted. Literature values and references are in parentheses.

$$\rho/\rho_0 - 1 = kC \qquad (3)$$

Values of A, B, and k, computed by the method of least squares, are given in Table II.[24]

Table II: Solution Parameters at 25°

Electrolyte	Solvent	k	A	B
NaI	Methanol	0.1736	0.028 ± 0.005	0.652 ± 0.010
NaI	1-Propanol	0.1580	0.077 ± 0.005	0.826 ± 0.010
NaI	2-Propanol	0.1651	0.094 ± 0.004	0.842 ± 0.009
NaI	1,3-Propanediol	0.1079	0.0156 ± 0.0005	0.415 ± 0.007
NaI	1,2-Propanediol	0.1049	0.016 ± 0.002	0.475 ± 0.003
NaI	1-Butanol	0.1539	0.099 ± 0.004	0.883 ± 0.007
NaI	1-Pentanol	0.1522	0.085 ± 0.004	0.989 ± 0.007
NaI	1-Hexanol	0.1475	0.032 ± 0.004	1.135 ± 0.008
NaI	Glycerol	0.07796	0.003 ± 0.001	0.357 ± 0.005
NaI	2-Aminoethanol	0.1136	0.010 ± 0.001	0.843 ± 0.007
NaI	2,2′,2″-Nitrilotriethanol	0.09567	0.043 ± 0.005	0.977 ± 0.007
KI	1,2-Propanediol	0.1166	0.037 ± 0.005	0.069 ± 0.002
KI	1,3-Propanediol	0.1125	0.024 ± 0.005	0.053 ± 0.002
KI	Water	0.1227	...	−0.0719
KI	Deuterium oxide	0.1005	...	−0.096
CsI	1,2-Propanediol	0.1938	0.043 ± 0.005	−0.106 ± 0.005
CsI	1,3-Propanediol	0.1937	0.009 ± 0.001	−0.116 ± 0.005
CsI	2-Aminoethanol	0.2021	0.035 ± 0.001	0.385 ± 0.003
CsI	2,2′,2″-Nitrilotriethanol	0.1768	0.024 ± 0.005	0.204 ± 0.010
CsI	Water	0.2017	...	−0.120
CsI	Deuterium oxide	0.1798	...	−0.134

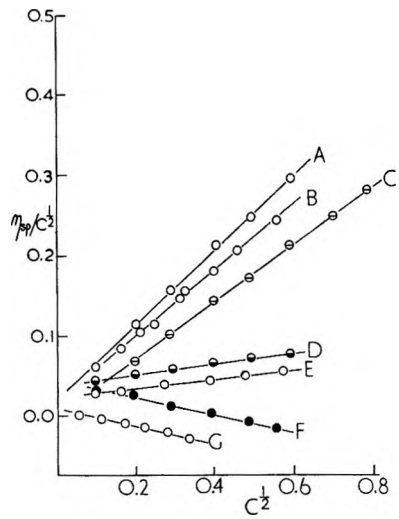

Figure 1. Viscosity B coefficient plot: A, NaI in 1,2-propanediol; B, NaI in 1,3-propanediol; C, NaI in glycerol; D, KI in 1,2-propanediol; E, KI in 1,3-propanediol; F, CsI in 1,2-propanediol; G, CsI in 1,3-propanediol.

Discussion

The presence in one water molecule of two hydroxyl protons and two pairs of nonbonded oxygen electrons results in the unusually high degree of intermolecular association in liquid water at room temperature. A single water molecule can participate in hydrogen bonding simultaneously with four other water molecules. The search for a generally acceptable model on which may be based an explanation of the behavior of liquid water continues in many laboratories. The fact that in dilute aqueous solution, alkali halides of high surface charge density give solutions more viscous than the solvent while those of low surface charge density give

(24) Listings of concentration, density, and specific viscosity will appear immediately following this article in the microfilm edition of this volume of the journal. Single copies may be obtained from the Business Operations Office, Books and Journals Division, American Chemical Society, 1155 Sixteenth Street, N.W., Washington, D. C. 20036. Remit check or money order for $3.00 for photocopy or $2.00 for microfiche.

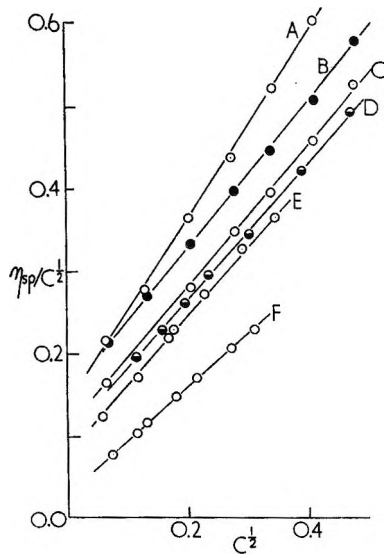

Figure 2. Viscosity B coefficient plot: NaI in 1-hexanol (A), 1-pentanol (B), 1-butanol (C), 2-propanol (D), 1-propanol (E), and methanol (F). The vertical scale has been lifted by 0.05 and 0.10 for 1-pentanol and 1-hexanol, respectively, for clarity.

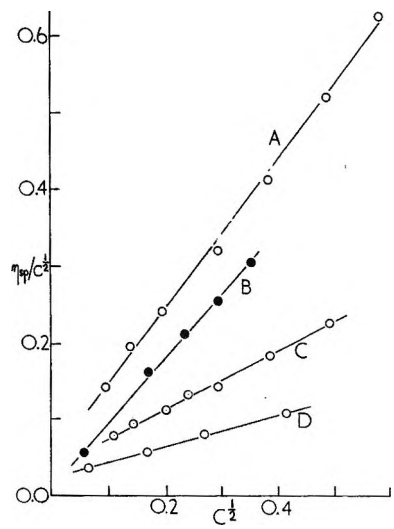

Figure 3. Viscosity B coefficient plot: A, NaI in 2,2′,2″-nitrilotriethanol; B, NaI in 2-aminoethanol; C, CsI in 2-aminoethanol; D, CsI in 2,2′,2″-nitrilotriethanol.

"negative viscosities" or solution viscosities less than the solvent has been explained in terms of the effect of the electrolyte on the quasicrystalline structure of water.[2]

A polyhydric alcohol molecule should also afford the opportunity for extensive intermolecular association, where each hydroxyl group could, in principle, hydrogen bond to two other molecules, resulting in a three-dimensional solvent structure similar to that in water. Table III summarizes the B coefficients for three alkali halides in four polyhydric alcohols and Figure 1 illustrates the validity of eq 1 for these systems. The

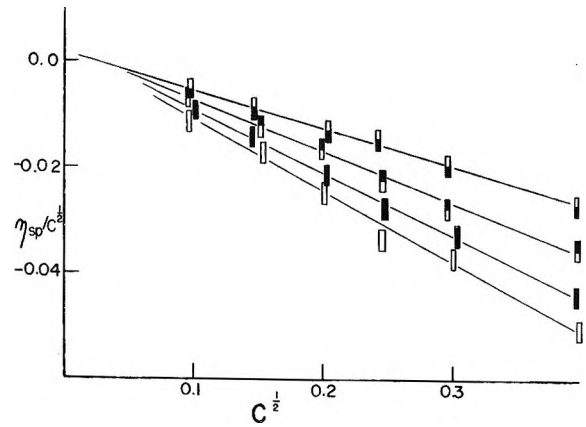

Figure 4. Viscosity B coefficient plot: ■, KI in H_2O; ▣, KI in D_2O; ▮, CsI in H_2O; □, CsI in D_2O.

Table III: B Coefficients in Polyhydric Alcohols at 25°

	NaI	KI	CsI
Glycerol	0.357	−0.185[a]	−0.408[a]
1,2-Ethanediol	...	0.033[a]	−0.080[a]
1,2-Propanediol	0.475	0.069	−0.106
1,3-Propanediol	0.415	0.053	−0.116

[a] Reference 12.

linearity of the $\eta_{sp}/C^{1/2}$ against $C^{1/2}$ plot for NaI in glycerol to concentrations in excess of 0.6 M corroborates our previous findings[12] in this solvent.

Two points can be made from these results. First, the B coefficient becomes less positive with decreasing surface charge density of the cation in agreement with behavior found in water. The cesium salt is the only one to exhibit negative B values in all four solvents, although B(KI) is negative in glycerol and close to zero in the other solvents. Second, the B coefficients in Table III are less positive than those for these electrolytes in any other solvent investigated to date, including those in this study. This suggests that in these four solvents the hydrodynamic effect of ion–solvent interaction is different from that in unassociated or weakly associated solvents, but similar to that exhibited in water. A search for further solvents in which this phenomenon will be present will probably be hampered by decreasing solubility of the lower surface charge density electrolytes with decreasing dielectric constant. Formamide (ϵ_{25} = 109.5) might, however, prove to be an interesting solvent from the point of view of negative or very small B coefficients as several of its properties are similar to those of water.

From a recent study of proton relaxation rates in aqueous and nonaqueous electrolytic solutions, Engel and Hertz[25] reported findings in good agreement with

(25) G. Engel and H. G. Hertz, *Ber. Bunsenges. Phys. Chem.*, 72, 808 (1968).

previous interpretations of positive and negative Jones–Dole B coefficients. In water, 1,2-ethanediol, and glycerol, those electrolytes which exhibited negative viscosity B coefficients also gave solvent–proton relaxation rates faster in solution than in the pure solvents. In methanol, ethanol, formamide, and N-methylformamide, the other solvents studied in which hydrogen bonding might be expected to be significant, evidence for a weakening of solvent structure was not found in the relaxation rate studies.

Intermolecular hydrogen bonding in monohydric alcohols will lead to dimeric or polymeric association[26] depending on the nature of the alkyl group. In neither case, would there result anything resembling the extensive three-dimensional solvent structure described above. These substances would be expected to be intermediate between the polyhydric alcohols and liquids such as dimethyl sulfoxide, propylene carbonate, and acetone where intermolecular interactions would be minimal.

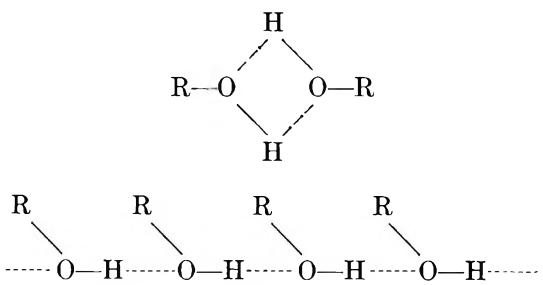

There have been a number of studies of electrolyte viscosities in methanol and ethanol. In three of these studies,[23,27] the data are either too scattered or at too high concentration to permit calculation of B coefficients. Jones and Fornwalt[5] reported values of B of 0.6747, 0.7396, and 0.7635 for KI, KBr, and KCl, respectively, in methanol at 25°. Their plot of $\eta_{sp}/C^{1/2}$ against $C^{1/2}$ for KI shows a distinct break at approximately 0.02 M and then a further linear portion with a smaller slope of 0.42. Cox and Wolfenden[28] reported a value of B of 1.15 for NaI in ethanol at 18°. A recalculation of B, excluding two points of large deviation, gives a value closer to 1.05. The authors are unaware of any viscosity studies on the alkali halides in any of the longer chain alcohols. Table IV gives B values for NaI, chosen because of its suitable solubility, in seven monohydric alcohols.

These results represent the first study of the Jones–Dole B coefficient in a homologous series of solvents. With one exception, the increase in B parallels the increase in the length of the alkyl chain (see Figure 2). As the size of the solvent molecule increases, the polar group remaining the same, the volume of the hydrodynamic entity consisting of the ion and the oriented solvent molecules will be expected to increase. Even in 1-hexanol a substantial degree of orientation of the hydroxyl groups about the cation must be present in order that the electrolyte dissolve approciably. Janz[29] reported viscosity data for NaI in acetonitrile, but again the concentrations were too great to permit an evaluation of B for comparison with the present work. Feakins[30] reported values of 0.608 and 0.573 for NaCl and NaBr in N-methylformamide, from which a value of 0.53 could be approximated for NaI. The B(NaI) values in the monohydric alcohols are, therefore, more positive than any values reported in other solvents.

Table IV: B Coefficients of NaI in Monohydric Alcohols

Methanol	0.652
Ethanol	1.15[a] (1.05)
1-Propanol	0.826
2-Propanol	0.842
1-Butanol	0.883
1-Pentanol	0.989
1-Hexanol	1.135

[a] Reference 28, 18°. Recalculation gives 1.05.

As part of our investigation of associated solvents, it was thought that the ethanolamines would present an interesting comparison with simple alcoholic solvents. These solvents have received little attention. Pearce and Berhenke[18] reported the dipole moments of the mono-, di-, and triethanolamines. Briscoe[31] reported some conductance results in monoethanolamine which were later found to be in error by Brewster[19] who made more careful correction for solvent conductance. Diethanolamine is a solid at 25° and therefore could not be included in the present study.

The B coefficients (see Table II) show the same strong dependence on cation, B(NaI) − B(CsI) being 0.458 and 0.773 in 2-aminoethanol and 2,2′,2″-nitrilotriethanol, as has been found in the highly associated polyhydric alcohols, but in all cases the B values are positive. Even in 2,2′,2″-nitrilotriethanol, a solvent similar to glycerol in its physical properties, B(CsI) is small but positive (0.204). The B(CsI) values of 0.385 and 0.204 in these two associated solvents are significantly below the value of 0.68 in dimethyl sulfoxide,[32] a solvent in which hydrogen bonding would not be expected to be present.

(26) (a) H. Eyring, M. S. Jhon, J. Grosh, and E. R. Van Artsdalen, *J. Chem. Phys.*, **47**, 2231 (1967); (b) M. Saunders and J. B. Hyne, *ibid.*, **29**, 1319 (1958); (c) G. E. McDuffie, Jr., and T. A. Litovitz, *ibid.*, **37**, 1699 (1962); (d) L. H. Thomas and R. Meatyard, *J. Chem. Soc.*, 1986 (1963).

(27) (a) F. H. Getman, *J. Am. Chem. Soc.*, **30**, 1077 (1908); (b) F. K. Ewart and H. R. Raikes, *J. Chem. Soc.*, 1907 (1926).

(28) W. M. Cox and J. F. Wolfenden, *Proc. Roy. Soc. Ser. A*, **145**, 475 (1934).

(29) R. P. T. Tomkins, E. Andalaft, and G. J. Janz, *Trans. Faraday Soc.*, **65**, 1906 (1965).

(30) D. Feakins and K. G. Lawrence, *J. Chem. Soc. A*, 212 (1966).

(31) H. T. Briscoe and T. P. Dirkse, *J. Phys. Chem.*, **44**, 388 (1940).

(32) M. D. Archer and R. P. H. Gasser, *Trans. Faraday Soc.*, **62**, 3451 (1966).

The B(NaI) values of 0.826, 0.843, and 0.415 in 1-propanol, 2-aminoethanol, and 1,3-propanediol, respectively, suggest that from the point of view of viscosity, the effects of the methyl and amino groups in the 2 position are indistinguishable, while the second hydroxyl group produces a much greater degree of solvent structure, disrupted by the electrolyte, giving the smaller value of 0.415.

A substantial amount of evidence[33-35] suggests that at room temperature, the intermolecular hydrogen bonding is more extensive in heavy water (D_2O) than in ordinary water (H_2O). For example, the viscosity (25°) of D_2O (1.096 cP) is about 20% greater than that of H_2O (0.890 cP). The temperatures of maximum density[33] of D_2O and H_2O are 11.23 and 3.98, respectively, suggesting that the quasi-crystalline solvent structure is more thermally stable in the deuterated solvent than in the protonated solvent.

A number of investigations of the properties of electrolytes in D_2O have been made.[36-38] The viscosities of D_2O solutions of various alkali metal salts have recently been reported.[39,40] However, in both cases, the concentrations used were greater than those for which the Jones–Dole equation is thought to be valid.

The B coefficients for the present investigation, together with values for several quaternary ammonium halides in H_2O[3] and D_2O,[37] are given in Table V. As far as the authors know, a comparison of the latter values has not been made. Although the viscosities of H_2O solutions of CsI[41] and KI[42] have been reported, it was decided to repeat the measurements in this laboratory for consistent comparison with the D_2O results.

Table V: B Coefficients in H_2O and D_2O (25°)

Electrolyte	H_2O	D_2O
KI	−0.0719	−0.096
	−0.0755[a]	
CsI	−0.120	−0.134
	−0.118[b]	
$(CH_3)_4NBr$	0.0855	0.08
$(C_2H_5)_4NBr$	0.349	0.3I
$(C_3H_7)_4NBr$	1.06	0.79
$(C_4H_9)_4NBr$	1.36	1.26

[a] Reference 42. [b] Reference 41.

The present values of the B coefficients in H_2O are in satisfactory agreement with the literature values. The values in D_2O for the potassium and cesium salts are approximately 30 and 10%, respectively, more negative than the corresponding H_2O values. This suggests that these electrolytes destabilize the solvent association to a greater extent in D_2O. Figure 5 compares the present results on KI in D_2O with those of Selecki.[40] It is interesting to note that the two most

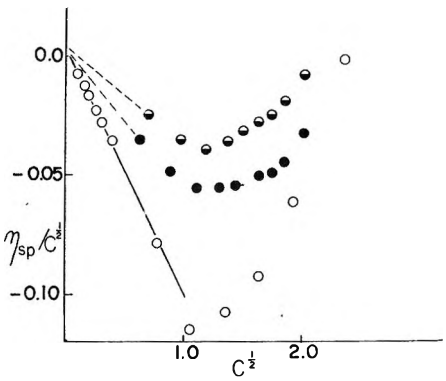

Figure 5. Viscosity B coefficient plot: ○, KI in D_2O; below $C^{1/2} = 0.5$, this work; above $C^{1/2} = 0.5$, ref 40; ◒, CsCl in H_2O, ref 39; ●, CsCl in D_2O, ref 39.

dilute points in Selecki's work are approximately collinear with the present results. Ostroff's[39] results on CsCl in H_2O and D_2O are also shown in Figure 5. The Falkenhagen expression[11] would predict very similar values of A, the ordinate intercept on this plot, for CsCl in the two solvents, so it appears probable that work at lower concentrations would show a more negative B(CsCl) in D_2O than in H_2O. The minimum and subsequent increase above about 1 M illustrate the need in the Jones–Dole equation for terms of higher order in concentration.

The B coefficients for the quaternary ammonium salts are less positive in D_2O than in H_2O in agreement with the alkali halide results.

When the present results are viewed in the light of the literature on viscosity B coefficients for alkali halides in aqueous and nonaqueous media, some tentative generalizations can be made. The interpretation of aqueous B coefficients presented by Frank and Wen[2] in terms of "structure makers" and "structure breakers" appears to be sound and has been widely accepted. Stokes[3] has utilized the Frank–Wen model for ion–solvent interactions in suggesting an explanation of electrolytic viscosities based on three separate contributions to the B coefficient: η^E, the viscosity increment resulting from the size and shape of the ions; η^A, an increase in viscosity resulting from ordering of

(33) G. Nemethy and H. A. Scheraga, *J. Chem. Phys.*, **41**, 680 (1964).
(34) M. Falk and T. A. Ford, *Can. J. Chem.*, **44**, 1699 (1966).
(35) H. A. Rizk and Y. M. Girgis, *Z. Phys. Chem. (Frankfurt am Main)*, **65**, 269 (1969).
(36) J. Greyson, *J. Phys. Chem.*, **66**, 2218 (1962); **71**, 2210 (1967).
(37) R. J. Kay and D. F. Evans, *ibid.*, **69**, 4216 (1965).
(38) C. G. Swain and D. F. Evans, *J. Amer. Chem. Soc.*, **88**, 383 (1966).
(39) A. G. Ostroff, B. S. Snowden, Jr., and D. E. Woessner, *J. Phys. Chem.*, **73**, 2784 (1969).
(40) A. Selecki, B. Tyminski, and A. G. Chmielewski, *J. Chem. Eng. Data*, **15**, 127 (1970).
(41) G. Jones and H. J. Fornwalt, *J. Amer. Chem. Soc.*, **58**, 619 (1936).
(42) M. Kaminsky, *Z. Phys. Chem. (Frankfurt am Main)*, **5**, 154 (1955).

the solvent molecules in the immediate vicinity of the ions as a result of the ionic field; and finally, η^D, a decrease in the solvent viscosity as a result of the disruptive presence of the ions. For alkali halides, the magnitude of η^E will reflect the extent of the solvation and the size of the solvent molecules in the cosphere of the ions. The relative sizes of the three terms resulting from ion–solvent interaction will determine the size and sign of the B coefficient.

In water, the B coefficients are all numerically small, ranging from B(LiCl) of 0.140 to B(CsI) of −0.120, and because the contribution to B from the η^E term will be small, the viscosity will be determined by the relative sizes of the η^A and η^D terms in the Stokes expression. If the structure enhancement term predominates, the B value will be positive while if structure disruption predominates, B will be negative. Hence, the sign of B has been used to distinguish the two classes of electrolytes. It should be noted, however, that this approach may require certain modifications in discussion of nonaqueous solutions.

Very little has been said about the applicability of the Frank–Wen model and the Stokes partition of the B coefficient for nonaqueous solutions. In these cases, the polar solvent molecules are larger than the water molecule and the ionic cosphere will be larger, giving more importance to the η^E term. Even if η^D is larger than η^A, the overall sign of B may be positive. The authors would suggest that in nonaqueous solvents, it is not possible to say that only when B is negative is the electrolyte participating in a net structure-breaking interaction with the solvent. For example, the small positive values of B(CsI) of 0.385 and 0.204, relative to the B(NaI) values, in 2-aminoethanol and 2,2′,2″-nitrilotriethanol should probably be interpreted as evidence for predominance of the η^D term over the η^A term with the η^E term fairly large (and positive) for both electrolytes.

In the interest of brevity, a complete tabulation of all the B values considered will not be made, but the relevant literature will be cited. First, fairly extensive work on the electrolytes NaI, KI, and CsI shows the wide range of values which the Jones–Dole coefficient can assume for a given electrolyte. B(KI) varies from −0.0719 in water to 1.30 in N-methylpropionamide[7] while B(CsI) varies from −0.408 in glycerol[12] to 0.68 in dimethyl sulfoxide.[32] This variation points to the complexity of the hydrodynamic phenomena for which an explanation is sought. Second, there is a fairly clear distinction between solvents in which the B coefficient shows a dependence on the alkali halide in question and those solvents in which the alkali halide B coefficients are all rather close together. The authors have interpreted this as evidence for the relative importance of intermolecular solvent association. In water, the polyhydric alcohols, and the ethanolamines, the results to date show that B always becomes less positive with increase in cation or anion size. In water, glycerol, 1,2-propanediol, and 2,2′,2″-nitrilotriethanol, the difference B(NaI) − B(CsI) is 0.128, 0.765, 0.581, and 0.773, respectively. Only in these solvents where B appears to depend on both the solvent and the electrolyte are negative values of B found. The dependence of B on electrolyte in dimethylformamide[7] (LiCl, 0.59; KI, 1.10; 25°) is difficult to explain in terms of solvent association because hydrogen bonding should not be possible in this case.

In the second group of solvents, where solvent association would be less pronounced, are dimethyl sulfoxide, the monohydric alcohols, N-methylformamide, N-methylacetamide,[7] N-methylproprionamide, and propylene carbonate.[6] In methanol, B values of 0.652, 0.7635, 0.7396, and 0.6747 have been reported[5] for NaI, KCl, KBr, and KI, respectively. In N-methylformamide values of 0.59, 0.608, 0.573, 0.634, 0.590, 0.56, and 0.60 have been reported[30,43] for LiCl, NaCl, NaBr, KCl, KBr, KI, and CsI while in N-methylproprionamide values of 1.25, 1.30, and 1.37 have been reported[7,44] for LiCl, KI, and KCl. In contrast to what was observed in the highly associated solvents, the B coefficients for the different alkali halides, in a given solvent, show only a small variation with surface charge density. Where comparison is possible in methanol, N-methylformamide, and N-methylproprionamide, B increases slightly with increasing cation size, in marked opposition to the trend in water, the polyhydric alcohols and the ethanolamines where the larger cations are the better "structure breakers." The hydrodynamic effect of cation–solvent interaction is quite different in this second group of solvents. The B coefficients decrease slightly in these solvents with increasing anion size.

It should be noted that in both groups of solvents, a given electrolyte will show considerable variation in the B coefficient in different solvents.

A simple explanation of the large variation in B with solvent for a given electrolyte and, secondly, of the classification of solvents into two groups depending on the sensitivity of B to the nature of the electrolyte, is not possible. One would predict that both η^E and η^A would become less positive and η^D would become more negative as the ion size increased with the corresponding decrease in coulombic field at the surface of the ion. These changes would all be expected to reduce B and would explain the sensitivity of B to the nature of the electrolyte in the highly associated solvents. In the unassociated solvents, η^A and η^D would be negligible and the magnitude of B would reflect primarily the size of the solvated ions. For a given solvent, one would expect the larger ions to be less

(43) P. P. Rastogi, *Bull. Chem. Soc. Jap.*, **43**, 2442 (1970).
(44) T. B. Hoover, *J. Phys. Chem.*, **68**, 876 (1964).

solvated and therefore to exhibit smaller B values. For a given electrolyte, the size of the η^E contribution could be interpreted in terms of the relative sizes of the solvent molecules in the solvation shell. As pointed out already, the B(NaI) values in the monohydric alcohols, with one exception, increase with increasing size of the solvent molecules. The values[7,43] of B(KI) of 0.56, 1.01, and 1.30 in N-methylformamide, N-methylacetamide, and N-methylproprionamide also appear to reflect the size of the solvent molecule. Some hydrogen-bonded association would be present in the amides, and it would probably be most pronounced in the least sterically hindered N-methylformamide. A case could be made for explanation of the increase in B in the amides as a result of decreasing importance of the η^D term, relative to the η^A term, in going from N-methylformamide to N-methylproprionamide.

Finally, the values of B(NaI) of 0.977, 0.826, 0.415, and 0.357 in 2,2′,2″-nitrilotriethanol, 1-propanol, 1,3-propanediol, and glycerol present an interesting series. The monohydric alcohol presumably represents a case where η^A and η^D are not important and B reflects the size of the solvated shell of the ion through the η^E contribution. In 1,3-propanediol, the ions would still be expected to interact with only one end of the solvent molecule and the size of the ionic cosphere would be similar to that in 1-propanol. The decrease in B(NaI) of 0.411 reflects the dominance of the η^D term over the η^A term, what Frank and Wen have referred to in water as net "structure breaking."[2] It would be unwarranted to predict the nature of the solvation in glycerol where the ion is exposed to a highly polar, strongly associated medium. It is unlikely that the presence of any ion could increase the degree of solvent association in a solvent already so extensively hydrogen bonded, making the η^A term negligible. Although η^D would be expected to be more important in glycerol than in 1,3-propanediol, it is not possible to estimate the relative importance of changes in η^E and η^D in bringing about the further small decrease of 0.058 in B(NaI). B(NaI) in 2,2′,2″-nitrilotriethanol (0.977) is an interesting example. The solvent molecules are large with four polar sites possible for ion–solvent interaction. The difference, B(NaI) − B(CsI), of 0.773 suggests that specific ion–solvent interactions are important. However, it again seems unlikely that an ion could increase the hydrogen bonding in a solvent already so associated. The value of B will be determined by the relative magnitudes of the η^E and η^D contributions, the former being more important for NaI giving $B = 0.977$ while the two terms achieve more equal weight for CsI giving a B value of 0.204.

The speculative nature of these suggestions emphasizes the need for much more investigation of ion–solvent interactions for a wider variety of electrolytes in nonaqueous media.

Acknowledgment. The authors gratefully acknowledge funds made available as part of a grant to Williams College by the Alfred P. Sloan Foundation.

Mobility of Excess Electrons in Liquid Hydrocarbon Mixtures[1]

by R. M. Minday,* L. D. Schmidt, and H. T. Davis

Department of Chemical Engineering and Materials Science, University of Minnesota, Minneapolis, Minnesota 55455 *(Received July 21, 1971)*

Publication costs assisted by the Petroleum Research Fund

In an effort to further elucidate the mechanism of excess electron transport in nonpolar hydrocarbons, electron mobilities are studied in mixtures of *n*-hexane and neopentane in both liquid and vapor and in liquid toluene, a molecule with a permanent dipole moment. Mobility measurements in the liquid mixtures as functions of mole fraction and temperature show that the mobility varies as $\exp[-x_h E/RT]$ where x_h is the mole fraction of hexane and E is a constant. The mobility in liquid toluene is almost the same as in benzene, showing that the permanent dipole moment of toluene does not significantly alter the transport process. From these results it is concluded that, while the mechanism of electron transport in liquid hydrocarbons appears to involve short lived traps in the fluid as suggested previously, these traps must be a collective property of the fluid rather than being associated with individual molecules.

Introduction

Stable excess electronic-charge carriers have recently been observed in carefully purified hydrocarbon liquids,[2] but their properties are considerably more complex than in the rare gas liquids.[3,4] In the alkanes the room temperature mobilities vary by as much as three orders of magnitude between isomers: from 0.07 in pentane to 70 $cm^2/(V\ sec)$ in neopentane. Electronic carriers have also been observed in liquid olefins and aromatics, with mobilities of 3.6 in 2-methylbutene-2 and 0.6 $cm^2/(V\ sec)$ in benzene.[1] Electron mobilities in all the hydrocarbons examined to date appear to show an Arrhenius dependence on temperature

$$\mu = \mu_0 e^{-E/RT} \qquad (1)$$

and possess larger activation energies in those liquids with lower mobilities.

The purpose of this paper is to describe additional experiments which give further insight into the mechanism of electron transport in hydrocarbon liquids. A preliminary report of these results has been published.[5]

Room temperature electron mobilities have been measured as a function of mole fraction in mixtures of *n*-hexane and neopentane; the temperature dependence of the mobilities in the mixtures has also been measured to determine activation energies. Free electrons have also been produced in liquid toluene, a molecule which possesses a permanent dipole moment; these results are compared with those in benzene, a molecule structurally similar to toluene but with no permanent dipole moment. Electron drift velocities were also measured in vapors of *n*-hexane and neopentane as a function of pressure and field to determine electron mobilities in these systems at low densities.

Experimental Section

The hydrocarbon liquids were purified in an ultrahigh vacuum system by contact with zeolite molecular sieves and evaporated barium films.[2a] Mobilities in the liquids were determined from the time of flight of photoinjected electrons across a drift space in a uniform electric field. The time of flight was measured by periodically interrupting the electron flow by either chopping the ultraviolet light source to the photocathode (single shutter method) or by electron shuttering within the mobility cell through use of a system of grids between the cathode and collector (double shutter method). Earlier publications[2a] give complete descriptions of the purification procedures and the two techniques of mobility measurement; however, the procedures followed in the hexane–neopentane mixing experiment involve techniques which require discussion in some detail.

The mixing experiment was performed in a system that contained two chambers connected to each other and to the pumps by three high-vacuum metal valves. One valve isolated from the pumps a manifold that connected the valves leading to the two sample chambers. Each chamber contained barium film getters, a cell for mobility measurements, and a cell calibrated for volume measurements. Hexane and neopentane samples of ~50 cm^3, >99 mol% initial purity (Phillips Petroleum Co.), were separately purified until electronic charge carriers were observed in each. Before any mixing, the mobility for each pure liquid was determined in

* Address correspondence to this author at the Esso Research and Development Laboratory, Linden, N. J.

(1) Acknowledgment is made to the donors of the Petroleum Research Fund, administered by the American Chemical Society–Petroleum Research Fund Fellows.

(2) (a) R. M. Minday, L. D. Schmidt, and H. T. Davis, *J. Chem. Phys.*, **50**, 1473 (1969); **54**, 3112 (1971); (b) W. F. Schmidt and A. O. Allen, *J. Chem. Phys.*, **50**, 5037 (1969); **52**, 4788 (1970).

(3) L. S. Miller, S. Howe, and W. E. Spear, *Phys. Rev.*, **166**, 871 (1968).

(4) J. A. Jahnke, L. Meyer, and S. A. Rice, *ibid.*, *A*, **3**, 734 (1970).

(5) R. M. Minday, L. D. Schmidt, and H. T. Davis, *Phys. Rev. Lett.*, **26**, 360 (1971).

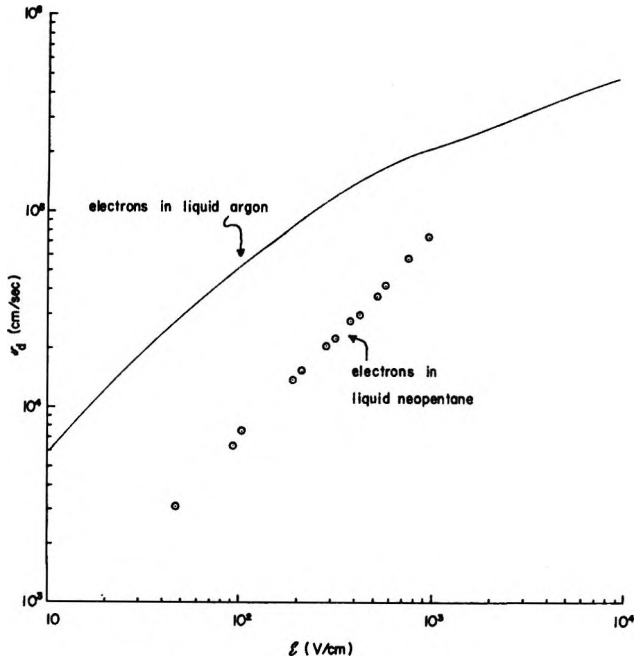

Figure 1. Plot of electron drift velocity in liquid neopentane *vs.* electric field. Drift velocities were measured using the electronic double shutter method. The solid line indicates measured drift velocities in liquid argon.[3] The variation of v_d with $\mathcal{E}$ shows that electrons in the polyatomic neopentane remain at thermal energy even at high fields.

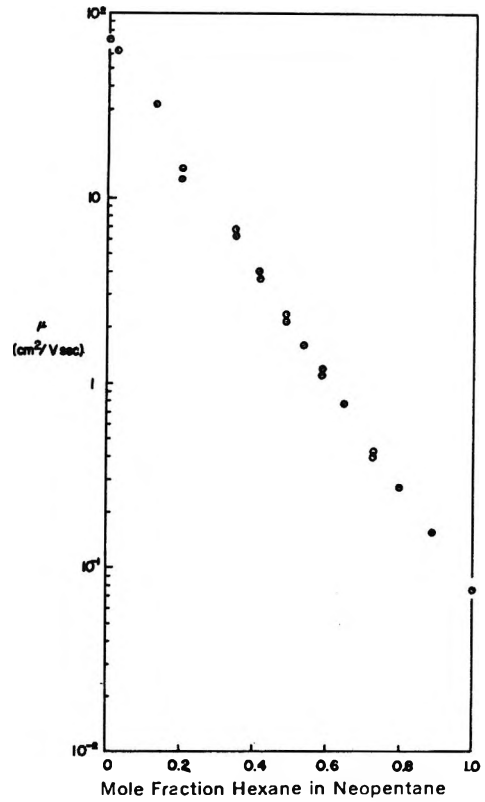

Figure 2. Plot of mobility *vs.* mole fraction of *n*-hexane in neopentane–hexane mixtures at 300°K.

the double shutter cell and the initial number of moles of each was determined from volume measurements and the densities. Inaccuracies of the double shutter method associated with measurement of grid spacings and with distortion of the electric field are estimated to be less than ±10%, but the precision obtainable with this method is ±2% in a given cell.

Portions of one liquid were cryogenically pumped from one sample chamber to another through the manifold, after which the valves were closed and the liquids allowed to warm to room temperature. The mole fraction of the mixture was determined from the volume of liquid transferred. Mobility measurements were made over time periods of several hours to ensure that the liquids were thoroughly mixed and at thermal equilibrium. Activation energies of the mixtures were determined by measuring the mobility as a function of temperature in the double shutter cell immersed in various baths in the temperature range from 180 to 300°K. The mixing experiment was performed twice: in one experiment successive amounts of *n*-hexane were added to neopentane, in another neopentane was added to *n*-hexane.

It was often desirable to obtain other mole fractions after the liquids were mixed. This could be accomplished by slow distillation from one sample chamber to another since the volatility of neopentane is more than seven times that of hexane. Assumption of Raoult's law and ideal differential distillation allowed determination of the mole fractions in the residue and distillate from volume measurements.

Vapor phase mobility measurements in hexane and neopentane were performed in an identical double shutter cell. The mobility was measured as a function of $\mathcal{E}/p$, the electric field divided by the pressure in the cell. Different pressures were obtained by maintaining the vapor-filled cell at 300°K in contact with a chamber containing the liquid thermostated at a known lower temperature. The pressure in the vapor cell was then calculated from the vapor pressure of the liquid at the thermostat temperature corrected for transpiration.

Results

Hexane–Neopentane Mixtures. Room Temperature Mobilities. Prior to the mixture experiment, mobilities in the pure components were determined by double shutter measurements. The mobility in *n*-hexane was found to be 0.076 cm²/(V sec), very close to the values reported previously.[2] Figure 1 shows the drift velocity in neopentane as a function of field. The mobility of 70 cm²/(V sec) is somewhat above the value previously reported,[2b] and is found to remain independent of field between 19 and 950 V/cm.

Figure 2 shows a plot of the logarithm of the mobility *vs.* the mole fraction of hexane in hexane–neopentane mixtures. The data lie on a straight line indicating that the mobility in the mixture can be expressed very well by an equation of the form

$$\mu_{mix} = \mu_{np} e^{Ax_h} \quad (2)$$

where $\mu_{np} = 70$ cm²/(V sec) is the mobility in pure neopentane, $A = -6.8$ is the slope of the line in Figure 2, and x_h is the mole fraction of hexane.

In Figure 1 we also show the electron drift velocity in liquid argon[3] at its normal boiling point. It is evident that v_d in argon (and in the other rate gas liquids) deviates from a linear dependence on $\mathcal{E}$ for $v_d > 10^5$ cm/(sec) while v_d in liquid neopentane remains precisely proportional to field up to at least 10^5 cm/sec. Even more striking are the measurements in liquid tetramethylsilane[2b] for which the drift velocity is constant up to $v_d = 10^6$ cm/sec. Deviations from linearity are due to excess kinetic energy of the electrons at high fields.[3,6] Above 10^5 cm/sec the data in the rare gases can be fit quite well by the $\mathcal{E}^{1/2}$ dependence predicted by the Schottky theory of hot electrons.[3] The absence of these deviations in the polyatomic fluids indicates that electrons remain at thermal energy even at very high fields and drift velocities. This is undoubtedly associated with the greater efficiency of energy transfer between electrons and the polyatomic molecules of the fluid either due to inelastic collisions or trapping.

Temperature Dependence. The temperature dependences of the mobilities are shown in Figure 3 for neopentane, 2-methylbutene-2, hexane, and two hexane–neopentane mixtures. Curves of log μ *vs.* $1/T$ are shown in compressed form to allow comparison on a single graph and extrapolation to $1/T = 0$; the actual determination of activation energies was performed on graphs with expanded scales. It is seen that data for all systems can be described quite well by an Arrhenius expression. The activation energies in kcal mol^{-1} for the pure liquids were 0.5 ± 0.1 in neopentane, 2.6 ± 0.3 in 2-methylbutene-2, and 4.3 ± 0.3 in hexane, while in the hexane–neopentane mixtures they were 1.6 ± 0.1 for $x_h = 0.35$ and 2.9 ± 0.15 for $x_h = 0.66$. It is uncertain whether the mobility in pure neopentane is truly given by an Arrhenius expression because the temperature range over which neopentane is liquid is small and the mobility varies only slightly with temperature. The possibility exists for some other temperature dependence for neopentane. For the other liquids the temperature dependences could only be fit assuming an Arrhenius dependence.

Figure 4 shows that the activation energy in mixtures of hexane and neopentane varies almost linearly with the mole fraction of hexane. In fact all data except that for neopentane can be fit by a straight line passing

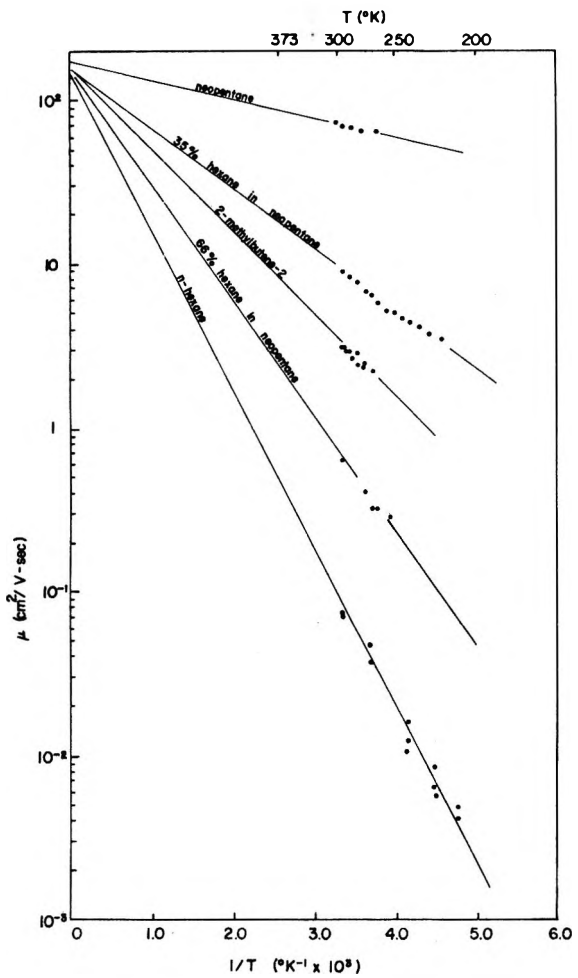

Figure 3. Arrhenius plots of the mobilities in various liquid hydrocarbons. All curves lie on straight lines which extrapolate to $\mu_0 \simeq 150$ cm² (V sec) at $1/T = 0$.

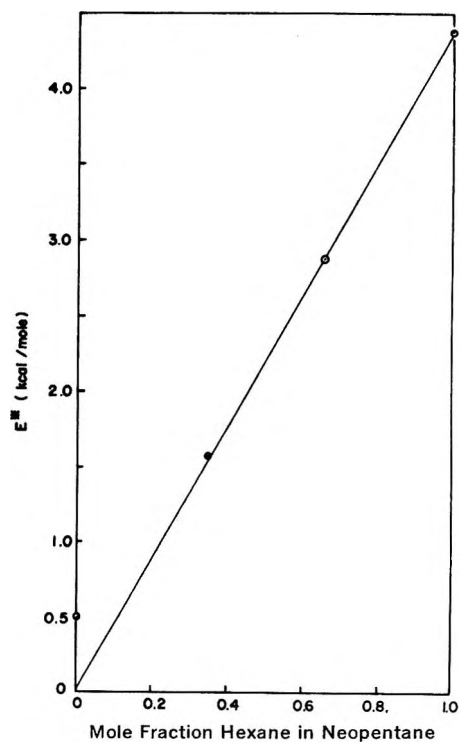

Figure 4. Variation of the mobility activation energy with x_h in hexane–neopentane mixtures.

(6) M. Cohen and J. Lekner, *Phys. Rev.*, **158**, 305 (1967).

through the origin; this suggests that the activation energy in neopentane may be zero and that the observed temperature dependence may have other causes.

The experimental results for electron mobilities in liquid *n*-hexane and neopentane mixtures may be summarized by the expression

$$\mu = \mu_{np} e^{-x_h E_0/RT} \quad (3)$$

with E_0 = 3.7–4.3 kcal/mol.

Toluene. Single shutter measurements of the drift velocity in toluene at fields between 1.6 and 3.3 kV/cm gave a mobility of 0.54 ± 0.1 cm²/(V sec). This mobility is only slightly below the value of 0.6 ± 0.1 cm²/(V sec) measured in benzene.[2a]

Purification of toluene, as well as benzene,[2a] was considerably more difficult than for the alkanes; many cycles of barium contact and vacuum pumping were required before electronic charge carriers were observed. At best, the current due to electrons was no more than 20% of the total current measured in the mobility cell. The remaining 80% of the current was ionic and probably resulted from electron scavenging impurities which could not be removed. All currents were shown to originate at the cathode, however, because reversing the voltage polarity caused reduction of currents by several orders of magnitude. Because electron currents were so low in toluene and benzene, accuracy of the mobility measurements was not as great as in the other liquids studied, and it was not possible to determine the temperature dependences of the mobilities.

Electron Mobilities in Gaseous Hydrocarbons. To determine whether the large difference in the mobilities between alkane isomers is only observed at the high densities of the liquids rather than being associated with radically different scattering cross sections for the molecules, electron drift velocities were also measured in *n*-hexane and neopentane vapors using the double shutter method. Extensive mobility studies have been carried out for simple gases.[7] Cottrell and Walker[8] have measured mobilities in polyatomic gases such as CH_4, C_2H_6, and C_2H_4, but to our knowledge no low-field measurements have been reported in the larger alkanes.

Room temperature drift velocities in pure *n*-hexane and neopentane vapors *vs.* $\mathcal{E}/p$ are shown in Figure 5. All data points for both systems lie on straight lines passing through the origin. In mixtures of *n*-hexane and neopentane vapors the drift velocity varied *linearly with mole fraction* as expected for single molecule scattering.

The temperature dependence of the drift velocity in *n*-hexane was also measured between 250 and 320°K. At constant $\mathcal{E}/p$ the drift velocity increased slightly with increasing temperature: a $T^{+3/2}$ dependence fit the data fairly well over this range. If the electron molecule scattering cross section were determined entirely by the polarization potential, a T^{+1} dependence would be observed. The observed dependence implies

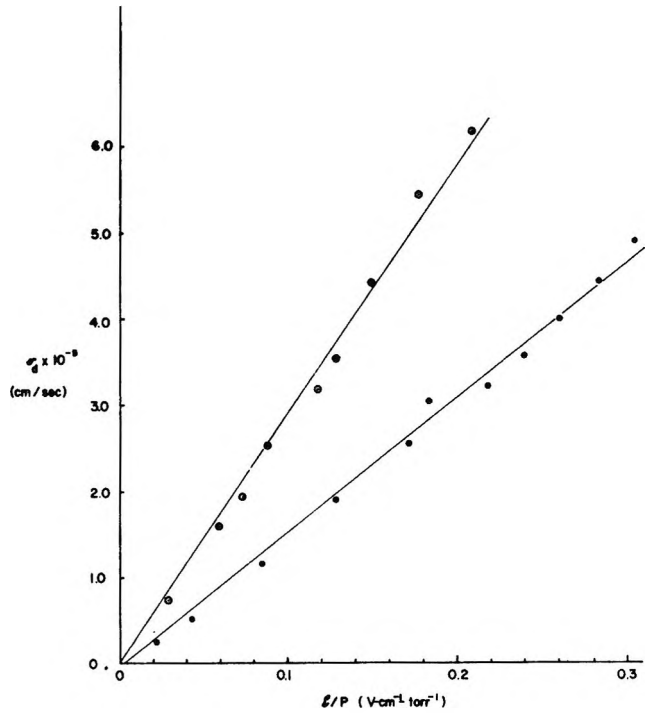

Figure 5. Drift velocity versus $\mathcal{E}/p$ for electrons in gaseous *n*-hexane (upper curve) and neopentane (lower curve) at 300°K.

that the scattering potential is a little "softer" than the polarization potential.

From the gas data it is clear that none of the anomalies in the electron mobilities found in these liquids are observed at low densities: the mobilities are almost the same for different isomers, the mobility in mixtures varies linearly with mole fraction, and the temperature dependence shows no activation energy.

It is also interesting to extrapolate the gaseous drift velocities up to the liquid densities to determine what the mobilities in liquids would be if electron scattering at high density were from isolated molecules. The data shown in Figure 5 give "liquid" mobilities of 30 and 15 cm²/(V sec) for *n*-hexane and neopentane, respectively. It should also be noted that in contrast to the liquids the mobility in hexane is slightly *higher* than in neopentane; this is as expected because the angle averaged cross section for the linear molecule should be slightly smaller than for the almost spherical neopentane molecule.

Discussion

Although no quantitative theory presently exists which explains the behavior of excess electrons in hydrocarbons, the fact that the mobilities obey an Arrhenius temperature dependence argues strongly that electron transport involves trapping or localized states. The temperature and composition dependences ob-

(7) H. S. W. Massey and E. H. S. Burhop, "Electronic and Ionic Impact Phenomena," Oxford University Press, London, 1952.

(8) T. L. Cottrell and I. C. Walker, *Trans. Faraday Soc.*, 61, 1585 (1965).

served in liquid *n*-hexane and neopentane mixtures (and summarized by eq 3) allow one to conclude that the trapping process giving rise to the activation energy of the mobility is a collective effect. If this were not true, *i.e.*, if the activation process were a single molecule process (*e.g.*, short-lived negative ion state, rotational resonance, etc., of a single molecule), then the activation energy at low neopentane concentration should be approximately equal to the *n*-hexane activation energy in contradiction to our observation that the activation energy is proportional to the mole fraction of *n*-hexane. In fact, eq 3 requires that the activation energy E^* of the mixture be of the form

$$E^* = E_h x_h + E_{np} x_{np} \tag{4}$$

where E_h and E_{np} are the activation energies of pure hexane and neopentane, respectively. Thus, as in water, ammonia and amines, the electron trap in hydrocarbons involves many molecules acting collectively. However, unlike the polar liquids, the long-range Landau potential, of the form

$$V = -\frac{e^2}{r}\left[\frac{1}{D_s} - \frac{1}{D_{op}}\right] \tag{5}$$

is not important in forming the trap since D_s and D_{op}, the static and optical dielectric constants, are very nearly equal for the hydrocarbons studied here. The traps must be due to local configurations of groups of molecules whose group-electron potential energy is favorable for trapping the electron.

We have previously suggested the following mechanism of electron transport in hydrocarbons.[2a] The electron moves as a quasi-free particle (*i.e.*, in the conduction band) until it is trapped by a group of molecules in a configuration favorable for trapping. The electron then remains in the relatively immobile trap until thermally promoted back to the conduction band. The activation energy of the mobility then arises from the thermal promotion step.

Another possible transport mechanism is electron tunnelling from trap to trap. In this picture the electron remains trapped until a thermal fluctuation (the activation step) provides a neighboring trap into which the electron may move by tunnelling. Theoretical investigation of these and other possible mechanisms suggested by recent work on amorphous solids will be the subject of a future publication.[9]

(9) NOTE ADDED IN PROOF. In a note to appear in *Chem. Phys. Lett.*, the authors have shown that a polyatomic version, the Cohen–Lekner quasi-free electron theory, accounts for the preexponential factor in eq 1 and for the observed field independence of electron mobilities in hydrocarbons.[2]

The Dimerization of a Copper(II)–Phthalocyanine Dye in Carbon Tetrachloride and Benzene

by Alan R. Monahan,* James A. Brado, and Allen F. DeLuca

Xerox Rochester Research Center, Rochester, New York 14603 *(Received July 19, 1971)*

Publication costs assisted by Xerox Corporation

Analyses of the absorption spectra of 4,4′,4″,4‴-tetraoctadecylsulfonamidophthalocyaninecopper(II) in carbon tetrachloride and benzene solutions demonstrate the existence of monomer–dimer equilibria in the 10^{-6}–10^{-4} M concentration range. The dimerization constants, $K_{eq} = C_d/C_m^2$, are $(2.97 \pm 0.02) \times 10^6$ M^{-1} and $(1.58 \pm 0.09) \times 10^4$ M^{-1} at 22 ± 2° in carbon tetrachloride and benzene, respectively. The absorption spectra of the pure monomer and pure dimer were calculated and found to be nearly identical in both solvent systems. A close correspondence was found to exist between the spectra of the resolved solution dimer and the solid state absorption spectrum of the phthalocyanine dye. The nature of the intermolecular interactions between phthalocyanine dye molecules in solution and the solid state is discussed.

The electronic spectroscopy of phthalocyanines and porphyrins has received a great deal of attention due to the similarity in structure between these molecules and chlorophyll and hemoglobin. In addition, the semiconduction and photoconduction properties of phthalocyanines as well as their importance as cyans in colored reprographic systems has added to the intensity of research on this class of compounds.[1]

(1) F. H. Moser and A. L. Thomas, "Phthalocyanine Compounds," Reinhold, New York, N. Y., 1963.

Since the dimeric and aggregated states of phthalocyanines,[2] chlorophylls,[3] etc., have been found to be important in both fluid and solid-state media, many investigations have focused on the mechanistic details of intermolecular interactions in phthalocyanine-type molecules. In general, it has been found that spectroscopic investigations in solution are more amendable to well defined studies since complications arising from polymorphism can be eliminated.[2,4]

Several water-soluble tetrasulfonated phthalocyanines have been chosen by other authors[5] as model compounds for equilibrium studies between monomer, dimer and higher order aggregates. The total dye concentration ranges studied have generally been of the order of 10^{-7}–10^{-4} M in aqueous media. The resolved pure component monomer and aggregate spectra have not been reported in the past.

In this paper we report a study on the monomer–dimer equilibria of a phthalocyanine dye molecule of the structure

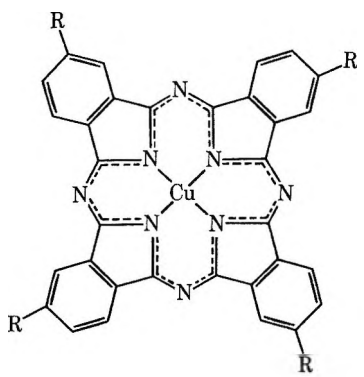

where R is $SO_2NH(CH_2)_{17}CH_3$. The equilibria studies were carried out in benzene and CCl_4 using total dye concentrations in the range 10^{-6}–10^{-4} M. Using this type of phthalocyanine molecule the dimerization process could be studied in solvents of low dielectric constant. Thus, the dye–dye interaction is the driving force for dimerization in these solvent systems since the screening of the dye–dye interaction is minimized in nonpolar solvents.[6] In the studies involving water as a solvent, the dye–dye interaction is in all probability not the major force causing the molecules to associate; instead the strong solvent–solvent interaction excludes the dye molecules from solution and causes them to aggregate.[7] The effects of phthalocyanine-dye dimerization were evaluated in CCl_4 and benzene by determining equilibrium constants for dimerization using previously reported[7] spectroscopic–computer techniques. In addition, pure monomer and dimer spectra were measured in each system and compared to the solid state.

Experimental Section

Preparation of Dye. The dye, 4,4′,4″,4‴-tetraoctadecylsulfonamidophthalocyaninecopper(II), was prepared by the method of Zickendraht.[8] Purification was achieved by solvation of the dye (5 wt %) in chloroform and precipitation in methanol. The purification procedure was repeated five times. The material was then vacuum dried at 50° for 12 hr. (*Anal.* Calcd for dye: C, 65.6; H, 8.7; N, 8.8; Cu, 3.3. Found: C, 65.9; H, 8.4; N, 9.1; Cu, 3.6.)

Preparation of Solutions and Absorption Spectra. For each experiment, fresh solutions were prepared by weighing a sample of phthalocyanine into a known volume of either Matheson Coleman and Bell Spectro quality carbon tetrachloride or benzene. The amount of water in each freshly prepared "master solution" was found by the Karl Fisher method to be 0.27 mg/ml (C_6H_6) and 0.21 mg/ml (CCl_4). Less concentrated solutions were then prepared by parallel dilution and run on a Cary Model 14R automatic spectrophotometer using 0.1-, 0.5-, 1-, 2-, 5-, and 10-cm matched quartz cells.

Results and Discussion

The unsubstituted copper phthalocyanine pigment and the substituted dye under consideration in this study both have D_{4h} symmetry. The lowest electronic transition in both compounds is observed at *ca.* 680 mμ in 1-chloronaphthalene. The extinction coefficients at peak maxima are *ca.* 1.1×10^5 l. mol^{-1} cm^{-1} for the dye and *ca.* 2.1×10^5 l. mol^{-1} cm^{-1} for the pigment. Vibrational satellites are noted at *ca.* 610 mμ and 650 mμ. In general, the phthalocyanine pigments are difficult to study in solution due to their negligible or limited solubility in organic solvents. In marked contrast to the phthalocyanine pigment, the dye analog has a solubility greater than 10^{-3} M in CCl_4, benzene, toluene, etc., and better than 10^{-2} M solubility in THF, DMF, and dioxane. Further work in the two solvent systems, *i.e.*, CCl_4 and benzene, indicated that dye concentrations of the order of 10^{-6} M in benzene produced spectra very similar to the dye spectrum in 1-chloronaphthalene, whereas in CCl_4 at 10^{-6} M there was enhanced absorption in the 16,000-cm^{-1} region.

The concentration dependences of the dye molecule in CCl_4 and benzene are shown in Figure 1. With increasing concentration both dye–solvent systems show a decreasing apparent extinction coefficient at 14,700

(2) J. H. Sharp and M. Lardon, *J. Phys. Chem.*, **72**, 3230 (1968).

(3) K. Sauer, *Proc. Nat. Acad. Sci. U. S.*, **53**, 716 (1965).

(4) E. A. Lucia and F. D. Verderame, *J. Chem. Phys.*, **48**, 2674 (1968).

(5) S. E. Sheppard and A. L. Geddes, *J. Amer. Chem. Soc.*, **66**, 1995 (1944); H. Kobayashi, Y. Torrii, and N. Fukuda, *J. Chem. Soc. Jap.*, **81**, 694 (1960); K. Bernauer and S. Fallub, *Helv. Chim. Acta*, **44**, 1287 (1961).

(6) K. Sauer, J. R. Lindsay Smith, and A. J. Schultz, *J. Amer. Chem. Soc.*, **88**, 2681 (1966).

(7) A. R. Monahan and D. F. Blossey, *J. Phys. Chem.*, **74**, 4014 (1970); A. R. Monahan, N. J. Germano, and D. F. Blossey, *ibid.*, **75**, 1227 (1971).

(8) C. Zickendraht and E. J. Koller, U. S. Patent 2,897,207.

Table I: Monomer–Dimer Equilibrium of Phthalocyanine Dye at 22°

	Benzene: $K_{eq} = (1.58 \pm 0.09) \times 10^4$ l. mol^{-1}					
Total dye concentrations, mol l.$^{-1}$ ($\times 10^6$)	4.89	9.78	24.5	48.9	97.8	489.0
Monomer concentrations, mol l.$^{-1}$ ($\times 10^6$)	4.32	7.84	15.8	26.8	43.0	107.1
Dimer concentrations, mol l.$^{-1}$ ($\times 10^6$)	0.284	0.971	4.33	11.0	27.4	191.0
Equilibrium constants, l. mol^{-1} ($\times 10^{-4}$)	1.52	1.58	1.73	1.53	1.48	1.67
	CCl_4: $K_{eq} = (2.97 \pm 0.02) \times 10^6$ l. mol^{-1}					
Total dye concentrations, mol l. ($\times 10^6$)	1.07	2.14	4.28	21.4		
Monomer concentrations, mol l. ($\times 10^6$)	0.349	0.520	0.772	1.81		
Dimer concentrations, mol l. ($\times 10^6$)	0.360	0.810	1.75	9.78		
Equilibrium constants, l. mol^{-1} ($\times 10^{-4}$)	296.7	299.3	294.0	298.7		

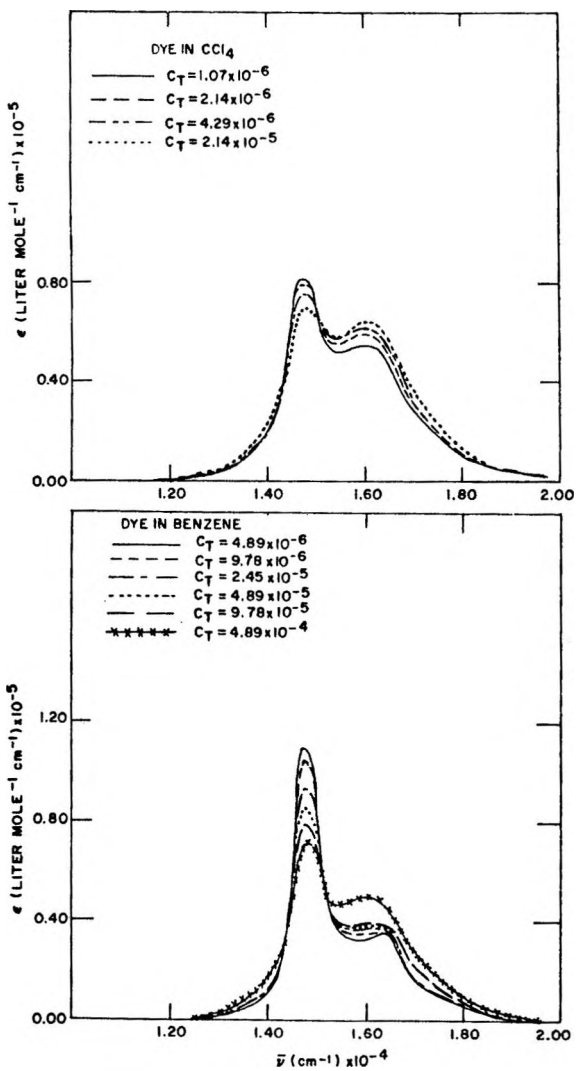

Figure 1. Concentration dependence of the phthalocyanine dye in benzene and carbon tetrachloride.

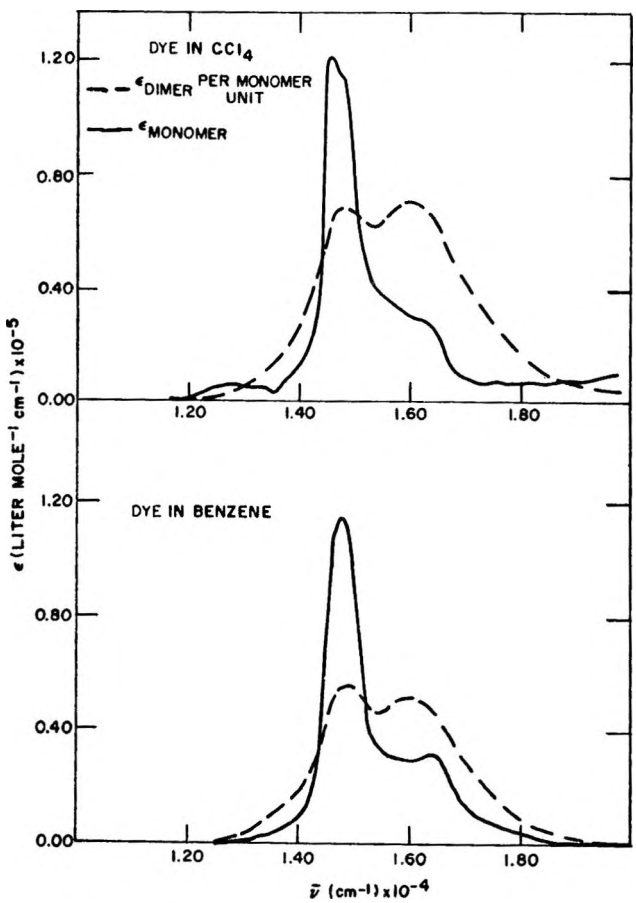

Figure 2. Calculated absorption spectra of pure phthalocyanine monomer and dimer in carbon tetrachloride and benzene.

$\pm$ 100 cm^{-1} with an increase in ϵ in the 16,000-cm^{-1} region. Isosbestic points occur at 14,200 $\pm$ 100 and 15,100 $\pm$ 100 cm^{-1} in each dye–solvent system. Based on the observations of monomer–dimer equilibria in-

volving sulfonated phthalocyanines in water,[5] a similar mechanism was assumed to be operative in these systems.

Monomer–Dimer Equilibrium. From each set of data, the pure monomer spectrum, pure dimer spectrum and the equilibrium constant can be calculated using a previously reported computer procedure.[7]

For each total concentration c_t, the monomer concentration c_m, dimer concentration c_d, and equilibrium constant K_{eq} was found. The best fit was obtained at equilibrium constants of $K_{eq} = (1.58 \pm 0.09) \times 10^4$ l. mol^{-1} for the dye–benzene system and $K_{eq} = (2.97 \pm 0.02) \times 10^6$ l. mol^{-1} for the dye–CCl_4 system. The best fit monomer and dimer spectra are shown in Figure 2. The results of the analyses are tabulated in Table I.

The equilibrium constants for the phthalocyanine in CCl_4 and benzene are in qualitative agreement with equilibrium constants reported for sulfonated phthalocyanines in water[5,9] and the chlorophylls in CCl_4.[6] The equilibrium constants obtained for these molecules were also realized by using the observed changes in the long wavelength electronic absorption bands as a function of concentration in the 10^{-6}–10^{-4} M range. For example, the monomer–dimer equilibrium of the tetrasodium salt of 4,4′,4″,4‴-tetrasulfophthalocyaninecobalt(II) has been investigated by equilibrium spectrophotometric measurements[5] and by stopped-flow relaxation techniques[9] in aqueous solution. The equilibrium constant was found by both techniques to be $(2.05 \pm 0.05) \times 10^5$ l. mol^{-1}. Sauer and Lindsay[6] have reported the dimerization of three chlorophylls in CCl_4 and found the association constants to be *ca.* 1×10^4 l. mol^{-1}.

Dimer formation in our system was observed and compared in solvents other than CCl_4 and benzene. This was accomplished by measuring the ratio of the solution optical density at 14,700 cm^{-1} relative to the 16,000 cm^{-1} density at nearly equivalent total dye concentrations (*ca.* 2×10^{-5} M). The order of decreasing phthalocyanine-dye dimerization in several solvent systems is CCl_4 > benzene > toluene > chloroform > dioxane > DHF > THF, etc. It is probably pertinent to note that the aggregation tendency of the dye is diminished in the solvents yielding the greatest dye solubility and, in general, the largest dielectric constant. To form the dimer, the dye–dye interaction must be strong enough to overcome any other forces which would favor solvation of the monomer. Thus, the lower the dielectric constant of the solvent, the less the screening of the dye–dye interaction by the solvent. Relative to benzene, the dye–solvent interaction is probably weaker in carbon tetrachloride. Therefore, the conditions for maximum dye association or interaction are maximized in the CCl_4 system, *viz.*, low dielectric constant and low solvation of the dye.

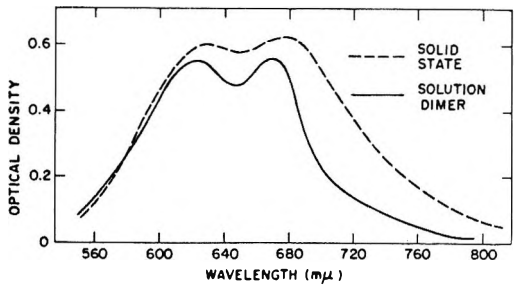

Figure 3. Comparison of melt cast solid-state absorption spectrum of dye with the benzene solution dimer spectrum.

By inspection of Figure 3, it can be concluded that the solid state is also composed of phthalocyanine molecules acting *via* similarly structured dimeric pairs. Thus, molecular interactions operative in the solid state can be simulated in solution if the solvent properties and structure–solubility characteristics of the dye are matched properly.

Acknowledgments. Stimulating discussions with Drs. D. F. Blossey and M. S. Walker are acknowledged with pleasure.

(9) Z. A. Schelly, R. D. Farina, and E. M. Eyring, *J. Phys. Chem.*, **74**, 617 (1970).

COMMUNICATIONS TO THE EDITOR

Near-Infrared Spectroscopic Study of the Interactions between Water and Acetone

Publication costs borne completely by The Journal of Physical Chemistry

Sir: McCabe, Subramanian, and Fisher have recently published "A Near-Infrared Spectroscopic Investigation of the Effect of Temperature on the Structure of Water." In order to support their interpretation, they have examined the near-infrared spectra of water–acetone mixtures.[1] We had studied absorption spectra, between 1000 and 11000 cm^{-1}, of H_2O, D_2O, and HOD as free

(1) W. C. McCabe, S. Subramanian, and H. F. Fisher, *J. Phys. Chem.*, **74**, 4360 (1970).

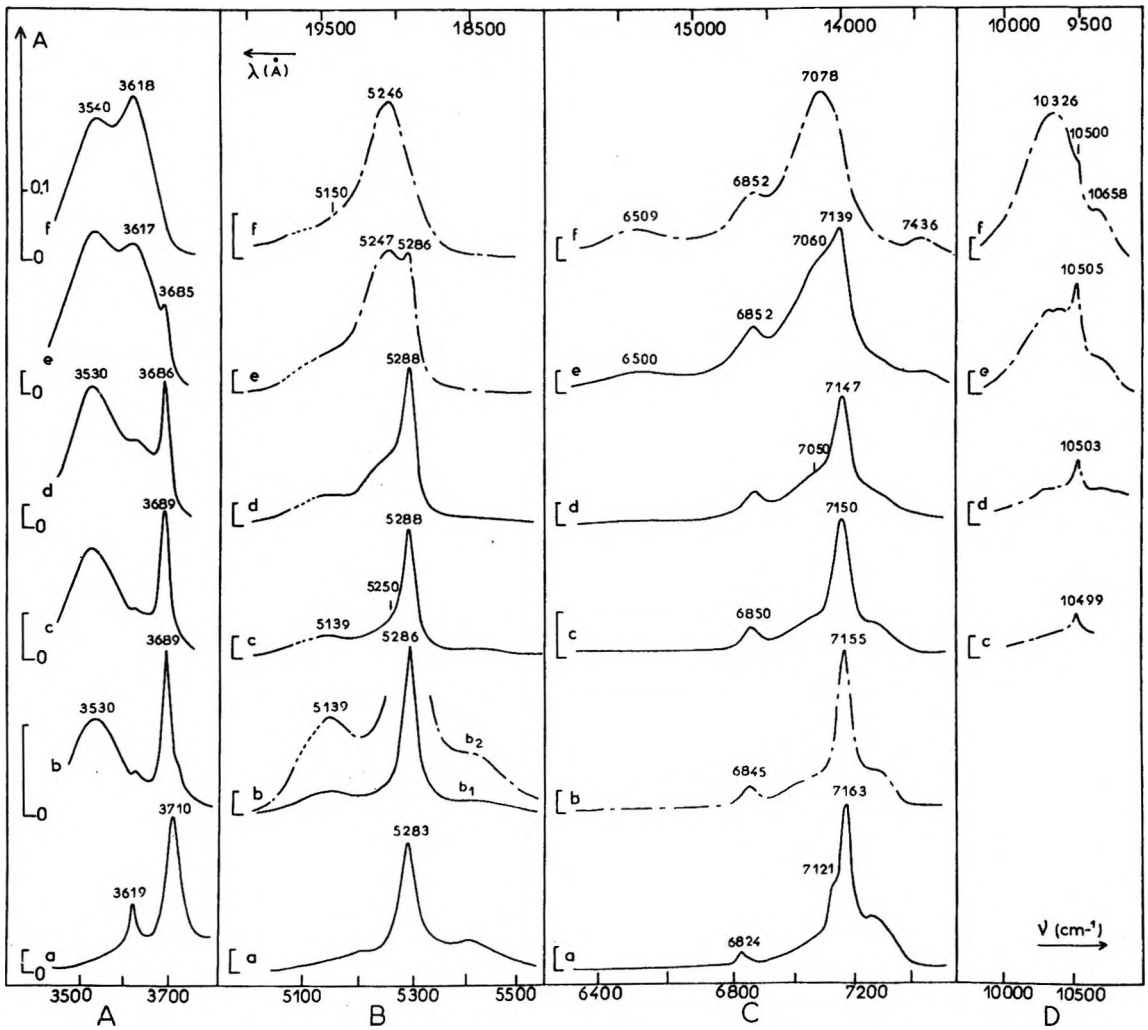

Figure 1. Spectra of H_2O molecules diluted in mixtures acetone–carbon tetrachloride. In Figures B, C, and D, the abscissas are linear with the wavelengths; however the maxima of the bands are expressed with cm^{-1}. The ordinates on the left of the spectra correspond to 0.1 or 0.01 unity of absorbance for the curves——— or —.—, respectively. The dashed spectra are doubtful on account of the absorption of the solvent. Acetone molar fraction in the mixture acetone–carbon tetrachloride: a, 0; b, 0.065; c, 0.13; d, 0.25; e, 0.57; f, 1; in Figure D (*f*), acetone-d_6 has been used. Figure A: H_2O concentration (*M*): a, 0.008; b, 0.01; c, 0.02; d, 0.04; e, f, 0.2; length of the cell (cm): a, 3; b, 0.5; c, d, 0.2; e, 0.0383; f, 0.0217. Figure B: H_2O concentration (*M*): a, 0.002; b, 0.02; c, 0.05; d, 0.04; e, 0.03; f, 0.2; length of the cell (cm): a, 100; b_1, 10; b_2, 5; c, 3; d, 5; e, 1; f, 0.1. Figure C: H_2O concentration (*M*): a, 0.007; b, 0.01; c, 0.05; d, 0.12; e, f, 0.2; length of the cell (cm): a, 100; b, c, d, e, 10; f, 1. Figure D: H_2O concentration (*M*): c, 0.05; d, 0.12; e, 0.5; f, 1; length of the cell (cm): c, d, e, f, 10.

molecules and in interaction with bases in dilute solutions.[2,3a] Our overall experimental evidence seems *a priori* in contradiction with their interpretation of the 7075-cm^{-1} absorption band of water in acetone. The aim of this paper is a demonstration of this statement from the spectra of ternary mixtures water–acetone–carbon tetrachloride.

The spectra have been recorded using, under 4000 cm^{-1}, a Beckman ir 12 spectrometer and, above 4000 cm^{-1}, a Cary Model 14 equipped either with a 0–2 or a 0–0.2 absorbance potentiometer. The spectral slit-width was less than one tenth of the band half-width. The stabilization temperature of the solutions in the beam was about 30°. The precision of the wavenumbers measured at the maxima of the absorption bands is approximately 1 cm^{-1} for narrow bands and 5 cm^{-1} for broad bands. The shape and frequency of some of the bands vary with water concentration.

Solutions have been prepared with spectroquality acetone and carbon tetrachloride from Prolabo. These solvents have been dried over 4 A Molecular Sieves and the mixtures made in a drybox in order to control the water content of the solutions. We have also used acetone-d_6 (99.7%) from C. E. A. France, but we were unable to study ternary solutions (H_2O–acetone-d_6–carbon tetrachloride) because of a fast exchange, probably catalyzed by trace amounts of HCl in carbon tetrachloride.

(2) A. Burneau, "Thèse de troisième cycle," University of Paris VI, Paris (1970); A. Burneau and J. Corset, *Chem. Phys. Lett.*, 9, 99 (1971).

(3) (a) A. Burneau and J. Corset, *J. Chim. Phys. Physicochim. Biol.*, 69, 142 (1972); (b) *ibid.*, 69, 153 (1972); (c) *ibid.*, 69, 171 (1972).

In the course of a systematic study of overtone and combination vibrational transitions of water interacting with bases of different strengths, we have examined, among others, the case of acetone. The spectra of Figure 1 can be interpreted without difficulty with the help of a detailed analysis of similar spectra related to interactions H_2O–hexamethylphosphorotriamide (HMPT).[3a] It can be seen that the spectra of the water molecule at low concentration in mixtures of acetone and carbon tetrachloride are clearly dependent on the molar fraction of the mixture. The evolution of the spectra is explained by equilibria between different species: the water molecule quasi free in pure carbon tetrachloride (curves a) yields mostly a 1–1 complex when acetone is added up to a molar fraction of 0.25 (curves d). When acetone concentration is still higher a 1–2 complex appears and becomes predominant at a molar fraction of 0.57 (curves e). This 1–2 complex is practically the only species present when water is diluted in pure acetone (curves f). From the study of the stretching fundamental vibrations, different authors[4] had already reached such conclusions for water interacting with different types of organic bases.

The infrared spectra of the water molecule in carbon tetrachloride solution (curves a) have already been discussed:[3a] the water molecule is considered as "quasi free" and is only submitted to weak nonspecific interactions. It is still able to rotate as indicated by wings on the sides of the bands, the one at higher frequency being more intense.[3a]

When acetone is added (curves b and c) the absorptions due to free molecules disappear and are replaced by new ones due to the 1–1 complex H–O–H···B (B stands for an acetone molecule). The relatively narrow bands are mainly related to the free OH bond:[5] $\nu(001)$ at 3689 cm^{-1}, $\nu(011)$ at 5288 cm^{-1}, $\nu(021)$ and $\nu(002)$ at about 6850 and 7150 cm^{-1}, $\nu(003)$ near 10500 cm^{-1}. The wider bands are mainly due to the hydrogen bonded OH: $\nu(100)$ at 3530 cm^{-1} and $\nu(110)$ at 5139 cm^{-1}. The decoupling between the two vibrators, however, is less pronounced than in the 1–1 complex with a strong base like HMPT.[3a,b]

From an acetone molar fraction of 0.25 (curves d to f) some new rather wide absorptions are due to the formation of a 1–2 complex B···H–O–H···B at the expense of the 1–1 complex, as can be seen from the intensity decrease of the narrow bands. Moreover the shoulder towards 5250 cm^{-1} shows that a slight amount of 1–2 complexes might be present from an acetone molar fraction of 0.13 (curve c, Figure 1B).[3a] At an acetone molar fraction of 0.57 (curves e), the bands at 3685, 5286 and 7139 cm^{-1} on the one hand, and at 3617, 5247 and about 7060 cm^{-1} on the other hand, show clearly the coexistence of 1–1 and 1–2 complexes. In pure acetone (curves f), the second group of absorptions is the only one left, due to the almost exclusive presence of 1–2 complexes. The question is whether the whole spectrum (f) must be related only to interactions between water and acetone. For instance, Karyakin, *et al.*, have assumed that, for relatively high water concentrations, the band at 7078 cm^{-1} is due to H_2O–acetone interactions and those near 6852 and 6509 cm^{-1} to H_2O–H_2O complexes, called "water in quasi emulsion," involving an indeterminate number of molecules.[6] The shape of the spectrum is as a matter of fact dependent on the whole water concentration. Nevertheless at the low concentrations used in Figure 1 (0.2 *M*) it is likely that the transitions of spectrum (f) correspond to 1–2 complexes between water and acetone, with the exclusion of more complex aggregates. The bands at 6852 and 7078 cm^{-1} are assigned to $\nu(021)$ and $\nu(101)$ in agreement with Greinacher, *et al.*,[7] but the whole region 6400–7500 cm^{-1} (Figure 1 C) needs a more detailed study.[3c,7a] In the other regions the bands at 3540, 3618, and 5246 cm^{-1} are due to $\nu(100)$, $\nu(001)$, and $\nu(011)$ for H_2O in the 1–2 complex; the shoulder near 5150 cm^{-1} could correspond to $\nu(110)$.

Figure 1 also shows that the more the sum of the quantic vibrational numbers of the final state increases the easier it is to detect the free vibrators, as we have already observed.[3a] It can indeed be noticed that the ratio of the extinction coefficients of the bands corresponding to the free and associated vibrators varies with the considered spectral region.[8,9] For instance, for an acetone molar fraction 0.57 (curves e), the narrow band at 3685 cm^{-1} is much less intense that the neighboring group of absorptions, whereas the bands at 5247 and 5286 cm^{-1} have a similar absorbance; finally, in the region of the first and second overtones of the stretching vibrations (Figure 1 C and D), the characteristic bands of the free vibrator clearly predominate. This is why the sharp change of slope near 10500 cm^{-1}, displayed by the absorption of water in acetone-d_6

(4) P. Saumagne and M. L. Josien, *Bull. Soc. Chim. Fr.*, 813 (1958); G. V. Yuknevich, A. V. Karyakin, and A. V. Petrov, *Zh. Prikl. Spektrosk.*, **3**, 142 (1965); S. C. Mohr, W. D. Wilk, and G. M. Barrow, *J. Amer. Chem. Soc.*, **87**, 3048 (1965); D. N. Glew and N. S. Rath, *Can. J. Chem.*, **49**, 837 (1971).

(5) Cold transitions are written $\nu(v_1, v_2, v_3)$, quantic vibrational numbers between brackets being those of the final state. The indexes 1 and 3 are used for stretching vibrations, 2 for bending.[3a]

(6) A. V. Karyakin, A. V. Petrov, and Yu. Gerlit, *Vodorodnaya Svyaz*, 181 (1964); *Chem. Abstracts*, **62**, 4783e (1965); A. V. Karyakin and A. V. Petrov, *Sovrem. Metody Anal.*, 185 (1965); *Chem. Abstracts*, **64**, 7367d (1966).

(7) E. Greinacher, W. Lüttke, and R. Mecke, *Ber. Bunsenges. Phys. Chem.*, **59**, 23 (1955).

(7a) NOTE ADDED IN PROOF. Since we have submitted this communication, we have shown that the absorption at about 6500 cm^{-1} is not to be assigned only to H_2O molecules: it corresponds to a combination transition simultaneously involving the vibrations of hydrogen-bonded water and acetone molecules [A. Burneau and J. Corset, *J. Chem. Phys.*, **56**, 662 (1972)].

(8) Analogous observations about the intensity of overtones have been done by different authors from the study of diatomic groups.[7,9]

(9) W. Lüttke and R. Mecke, *Z. Elektrochem.*, **53**, 241 (1949); R. Mecke, *Disc. Faraday Soc.*, **9**, 161 (1950); M. Couzi, "Thèse de troisième cycle," University of Bordeaux, Bordeaux (1966); C. Bourderon and C. Sandorfy, *54th Can. Chem. Conf.*, Halifax (1971).

(curve f, Figure 1D) could correspond to traces of 1–1 complexes.

The spectra of ternary solutions water–acetone–carbon tetrachloride show that, for acetone molar fractions lower than 0.25, water and acetone interact essentially by following a 1–1 stoichiometry. On the contrary, in pure acetone, water at low concentration is almost totally involved in 1–2 complexes and the band around 7078 cm^{-1} must be related to such complexes, contrary to the hypothesis of McCabe, *et al.* These authors have indeed made an erroneous extension to water–acetone binary solutions of results obtained, by different techniques, with ternary mixtures water–acetone–1,2-dichloroethane where the acetone formal concentration was lower than 0.6 *M* (molar fraction $\approx$ 0.05).[10]

Acknowledgments. We wish to thank Professor M. L. Josien for helpful discussions and Mrs. R. M. Moravie for her assistance with the experimental work.

(10) T. F. Lin, S. D. Christian, and H. E. Affsprung, *J. Phys. Chem.*, **69**, 2980 (1965); T. F. Lin, S. D. Christian and H. E. Affsprung, *ibid.*, **71**, 1133 (1967).

LABORATOIRE DE SPECTROCHIMIE MOLÉCULAIRE
UNIVERSITÉ PARIS VI
PARIS V^{e}, FRANCE

ANDRÉ BURNEAU*
JACQUES CORSET

RECEIVED SEPTEMBER 22, 1971

Reply to "Near-Infrared Spectroscopic Study of the Interactions between Water and Acetone," by Burneau and Corset

Publication costs assisted by the Veterans Administration

Sir: Burneau and Corset's studies[1] of CCl_4–acetone–water mixtures in the medium and near-infrared spectral regions demonstrate the sequential formation of 1–1 and 1–2 water–acetone complexes as the mole fraction of acetone is increased. While their assignments are correct in the fundamental region, they are subject to certain doubts in the overtone region. The assignment of the 7163-cm^{-1} band to ν(101) is in agreement with other studies.[2] They do not consider the possibility of a ν(200) band due to the bonded OH in the 1–1 complex while assigning the 7150-cm^{-1} band to ν(002) of the free OH in the 1–1 complex and the 7078 cm^{-1} band to ν(101) of the 1–2 complex. The shoulder at 7050 cm^{-1} observed at moderate acetone concentrations moves toward higher frequencies and appears as a peak at 7078 cm^{-1} in pure acetone as solvent. The peak at 7078 cm^{-1} (similar to Figure 5 in our paper[3]) is broad and asymmetric and can be resolved into two Gaussian peaks—one at 7075 cm^{-1} and another at $\sim$6980 cm^{-1}. This is also obvious from Figure 5 in our paper.[3] In the fundamental region, the 1–2 complex gives[1] a shift of $\sim$90 cm^{-1} towards lower frequencies for each of the ν_1 and ν_3 vibrations from those for "free" water in CCl_4. However, in the overtone region, the shift for the ν(101) band for the 1–2 complex from that of "free" water in CCl_4 is only 85 cm^{-1}. This shift is about half the expected value. The anharmonicity factor would not, we believe, account for this drastic reduction. This, taken together with the fact that the intensity of bonded OH is higher than free OH in the fundamental while the opposite is true in the overtone region,[4] suggests that the peak at 7078 cm^{-1} could be a composite of a sharp peak (at $\sim$7075 cm^{-1}) due to a small amount of a 1–1 complex and a small broad peak at $\sim$6980 cm^{-1} due to the major 1–2 complex.

We extended the arguments of a 1–1 complex in water–acetone 1,2-dichloroethane mixtures[5] to water-in-acetone mixtures to show the spectral contribution at 7075 cm^{-1} is due to a 1–1 complex but did not deny the existence of a 1–2 complex for small amounts of water in large amounts of acetone. There was also another basis for assigning the 7075 cm^{-1} Gaussian component in Figure 5 of our paper to a 1–1 complex. Worley and Klotz,[6] in their near-infrared studies of HOD in D_2O, assigned the peak at 7063 cm^{-1} to the overtone of free OH. Our water-in-acetone spectra had a major peak at 7075 cm^{-1}. Recognizing a small difference due to isotopic substitution and dielectric constant of the medium, we assigned the 7075-cm^{-1} band to the ν(101) of the 1–1 complex.

(1) A. Burneau and J. Corset, *J. Phys. Chem.*, **76**, 449 (1972).

(2) D. P. Stevenson, *ibid.*, **69**, 2145 (1965).

(3) W. C. McCabe, S. Subramanian, and H. F. Fisher, *ibid.*, **74**, 4360 (1970).

(4) W. A. P. Luck, *Discuss. Faraday Soc.*, **43**, 134 (1967).

(5) T. F. Lin, S. D. Christian, and H. E. Affsprung, *J. Phys. Chem.*, **69**, 2980 (1965); T. F. Lin, S. D. Christian, and H. E. Affsprung, *ibid.*, **71**, 1133 (1967).

(6) J. D. Worley and I. M. Klotz, *J. Chem. Phys.*, **45**, 2868 (1966).

VETERANS ADMINISTRATION HOSPITAL
KANSAS CITY, MISSOURI 64128

S. SUBRAMANIAN
H. F. FISHER*

RECEIVED OCTOBER 21, 1971

Bicipital Relaxation Phenomena

Publication costs assisted by the National Institutes of Health

Sir: In investigating the kinetics of metal–ligand reactions using the temperature-jump relaxation method,[1] we have recently observed unusual behavior in the relaxation curves which does not appear to have been

(1) (a) D. B. Rorabacher, *Inorg. Chem.*, **5**, 1891 (1966); (b) W. J. MacKellar and D. B. Rorabacher, *J. Amer. Chem. Soc.*, **93**, 4379 (1971); (c) D. B. Rorabacher and C. A. Melendez-Cepeda, *ibid.*, **93**, 6071 (1971); (d) D. B. Rorabacher and R. B. Cruz, Abstracts INOR-43, 162nd National Meeting of the American Chemical Society, Washington, D. C., Sept., 1971; (e) F. R. Shu and D. B. Rorabacher, *Inorg. Chem.*, accepted for publication.

noted in any of the previous literature. Not only are the amplitudes of the observed relaxation curves dependent upon the solution conditions, but a complete inversion of the curves may be generated with an appropriate adjustment of these conditions. In fact, for some reaction systems the amplitude of these inverted curves, which are obtained under conditions which might be considered to be extremely unfavorable, can be made larger than the curves which are normally observed resulting in an improvement in the experimental data.

The observed behavior, which occurs only with systems containing coupled reactions, is in accord with previously described relaxation theory.[2,3] Thus, the chemical relaxation for each of two coupled reactions is governed by the combined result of two perturbing forces—the changing state function (temperature, pressure, electric field) and the changing concentrations of the commonly shared species (resulting from the equilibrium shift of the coupled reaction). We propose to call such a process a *bicipital* relaxation (*i.e.*, arising from two sources).

The two perturbing forces may tend either to reinforce or to oppose one another. In the latter case, the net response may be a drastic reduction or even a complete cancelation of the desired equilibrium shift, thereby making it difficult or impossible to obtain the desired kinetic data.

As applied to the temperature-jump method, the conditions for an opposing bicipital relaxation should exist whenever the enthalpies of two parallel coupled reactions

$$A + B \rightleftharpoons E \quad (1)$$

$$A + C \rightleftharpoons F \quad (2)$$

have the same sign. If these two reactions are of the same molecularity and are not coupled to any other reactions, the magnitude of the net equilibrium shift can be shown to depend directly on the relative magnitude of the two ΔH values and cannot be altered by a change in conditions. Under such circumstances a complete cancelation of the equilibrium shift can be shown to occur only under the specific condition where $\Delta H_1 = \Delta H_2$. If, however, the molecularities of the two reactions differ or if other reactions are coupled to these two, the net equilibrium shift can, in theory, be altered by a change in solution conditions (*i.e.*, altering relative concentrations or varying the magnitude of the temperature increase). By a judicious choice of conditions, therefore, the magnitude of the net equilibrium shift of a desired reaction may be enhanced or the direction of the shift may be completely reversed. It follows that there also exists the possibility of achieving a null relaxation point where no net shift occurs. Neither the prediction nor the observation of these phenomena has been previously described.

As a specific example, we have examined in some detail *via* the temperature-jump method the reaction of aquocobalt(II) ion with ammonia to form the monoammine complex in aqueous solution. Under pH conditions equivalent to those used in the previous study of this system,[1a] the ammonia is almost entirely protonated yielding two coupled reactions each of which possesses a negative enthalpy

$$Co^{2+} + NH_3 \rightleftharpoons Co(NH_3)^{2+}; \quad \Delta H_1 = -2.0 \text{ kcal/mol} \quad (3)$$

$$H^+ + NH_3 \rightleftharpoons NH_4^+; \quad \Delta H_2 = -12.4 \text{ kcal/mol} \quad (4)$$

Since the latter reaction equilibrates much faster than the former following the temperature jump, the net effect upon reaction 3 is that of a concentration jump of the ligand, NH_3, which tends to oppose the temperature-induced shift of this reaction. Thus the conditions for an opposing bicipital relaxation are present.

The introduction of an acid–base indicator into the system to permit spectrophotometric monitoring of reaction 3[1a] provides a third coupled reaction

$$H^+ + In^- \rightleftharpoons HIn \quad (5)$$

which then permits the net shift of the reaction 3 equilibrium to be altered upon changing solution conditions. (The autoprotolysis equilibrium of water may also be significant as a fourth coupled reaction.)

As illustrated in Figure 1, a significant reversal of the equilibrium shift for reaction 3 is obtained within a narrow pH range (the amplitude being significantly enhanced at still lower pH). The system is sufficiently sensitive that slight deviations from the null relaxation point can be observed upon changing the pH of the solution by ± 0.05 unit from the null conditions. In further experiments it has been demonstrated that a relaxation reversal can also be obtained at constant pH either by varying the concentration of the reactants (Co^{2+}, NH_3) or the magnitude of the temperature jump (the final temperature being kept constant). The amplitude of the "inverted" relaxation curve is sufficiently large that useful data may be obtained at pH 4.5 where the ratio of $Co(NH_3)^{2+}$ to uncomplexed Co^{2+} is 10^{-4}.

That the inverted relaxation curves represent the same relaxation process is confirmed by the equivalence of the relaxation times. Furthermore, the conditions existing at the null relaxation point are in accord with the mathematically derivable equation[4]

$$\ln([H^+]^*/[H^+]) = (\Delta H_1 - \Delta H_2)\Delta T/RT^2 \quad (6)$$

where $[H^+]^*$ and $[H^+]$ represent the hydrogen ion

(2) M. Eigen and L. deMaeyer in "Technique of Organic Chemistry," Vol. VIII, S. L. Friess, E. S. Lewis, and A. Weissberger, Ed., 2nd ed, Interscience, New York, N. Y., 1963, Part II.

(3) G. H. Czerlinski, "Chemical Relaxation," Marcel Dekker, New York, N. Y., 1966.

(4) D. B. Rorabacher and R. W. Taylor, to be published.

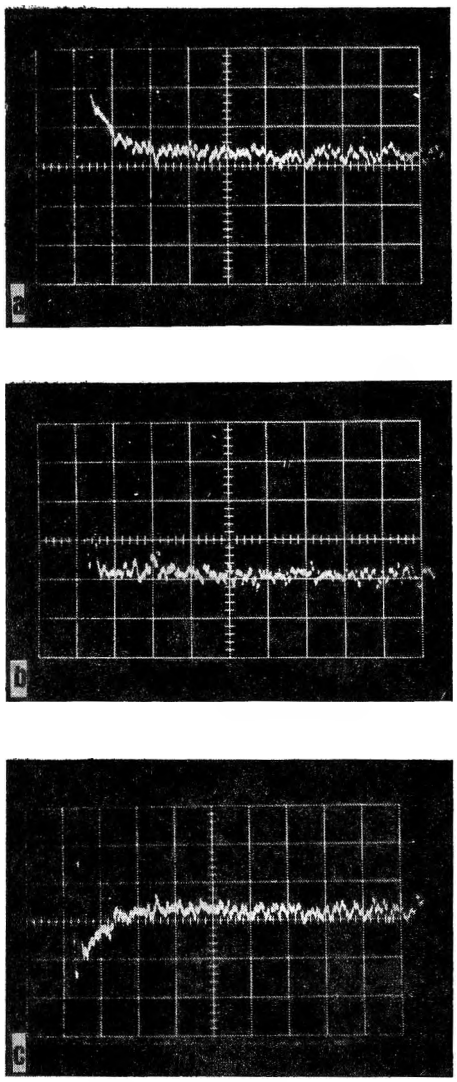

Figure 1. Relaxation curves for the aqueous cobalt(II)–ammonia system obtained at pH (a) 5.36 (top), (b) 5.65 (center), (c) 5.96 (bottom). All solutions contain 0.020 *M* $Co(ClO_4)_2$, 0.10 *M* NH_4ClO_4, 8×10^{-5} *M* bromocresol green plus $NaClO_4$ to achieve 0.2 *M* ionic strength. Conditions for each spectrum are: $\Delta T = 4.6°$ (final temp = 25°), sweep rate = 0.5 msec/div, amplitude = 5 mV/div, $\lambda = 592$ nm.

concentration before and after the temperature-jump, respectively.

In view of the widespread use of coupled indicator systems in relaxation studies, the bicipital relaxation phenomena described above suggest that systems which may previously have been abandoned as unobservable should be reexamined under varying solution conditions to ascertain whether the difficulty may be attributable to the inadvertent use of conditions close to the null relaxation point. In addition, investigators working with coupled systems might be well advised to establish the existence of a null relaxation point as confirming evidence that only a single relaxation is occurring in the observed time range, it being extremely unlikely that identical null relaxation points would be exhibited by closely overlapping relaxation processes which might otherwise go undetected.

Acknowledgment. This work was supported by the National Institute of General Medical Sciences under Grant No. GM-12596. The authors also gratefully acknowledge the support of R. W. T. by a National Science Foundation Graduate Traineeship.

DEPARTMENT OF CHEMISTRY
WAYNE STATE UNIVERSITY
DETROIT, MICHIGAN 48202

R. W. TAYLOR
D. B. RORABACHER*

RECEIVED OCTOBER 1, 1971

Anomalous Isotope Shifts in the Vibrational Spectrum of Hydrogen Cyanide in Argon Matrices[1]

Publication costs assisted by Ames Laboratory, U. S. Atomic Energy Commission

Sir: The matrix spectra of isotopic species of small molecules have been used widely to deduce the molecular geometry of labile molecules *via* the Redlich–Teller product rule.[2] Structures so obtained correspond to the geometry of the free molecule only if the vibrational model of the free molecule adequately describes the molecular vibrations in the matrix. If this prerequisite is fulfilled, the isotopic shifts of the vibrational frequencies in the matrix spectra will be the same as those in the gas phase vibrational spectra; if it is not fulfilled, the isotope shifts will differ. Verification of this prerequisite is crucial to the validity of matrix isolation structural studies because small changes in the isotopic frequency shifts in the matrix would be incorrectly interpreted in terms of the geometry of the molecule rather than attributed to the use of an inappropriate vibrational model. The gas phase and matrix spectra of only a few molecules have been sufficiently well characterized to provide an unambiguous test of this prerequisite. The isotopic species of HCN offer one such case.

Careful measurement of the infrared spectra of HCN isotopes isolated in an argon matrix at 8°K were made using a Perkin-Elmer E-13 monochromator. The concentration of the samples varied from 0.0015 to 0.0030 mole ratio HCN:Ar. All the fundamentals were observed except the ν_1 vibration of the hydrogen isotopes. The intensity of this vibration is very weak; however upon deuteration the intensity increases markedly so that the vibration was observed in the deuterium isotopes. In addition certain other features attributable to dimers and polymers[3] were observed. The assignment of the monomer absorptions was made by analogy

(1) Work was performed in the Ames Laboratory of the Atomic Energy Commission. Contribution No. 3110.

(2) G. Herzberg, "Molecular Spectra and Molecular Structure. II. Infrared and Raman Spectra of Polyatomic Molecules," Van Nostrand, Princeton, N. J., 1945, p 227 ff.

(3) Charles M. King and Eugene R. Nixon, *J. Chem. Phys.*, **48**, 1685 (1968).

Table I: Vibrational Frequencies of HCN Isotopes in Argon Matrices and the Gas Phase

	Matrix								Gas[c]		
	ν_1	A.D.[a]	No.[b]	ν_2	A.D.[a]	No.[b]	ν_3	A.D.[a]	No.[b]	ν_1	ν_2	ν_3
$H^{12}C^{14}N$				720.96	0.05	10	3305.66	0.07	4	2096.85	712.35	3311.45
$H^{13}C^{14}N$				714.94	0.03	8	3288.08	0.13	6	2063.05	706.34	3293.46
$H^{12}C^{15}N$				719.74	0.04	4	3304.61	0.10	4	2064.35	711.41	3310.13
$D^{12}C^{14}N$	1925.17	0.03	4	576.02	0.05	4	2626.43	0.05	4	1925.24	569.30	2630.34
$D^{13}C^{14}N$	1911.91	0.01	3	568.01	0.06	4	2585.85	0.03	6	1911.81	561.60	2590.05
$D^{12}C^{15}N$	1900.16	0.01	3	574.44	0.02	6	2616.99	0.02	4	1900.12	568.06	2621.22

[a] Average deviation from the mean. [b] Number of times the frequency was calibrated. [c] From ref 3 and citations therein.

Table II: Isotope Shifts of HCN Vibrational Frequencies in the Matrix and Gas and the Discrepancy between Them

	$\Delta\nu_1$			$\Delta\nu_2$			$\Delta\nu_3$		
	Matrix	Gas	δ	Matrix	Gas	δ	Matrix	Gas	δ
$H^{12}C^{14}N$									
				6.02	6.00	0.02	17.53	17.99	−0.46
$H^{13}C^{14}N$									
$H^{12}C^{14}N$									
				1.22	0.94	−0.28	1.00	1.32	−0.32
$H^{12}C^{15}N$									
$D^{12}C^{14}N$									
	13.26	13.43	−0.17	8.01	7.70	0.31	40.58	40.29	0.29
$D^{13}C^{14}N$									
$D^{12}C^{14}N$									
	25.01	25.12	−0.11	1.58	1.24	0.24	9.44	9.12	0.32
$D^{12}C^{15}N$									
$H^{12}C^{14}N$									
				144.94	143.05	1.89	679.18	681.11	−1.93
$D^{12}C^{14}N$									
$H^{13}C^{14}N$									
				146.93	144.74	2.19	702.23	703.41	−1.18
$D^{13}C^{14}N$									
$H^{12}C^{15}N$									
				145.30	143.35	1.95	687.62	688.91	−1.29
$D^{12}C^{15}N$									

to the location of the bands in the gas phase, by diffusion experiments, and by observing the relative intensities of features as a function of concentration. Each feature was calibrated from three to ten times using HCN, DCN, and in one case, H_2O vapor as a calibrant.[4] The spectral resolution was 1.5, 0.7, and 0.3 cm^{-1} in the 3000, 2500, and 700 cm^{-1} regions, respectively. The experimental data, the number of calibrations, the average deviation of the calibrations from the mean, and the gas phase band centers[5] are summarized in Table I.

The isotopic shifts of the matrix and gas phase frequencies and the discrepancies between them, δ, are tabulated in Table II for various isotopic combinations. The discrepancies are small for isotopic combinations involving mass changes of the heavy atoms. On the other hand, for isotopic combinations involving H and D, the discrepancies are about 2 cm^{-1}. This far exceeds the combined uncertainty of the gas and matrix data.

While these inconsistencies have little effect on the value of the force constants for HCN evaluated from the matrix spectra, the effect on the calculated molecular geometry using the product rule is much more serious. Because of the sensitive dependence of the calculation on the isotopic shift, an error of even a few tenths of a cm^{-1} represents a substantial uncertainty in the calculated geometry. For example, application of the Redlich–Teller Product Rule to the bending vibration of HCN in the matrix yields ratios of the CN and CH bond lengths that are not only mutually inconsistent but also are in serious disagreement with the analogous computation using the gas phase data. As

(4) K. N. Rao, C. J. Humphreys, and D. H. Rank, "Wavelength Standards in the Infrared," Academic Press, Washington, D. C., 1966; P. Fraley and K. N. Rao, *J. Mol. Spectrosc.*, **26**, 312 (1969); P. B. Checkland and H. W. Thompson, *Trans. Faraday Soc.*, **51**, 1 (1955).

(5) T. Nakagawa and Y. Morino, *Bull. Chem. Soc. Jap.*, **42**, 2212 (1969).

shown in Table III, no improvement in the value of the bond length ratio in the *matrix* accrues when anharmonicity is compensated for by applying the appropriate anharmonic constants obtained from the overtone-combination analysis in the gas phase,[5] although the gas phase data showed excellent consistency when this correction was applied.

Table III: Ratios of Gas Phase and Matrix Bond Lengths Calculated from the Observed and Harmonic Frequencies Using the Redlich–Teller Product Rule

	Matrix (r_{CN}/r_{CH})		Gas[a] (r_{CN}/r_{CH})	
	Observed	Harmonic	Observed	Harmonic
$H^{12}C^{14}N$–$D^{12}C^{14}N$	1.01	0.96 ± 0.03	1.145	1.079
$H^{12}C^{14}N$–$H^{12}C^{15}N$				
$H^{12}C^{14}N$–$D^{12}C^{15}N$	0.99	0.97 ± 0.03	1.116	1.082
$H^{12}C^{14}N$–$D^{12}C^{14}N$	1.13	1.09 ± 0.02	1.119	1.081
$H^{12}C^{14}N$–$H^{13}C^{14}N$				
$H^{12}C^{14}N$–$D^{12}C^{14}N$	1.07	1.05 ± 0.02	1.095	1.081
$D^{12}C^{14}N$–$D^{13}C^{14}N$				
$H^{12}C^{14}N$–$H^{13}C^{14}N$	0.91	0.85 ± 0.05	1.169	1.077
$H^{12}C^{14}N$–$H^{12}C^{14}N$				
$D^{12}C^{14}N$–$D^{13}C^{14}N$	0.93	0.89 ± 0.05	1.135	1.082
$D^{12}C^{14}N$–$D^{12}C^{15}N$				
Average	1.00	0.97 ± 0.04	1.130	1.080

[a] Microwave measurements give a value 1.083 for this ratio.

It does not seem plausible that the discrepancies of the isotope shifts can be accounted for by a change in the geometry of HCN in argon. The van der Waals forces that exist between the molecule and the matrix environment are not strong enough to deform the HCN bonds 0.1 Å.

The discrepancy most likely results from the failure of the linear *x–y–z* vibrational model to describe the vibrations of the matrix isolated molecule adequately. If this is true, one is forced to conclude that molecular geometries based on the analysis of isotopic shifts in matrices are likely to be in serious error when light isotopic substitutions are involved, *e.g.*, H and D, no matter how precisely the frequencies are measured and no matter how well anharmonicity is accounted for.

INSTITUTE FOR ATOMIC RESEARCH AND DEPARTMENT OF CHEMISTRY
IOWA STATE UNIVERSITY
AMES, IOWA 50010

JACOB PACANSKY
G. VINCENT CALDER*

RECEIVED OCTOBER 25, 1971

Polywater

Publication costs assisted by the Naval Research Laboratory

Sir: Recently, Brummer, *et al.*,[1] gave a detailed description of their procedure for preparing "polywater" or anomalous water in high yields. Their results may be interpreted as merely adding to the evidence that this material is not a modified or polymeric form of water but is simply the corrosion product of the Pyrex or quartz capillaries in which it is formed as suggested by Bascom, Brooks, and Worthington.[2] One of the principal points made by Brummer, *et al.*, is that the yield of "polywater" is greatest in strained regions of the glass or quartz capillary. For example, their yield was particularly high at the tapered ends of thick walled capillaries that had been sealed by melting and drawing. Annealing the capillaries removed this enhanced activity. In the earlier work of Bascom, *et al.*,[2] it was pointed out that strained siloxane bonds would be especially susceptible to attack by adsorbed water made alkaline by cations present in the Pyrex (or in the case of quartz by electrolytes that had surface-diffused into the capillaries). The product of this surface corrosion would be an alkaline silicate sol or gel.

Brummer, *et al.*, and others before them[3] claim that the infrared spectrum of "polywater" is unique and cannot be attributed to inorganic salts. However, Bascom, *et al.*, have shown that spectra of bicarbonate–silicate mixtures closely resemble the polywater spectra. They argue that the alkaline condensate formed in glass and silica capillaries absorbs atmospheric CO_2 to form the bicarbonate ion. An example of the bicarbonate–silicate spectra is given in Figure 1. It closely resembles the spectrum of the Pyrex-grown polywater given by Brummer, *et al.* (Figure 2C, reference 1). The bands at 1650 cm^{-1} and 1425 cm^{-1} originally attributed to "polywater"[3] are due to the symmetric and antisymmetric O–C–O stretching vibrations. The band at 1000–1100 cm^{-1} is due to the Si–O–Si stretch of the silicate constituent. This band and the sharp bands between 800 and 900 cm^{-1} are also present in the "polywater" spectra.[1,3] It should also be noted that the 1425-cm^{-1} band appears to be a doublet in both the bicarbonate–silicate spectrum and the "polywater" spectra.

The salt solution used to obtain Figure 1 was made by mixing equal amounts of a 10% (by weight) solution of $KHCO_3$ and a 15% solution of SiO_2 and Na_2SiO_3 at a 3.3:1 mole ratio. This mixture was diluted to about 0.5% with distilled water. Approximately 0.25 ml of this final solution was then dried to a gel on an Irtran

(1) S. B. Brummer, G. Entine, J. I. Bradspies, H. Lingertat, and C. Leung, *J. Phys. Chem.*, 75, 2976 (1971).

(2) W. D. Bascom, E. J. Brooks, and B. N. Worthington, *Nature (London)*, 228, 1290 (1970).

(3) E. R. Lippincott, R. R. Stromberg, W. H. Grant, and G. L. Cessac, *Science*, 169, 1482 (1969).

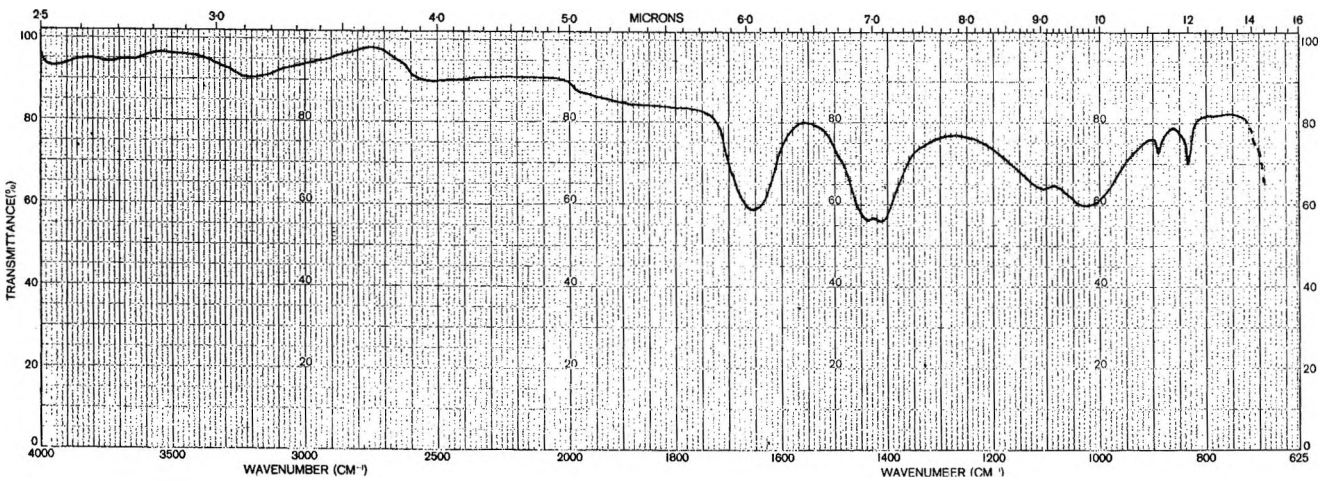

Figure 1. Infrared spectrum of the residue of a bicarbonate–silicate solution.

plate. As noted previously[2] the positions and the relative intensities of the bands depend on the composition and the history of the bicarbonate–silicate mixture.

It would appear that "polywater" could easily result from the surface corrosion of the capillaries to form an alkaline product that absorbs CO_2 from the air. This explanation reasonably accounts for the reported presence of carboxylic acid groups[4] and a high carbon content[5] of polywater samples. Furthermore, we would expect a solution of inorganic ions to increase the surface tension of water—a property recently attributed to anomalous water.[6] Finally, "polywater" formed from D_2O has an infrared spectrum identical with that of H_2O[7] which is difficult to understand if the material is a polymeric form of water but easily explained if it is a mixture of bicarbonate and silicate ions. There are objections to explaining "polywater" in terms of bicarbonate–silicate mixtures. Rousseau[7] notes that when compared to the "polywater" spectra, the bicarbonate band is at 1650 cm^{-1} rather than at 1600 cm^{-1} and that the 1400-cm^{-1} band tends to be the more intense of the two whereas it is usually the opposite in the polywater spectra. However, recent spectra claimed for "polywater" show the 1400-cm^{-1} band to be equal or stronger than the 1600-cm^{-1} band[1,5] and in one case[5] the latter band appears to be shifted to a higher frequency.

(4) R. E. Davis, D. L. Rousseau, R. O. Board, *Science*, 171, 167 (1971).

(5) T. F. Page, and R. J. Jakobsen, *J. Colloid Interface Sci.*, 36, 427 (1971).

(6) B. V. Deryagin, Z. M. Zorin, V. V. Karasev, V. D. Sobolev, E. N. Khromova, and N. V. Churaev, *Dokl. Akad. Nauk SSSR*, 187, 605 (1969).

(7) D. L. Rousseau, *J. Colloid Interface Sci.*, 36, 434 (1971).

SURFACE CHEMISTRY BRANCH
CODE 6170, CHEMISTRY DIVISION
NAVAL RESEARCH LABORATORY
WASHINGTON, D. C. 20390

WILLARD D. BASCOM

RECEIVED OCTOBER 26, 1971

Polywater, an Organic Contaminant

Publication costs borne completely by The Journal of Physical Chemistry

Sir: Bascom raises two important points about anomalous water—that it is not polymeric water and that it is in fact dissolved glass, specifically a silicate–bicarbonate residue. It is pertinent to examine the evidence for these views.

The only remaining evidence of any substance to suggest that anomalous water may be polymeric water is that of Deryagin, *et al.*[1] We have attempted to reproduce many of their results, including the quantitative conversion of anomalous water to water, and the preparation of anomalous water under conditions of rigorous organic exclusion. Our findings do not agree with the Russian work and we concur with Bascom that anomalous water is not a polymeric form of water.

However, we disagree with the proposal that the phenomenon is due to an inorganic contaminant, in particular silicate–bicarbonate. Thus, both Rousseau[2] and Lippincott, *et al.*,[3] have shown conclusively that there was very little silicon in their material. In addition, we have produced anomalous water from a ZrO_2-based glass (Corning #7280) which does not exhibit the 1000–1100-cm^{-1} ir band attributed to silicate (Figure 1).

We would say also that the ir spectrum on which Bascom bases his argument is not typical of the anomalous water spectrum. Thus, his band at ~1650 cm^{-1} is more usually found at ~1590 cm^{-1}—except, we have found, on acidification, when it shifts to ~1700 cm^{-1} and the material becomes volatile in the ir beam, which behavior is typical of carboxylic acids. Also, his spectrum shows a peak at ~880 cm^{-1}. This peak is characteristic of ionic carbonate and would be expected to oc-

(1) B. V. Derjaguin and N. V. Churayev, *J. Colloid Interface Sci.*, 36, 415 (1971).

(2) D. L. Rousseau and S. P. S. Porto, *Science*, 167, 1715 (1970).

(3) E. R. Lippincott, R. R. Stromberg, W. H. Grant, and G. L. Cessac, *Science*, 164, 1482 (1969).

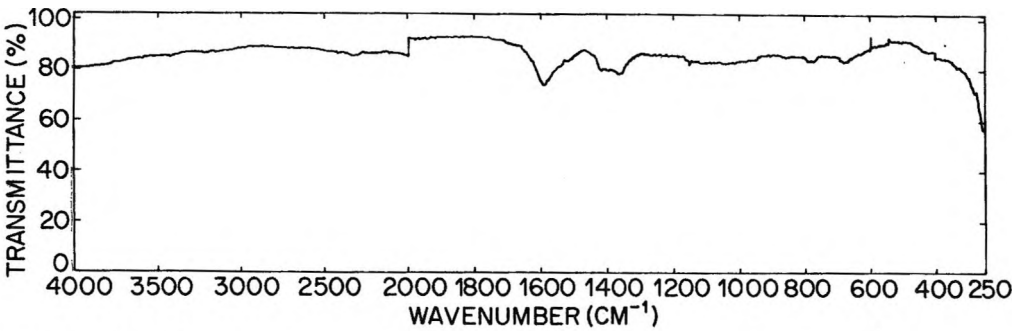

Figure 1. Material from zirconia cones.

cur as the result of CO_2 absorption from the atmosphere in an alkaline condensate. This peak is never observed in the spectrum of our material. Therefore, the ir data do not support the silicate–bicarbonate hypothesis. Nor will his model fit the tendency of the ir-active component of anomalous water to char, its spectral shift on acidification, its volatility, or our observations with ZrO_2 glass.

Therefore, although we have observed instances of inorganic contamination, particularly by borates, these contaminants are not, we feel, responsible for the "polywater" phenomenon. Rather, we believe that the infrared spectrum most usually identified with "polywater" results from the products of the reaction of hot glass with organic materials in the atmosphere when the glass is being blown. "Annealing," which eliminates the activity of the glass, certainly influences its solubility but its principal effect in this regard, we feel, is to destroy this organic residue. Thus, we find quite different ir spectra when the glass is pulled out of contact with the atmosphere—not typical of anomalous water. In addition, the charring of the product upon heating, the spectral shift on acidification, and the observations with ZrO_2 glass mentioned above are all consistent with an organic product. Thus, while we have some disagreements in detail with the conclusions of Rousseau, *et al.*,[4] we agree with the basic conclusion that anomalous water is an organic rather than an inorganic phenomenon.

Finally, we believe that to resolve the problem completely, it is necessary to tie the American research to that of the Russians. By demonstrating that the organic contaminant produced here is the same as the Russian material and is not a polymer of water, the case can be concluded. In this regard, we have measured the molecular weight of our material[5] and found it similar to theirs.[6] More recently we have determined the refractive index (tentatively, 1.4–1.5 compared with 1.48[7]) and repeated the distillation experiments. The latter are as yet inconclusive; certainly the material is volatile and decomposes, apparently to form H_2O. With rigorous exclusion of O_2, however, the volatile component ($\ll$ 1 mm vp at 300°) appears to carbonize on heating to 600°. We intend to report these experiments in some detail at a later date.

Acknowledgments. We are pleased to acknowledge that the work reported above was supported by The Advanced Research Projects Agency of The Department of Defense (Contract No. DAAH01-71-C-1216) and by the Office of Saline Water, Department of the Interior (Contract No. 14-01-0001-2259).

(4) R. E. Davis, D. L. Rousseau, and R. O. Board, *Science*, **171**, 167 (1971); D. L. Rousseau, *ibid.*, **171**, 170 (1971).

(5) S. B. Brummer, G. Entine, J. I. Bradspies, H. Lingertat, and C. Leung, *J. Phys. Chem.*, **75**, 2976 (1971).

(6) B. V. Deryagin, B. V. Zhelezny, N. N. Zakhavaeva, O. A. Kiseleva, A. I. Konovalov, D. S. Lychnikov, Ya. I. Rabinovich, M. V. Talaev, N. V. Churaev, *Dokl. Akad. Nauk SSSR*, **189**, 1282 (1969); B. V. Deryagin, B. V. Zhelezny, Ya. I. Rabinovich, V. K. Simonova, M. V. Talaev, and N. V. Churaev, **190**, 372 (1970).

(7) B. V. Deryagin, Z. M. Zorin, and N. V. Churaev, *ibid.*, **182**, 811 (1968).

TYCO LABORATORIES, INC.
WALTHAM, MASSACHUSETTS 02154

S. B. BRUMMER*
J. I. BRADSPIES
G. ENTINE
C. LEUNG
H. LINGERTAT

RECEIVED NOVEMBER 8, 1971

Two New Texts From Harper & Row

Modern Theory of Polymer Solutions/HIROMI YAMAKAWA, Kyoto University. Systematically describes the theoretical advances of the last 20 years in the study of the equilibrium and nonequilibrium properties of dilute polymer solutions. Emphasis throughout is on physical pictures and theoretical methods, which are carefully developed and explained. 1971. 619 pp.; $19.95.

Introductory Quantum Chemistry/S. R. LA PAGLIA, Georgetown University. This modern text emphasizes observables and real chemical systems. Covered in depth: the chemical bond, development of the wave theory of matter, principles of quantum mechanics, atoms and the periodic system, the diatomic molecule, molecular spectra and molecular structure, polyatomic molecules, PI electron theory, Ligand field theory. Prerequisite: One year of college calculus. 1971. 416 pp.; $13.95

For more information on these and other texts write Dept. 275G
Harper & Row, 49 E. 33d St. New York 10016.

1817

ISOTOPE EFFECTS IN CHEMICAL PROCESSES

ADVANCES IN CHEMISTRY SERIES NO. 89

Thirteen papers from a symposium by the Division of Nuclear Chemistry and Technology of the American Chemical Society, chaired by William Spindel. Includes:

- Separating isotopes by chemical exchange, distillation, gas chromatography, electromigration, and photochemical processes
- Methods for fractionating isotopes of hydrogen, lithium, boron, carbon, and nitrogen
- Thermotransport in monatomic and ionic liquids
- Statistical-mechanical theory determining isotope effects

278 pages with index Clothbound (1969) $13.00

Postpaid in U.S. and Canada; plus 30 cents elsewhere.

Free set of L. C. cards with library orders upon request.

Order from:

SPECIAL ISSUES SALES
AMERICAN CHEMICAL SOCIETY
1155 SIXTEENTH ST., N.W.
WASHINGTON, D.C. 20036

Inorganic Chemistry is the one...

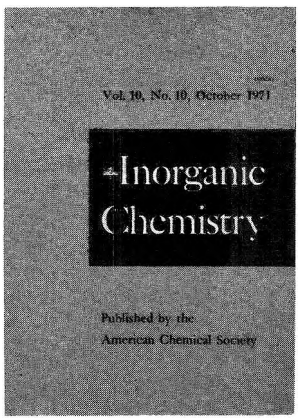

that publishes both experimental and theoretical fundamental studies in *all phases of inorganic chemistry.*

These studies include synthesis and properties of new compounds, quantitative studies regarding structure, and thermodynamics and kinetics of inorganic reactions. Articles may range from the borders of organic chemistry to the borders of theoretical physics . . . giving you a broad expanse of authoritative information.

Besides the 35 or more papers presented in each monthly issue, you'll also profit from the shorter *Notes* and the *Correspondence* sections, that provide an informal medium of exchange for scientific views and ideas.

Inorganic Chemistry is the one . . . to order right now for your own professional interests. Simply complete and return the form below.

American Chemical Society
1155 Sixteenth Street, N.W., Washington, D.C. 20036

Please enter my subscription to **Inorganic Chemistry** at the rates checked below.

ACS Members:	Nonmembers:
☐ U.S. $18.00	☐ U.S. $54.00
☐ Canada, PUAS $22.00	☐ Canada, PUAS $58.00
☐ Other Nations $23.00	☐ Other Nations $59.00

☐ Bill me ☐ Bill employer

☐ Payment enclosed (Payable to American Chemical Society)

Name _____ Title _____

Employer _____

Address: ☐ Home ☐ Business _____

City _____ State/Country _____ Zip _____

Nature of employer's business?
☐ Manufacturing or processing ☐ Academic ☐ Government
☐ Other _____
(Please indicate)

☐ I am an ACS member ☐ I am not an ACS member

Payment must be made in U.S. currency, by international money order, UNESCO coupons, U.S. bank draft; or order through your book dealer.

Note: Subscriptions at ACS Member Rates are for personal use only. P3B

NEED

A HIGH RESOLUTION ELECTRON ENERGY ANALYZER?

or ac electron source*?

Then ask ARIS about the EEA Series HIGH RESOLUTION ELECTRON ENERGY ANALYZERS and the MES Series HIGH RESOLUTION MONOCHROMATIC ELECTRON SOURCE (AC)*.

Both Series devices provide energy resolution better than 30meV independent of electron energy from less than 0.1eV on up. And its all done electrostatically in a compact package which mounts on a single 6" O.D. vacuum flange.

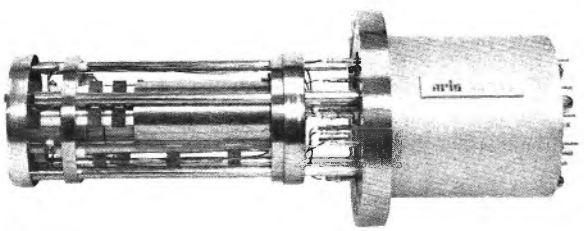

The ARIS Model EEA2000 High Resolution Electron Energy Analyzer. A Modulated Retarding Potential type analyzer. It incorporates a unique electrostatic lens system which acts as a crude monochromator to eliminate beam noise associated with other modulated RPD type analyzers.

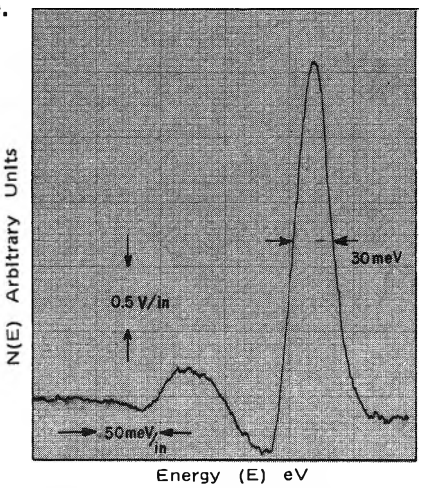

EEA2000 Energy Scan of 2000eV electrons from a monochromatic source. Resolution of the combination was better than 30meV (0.0015%) and limited by the source which was not a standard ARIS source.

Features

- Energy resolution of better than 30meV AT ALL ENERGIES with 6° cone of acceptance
- Constant transmission
- Output signal automatically provides energy distribution
- Uses Modulated Retarding Potential technique, no magnets, completely electrostatic
- Energy range 0-3000 volts
- MES Series Electron Source produces 5×10^{-6} amps of current (AC) per electron volt of resolution to a maximum of 1 microamp.
- A complete operating system
- Ideally suited for both UV and X-Ray ESCA, high resolution AUGER spectroscopy, elastic and inelastic scattering of atoms and molecules, and many other experimental applications requiring an Energy Analyzer
- Electron Source combines with the Energy Analyzer for energy loss system

*Produces a highly monochromatic AC beam superimposed on a non monochromatic DC beam and requires the detection system to be sensitive to AC only; i.e., a lock in type amplifier is required.

for further information, write or call Tom Conklin at

ADVANCED RESEARCH INSTRUMENT SYSTEMS, INC.

6500 Tracor Lane, Austin, Texas 78721 AC512–926-6130